



Land Subsidence

- by fluid withdrawal
- by solid extraction
- theory and modelling
- environmental effects and remedial measures

Edited by

FRANS B. J. BARENDS

Delft Geotechnics, PO Box 69, 2600 AB Delft, The Netherlands

FRITS J. J. BROUWER

*Ministry of Transport, Public Works and Water Management,
PO Box 5023, 2600 GA Delft, The Netherlands*

FRANS H. SCHRÖDER

*The Netherlands Geodetic Commission, PO Box 5030, 2600 GA Delft,
The Netherlands*

Proceedings of the Fifth International Symposium on
Land Subsidence, held at The Hague, The
Netherlands, 16-20 October 1995.

The symposium was convened by the International
Association of Hydrological Sciences and the United Nations
Educational, Scientific and Cultural Organization
(UNESCO), as part of the International Hydrological
Programme, and The Netherlands Geodetic Commission.
Support and co-sponsorship for the symposium was provided
by many international and Dutch national organizations.



*UNESCO provided financial sponsorship for this
publication within the framework of the International
Hydrological Programme under project M.3.5(C) on
"Groundwater assessment and environmental impact due
to over-development"*

**Published by the International Association of
Hydrological Sciences 1995.**

IAHS Press, Institute of Hydrology, Wallingford, Oxfordshire
OX10 8BB, UK.

IAHS Publication No. 234.

ISBN 0-947571-74-4

British Library Cataloguing-in-Publication Data.

A catalogue record for this book is available from the British Library.

IAHS is indebted to the employers of the Editors for their invaluable support and the services provided that enabled the Editors to function effectively and efficiently. Support from Delft Geotechnics, PO Box 69, 2600 AB Delft, The Netherlands, for the first Editor, is particularly appreciated and acknowledged.

The designations employed and the presentation of material throughout the publication do not imply the expression of any opinion whatsoever on the part of IAHS concerning the legal status of any country, territory, city or area or of its authorities, or concerning the delimitation of its frontiers or boundaries.

The use of trade, firm, or corporate names in the publication is for the information and convenience of the reader. Such use does not constitute an official endorsement or approval by IAHS of any product or service to the exclusion of others that may be suitable.

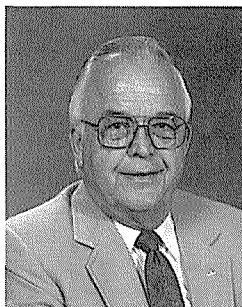
The Editors would like to express their appreciation to the many people who gave their time, effort, and knowledge to produce the successful programme and field trips. Special thanks go to IAHS Secretary General (until July 1995) Henny Colenbrander (The Netherlands), to Jolanda Hey who provided the considerable secretarial assistance needed for the symposium. The front cover and FISOLS 95 logo were designed by Jos Rietveld and Hans Hooghart. Finally, this proceedings would not have been possible without the publication assistance of Penny Kisby at IAHS Press, Wallingford, UK.

The Editors would also like to express their thanks for the support and sponsorship provided for the symposium by the following companies and organizations:

AKZO Nobel Chemicals	Netherlands Ministry of Foreign Affairs
AMOCO Netherlands Petroleum Company	Netherlands Society for Soil Mechanics and Foundation Engineering
Delft Geotechnics	Royal Dutch Academy of Sciences (KNAW)
Delft University of Technology	Royal Dutch Shell
Elf Petroland	Royal Institute of Engineers in the Netherlands (KIVI)
Geological Survey of the Netherlands (RGD)	State Supervision of Mines (STodM)
Harbour of Delfzijl	Rijkswaterstaat, Ministry of Transport, Public Works and Water Management
International Institute for Infrastructural, Hydraulic and Environmental Engineering, Delft (IHE)	TNO Institute of Applied Geoscience
International Association of Geodesy (IAG)	U.S. National Committee for Scientific Hydrology
Municipality of The Hague	Waterboard of the Province of Groningen
Nederlandse Aardolie Maatschappij (NAM)	
Netherlands Ministry of Economic Affairs	

The camera-ready copy for the papers was prepared at the authors and improved and completed at Delft Geotechnics (by Jolanda Hey, Letty van der Meer, Peter Ruygrok, Gert Greeuw) and assembled by Penny Kisby at IAHS Press, Institute of Hydrology, Wallingford, Oxfordshire, UK.

In honour of the many years of research and education on land subsidence this proceedings volume is dedicated to A. Ivan Johnson and Soki Yamamoto



This dedication provide high praise and recognition to A. Ivan Johnson for his long personal history of teaching, research and stimulation in the field of hydrology.

Ivan Johnson served 31 years with the Water Resources Division of the US Geological Survey, primarily dealing with groundwater studies and research related to artificial recharge, land subsidence and water in the vadose zone.

He was Chief of the US Geological Survey National Hydrologic Laboratory, of the National Special Purpose Equipment Unit and of the National Water Resources Training Center in Denver. He also served for eight years as Assistant Chief of the Office of Water Data Coordination in Washington, DC, where he was responsible for coordinating water activities amongst some 30 USA Federal Agencies.

Throughout his career Ivan had the responsibility for training many international scientists and engineers at his various US Geological Survey offices and in the Training Center.

Ivan was involved in the 1950s and early 1960s in some of the pioneering research on artificial recharge in Arkansas, New York and California. He is the author, co-author or editor of over 130 published reports and papers.

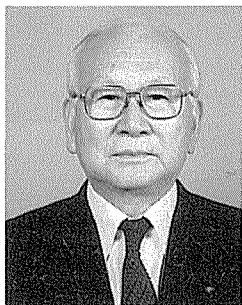
Following his retirement from the US Geological Survey in 1979 he became a consultant and formed his own water and soil consulting company, A. Ivan Johnson Inc., in Arvada, Colorado.

Ivan Johnson is a registered professional engineer and is certified by the American Institute of Hydrology (AIH) as a Professional Hydrologist. He has been a member of the AIH Advisory Board since 1987.

Ivan is Honorary President of the International Association of Hydrological Sciences, and is Chairman of the UNESCO IHP Working Group on Land Subsidence. He was the initiator of the series of international symposia on land subsidence held in Tokyo 1969, Anaheim 1976, Venice 1984 and Houston 1991. He also was involved in the organization of many other international and national meetings with IAHS, the American Geophysical Union, the American Water Resources Association and other bodies.

He holds a large number of awards for merit and service presented by a wide range of scientific and engineering associations. In his many activities he was always greatly supported by his wife Betty.

Because of Ivan Johnson's ever-lasting enthusiasm to inspire organizations and individuals, both national and international, recognition of his achievements is given by this dedication of the proceedings of the Fifth International Symposium on Land Subsidence.



This dedication provides high praise and recognition to Dr Soki Yamamoto, Professor Emeritus of the University of Tsukuba, Professor of Tokyo Seitoku College, Tokyo, Japan, for his long personal history of research and teaching in the fields of hydrology and geography.

Dr Yamamoto has been involved in the UNESCO Working Group on Land Subsidence as well as all five of the IAHS/UNESCO symposia on land subsidence from the beginning of such activities in the early 1970s.

Dr Yamamoto worked for six years for the Water Resources Survey and Planning Division of the South Manchurian Railway Company. He received his Doctorate of Science from the University of Tokyo in 1952, while working from 1947 to 1963 in the Ministry of Agriculture and Forestry. His thesis was entitled "Groundwater in Manchuria". In 1962, Dr Yamamoto was appointed Professor of Hydrology in the Department of Geography, Tokyo University of Education, where he was heavily involved in both research and education. After retiring in 1978, Dr. Yamamoto served as Professor at the University of Rishso until 1985, when he moved to his present position as Professor at Tokyo

Seitoku College. Under his educational leadership, many researchers in hydrology and subsidence have received their Doctor's degrees.

Dr Yamamoto has been very active as an officer in the Japan Science Council, Natural Resources Council of the Ministry of Science and Technology, Atomic Energy Council, and the Central Committee for Environmental Protection. Participation in technical professional organizations included officerships in both the IAHS International Commission on Groundwater and the IAHS Bureau, Association of Japanese Geographers, Japan Association for Quaternary Research, and the Japan National Committees for the International Hydrological Programme (IHP) and the International Union of Geodesy and Geophysics.

Dr Yamamoto has been a prolific author of technical papers and reports and also as editor of books, many of which have been on the subject of land subsidence. He received a United Nations Fellowship for work with the US Geological Survey in 1956.

In 1969 Soki Yamamoto, together with Joseph Poland and Ivan Johnson, organized the IAHS First International Symposium on Land Subsidence. Several years later, he joined Poland, Johnson, and several other subsidence researchers on the newly formed UNESCO/International Hydrological Decade Working Group on Land Subsidence. Since that time, Dr Yamamoto contributed much to the Working Group's activities: symposia, workshops, and publications. Because of Dr Yamamoto's outstanding scientific stature and reputation, both nationally and internationally, recognition of his achievements is given by this dedication of the proceedings of the Fifth International Symposium on Land Subsidence.

Symposium Committees

The organization of the symposium took place in three committees: the Symposium Advisory Committee (SAC), the International Scientific Committee (ISC), and the Local Organizing Committee (LOC). On behalf of IAHS/UNESCO and The Netherlands Geodetic Commission appreciation is expressed to all the staff members and contributors in the various committees, in particular to:

Symposium Advisory Committee

	organization
F. A. Bierman	<i>AKZO Nobel Chemical</i>
H. J. Colenbrander	<i>International Association of Hydrological Sciences</i>
C. W. M. Dessens	<i>Ministry of Economic Affairs</i>
P. J. D. van Ditzhuijzen	<i>Royal Dutch Shell</i>
A. van den Ende	<i>Association of Waterboards</i>
J. M. H. van Engelshoven	<i>Royal Dutch Institution of Engineers</i>
R. A. Feddes	<i>National Committee IHP/UNESCO</i>
T. F. Happel	<i>Elf Petroland</i>
A. J. E. Havermans	<i>Municipality of The Hague</i>
L. M. L. H. A. Hermans	<i>Province of Friesland</i>
J. R. Hoogland	<i>Rijkswaterstaat</i>
J. A. Oele	<i>Nederlandse Aardolie Maatschappij</i>
W. A. Segeren	<i>IHE Delft</i>
H. Speelman	<i>TNO Institute of Applied Geoscience</i>
Chr. Staudt	<i>Geological Survey of the Netherlands</i>
W. Stevelink	<i>Delft Geotechnics</i>
P. J. G. Teunissen	<i>Netherlands Geodetic Commission</i>
A. K. van der Tuin	<i>State Supervision of Mines</i>
H. J. L. Vonhoff	<i>Province of Groningen</i>
K. F. Wakker	<i>University of Technology Delft</i>
V. P. Whitfield	<i>AMOCO Petroleum Company</i>

International Scientific Committee

	discipline
A. I. Johnson (Co-Chairman)	hydrology
F. J. J. Brouwer (Co-Chairman)	geodesy
F. B. J. Barends (Secretary)	geotechnics
L. Carbognin	groundwater
S. A. P. L. Cloetingh	geophysics
G. Figueroa Vega	groundwater
J. A. M. van der Gun	geohydrology
M. Hofman	geodesy
J. M. Marquenie	environment
P. M. Maurenbrecher	informatics
J. J. E. Pöttgens	mining
N. Rengers	engineering geology
F. Schokking	geology
P. M. T. M. Schutjens	reservoir deformation
S. Yamamoto	groundwater
H. Wassmann	salt mining

Local Organizing Committee

	task
F. B. J. Barends	Chairman
F. H. Schröder	Secretary
G. K. Lorenz	Treasurer
J. A. Boswinkel	Public relations
A. Lokhorst	Social programme
P. M. T. M. Schutjens	Accommodation
H. J. Gussinklo	Excursion
J. J. E. Pöttgens	Excursion
J. van de Kamp	Registration

Preface

Subsidence (land surface sinking) occurs in many parts of the world, particularly in densely populated deltaic regions, causing extremely expensive damage. Subsidence has resulted from natural causes, such as tectonic motion and sea level rise, from man-induced causes, such as the heavy withdrawal of groundwater, geothermal fluids, oil, and gas, or the extraction of coal, sulphur, gold, and other solids through mining, or underground construction (tunnelling), or from other mixed causes, such as the hydro-compaction of loosely deposited sediments, oxidation and shrinkage of organic deposits, or the development of sinkholes in karstic terrain.

Over 150 areas of contemporary subsidence are known, some with as much subsidence as 10 m in countries such as Mexico, Japan, and the United States. Many more areas of subsidence are likely to develop in the next few decades as a result of accelerated exploitation of natural resources in order to meet the demands of increasing population and industrial development in many developed countries of the world. As developing countries expand their industry, subsidence is likely to occur in many more areas.

Most of the major subsidence areas around the world have developed in the past half century, probably starting to a great extent during World War II and continuing since then, at accelerated rates due to the rapidly increasing use of groundwater and of oil and gas. Most areas of known subsidence are along coasts where the phenomenon becomes quite obvious when the ocean or lake waters start coming further up on the shore. In some such areas, the usually dense population and intensive industrial development are protected from being flooded by several metres of water only by construction of extensive and expensive systems of dikes, flood walls, and pumping stations. The most common subsidence, that due to underground fluid withdrawal, is such a subtle phenomenon – often of large areal extent and at a slow rate – that the problem is not evident in inland areas until new precise levelling takes place or underground pipelines crack, well casings fail or stand above ground level, surface drainage patterns change, or canals no longer carry original design flows.

Developers, as well as the engineers and scientists making the studies and plans for industrial complexes, urban developments, water supply systems, and natural resource extractions need to know about the potential hazards, costs, and socio-environmental impacts that can result from land subsidence.

The Fifth International Symposium on Land Subsidence (FISOLS 95) is the fifth in the series of land subsidence symposia convened by IAHS/UNESCO with the main emphasis on hydrology and fluid withdrawal from underground reservoirs. The disciplines of mining/reservoir engineering and geotechnical engineering organized in the last 15 years other conferences on the subject of land subsidence which are also worthwhile mentioning: Pensola Beach (1979), Fountainhead (1982), Boulder (1984), Henniker (1984), Newark (1985), Dhanbad (1989).

The main objective of FISOLS 95 was to gather specialists of all relevant

disciplines – scientists, engineers and authorities – to discuss and to study the occurrence of land subsidence, its causes and effects, including remedial measures. In this era of increasing awareness by mankind of the relevance of sustainable growth, special emphasis was put on ecological and monitoring aspects of land subsidence, anticipating the need for a broad multidisciplinary approach to new problems and modern solutions related to land subsidence.

From the large number of contributions received (168 scientific and technical contributions from over 30 countries), 91 have been selected for inclusion in the proceedings. These are published in two separate volumes, this volume published by IAHS and a second volume published by Balkema, Rotterdam. The contents of these volumes are as follows:

Main theme	Subthemes	IAHS volume	Balkema volume
Causes of land subsidence	Natural causes of subsidence		*
	Subsidence by fluid withdrawal	*	
	Subsidence by solid extraction	*	
Determination of land subsidence	Measuring techniques		*
	Theory and modelling	*	
Effects of land subsidence	Environmental effects and remedial measures	*	
	The Groningen Gas Fields		*

The last theme encompasses contributions on various aspects related to one of the world largest gas reservoirs: the Groningen Gas Fields.

The symposium was held at the beautiful Atlantic Hotel in Kijkduin, the Hague, built on the dunes along the North Sea coast. The Municipality of the Hague offered a warm welcome reception at the new Town Hall. Three technical excursions were organized by the Nederlandse Aardolie Maatschappij and Elf Petroland oil/gas companies, visiting the Groningen Gas Fields including the harbour of Delfzijl, which is subjected to subsidence, or visiting the gas production plant on the island of Ameland passing the Waddenzee, a unique natural marine resort, or visiting the remote-controlled Zuidwall production platform specially equipped to prevent damage to an area of great ecological importance. A post-symposium tour took place to the former Dutch coal mining district near the city of Maastricht.

We hope all readers find this publication interesting and informative.

Frans B. J. Barends

Chairman of the Local Organizing Committee and Secretary of the International Scientific Committee, FISOLS 95

Frits J. J. Brouwer

Co-Chairman of the International Scientific Committee, FISOLS 95

Frans H. Schröder

Secretary of the Local Organizing Committee, FISOLS 95

A quarter century of IAHS/UNESCO technology transfer regarding land subsidence occurrence and research

Because of the wide international distribution of land subsidence and the resultant extensive problems, land subsidence was one of the topics included by UNESCO (United Nations Educational, Scientific, and Cultural Organization) in its list of projects needing research and technology transfer. The UNESCO long range programme for land subsidence eventually included its International Hydrological Decade (IHD), which began in 1965, and four International Hydrological Programmes (IHP) – continuing UNESCO programmes beginning in 1975, with each subsequent programme segment being 5 years long. To provide a forum for exchange of subsidence information and research from those specialists who have had to deal with the problems, UNESCO organized in April 1974 under IHP-I, project 8.4: "Working Group on land subsidence due to groundwater exploitation", with the objective of organizing symposia, collecting worldwide data, and writing a casebook on land subsidence. The Working Group Chairman was Joseph Poland, US Geological Survey, Sacramento, California, USA; with members A. Ivan Johnson, US Geological Survey, Denver, Colorado, USA; Laura Carbognin, National Research Council of Italy, Venice, Italy; German Figueroa-Vega, Water Commission of the Valley of Mexico, Mexico City, Mexico; and Soki Yamamoto, University of Tokyo, Tokyo, Japan. UNESCO Staff Liaison to the Working Group was Jose da Costa. These Working Group members had previously spent many years in study of land subsidence and were still actively involved in trying to solve a variety of problems resulting from subsidence in their countries, as well as other parts of the world.

The objectives for the Working Group, as stated in UNESCO IHD project documents, resulted in the Working Group inviting the International Association of Hydrological Sciences to co-sponsor an International Symposium on Land Subsidence, convened in Tokyo, Japan, during 1969. That first symposium was followed by a series of symposia: The Second International Symposium on Land Subsidence at Anaheim, California, USA, in 1976 (IHP-I); The Third International Symposium at Venice, Italy, in 1984 (IHP-II), The Fourth International Symposium at Houston, Texas, USA, in 1991 (IHP-III), and now The Fifth International Symposium at The Hague, The Netherlands, in 1995 (IHP-IV). All five symposia have been held at locations with major subsidence problems and all five symposia included 2-to-3-day field trips to areas of subsidence. Selected papers presented in the first four symposia were published by IAHS as Publications no. 88-89, 121, 151 and 200, respectively, in the "Red Book" Series of Proceedings and Reports.

During the period from 1969 to the present, the Working Group has circulated a detailed 4-page questionnaire to collect data on occurrence, research, and remedial work on land subsidence throughout the world. The questionnaire was sent to geological, hydrological, and petroleum agencies throughout the world. In addition, the questionnaire was advertised widely as being available on request and also was provided to all authors in each of the first four symposia. Hundreds of the

questionnaires have been collected from many parts of the world and the Working Group hopes to summarize and publish the collected data.

Also since the formation of the UNESCO Working Group, the members completed a 1327-page report published in 1984 by UNESCO entitled *Guidebook to Studies of Land Subsidence Due to Ground-Water Withdrawal*. The members, with Dr Joseph Poland as chief editor, wrote most of the sections and used much of the data collected through the previously circulated questionnaires.

In 1979 the UNESCO/IHP Working Group members, with assistance from several Mexican specialists, presented a UNESCO-sponsored week-long "Workshop on Land Subsidence" at Mexico City, primarily for attendees from South and Central America. The workshop also included a subsidence field trip in Mexico City and adjacent areas. Also in 1979, the Working Group and the American Society of Civil Engineers co-sponsored a "Seminar on Legal, Socio-Economic, and Environmental Significance of Land Subsidence in the United States", held in Atlanta, Georgia.

For the beginning of UNESCO's IHP-IV in 1991, land subsidence was continued as IHP/IV project M.3.5(C): "Groundwater assessment and environmental impact due to over-development". Due to the illness of Joseph Poland, Ivan Johnson was requested to take over the chairmanship, and all members of the previous working group continued as members for Working Group M.3.5(C). Dr Poland died in June 1991, only one month after the Fourth Symposium in Houston.

During the Houston Symposium, informal invitations were received to convene the Fifth International Symposium on Land Subsidence in either China or The Netherlands. These offers were discussed by the UNESCO/IHP Working Group members at the end of the Houston meeting and again during the 1993 IAHS Fourth Scientific Assembly in Yokohama, Japan. After due deliberation of detailed proposals received from each country, the Working Group members selected The Netherlands for the Fifth Symposium and action subsequently was initiated to convene FISOLS 95 at The Hague in October 1995. This proceedings with many excellent contributions shows that the Fifth Symposium on Land Subsidence was a success. The subject of land subsidence is currently at the centre of significant technical development and the results of this activity will be of importance for the future.

A. Ivan Johnson

Honorary President IAHS

Co-Chairman International Scientific Committee, FISOLS 95

Ground movements over the coal mines of southern Limburg, The Netherlands, and their relation to rising mine waters

R. F. BEKENDAM

Delft University of Technology, Section of Engineering Geology, Faculty of Mining and Petroleum Engineering, PO Box 5028, 2600 GA Delft, The Netherlands

J. J. PÖTTGENS

State Supervision of Mines, Voskuilenweg 131, 6416 AJ Heerlen, The Netherlands

Abstract In southern Limburg coal mining has been undertaken for more than 500 years at depths ranging from 0 to more than 800 m. Extensive subsidence, locally exceeding 10 m, resulted in considerable damage. This damage was generally caused by longwall mining at deeper mining levels and can be referred to as sag or through subsidence. After the abandonment of the mines in the 1970s most mine water pumps were switched off and the deeper mines became flooded. Due to the rising mine waters a small vertical lift occurred at the surface of up to 25 cm, which did not bring about additional damage. At the beginning of 1994 pumping ceased completely and the mine waters will reach the shallow mines in the near future. The presence of water in the shallow mines, which are still open, and its overburden will adversely affect the stability of roof, pillars and shafts. This may result in the formation of sinkholes or subsidence troughs threatening structures at the surface. Also the water-supply might be impeded. This article gives an overview of the consequences of the mining activities which arose in the past and deals with the effects of flooding of the shallow mines and eventual saturation of its overburden which can be expected in the future.

INTRODUCTION

In southern Limburg the first mining was undertaken more than 500 years ago in the southeastern part where coal fields had been discovered close beneath the topographical surface. In the shallow seams, which generally dip about 10 to 30° towards the south-east, the long pillar mining system (in German: Langkammerpfeilerbau) was applied. This resulted in an underground pattern of alternating galleries and pillars of a few hundred metres length, orientated parallel to the strike of the seam and interconnected locally by transverse galleries. The mine workings are considered to be still open.

During the beginning of the twentieth century there was a change over to longwall mining. In the course of time coal was mined down to depths of more than 800 m. Pneumatic stowing of panels occurred when unacceptable damage at the surface was expected. The discovery of the enormous natural gas resources in the 1960s marked the end of coal production. In 1974 the last mine was closed. The total coal production, of

the 12 mines within the south Limburg coal fields altogether, from the beginning of this century till 1975 measured $600 * 10^6$ tonnes.

The mining of coal brought about a range of ground movements. The longwall mining resulted in extensive subsidence, causing substantial damage at surface structures. After abandonment of the mines the mine water economy was terminated for the greater part. The deeper mines became flooded, which induced a small uplift at the surface. Since the pumping of mine water has ceased now completely the shallow mines will be flooded as well in the near future. Considering subsurface stability the water will have a negative effect not only on the behaviour of the rock masses in the direct vicinity of the still open mine workings, but also on the behaviour of the overlying rock and soil units and eventual support structures. The formation of sinkholes might be the result.

SUBSIDENCE DUE TO LONGWALL MINING

The deformation of the rock mass overlying a mined longwall panel is illustrated in Fig. 1. According to Kratzsch (1983) the overburden can be divided into four zones on the basis of characteristic deformation behaviour. These zones are, from bottom to top:

- the immediate roof layer, which separates from the rock mass above and collapses either on top of the stowing material or, if no stowing has been applied, on the floor filling the mine opening with rock debris
- the main roof, which deflect downwards gradually over the underlying disintegrated rock mass, resulting in movements along discontinuities, predominantly near-vertical joints;
- the intermediate zone, which deflects downwards more or less elastically with only minor movements along some bedding planes;
- the surface zone, consisting of soil which behaves plastically. This zone deflects gradually over the solid bedrock resulting in a subsidence trough at the surface.

The extent of a subsidence area is determined by the angle of draw, which is about 45° for the coal fields of south Limburg. The maximum subsidence at the surface was observed to be nearly equal to the seam thickness. Pneumatic stowing proved to reduce the surface subsidence with about 50%. The subsidence at an arbitrary point is calculated according to the empirical integration-grid method (see e.g. Kratzsch, 1983). For south Limburg the integration grid consists of five concentric rings and is radially subdivided into eight sectors. The radius of the outer ring is equal to the seam depth. The contribution to subsidence within the concentric rings is respectively 40, 28, 16, 12 and 4% of the seam thickness.

The subsidence measured locally more than 10 m and brought about considerable damage in one of the most densely populated areas of The Netherlands. Most damage was the result of the dynamic character of the mining process, i.e. the daily advance of the coal face. Figure 2 shows the subsidence due to coal mining in south Limburg.

UPLIFT DUE TO RISING MINE WATER

The mines of southern Limburg were abandoned in phases and mine water pumps were switched off one by one. To protect the still operating mines against flooding dams were built at various locations which resulted in a repartition of the coal fields into a series

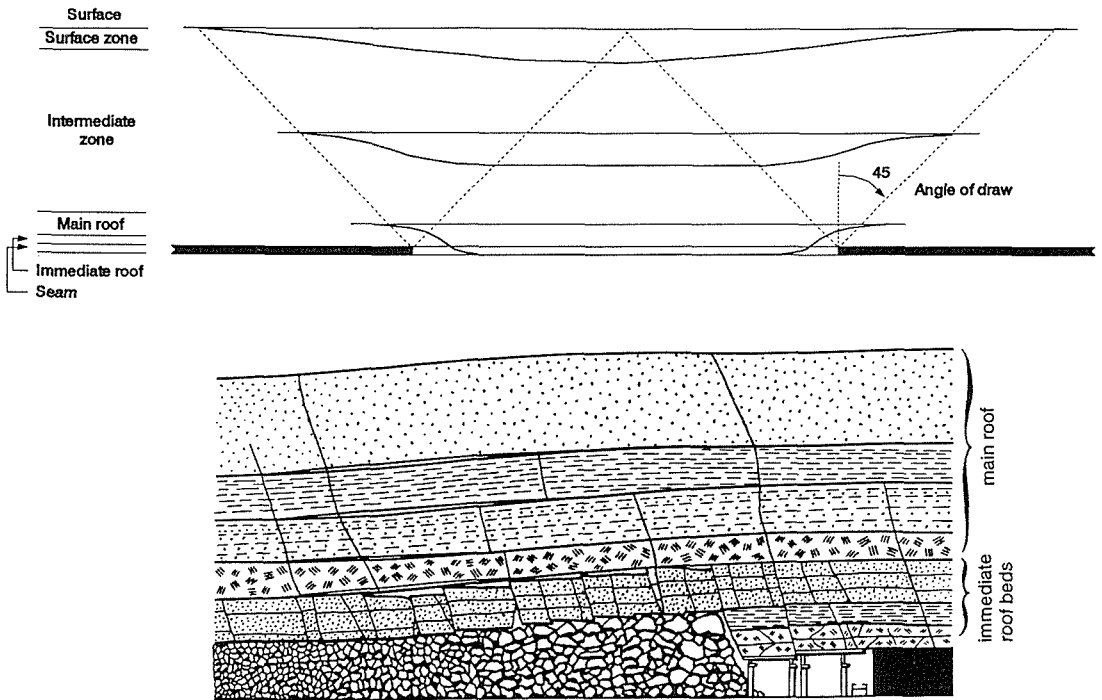


Fig. 1 Zones of deformation over an undermined rock mass, critical case (after Kratzsch, 1983).

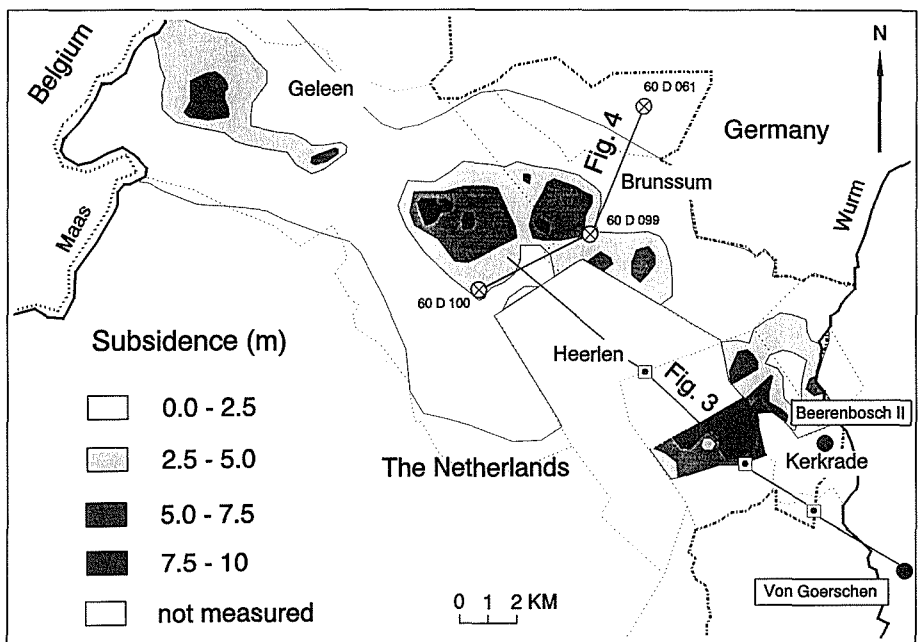


Fig. 2 Map of the coal mining area of southern Limburg showing the amount of surface subsidence.

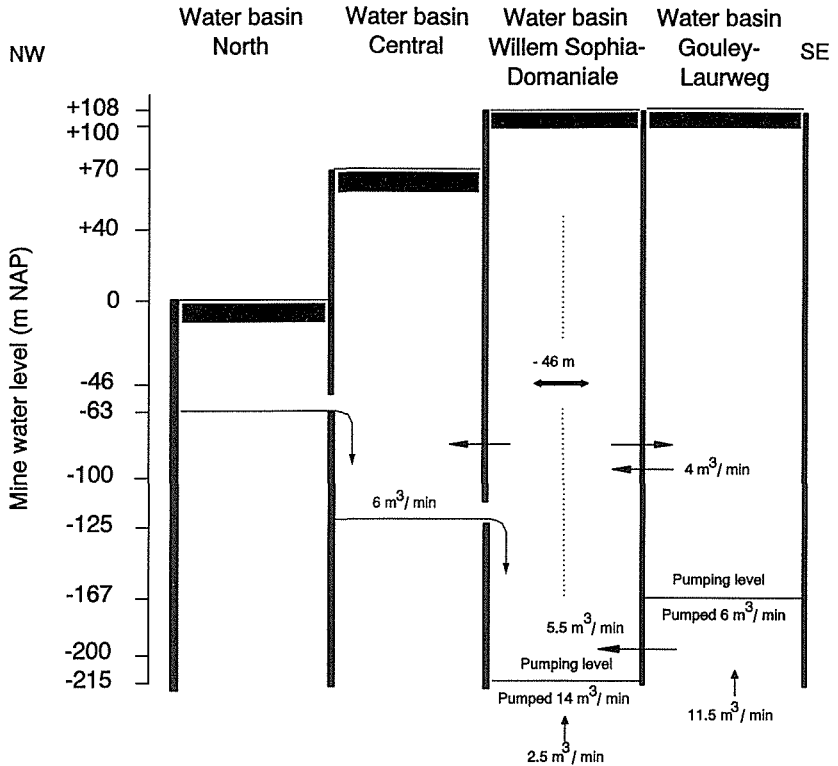


Fig. 3 Profile of the mine water basins showing overflow levels and discharges. The section is indicated in Fig. 2.

of separate basins. The mines out of production became flooded up to a series of overflow levels. The mine water economy is explained in Fig. 3. In the western basins the mine water rose to -61 m NAP. An overflow at -63 m NAP connects the western basins with the central basin, where the mine water reached a level of -125 m NAP. The water in this basin flows over at -138 m NAP into the basin of the Willem-Sophia Domaniale, which is also in hydraulic connection with the German Gouley-Laurweg basin. Till the beginning of 1994 the neighbouring mines Anna and Emil Mayrisch near Aachen, just across the Dutch-German border, were still in operation. To protect these mines mine water was pumped respectively through the shaft of Beerenbosch II from -220 m NAP and through the shaft of Von Goerschen from -169 m NAP and drained off into the River Wurm.

As a result of the rising mine water the mine workings became flooded, which brought about some uplift. This uplift is explained by an increase of pore pressure in the disturbed rock over the longwall panel (Pöttgens, 1985). The zone of main roof layers contains open fractures and the zone of immediate roof layers is even disintegrated. Hence in both zones the porosity and permeability is increased considerably and this disturbed rock mass becomes prone to the ingress of mine water. The total thickness of both zones together is estimated at about four times the seam thickness. The pore pressure in the disturbed rock mass can increase up to the hydrostatic pressure if the mine water reaches the topographic surface. This pore pressure increase brings about

an expansion of the zone of disturbed rock. As a consequence uplift will occur at the surface.

The surface uplift is analysed with the help of the theory of poro-elasticity, which considers a linear relation between the increase of pore water pressure and the vertical expansion of a rock mass of infinite horizontal extent:

$$\Delta h = h * D_m * \Delta p \quad (1)$$

where:

h = thickness of the zone of disturbed rock, taken as four times the seam thickness;

D_m = uniaxial dilation coefficient (bar^{-1}) of the disturbed rock mass;

Δp = increase of pore pressure (bar) within the disturbed rock mass.

The uplift at the surface is linearly dependent of Δh and thus increases linearly with the rise of the mine water level. This is in contrast with uplift related to swelling of the disturbed rock mass due to water absorption of the rock material. According to this mechanism, suggested by Oberste-Brink (1940), surface subsidence is expected to be independent of the mine water level, once the zone of disturbed rock has been completely flooded. The field data will demonstrate that the latter mechanism is of minor importance.

In order to determine the uplift at the surface the theory of subsidence due to reservoir compaction of Geertsma (1973) is applied. The application of this theory, based on the concept of strain nuclei, involves the assignment of linear elastic properties to both disturbed rock mass and surrounding rock and soil. Additionally the elastic constants inside and outside the disturbed rock mass are assumed to be identical, which is probably not correct but justifiable for a rough estimation of the surface uplift.

The surface uplift over the centre of a circular zone of disturbed rock of radius R and thickness h at a depth c , where $C = c/R$, is equal to:

$$u_z(0,0) = 2(1-\nu)\left(1 - \frac{C}{\sqrt{1+C^2}}\right) * D_m * h * \Delta p \quad (2)$$

where ν is Poisson's ratio. The value of D_m has been determined indirectly, by relating the measured surface uplift near shafts with the mine water level. A rough estimation of D_m is 0.35 bar^{-1} . This value proved to apply more or less for the whole area, despite the varying composition of the overburden.

It has to be noted that the ratio of uplift due to rising mine water and subsidence developed before is not constant. Uplift and subsidence are affected in a different way by a change in depth and horizontal extent of a mined seam. Moreover, uplift increases at a mine water rise. If we consider the critical case ($C = 1$ at an angle of draw of 45°) the surface subsidence over the middle of the mined area is approximately equal to the seam thickness if no stowing has occurred. Equation (2) shows that in this case the surface uplift is only 29% of the surface uplift over a mined area of infinite horizontal extent. It can be determined that, if the mine water has reached the surface and assuming $D_m = 0.35 * 10^{-3} \text{ bar}^{-1}$ and $\nu = 0.25$, the surface uplift over a panel of critical width and at 500 m depth is about 3% of the surface subsidence.

In the profile of Fig. 4 are depicted the surface subsidence resulting from mining from 1915 to 1974, the surface uplift from 1974 to 1984 and the mined coal seams. The thickness and depth of the coal seams at levelling point 60D099 are shown in Fig. 5.

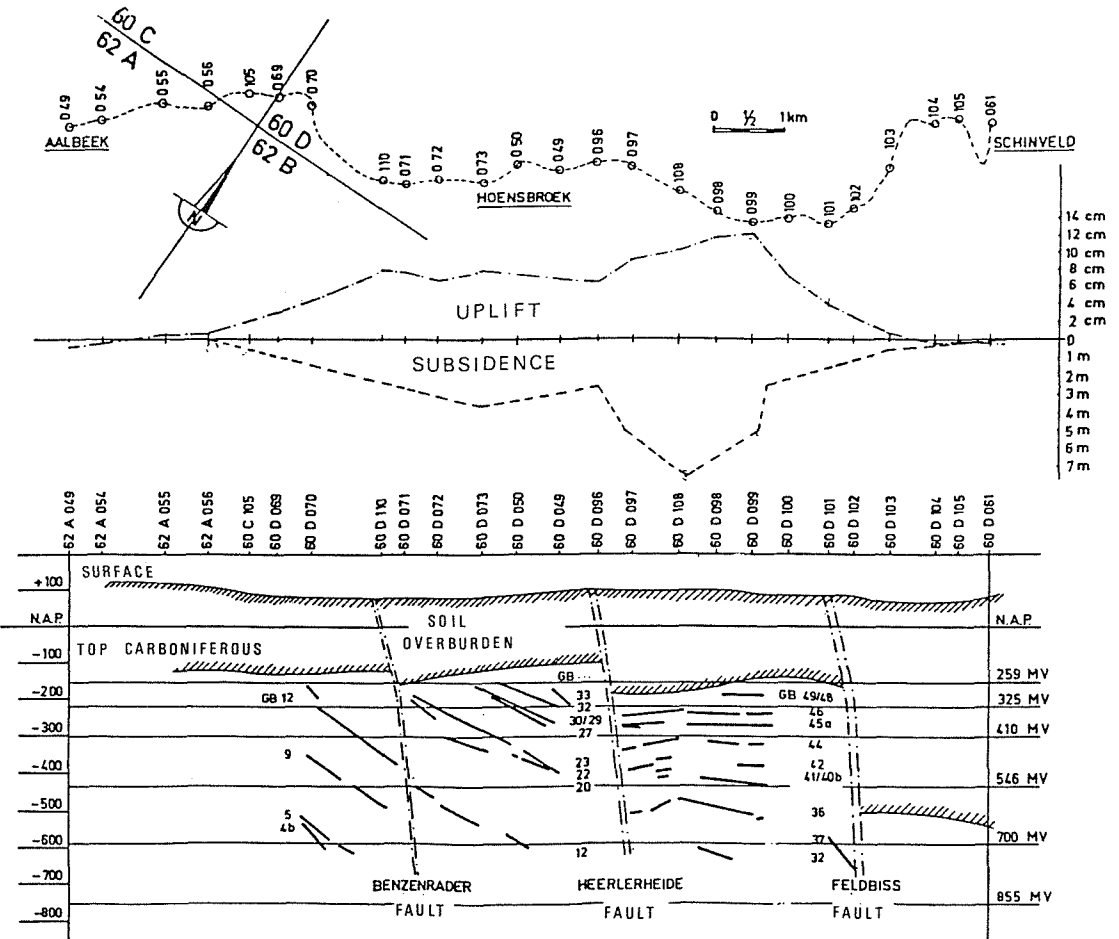


Fig. 4 The section Aalbeek-Hoensbroek-Schinveld showing the measured subsidence and uplift due to coal mining. The section is indicated in Fig. 2.

Obviously a rough correlation exists between surface subsidence and uplift but the uplift/subsidence ratio is varying considerably from point to point. The point of maximum subsidence, point 60D108, does not coincide with the point of maximum uplift, which is point 60D099. However, it should be noted that subsidence has been measured less accurately because at that time less levelling points were available. Generally the uplift is 2 to 4% of the subsidence. Detailed profiles have shown that faults and locations of maximum horizontal extension are accompanied by a sudden "subsidence step" of up to 0.5 m at the surface. Irregularities of surface uplift have not been measured up to now and are not to be expected if the theory of uplift mentioned before is assumed.

The uplift in the course of time of point D099 is shown in Fig. 5. The theoretical results are in good agreement with the measured data. A mine water rise is immediately followed by a surface uplift. In 1990 the mine water reached the overflow level at -63 m NAP. The mine water level did not rise any more and no further uplift has developed accordingly. But, since the pumps have been switched off in the beginning

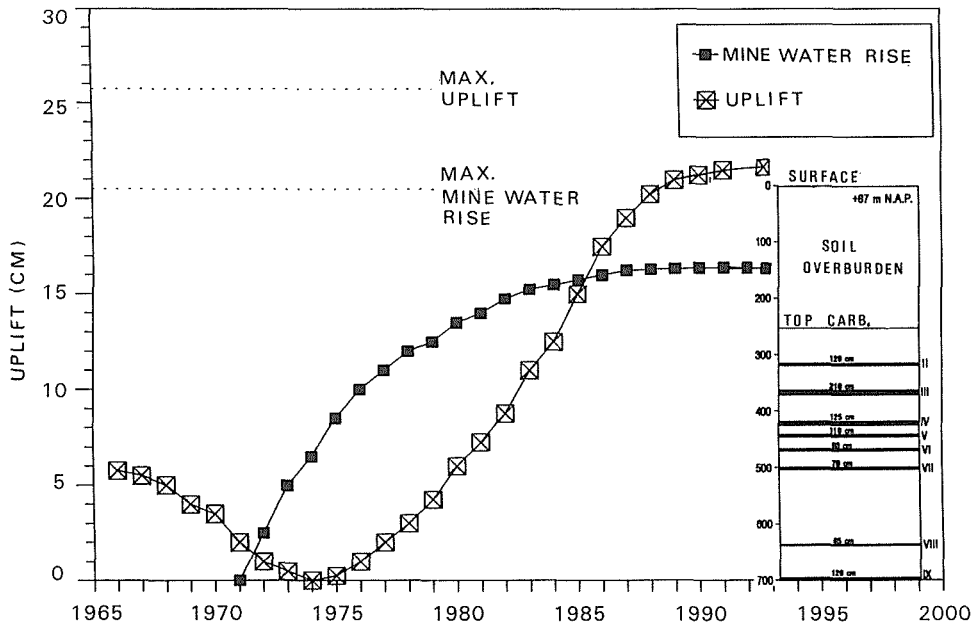


Fig. 5 Mine water level and uplift as a function of time at levelling point of 60D099.

of 1994, the mine water will rise again in the near future and uplift will attain a final value of about 26 cm.

RISK OF SINKHOLE DEVELOPMENT DUE TO RISING MINE WATERS

When pumping through the shafts of Beerenbosch II and Von Goerschen was stopped in the beginning of 1994 the mine water started to rise. In January 1995 levels of -75.85 and -69.45 m NAP were reached in the Willem Sophia-Domaniale and Gouley-Laurweg basins respectively (Fig. 6). The mine water level reached the -125 m NAP level in the spring of 1994. Hence also the level in the central basin has started to rise (Fig. 3). The mine water is expected to reach the overflow level of the northern basins at -63 m NAP in the summer of 1995.

The rise of mine water towards the surface will bring about a risk of sinkhole development in the southeastern concession areas of the Domaniale-Neu Prick and Gouley-Laurweg, situated in the Dutch-German borderland. As mentioned before, coal was to be found here close to the surface and the heritage of former coal mining comprises many shallow, still open long pillar mines and shafts often not adequately filled and plugged.

Although the water will give some support pressure inside the galleries all in all the presence of water in the shallow mines and its overburden will reduce the stability of roof and pillars. Especially roof collapses at gallery intersections might occur. For example effective stresses inside the rock mass will decrease, and cohesion and angle of friction, both internal and in discontinuities, will diminish. As a consequence the failure envelope and Mohr circle will shift towards each other, increasing the probability

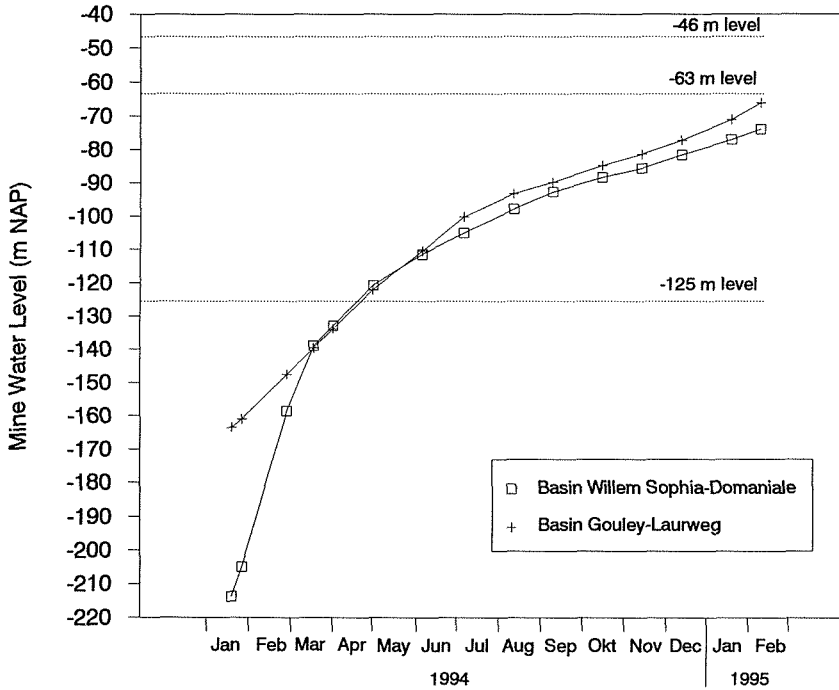


Fig. 6 Graph depicting the mine water rise in the basins of Willem Sophia-Domaniale and Gouley-Laurweg.

of failure. It is known that the presence of water brings about a reduction of unconfined compressive strength for all types of rock. This loss of strength varies significantly per rock type and can amount to 78% for certain sandstones (Hawkins & McConnell, 1992). Furthermore, saturation of the soil overburden brings about an increase of vertical stress at depth resulting in less stable roof conditions.

A roof collapse might result in sinkhole development at the surface if the cavity resulting from the collapse reaches the rock-soil interface. Whether this occurs or not depends on the dimensions and shape of the roof collapse, the height of the gallery, the distance between the gallery roof and the top of the solid rock, and the scree angle and bulking factor of the roof debris. Important contributions in this field have been established amongst others by Fenk (1981), Garrard & Taylor (1988) and Meier (1988). Water entered into the mine may reduce the scree angle of the debris pile. In the galleries generally inclined at about 10 to 30° the debris may even be washed away. Consequently more roof material may accumulate into the gallery and the probability of cavity migration towards the rock-soil interface might increase. Finally, it has to be noted that, if the cavity and the water level reach the soil overburden, cavity migration towards the surface and hence sinkhole formation become more likely because soil becomes less stable on saturation.

Experience acquired in the Westphalian coal fields (Hollmann & Nürenberg, 1972), similar in many aspects to the coal fields considered here, indicate that instability of a shallow mine can result in the formation of a sinkhole if the mine has been excavated within 20 m under the top of the rock-soil interface, which is in this case the boundary

between the Carboniferous sandstone/shale strata and the overlying sands, gravels and clays of the Quaternary and Tertiary. Within the concession of the Domaniale this applies to more than 20 mine workings, which corresponds with a total area of more than 150 ha in a densely populated area. Up to now a few sinkholes have been formed over these mine workings. It has to be found out now how much the probability of sinkhole development might increase as a result of rising mine water.

Within the concession areas of the Domaniale-Neu Prick and Gouley-Laurweg more than 900 shafts, most of them located in Germany, are to be found. In contrast to the other concession areas, here the shallow shafts have been filled with soil and rubble and have not been provided with an adequate concrete cover. Rising mine water would reduce the friction angle of the filling material, which might flow into the open mine workings resulting in a sinkhole at the surface.

In the end of 1995 the mine water is expected to reach the open connection at -46 m between the Dutch and German coal fields. At a further rise of the water much more shafts would be flooded. At the moment the German authorities investigate if all of the about 30 shafts with a base below the -46 m level have been closed off adequately. Whether the mine water will be allowed to rise beyond the -46 m level depends on the outcome of this study. It has become clear already in February 1995 that not all shafts are safe. During remedial works at an old shaft in a district of Kohlscheid it was discovered that the ancient filling material had, possibly due to the rising mine water, collapsed about 110 m into the 270 m deep shaft. In one day about 542 m³ of concrete fill was applied. This shaft had collapsed earlier, in 1861, when eighteen people were killed.

Within the Dutch coal fields only one shaft, the Catharine shaft in the city of Kerkrade, has its base below the -46 m level. The base of this shaft at -98 m NAP has been reached by the mine water in the summer of 1994. The terrain over the shaft has been closed off and remedial measures are planned.

During many centuries the mine water has been drained off through canals into the River Wurm. When the mine water is allowed to rise further the old drainage canals might function again. Then the mine water will reach a final level of $+108$ m NAP at the beginning of the twenty-first century and a few hundred shafts, including about 35 within the Dutch coal fields, will be flooded additionally. Additional research must ascertain if such a rise can be tolerated in view of the safety at the surface.

Finally, it has to be noted that part of the water supply might be affected by the rising mine water. At a few sites water has been pumped since long from reservoirs situated in the Tertiary overburden. In 1995 the mine water will reach the base of one of the reservoirs. To detect pollution of the drinking-water salt concentrations are measured in four wells.

REFERENCES

- Fenk, J. (1981) A theory of sinkhole development over cavities in soils (in German). *Freiberger Forschungshefte* A639, 1-139.
- Garrard, G. F. G. & Taylor, R. K. (1988) Collapse mechanisms of shallow coal-mine workings from field measurements. In: *Engineering Geology of Underground Movements* (ed. by F. G. Bell *et al.*), 181-192. Geological Society Engineering Geology Special Publication 5.
- Geertsma, J. (1973) A basic theory of subsidence due to reservoir compaction: the homogeneous case. *Verh. Kon. Ned. Geol. Mijnbouwk. Gen.* 28, 43-62.

- Hawkins, A. B. & McConnell, B. J. (1992) Sensitivity of sandstone strength and deformability to changes in moisture content. *Quart. J. Engng Geol.* **25**, 115-130.
- Hollmann, F. & Nürenberg, R. (1972) Undeep mining as a technical problem in the execution of safety measures (in German). *Mitteilungen der Westfälischen Berggewerkschaftskasse* **30**, 1-29.
- Kratzsch, H. (1983) *Mining Subsidence Engineering*. Springer, Berlin.
- Meier, G. (1988) On the assessment of sinkhole hazards in rock (in German). *Neue Bergbautechnik* **18**(9), 352-354.
- Oberste-Brink, K. (1940) Surface uplift due to ground movements as a result of mining. *Glück Auf* **76**, 249-256.
- Pöttgens, J. J. E. (1985) Uplift as a result of rising mine waters (in German). In: *The Development Science and Art of Minerals Surveying* (Proc. 6th Int. Congr. Int. Soc. for Mine Surveying, Harrogate, UK), vol. 2, 928-938.

Land subsidence due to gas production in the on- and off-shore natural gas fields of the Ravenna area, Italy

WERTHER BERTONI

Municipality of Ravenna, Ravenna, Italy

GIOVANNI BRIGHENTI

Istituto di Scienze Minerarie, Viale Risorgimento 2, I-40156 Bologna, Italy

GIUSEPPE GAMBOLATI, GIUSEPPE RICCERI

Department of Mathematical Models for Applied Sciences, University of Padova, Beloni 7, I-35100 Padova, Italy

FIorenzo VUILLERMIN

University of Ferrara, Ferrara, Italy

Abstract Over the past 40 years the Ravenna area has experienced an alarming land subsidence with a severe impact on the coastal environment. The sinking rate achieved a maximum value of 6-7 cm the mid 1970s. At present settlement is still occurring in some areas, although at a much reduced rate. The subsidence is mainly related to groundwater withdrawal. However, a significant local contribution may arise because of the natural gas production from a number of deep reservoirs scattered inland and off-shore. In view of the important role that anthropogenic subsidence may play in enhancing the coastline regression, the Authors have studied the impact from three gas fields near the shoreline: Dosso degli Angeli, Angela-Angelina and Porto Corsini. Overall production to date is quite different from one reservoir to the other as is their depth which ranges over the wide interval 1750-4000 m. The results from the present investigation show that a significant land subsidence may have occurred over these fields. The extent of the subsiding bowl may affect areas which host infrastructures and activities of high social, economical and tourist relevance.

INTRODUCTION

The Ravenna area is located in the Southeast part of the Po River Valley (Fig. 1) and in the last 40 years has experienced a widespread land sinking with a severe impact on the environment. The occurrence achieved its peak value during the early 1970s and is still under way, although at a much slower rate.

The maximum land subsidence has exceeded 1 m, causing serious damages to urban, industrial and harbour infrastructures, as well as to the coastal environment. The event was studied in detail by Carbognin *et al.* (1978), who identified the main causes with the extensive groundwater withdrawal and gas production from natural gas reservoirs scattered over the area (Fig. 2). However apportioning of the responsibility of land settlement between groundwater and gas production was highly uncertain. In April 1980,



Fig. 1 Map of the eastern end of the Po River basin.

the Ravenna Municipality appointed the "Committee for the Study of the Subsidence of Ravenna" with the purpose of systematically studying the problem and quantifying the factors responsible for the phenomenon.

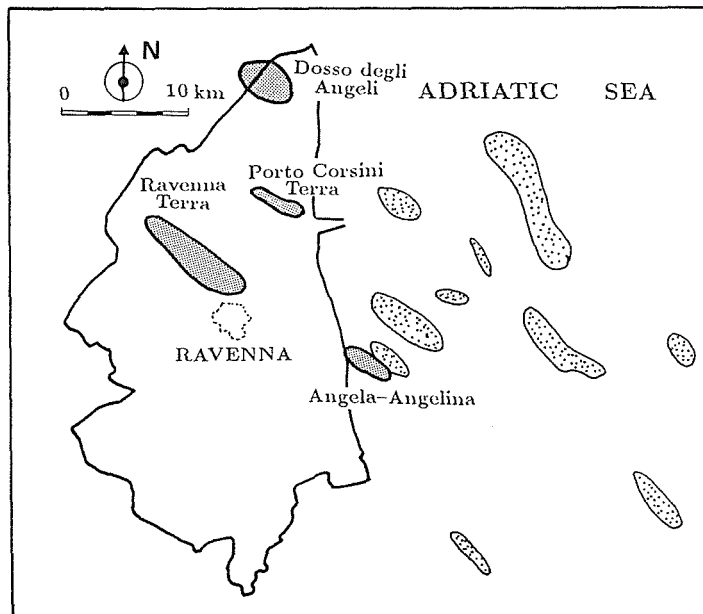


Fig. 2 Location of the main gas fields in the Ravenna area and neighbouring sea.

In particular, the Ravenna groundwater aquifer system was analysed and the regional geology, the Ravenna stratigraphy and the geotechnical soil characteristics were determined. Further periodic surveys have made it possible to draw contour maps of both piezometry and land subsidence.

As far as the effect of gas withdrawal was concerned, the Committee decided to analyse one of the most representative reservoirs. For this purpose the Ravenna Terra gas field, one of the oldest reservoirs detected and exploited by AGIP in this area, was deemed to be particularly suitable because of the large size and because, at that time, its production was completed and AGIP was willing to release all the information regarding the field and the data on its production (over a 30 year period).

The field was made of several pools, with two major pools containing more than 95% of initial in-place gas. The depth ranges between 1720 and 1957 m and the production amounted to $21.77 \cdot 10^9$ SCM, with the maximal pressure decline in the two main pools equal to 8.9 and 9.4 MPa respectively.

The study was performed using a three-dimensional numerical simulation (Gambolati *et al.*, 1991b) and a maximum land sinking more than 60 cm was calculated over the Ravenna gas field.

The main results of the research were submitted to the Municipality in 1988 (Committee for the Study of the Subsidence of Ravenna, 1988) and were also presented in a communication given at FISOLS 91 (Gambolati *et al.*, 1991a). These results showed that the main cause of the regional land subsidence was the extensive pumping of groundwater, which occurred during the 1970s. Gas production played a role restricted to the area overlying the field, while the actual subsidence is related to the reservoir depth, geometrical size and pore pressure decline. Nonetheless, the settlement can be significant and cause damages to the environment especially if it occurs in the vicinity of the coastline.

Since the Ravenna setting is quite precarious along the littoral zone and even a modest land settlement can lead to a severe regression of the coastline and to large economical damages to the irrigation and drainage system as well as to the infrastructures and to man-made installations, the Ravenna Municipality decided to entrust the Committee with a more detailed study, with the aim of examining the risk on the coastal area related to the production of existing on- and off-shore gas fields. The most significant results (Committee for the Study of the Subsidence of Ravenna, 1994) are shortly presented in this contribution.

ORGANIZATION OF THE STUDY

The Committee decided to extend the study to various reservoirs located on- and off-shore in the Ravenna area. More precisely three major fields were studied: Dosso degli Angeli, Angela-Angelina and Porto Corsini Terra (their location is given in Fig. 3). These fields are located mostly in Pliocene series and are made of alternating series of coarse clastic sediments and fine pelagian deposits. The presence of clay layers allows for the formation of multiple pools in the same field that are more or less interconnected. Gas is practically pure methane. Cumulative production and pressure decline vs. time, and other important data were made available by AGIP.

The **Dosso degli Angeli** field, located under the Comacchio Marshes, is made of eight main pools, of which the three most important ones are situated at an average

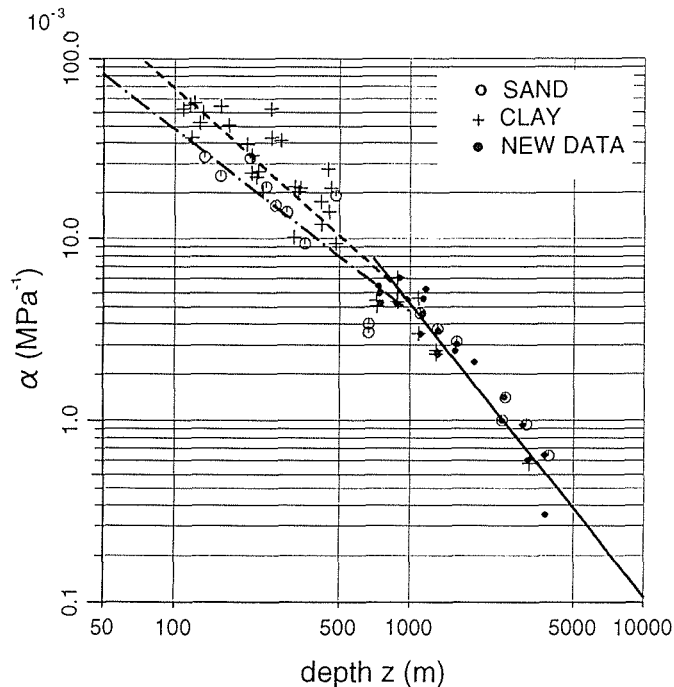


Fig. 3 Vertical soil compressibility α vs. depth.

depth ranging from 3033 to 3232 m, with an initial pressure between 36.3 and 33.7 MPa, and contain more than 85% of the gas in place.

In view of the purpose of the research, the study was limited to the impact of these three major pools. Their cumulative gas production from 1971 to 1991 amounted to $26.7 \cdot 10^9$ SCM with a pressure drop between 25 and 30 MPa, according to the pool. The production history points to the possible presence of an active edge water drive.

The off-shore **Angela-Angelina** field, located at about 2 km from the shoreline south of Ravenna, with an extension below the coastline, is made of 68 pools, five of which only are in production and contain about $8.7 \cdot 10^9$ SCM of gas. Their average depth ranges from 2974 to 3934 m, with an initial pressure between 33.1 and 47.7 MPa.

During the period 1973-1991 the pressure drop was between 5 and 30 MPa approximately, with a cumulative production of about $4.5 \cdot 10^9$ SCM.

The **Porto Corsini Terra** field, located 6 km northeast of Ravenna, is composed of five main pools, with an average depth between 1772 and 2040 m, and initial pressure between 26 and 31 Mpa. From 1969 to 1991, pore pressure declined in the range of 5 to 13 Mpa approximately and cumulative production was about $772 \cdot 10^6$ SCM.

The study of land subsidence over these three fields was performed by a 3-D numerical analysis, similar to that used to predict the subsidence over the Ravenna Terra reservoir (Gambolati *et al.*, 1991b). A 2-D finite element model, developed for each of the simulated pools, provided the corresponding fundamental solution which was then integrated over the actual shape of the reservoirs.

In the case of the Dosso degli Angeli reservoir, where an active water drive may be present, this model was supplemented by a hydrologic finite-element model to calculate

the associated pressure decline in the edge aquifer. The properties of the aquifer surrounding each pool were determined by requiring that the water influx calculated by the model be equal to the water influx calculated by AGIP on the basis of the material balance.

As far as the vertical soil compressibility α is concerned, the values used in the previous study (Gambolati *et al.*, 1991a) were preserved down to approximately 1000 m (α is higher in cohesive soils than in granular soils) while, on the basis of new measurements carried on deep boreholes in the Ravenna area (Brighenti, 1994), for greater depths a new correlation law, holding for both cohesive and granular soils as used also by Van der Van der Knaap & Van der Vlies (1967), was determined. Figure 3 shows values of α vs. depth as were implemented into the mathematical models.

RESULTS AND CONCLUSIONS

The main results of the simulation are given in Figs 4-6. For further details see the report of the Committee (Gambolati *et al.*, 1993). More specifically Fig. 4 shows the 1992 land subsidence over the Dosso degli Angeli field, as predicted by the mathematical model taking into account only the pressure decline in the gas reservoir. In the presence of an active edge water influx, as indicated by AGIP, the maximum settlement may increase by approximately 45 cm. Figure 5 shows the land sinking predicted over the Angela-Angelina reservoir in 1991, while Fig. 6 gives the subsidence predicted over the Porto Corsini Terra reservoir in 1992. Note that maximum settlement over these two fields is actually markedly less than that of Dosso degli Angeli, consistent with the much more limited production and pore pressure decline.

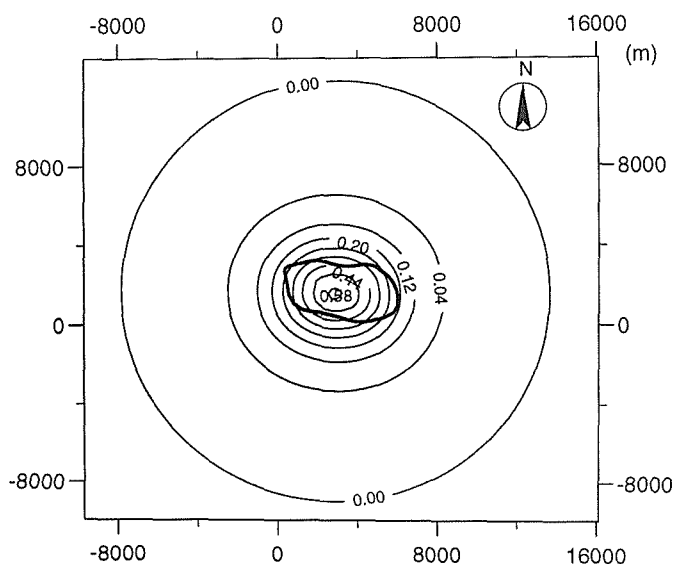


Fig. 4 Contour lines of equal land subsidence (m) due to gas production over the Dosso degli Angeli field in 1992 as predicted by the mathematical model.

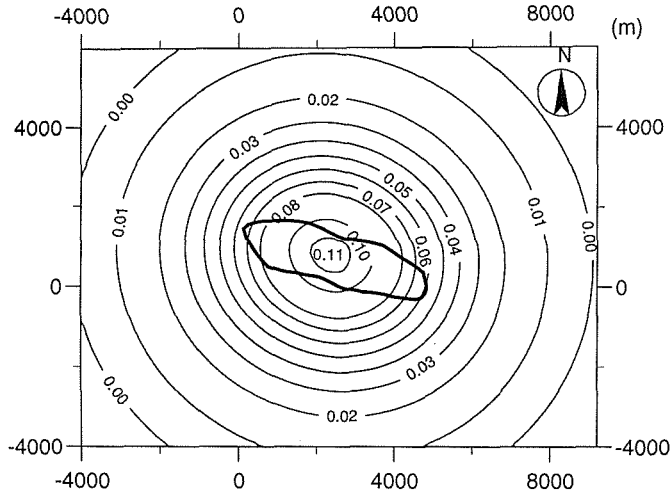


Fig. 5 Contour lines of equal land subsidence (m) due to gas production over the Angela-Angelina field in 1991 as predicted by the mathematical model.

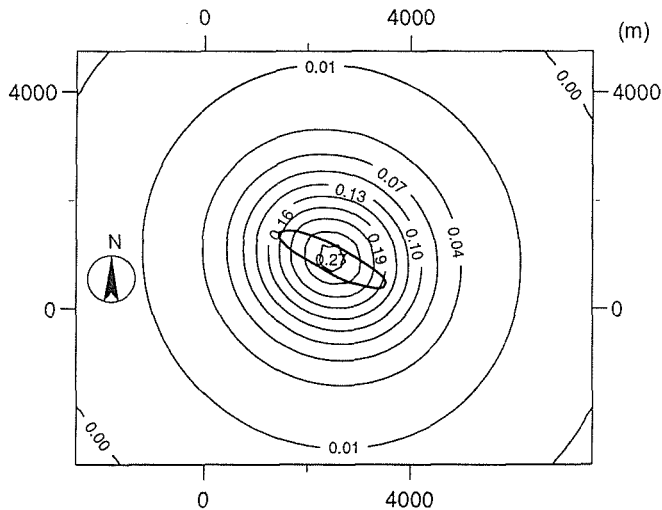


Fig. 6 Contour lines of equal land subsidence (m) due to gas production over the Porto Corsini Terra field at the end of 1992 as predicted by the mathematical model.

Table 1 summarizes the main features and the maximum land subsidence due to gas production for Ravenna Terra, Dosso degli Angeli, Angela-Angelina and Porto Corsini Terra as simulated using the mathematical model.

Careful inspection of Figs 4, 5 and 6 shows that:

- gas production from the Ravenna reservoirs can cause serious subsidence;
- the magnitude of the subsidence bowl depends to a large extent on the size of the reservoir, its depth, overall pore pressure decline and mechanical soil properties (including the mechanical properties of the neighbouring formations);
- for a given reservoir depressurization the presence of an edge aquifer may lead to an increase of land settlement.

Table 1 Representative data and maximum subsidence over some Ravenna area gas fields as predicted by the mathematical model.

Gas field	Average depth (m)	P_i (Mpa)	G_p (10^9 SCM)	Δp (Mpa)	Maximum land subsidence (cm)
Ravenna Terra	1735-1920	20-22	21.8	9	65
Dosso degli Angeli	3033-3232	34-36	26.7	25-30	58*
Angela-Angelina	2974-3934	33-48	4.5	5-30	11
Porto Corsini Mare	1772-2040	26-31	0.8	5-13	27

P_i = initial pore pressure; G_p = cumulative gas production; Δp = final pore pressure decline in the reservoir.

*The influence of an active water drive is not included.

Compressibility data are affected by sample disturbance, improper laboratory stress conditions, anisotropic samples and other experimental inaccuracies (Brighenti, 1994). Moreover, the use of a constant a value for each pool is not entirely correct because this value is taken from a profile obtained by interpolation of fairly scattered experimental data and is related to the initial reservoir pressure, while a is known to vary when the pore pressure undergoes a large variation. For example a variation of more than 30 Mpa was recorded in one of the pools of Dosso degli Angeli field.

The use of a non-linear stress-strain behaviour allowing for a values that decrease as the pore pressure decreases, could improve the outcome from the numerical analysis. However, a better more decisive improvement could be obtained by in situ measurements of reservoir compaction followed by a model calculation of the true reservoir compressibility.

With this premise, the land subsidence values predicted by the present model are nonetheless considered to be representative of the actual occurrence, with an approximation that is consistent with the objective of the investigation. They emphasize that ground settlement due to gas production from gas fields underlying the coast-line can have a significant impact on the stability of the Ravenna coast and can affect areas which host infrastructures and activities with great social, economic and tourist importance. Therefore a more detailed and advanced numerical study of each individual gas field would be most appropriate and is to be highly recommended.

Acknowledgements The authors are indebted to AGIP S.p.A. for providing part of the data used and to the Municipality of Ravenna for financial and technical support.

REFERENCES

- Brighenti, G. (1994) Criteria for soil-compressibility evaluation in the case of subsidence due to fluid withdrawal (in Italian). In: *Geoengineering* (Proc. IV Geoengineering International Congress, Torino, March 1994), 37-42.
- Carbognin, L., Gatto, P., Mozzi, G. & Gambolati G. (1978) Land subsidence of Ravenna and its similarities with the Venice case. In: *Evaluation and Prediction of Subsidence* (ed. by S. K. Saxena), 254-266. ASCE, New York.
- Committee for the Study of the Subsidence of Ravenna (W. Bertoni, G. Brighenti, G. Gambolati, G. Ricceri & F. Vuillermin) (1988) Final report to the Municipality of Ravenna (in Italian).
- Committee for the Study of the Subsidence of Ravenna (W. Bertoni, G. Brighenti, G. Gambolati, G. Ricceri, G. & F. Vuillermin) (1994) Second report to the Municipality of Ravenna (in Italian).

- Gambolati, G., Ricceri, G., Bertoni, W., Brighenti, G. & Vuillermin, F. (1991a) Numerical analysis of land subsidence at Ravenna due to water withdrawal and gas removal. In: *Land Subsidence* (Proc. Fourth Int. Symp. on Land Subsidence, Houston, May 1991), 119-129. IAHS Publ. no. 200.
- Gambolati, G., Ricceri, G., Bertoni, W., Brighenti, G. & Vuillermin F. (1991b) Mathematical simulation of subsidence of Ravenna. *Wat. Resour. Res.* **27**(11), 2899-2918.
- Gambolati, G., Putti, M., Teatini, P. & Bau, D. (1993) Programme with the Municipality of Ravenna for the realization of numerical models to study the risk of land subsidence on the coastline as related to gas production from in land and off-shore reservoirs. Final Technical Report (in Italian). University of Padova.
- Van der Knaap, W. & Van der Vlies, A. C. (1967) On the cause of subsidence in oil producing areas. In: *Proc. VII World Petroleum Congress* (Mexico City), vol. 3, p. 85.

An extensive investigation of land subsidence in the Euganean geothermal basin, Italy

G. GOTTARDI, P. PREVIATELLO & P. SIMONINI

Istituto di Costruzioni Marittime e di Geotecnica, Università di Padova, Via Ognissanti 39, I-35129 Padova, Italy

Abstract In order to characterize the phenomenon of man-induced land subsidence taking place in the Euganean geothermal basin, an extensive investigation has been carried out at the University of Padova. This phenomenon was observed in the recent past and related to the withdrawal of hot waters (85°C) from the subsoil. The currently exploited aquifers are located in the deep calcareous bedrock, hydraulically interconnected to the alluvial Quaternary deposits. In the 1960s the production of hot waters for mud bath treatments caused the progressive piezometric lowering (2.5 m year⁻¹) and the shallow layers cooling. A marked phenomenon of land subsidence thus developed, notwithstanding the deepening of draining wells. A 300 m-deep borehole was drilled and continuously sampled in order to investigate the geotechnical properties of the alluvial soils; at the same time an accurate measurement of water withdrawal and piezometric levels was also planned. The effects of high temperatures on soil parameters and on land subsidence occurrence are also taken into account in the paper.

INTRODUCTION

Phenomena of soil lowering in the Euganean geothermal basin – located at the foot of the Euganean Hills, southwest of Padova (Fig. 1) – had been observed several times in the past and were soon related to the withdrawal of hot waters from the subsoil. The area has been well known since Roman times, as reported by many archaeological finds and witnessed by Latin authors like Lucretius, Titus Livius, native of this country, Plinius Maior and others.

The present hills are mainly composed of volcanic rocks of Upper Eocene and Oligocene age, whereas the present sedimentary rocks are from Upper Jurassic to Lower Oligocene. The whole area is characterized by a close system of intersecting block faults, which caused step-like displacements of the rock formations situated under the alluvial Quaternary sediments. Due to the morphology of the bedrock, the Quaternary deposits – mainly sandy and clayey loose materials – have different thicknesses: in Abano Terme they range from about 100 to a maximum of 230 m, whereas in Montegrotto Terme from 0, where bedrock locally crops out, to a maximum of 180 m.

Discovering the source origin of thermal waters has always fascinated the researchers: earliest assumptions connected the water heat to the natural burning of imagined underground deposits of sulphur and coal. Until the beginning of this century

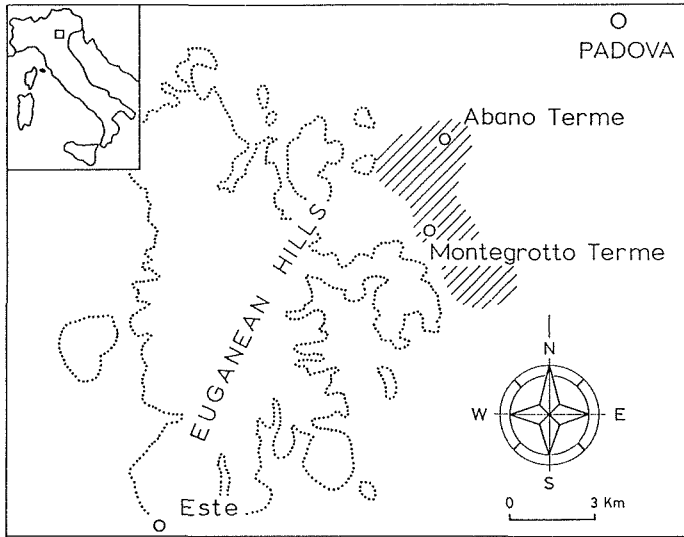


Fig. 1 Location of the Euganean geothermal basin (hatched area).

the heating source was ascribed to the possible presence of magmatic waters; subsequently the idea of the geothermal gradient as main heating cause of the infiltrating rain waters began to develop. In 1973, Piccoli *et al.* carried out an exhaustive research which led to a novel interpretation – now widely accepted – of the Euganean hydrothermal phenomenon. According to the authors the thermalism source is related to the rain waters that, in infiltrating into the subsoil in the "Piccole Dolomiti" area and nearby zones (about 100 km northwest), gain temperature and salinity. In particular the high temperature of the water (varying from 80°C to 87°C) would be produced by the terrestrial heat at depths – around 5000 m – reached by their circulation. Deep waters, moving towards the southeast, reach the area around the Euganean Hills and suddenly go back up through the described system of faults and fractures existing in the local subsoil.

LAND SUBSIDENCE IN THE EUGANEAN BASIN

Until the end of the last century the waters used for thermal baths spontaneously emerged from springs and lakes, thus confirming that the average piezometric head was originally above the ground level. The increasing demand of water for thermal treatments made it subsequently necessary to drill numerous wells into the shallow Quaternary alluvial sediments. This produced the progressive lowering of the piezometric level at an escalating rate, which reached a maximum in the 1970s. In order to withdraw the waters with higher temperature and salinity levels, many wells were finally deepened into the fractured carbonatic bedrock (mainly the "Biancone" formation, Upper Cretaceous-Upper Jurassic, and in part the "Scaglia Rossa", Lower Eocene p.p.-Upper Cretaceous) which now represents the only exploited aquifer with a rather high "equivalent" permeability $k_{eq} = 10^{-3} \text{ m s}^{-1}$. However small cracks in some well casings could cause a slight withdrawal of groundwater from the alluvial sediments too.

Due to its economical and environmental importance, in 1966 the Italian Department of Industry decided to impose a united management of the local geothermal resources. Only after that date piezometric levels over the entire region together with the total production of hot waters began to be systematically monitored and recorded.

The volume of water pumped in the two urban centres of Abano and Montegrotto in the period 1978-1992 – satisfying the demands from more than 2 million daily visitors per year – was about 20 millions $\text{m}^3 \text{ year}^{-1}$ with a maximum of over 25 millions in 1985 (Fig. 2). Since the exploitation was mainly concentrated in such area of about 20 km^2 , the upper solid line in Fig. 2 represents the 90% of the total amount withdrawn from the entire basin (about 30 km^2).

The average piezometric level trend showed in the same period not only a progressive reduction – especially in the 1970s (up to 2.5 m year^{-1}) – but also clear seasonal cycles as a consequence of the corresponding demand and touristic flow (Ballestrazzi *et al.*, 1991). It was apparent how quick the system could reply to substantial variations of the volume of water withdrawn. This would suggest that aquifers are in general rapidly and continuously supplied with the previously described deep circulation system and therefore that their exploitation is still possible, even if only partially and under controlled conditions: it is now estimated that, if all the wells were shut down, there would be a sudden recovery of the piezometric head up to above the ground level again.

The elevation measures in the thermal area started not organically in 1959, but high precision levelling began only in 1985. The last survey was carried out in 1991. Main results are summarized in Fig. 3 (Antonelli *et al.*, 1995), where the isokinetic lines representing the total settlement in the period 1988-1991 are drawn. Two marked subsidence cones are clearly identifiable, located in the centres of Abano and

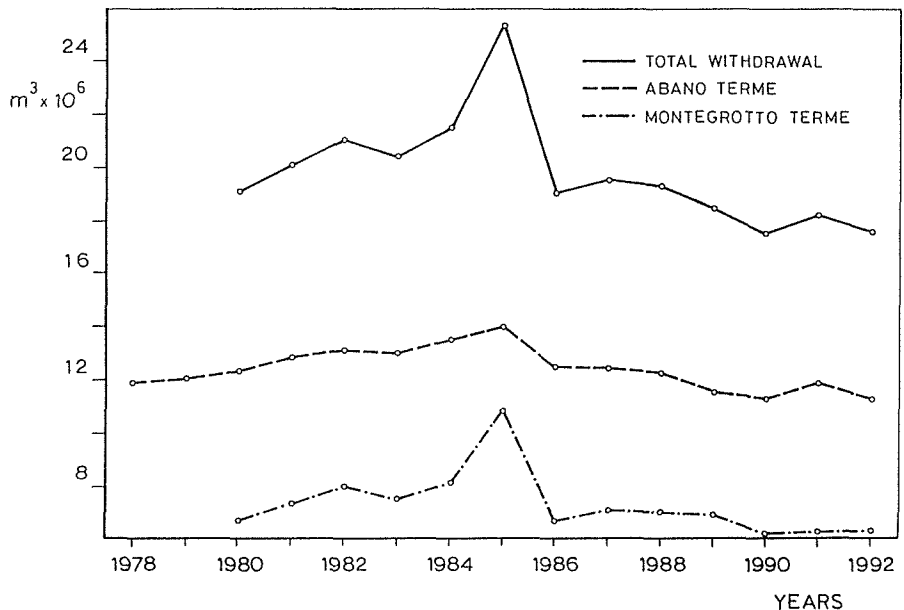


Fig. 2 Withdrawal in the period 1978-1992.

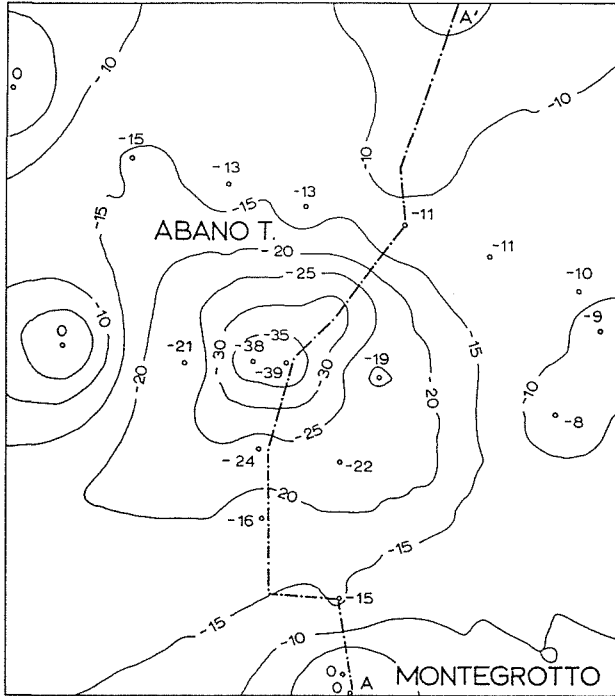


Fig. 3 Isokinetic lines during 1988-1991 (Antonelli et al., 1995).

Montegrotto. Data from repeated levellings during 1985-1991 along the north-south profile indicated with the A-A' line in Fig. 3 are plotted in Fig. 4. The subsidence rate, which has been estimated to have exceeded 20 mm year⁻¹ in the recent past, appears to have turned into a decreasing trend in the late 1980s.

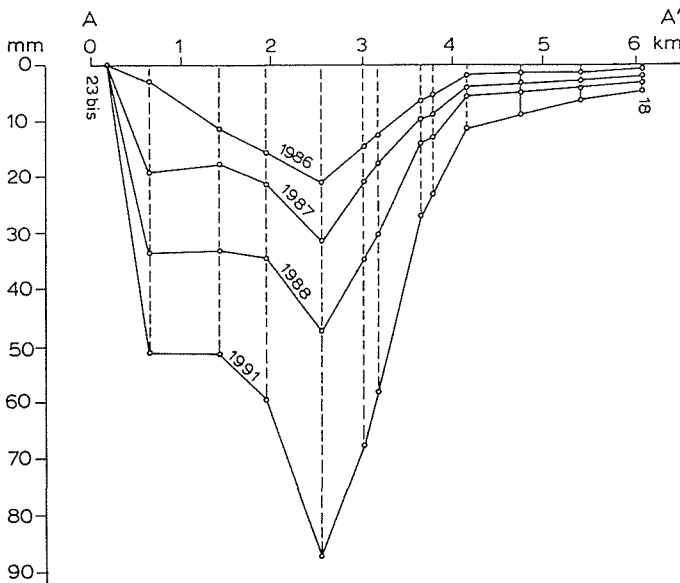


Fig. 4 Settlement profile in 1985-1991 along the A-A' line (Antonelli et al., 1995).

SITE INVESTIGATION OF ALLUVIAL SEDIMENTS

With the aim of keeping under control the land subsidence occurrence in the Euganean basin and, more generally, of optimizing the management of geothermal resources, a detailed and multidisciplinary investigation was therefore promoted by the local authority (the "Regione Veneto") and commissioned to the University of Padova. One of the main objectives was the investigation of the geotechnical properties of soils forming the alluvial Quaternary deposit, in order to provide as accurate as possible parameters for the calibration of the finite element model which represents the final and most attractive step of the research.

A borehole named "Aponus 2" and 300 m deep – a depth never achieved previously in the area – was therefore drilled and continuously sampled. The engineering simplification of the soil profile, stressing the permeability and compressibility properties, is proposed in Fig. 5 (Gottardi *et al.*, 1994); the layer subdivision is not always unambiguous because of the silty nature of most sediments.

The Quaternary deposit extends locally as far as 196 m and is followed by the carbonatic fractured bedrock indicated as "Biancone". Three main aquifers, alternating with more or less impervious aquitards composed of silty clay and clayey silt of low plasticity, can be singled out within the alluvial sediments: the first one (10-13 m), composed of silty sand, is too shallow to be of practical interest for thermal purposes, while the other two (48-57 m and 117-141 m), made by medium and fine sand, provide rather satisfying characteristics of permeability ($k = 10^{-5}$ - 10^{-4} m s⁻¹). It was already noticed that they are no longer exploited.

In correspondence to each aquifer a standpipe piezometer was then installed (labelled P1, P2 and P3 in Fig. 5), both to check the possible hydraulic interconnections and to measure water level variations during the year. Figure 6 shows these records starting from July 1990: measures labelled P4 refer to the borehole itself which was subsequently deepened as far as 465 m into the bedrock. All water levels lie well below the ground surface and show a clear seasonal trend according to the corresponding volume withdrawn; furthermore depressions generated in the deep aquifer appear to propagate towards the other shallower aquifers. A general recovery in reply to recent withdrawal limitations is also evident.

Finally, on the right-hand side of Fig. 5, the temperature log represents the result of one of the many geophysical tests performed in the deep borehole: starting from about 45°C at the top, the water temperature reaches (and in many cases exceeds) 80°C in correspondence of the bedrock. Unfortunately no data measured directly in the Quaternary deposits are available, but the actual temperature gradient should not be dissimilar from the borehole trend of Fig. 6.

GEOTECHNICAL CHARACTERIZATION

A total of 113 samples (33 undisturbed and 80 remoulded) were obtained from the deep borehole. Figure 7 summarizes the main geotechnical properties of the alluvial sediments. Atterberg limits show that most samples lie within the category of very silty clays ($10 < \text{plasticity index } (I_p) < 22$, $35 < \text{liquid limit } (w_L) < 50$) and very few samples are high plastic clays. The water content profile indicates that the soil below

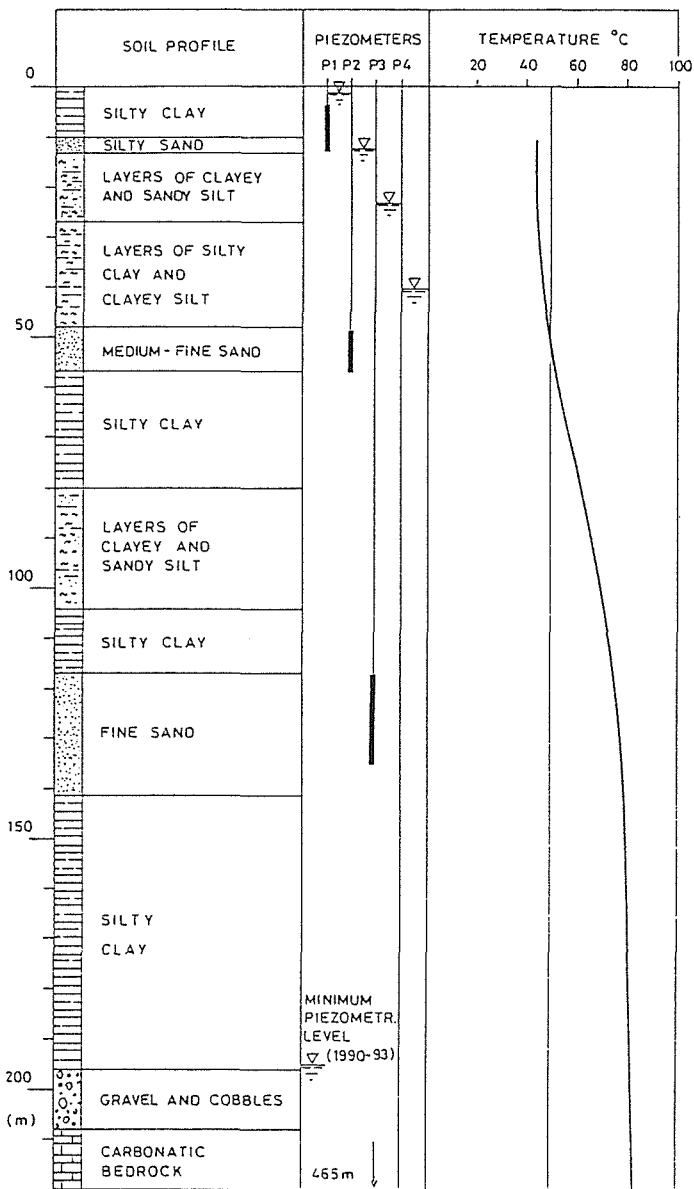


Fig. 5 Simplified soil profile from the deep borehole.

90 m has a natural water content either at or under its plastic limit and that the liquidity index (I_L) generally tends to decrease with depth. This is due to the large vertical effective stress at those depths and does not necessarily imply extremely over consolidated deposits.

Standard one-dimensional oedometer compression tests were performed on twenty-six 70 mm diameter specimens. In Fig. 7 the vertical preconsolidation stresses determined from e -log σ' plots using the Casagrande method is reported. On the same figure the trend of vertical effective stress is drawn, considering both a linear ($u = \gamma z$,

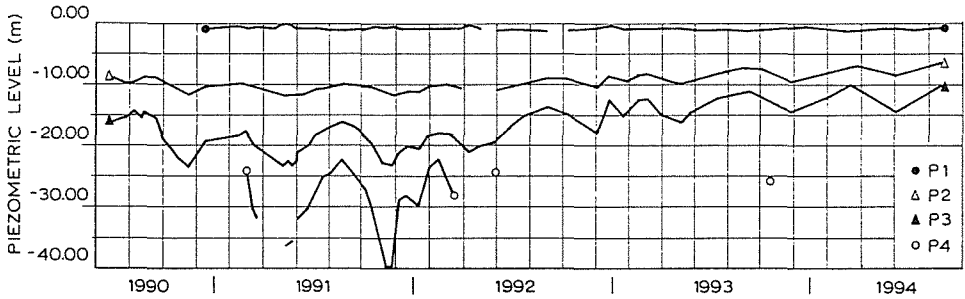


Fig. 6 Water level measurements in 1990-1994.

where: $\gamma = 9.81 \text{ kN m}^{-3}$ and $z = \text{depth}$) and *in situ* measured piezometric pore pressure distributions. Total vertical stresses were calculated using an average soil density equal to 19 kN m^{-3} . Note that only few samples are slightly overconsolidated, especially in the upper layers of the Quaternary deposit, whereas the others appear to be normally consolidated or slightly under consolidated with respect to the present effective stress situation.

The oedometric modulus M was calculated in correspondence of the *in situ* vertical effective stress and its values are also reported in Fig. 7. Even if experimental data are rather scattered, a general increase of M with depth can be observed. The power equation $M = 490 z^{0.84}$ (where if z is in m, M is in kPa), fitting the experimental data, was assumed as a reasonable trend of soil stiffness with depth.

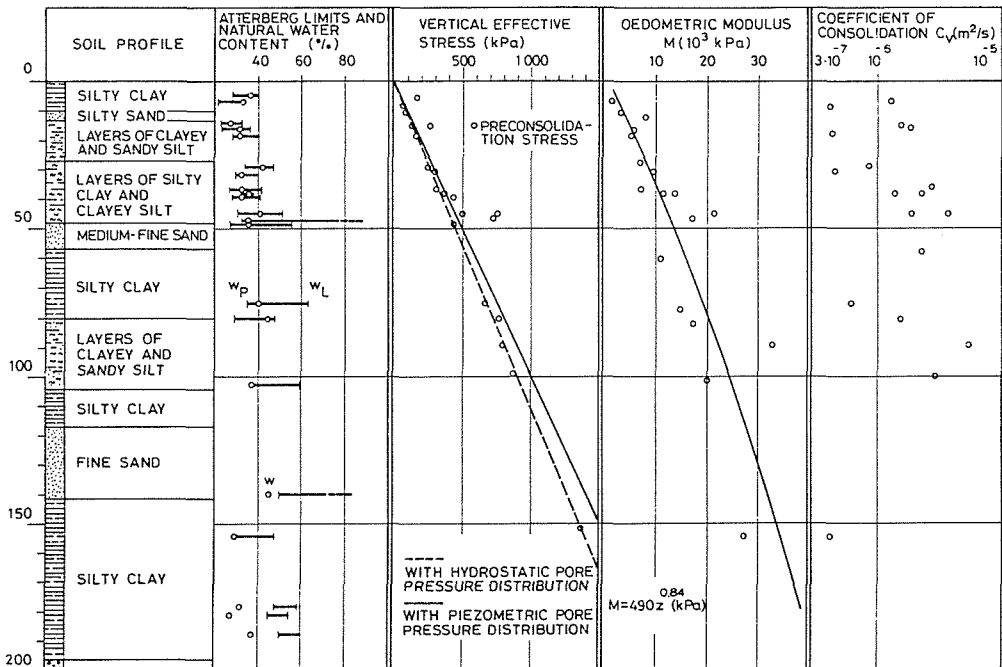


Fig. 7 Main geotechnical parameters of alluvial sediments from laboratory tests.

Finally values of the coefficient of consolidation C_v have been determined from oedometric settlement-time plots – in the normally consolidated range – using the Terzaghi one-dimensional consolidation theory and the Casagrande method. The values of C_v vs. depth range from about $4.5 \cdot 10^{-7}$ to $8.5 \cdot 10^{-6} \text{ m}_2 \text{ s}^{-1}$ (Fig. 7). A large scatter of experimental data is again observed and no particular trend of C_v with depth appreciated.

THERMAL EFFECTS ON CONSOLIDATION PROPERTIES

It should be kept in mind that the Quaternary deposits are permeated by hot water, characterized by a temperature level up to 85°C , which is substantially different from standard long-term geotechnical laboratory tests. Many studies have established that soil behaviour is significantly influenced by temperature and particularly the consolidation rate.

Two types of conditions can be considered in relation to the temperature influence on soil behaviour: isothermal and non-isothermal. In the case of the Euganean basin no changes of the temperature profile have been developed for the last 20 years and, consequently, isothermal conditions in the alluvial Quaternary deposits seem to take place.

In such conditions the coefficient of compressibility C_c can be assumed constant for a given soil, independently of the temperature level (Campanella & Mitchell, 1968). Therefore, also the oedometric modulus $M = 2.3(1 + e)\sigma'/C_c$ is practically not affected by temperature even if a slight decrease of the void index is observed when temperature is increased.

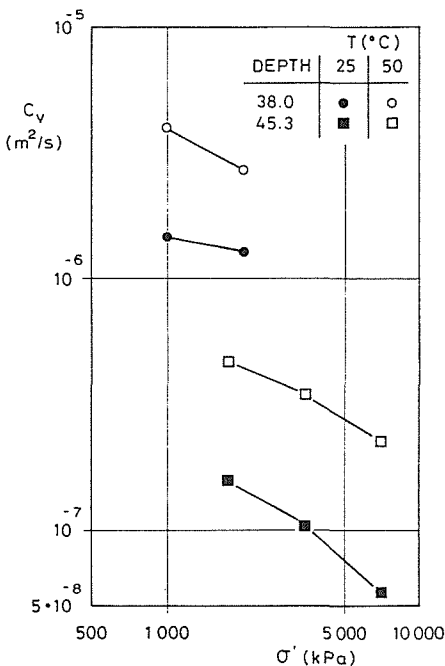


Fig. 8 Influence of temperature on consolidation rate.

In order to characterize the variation of consolidation rate with temperature, some special oedometer tests were also carried out. In this case the oedometer apparatus was installed in a thermostatic cell, capable of maintaining the soil sample at constant temperature (25°C and 50°C in this case): C_v -values at 50°C in the normally consolidated range (Fig. 8) are higher than those obtained from oedometric tests performed at 25°C, for soils sampled at 38.0 and 45.3 m. Similar results have been found by Burghignoli & Desideri (1988), and can be partially explained taking into account the variation of water viscosity and specific weight, which considerably affects the hydraulic conductivity of soils.

The secondary compression coefficient C_α was finally measured in all the oedometric tests and for the Quaternary cohesive deposits lies between 0.003 and 0.010. No appreciable differences of C_α -values were detected in samples tested at 25°C and 50°C, thus confirming the experimental work of Miliziano (1992).

CONCLUDING REMARKS

The heavy exploitation of hot water and the consequent piezometric lowering are responsible for the widespread phenomenon of land subsidence in the Euganean geothermal basin, which has been detected and monitored over about the last 20 years.

On the basis of the detailed mechanical characterization of cohesive soil layers, a rough estimate of the final consolidation settlement produced by the maximum piezometric lowering has been produced simply by assuming one-dimensional vertical deformations and by using the proposed trend of the modulus M with depth. The following hypotheses were also introduced in calculating consolidation settlements: homogeneous and uniform soil within each layer, incompressible granular materials and linear increasing with depth of the vertical effective stress increment induced by the piezometric lowering (Gottardi *et al.*, 1994). The total final settlement s_{tot} thus emerges from the following simple expression:

$$s_{tot} = \sum_{i=1}^n \frac{H_i \Delta \sigma'_i}{M_i} \quad (1)$$

where H_i , M_i are respectively, the thickness and oedometric modulus of the n compressible layers and $\Delta \sigma'_i$ is the vertical effective stress increase.

The so computed settlement is equal to about 50 cm, but it should be observed that all the above approximations lead to an upper limit of the total settlement (Ricceri & Butterfield, 1974). In fact the hypothesis of homogeneity and uniformity within each cohesive layer is unfortunately far away from the actual *in situ* soil profile, where thin sub-layers of silt and silty sand may easily modify the behaviour of the whole layer. A better estimate of subsidence settlement can be obtained by the three-dimensional finite element numerical model (Antonelli *et al.*, 1995), which has been calibrated on the basis of the above mentioned geotechnical parameters.

Unfortunately accurate measurements of ground level variations have not been available since the beginning of the phenomenon of land subsidence, which had already been recognized in the early 1960s. However the subsidence rate, estimated to have exceeded 20 mm year⁻¹ in the recent past, has been found to show a decreasing trend in the late 1980s.

A comparison of the two orders of magnitude – measured and computed – would suggest that most of the expected settlements have already taken place and that the phenomenon is now being exhausted, as confirmed also by the most recent levellings. Therefore, land subsidence in the Euganean region appears to be in its final stage, provided that no further piezometric level lowering in the aquifers of the alluvial deposits occurs.

Finally the land-subsidence phenomenon, which normally takes long time to fully develop, in the Euganean basin is speeded up by the presence of hot groundwaters: lower water viscosity and specific weight at high temperature imply higher permeability and thus higher rate of consolidation.

Acknowledgement The work has been kindly supported by the "Regione Veneto – Segreteria Regionale per il Territorio, Dipartimento per la Geologia e le Attività Estrattive".

REFERENCES

- Antonelli, R., Fabbri, P., Illiceto, V., Majorana, C., Preatello, P., Schrefler, B. & Sedeà, R. (1995) The geothermal Euganean field. A subsidence modelling approach. In: *Proc. World Geothermal Congress* (Florence) (in press).
- Ballestrazzi, P., Brighenti, G., Ciancabilla, F., Dainese, A. & Schiesaro, G. (1991) Ricerca sulla subsidenza nell'area termale di Abano Terme (PD). Investigation Pei Ed., Parma.
- Burghignoli, A. & Desideri, A. (1988) Influenza della temperatura sulla compressibilità delle argille. In: *Proc. of the Conf. "Deformazioni dei terreni ed interazione terreno-struttura in condizioni di esercizio"* (Monselice, Padova), 19-34.
- Campanella, R. G. & Mitchell, J. K. (1968) Influence of temperature variations on soil behaviour. *J. Geotech. Engng ASCE* **94**(3), 709-734.
- Gottardi, G., Preatello, P. & Simonini, P. (1994) Geotechnical characterization of land subsidence in the Euganean thermal basin. In: *Proc. 7th Int. Congr. IAEG* (Lisbon), 1915-1923.
- Miliziano, S. (1992) Effetti della temperatura sul comportamento meccanico delle terre coesive. PhD Thesis, Università di Roma "La Sapienza".
- Piccoli, G., Dai Prà, A., Sedeà, R., Bellati, R., Di Lallo, E., Cataldi, R., Baldi, P. & Ferrara, C. (1973) Contributo alla conoscenza del sistema idrotermale Euganeo-Berico. *Proc. Acc. Naz. Lincei, VIII, Roma* **11**, 103-131.
- Ricceri, G. & Butterfield, R. (1974) An analysis of compressibility data from a deep borehole in Venice. *Géotechnique* **24**(2), 175-192.

Relation between groundwater withdrawal and land subsidence in Kelantan, Malaysia

HARYONO

National University of Malaysia, Department of Geology, Faculty of Physical and Applied Sciences, 43600 UKM Bangi, Selangor Darul Ehsan, Malaysia

Abstract As a result of intensive abstraction of groundwater in Kelantan, the author is afraid that the land in the area is subsiding. To monitor the phenomena, the author will use the Global Positioning System technique.

INTRODUCTION

Many Kelantanese people use groundwater. The people dig private wells and draw water from a shallow aquifer while the Water Supply Department takes the groundwater from

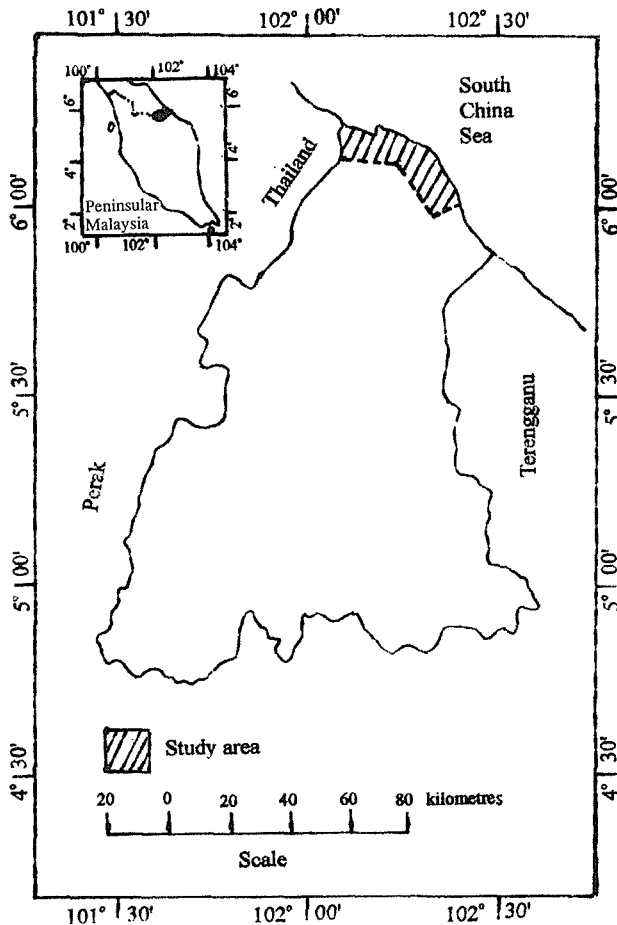


Fig. 1 A description of the study area.

the deeper aquifer. If too much groundwater is extracted, we are afraid that land subsidence will occur in the area.

STUDY AREA

Figure 1 is a description of the study area. To the north of the study area is the South Chinese Sea and to the west is Thailand.

DATA

Table 1 describes the groundwater abstraction in Kelantan.

Table 1 Groundwater abstraction in Kelantan.

Group	No.	Well field	Water abstraction (Ml day ⁻¹) in:			
			1974	1980	1985	1988
A	1	Pengkalan Chepa	2.55	3.64	1.36	6.27
	2	Kampung Puteh	10.46	26.14	28.64	28.91
	3	Pt. Geng (shallow)		4.55	3.64	2.50
	4	Kubang Kerian	1.46	4.55	7.27	19.54
	5	Kampung Puteh				
	6	Kampung Tok Jaafar				
	7	Kampung Kota				
	8	Kampung Pasir Nor				
	9	Kg. Pasir Tumbuh				
	10	Kampung Kenali				
	11	Kampung Seribong				
	12	S.K. Kubang Kerian				
	13	Kg. Pdg. Penyadap				
	14	Jalan Merbau				
	15	Kampung Teluk				
	16	Kg.Rambutan Redang				
Total abstraction of group A			14.47	38.88	40.91	57.22
B	1	Tanjung Mas		3.18	3.18	2.59
	2	Pintu Geng (deep)				
Total abstraction of group B				3.18	3.18	2.59
C	1	Wakaf Baru	0.18	0.09	5.45	3.77
	2	Kampung Sedar				
	3	Kg. Pdg. Rokma				
	4	Kg. Alor Durian				
	5	Kampung Binjai				
Total abstraction of group C			0.18	0.09	5.45	3.77
D	1	Kampung Chap	0.09	0.14	1.68	1.68
	2	Jelawat			0.50	0.72
Total abstraction of group D			0.09	0.14	2.18	2.40

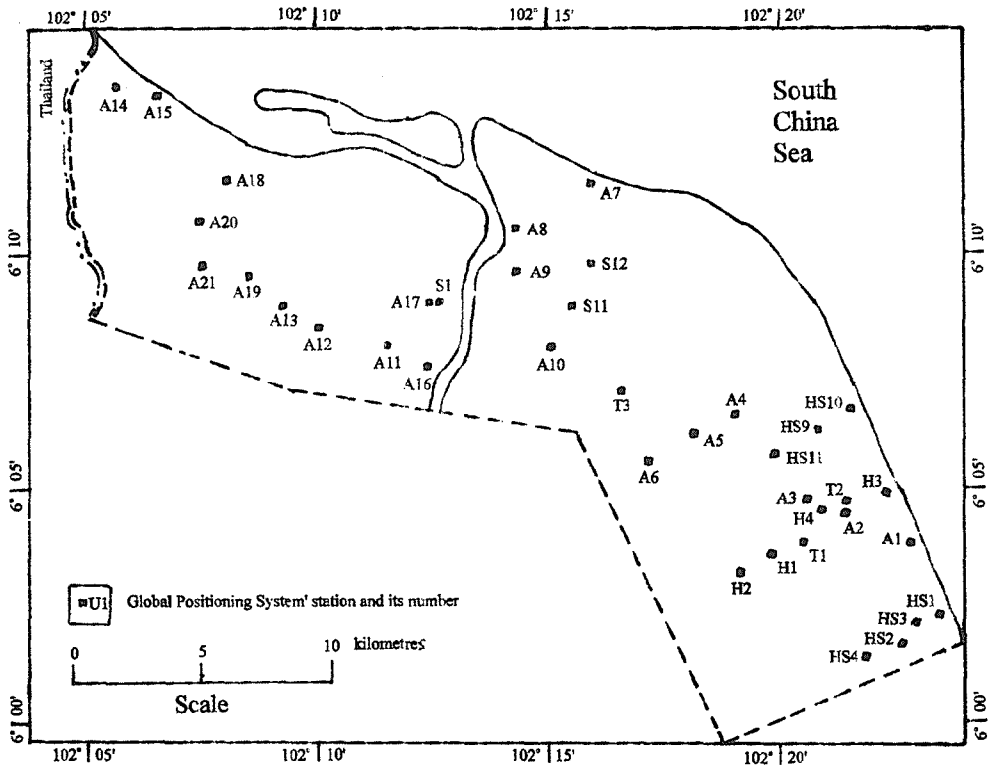


Fig. 2 A map of the GPS network of stations.

METHODOLOGY

To monitor the land subsidence, a network of stations was established. We plan to monitor the land subsidence by the GPS (Global Positioning System) technique.

RESULTS

Figure 2 shows the GPS network of stations. In the future, we will observe the stations from time to time.

DISCUSSION

Although our activity is only a first step to monitor the land subsidence, we are determined to see it through. There are many obstacles to the operation of the project, such as financial problems, lack of experience etc., but we shall continue to achieve the objectives of the project.

Investigation of aquifer-system compaction in the Hueco basin, El Paso, Texas, USA

CHARLES HEYWOOD

US Geological Survey, Water Resources Division, 4501 Indian School Road NE, Suite 200, Albuquerque, New Mexico 87110, USA

Abstract The Pleistocene geologic history of the Rio Grande valley in the Hueco basin included a cycle of sediment erosion and re-aggradation, resulting in unconformable stratification of sediment of contrasting compressibility and stress history. Since the 1950s large groundwater withdrawals have resulted in significant water-level declines and associated land subsidence. Knowledge of the magnitude and variation of specific storage is needed for developing predictive models of subsidence and groundwater flow simulations. Analyses of piezometric and extensometric data in the form of stress-strain diagrams from a 16 month period yield *in situ* measurements of aquifer-system compressibility across two discrete aquifer intervals. The linear elastic behaviour of the deeper interval indicates over-consolidation of basin deposits, probably resulting from deeper burial depth before the middle Pleistocene. By contrast, the shallow aquifer system displays an inelastic component, suggesting pre-consolidation stress not significantly greater than current effective stress levels for a sequence of late Pleistocene clay. Harmonic analyses of the piezometric response to earth tides in two water-level piezometers provide an independent estimate of specific storage of aquifer sands.

INTRODUCTION

The Hueco basin is a fault-bounded structural depression associated with the Rio Grande Rift (Fig. 1). From the late-Tertiary to the middle Pleistocene, the basin aggraded with alluvial deposits associated with an ancient fluvial system. In the middle Pleistocene, the modern Rio Grande penetrated the basin and eroded approximately 150 m of early Pleistocene basin fill to form the Rio Grande valley. The river has since deposited approximately 60 m of gravel, sand and clay. This cycle of erosion and deposition has resulted in unconformable stratification of unconsolidated late Pleistocene and Holocene sediment above over-consolidated early Pleistocene alluvium.

The two million inhabitants of El Paso, Texas, and Juarez, Mexico, create a large demand for water in an arid environment. Much of this demand is supplied by groundwater pumpage from the Hueco basin aquifer system underlying El Paso and Juarez, resulting in water table declines of more than 50 m. Precision geodetic measurements indicate land subsidence of as much as 0.3 m since the mid 1950s. Adverse effects have occurred in local areas of shallow differential compaction of late Pleistocene sediments (Land & Armstrong, 1985).

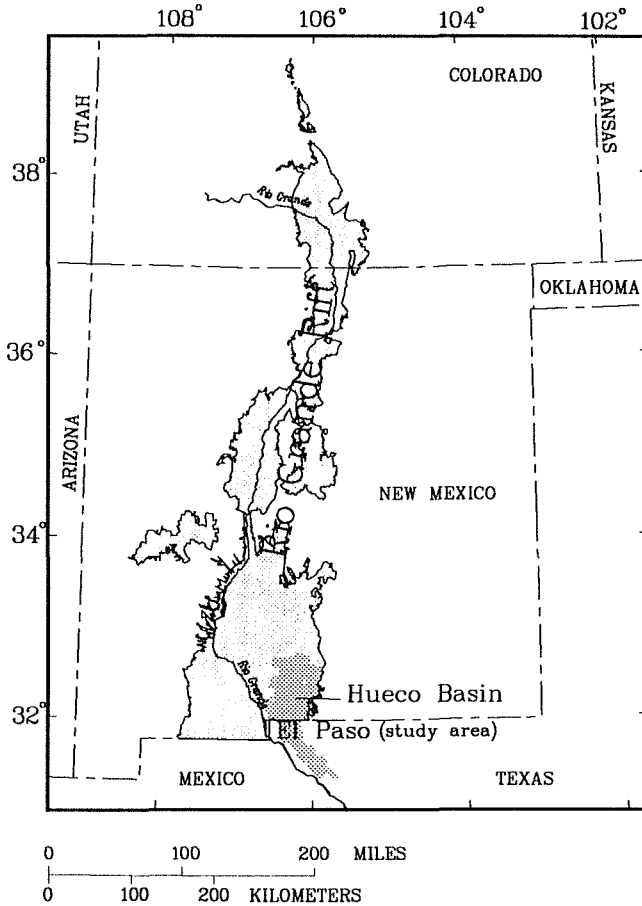


Fig. 1 Map showing location of Rio Grande rift, Hueco Basin and El Paso study area.

STRAIN AND PRESSURE MEASUREMENT

In order to discriminate the components of vertical deformation due to groundwater production in the deeper early Pleistocene alluvium from those occurring in the Holocene river alluvium, a pair of highly-sensitive vertical extensometers was installed in the aquifer system adjacent to the Rio Grande in 1992. Riley (1986) elucidated the fundamental requirements for precision borehole extensometry, which Heywood (1994) applied to the installation in El Paso (Fig. 2). A shallow extensometer spans the interval 6-100 m depth, which includes the recent river alluvium (Fig. 3). A deeper extensometer spans the interval 6-340 m, which also includes the interval of production from the regional aquifer system. Bi-hourly displacement measurements made with linear potentiometers have a resolution of several microns. Tests of displacement sensitivity indicated frictional deadband less than 20 microns in either extensometer, corresponding to strain sensitivity less than 2×10^{-7} for the shallow extensometer and 6×10^{-8} for the deep extensometer. A 16 month record of the displacement time series for both extensometers is depicted in Fig. 4(a). (Digital data for September 1993 were lost due



Fig. 2 Photograph of deep extensometer, counter-weight lever arm, and surface datum table.

to failure of data logger electronics.) A key feature of this extensometer installation is the precise reference of both extensometers to the same surface datum, thus the difference between the two extensometer signals measures vertical compaction in the 100-340 m interval of the regional aquifer system. Because the mechanical components of both extensometers are nearly identical at the surface, the small temperature effects in each extensometer are largely cancelled in this signal-difference measurement.

Seven piezometers were installed to measure pore pressure at various depths in the aquifer system. Figure 3 displays a geophysical log of electrical resistivity obtained from the deepest extensometer hole. The depth and thickness of sand (high resistivity) vs. clay (low resistivity) strata may be inferred in the shallow brackish and fresh-water zones to approximately 230 m depth. Increasingly saline water below this depth causes low apparent electrical resistivity of the formation. (TDS of water in the piezometer screened at 320 m depth was $1 \times 10^4 \text{ mg l}^{-1}$.) Piezometer screens 3 m in length were placed in selected sand intervals, the depths of which are indicated by accented shades in Fig. 3. The inverted solid triangles in Fig. 3 indicate the average piezometric head for each piezometer. A large downward vertical hydraulic gradient exists from the river to the production interval of the regional aquifer system, which is between 100-230 m depth. Water is also occasionally injected into this fresh water interval for storage and to retard vertical diffusion of overlying brackish and underlying saline groundwater. Bi-hourly pressure measurements resolved 20 Pa of pressure or 2 mm of water level change. Maximum amplitudes of pore-pressure change were measured in the piezometer screened at 201-204 m depth, in response to withdrawal from and injection into the regional aquifer system. A 16 month record of piezometric drawdowns at 55-58 and 201-204 m depth is depicted in Fig. 4(b). The similarity in form of the piezometric hydrograph for 201-204 m depth (Fig. 4(b)) with the deep extensometer displacement

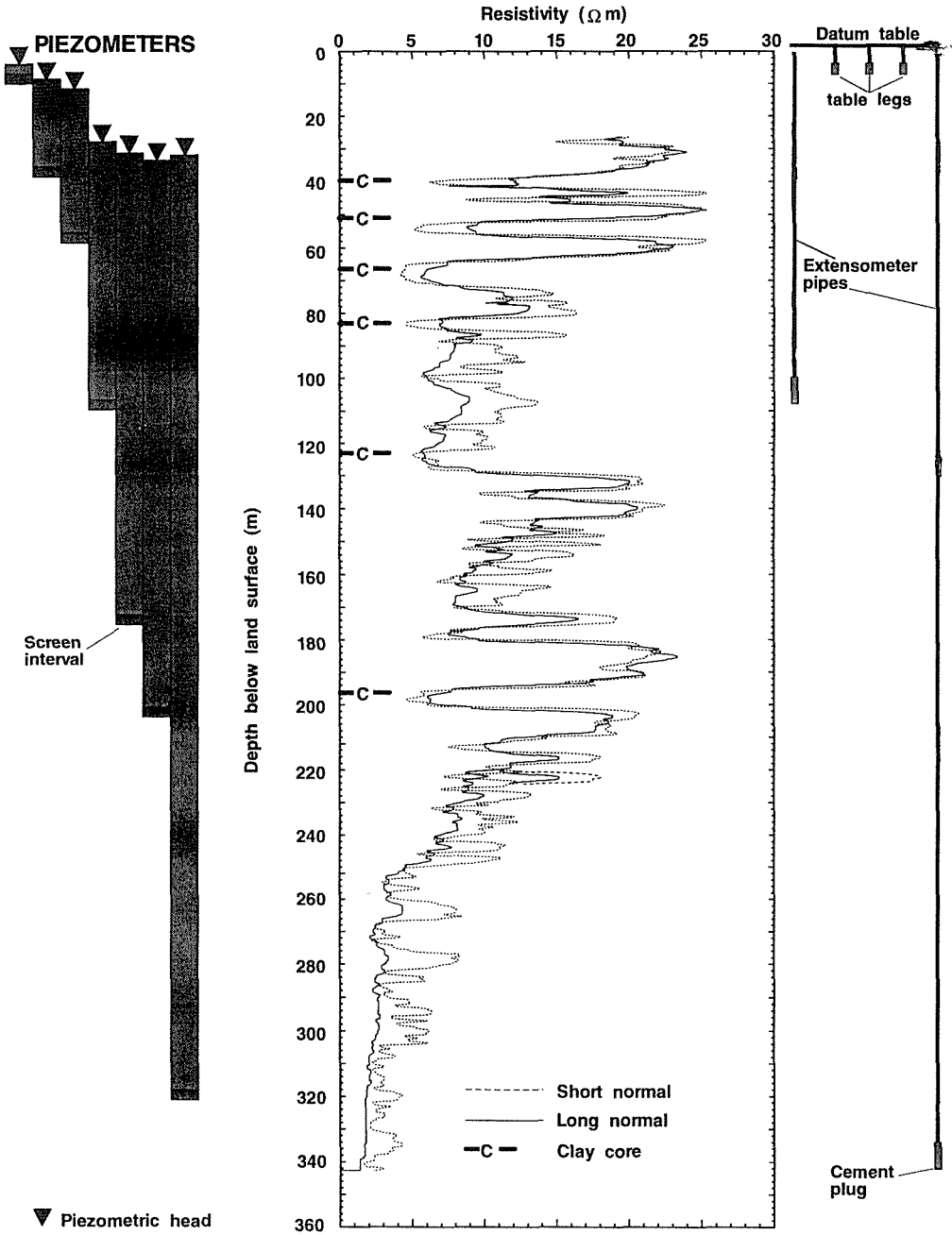
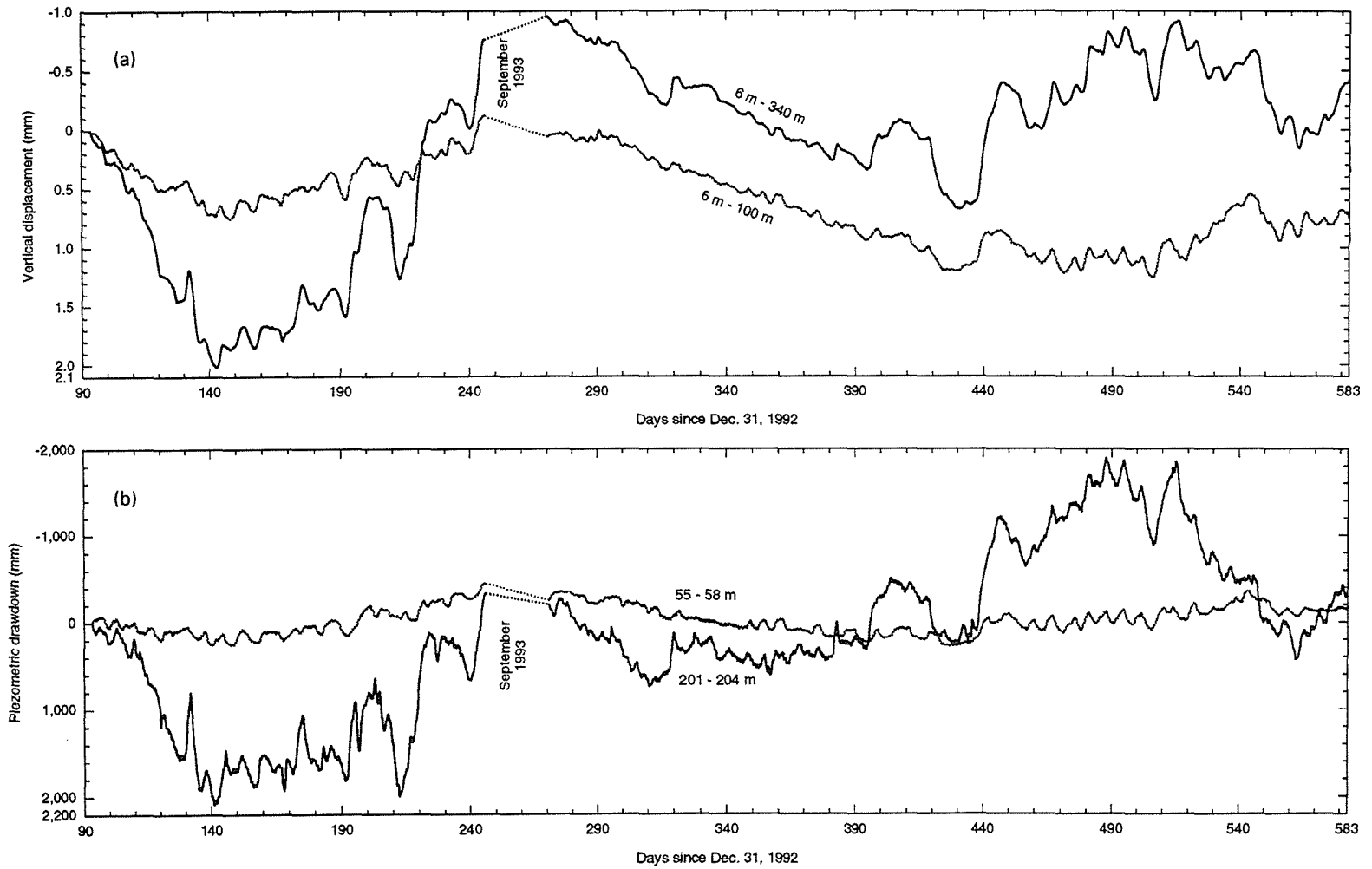


Fig. 3 Resistivity logs with piezometer and extensometer depth intervals (explained in text).

record for the same time period (Fig. 4(a)) indicates that pressure changes in this interval principally effect gross aquifer-system compaction at the extensometer site.



Aquifer-system compaction in the Hueco basin, El Paso, Texas

Fig. 4 (a) Sixteen month displacement records from shallow and deep extensometers. (b) Sixteen month hydrographs of piezometers screened at 55-58 and 201-204 m depth.

DETERMINATION OF AQUIFER-SYSTEM SPECIFIC STORAGE

The specific storage of porous media is given by $S_s = \rho g (\alpha + n \beta)$, where ρ is the density of water, g is the acceleration of gravity, α is the vertical compressibility of the granular matrix, β is the compressibility of water, and n is the porosity. This definition of S_s includes a skeletal portion S_{sk} governed by the matrix compressibility, and a portion S_{sw} due to the compressibility of water contained in the matrix pore space. Solid grains are much stiffer than the alluvial skeletal matrix they comprise, and are considered incompressible. The skeletal portion S_{sk} may have both elastic S_{ske} and inelastic S_{skv} components, the magnitude of which depend on both the magnitude and frequency of the applied stress and the stress history of the compressible materials (Helm, 1976; Galloway, 1994).

Extensometric-piezometric determination of aquifer-system matrix compressibility

Riley (1970) demonstrated the utility of plots of piezometric head vs. vertical compaction data for determining elastic and inelastic components of aquifer system skeletal specific storage. Vertical strain ϵ_{33} for the interval 100-340 m depth was calculated from the difference between the deep and shallow extensometer displacement time series, divided by 240 m (the difference in length between the deep and shallow extensometers). Figure 5(a) is a plot of decrease in pore pressure at 201-204 m depth vs. ϵ_{33} for the data depicted in Figs 4(a) and 4(b). Because the water table did not change during the periods of these pressure fluctuations, a unit decrease in pore pressure results in a unit increase in effective stress. The ordinate of Fig. 5(a) is therefore equivalent to increased effective stress in the aquifer matrix at 201-204 m depth. The inverse slope $2.7 \times 10^{-10} \text{ Pa}^{-1}$ in this plot under-estimates the average matrix compressibility α for the aquifer system between 100-340 m depth because the distribution of pore pressure variation over this interval is non-uniform and generally smaller in magnitude than that measured at 201-204 m depth. A vertical distribution of pore pressure variation constrained by hydrographs at four depths between 100-340 m depth was assigned according to the distribution of sand and clay inferred from the borehole geophysical logs (Fig. 3). The average pore-pressure variation was approximately 35% of that measured in the piezometer screened from 201-204 m depth, resulting in an adjusted $\alpha = 7 \times 10^{-10} \text{ Pa}^{-1}$, corresponding to $S_{ske} = 7 \times 10^{-6} \text{ m}^{-1}$ for the interval from 100-340 m depth.

Because of negligible frictional deadband in either extensometer, the loops in Fig. 5(a) represent hydrodynamic lag between the change in stress measured in the permeable sand at 201-204 m depth and strain in the less permeable fractions of the aquifer system. The width of these loops is related to the permeability and thickness of aquitards within the aquifer system (Riley, 1970).

Over the 16 month period from 3 April 1993 to 5 August 1994, a net expansive strain of 4×10^{-6} occurred with increased pore pressure of only 2 kPa at 201-204 m depth. This elastic expansion may have resulted from either:

- (a) net lowering of the water table, which decreased the geostatic stress in the deeper aquifer system interval, or
- (b) groundwater injection resulting in greater pore pressure increase in a stratigraphic zone above or below that measured at 201-204 m depth.

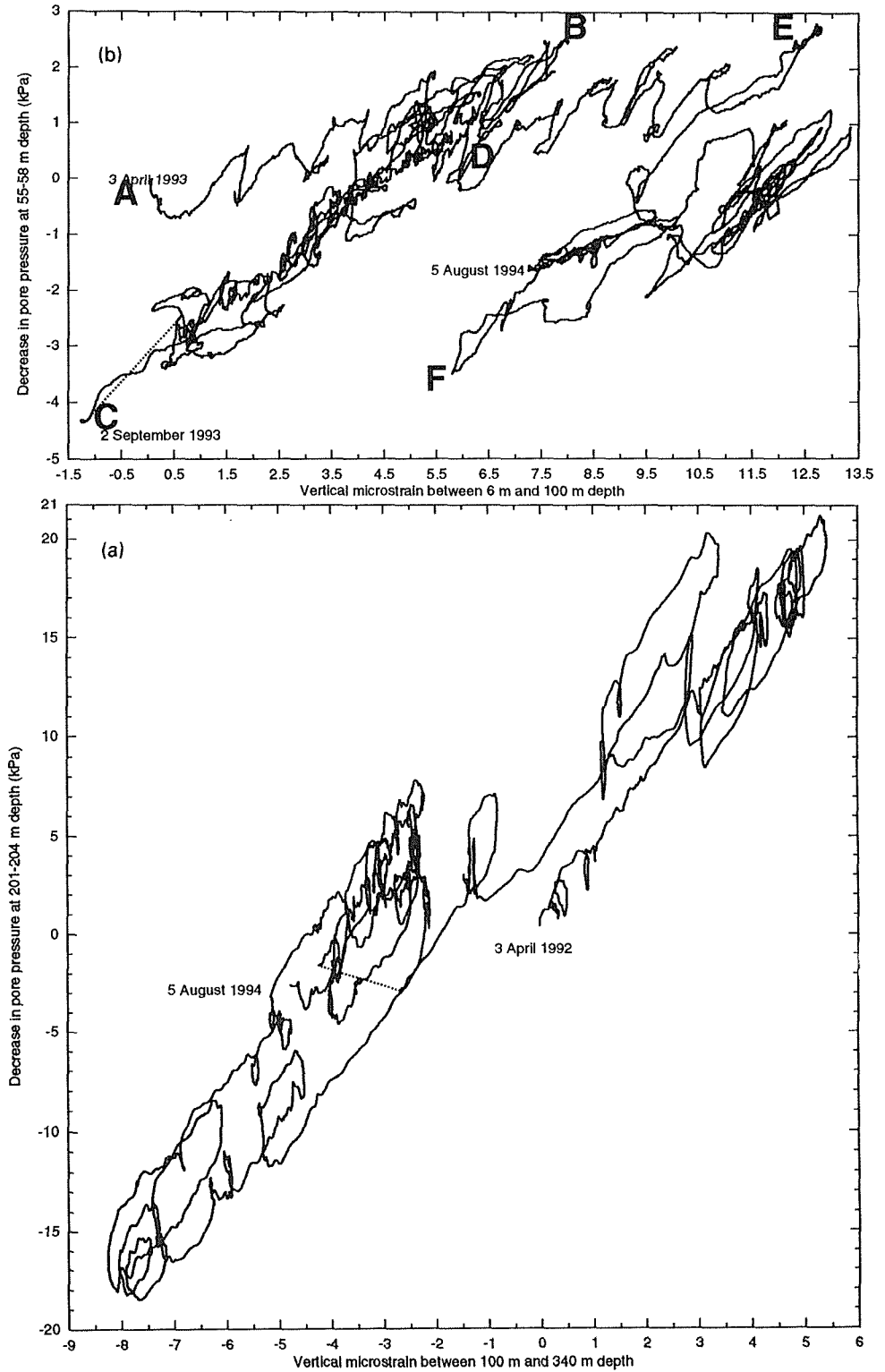


Fig. 5 (a) Stress-strain diagram (explained in text) for aquifer depth interval 100-340 m. (b) Stress-strain diagram (explained in text) for aquifer depth interval 6-100 m.

Two distinct slope trends are apparent in Fig. 5(b), which plots decrease of pore pressure measured in the piezometer screened from 55-58 m depth vs. strain measured by the shallow extensometer between 6 and 100 m depth. The shallow trends of limbs A-B and D-E reflect virgin consolidation of late Pleistocene clays above 60 m. The initial limb A-B of generally declining pore pressure attains a maximum increase in effective stress near point B, which is followed by a second limb B-C of cyclical recovery and drawdown. These two limbs have distinctly different slope, suggesting a stiffer mechanical response along limb B-C at effective stress levels less than the preconsolidation stress attained at point B. Subsequent drawdown increased effective stress levels near that attained at B and resulted in further inelastic consolidation along limb D-E, with preconsolidation stress set slightly higher at the time of point E. Further drawdown and recovery until 5 August 1994 on limb E-F occurred with compressibility similar to limb B-C.

Right leaning cusps between points A and E may represent virgin consolidation of late Pleistocene clays above 60 m depth superimposed upon the stiffer elastic response of coarse interbeds and underlying early Pleistocene sediment. Gently sloping cusp tops result from virgin consolidation and trend parallel to the net displacements from A to B and D to E. Geophysical logs suggest aggregate clay thickness of 20 m above 60 m depth. If inelastic deformation is occurring in this sequence of clays, α is approximately $1 \times 10^{-8} \text{ Pa}^{-1}$ for virgin consolidation of late Pleistocene clay, corresponding to $S_{skv} = 1 \times 10^{-4} \text{ m}^{-1}$. The steeper cusp flanks with inverse slope $\alpha = 6 \times 10^{-10} \text{ Pa}^{-1}$ suggest $S_{ske} = 6 \times 10^{-6} \text{ m}^{-1}$ for the older and coarse sediment fraction in the interval from 6-100 m depth. Limbs B-C and E-F have a slightly shallower slope than the steep cusp flanks, reflecting the somewhat softer elastic response of the entire stratigraphic sequence between 6-100 m compared the coarse fraction. The inverse slope $\alpha = 1 \times 10^{-9} \text{ Pa}^{-1}$ of these limbs corresponds to $S_{ske} = 1 \times 10^{-5} \text{ m}^{-1}$.

Determination of sand specific storage from piezometric earth-tide response

Piezometers screened from 106-109 and 201-204 m depth responded to solid earth tides. The magnitudes of the measured responses were analyzed to constrain S_s of aquifer sands at these depths. Piezometric data were resampled at an hourly interval for each well and grouped into equal length time series of 42.67 days. Corresponding time series of theoretical horizontal strain ($\varepsilon_{11} + \varepsilon_{22}$) due to solid earth tides at the piezometer location were calculated with the algorithm of Harrison (1971). To determine the piezometric response due to each earth-tide harmonic, each time series was filtered with a 7th order Butterworth high-pass filter using a cutoff frequency of 0.7 cycles day⁻¹ and fit to a sum-of-sines-and-cosines function using least squares:

$$x(t_j) = \sum_{n=1}^N a_k \cos(2\pi\omega_k t_j) + b_k \sin(2\pi\omega_k t_j) + R_j$$

where: $x(t_j)$ represents the reduced data at time t_j , t_j is the time of data point j , $N = 6$ (the number of tidal harmonics in the analysis), ω_k is the frequency of the k th tidal harmonic (Table 1), a_k and b_k are regression coefficients, and R_j is the residual of data point j in the reduced record. The amplitude of the piezometric response to a particular

Table 1 Tidal harmonics used in regression analysis (Bartels, 1957).

Tide	Frequency (day ⁻¹)	Period (hours)
S2 Principal solar	2.000000000	12.00000000
M2 Principal lunar	1.932273614	12.42060121
N2 Lunar ellipticity	1.895981969	12.65834823
K1 Lunisolar	1.002737909	23.93446961
O1 Lunar declination	0.929535706	25.81934169
Q1 1st order elliptic from O1	0.893244067	26.86835647

Table 2 Piezometric sensitivities to earth tides and calculated S_s for M2.

Piezometer screen interval (m)	N	$p(\epsilon_{11} + \epsilon_{22})^{-1}$ for M2 (GPa)		$p(\epsilon_{11} + \epsilon_{22})^{-1}$ for O1 (GPa)		S_s for M2 (m ⁻¹)
		Mean	Std. error	Mean	Std error	
106-109	5	1.1	0.3	2.2	1.3	5.9 x 10 ⁻⁶
201-204	11	1.4	0.1	1.6	0.8	4.6 x 10 ⁻⁶

harmonic was found from the regression coefficients $A_k = (a_k^2 + b_k^2)^{1/2}$ and the phase from $\phi_k = \text{atan}(-b_k/a_k)$ (Cryer, 1986). A similar regression fit determined the amplitude and phase of each tidal harmonic in the theoretical horizontal strain ($\epsilon_{11} + \epsilon_{22}$) associated with each sample time series. The ratios of piezometric responses (p) to horizontal strain amplitudes, or horizontal strain sensitivities ($p(\epsilon_{11} + \epsilon_{22})^{-1}$), were calculated for the M2 and O1 frequencies and are summarized in Table 2. Standard errors of horizontal strain sensitivity were larger for O1 than M2 because the amplitude of tidal horizontal strain at the O1 frequency is approximately one half the amplitude at the M2 frequency. By assuming a Poisson ratio = 0.25, specific storage was calculated for the M2 frequency using the relation (Bredehoeft, 1967; Hsieh *et al.*, 1988):

$$S_s = \rho g \frac{1 - 2\nu}{1 - \nu} \frac{(\epsilon_{11} + \epsilon_{22})}{p}$$

Pressure diffusion can attenuate horizontal strain sensitivity, causing magnitudes of specific storage to appear frequency dependent at tidal frequencies. Although the magnitudes of horizontal strain sensitivity for O1 and M2 agree within the range of the standard error for O1, this standard error is relatively large. Therefore, some frequency dependence of S_s may exist at these tidal frequencies. Drainage effects may also be quantified by examining the frequency dependence of the barometric efficiency (Galloway, 1994; Rojstaczer, 1988). At the piezometer location in El Paso, random pumping stress contaminated the piezometric response to atmospheric loading, causing incoherent frequency response of the barometric efficiency. It was therefore not possible to further quantify the magnitude of possible attenuation of horizontal strain sensitivity.

COMPARISON OF ELASTIC SPECIFIC STORAGE ESTIMATES

The stress-strain plots provide estimates of S_{ske} integrated over aquifer system intervals from 6-100 and 100-340 m depth and S_{skv} for late Pleistocene clay above 60 m depth. If a porosity of 0.3 is assumed and $\beta = 4.4 \times 10^{-10} \text{ Pa}^{-1}$, $S_{sw} = 1.3 \times 10^{-6} \text{ m}^{-1}$ may be added to these skeletal components to estimate the average S_s for these intervals, which are summarized in Table 3. The average S_s measured by extensometric-piezometric analysis decreases between the 6-100 m interval and the 100-340 m interval. This trend is also apparent from the magnitudes of S_s for sands at 106-109 and 201-204 m depth determined from earth tide analyses, and probably reflects a general trend of smaller matrix compressibilities with larger confining pressures.

Table 3 Summary of elastic specific storage estimates.

Depth interval (m)	Method	Lithology	$S_{ske} \text{ (m}^{-1}\text{)}$	$S_s \text{ (m}^{-1}\text{)}$
6-100	Extensometric	sands and clays	1.0×10^{-5}	1.1×10^{-5}
6-100	Extensometric	sands	6×10^{-6}	7.3×10^{-6}
106-109	Tidal response	sand		5.9×10^{-6}
201-204	Tidal response	sand		4.6×10^{-6}
100-340	Extensometric	sands and clays	7×10^{-6}	8×10^{-6}

The magnitudes of S_s for sands at 106-109 and 201-204 m depth are smaller than the average for the interval 100-340 m depth determined from extensometric-piezometric analysis. This suggests that the clay fraction in this interval has somewhat higher S_s than the average for the interval as a whole. A similar difference is observed in the upper aquifer-system interval from 6-100 m depth, for which the S_s inferred for sands is elastically stiffer than the average for sand and clay in the interval. It is noteworthy that S_s for sands in either interval is approximately $2.8 \times 10^{-6} \text{ m}^{-1}$ less than the average for sand and clay in the corresponding interval. The larger S_s determined from extensometric-piezometric analysis may partly result from the lower frequencies of stress changes measured by this method (Galloway, 1994). At the lower frequencies pore pressures within the clays can more nearly approach equilibrium with adjacent sands. As a result, average changes in effective stress are larger and the concomitant changes in strain are greater.

REFERENCES

- Bartels, J. (1957) Tidal forces. In: *Earth Tides* (ed. by J. C. Harrison), 25-63. Van Nostrand Reinhold Co., New York.
- Bredehoeft, J. D. (1967) Response of well-aquifer systems to earth tides. *J. Geophys. Res.* **72**(12), 3075-3087.
- Cryer, J. D. (1986) *Time Series Analysis*. Duxbury Press, Boston, Massachusetts.
- Galloway, D. L. (1994) The frequency dependence of aquifer-system elastic storage coefficients, implications for estimates of aquifer hydraulic properties and aquifer-system compaction. In: *U.S. Geological Survey Subsidence Interest Group Conference* (ed. by K. R. Prince, D. L. Galloway & S. A. Leake) (Edwards Air Force Base, Antelope Valley, California, November 18-19, 1992), Abstracts and Summary. *USGS Open-File Report 94-532*.
- Harrison, D. H. (1971) New computer programs for the calculation of earth tides, Cooperative Institute for Research in Environmental Sciences, NOAA/University of Colorado.

- Helm, D. C. (1976) One-dimensional simulation of aquifer system compaction near Pixley, California. 2. Stress dependent parameters. *Wat. Resour. Res.* 12(3), 375-391.
- Heywood, C. E. (1994) Monitoring aquifer compaction and land subsidence due to groundwater withdrawal in the El Paso, Texas - Juarez, Chihuahua area. In: *U.S. Geological Survey Subsidence Interest Group Conference* (ed. by K. R. Prince, D. L. Galloway & S. A. Leake) (Edwards Air Force Base, Antelope Valley, California, November 18-19, 1992), Abstracts and Summary. *USGS Open-File Report 94-532*.
- Hsieh, P. A., Bredehoeft, J. D. & Rojstaczer, S. A. (1988) Response of well aquifer systems to earth tides: problem revisited. *Wat. Resour. Res.* 24(3), 468-472.
- Land, L. F. & Armstrong, C. A. (1985) A preliminary assessment of land-surface subsidence in the El Paso area, Texas. *USGS Water-Resources Investigations Report 85-4155*.
- Riley, F. S. (1970) Analysis of borehole extensometer data from central California. In: *Land Subsidence* (Proc. Tokyo Symp., 1969), vol. 2, 423-431. IAHS Publ. no. 89.
- Riley, F. S. (1986) Developments in borehole extensometry. In: *Land Subsidence* (ed. by A. I. Johnson, L. Carbognin & L. Ubertini) (Proc. Venice Symp., March 1984), 169-186. IAHS Publ. no. 151.
- Rojstaczer, S. A. (1988) Determination of fluid flow properties from the response of water wells to atmospheric loading. *Wat. Resour. Res.* 24, 1927-1938.

Land subsidence due to groundwater withdrawal from the semi-confined aquifers of southwestern Flanders

L. LEBBE

Laboratory for Applied Geology and Hydrogeology, University of Gent, Krijgslaan 281 S8, B-9000 Gent, Belgium

Abstract Due to the heavy water withdrawal from the confined aquifers of southwestern Flanders, a subsidence cone has developed. This subsidence cone was mapped by comparing the levels of the first order of the National Geographical Institute (Belgium) between the levels of 1946-1948 and 1976-1980. In the centre of the subsidence cone, the drawdowns in the semi-confined aquifers have reached their maximum values. By means of an axi-symmetric hybrid finite-difference finite-element numerical model, the evolution of the drawdown around a pumped well can be calculated. In this axi-symmetric model the groundwater reservoir can be discretized in a large number of layers, which are supposed to be laterally homogeneous. So the evolution of the drawdown can be simulated at different levels of thick semi-pervious layers. In this way, the evolution of the subsidence, which is mainly due to the compaction of the semi-pervious layers, can be simulated. Here, the evolution of the subsidence is calculated for two cases: for a pumping in the lower semi-confined aquifer and a pumping in the upper semi-confined aquifer with the same discharge rate. The hydraulic parameters of the pumped aquifers were derived from pumping test analyses. However, the hydraulic parameters of the thick semi-pervious layers had to be estimated. Thus, their specific elastic storages were estimated by means of the Van der Gun relation. These values were verified by the comparison of the calculated and the observed subsidence in the area of maximum drawdowns. The subsidence due to pumping in the lower semi-confined aquifer has proved to be very different from the subsidence caused by a pumping in the upper semi-confined aquifer. This is the case both for the radial extension and for the evolution of the subsidence.

INTRODUCTION

Comparison of the eighteen hundred first order level marks of the National Geographical Institute (Belgium) between the levels of 1946-1948 and 1976-1980, made it possible to draw a recent ground level movement map (Pissart & Lambot, 1989). These movements are all derived with respect to the reference point at Ukkel. The absolute movement of this reference point is, however, not known. On this map, one can distinguish two large areas of ground lowering. One of this areas is located in the southwestern part of Flanders (Fig. 1). There, an almost circular area of subsidence occurs. In the centre of this area, the subsidence reaches maximum values which range between 80 and 100 mm.

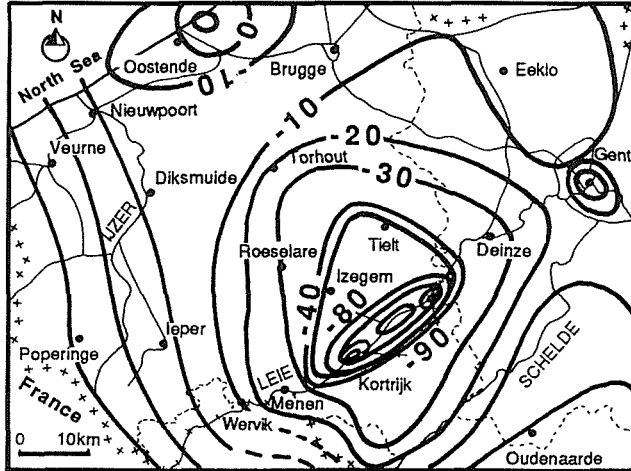


Fig. 1 Height changes of the first order level marks of the National Geographical Institute (Belgium) between the levelling of 1949-1948 and 1976-1980 (Pissart & Lambot, 1989).

This subsidence area coincides with the area of minimum hydraulic heads in the two underlying semi-confined aquifers (Fig. 2).

The groundwater reservoir consists of two semi-confined aquifers, which are separated by a semi-pervious layer. They are covered with a relatively thick semi-pervious layer (Fig. 3). At the top of the groundwater reservoir, a thin phreatic aquifer occurs. In the centre of the subsidence cone, the consolidated rocks of the Cambro-Silurian Brabant Massif occur at about 140 m below the ground surface. The upper part of this massif is fractured and forms the lower semi-confined aquifer. The massif is covered by Cretaceous and Tertiary unconsolidated rocks. The approximately 10 m thick Cretaceous deposits in the centre of the subsidence cone consist mainly of chalk and are semi-pervious. The overlying Tertiary deposits, which are principally composed of silt and clay, can also be considered to be semi-pervious. Between a depth of 86 and 100 m, silty fine sands occur that form the upper semi-confined aquifer. This aquifer is covered by Tertiary clayey and silty deposits. This semi-pervious layer has a very large areal extension and a considerable thickness under nearly the whole of the Belgian provinces West- and East-Flanders. This clay and silt layer has the same geological age as the London Clay. The superficial Quaternary sediments (sand, silt and clay) are generally thin, mostly between 2 and 13 m. In the river valleys, these sediments can be thicker. They form the phreatic aquifer. From both semi-confined aquifers, large groundwater quantities are withdrawn which cause large depression cones in the hydraulic head of both aquifers. In the centre of the cones, the drawdown since the start of the pumpings is estimated at 140 m in the lower semi-confined aquifer and about 85 m in the upper semi-confined aquifer (Lebbe *et al.*, 1988) (Fig. 2).

DRAWDOWN CALCULATED BY A NUMERICAL MODEL

The applied numerical model is two-dimensional and axi-symmetric. In this model, the groundwater reservoir is discretized in a number of homogeneous layers which are

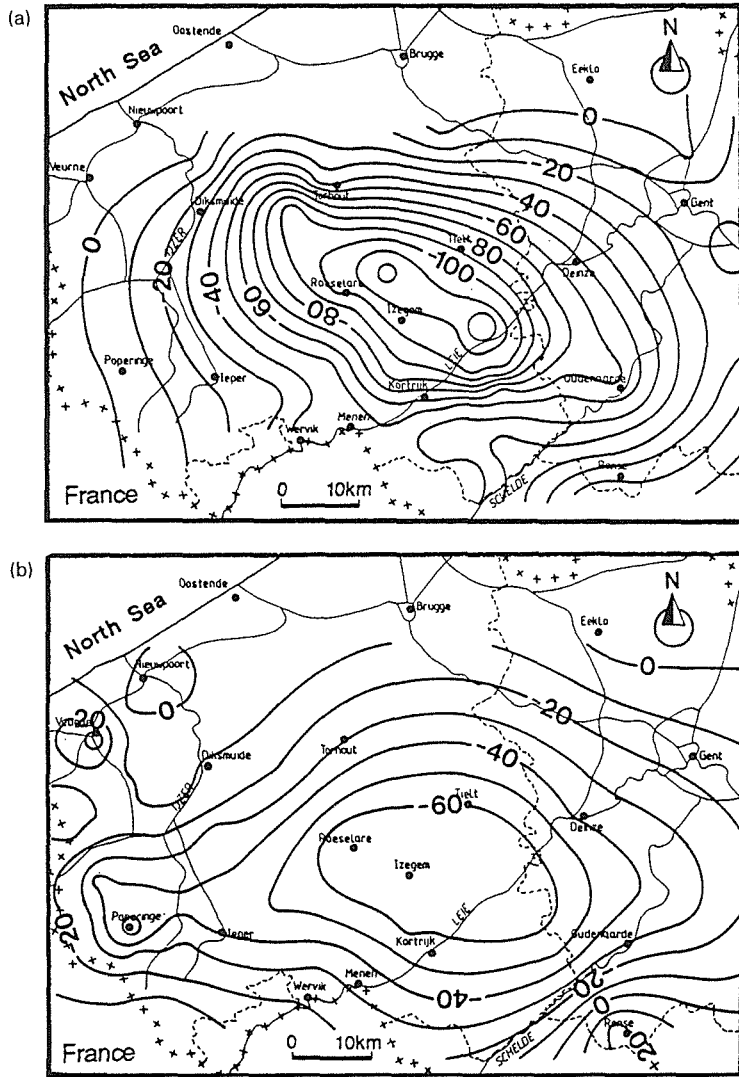


Fig. 2 Hydraulic head contour lines of the lower (a) and the upper (b) semi-confined aquifers in the southwestern part of Flanders (Lebbe *et al.*, 1988).

numbered from bottom to top. Each layer is subdivided in a number of concentric rings. The lowest layer, layer 1, is bounded below by an impervious boundary. The water table always equals the top of the uppermost layer. The horizontal flow and the storage change in each layer are characterized, respectively, by one value of the horizontal conductivity and one value of the specific elastic storage. The vertical flow between two layers is governed by one value of the hydraulic resistance between those layers. The hydraulic resistance is the thickness of the layer divided by its vertical conductivity. The amount of water delivered by a unit decline of the water table is given by one value of the specific yield. In the block centred nodal circles of each ring, the drawdowns are calculated with a hybrid finite-difference finite-element model. The input parameters that define the space-time grid are the number of layers, the number of rings per layer, the

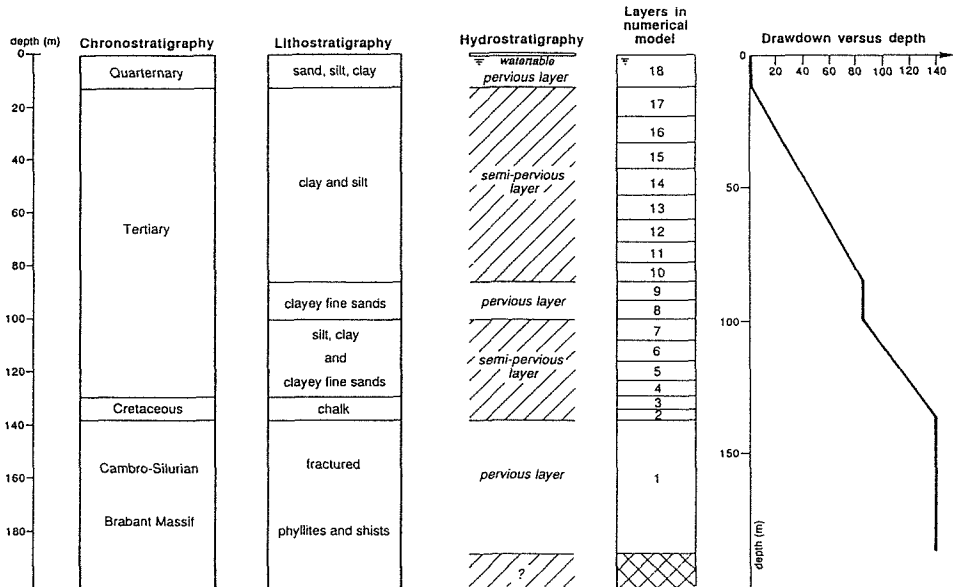


Fig. 3 Chrono- and lithostratigraphical data and hydrogeological schematization of the groundwater reservoir in the centre of the subsidence area of southwestern Flanders. The vertical discretization of the groundwater reservoir in the numerical model along with the maximum drawdown vs. the depth.

number of time steps, the initial radius, RI , the initial time, TI , and the factor A . The initial radius is the inner radius of the smallest ring in the numerical model. The factor A determines the ratio of the outer and inner radii of all the rings and the ratio between the final and the starting time of the considered time steps. It is assumed that between two successive nodal circles of one layer the drawdown changes linearly with the logarithm of the distance from the pumped well. A detailed description of the numerical model is given in Lebbe (1988). In this work, the validation of this numerical model was shown by the simulation of the classical models of Theis, Jacob, Hantush & Jacob, Hantush and Boulton.

SUBSIDENCE DUE TO DRAWDOWN OF THE HYDRAULIC HEAD

In this paper, the real three-dimensional deformation of the groundwater reservoir is simplified to a one dimensional compression in the vertical direction. It is further assumed that the solids are incompressible and consequently, that the change in thickness of a layer is fully accounted by the change in void ratio. According to these, one can derive from Domenico & Schwartz (1990) that the thickness of a layer J , $D(J)$, reduces with a value $\Delta D(J)$:

$$\Delta D(J) = D(J)(S_s(J) - \rho_w g n(J)\beta_w)\Delta s \quad (1)$$

where $\Delta D(J)$ is the thickness reduction of layer J , $D(J)$ is the thickness of layer J , $S_s(J)$ is the specific elastic storage of layer J , $\rho_w g$ is the specific weight of the water, $n(J)$ is the porosity of layer J , β_w is the water compressibility and Δs is the drawdown increase.

Applying this formula, it is assumed that the specific elastic storage at every level is constant during the compaction and also independent of the drawdown. The thickness reduction of every layer can be found by calculating the drawdown for every layer with the numerical model. The subsidence undergone by the middle of a layer is now the sum of the thickness reductions of all the underlying layers increased with half the thickness reduction of the considered layer. For the uppermost layer of the numerical model, the calculated subsidence corresponds with the subsidence at the top of this layer.

DISCRETIZATION IN THE NUMERICAL MODEL

In the numerical model, the groundwater reservoir is discretized in eighteen layers (Fig. 3). The lowermost layer corresponds with the fractured top zone of the Brabant Massif. The Cretaceous deposits are discretized in two layers of respectively 4 and 5 m thick. The lower part of the Tertiary deposits, which form a semi-pervious layer, is discretized in five layers of respectively 6, 7, 8, and 7 m thick. The Tertiary fine sands between the depths of 86 and 100 m, are discretized in two layers of the same thickness. The thick upper part of the Tertiary deposits, which consists primarily of clay and silt, forms a semi-pervious layer. These deposits are discretized in eight layers with thicknesses between 7 and 11 m. The uppermost layer of the numerical model coincides with the phreatic aquifer and has a thickness of 12 m.

HYDRAULIC PARAMETERS

Only the horizontal conductivities and the specific elastic storages of the pervious layers are well known. They were measured by means of pumping tests in the Brabant Massif (Lebbe *et al.*, 1991) and in the Tertiary deposits (Lebbe *et al.*, 1989; De Ceuckelaire *et al.*, 1991). The other hydraulic parameters are estimated. This is particularly true for the horizontal conductivities of the semi-pervious layers and the vertical conductivities of the semi-pervious and pervious layers.

The horizontal conductivity of layer 1 is equal to 0.8 m day^{-1} . According to the assumed thickness of the layer (50 m), the transmissivity of the pervious layer is equal to $40 \text{ m}^2 \text{ day}^{-1}$. This is about the average transmissivity found in five pumping tests executed in the Brabant Massif (Lebbe *et al.*, 1991). The average specific elastic storage found in these tests is $5.0 \times 10^{-7} \text{ m}^{-1}$. This very small specific elastic storage is probably only due to the elasticity of the water. If the consolidated rocks are completely inelastic, they must have a porosity of about 11%. The horizontal conductivity of the Tertiary fine sands, which form the upper semi-confined aquifer, is equal to 0.16 m day^{-1} . The specific elastic storage of this layer is $9.8 \times 10^{-6} \text{ m}^{-1}$. This is the average value found by two pumping tests in these fine sands.

Because the semi-pervious layers are horizontally stratified, they are considered as anisotropic with respect to the hydraulic conductivity. The horizontal conductivities of these layers are assumed to be two times larger than the vertical conductivity. The vertical conductivity of the Cretaceous deposits is estimated at a value of $4.0 \times 10^{-4} \text{ m day}^{-1}$. The lower part of the Tertiary deposits has a vertical conductivity of $2.0 \times 10^{-4} \text{ m day}^{-1}$. The upper part of the Tertiary deposits, which consists

principally of silt and clay, has the smallest vertical conductivity, about $8.0 \times 10^{-5} \text{ m day}^{-1}$.

ESTIMATION OF THE SPECIFIC ELASTIC STORAGES

The specific elastic storages of the semi-pervious layers were not directly deduced from the pumping test analyses. These values are first derived with the help of the relation between the specific elastic storage and the depth of the sediments proposed by Van der Gun (1979). Based on the work of Van der Knaap (1959), Van der Gun (1979) proposes a relation between the specific elastic storages of sandy aquifers, S_s , and the depth, d :

$$S_s = 1.8 \times 10^{-6} + 2.59 \times 10^{-4} d^{-0.7} \quad (2)$$

The values derived from the specific elastic storages were verified by the comparison of the calculated and the observed subsidence in the area of maximum subsidence. The subsidence was calculated according to the method proposed by Domenico & Schwartz (1990). For this calculation the groundwater reservoir is discretized in the same way as in the numerical model. The specific elastic storages of each layer are calculated with the Van der Gun relation given above, according to the depths of the middle of the layer. The thickness reduction of every layer is then calculated by means of equation (1) with the drawdowns that occur now in the centre of the subsidence cone around Waregem.

The estimated drawdowns in the pervious layers are equal to the differences between the observed hydraulic heads in these layers (Fig. 2) and the calculated head for the unpumped state of the groundwater reservoir (Lebbe *et al.*, 1988). In the centre of the subsidence cone, the drawdowns have reached their maximum values. In the lower semi-confined aquifer they have a value of 140 m, in the upper semi-confined aquifer they reach a value of 85 m. The drawdown of the uppermost layer, which correspond with the phreatic aquifer, is put equal to 0.5 m. The drawdowns in the semi-pervious layers are calculated by linear interpolation between the drawdowns of the aquifers (Fig. 3). So, a steady state flow through the semi-pervious layer is assumed.

In the calculation, a constant porosity of 0.4 was considered. The resulting subsidence is then equal to 106 mm. This value is a little higher than the observed change of the level marks between the levels of 1946-1948 and 1976-1980. It should be mentioned that there was already a very small subsidence before 1947 and that the subsidence had not reached his maximum value in 1978. The used drawdowns values were observed in 1986. Because the values for the specific elastic storage, estimated with the Van der Gun relation, result in calculated subsidence which is in accordance with the observed changes, these values can be used for a first attempt to simulate the subsidence due to pumping in one of the aquifers.

SUBSIDENCE CALCULATED WITH THE NUMERICAL MODEL

The evolution of the subsidence is calculated for a pumping in the lower semi-confined aquifer formed by the Palaeozoic Brabant Massif and secondly for a pumping in the upper semi-confined aquifer. In both calculations, a discharge rate of $192 \text{ m}^3 \text{ day}^{-1}$ is chosen. This is the maximum possible withdrawal for a pumping well in the upper semi-confined aquifer. For a pumping well in the lower aquifer, however, it is a rather

small discharge rate. The parameters that define the space-time grid are also the same in both calculations. The initial radius was 0.16 m, the factor which defines the ratio of the inner and the outer diameter was 0.126 and fifty-eight rings were considered. This means that the outer boundary of the numerical model is situated at 100 km from the axis of the pumped well. The initial time of the calculation is equal to one minute and the drawdowns and the subsidence are calculated till 10^7 minutes, or about 19 years, after starting the pumping.

The calculated subsidence are represented in subsidence-time and subsidence-distance graphs for both tests (Fig. 4). All axes of the graphs are logarithmic. In the subsidence-time graphs the evolution of the subsidence is represented for different times after the start of the pumping test. In the subsidence-distance graphs, the lateral variation of the subsidence is represented for different times after the start of the pumping.

Comparing the graphs of both tests, one can draw the following conclusions. In the case of pumping in the upper semi-confined aquifer, the subsidence reaches its maximum value after about two years of pumping and for distances smaller than 500 m from the pumped well. At larger distances, the subsidence continues to increase after a longer pumping time. If the lower semi-confined layer is pumped, the subsidence has not reached his maximum value, even after a period of about 20 years of pumping and this for all distances from the pumped well. At relative large distance from the pumped

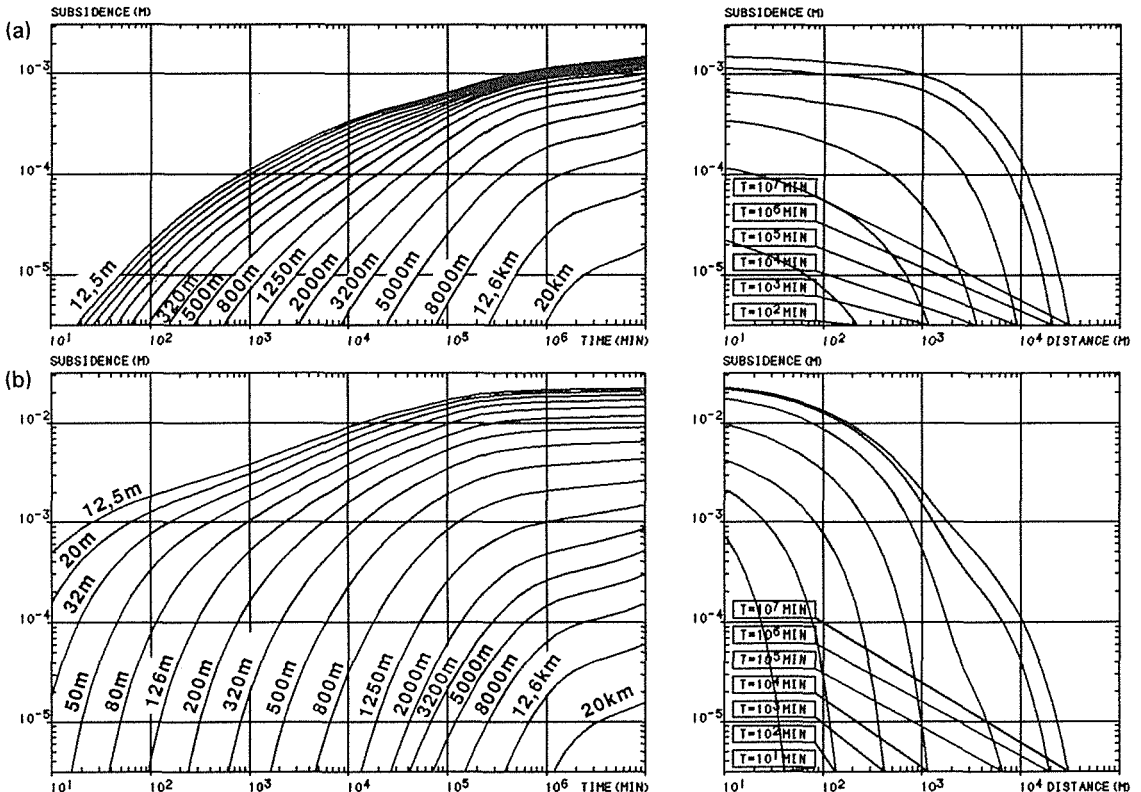


Fig. 4 Subsidence-time and subsidence-distance graphs for the pumping test in the lower (a) and the upper (b) semi-confined aquifer both with a same discharge rate of $192 \text{ m}^3 \text{ day}^{-1}$.

well and after a long period of pumping, the subsidence due to pumping in the lower semi-confined aquifer is about equal to the subsidence caused by pumping in the upper semi-confined aquifer. For distances smaller than 2 km, the change of the subsidence versus the distance from the pumped well is much smaller in the case that the lower semi-confined aquifer is pumped then in the other case.

CONCLUSION

The subsidence due to pumpings in two different semi-confined aquifers in southwestern Flanders was studied by means of a numerical model. The evolution of the drawdowns was calculated at a large number of different levels in the thick semi-pervious layer. With these drawdowns, the evolution of the subsidence due to pumping can be calculated. First, the subsidence due to a pumping in the lower semi-confined aquifer of southwestern Flanders is calculated. The subsidence caused by pumping in the upper semi-confined aquifer is considered in the second simulation. The evolution and the lateral extension of the subsidence of both pumpings are very different. At relatively small distances from the pumped well, the subsidence is many times smaller in the first case than in the second case. At such distances, the subsidence reaches equilibrium later in the first case than in the second case. At relatively large distances the subsidence continues to increase after relatively large pumping times. At large distances from the pumped well, the subsidence of both pumpings does not differ much. This study must be considered as a first attempt to treat numerically the subsidence due to groundwater withdrawal from the semi-confined aquifers of southwestern Flanders. In a following step this subsidence should be treated taking the stress-dependence of the hydraulic parameters into account.

Acknowledgements The author would like to thank the National Fund for Scientific Research (Belgium) under whose auspices the study was carried out. He wishes also to express his gratitude to Prof. W. De Breuck, Head of the Laboratory of Applied Geology and Hydrogeology, for the support given for the preparation of this paper.

REFERENCES

- De Ceuckelaire, M., Lebbe, L., Bolle, I. & De Breuck, W. (1991) *Results of the Pumping Test of the Dairy Factory INCO at Langemark* (in Dutch). Report TGO 90/53, State Univ. Gent, Lab. Appl. Geol. and Hydrogeology.
- Domenico, P. A. & Schwartz, F. W. (1990) *Physical and Chemical Hydrogeology*. John Wiley & Sons, New York.
- Lebbe, L. (1988) Execution of pumping tests and interpretation by means of an inverse model (in Dutch). Thesis Geagg. Hoger Onderw. Geologisch Instituut, Univ. Gent, Gent.
- Lebbe, L., Van Camp, M., Van Burm, P., De Ceuckelaire, M., Wattiez, R. & De Breuck, W. (1988) The groundwater in the Palaeozoic Basement Complex and in the Landenian aquifer in West- and East-Flanders (in Dutch). *Water* **41**, 104-108.
- Lebbe, L., Mahauden M. & De Breuck, W. (1989) *Results of the pump and recovery test in the Benedictine sister's convent at Poperinge* (in Dutch). Report TGO 89/53, State Univ. Gent, Lab. Appl. Geol. and Hydrogeol.
- Lebbe, L., Mahauden M. & De Breuck, W. (1991) Interpretation of pumping tests in the anisotropic Brabant Massif by means of a numerical inverse model. *Ann. Soc. Géol. Belgique* **114**(1), 277-282.
- Pissart, A. & Lambot, P. (1989) Les mouvements actuels du sol en Belgique; comparaison de deux nivellements IGN (1946-1948 et 1976-1980). *Ann. Soc. Géol. Belgique* **112**(2), 495-504.
- Van der Gun, J. A. M. (1979) Estimation of the elastic storage coefficient of sandy aquifers (in Dutch). *TNO Dienst Grondwaterverkenning, Jaarverslag 1979*, 51-61.
- Van der Knaap, W. (1959) Non-linear behaviour of elastic porous media. *Trans AIME*, **216**.

Land subsidence due to groundwater withdrawal in Hanoi, Vietnam

TUNG Q. NGUYEN & DONALD C. HELM

Nevada Bureau of Mines and Geology, University of Nevada-Reno, Mail Stop 178, Reno, Nevada 89557-0088, USA

Abstract Groundwater has been exploited since the beginning of this century to supply water for the Hanoi urban area from two porous unconfined and confined aquifers. These aquifers occur in Quaternary unconsolidated sediments and are separated by a virtually impervious clay layer. Most of the water used in Hanoi is extracted from the confined aquifer which is underlain by bedrock of Tertiary age. Due to socio-economic growth, the groundwater extraction system has been broadened from 9 to 11 water plants in order to increase the amount of water development. As a consequence of this action, water levels within the aquifers have declined to about 35 m below the initial level. This leads to land subsidence, which has been observed since 1988 by levelling. It shows that the ground surface has declined more in the centre, where water extraction wells are located, than in the surrounding adjacent areas. In some places the magnitude of subsidence reaches about 10 to 15 cm – damaging houses, schools and factories. Land subsidence due to groundwater withdrawal is a new field of research in Vietnam. Future research should clarify our understanding of land subsidence mechanisms and predict subsidence for groundwater management and city planning.

INTRODUCTION

Hanoi is located in the centre of Bacbo plain at an elevation of about 5 to 12 m above mean sea level. The climate is characterized by a monsoon regime, which is divided into two seasons: a dry season from November to April and a rainy season from May to October. The mean annual precipitation is about 1500 mm and is unevenly distributed through the year: 84% during the rainy season and 16% during the dry season. The seasonal precipitation water serves as a natural replenishment of the unconfined aquifer but is restricted by impervious areas such as houses and streets, as well as evaporation from the surface, which can reach 1100-1300 mm annually. The major drainage system of the area is the Red River with its distributaries.

Groundwater is the only source of water supply to Hanoi City. Since 1978, the process of water exploitation has increased, especially during the last decade due to socio-economic development. Along with this, urban hazards such as land subsidence, floods, and fissuring become increasingly serious and dangerous to the city causing great damage (Tran & Nguyen, 1990).

GEOLOGY

The Hanoi area is underlain by unconsolidated sediments of Holocene to Pleistocene age Q_{1-4} about 45 to 120 m thick that overlie a basement of Tertiary age N. The basement is composed of gravelstone, sandstone and claystone which have not been well investigated. Quaternary unconsolidated sediments of coarse-grained size in the deeper part and fine to small-grained size in the upper part are of primary interest. The deeper part consists of Lower to Middle Pleistocene Q_{1-2} pebble, gravel, coarse sand and alternating clay lens of alluvial origin that dip and generally thicken in the south-east direction. The upper part consists of Upper Pleistocene and Holocene Q_{3-4} soils of marine, lacustrine and alluvial genesis: fine and small-grained sands, clayey sand, sandy clay, clay, peat and silt. Clay of Upper Pleistocene Q_3 is the principal confining bed in the Hanoi area, which in some places bares at the surface. A stratigraphic column is generalized and illustrated in the Table 1.

Table 1 General stratigraphy in Hanoi area.

Geologic age		Approximate thickness (m)	Description
Cenozoic	Holocene- Upper Pleistocene Q_{3-4}	0-30	Fine and small-grained sands, clayey sand, sandy clay, soft clay, peat and silt
	Upper Pleistocene Q_3	0-15	Clay
	Middle-Lower Pleistocene Q_{1-2}	40-70	Pebble, gravel, coarse-grained sand and clay lens
Tertiary	Pliocene-Miocene N	> 1000	Gravelstone, sandstone and claystone

HYDROLOGY

Two aquifers, leaky unconfined and confined, are classified to correspond to Q_{3-4} and Q_{1-2} respectively in the stratigraphic column (Fig. 1).

The unconfined aquifer is supplied by rainfall and lateral recharge from Red River. Evaporation is its main way of drainage. The specific yield of wells is less than $1.0 \text{ l s}^{-1} \text{ m}^{-1}$. The water is mainly used for agriculture and houses and is extracted by sparsely distributed private wells.

The confined aquifer is separated from the unconfined aquifer by a virtually impervious stratum of clay. Most supplies of industrial and municipal water in the Hanoi urban area are drawn from this aquifer, which gets recharge through leakage from the above unconfined aquifer and from lateral flow of groundwater. The specific yield ranges from 5 to $15 \text{ l s}^{-1} \text{ m}^{-1}$.

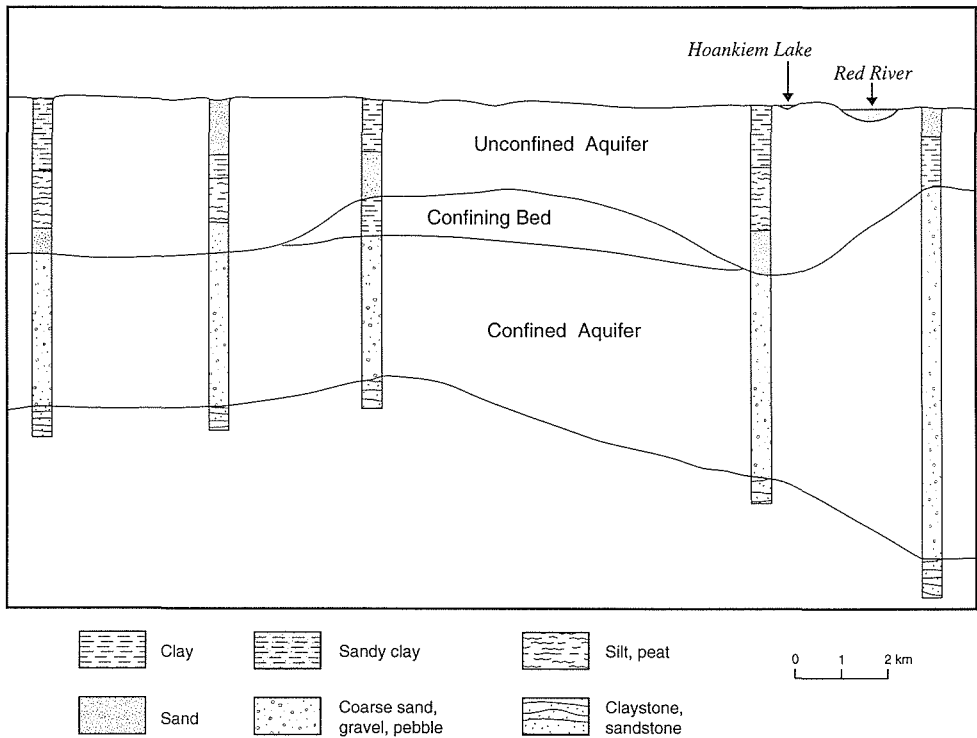


Fig. 1 Hydrogeological cross section of the Hanoi urban area.

GROUNDWATER EXTRACTION AND LAND SUBSIDENCE

Groundwater began to be exploited in the beginning of this century by the French on a small scale. The primary rate of pumpage was about $20\,000\text{ m}^3\text{ day}^{-1}$. This rate doubled by 1954 and increased further to $164\,000\text{ m}^3\text{ day}^{-1}$ by 1978. Since 1985, the groundwater extraction system has been broadened from 9 to 11 water plants with the assistance of the Finnish Government in order to increase the amount of water extraction. It reached a rate of $300\,000\text{ m}^3\text{ day}^{-1}$ in 1988 and about $400\,000\text{ m}^3\text{ day}^{-1}$ in 1991. However, this amount satisfies only about 60% of water demand. Therefore, it will be increased in the future (Rau *et al.*, 1991).

The heavy pumping has resulted in a substantial decline of piezometric head to form a large drawdown cone beneath the Hanoi urban area. The piezometric head in deep wells initially was 2-5 m below land surface, but by 1993 it had dropped to 37-40 m (Fig. 2). Meanwhile, the water table of the $Q_{3,4}$ aquifer has declined by 2-6 m. The drawdowns of piezometric head as well as of the water table have caused a significant increase in effective stress within the aquifers themselves with an accompanying decrease of pore water pressure and increase in effective stress within the confining bed. Stress transfer results from the release of stored water in highly compressible clay layers and their subsequent compaction (Helm, 1984). Therefore, the occurrence of land subsidence can not be avoided. The first evidence of subsidence was observed during the 1988-1989

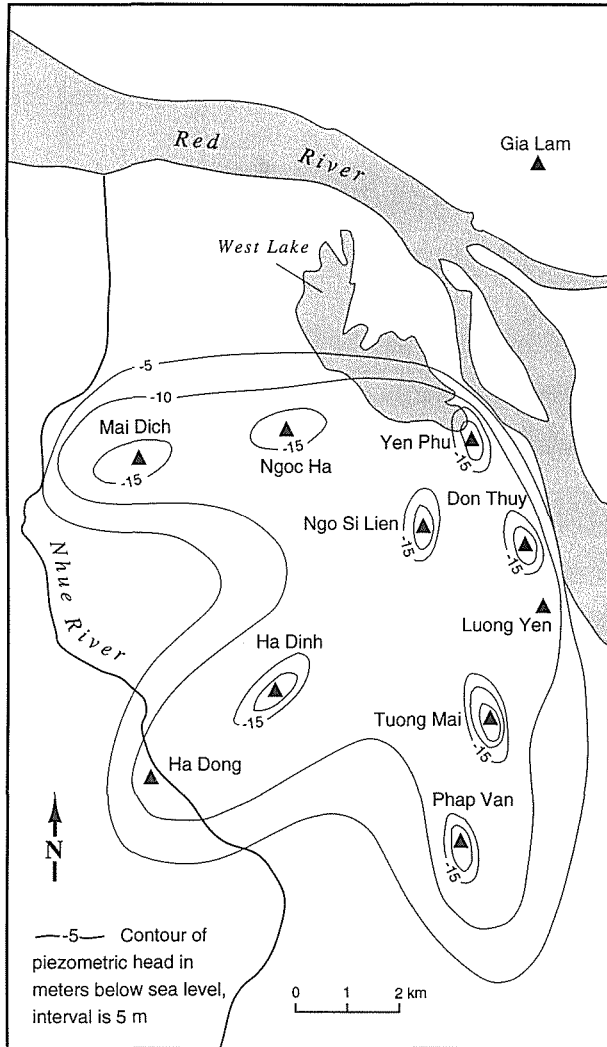


Fig. 2 Map of the Hanoi urban area showing the piezometric head in 1993. Contour lines show the piezometric head in m below sea level, interval 5 m. ▲ : location of water plant.

levelling of land surface over the Hanoi urban area. It showed that land surface has declined more in the centre, where water extraction wells are located, than in the adjacent areas. During this period subsidence reached about 10-15 cm and has formed a subsidence bowl that coincides with the cone of depression of piezometric head (Fig. 3). Land subsidence has damaged several houses, schools and factories in the central and southern parts of Hanoi. Related to land subsidence, fissures have been found in southwest part of the city, which were never observed before. Moreover, in the centre of the land subsidence area, surface water can not be drained in a timely manner during the rainy season, which adversely influences city traffic. In summary, land subsidence has brought a great damage to the city. Because of the time lag (due to low permeability)

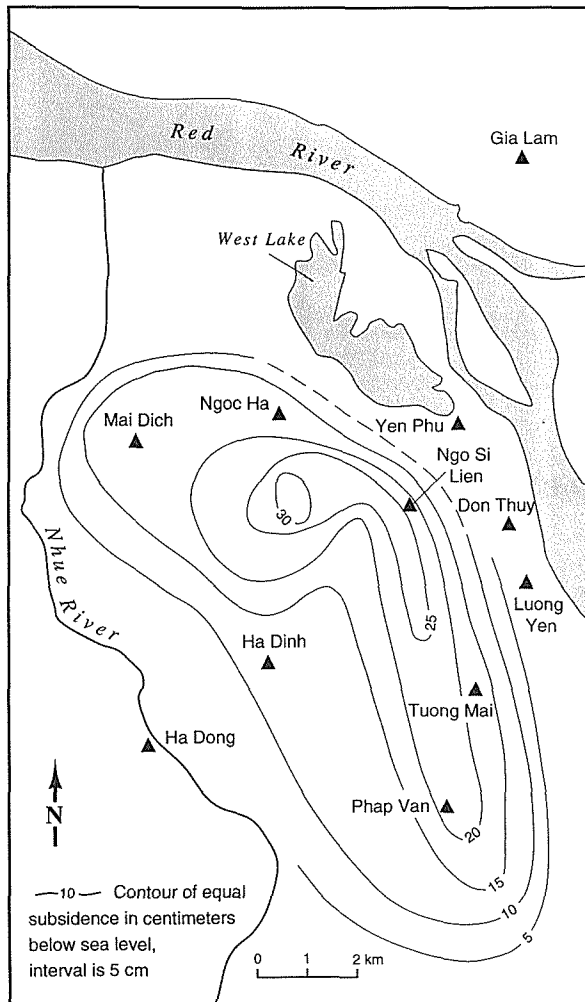


Fig. 3 Map of the Hanoi urban area showing the subsidence bowl. Contour lines show subsidence in cm, interval 5 m. ▲: location of water plant.

in pressure changes progressing vertically through the clay confining bed (Q_3), the highly compressible confining layer is not a hundred percent consolidated. Hence, even if water levels decline no further in the two aquifers, latest subsidence can be expected to continue for years (even decades) into the future. Increased drawdown in the future within the two aquifers will only increase the subsidence further. The 10-15 cm subsidence already observed may only be a fraction of what can be expected during the coming decades if steps are not taken quickly to plan wisely for the future.

CONCLUSION

Groundwater extraction in the Hanoi urban area is the main cause of land subsidence. In contrast to many other places throughout the world, land subsidence in Hanoi has not

yet been controlled. Therefore, land subsidence investigations are urgent by needed to clarify its mechanism and predict subsidence for effective and timely groundwater management and city planning.

REFERENCES

- Helm, D. C. (1984) Field-based computational techniques for predicting subsidence due to fluid withdrawal. In: *Man-Induced Land Subsidence* (ed. by T. L. Holzer), 1-22. Reviews in Engineering Geology 6, Geological Society of America.
- Rau, J. L., Nutalaya, P., Tran, H. V. & Nguyen, T. Q. (1991) The problem of land subsidence in the world and Vietnam. In: *Proc. Second Conference on Geology of Indochina*, vol. 1, 421-428.
- Tran, H. V. & Nguyen, T. Q. (1990) *The Alteration of Geological Environment in the Hanoi Area in the Process of Urbanization* (in Vietnamese). Centre for Applied Geophysics, National Centre for Scientific Research, Hanoi, Vietnam.

Land subsidence and well failure in the Belridge Diatomite Oil Field, Kern County, California. Part I. Experiments, model and verification

E. DE ROUFFIGNAC

*Shell Exploration Co., Bellaire Technology Center, PO Box 481, Houston,
Texas 77001-0481, USA*

P. L. BONDOR

CalResources LLC

Abstract Depleting fluids from shallow and thick reservoirs composed of low strength rock can cause substantial compaction leading to surface subsidence and well failure. This is the case for the Diatomite reservoir, where over 10 ft of subsidence has occurred in some areas. Well failure rates have averaged over 3 % per year, resulting in high well replacement and repair costs. A team effort has been underway to address this issue, including experimental work, modelling, and subsidence calculations. This paper labelled Part I deals principally with isothermal experimental results and the constitutive model derived from them.

UNITS

1 psi = 6900 Pa

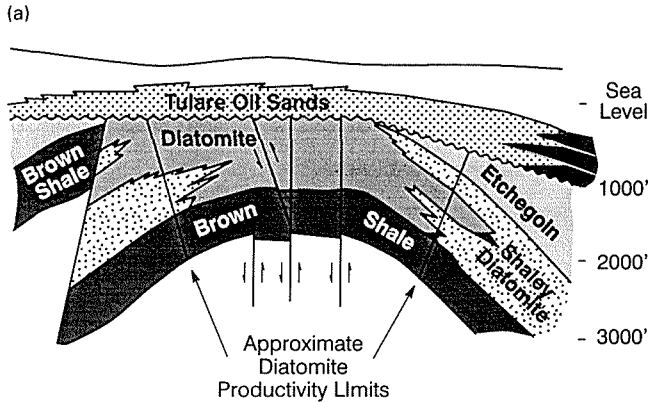
1 foot (ft) = 30.5 cm

1 inch (in.) = 2.54 cm

1 MD = 10^{-11} cm²

INTRODUCTION

The South Belridge field is located approximately 50 miles west of Bakersfield in central California. It is a giant field, with more than 2 billion barrels of oil in place in the diatomite horizon alone. Figure 1(a) shows a vertical cross section of the reservoir. Total diatomite reservoir thickness ranges from 800 to 1000 ft and is overlain by 200 to 400 ft of air sands on top of 400 to 600 ft of sands and shales, the latter being the Tulare formation. The Diatomite formation is a very fine-grained mixture of biogenic silica (40%-75%), and other minerals (Schwartz, 1988) as listed on Fig. 1(b). The depositional environment generated a reservoir with distinct layers (Schwartz, 1988) which we have labelled alphabetically from "G" at the top of the Diatomite to "M" at the bottom. The silica in these layers comes in the form of "pill-shaped" diatoms embedded in their own skeletal fragments which were mostly broken but only partially compacted during burial and tectonic activity. This has generated an unusually porous rock with low Young's modulus (see Fig. 1(b)) as compared to sandstones. This combination of large thickness and low Young's modulus results in substantial compaction of the Diatomite during fluid depletion leading to subsidence and surface fissures as shown on Fig. 2(a).



(b)

- Mineralogy

OPAL-A	50%
Quartz + Feldspar	25%
Carbonates	10%
Clays	15%
- Deposition

Twelve sedimentary cycles 30-180 feet thick and extending over twenty square miles occur in the Belridge Diatomite.
- Main Rock Characteristics

Low Young Modulus	25,000 – 80,000 psi
High Porosity	55 – 60%
Low grain density	2.2 – 2.5 gm/cm ³
Low permeability	0.03 – 0.3 md
High avg. oil sat.	45%
Avg. water sat.	45%
Avg. gas sat.	10%

Fig. 1 (a) Belridge Diatomite and (b) Diatomite properties.

DATA

Compaction experiments

Diatomite in the reservoir compacts as effective stresses supported by the rock frame increase due to depletion. The three principal mechanisms involved are:

- (a) the elastic deformation of the grains which constitute the rock frame;
- (b) the shear deformation caused by unequal horizontal and vertical stresses;
- (c) the breakage of the frame itself (pore collapse) which leads to volumetric reduction even under hydrostatic stress conditions (and is only significant in relatively weak rocks like Diatomite or Chalks).

The first mechanism is reversible and can be readily understood based on elastic theory. Shear failure and pore collapse are irreversible mechanisms that can be quantified by a plastic formulation (Chen & Baladi, 1985). Previous work (Hansen *et al.*, 1993) has included the first two mechanisms only. Inclusion of pore collapse in our new formulation results in a significantly improved subsidence match and prevents overestimation of surface rebound, as will be discussed later.

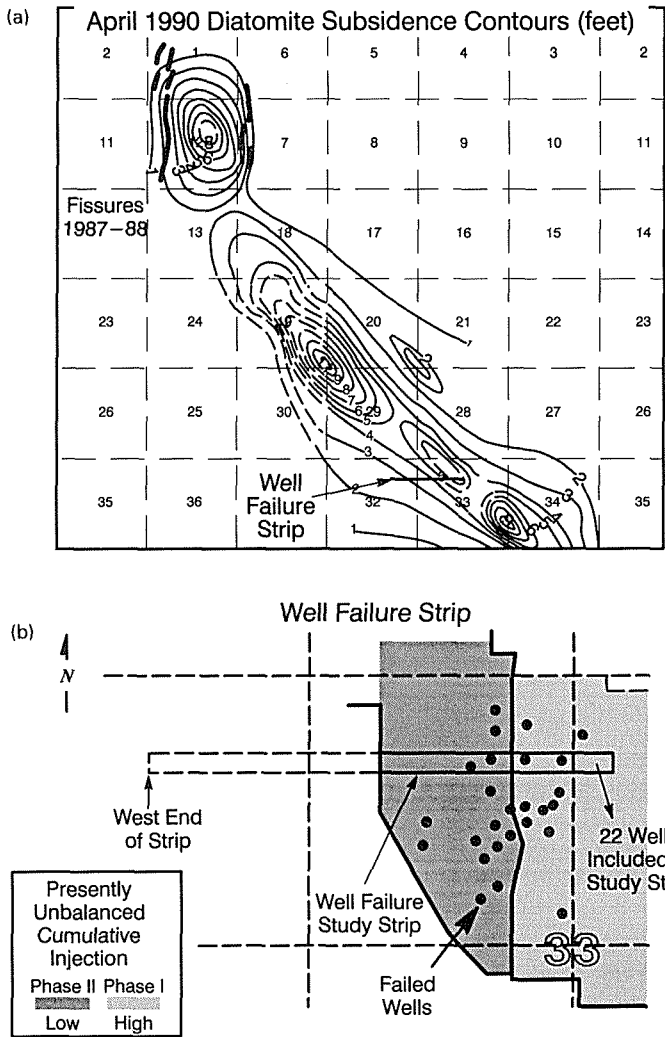


Fig. 2 (a) April 1990 Diatomite subsidence contours (feet).
 (b) Well failure strip.

We conducted a large number of room temperature triaxial and uniaxial experiments to determine the main failure mechanisms. Is Diatomite similar to other rocks where shear failure is the dominant mechanism? Figure 3(a) shows typical triaxial data for G-cycle Diatomite cores from two different wells. The failure envelope drawn is a straight line fit through the data. The same applies for J, L and M core as shown on Figs 3(b) and 3(c). The cohesion (Y-axis intercept) is about 14 kPa for G-J material and nearly 21 kPa for L-M. These results suggest using a Drucker-Prager type constitutive law to describe the rock. But further insight was gained by performing uniaxial experiments as shown on Figs 3(d) and 4(a). These are uniaxial compaction experiments at zero radial strain. The unloading part of the curve (particularly on Fig. 4(a)) shows a very small linear region up to perhaps 7 kPa (≈ 100 psi). On reloading the sample behaviour is nearly linear but shows substantial hysteresis. This behaviour is characteristic of a

Failure Envelope

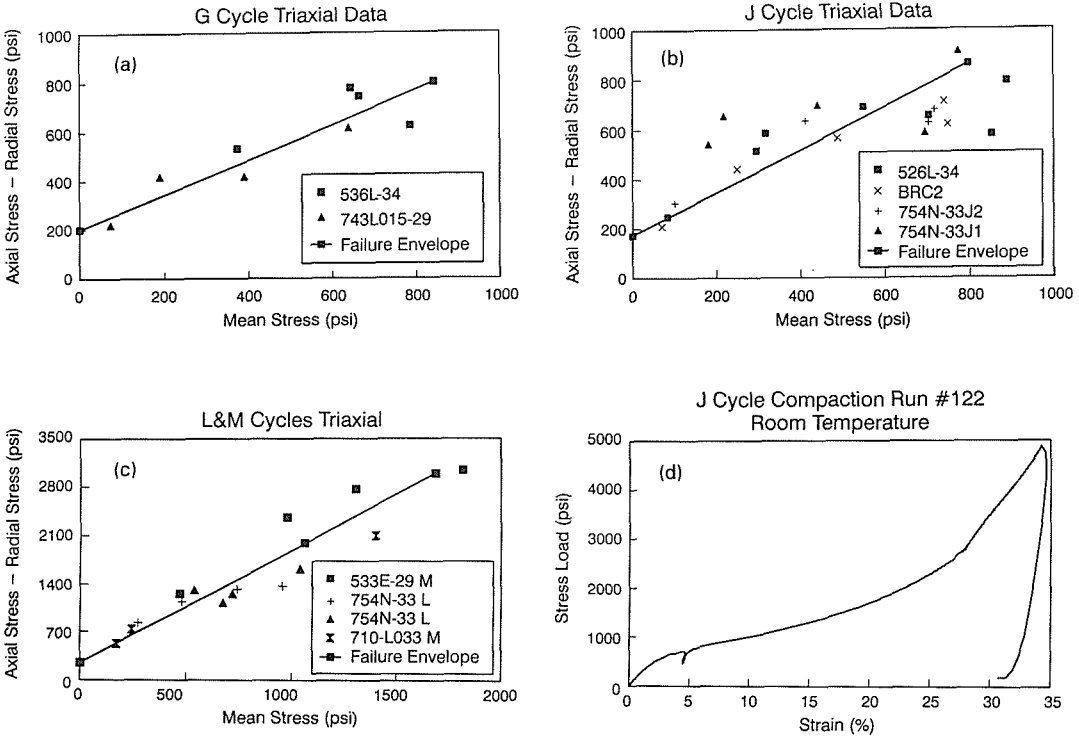


Fig. 3 (a) G cycle triaxial data.
 (b) J cycle triaxial data.
 (c) L&M cycle triaxial data.
 (d) J cycle compaction run 122, room temperature.

material which exhibits elastic and irreversible plastic deformation when the stress increases but a purely elastic behaviour when the stress goes down. The small linear elastic region during loading makes it difficult to model with only a shear failure mechanism during uniaxial loading. We believe that in fact diatoms and diatom fragments break during the loading causing "pore collapse" of the material and leading to an irreversible reduction in porosity. Figure 3(d) shows the results for a sample taken to stress levels well beyond the 50 Kpa level expected during field depletion. Porosity decreased irreversibly from 55% initially to 31% after 35% vertical compacting strain. It is apparent that as the rock loses porosity it becomes stiffer and its stress-strain slope eventually reaches values appropriate for matrix grain material. Figures 3(b) and 3(c) show similar results to Fig. 3(a), for cycles J and M. In order to capture both the triaxial and uniaxial behaviour we use the Drucker-Prager model suggested above with a "cap" added to generate the pore collapse. We chose an elliptical cap that closes the Drucker-Prager cone in deviatoric space, as shown on Fig. 5(a). Poisson's ratio ν and failure surface parameters d and b are obtained from the triaxial data. The Young's Modulus is derived from the downloading branch of the uniaxial experiments. The parameters for the cap F_c are obtained by fitting a simple finite element model of the uniaxial experiment to the results of Figs 4(a) through 4(c); the black dotted line on the figures

Isothermal Uniaxial Compaction of Diatomite

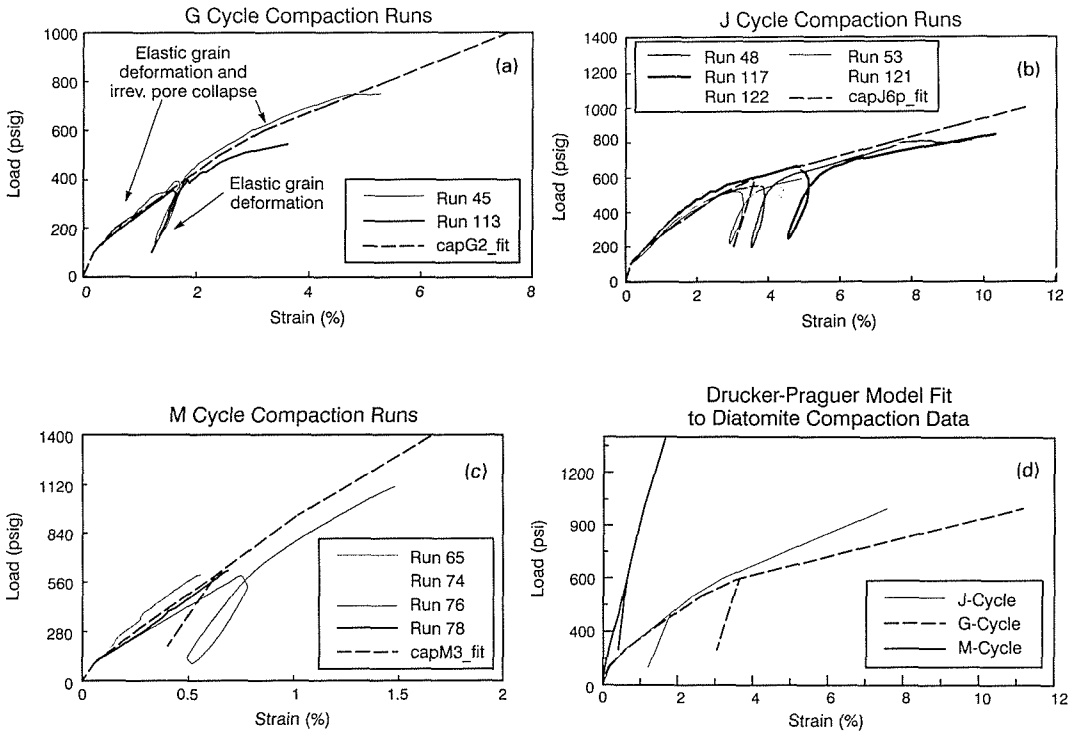


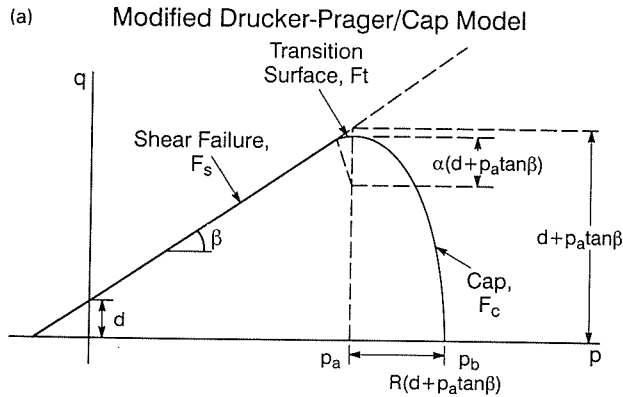
Fig. 4 (a) G cycle compaction runs.
 (b) J cycle compaction runs.
 (c) M cycle compaction runs.
 (d) Drucker-prager model fit to Diatomite compaction data.

represents the fit to those data. Figure 4(b) gives typical values for these parameters. The transition surface F_t (Hibbitt, Karlsson & Sorensen Inc., 1994) is used to smooth the algorithm and has little effect on results.

Notice in Fig. 4(d) that the behaviour of M-cycle rock is substantially "stiffer" than that of shallower layers. This result is consistent with a geologically well-defined (Schwartz, 1988) diagenetic transition from shallow "Opal A" Diatomite to less hydrated, denser and stronger "Opal CT" (or "Porcelanite") Diatomite at greater depth. The elastoplastic deformation just described so far is time independent in the sense that it occurs immediately after depletion or injection (or immediately after application of a load in the experiments) and appears to be the main cause for subsidence and well failure. However, laboratory experiments currently under way indicate that time dependent deformation or "creep" will also be a factor. Based on preliminary results we have allowed for an additional 20% creep-induced vertical displacement in the subsidence calculations discussed below.

Subsidence

An area in the northwest quadrant of Section 33 was selected to calibrate our compaction



(b) Cap Model Parameters for Diatomite
G Cycle, Room Temperature

Poisson's Ratio	ν	0.17
Young's Modulus	E	47700
Angle of Friction	β	36.9
Cohesion	d	200
Transition Surface Radius	α	0.01
Cap eccentricity	R	0.33

Cap Hardening Law

hydrostatic Stress (psi)	Volumetric Plastic Strain
initial cap position → 69	0
200	0.00712
400	0.015
800	0.055
900	0.065

(c) Well Failure Study Strip Layering Scheme

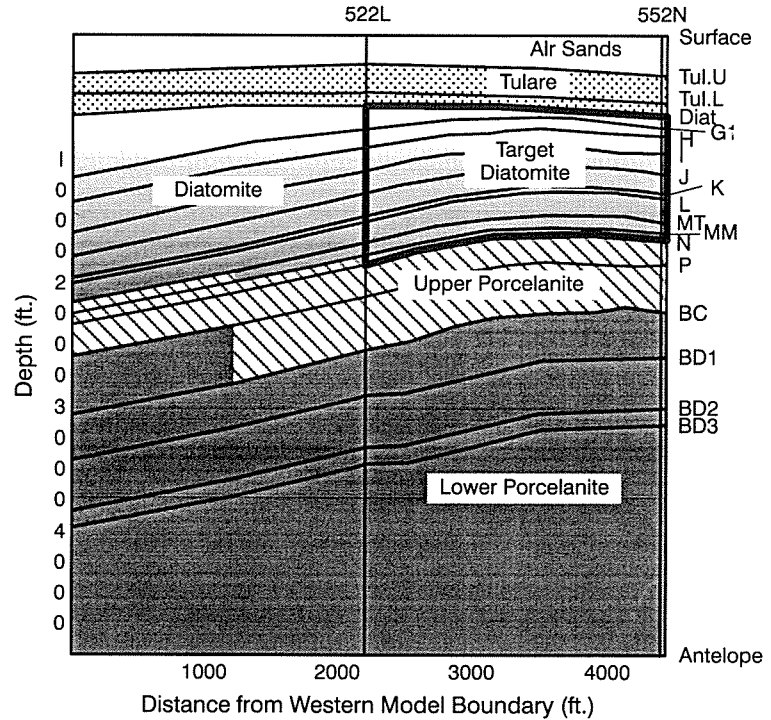


Fig. 5 (a) Modified Drucker-prager/cap model.
(b) Cap model parameters for Diatomite, G cycle, room temperature.
(c) Well failure study strip layering scheme.

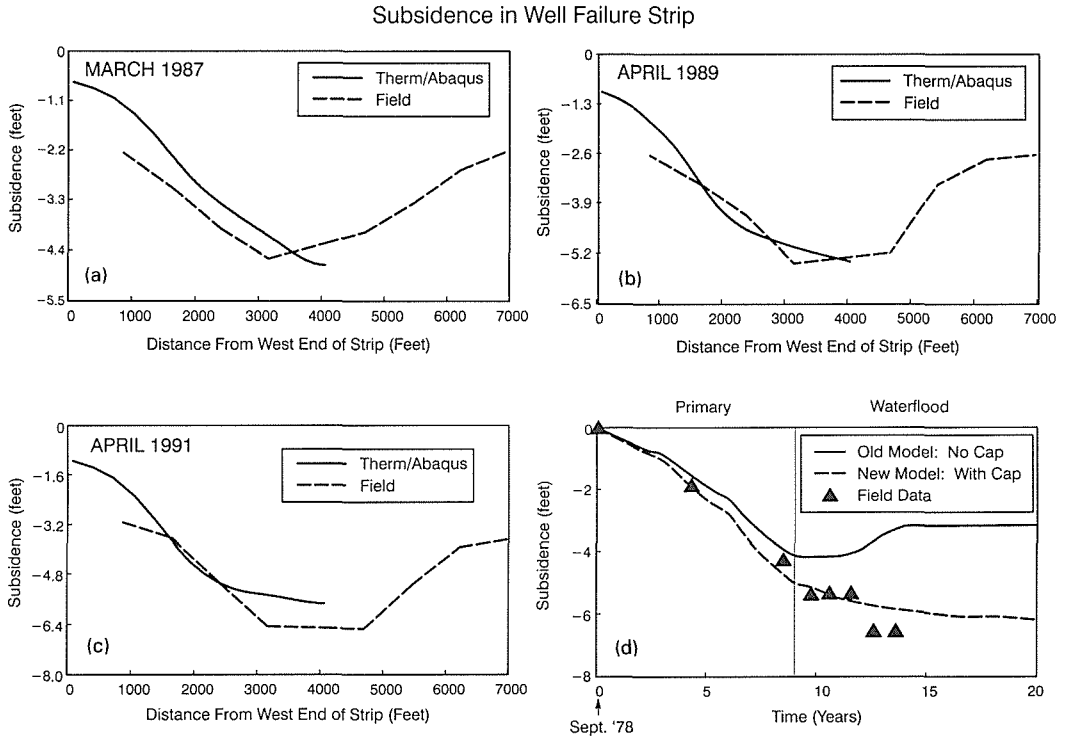


Fig. 6 Subsidence in well failure strip: (a) March 1987, (b) April 1989, (c) April 1991, (d) centre of bowl.

model against field data. This area, shown on Fig. 2(a) and expanded on Fig. 2(b), has been labelled the "black hole area" due to numerous well failures reported over the last five years. This area was under primary production since 1978 followed by a $1\frac{1}{4}$ acre water flood approximately nine years later. This area straddles the boundary between the initial (Phase 1) water flood development and its subsequent extension, labelled Phase 2. It was postulated that the resulting regional imbalance in water injection could be the cause of the high frequency of well failures. A 2D vertical cross section (well failure strip) perpendicular to the Phase 1-Phase 2 boundary was modelled using the finite element code mentioned above to calculate subsidence. The strip extends eastward from well 522L to well 552N and includes 17 wells. The vertical layering of this cross section is shown on Fig. 5(c); measured mechanical properties for all rock types shown were used in the model, including differing layer properties in the Diatomite; this was done by using the matched constitutive laws mentioned above. Details of the model are given elsewhere (De Rouffignac *et al.*, 1995). Surface subsidence as a function of distance along the strip is obtained as shown on Fig. 6(a) for 1987, one year after the end of the Primary phase. Approximately 20% of the predicted subsidence is due to creep. The calculated subsidence bowls for 1989 and 1991, shown on Figs 6(b) and 6(c), compare favourably with field measurements. They show a substantial decrease in subsidence rate after 1987 due to initiation of the water flood. The plot on Fig. 6(d) tracks observed and calculated subsidence at the centre of the bowl as a function of time; it shows that subsidence decreases from 7 in. year⁻¹ during Primary to less than 1

in. year⁻¹ after water flood, and that the new cap model both removes the rebound (not observed in the field) and improves the fit to the data. Applications of this model to different field development scenarios are discussed in a companion Part II paper (Bondor & De Rouffignac, 1995).

SUMMARY AND CONCLUSIONS

The mechanical properties of the Diatomite coupled with its thickness cause substantial compaction to occur. This has resulted in subsidence bowls over 10 ft deep, large fissures near bowl edges and over 3% annual well failure rates. A subsidence and reservoir deformation forecasting tool was developed for primary/water-flood processes in Diatomite based on extensive laboratory data and finite element analysis. An important feature of the model is the inclusion of a "cap" to capture the effect of pore collapse. The model was tested favourably against field measured subsidence from 1978 to 1993 in Section 33 and showed that including pore collapse as a mechanism substantially improves the subsidence forecast.

Acknowledgements Technical assistance in experimental work from Art A. Cherubini and George E. Hill is gratefully acknowledged. The authors also wish to thank the management of Shell Western E&P Inc. and Shell Development Co. for permission to publish this work.

REFERENCES

- Bondor, P. L. & De Rouffignac, E. (1995) Land subsidence and well failure in the Belridge Diatomite Oil Field, Kern County, California. Part II. Applications. In: *Land Subsidence* (ed. by F. Barends *et al.*) (Proc. FISOLS 95 Symp., The Hague, October 1995), this volume. IAHS Publ. no. 234.
- Chen, W. F. & Baladi, G. Y. (1985) *Soil Plasticity, Theory and Implementation*. Developments in Geotechnical Engineering 38, Elsevier.
- Hansen, K. S., Prats, M. & Chan, C. K. (1993) Finite element modelling of depletion-induced reservoir compaction and surface subsidence in the South Belridge Oil Field, California. SPE paper 26074 presented at the Western Regional Meeting held in Alaska, USA, 26-28 May 1993.
- Hibbit, Karlsson & Sorensen Inc. (1994) *ABAQUS Theory Manual*, version 5.3, Pawtucket, RI.
- De Rouffignac, E., Karanikas, J. M., Bondor, P. L. & Hara, S. K. (1995) Subsidence and well failure in the South Belridge Diatomite Field. SPE paper 29626 presented at the 1995 Western Regional Meeting in Bakersfield, California, 8-10 March 1995.
- Schwartz, D. E. (1988) Characterizing the lithology, petrophysical properties and depositional setting of the Belridge Diatomite, South Belridge Field, Kern County, California. In: *Studies of the Geology of the San Joaquin Basin*, Pacific Section SEPM, vol. 60, 281-301.
- Scientific Software-Intercomp (1984) *THERM User's Manual*, Release 2.2. Scientific Software-Intercomp, Denver.

Land subsidence and well failure in the Belridge diatomite oil field, Kern county, California. Part II. Applications

P. L. BONDOR & E. DE ROUFFIGNAC

Shell Development Co., Bellaire Technology Center, PO Box 481, Houston, Texas 77001-0481, USA

Abstract In the Diatomite reservoir, over 10 ft of subsidence and well failure rates averaging over 3% per year have occurred in some areas, resulting in several million dollars per year in well replacement and repair costs. An active effort, including both research and field operations, is underway to develop methods to understand the subsidence process and reduce its economic impact. This paper, labelled Part II, addresses the monitoring efforts and the use of finite element models to understand the effect of operating policy on subsidence and well failure. A companion paper labelled Part I (de Rouffignac & Bondor, 1995) discusses the experimental effort and the development of finite element models of the Diatomite.

UNITS

1 ft (foot) = 30.5 cm

1 in. = 2.54 cm

1 acre = 0.4047 ha

INTRODUCTION

The South Belridge Diatomite field is located approximately 50 miles west of Bakersfield in central California. Details of the formation comprising the reservoir have been described in the companion paper (de Rouffignac & Bondor, 1995). In brief, the reservoir is composed of a very thick, soft rock with a low Young's modulus. This combination results in substantial compaction of the diatomite during fluid depletion; this compaction is believed to be the primary cause of the surface subsidence and well failures observed to date. Aggressive production by an offset operator in the mid-1980s resulted in the development of a bowl with a maximum subsidence of some 20 ft (6.1 m) in its centre; 20% of the operator's wells failed annually over a four-year period, and large surface fissures developed on the edges of the bowl (Bowersox & Shore, 1990).

SUBSIDENCE MEASUREMENTS

An array of 200+ level survey monuments is in place throughout North, Middle and South Belridge fields. Field-wide measurements of subsidence have been carried out (at

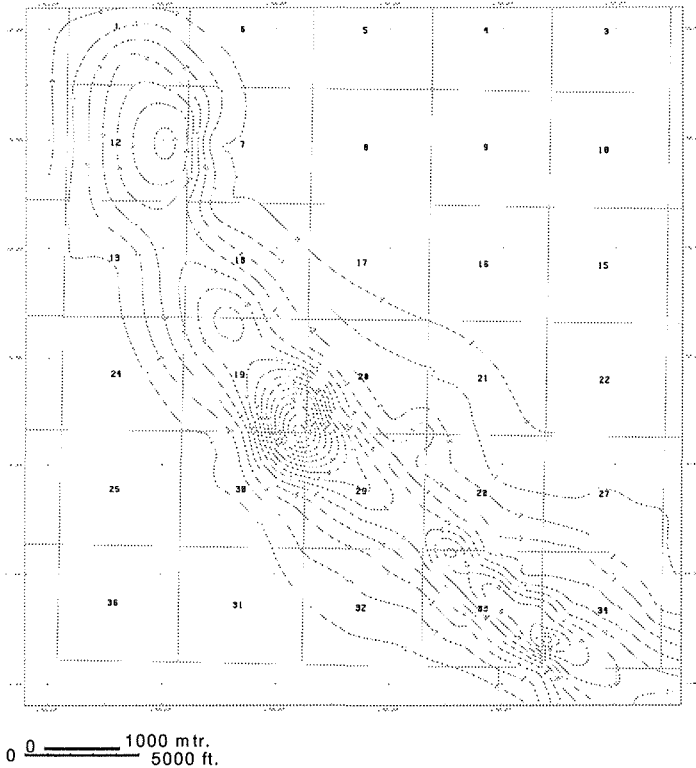


Fig. 1 Cumulative subsidence in the Belridge Field through May 1994 (C.I. = 1 ft = 30.5 cm).

least annually) since 1988. Figure 1 shows cumulative subsidence through the Spring, 1994 survey. Some areas of the field have subsided in excess of 10 ft from the 1942 zero level. Prior to the initiation of waterflooding operations on 1 ¼ acre (0.5 hectare) well spacing in the late 1980s, field subsidence in some areas was in excess of 18 inches (45 cm) per year. The waterflood project has been successful at substantially reducing subsidence; in some areas, annual data even show limited rebound. Figure 2 shows incremental subsidence between April 1993 and May 1994; in general, subsidence has been reduced to some 5 to 10 cm year⁻¹. While the monument surveys have been very valuable in monitoring the large-scale subsidence, the definition provided by the necessarily coarse array, and the limitations of instrument sensitivity, preclude use of the survey data to carry out a detailed examination of the relationship between individual well failures and subsidence.

MODELLING OF FIELD PROJECTS

Subsidence

The South Belridge field is currently developed with a pattern waterflood on 1 ¼ acre spacing, with a producer-to-injector ratio of 1/1. The field operating plan includes the

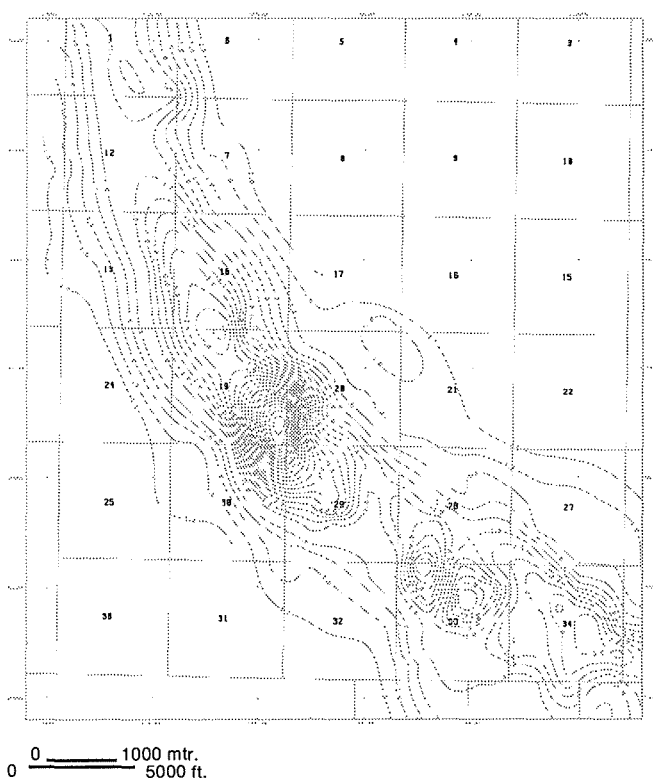


Fig. 2 Differential subsidence in the Belridge Field April 1993-May 1994 (C.I. = 0.5 in. = 1.27 cm).

implementation of infill drilling to 5/8-acre spacing over the next 5 years, reducing anticipated waterflood project life. Oil recovery will be accelerated, and project economics significantly improved, if the development could utilize a 3/1 producer-to-injector ratio rather than the 1/1 ratio currently in place. However, a significant increase in well failure rate, increased surface subsidence, and potentially damaging surface fissures would adversely impact the project economics. The sensitivity of in-situ stresses and compaction/subsidence behaviour to producer/injector ratio was examined using simplified 2-D simulation models. These models, similar to the strip model described in the companion paper (de Rouffignac & Bondor, 1995), use a flat layer-cake grid structure and different process timing. No history match was attempted. The model was run to simulate 20 years of production from the field, including 14 years of history and 6 years of forecast.

The operating policy was modeled as follows: primary production on 2½ acre spacing for 7 years. At 7 years, 1¼ acre infill wells are drilled and put on production, and the original 2½ acre wells are converted to water injection. At 15 years, 5/8 acre infill wells are drilled and put on production for an additional 5 years. Two scenarios are examined. In the first, the old 1¼ acre production wells are converted to injection with only the new wells remaining as producers (resulting in a 1/1 producer/injector ratio). In the second, both the 1¼ acre and 5/8 acre wells are retained as producers,

resulting in a 3/1 producer/injector ratio. Both policies are compared to the continuation of the present 1 ¼ acre project.

The results are shown in Figs 3 and 4. Figure 3 compares the maximum surface subsidence at the end of 20 years of production for the three cases. At 15 years, cumulative surface subsidence is 5.12 ft; after 5 additional years of production under 5/8-acre spacing, the 1/1 producer/injector ratio results in 1.03 ft, and the 3/1 ratio 3.15 ft, of additional subsidence. By comparison, continuation of the 1 ¼ acre flood results in just 0.6 ft of additional subsidence. As one would expect, the effect is most marked immediately after the infill wells are put on production; in the first year, the 3/1 pattern subsides 1.22 ft compared to 0.4 ft for the 1/1 pattern. Figure 4 shows the surface contour over the model at 7 years (installation of 1 ¼ acre waterflood), 15 years (installation of 5/8-acre waterflood) and 20 years, for the three cases considered. Not only the subsidence, but also the surface slope, is steepest for the 3/1 pattern case.

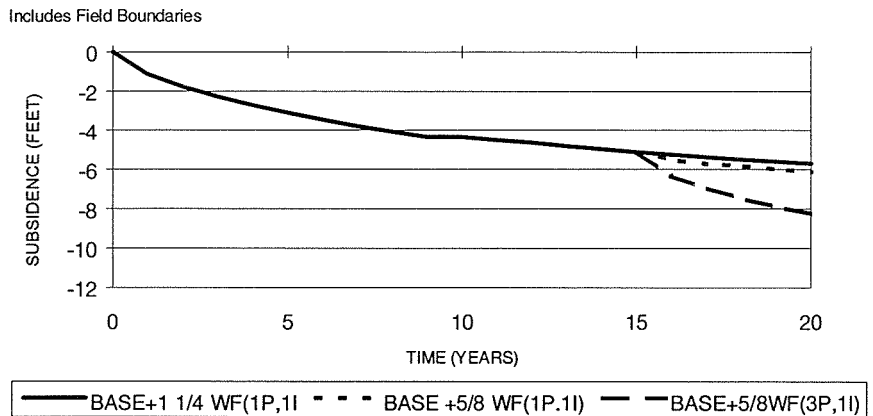


Fig. 3 Subsidence sensitivity to 5/8 acre infill scenario for Section 33.

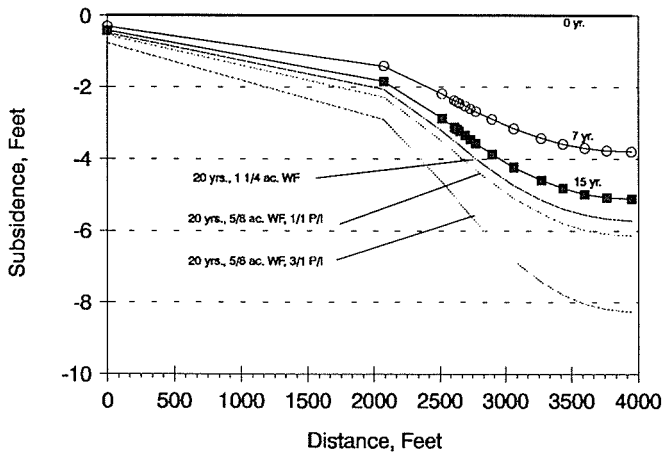


Fig. 4 Subsidence sensitivity: 1 ¼ acre vs. 5/8 acre waterflood infill scenarios.

Well failure

At present, we have no quantitative causal relationship established between surface subsidence and well failure. Qualitatively, however, we anticipate greater well failure rates in areas of high subsidence rate. Also, many observed well failures are doglegs, which suggest a shear mechanism. High shear strains are calculated in situ beneath the areas of highest surface gradient. The models developed can be used to explore the development of strains in the reservoir as a result of operating policies. Shear strain development may be related to doglegs, while vertical strains could lead to buckling failures. Figures 5(a) and (b) depict the shear strain distribution in the two weakest layers (the lower Tulare and the uppermost layer (G) of the Diatomite) for the first two years of the 5/8 acre infill project. There is a substantial increase in shear strain over time in the 3/1, compared to the 1/1, development policy. In addition, the results show increased shear strain differences at different locations in the model, specifically on different sides of a well. Figures 6(a) and (b) depict the vertical strain distribution in the

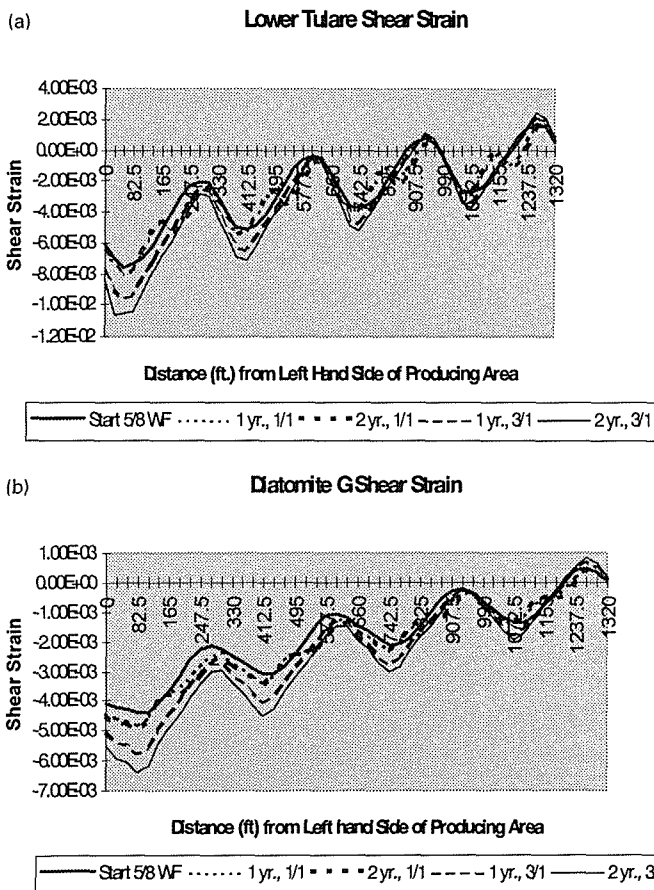


Fig. 5 Shear strain distribution in (a) the lower tulare layer during the first two years of waterflood on 5/8 acre spacing, and (b) the Diatomite G layer during the first two years of waterflood on 5/8 acre spacing.

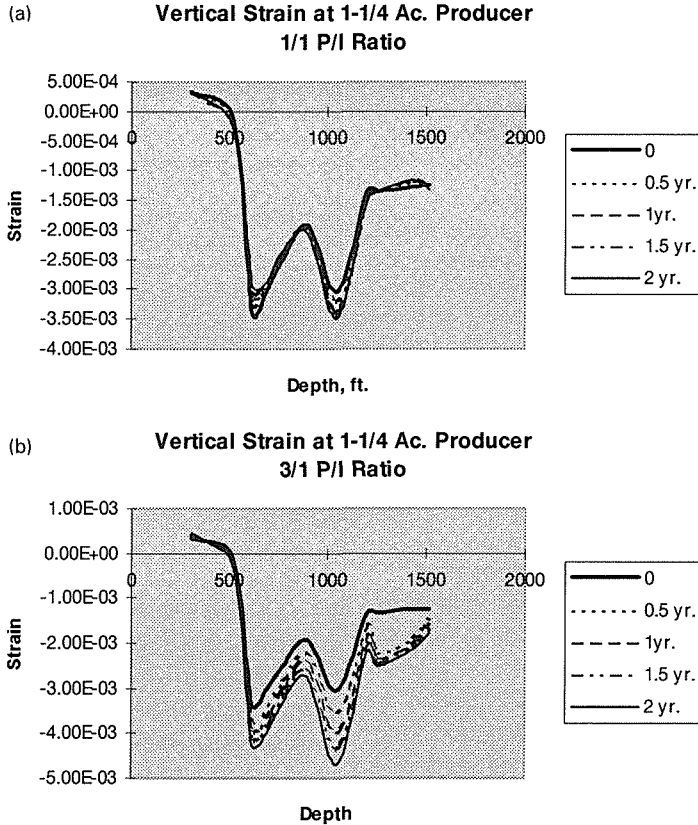


Fig. 6 Vertical strain distribution at location of 1-1/4 acre producer (a) converted to injector for 5/8 waterflood, and (b) retained as producer for 5/8 waterflood.

models. These data also show substantially higher strains in the 3/1 policy than in the 1/1 case. The vertical strains may be used to calculate differential compaction within the formation as a function of time, and thus forecast differential compaction rates under different operating policies.

FIELD MONITORING

Permanent tiltmeter arrays

The implementation of the 5/8 acre waterflood will take place in stages, at roughly 50 acres per year through the end of the decade. In 1994, two 25-acre areas have been converted; in one (in Section 33), the flood will be installed with a 3/1 producer-to-injector ratio; in the other (in Section 34) a 1/1 producer-to-injector ratio will be used. To determine the influence of operating policy on subsidence, arrays of tiltmeters were installed in both areas to provide a more detailed, more frequent monitoring of field subsidence. Figure 7 shows the (approximate) locations of the tiltmeters. In Section 33, twenty tiltmeters were installed in February and March 1994. In Section 34, twelve

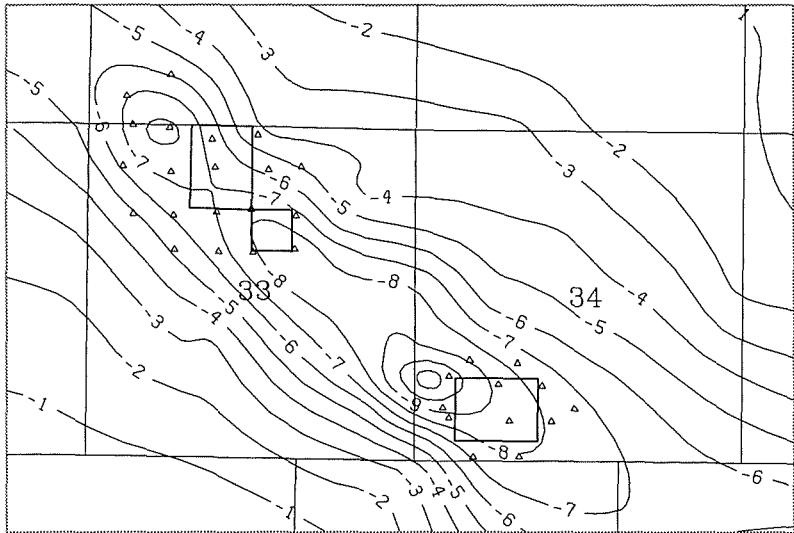


Fig. 7 Location of permanent tiltmeters in Sections 33 and 34 (triangles are tiltmeter locations).

tiltmeters were installed in August 1994. It is intended to use the tiltmeter arrays to monitor the surface subsidence of the two projects over the next two years, and obtain a direct comparison of the behaviour of the 1/1 versus the 3/1 ratios.

Figures 8, 9 and 10 illustrate monthly data obtained by the tiltmeter array in Section 33. In late June through July, the new 5/8 acre infill wells were put on production. The

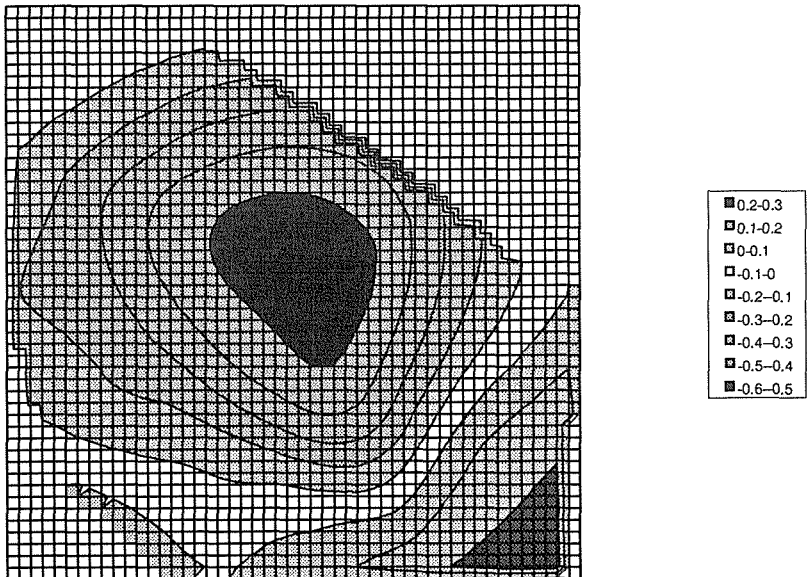


Fig. 8 Surface subsidence contours (units: inches) from Section 33 tiltmeter array, 1-31 July 1994.

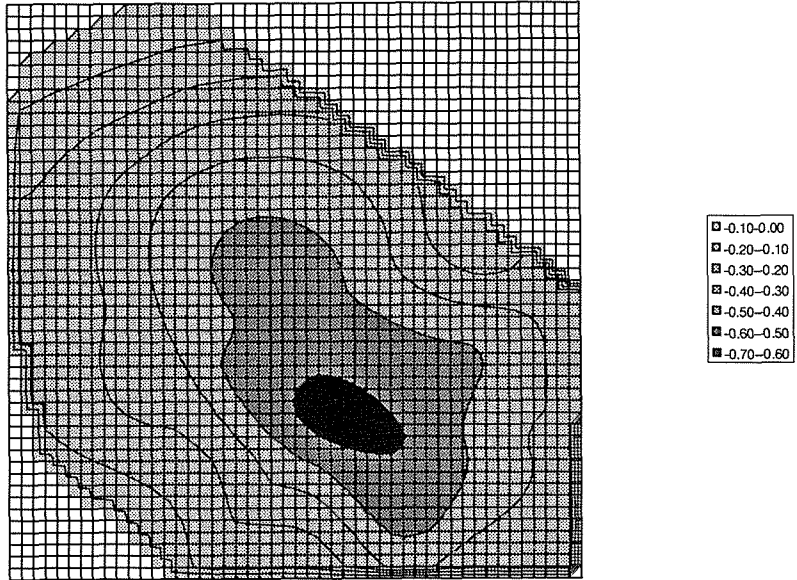


Fig. 9 Surface subsidence contours (units: inches) from Section 33 tiltmeter array, 1-31 August 1994.

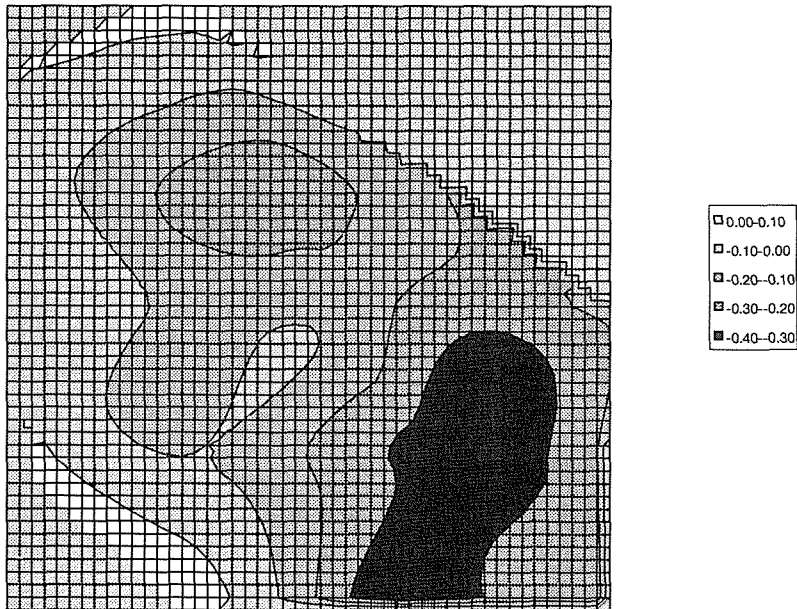


Fig. 10 Surface subsidence contours (units: inches) from Section 33 tiltmeter array, 1-31 December 1994.

flush production resulting appears to be reflected in the subsidence bowl seen in Fig. 8 (July 1995), as wells in the central and northern part of the project come on stream in early to mid-July. The wells in the southern part of the project came on stream in late

July; and the shift in maximum subsidence to the south seen in Fig. 9 (August 1995) reflects their flush production. September's data are very similar to August; by December, flush production from new wells no longer is apparent, and the contours shown in Fig. 10 appear to be more closely aligned with the balance of injection and production occurring in localized areas of the field. The December data, however, seem to confirm that the 3/1 producer-injector ratio is resulting in a higher average subsidence than has been seen in the 1-1/4 acre waterflood.

The tiltmeter array to date has given encouraging results. Twenty tiltmeters have been in place for one year (as of March 1995), with no failures, and have provided reliable data throughout. As the Section 34 project, with a 1/1 producer-injector ratio, comes on stream, it is expected that data from that tiltmeter array will provide similar information to allow comparison between the effect of different operating policies. In addition, results to date (Wright *et al.*, 1995) indicate that the surface subsidence, as measured by the tiltmeter array, can provide information regarding the changing stress state in the reservoir. Such information can be used to predict the direction of hydraulic fractures to be induced in new infill wells, allowing optimum placement of the new well.

Compaction monitoring

As shown above, the model provides data on the compaction of individual geological layers within the reservoir. To verify these data, two observation wells (one in the Section 33 project, one in the Section 34 project) will have 16 radioactive bullets permanently installed at intervals throughout the productive zone; the vertical location of these markers will be surveyed quarterly to detect differential compaction within the reservoir. In addition, the observation wells will have 20 pressure transducers installed at various depths throughout the productive zone, to allow comparison between simulation pressures and field data.

Well damage monitoring

Our understanding of the onset of well damage and failure, and timing of occurrence, is very low. Well damage and failure are discovered only in the course of normal operations (pump changes, etc.) when it is found that equipment cannot be run to (or removed from) operating depths in the well. Whether damage is gradual or episodic is not known. To answer these questions, a regular well survey program will be carried out on 15 selected wells in each of the two projects. Each well will be surveyed a minimum of once a year, and deviations (well deflection, casing diameter and eccentricity, degree of corrosion) will be measured. By comparing survey data with predicted reservoir strain state, it is hoped that model, survey and production/injection data can be integrated to give a clear understanding of the mechanisms operating in the field to cause well failure.

CONCLUSION

Simulation models can be applied to the prediction of both subsidence and well failures. Two-dimensional simulations have been applied to examine the impact of different

operating policies on subsidence, and to generate predictions of in-situ strains caused by those policies. Two field projects using different operating policies have been instrumented to monitor subsidence, compaction and well damage. The installation of long-term tiltmeter arrays has been shown to be a reliable way to obtain detailed subsidence data with precision and resolution far exceeding that possible from level monument surveys. The data from these arrays can be used to study the details of the response of the reservoir and overburden to injection and production.

Acknowledgements The installation and monitoring of the tiltmeter arrays has been carried out by Pinnacle Technologies, Inc., of San Francisco, California. The insight obtained from discussions with Chris Wright and Rob Conant of Pinnacle is gratefully acknowledged.

REFERENCES

- Bowersox, J. R. & Shore, R. A. (1990) Reservoir compaction of the Belridge Diatomite and surface subsidence, South Belridge Field, Kern County, California. In: *Structure, Stratigraphy and Hydrocarbon Occurrences of the San Joaquin Basin, California* (ed. by J. G. Kuesport & S. A. Reid), 225-230. Pacific Section of SEPM and AAPG, Bakersfield, California.
- de Rouffignac, E. & Bondor, P. L. (1995) Land subsidence and well failure in the Belridge Diatomite Oil Field, Kern County, California. Part I. Experiments, model and verification. In: *Land Subsidence* (ed. by F. B. J. Barends, F. J. J. Brouwer & F. H. Schröder) (Proc. Fifth Int. Symp. on Land Subsidence, The Hague, The Netherlands, October 1995), this volume. IAHS Publ. no. 234.
- Wright, C. A., Conant, R. A., Golich, G. M., Bondor, P. L., Murer, A. S. & Dobie, C. A. (1995) Hydraulic fracture orientation and production/injection induced reservoir stress changes in Diatomite waterfloods. *SPE Paper 29625 presented at the 1995 Western Regional Meeting* (Bakersfield, California, March 1995).

Cause of local subsidence in the Sagami-gawa alluvial plain, Kanagawa, Japan

**TAKAHIDE YOKOYAMA, KAZUHIRO ITADERA,
KAZUO NAGASE**

*Hot Springs Research Institute of Kanagawa Prefecture, 586, Iriuda, Odawara 250
Japan*

OKADA HISASHI

*Environment Division, Kanagawa Prefectural Government, 1, Nihon-odori,
Naka-Ku, Yokohama 231, Japan*

Abstract Because of regulated groundwater extraction, severe land subsidence in the Sagami-gawa alluvial plain has almost decreased to a minimum since 1973. The government, however, has had to pay attention to local land subsidence in the upper part of the plain around Atsugi. Average subsidence rates for the 19 year period from 1977 to 1994 ranged from 10 mm year⁻¹ to 18 mm year⁻¹. It was found that an area of the city extending to the back swamps of the Sagami River suffered severe subsidence because of a widely distributed compressive mud layer 2 m to 4 m thick. Compressibility of mud soil classified as follows: low N values below 1, compression indices (C_c) ranging more than 1.0 and natural high water contents (W_n) over 150%. In 1978, 1985, 1990 and 1993, severe land subsidence and low annual precipitations of less than 1500 mm were recorded. Analysing the relations between subsidence and lowering groundwater level by a one-dimensional compression model, it was estimated that the local subsidence was mainly caused by a decrease ranging from 0.5 m to 1.2 m in the groundwater head due to groundwater extraction for reconstructing buildings and was accelerated by low rainfall.

INTRODUCTION

Severe land subsidence occurred throughout the Sagami-gawa alluvial plain until 1973. A 30 mm year⁻¹ subsidence was observed in 1971 at the Ebina monitoring station. This severe subsidence was caused by a drastic increase in groundwater extraction by industries. Open ground cracks occurred along the terrace of Ebina in 1969 (Mikami & Imanaga, 1971) and many rise-ups of well-tops were observed in Hiratsuka city, forcing Kanagawa prefectural government to introduce regulations to check the over-extraction of groundwater. Due to effective regulations and a simultaneous decline of industry, pumping rates over the plain have decreased dramatically. Groundwater heads consequently have recovered 5 m to 20 m since 1971 (Yokoyama, 1982), and since 1973 land subsidence has almost ceased.

In contrast to the general trend of subsidence over the plain, local subsidence has become a severe problem in the centre of Atsugi. Land subsidence more than

50 mm year⁻¹ was observed in 1984, 1990 and 1993 (Kanagawa Prefectural Government, 1995), forcing the local government to pay attention to the problem of severe local land subsidence. This study aims to investigate the causes of local subsidence in the city area (Fig. 1).

HYDROGEOLOGY

Gravel deposits of natural levees were classified along the Sagami River and the muddy deposits of back swamps were distributed on both side of the river (Moriyama, 1972). The centre of Atsugi has extended to the back swamps. An organic mud layer 10 m to 30 m thick is widely distributed over the upper part of Sagami River alluvial plain.

A typical geological log of Atsugi is shown in Fig. 2. The thick mud layer was characterized as a layer of low N values below 10. This mud layer is underlain by one of gravel, which is classified a good aquifer for industrial water. The groundwater level of the study area is shallow. The level of the mud layer is 3 m or less and that of the gravel aquifer is within 5 m or less.

The upper 1 m to 5 m of this mud layer is particularly high in organic materials. The distribution of this high organic layer is clarified in Fig. 3 (Yokoyama, 1985). This mud

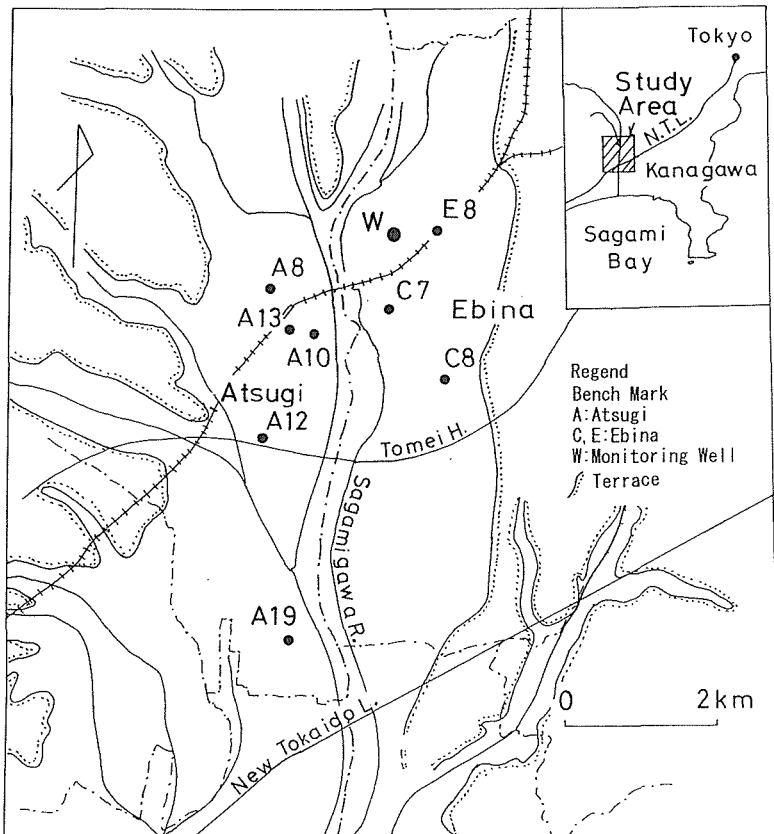


Fig. 1 Location of benchmarks (●) and the Ebina monitoring station (W).

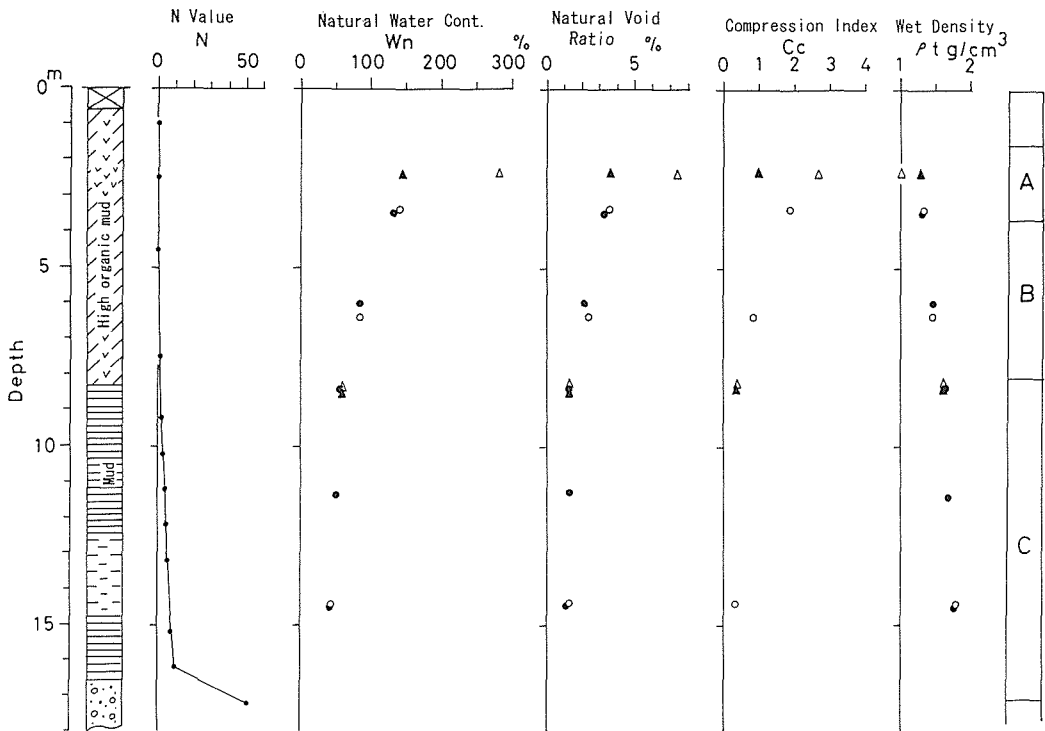


Fig. 2 Typical geological log and characteristics of soil samples in Atsugi.

layer is classified as compressive because compression indices (C_c) range over 1.0 and natural water content (W_n) ranges over 150%. Thick compressive organic layers over 2 m thick are recognized in Atsugi and Ebina. The thickness of the high organic layer in Atsugi ranges from 3 m to 4 m and the one in Ebina ranges from 3 m to 6 m. These qualities indicate that the vulnerability of subsidence is very high in the study area.

DROPS IN THE GROUNDWATER HEAD

Groundwater head data in the Atsugi area were not accurate because they were collected from an industrial pumping well. According to the data of the Ebina monitoring station, indicated by "W" in Fig. 1, due to a lack of rainfall the groundwater head decreased by 0.5 m in 1984 and 0.3 m in 1987 (Fig. 4). As the recent pumping rates of Ebina remain steady, these drops are considered to be a natural lowering caused by rainfalls below 1500 mm year⁻¹. The decrease in years of little rainfall in Atsugi is estimated to be more than 0.5 m. Because groundwater has been occasionally extracted to lower the groundwater head when constructing buildings, it is estimated that the groundwater head in the centre of Atsugi has been lowered by more than 1 m.

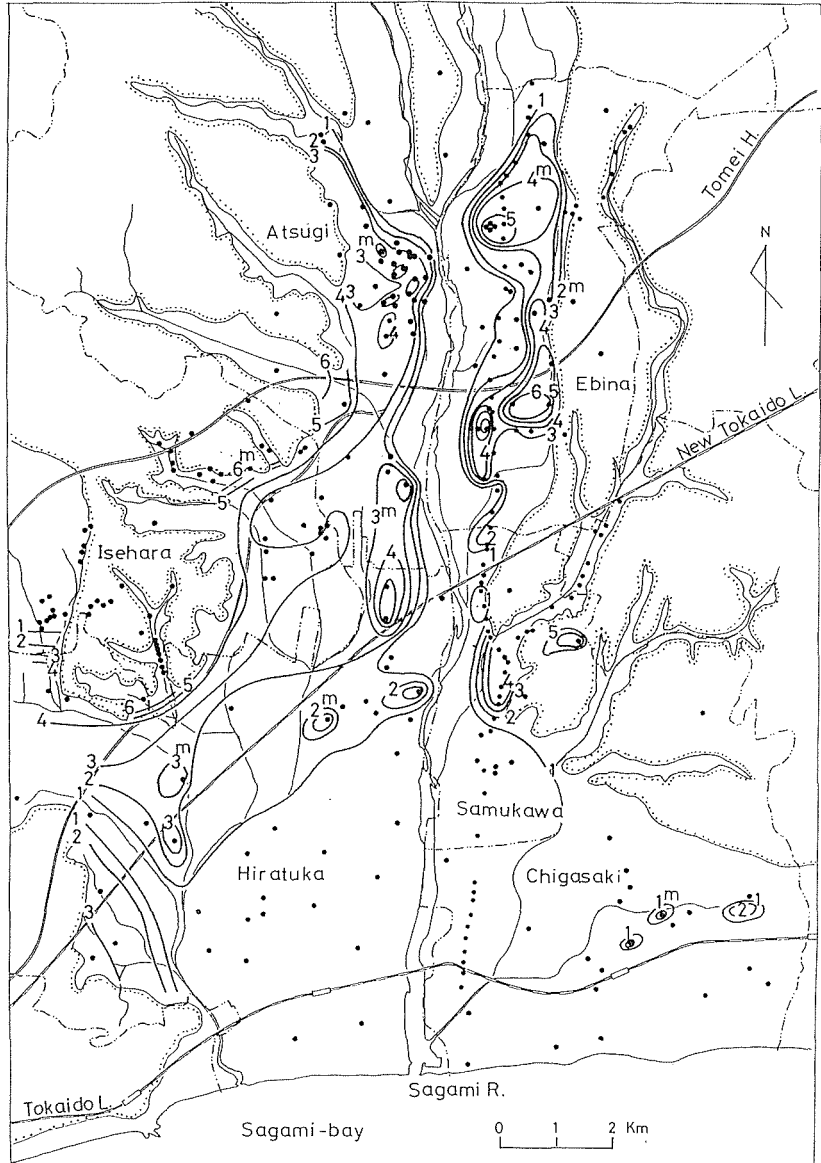


Fig. 3 Distribution of high organic mud soil (thickness: m).

LAND SUBSIDENCE

Severe land subsidence was reported in Atsugi in the latter half of the 1970s. A distribution of the total land subsidence over Atsugi and Ebinai for the 14 year period from 1980 to 1994 are shown in Fig. 5. Areas of land subsidence more than 50 mm widely cover the alluvial plain in Atsugi, but do not extend over that large of an area in Ebinai. An area of large subsidence in Atsugi corresponds to one of thick organic mud

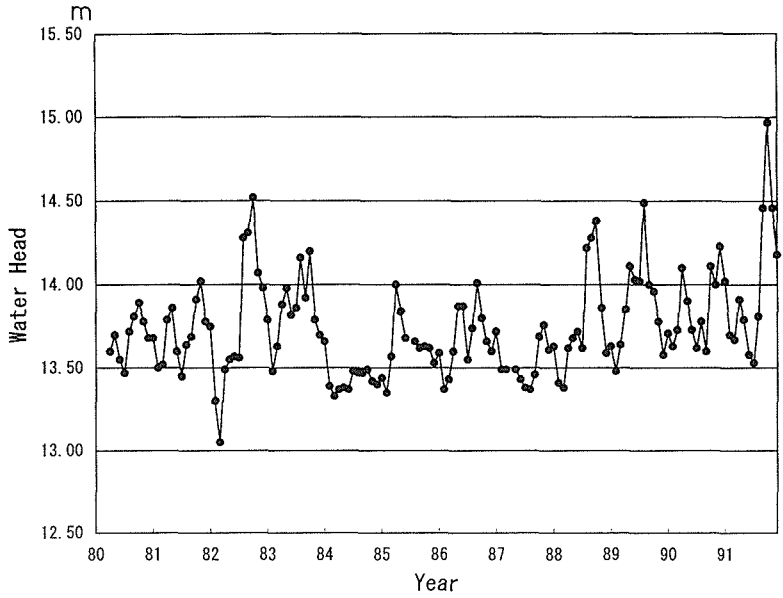


Fig. 4 Groundwater fluctuation at Ebina monitoring station.

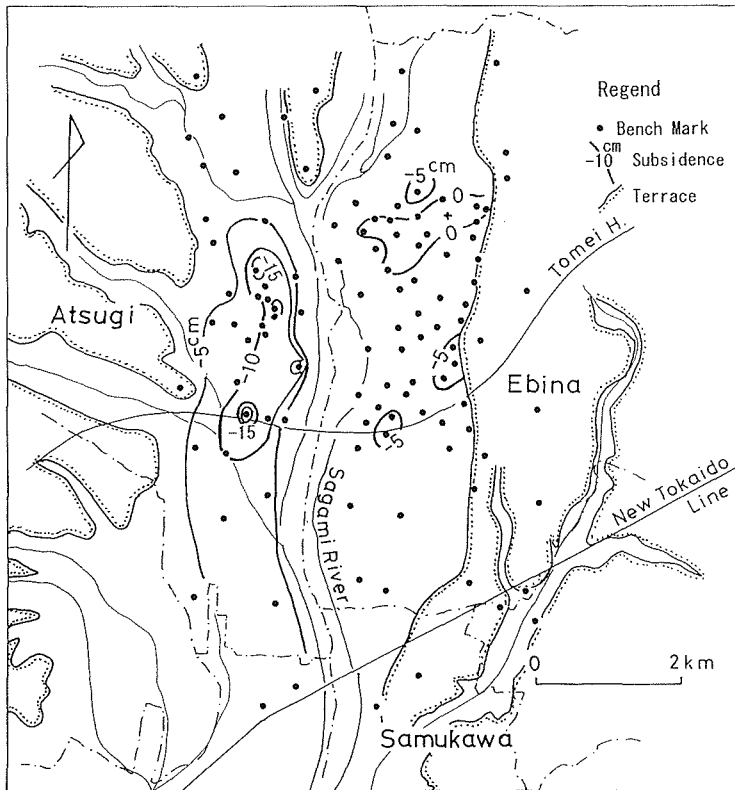


Fig. 5 Distribution of total land subsidence for the 14-year period from 1980 to 1994.

layers shown in Fig. 3. It was estimated that this high organic soil was affected by the lowering of groundwater heads.

Occurrences of severe land subsidence over 200 mm are shown in Fig. 5. Accumulative land subsidence at benchmarks of A8, A12, A13, E8, C7 and C8 for the period from 1975 to 1994 is shown in Fig. 6. The average rates of land subsidence at A8, A12 and A13 in Atsugi range from 10 mm to 18 mm per year. Looking over the accumulative subsidence lines of A8, A12 and A13 in Fig. 6, declining lines steeper than the one in the proceeding year were recognized to be simultaneous concave changes in 1979, 1985 and 1993. A13 alone showed a large drop in 1991.

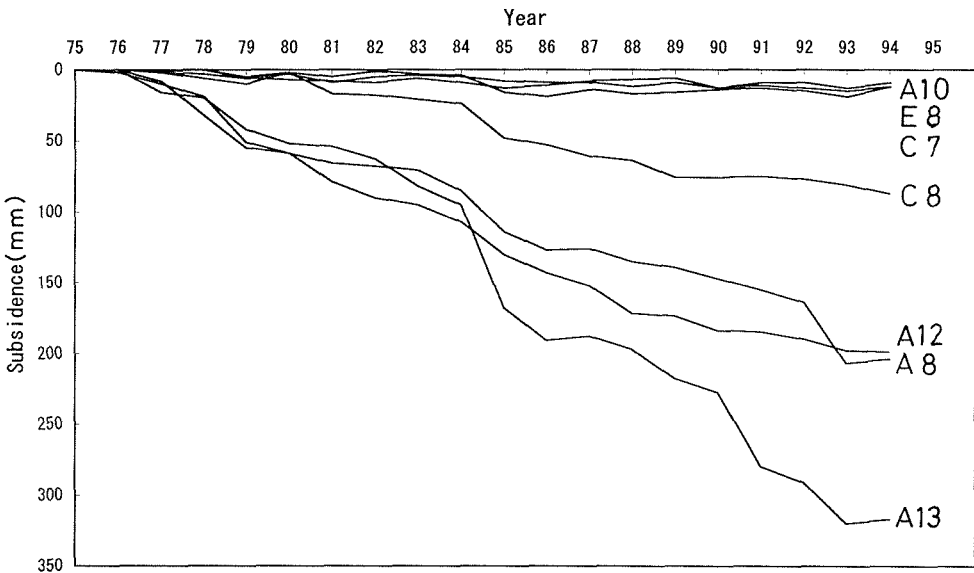


Fig. 6 Accumulative land subsidence observed at each benchmark (locations are shown in Fig. 1).

Comparing annual subsidence rates and annual rainfalls, the large subsidence occurrences classified in 1979, 1985 and 1993 correspond to small annual rainfalls (Fig. 7). In order to understand the natural effect of a reduction in rainfall, correlation between annual subsidence rate at benchmark A19 and annual rainfall at Ebina are shown in Fig. 8 because A19 is located on the thick high organic mud layer and is far from the centre of Atsugi city. It is clearly shown that less than average rainfall affected land subsidence.

CAUSE OF LOCAL SUBSIDENCE

In general, the following three causes of local land subsidence are recognized: an increase in industrial groundwater extraction, groundwater pumping for construction and little rainfall which caused a lowering of the groundwater head in the study area.

Though annual amounts of groundwater extraction in Atsugi slightly increased from 1981 to 1985, no noticeable lowering in the groundwater head was reported to the

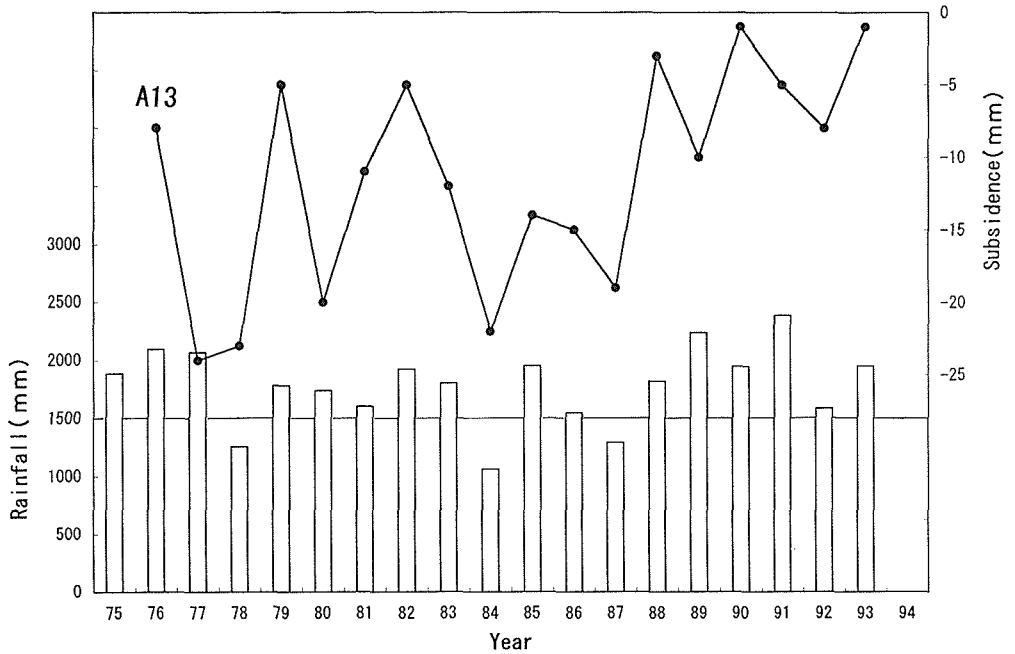


Fig. 7 Comparison of annual land subsidence at A13 and annual rainfall at Ebina.

government by industries. Consequently, increases in industrial groundwater extraction are not considered to be a cause of local land subsidence.

Considering the average rates of land subsidence at Atsugi, groundwater extraction for reconstructing building has been an important factor in lowering the groundwater heads since 1970s, though it is difficult to discern the exact amount of groundwater

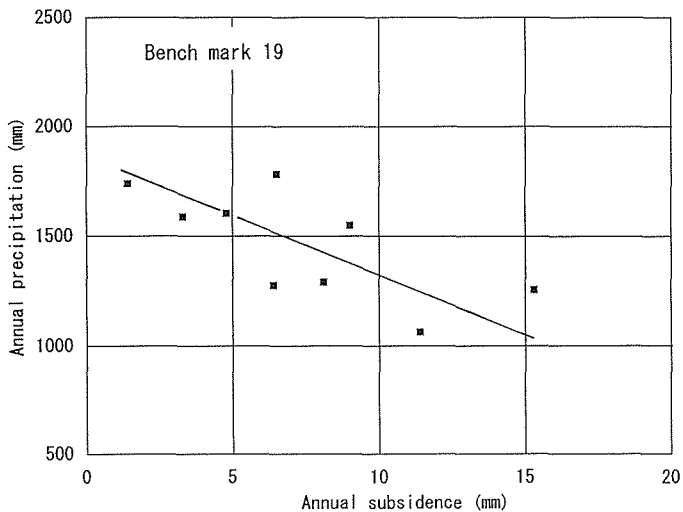


Fig. 8 Correlation between annual subsidence and annual rainfall at bench mark A19. Subsidence data are collected in the years of less than average rainfall.

extraction due to reconstruction. Investigating reconstruction around central Atsugi, remarkable developments were undertaken in the 1980s and 1990s. Because significant land subsidence was recognized around the central part of Atsugi, the main cause should be the lowering of groundwater heads by extraction for reconstruction accelerated by little rainfalls.

COMPACTION OF HIGH ORGANIC MUD SOIL

To investigate the influence of groundwater head lowering on the high organic mud layer, the amounts of land subsidence were simulated by a one-dimensional compaction model which was made from the typical geological log shown in Fig. 3. The simulation method used was Mikasa's method (Mikasa, 1963).

Mikasa generalized the Terzaghi theory on the one-dimensional consolidation of soft clay and obtained a differential equation of heat conduction type derived in terms of compression strain ε . In the case of soft clay consolidation, coefficient of volume compressibility (m_v), permeability (k) and depth of clay layer are variable. Using Takada's one-dimensional consolidation model (Takada, 1985), subsidence of the high organic layer in Atsugi was estimated.

A drop in the groundwater head corresponding to land subsidence was estimated by results of this model. The average coefficients of the soil shown in Fig. 3 were used for calculation. Considering the effect of groundwater lowering, calculations of land subsidence were carried out for two cases. One case assumed groundwater head drops in the A-layer and the other case assumed drops in the aquifer underlying the C-layer. Though compaction in the C-layer shown by open circles is 10 mm or less, subsidence in the A-layer shown by solid circles is calculated to be 200 mm due to a drop of 1.2 m in the groundwater head. According to these results (Fig. 9), it was found that drops in the A-layer have had more effect on subsidence than the ones in the aquifer. In the former assumption, drops in groundwater heads causing annual subsidence rates ranging from 10 mm year⁻¹ to 20 mm year⁻¹ were calculated to be 0.5 m to 1.2 m. These estimates agree with the monitoring data on groundwater heads.

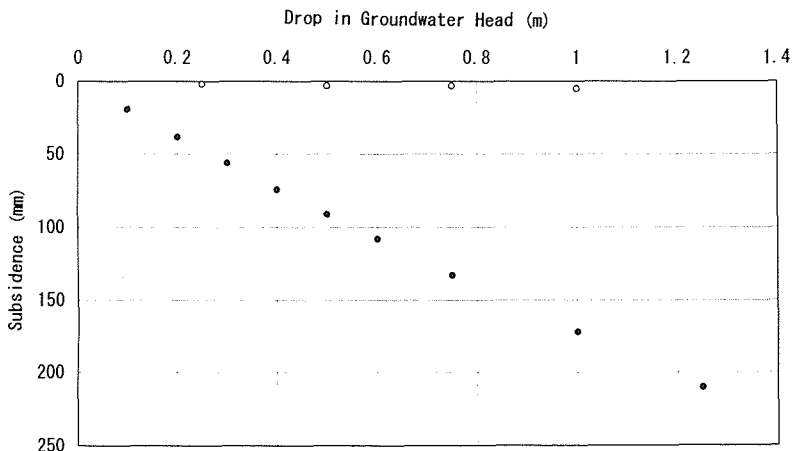


Fig. 9 Results of land subsidence calculation. ●: subsidence of the A-layer, ○: subsidence of the C-layer.

CONCLUSIONS

Compressive high organic mud layers 2 m to 6 m thick are distributed throughout the study area. These layers are caused by severe land subsidence. Land subsidence has high correlation with low rainfall. Rainfall less than 1500 mm year⁻¹ lowered the groundwater head 0.3 to 0.5 m from the average. According to the estimation of drops in groundwater head by a one-dimensional compaction model, land subsidence ranging from 10 mm year⁻¹ to 20 mm year⁻¹ was explained by 1.2 m drops of 0.5 m to 1.2 m in the groundwater head. It is estimated that the cause of local subsidence in the study area is compaction of the high organic mud layer due to about a 1 m drop in the groundwater head.

Acknowledgements The authors are indebted to the staff of the Hot Springs Research Institute for kind advice and to Miss C. Yamamoto and M. Suzuki for providing useful data.

REFERENCES

- Kanagawa Prefectural Government (1994) Report of investigating land subsidence in Kanagawa Prefecture.
- Mikami, K. & Imanaga, I. (1971) Open ground cracks occurred at Oya and its adjacent area, Ebina Town, Kanagawa Prefecture. *Bull. Kanagawa Pref. Mus.* **1**, 54-60.
- Mikasa, M. (1963) The consolidation of soft clay. *Kajima Shuppankai*. Tokyo.
- Moriyama, A. (1972) Micro-landforms of recent alluvial plain. *Mem. Geol. Soc. Jap.*, 197-211.
- Takada, N. (1985) Consideration of consolidation. In: *Simple Soil Mechanics*, 55-77. Japan. Soc. Soil Mech. Found. Engng, Osaka.
- Yokoyama, T. (1982) Basic investigation for the groundwater conservation in the Sagami-gawa alluvial plain. *Joint Research Report of Environment Section of Kanagawa Prefecture no. 5*, 15-24.
- Yokoyama, T. (1985) Distribution of the peat layers in the Sagami alluvial plain. *Bull. Hot Springs Res. Inst.* **16**, 201-208.

Groundwater abstraction-induced land subsidence prediction: Bangkok and Jakarta case studies

RAYMOND N. YONG, EDUARDO TURCOTT

Geotechnical Research Centre, McGill University, Montreal, Québec, Canada H3A 2K6

HARM MAATHUIS

Groundwater Research Division, Saskatchewan Research Council, Saskatoon, Saskatchewan, Canada S7N 2X8

Abstract Studies conducted in Bangkok and Jakarta show the problems of predicting subsidence with a model developed for one region, for application to another region, without proper recognition of the differences in the geologic and hydrogeologic settings. The subsidence model developed for the Quaternary deposit underlying Bangkok accounts for the alternating layers of incompressible aquifers and compressible aquitards, i.e. measured subsidence results from subsidence occurring only in the aquitards. The model has been successful in correlating subsidence predictions with actual observations. Direct application of the Bangkok model to the Jakarta setting is inappropriate, principally because the Quaternary deposits underlying Jakarta are characterized by a complex sequence of marine and non-marine deposits. Individual aquifers and aquitards can be only be traced over very short distances. The Jakarta model considers subsidence as the result of the compression of the total complex substrate.

INTRODUCTION

In the evaluation and prediction of land subsidence resulting directly from abstraction of groundwater via pumping wells, some of the more important factors and pieces of information required include:

- (a) the geologic and hydrogeologic settings;
- (b) the yield, storage and recharge information and conditions associated with the water bearing substrate;
- (c) the various parameters and boundary conditions associated with the abstraction wells.

Analytical/mathematical models can be successfully implemented if the physical situation is properly modelled, i.e. if the model accurately reflects the physical setting and boundary conditions.

This study considers two major coastal cities in southeast Asia (Bangkok and Jakarta) where ground subsidence has occurred as a result of the phenomenon described above. Comparison of data for the two cities show common features concerning urbanization and metropolitan growth, well pumping and usage, distribution and control of well pumping. However the geologic and hydrogeological settings for both cities are

significantly different. Unless this is properly recognized, subsidence prediction models developed from one particular hydrogeologic setting for application to another completely different setting can lead to considerable error. In this study, the model developed for the analysis and prediction of land subsidence based upon the geologic and hydrogeologic settings for Bangkok is discussed in light of the different settings for Jakarta, and the requirements for model refinement or redevelopment are examined as necessary inputs for development of the more appropriate model for the Jakarta setting.

DATA

Bangkok and Jakarta geologic and hydrogeologic settings

The Lower Central Plain (lower Chao Phraya basin), upon which the metropolis of Bangkok is founded, extends about 200 km northward from the Gulf of Thailand. The exact configuration of the basin floor is not well known, but is generally understood to consist of quartzite, gneiss, and granitic gneiss. The fault block tectonics which formed this basin during Tertiary time is apparently filled with clastic sediments from the Tertiary to Quaternary age, with depositional environments considered to be river plain and deltas. Occasional incursions of thin marine clay lenses have been noted in the sediments which show a total thickness ranging from about 400 m in the northern portion to more than 1800 m in the south. The geologic setting portrays a lithology which consists of thick sand-gravel layers separated by less thick clay layers. Hydrogeologists have noted nine individual and distinct aquifers consisting of sand and gravel beds, with strata of clay separating the aquifers as shown in Table 1.

The aquifers are very permeable, and can yield water at the rate of 100 to 300 m³ h⁻¹. The specific capacity of wells in the various aquifers is similar, and is in the range of 15 to 40 m³ h⁻¹ m⁻¹ drawdown, depending on well design and construction. The transmissibility of the upper three aquifers ranges from 1500 to 3600 m² day⁻¹, and the storage coefficient of the aquifers is about 10⁻⁴ for all water bearing formations, with an exceptionally high value of 3 × 10⁻³ for the third aquifer. Lithological correlations based on existing well log data indicate the possibility of interconnection of the aquifers. There is considerable evidence that the clay layers are distributed in a random manner and that while many clay layers are pinched over a considerable lateral distance, the third, fourth and fifth aquifers are interconnected (Metcalf & Eddy, 1977).

The geological and hydrogeological setting of the Jakarta basin consists of a 200 to 300 m thick sequence of Quaternary deposits which overlies Tertiary sediments. The top is considered to be the base of the groundwater basin. Although no formal stratigraphical framework exists, the Quaternary sequence can be subdivided into three major units, in ascending order (after JWRMS, 1994a): a sequence of Pleistocene marine and non-marine sediments, a Late Pleistocene volcanic fan deposit, and Holocene marine and floodplain deposits. The Pleistocene marine and non-marine sediments were deposited in near-shore and deltaic environments. Dispersed between these sediments are deposits of volcanic origin. The unit is mainly composed of silts and clays, with thin interbeds of silty/clayey sands. According to Soefner *et al.* (1986), borehole logs indicate that total thickness of sandy layers constitute only 20 to 25% of the entire thickness of the unit. Individual sandy layers are typically less than 5 m thick, and are composed of fine-

Table 1 Aquifer description (after Metcalf & Eddy Inc., 1977).

Aquifer	Depth to top of aquifer (m)	Total thickness (m)	Description
Bangkok (upper), 30 m	20 to 30	<1 to 30	Fine to coarse sand with gravel. Directly underlies Bangkok in most places. Aquifer missing in some areas or too fine-grained to be a source of supply.
Bangkok (lower), 50 m	30 to 50	<1 to 50	Predominantly fine to coarse sand with gravel and clay layers. In many places directly interconnected with 30 m aquifer.
Phra Pradaeng (100 m zone)	60 to 100	<1 to 70	Fine to coarse white sand with gravel and clay layers. In some places directly interconnected with the 50 m aquifer. Occasionally missing in eastern and western parts of the basin.
Nakhon Luang (150 m zone)	110 to 160	<5 to 70	Fine to coarse sand and gravel interbedded with clay layers which are locally extensive. Individual sand layers up to 30 m thick.
Nonthaburi (200 m zone)	180 to 200	<5 to 60	Fine to coarse sand and gravel layers interbedded with clay and silt.
Sam Khok (250 m zone)	240 to 250	10 to 55	Sand and gravel layers interbedded with clay.
Phaya Thai (350 m zone)	295 to 320	10 to 40	Sand and gravel layers interbedded with clay.
Thon Buri (400 m zone)	350 to 435	50 to 110	Sand and gravel layers interbedded with clay. Aquifer section may contain several distinct water bearing zones.
Pak Nam (550 m zone)	530	30	Variable thick layers of sand and gravel interbedded with clay. Individual sand layers as little as 5 m thick.

grained, silty sands. Because of the depositional environment, the lack of a stratigraphical framework and the often poor quality of the description of sediments by drillers, individual sand and silt/clay layers can only be traced over short distances (e.g. JWRMS, 1994a). The Late Pleistocene volcanic fan deposit was identified as a separate geological unit by JWRMS (1994a). However, its continuity beneath the coastal area of Jakarta remains a matter of speculation. The base of this unit is about 40 m below ground surface. The Holocene sediments are composed of marine silts and clays, overlain by floodplain deposits. Sands are encountered in channel deposits and in beach ridges. The sediments are between 10 and 20 m thick.

The hydrogeological setting proposed by Soekardi (1982) and ILN (1987) consists of a six-layer model for the Quaternary deposits: an upper aquifer (0 to 40 m), an aquifer-aquitard system with the aquifer bounded at the top and bottom by an aquitard (40 to 150 m) and an aquifer-aquitard system (150 to 250 m). Soefner *et al.* (1986), JWRMS (1994b), Maathuis & Yong (1994) consider the Pleistocene sediments underlying the volcanic fan deposits as a single hydrogeological unit. At a regional scale, this unit can be described as a complex, but homogeneous, aquifer-aquitard system, with significant anisotropy. Although there is no physical basis, for practical reasons, Soefner *et al.* (1986), JWRMS (1994b), Maathuis & Yong (1994) subdivide

this hydrogeological unit into aquifer "zones/horizons" similar to those used by Soekardi (1982) and ILN (1987). Despite the fact that individual sand layers cannot be traced, lateral and perhaps vertical continuity must exist as there are no reports of wells going dry. The Late Pleistocene volcanic fan deposits can be considered as an individual aquifer, but its extent and continuity beneath the northern part of the basin remains to be confirmed. The Holocene deposits form an aquitard.

In contrast to the Bangkok area, the transmissivities in the Jakarta area are much smaller. Soefner *et al.* (1987) estimate that the transmissivity of the entire Quaternary sequence ranges from about $250 \text{ m}^2 \text{ day}^{-1}$ in the coastal area of Jakarta to $500 \text{ m}^2 \text{ day}^{-1}$ 20 km from the shore. Based on a numerical model, JWRMS (1994b) suggests that these transmissivities may be up to a factor of two too high. The horizontal hydraulic conductivity of the sands typically is in the order of 1.5 m day^{-1} , and is seldom larger than 10 m day^{-1} . Values for the vertical hydraulic conductivity of clay/silt units are typically about $8.5 \times 10^{-5} \text{ m day}^{-1}$. Review of numerous results of geotechnical tests on core samples from depths less than 70 m indicate an average vertical hydraulic conductivity at reconsolidation pressure of about $1.3 \times 10^{-4} \text{ m day}^{-1}$ (Maathuis & Yong, 1994). No data are available on the vertical hydraulic conductivity of clay/silt layers at depth of more than 70 m. Values for the storativity of sands layers and the elastic storage coefficient of clay layers are also taken from the literature. Aquifer storativity values used for the Jakarta area range from 10^{-3} to 10^{-6} , and those for the elastic storage coefficient of clay layers between 10^{-2} and 10^{-3} m^{-1} .

Subsidence and groundwater abstraction

The report by Cox (1968) provides an early intimation of the problem of subsidence in the Bangkok region resulting from groundwater abstraction. Quantitative assessment of land subsidence however was not conducted until early in 1978. From mid-1978 until 1982, the Royal Thai Survey Department (RTSD) conducted seven runs of first order surface levelling at half-year intervals to monitor benchmarks. These results, together with measurements undertaken by the Asian Institute of Technology at 27 observation stations in 1978 and at four additional stations in 1981 and onward, provide useful information regarding subsidence in the Bangkok area (AIT, 1982). The greatest amount of groundwater abstraction in the Bangkok metropolitan region was found to be about $1.39 \text{ Mm}^3 \text{ day}^{-1}$ in 1982. The amount of abstraction in 1988 was estimated at about $1.2 \text{ Mm}^3 \text{ day}^{-1}$ with about $1 \text{ Mm}^3 \text{ day}^{-1}$ being withdrawn by "private" wells.

The situation is somewhat similar in Jakarta where about 30% of the population of Jakarta is connected to the water supply distribution system, and groundwater is a major source of water supply for domestic, industrial and commercial purposes. Since the early 1900s groundwater has been used as a water supply source, but a dramatic increase in groundwater withdrawals occurred since the early 1970s, as a result of the rapid urbanization and industrialization of the Jakarta area. In turn, the withdrawals resulted in the creation of significant drawdown cones in the hydrogeological unit deeper than 40 m as the hydraulic heads in this zone declined by as much as 40 to 60 m. This changed the basin recharge-discharge pattern in that the coastal region of Jakarta, originally a discharge area, became a recharge area. The large drawdowns raised concerns regarding seawater intrusion and land subsidence. In contrast to reported seawater intrusions extending 10 to 15 km from the shoreline (e.g Soefner *et al.*, 1986;

Tjahjadi, 1991), recent studies suggest that seawater intrusion may only be a minor problem, if occurring at all (JWRMS, 1994c; Maathuis & Yong, 1994). Relative benchmark surveys conducted between 1974/1978 and 1989/1990 indicate subsidence in the order of 50 cm over large areas of northern Jakarta, and locally up to 100 cm. Reliable data on subsidence are currently not available. Relating the subsidence to groundwater withdrawals from depth greater than 40 m is in particular hampered by the lack of geotechnical/hydrogeological data below this depth, and by uncertainties in the distribution of wells and volumes withdrawn. Information on the distribution of and production from wells is only available for the period 1985-1990. Deriving an idea of the spatial distribution of withdrawals is difficult as, for example, for 35% of the registered wells (i.e. non domestic wells) in 1990 no completion data were reported. Furthermore, survey data reported by JWRMS (1994a) suggest that there are more unregistered wells than registered and that volumes withdrawn are higher than the reported data.

Groundwater-abstraction and land subsidence modelling

The two different geologic settings as typified by Bangkok and Jakarta are summarized as follows:

- For Bangkok, one obtains a multiple aquifer-aquitard system which is somewhat well ordered. The aquifers are relatively incompressible, whereas the aquitards are compressible, i.e. can consolidate as a result of depletion of the water content in the aquitards.
- The geologic setting for Jakarta is seen to be comprised of a complex mixture of aquifers with intercalated clay lenses. The water bearing strata cannot be readily demarcated into distinct aquifers, and the assumption that the entire substrate is water bearing requires a judicious evaluation of the various transmissibility-compression coefficients.

The multiple aquifer-aquitard subsidence physical model (i.e. "Bangkok model") shown in Fig. 1 provides the basis for the development of the analytical procedures for the Bangkok setting. The basic idea in the development of the model is similar to that of boundary integral techniques, i.e. one assumes that the characteristics of the hydraulic head are directly related to the abstraction or recharge of the aquifer, and that subsidence occurs principally because of the compressibility (consolidation) of the aquitards. The technique is one of boundary analysis as opposed to domain analysis. The details of the analytical model have been reported previously (Yong *et al.*, 1989) and will not be repeated herein. In testing or applying the Bangkok model, unless one is cognizant of the particular incompressible aquifer-compressible aquitard nature of the problem, there exists the possibility that consolidation-subsidence calculations will be carried over the entire aquifer-aquitard sequences. This leads to considerable error, i.e. a magnified subsidence value is generally obtained. The three-step sequence shown in Fig. 1, in a simplistic sense, includes:

- Withdrawal of water from the aquifer from the pumping well which creates a drawdown cone.
- Drawdown in the aquifer which creates a negative pore pressure gradient in the overlying aquitard (Fig. 2).

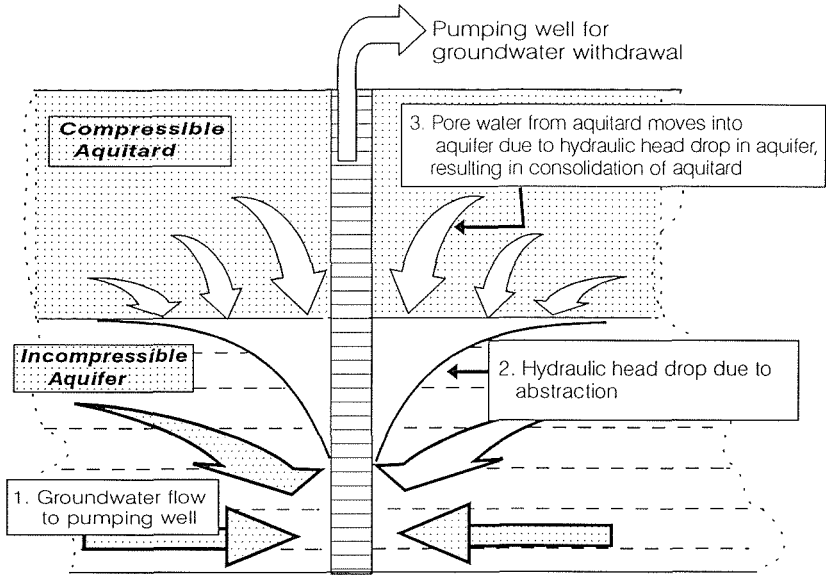


Fig. 1 Schematic drawing showing developed hydraulic heads in aquifer and aquitard.

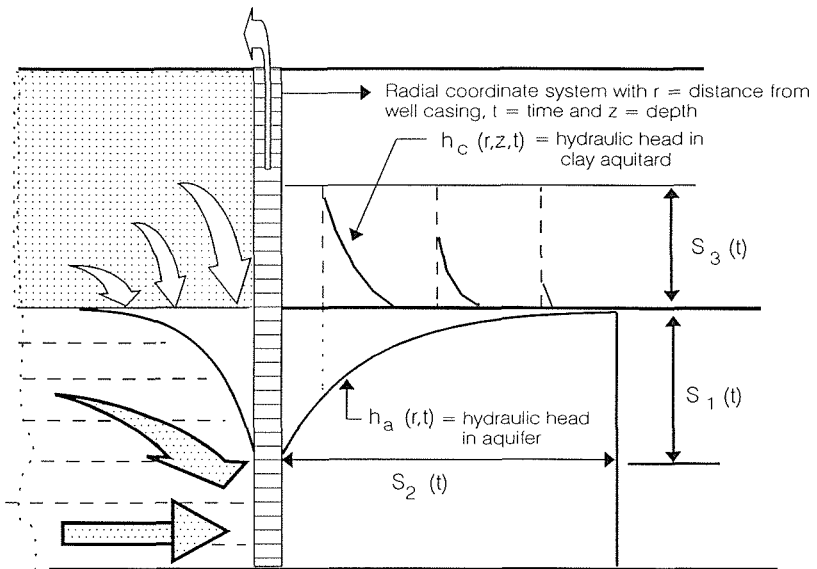


Fig. 2 Characteristics used for modelling "compressible" aquitard and incompressible aquifer.

- Downward movement of pore water in the aquitard into the aquifer in response to the gradient, creating thereby a consolidation effect.

The characteristic pressure heads in the aquifer h_a and aquitard h_c developed as a result of abstraction in the aquifer (Fig. 2) are given as:

$$\begin{aligned}
 h_a(r,t) &= -S_1(t) \left[1 - 2 \frac{r}{S_2(t)} + \frac{r^2}{S_2^2(t)} \right] \\
 h_c(r,z,t) &= -S_1(t) \left[1 - 2 \frac{r}{S_2(t)} + \frac{r^2}{S_2^2(t)} \right] \left[1 - 2 \frac{z}{S_3(t)} + \frac{z^2}{S_3^2(t)} \right]
 \end{aligned} \quad (1)$$

and can be established by determining the appropriate $S_n(t)$ conditions that would satisfy the initial and boundary conditions. Note that for $r \geq S_2(t)$, h_a becomes zero. Similarly, for $z > S_3(t)$, h_c becomes zero. The solution of these relationships and method of application have been given by Yong *et al.* (1989).

The underlying geology and hydrogeological setting for Jakarta differs markedly from that of Bangkok. Since there are no clear demarcations separating aquifers from aquitards, the multiple aquifer-aquitard Bangkok model is not appropriate. Considering the Jakarta underlying substrate to be entirely water bearing, the principal assumptions invoked for development of the governing relationships and solution for the Jakarta geological and hydrogeological settings (identified as the Jakarta model) include:

- flow in the water bearing substrate obeys Darcy's law;
- the confined water bearing substrate is visco-elastic, "homogeneous" and of approximate constant thickness;
- the storativity S is constant;
- the amount of water derived from storage due to an increment of drawdown Δs during an interval of time from τ to $\tau + \Delta\tau$ consists of two parts; namely a volume of water instantaneously released from storage and a delayed yield from storage at any time $t > \tau$ from the onset of pumping;
- a constant rate pumped from the fully penetrating wells.

The governing relationships are developed in accord with visco-elastic theory and are shown in a polar coordinate format for a multiple-well pumping case as:

$$\frac{\partial^2 s}{\partial r^2} + \frac{1}{r} \frac{\partial s}{\partial r} - \frac{W}{T} f(r) = \frac{S^*}{T} \frac{\partial s}{\partial t} + \frac{\gamma w}{\eta k} \frac{\partial}{\partial t} \int_0^t s(\tau) \exp\left[-\frac{(t-\tau)}{\alpha_2 \eta}\right] d\tau \quad (2)$$

where the output of the groundwater from the aquifer per unit area with a circular well field is given as $W = \Sigma Q/A$, (Q = flow rate, A = area) and where s = drawdown, r = radial coordinate, R = radius of the circular well field, $S^* = M\gamma_w(\mu\beta + \alpha_1)$, η = apparent viscosity of the "visco-elastic" material representation of the water bearing layer, α_1 and α_2 are the parameters that represent primary and secondary consolidation of the layer, k is the coefficient of permeability, and $f(r) = 1$ for $0 < r < R$, and $f(r) = 0$ for $r > R$.

The solution to equation (2) for the standard boundary conditions of zero drawdown at time equals zero and at infinite distance from the drawdown source, and drawdown gradients of zero t infinite r and $r = 0$, combines the Laplace transform, the convolution theorem and the Hankel transform to give the following:

$$s = -\frac{WR}{T} \int_0^\infty \frac{J_0(\xi R) J_1(\xi r)}{\xi^2 + L/2t} d\xi \quad (3)$$

Equation (3) is not analytically integrable, but can be solved numerically (Yong *et al.*, 1994).

DISCUSSION AND CONCLUDING REMARKS

This simplistic aquifer-aquitard Bangkok model has been tested using input obtained through physical testing of the consolidation-compression of representative cores from the aquifers and aquitards. Reasonable correlations between "predicted" and measured subsidence have been obtained over a period of years as shown by Yong *et al.* (1991). Application of the Bangkok subsidence prediction model to the Jakarta setting is difficult, not only because of its more complex hydrogeological setting, but also because of the lack of reliable geotechnical data for depths greater than 40 m, uncertainty in both the distribution and amounts of withdrawals, and absence of reliable subsidence measurements. To test the capability of the Jakarta model, field results from Bangkok were used. The predictions obtained by the Jakarta model have been reported in Yong *et al.* (1994). They are seen to be less well correlated with the field data – in comparison to those obtained by the Bangkok model. This is not surprising since the Bangkok model deals with the resulting consolidation of the aquitard in relation to the hydraulic head drop in the aquifer – as opposed to the Jakarta model which considers the basic setting as an "average" compressible layer with water bearing characteristics. Comparison with measurements obtained from the well withdrawal studies are presently underway and will be reported at a later time.

Acknowledgements The financial support for the study was provided by the International Development Research Centre (IDRC) of Canada. The authors are indebted to (a) Dr Aung Gyi of IDRC for his invaluable support and guidance, and (b) the research partners in both Bangkok and Jakarta for their input and assistance in the course of the studies.

REFERENCES

- Asian Institute of Technology (AIT) (1982) Groundwater resources in Bangkok area: development and management study. *Comprehensive Report 1978-1982*, submitted to the Office of the National Environment Board.
- Cox, J. B. (1968) A review of engineering properties of the recent marine clays in Southeast Asia. *Research Report no. 6*, Asian Institute of Technology, Bangkok.
- ILN (Indec & Associates Ltd, Lavalin International Inc. & Nippon Koei Co. Ltd, Ministry of Public Works, Directorate General of Water Resources Development, Indonesia) (1987) Cisadane River basin feasibility study. *Groundwater 3*.
- JWRMS (1994a) Jabotabek Water Resources Management Study. *Final Report*, vol. 6, annex 10: *Groundwater Resources*. Ministry of Public Works, Directorate of Water Resources Development, Indonesia.
- JWRMS (1994b) Jabotabek Water Resources Management Study. *Final Report*, vol. 6, annex 11: *Groundwater Models*. Ministry of Public Works, Directorate of Water Resources Management, Indonesia.
- JWRMS (1994c) Jabotabek Water Resources Management Study. *Final Report*, vol. 7, annex 12: *Groundwater Salinity*. Ministry of Public Works, Directorate of Water Resources Development, Indonesia.
- Maathuis, H. & Yong, R. N. (1994) Development of groundwater management strategies in the coastal region of Jakarta, Indonesia. *Year II Report (1993)*. Saskatchewan Research Council, Saskatoon, Canada.
- Metcalf & Eddy Inc. (1977) Report on groundwater monitoring, well construction and future programs for MWWA. *Report for Metropolitan Water Works Authority, Bangkok*.
- Soefner, B., Hobler, M. & Schmidt, G. (1986) Jakarta groundwater study. *Final report. Federal Institute of Geosciences and Natural Resources, Hannover & Directorate of Environmental Geology, Bandung*.
- Soekardi, R. (1982) Aspek geologi terhadap perkembangan pantai dan tata airtanah daerah Jakarta. Sarjana-Thesis, Universitas Padjadjaran, Bandung.
- Tjahjadi, B. (1991) *The Impact of Abstraction on Groundwater Quality and Monitoring in the Jakarta Region, Indonesia*. Directorate of Environmental Geology, Bandung.

- Yong, R. N., Xu, D. M. & Mohamed, A. M. O. (1989) Groundwater resource management model; Final report. *Report for International Development Research Centre, Canada.*
- Yong, R. N., Nutalaya, P., Mohamed, A. M. O. & Xu, D. M. (1991) Land subsidence and flooding in Bangkok. In: *Land Subsidence* (ed. by A. I. Johnson) (Proc. Fourth Int. Symp. on Land Subsidence, Houston, May 1991), 407-416. IAHS Publ. no. 200.
- Yong, R. N., Turcott, E. & Gu, D. (1994) Artificial recharge subsidence control, Bangkok, Thailand. *Report for International Development Research Centre, Canada.*

Strategies to assess the hazards presented by abandoned room and pillar mines

DAVID G. PRICE

199 Orchard Way, Wymondham, Norfolk NR18 0NZ, UK

Abstract Abandoned mines present problems of surface instability which form a major handicap to the development of areas underlain by them. In theory the stability of pillars and roofs of the mine openings can be calculated providing the parameters describing rock mass strength and structure are available. In practice, flooding and collapse make it impossible to obtain the data necessary for analysis and even if access is possible certain necessary information is almost always unobtainable. In consequence reliance is mostly placed on "rule of thumb" experience. The author argues for the institution of an internationally organized experience database which might lead to the quantification of hazard via a form of rock mass classification.

THE PROBLEM

Early mines were mostly located outside the towns in which the miners lived. The mining methods used in such mining were often variants of room and pillar techniques and left openings abandoned on withdrawal from the mine. Subsequently town limits expanded over these mines which, in time, collapsed. The time between abandonment and collapse may be of the order of hundreds of years so that generations of structures may function in apparent safety before collapse occurs.

Instability of the mine roof brings about local collapses of limited extent by migration of the mining void to surface, while if one pillar collapses this may, by a domino effect, cause other pillars to fail and result in a more widespread subsidence (Fig. 1). If support platforms to partially infilled shafts fail surface soil may flow into the shaft. The stability of any mine opening depends on the location of the water table and the degree of saturation of overlying strata; groundwater movements and rainfall contribute significantly to mine stability.

THEORY

To determine the stability of an abandoned mine it is necessary to calculate the stability of the mine roofs between pillars and of the pillars themselves. It seems to be generally accepted that the strength of the mine roof depends, in the most simple case, on the thickness of the roof beam of rock, the elasticity of the rock and the tensile strength of the beam rock. Equations presented by Obert & Duvall (1967) are given in Fig. 2 to illustrate the data required to solve these equations. Stability of the roof also depends upon the horizontal stresses acting.

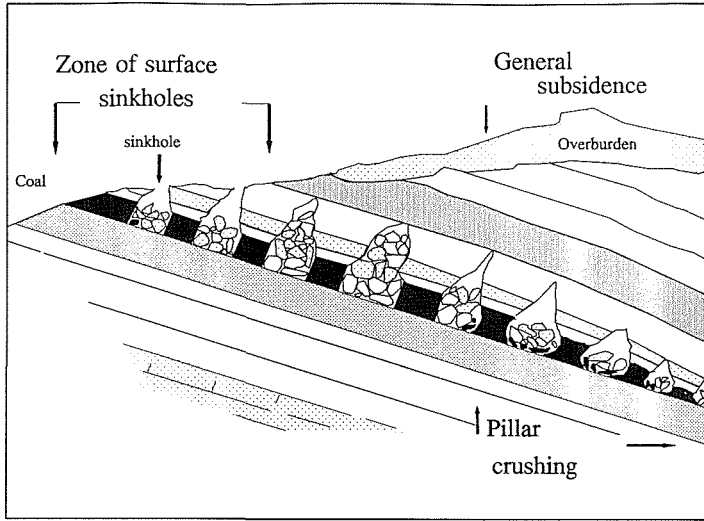


Fig. 1 Subsidence resulting from the collapse of old room and pillar mines.

Many different formulae exist to calculate pillar strength; most are of the form indicated in Fig. 2 and include pillar dimensions and rock strength as their measurable parameters. While the stresses that may bring about roof failure are, in theory, due to the self weight of the roof beam, those that bring about pillar crushing come from the weight of the strata supported by the pillar. Stresses on the pillar may be conveniently, but only approximately, calculated by the tributary area method, assuming that the distribution of the strata above and the unit weights of the various strata types are known.

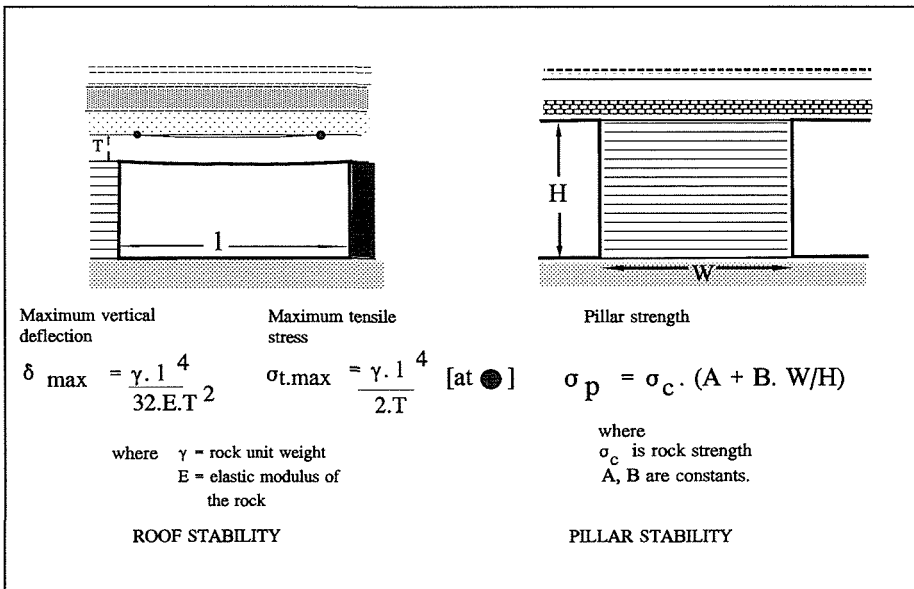


Fig. 2 Typical formulae to assess roof stability and pillar strength.

Most modern pillar strength formulae have been devised to aid design of mine pillars to give the most profitable extraction. Any uncertainties regarding strata load and pillar strength may be accommodated by increased safety factors and thence modified by experience. In the same way gallery span may be calculated and modified by experience as mining progresses, so that eventually a uniform logical mine design is achieved. In the case of the long abandoned ancient mine, mine design, if ever undertaken, was based on experience alone. Mining may have been intermittent so that the mine layout was not uniform.

The roof

Roof collapse leads to upward void migration (Fig. 1) to some limiting height determined by rock mass characteristics. The main characteristics are the thicknesses of beds which will serve as beams (Fig. 2), their strength and, not shown in Fig. 2, the frequency, orientation and strength of any joints traversing the beds. It may be assumed that the miners had, by experience, determined the span dimensions for a reasonably safe tunnel for their particular conditions. This span may have been increased by pillar robbing on withdrawal from the mine but later roof collapse has been caused by agencies acting through time to weaken the roof beam. Once the initial failure has taken place this may be repeated with successive beams until either a stratum of high mass strength is encountered or the fallen material, occupying a greater volume fallen than in situ, bulks sufficiently to support the roof. It is essential for surface construction to estimate how far the mining void may rise above the workings. This will depend upon mine height and span, local rock mass characteristics and the bulking properties of the roof rock. It is generally considered that migration up to 3 to 5 times the height of the mining void is usual (Bell, 1988) but may extend far above this in particular circumstances.

In bedded and jointed relatively strong rocks it is usually assumed that roof collapse is mostly related to the properties of the roof rock mass. However, Bekendam & Price (1993), observing the collapse of mines in the more-or-less unjointed calcarenites of the Maastrichtian of The Netherlands, noted that roof collapse was sometimes associated with the stress cracks, developed in the pillars, passing upwards into the roof beam.

Pillars

At the time of abandonment the mine pillars are sufficiently strong to support the load of the overburden, but may thence then deteriorate and weaken until they fail. Bekendam & Price (1993) in their specific study, attributed decay in calcarenite pillars to creep; other authors reviewing the topic, such as Bell (1988), recognize that pillar strength deterioration may have many causes.

The factor of safety of a system of pillars in a mine will depend upon the contrast between strength of the pillars and the stresses upon them, which must be calculated to make this comparison. Most pillar design formulae assume rectangular pillars; many very old mines show pillars of very irregular form, to which the mine design formulae have limited applicability. A formula for irregular pillars has been produced by Bekendam & Price (1993) but this may not be appropriate for jointed rocks. In the West Midlands of England it has been observed (Anon, 1983) that mining voids in the Upper

Wenlock Limestone may migrate upward into the overlying weaker Ludlow Shales, which then form the pillars which, being weaker, may crush under the overburden load.

LIMITATIONS

Abandoned mines, particularly coal mines, are often flooded and cannot be entered. Roof collapse, or a general collapse due to pillar crushing, may also prohibit entry to every part of the mine. As a consequence of this it is commonly not possible to obtain data on mine dimensions, which are essential parameters to both roof and pillar stability formulae. In some cases it may be possible to assess horizontal dimensions from old mine plans, but these, if they exist, are seldom sufficiently accurate for stability calculations, and very seldom include any indications of pillar height. They usually also lack indications of the depth of the workings below surface and the inclination of the mine floor.

For certain mines, particularly coal mines, geological studies aided by boreholes may establish the depth and orientation of the seam within which the mine is to be found, but for other mines, such as those in chalk, the mined horizon is not easily distinguished and, in any case, the mine may not be confined to a single stratigraphic layer. In the latter case it is exceedingly difficult to determine the location of the mine by any means other than directly encountering it via a shaft, pit or borehole. It is not often possible to enter a mine to produce a detailed plan showing all the dimensions necessary for calculation. It is equally difficult to obtain the geological data required, particularly regarding roof conditions. Most investigations are undertaken in mines, already in a distressed condition, to assess their collapse potential; extracting rock samples for testing from sagging mine roofs and deteriorating mine pillars is not a pastime to be recommended to the reader.

Thus, while the theory to determine stability is, to a certain degree, available, the necessary data is seldom present.

STRATEGY

While research into mining and rock mass mechanics must continue to find ways to calculate the stability of abandoned room and pillar mines, much is to be gained from the assembly and analysis of experience. Subsidence from the collapse of old mines and their associated shafts threatens the property and the life of the citizen, who has at least the moral, if not the legal, right to be informed of these hazards. Accordingly the citizen dwelling in areas affected by this problem must be made aware that it exists, where it is to be found and the hazards it poses. To do this catalogues of mine locations and explanations of the hazards they present, written for the non-specialist, should be published.

The development of awareness

The first stage in developing a strategy to deal with the problems presented by abandoned mines is to define and describe these problems in the particular areas in

which they are found. Such a description (Anon, 1993) has been produced with regard to the subsidence problems faced by the city of Norwich in Norfolk, Great Britain.

Norwich, a city of some 125 000 inhabitants, lies in the valley of the River Wensum. Upper Cretaceous chalk is exposed in the lower valley sides which are capped by Pleistocene and younger deposits. Open pit and underground mines have won chalk and flint, the former being used as source for lime and the latter as construction stone. Mining may have begun as long ago as the Neolithic and was certainly well established in the thirteenth century. The last mine closed in 1945. The mine galleries were of the order of 2 to 3 m wide and typically 2 to 2.5 m high, although more recent workings range up to 6 m high. In profile some are horseshoe shaped and others have a flat roof connecting at a sharp angle to vertical or steeply outwardly inclined side walls. Such plans of the workings as exist indicate that the galleries were excavated parallel to the shallow dip and strike of the beds, giving right-angled intersections which occasionally formed pillars although it appears that no regular room and pillar mining system was developed. The chalk/overburden surface is marked by infilled solution pipes which may have been encountered in the workings. The mines contain some inscriptions suggesting their age and there are many descriptions of the tunnels in the literature, such as those by Woodward (1831) and Atkins (1983). These descriptions are of historical interest but contain little information regarding the mining methods used and the reasons for the selection of mine locations.

There have been numerous subsidences, mostly as the result of void migration following roof collapse, causing building damage and, in one case, two fatalities. Norwich has, of course, other examples of subsidence damage resulting from other causes and the report "Subsidence in Norwich" deals with these as well as those resulting from past mining. While the most severe subsidence events are associated with past mining, the number of these events is relatively small in comparison with those connected with other causes such as leaking pipes, sewer collapse and solution features in the Chalk. The report is intended to make developers, planners and the general public aware of the subsidence problems in Norwich so that future works may be undertaken with proper regard to such potential hazards.

The description and correlation of experience

National mining agencies usually have a duty to inspect accessible mines and they, and local authorities, have the duty to describe and catalogue subsidence events. To gain from the experience of others it is necessary to establish the basic parameters which are necessary to describe the situation, with the hope of perhaps being able eventually to devise techniques of stability analysis similar to those incorporated in the rock mass classifications developed for tunnel design (Bieniawski, 1989). The rock mass classification approach has been used in one case, that of the calcarenite mines in South Limburg, The Netherlands, where "stand-up times" to collapse calculated using a rock mass classification system showed a quite good correlation with the recorded ages of collapsed mines (Hack & Price, 1990).

The parameters to be included in such a system would include the following:

- (a) *Mine geometry* Dimensions of rooms and pillars, height of pillars, elevations and slopes of floor and roof;

- (b) *Collapse geometry* Dimensions of collapse features relative to the mine geometry and the landscape;
- (c) *Rock mass* Thickness of beds, rock types, strength of the rock types, joint characteristics spacing and orientation, mass and material weathering;
- (d) *Soil overburden* Types, grading and strengths of soils involved in the collapse characteristics;
- (e) *Groundwater* Mine flooded or dry, position of the water table;
- (f) *Age of the mine* The dates of opening and abandonment of the mine and any indications of mine progress;
- (g) *Collapse event details* Associations with heavy rainfall, blasting, earthquakes etc.

It is unlikely that accurate values for the data mentioned above could be provided for every site with collapse problems, but some estimates could be given. Thus mine geometry could be perhaps assessed from a combination of seam thickness and knowledge of mining practice at the time of mining, while geological details could be estimated from nearby boreholes or exposures. At present accounts of collapses at one location usually lack some element of data vital to the use of this experience at some other site. The systematic collection of data including the parameters (a) to (g) would provide a data base which, when manipulated, might lead to empirical assessment of collapse hazard. The rock mass classification systems for tunnel design successfully applied today are empirical, based on much information. To develop a similar system appropriate to subsidence problems arising from collapsing room and pillar mines would require much data, derived from experiences in many different geological and mining situations. The collection of such an extensive data base requires co-operation at international rather than regional or national level. Within Europe such an endeavour could be sponsored by the European Union.

REFERENCES

- Anon (1983) *Limestone Mines in the West Midlands: the Legacy of Mines Long Abandoned*. Department of the Environment, London.
- Anon (1993) *Subsidence in Norwich*. Report of the Study on the Causes and Mechanisms of Land Subsidence. HMSO, London and Norwich.
- Atkins, M. W. (1983) The Chalk tunnels of Norwich. *Norfolk Archaeology* **38**, 313-320.
- Bekendam, R. & Price, D. G. (1993) The evaluation of the stability of abandoned calcarenite mines in South Limburg, Netherlands. *Eurock '93* (ed. by L. Ribeiro e Sousa & N. F. Grossman), 771-778. Balkema.
- Bell, F. G. (1988) The history and techniques of coal mining and the associated effects and influence on construction. *Bull. Assoc. Engng Geol.* **25**, 471-504.
- Bieniawski, Z. T. (1989) *Engineering Rock Mass Classifications*. Wiley-Interscience, New York.
- Hack, H. R. G. K. & Price, D. G. (1990) An extension of the stand-up time in the Q-system rock mass classification up to 200 years based on the limestone mines in The Netherlands. In: *Proc. of the 6th. Int. Congr. Int. Assoc. Engng Geol.*, vol. 5, 3559-3562.
- Obert, L. & Duvall, W. I. (1967) *Rock Mechanics and the Design of Structures in Rock*. John Wiley & Sons, New York.
- Woodward, S. (1831) The Chalk vaults near St. Giles' Gate, Norwich. *Archaeologia*. **23**, 411-412.

Historique de l'incident d'Okn 32, à la partie du nord du Sahara Algérien

SAID AKRETCHE

Ministère de l'Énergie, 80 Avenue Ahmed Ghermoul, Alger, Algérie

LYNDA OKBI

SONATRACH, Division Production, 8 Chemin du Réservoir Hydra, Alger, Algérie

Abstract On 26 October 1986 a land subsidence incident occurred at Haoud Berkaoui Oil Field in the northern part of the Algerian Sahara, which swallowed up the Okn-32 oil well and the core drill-2. The resulting crater was 80 m deep and 200 m in diameter. Six months later after subsequent subsidence events destroyed Okn-32 bis situated 80 m from Okn-32, the crater was 320 m in diameter. The origin of this event is discussed.

SITUATION

Le champ de Haoud Berkaoui est situé à l'ouest de Ouargla (Fig. 1). Le puits Okn 32 découvert en 1964, a produit de l'huile dans les grès Ordovicien se trouvant à 3200 m de profondeur.

Le forage du puits Okn 32, en Février 1978, à mis accidentellement en contact l'aquifère éruptif du Continental Intercalaire (Albo-Barrémien) et celle du complexe terminal (Sénonien carbonaté). La différence de charge de ces deux nappes de l'ordre de 250 m, a provoqué une circulation ascendante de l'eau Albienne à travers le sel Sénonien épais de 150 m (Fig. 2), dont le débit est évalué en 1990 entre 2500 et 2800 m³ h⁻¹. L'écoulement se faisant à travers le sel du Sénonien salifère, a créé une cavité de dissolution située entre 450 et 600 m de profondeur.

Cette dernière en s'agrandissant, a engendré l'effondrement de la couche sénonienne en Octobre 1986 créant ainsi en surface un cratère de 200 m de diamètre (Figs 3 et 4).

L'injection massive de sel dans le Sénonien carbonaté, a entraîné la pollution de cet aquifère qui constitue une ressource essentielle aussi bien pour l'agriculture que pour l'approvisionnement de la ville de Ouargla, située à 32 km au nord-est du puits Okn 32. Aussi, SONATRACH a confié à une société étrangère spécialisée, en Août 1988, une première étude de 18 mois visant à mettre en place les suivis d'urgence basés sur le cratère (subsidence et sismique) et sur le Carbonaté (interprétation des sondages électriques).

FORMATION DU CRATERE

Le cratère d'Okn 32 s'est formé brutalement au moment où le fontis engendré par lessivage de la cave s'est développé par effondrement progressif des terrains situés au dessus du sel, au fur et à mesure de sa dissolution.

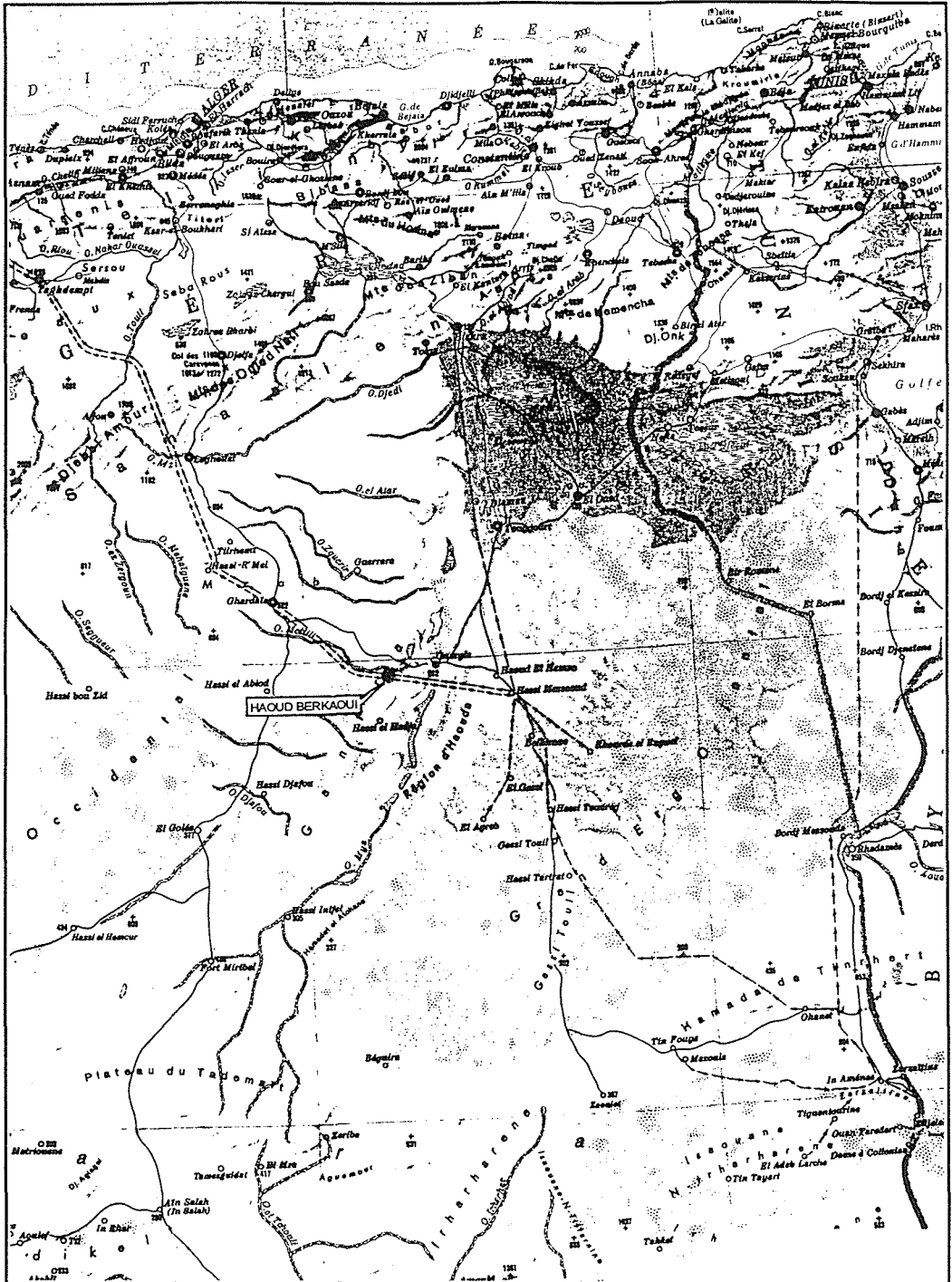


Fig. 1 Plan de situation.

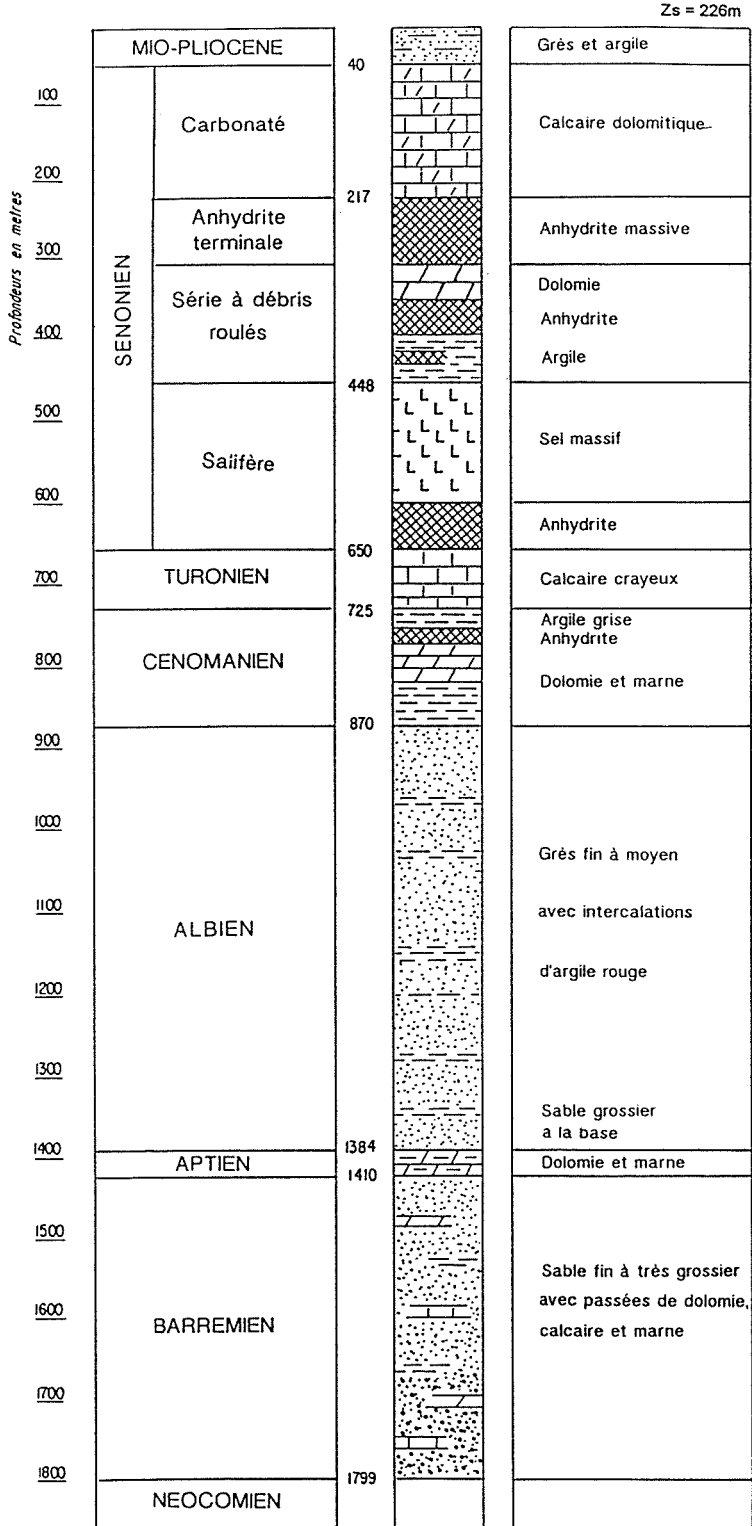


Fig. 2 Log lithostratigraphique du forage Okn 32.

La cave s'agrandissant, les matériaux sus-jacents s'effondrent progressivement jusqu'au dégagement de la dalle d'anhydrite terminale. Cette dernière retenait les terrains du Sénonien carbonaté et s'est rompu, le 26 Octobre 1986, entraînant la formation d'un cratère d'environ 600 m de diamètre. Il s'ensuit un découpage quasi-vertical du Sénonien carbonaté dont la stabilité provisoire revient à l'accumulation de débris d'éboulement dans la cheminée. Toutefois, il reste du vide qui en s'agrandissant, probablement par lessivage, peut créer de nouveaux effondrements (Figs 3 et 4).

ESTIMATION DU DEBIT DE L'ALBIEN

Le forage d'un sondage de reconnaissance a fourni par des mesures de RFT (Repeat Formation Tester) le profil de pressions dans l'Albo-Barrémien et par des tests de production, la perméabilité des différentes formations rencontrées. Le profil de débit

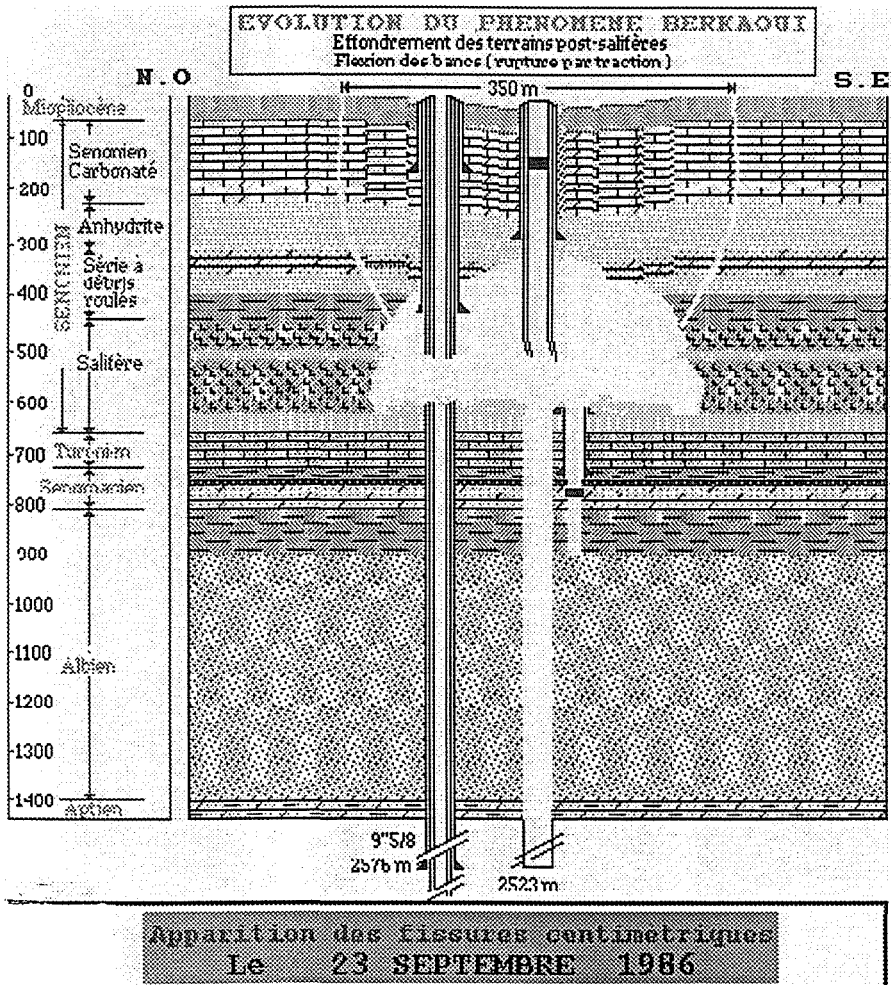


Fig. 3 Evolution du phénomène Berkaoui. Effondrement des terrains post-salifères.

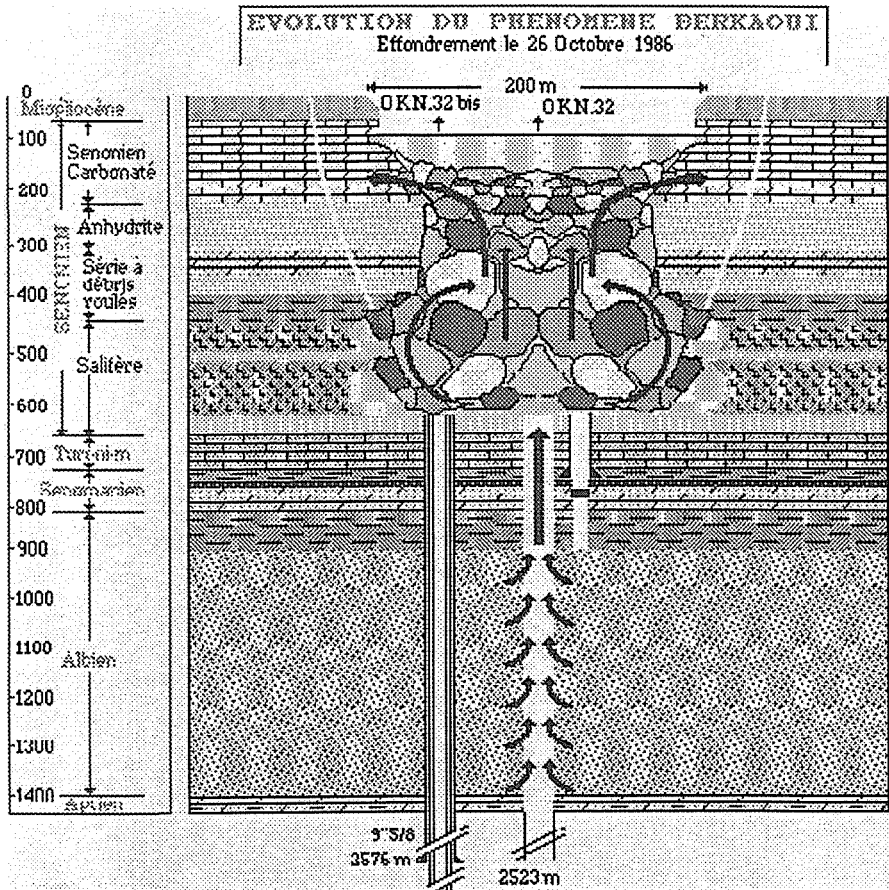


Fig. 4 Evolution du phénomène Berkaoui. Effondrement le 26 Octobre 1986.

calculé, présente une augmentation depuis la base du Barrémien jusqu'au top de l'Albien où il atteint 2000 et 2800 m³ h⁻¹ selon le potentiel de référence retenu pour l'Albien.

Ce même profil montre que deux tiers de la production du puits Okn 32 reviennent à l'Albien et un tiers au Barrémien (Fig. 5).

PROFONDEUR DU CRATERE

Le cratère a été exploré à l'aide d'un dispositif à ballon captif dirigé par trois treuils. Cette exploration a permis de sonder le cratère dont la profondeur est comprise entre 9 et 14 m. La cheminée entre le lac de surface et la cave, est complètement obstruée par les éboulis qui continuent de s'accumuler dans le cratère.

FORME DU CRATERE

Etude par la méthode de sismique

En l'absence actuelle de conclusions de la sismique 3D, qui est en fait la méthode

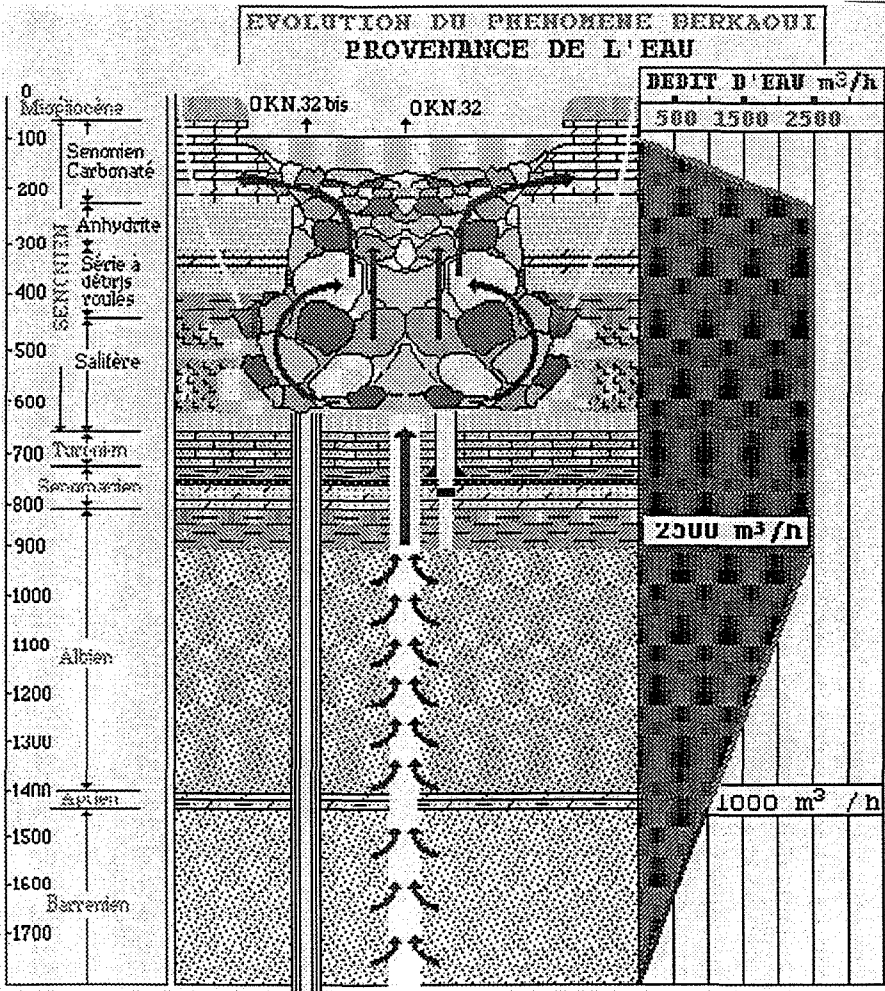


Fig. 5 Evolution du phénomène Berkaoui. Provenance de l'eau.

d'estimation la plus précise, on se basera sur les résultats de la campagne de sismique réfraction.

L'interprétation des profils sismiques traversants le cratère a permis d'estimer la taille de la cave (existante dans le Sénonien salifère entre les côtes 450 et 600 m). Celle-ci s'étend sur un diamètre minimal de 480 m et maximal de 740 m environ dans la direction nord-ouest/sud-est et un diamètre minimal de 360 m et maximal de 620 m environ dans la direction nord-est/sud-ouest. Sa forme évasée en son sommet est due à la migration de l'eau douce vers le haut (Fig. 6). Toutefois, il est utile de mentionner que le diamètre du cratère en surface a augmenté de 230 à 350 m durant la période s'étalant entre Décembre 1987 et Décembre 1994, soit une moyenne de 20 m an⁻¹ (Fig. 7).

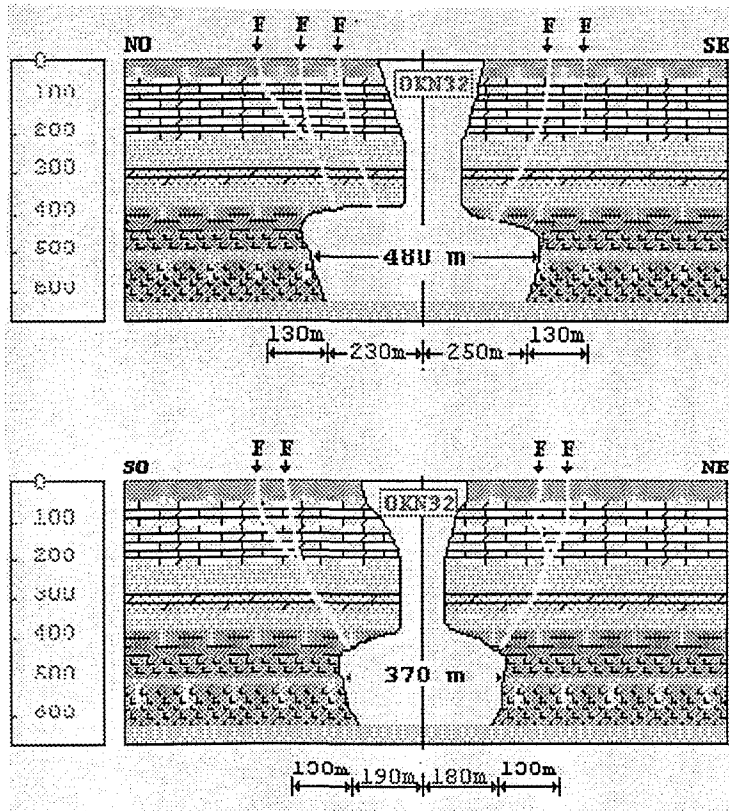


Fig. 6 Evolution du phénomène Berkaoui. Sismique réfraction.

Etude par la méthode gravimétrique

L'étude gravimétrique réalisée par l'entreprise Algérienne ENAGEO en 1991, a mis en évidence:

- Une extension de la cavité plus prononcée vers le nord-ouest, réduite vers le sud-est et de même ampleur vers le nord-ouest/sud-est.
- Des extensions maximales d'environ 740 m dans la direction sud-ouest/nord-est.
- Une surface maximale de l'anomalie estimée à 4 000 000 m³.

EVOLUTION DU PHENOMENE DE BERKAOUI

Afin de suivre l'évolution du phénomène d'éboulement et de subsidence, il a été procédé à:

- suivi de topographie,
- un suivi par écoute sismique,
- un suivi de résistivité.

Berkaoui

Année	Densité Saumure kg/l	Volume Cavité $m^3 \cdot 10^6$	Sel produit $T \cdot 10^6$	Rayon Profondeur (m)				
				485 m	515 m	545 m	575 m	605 m
1979	1.1027	1.38	2.76					
1980	1.1203	3.47	6.86	93	90	86	83	78
1981	1.1296	5.84	11.45					
1982	1.1357	8.36	16.32	146	140	134	128	119
1983	1.1400	11.00	21.40					
1984	1.1434	13.73	26.63	189	181	173	164	153
1985	1.1461	16.53	31.98					
1986	1.1483	19.37	37.43	223	214	204	193	180
1987	1.1502	22.27	42.95					
1988	1.1518	25.19	48.53	255	244	233	219	204
1989	1.1532	28.16	54.19					
1990	1.1544	31.16	59.89	285	272	259	243	225
1991	1.1555	34.16	65.61					
1992	1.1564	37.22	71.41	312	298	283	265	246

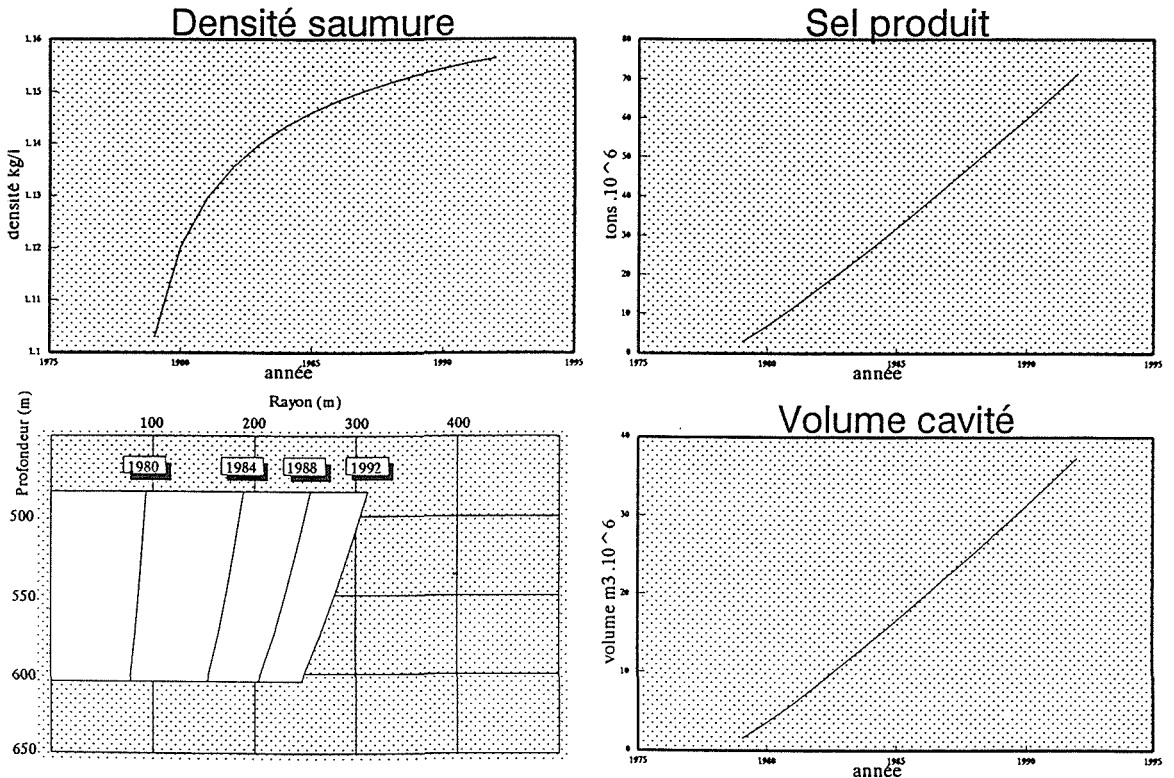


Fig. 7 Un affaissement variable des bases qui atteint pour certaines, placées à 20 m d'Okn 32, 60 cm en trois ans.

Suivi topographique

L'entreprise algérienne ENAGEO a régulièrement entrepris des campagnes de mesures de nivellement sur un réseau permanent de bases géodésiques qui permettent de suivre

l'affaissement des terrains environnants. Ce réseau a été complété par des mesures extensométriques sur les fissures existantes. Celles-ci, font apparaître un affaissement variable des bases qui atteint pour certaines, placées à 20 m d'Okn 32, 60 cm en trois ans (Fig. 7). L'axe principal de cette subsidence est orienté nord-ouest/sud-est. Ce phénomène est probablement lié au tassement des déblais qui soutiennent les abords de la cave. Par ailleurs, les mesures extensométriques montrent que:

- Les grandes fissures observées en surface autour du cratère, sont comprises dans une couronne d'épaisseur de 40 m.
- La fissure apparue en Octobre 1991, du côté nord-ouest à 520 m d'Okn 32, ne cesse de s'élargir et de s'étendre couvrant actuellement un angle de 120° soit une longueur de 1000 m.
- Le grand pan de 250 m de longueur dérivant de la fissure située à 25 m au nord-ouest du cratère, continue à s'affaisser. En effet, il était à 0 cm en Juin 1990, 70 cm en Juin 1991, 135 cm en Juin 1993 et 250 cm en Décembre 1994.

Suivi par écoute sismique

Le réseau de surveillance sismique a été installé autour du cratère en Août 1989. L'auscultation du cratère a permis de mettre en évidence l'existence d'une forte activité microsismique due, principalement à de simples réajustements des fissures de surface dans le Mio-Pliocène et le Carbonaté supérieur, essentiellement dans la partie nord-ouest ainsi qu'à quelques décollements au niveau de la dalle d'anhydrite terminale et enfin à un petit nombre d'événements profonds en relation avec le toit du sel qui semble encore en mouvement.

Suivi de résistivité

Depuis l'effondrement en Octobre 1986, cinq campagnes de résistivité ont été réalisées:

- La première effectuée en 1987, a décelé la propagation de la contamination par les eaux salées suivant les quatre directions à partir d'Okn 32 et dont les limites se situent:
 - vers l'est, à environ 3 km;
 - vers le sud, à environ 2.5 km;
 - vers le nord, à environ 1.5 km;
 - vers l'ouest à environ 1 km.
- La deuxième campagne réalisée en Mars 1988, a montré l'extension de la zone contaminée.
- La troisième campagne effectuée en 1989, a mis en évidence l'arrêt du front de contamination sur les profils et son extension sur le reste des autres profils.
- La quatrième réalisée en Mars 1990, a montré qu'il existe un avancement du front dans toutes les directions sauf la partie ouest.
- La dernière datant de Mars 1992, a déterminé une diminution des résistivités dans la zone faiblement saturée par rapport à la quatrième campagne assimilée à la propagation de la contamination due aussi bien à l'envahissement du Sénonien lagunaire ainsi que la partie basse du Sénonien carbonaté par les eaux salées, qu'à un passage latéral de faciès.

CONCLUSION – MESURES A PRENDRE

L'éruption de l'Albien à Okn 32 est devenue un phénomène très complexe à étudier surtout, en terme d'évolution de ses conséquences. Les résultats actuels montrent que le phénomène est en régression sur le plan de lessivage du sel et que la cave souterraine est en cours de stabilisation. Néanmoins, la stabilisation géomécanique des terrains de surface va probablement entraîner un agrandissement important du cratère. Aussi, le réseau de surveillance hydrogéologique, géotechnique et sismique permettant de suivre l'évolution de l'impact de ce phénomène sur l'environnement doit être nécessairement entretenu et complété en entreprenant certaines actions à savoir:

- La condamnation de l'accès à la zone du cratère surplombant la cave et l'adaptation du système de surveillance sismique au nouveau danger que représente une possible rupture du surplomb de la cave.
- L'amélioration de la surveillance de l'exutoire du carbonaté par la reprise partielle des piézomètres existant et par le forage de piézomètres complémentaires.
- La poursuite des modèles de transport de sel dans le carbonaté afin d'introduire les nouvelles données de suivi et d'affirmer notre prédiction de comportement.

La faisabilité de la maîtrise ne sera validée que par l'exécution d'un forage qui intercepte le trajet du puits Okn 32 ainsi que des fluides de maîtrise.

La mise en application du principe de maîtrise d'Okn 32 doit se faire en phases, après la réalisation d'un puits de reconnaissance qui conclut la phase de faisabilité et participe à l'opération de réparation:

- forage d'un ou plusieurs puits de maîtrise;
- mise en communication du ou des puits de maîtrise avec Okn 32;
- forage de puits d'observation;
- maîtrise par injection d'un fluide lourd. A ce stade, l'équilibre nécessite un pompage;
- colmatage définitif sur toute la hauteur de l'Albien et jusqu'au conduit Cénomaniens-Turonien par l'injection d'un ciment qui bouchera définitivement Okn 32.

Le passage entre la phase maîtrise de débit et le colmatage doit être quasiment instantané car tout arrêt prolongé favoriserait la production de l'Albien et ainsi la réduction à néant des effets de la phase préparative de blocage des écoulements. Il est cependant nécessaire de rappeler l'importance des fluides qui peuvent traiter ce problème. Ces derniers dépendront évidemment de l'objectif à atteindre.

REFERENCES

Suivi de l'évolution de l'effondrement d'Okn 32. Rapport internes, SONATRACH, division production 1990, 1992, 1994, 1995.

Simulation of subsidence in soil layers in a geotechnical centrifuge

H. G. B. ALLERSMA

Delft University of Technology, Civil Engineering, Stevinweg 1, Delft, The Netherlands

Abstract Tests were performed in the small geotechnical centrifuge at the University of Delft in order to examine the behaviour of soil layers that are subjected to a large localized settlement at a large depth. Uniform soil layers as well as soil with a clay layer and a layer of rocky material were tested. The tests clearly show the interaction between the different soil types. It is believed that this test technique is a good tool for investigating this phenomenon.

INTRODUCTION

For a better understanding of the structure of the earth, knowledge is required of how discontinuities at a great depth are influencing the upper soil layers. This phenomenon is also of interest when predictions have to be made of how local settlements at deep soil layers i.e. due to gas production influence the soil surface. The influence of local settlements at deep layers has been investigated by several researchers (i.e. Terzaghi, 1936; Horsfield, 1977; and Vardoulakis *et al.*, 1981). Small scale tests have been reported which are used to support the theoretical analyses. The tests, however, were performed at 1g so that it is not sure in how far the stress dependent behaviour of the soil is taken into account. Furthermore, it is not possible to simulate the behaviour of clay layers or rocky materials in small scale tests. In the small geotechnical centrifuge of the University of Delft a test technique has been developed which enables the simulation of a large discontinuous displacement of an earth segment at a large depth. The advantage of centrifuge tests is that shear stresses can be realized which are of the same magnitude as in a soil layer with a thickness of more than 40 m. This also means that the behaviour of a clay layer or soft rock can be studied and that the stress dependent behaviour of sand is modelled in a better way.

TESTING TECHNIQUE

The tests are performed in a small geotechnical centrifuge (Fig. 1). This device has been developed at the Geotechnical Laboratory of the Faculty of Civil Engineering of the University of Delft (Allersma, 1994a,b). The design concept was to obtain a device which is flexible and cheap in operation. The centrifuge, which has a diameter of 2.4 m, contains two swinging platforms to carry the samples. Samples with a weight of more than 300 N and a volume of 15 x 40 x 40 cm can be accelerated up to 150 times earth's gravity. In most cases the weight of the model containers is less than 200 N, so that they can be handled by one person. This means that the centrifuge is very convenient in use.

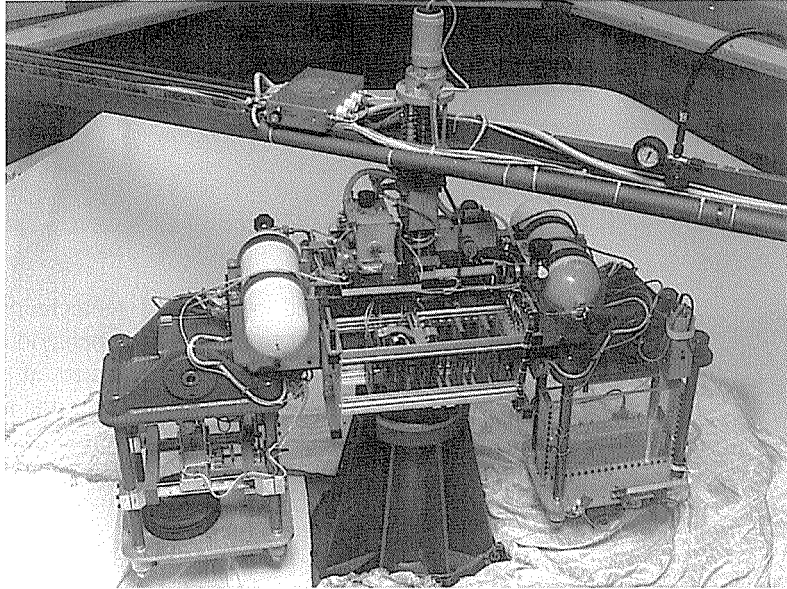


Fig. 1 Photograph of the small geotechnical centrifuge of the University of Delft.

Due to the artificial gravity, the self-weight of the soil and therefore the soil stress increases, so that a soil layer of 30 cm at an acceleration of 100g is subjected to the same stress gradient as a soil layer with a thickness of 30 m. The small model now also simulates the stress dependent behaviour of the soil, which is particularly important when cohesive materials, such as clay or wet sand, have to be tested.

An advanced electronic system, containing a single-board IBM PC compatible computer (486 central processor, 66 Mhz), is installed in the spinning part of the centrifuge in order to control the tests. A monitoring system, which uses image processing techniques to digitise displacements, has been developed to watch the course of the tests in more detail during spinning (Allersma, 1990, 1991). Several devices have been developed in order to perform tests in flight (Allersma, 1994a). In this test program, a computer controlled air supply system is used to manipulate the course of the test.

MEASURING SETUP

Because the centrifuge contains advanced computer controlled devices, a very simple test device could be developed to simulate the localized deformation. A photograph of the test cell is presented in Fig. 2. Two perspex sheets at a distance of 60 mm apart form a container with dimensions of 60 x 400 x 400 mm. A platform is made in the cell to create a space under the soil layer. At the centre a conical opening has been made in the platform. The outlet of the cone ends a few centimetres above the bottom of the container. Furthermore, a metal tube with small holes is placed under the cone, where the space between tube and cone is sufficiently wide to permit sand to flow out of the cone. Due to the internal friction the flow through the cone will stop when the sand has

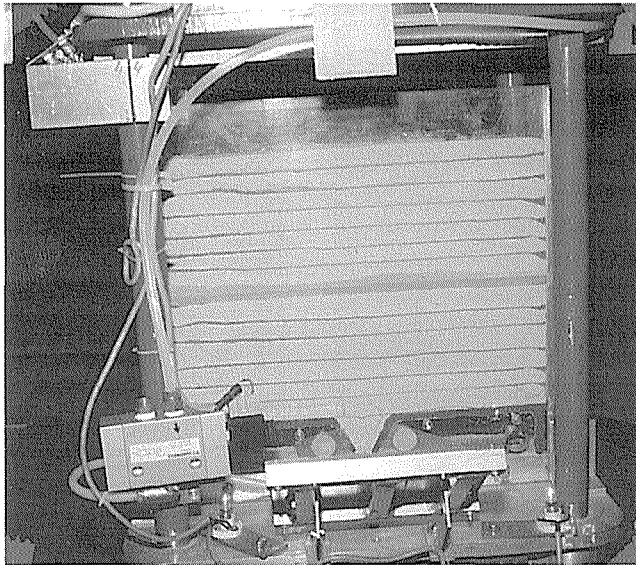


Fig. 2 Diagram of the test box. The sand flow is activated by air shots via the central tube.

formed the natural slope. The flow can now be activated by disturbing the natural slope, which can be forced by pressurizing the metal tube, so that air blows through the holes displacing the sand. The settlement of the sand at the bottom of the sand sample is quite uniform over the length and width of the outlet, so that a good simulation of the so called trap-door mechanism is obtained. An advantage compared to a mechanical control system is that very large displacements can be achieved by using only a small space under the sample.

RESULTS

Homogeneous sand layer

Tests have been performed with a homogeneous layer of Dune sand. The internal friction angle of a medium dense packed sample with a porosity of 34% is 35° . The median grain size D_{50} is 0.2 mm. To visualise the behaviour of the sand in more detail grid lines of black coloured sand are sprinkled in the sample during preparation. To demonstrate the influence of the stress gradient, similar tests on dense packed sand are performed at 1g (Fig. 3(a)) and 100g (Fig. 3(b)). It appears that the results are quite different. At 100g the discontinuities in the field are more pronounced and a larger area is effected by the discontinuous displacement of the boundary than in the 1g test. The difference is probably mainly caused by the fact that sand behaves more frictional at a low stress level. The higher friction angle can be a result of roughness of the particle surface. This roughness is not so effective at higher stresses due to micro crushing. The difference will also be strong if some cohesion is introduced, i.e. by dust in the sand.

In Fig. 4 two tests at 100g on a dense (a) and a loose (b) sand bed with heights of 25 cm each are presented. The displacements are made visible by subtracting images of

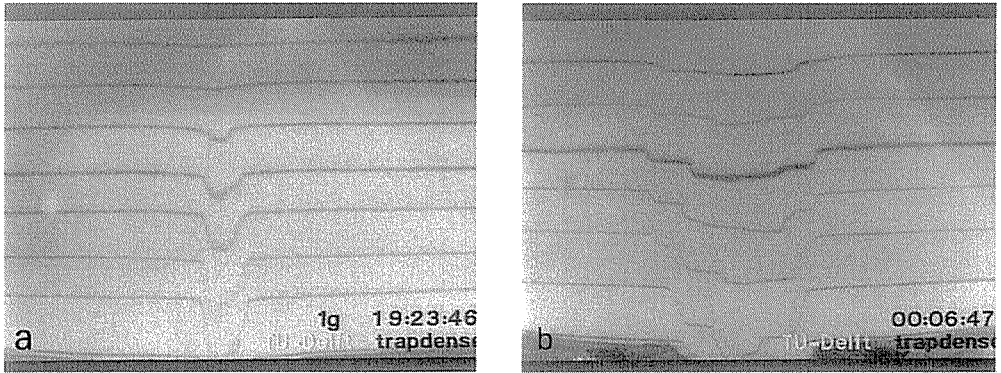


Fig. 3 Comparison of a 1g test and a 100g test on a layer of homogeneous dense sand.

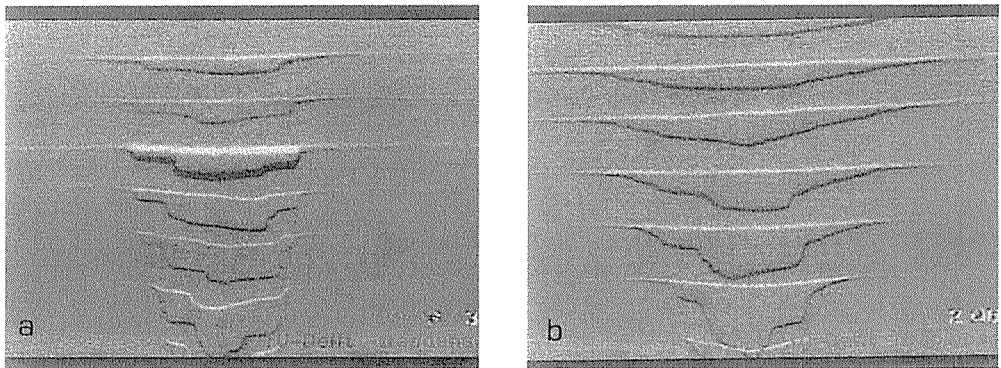


Fig. 4 Comparison of the behaviour of dense (a) and a loose (b) sand in a test at 100g.

two test stages. Typical is that the width of the column that is influenced by the displacement increases at lower depth in case (a). This indicates a mechanism which reduces the displacement to almost zero at a large distance from the source. However, when the displacements became larger the effect seemed to be concentrated to a more narrow column. It seems that, in the case of dense packed sand, the initial discontinuous deformation is continued over a long distance from the source. In the case of loose packed sand, however, the vertical displacements become smooth at a much smaller distance from the source. The differences can be explained by the more dilatant behaviour of dense sand. In dense sand shear can occur only if the volume increases. Because this takes lots of energy the sand prefers to deform in more localized shear zones than is the case in loose packed sand. The increment of the volume in dense packed sand can be deduced from the fact that the displaced area decreases at larger distances from the source.

Sand with clay layer

In Fig. 5 a test at 100g is presented on a sand bed with a clay layer. The cohesion of the

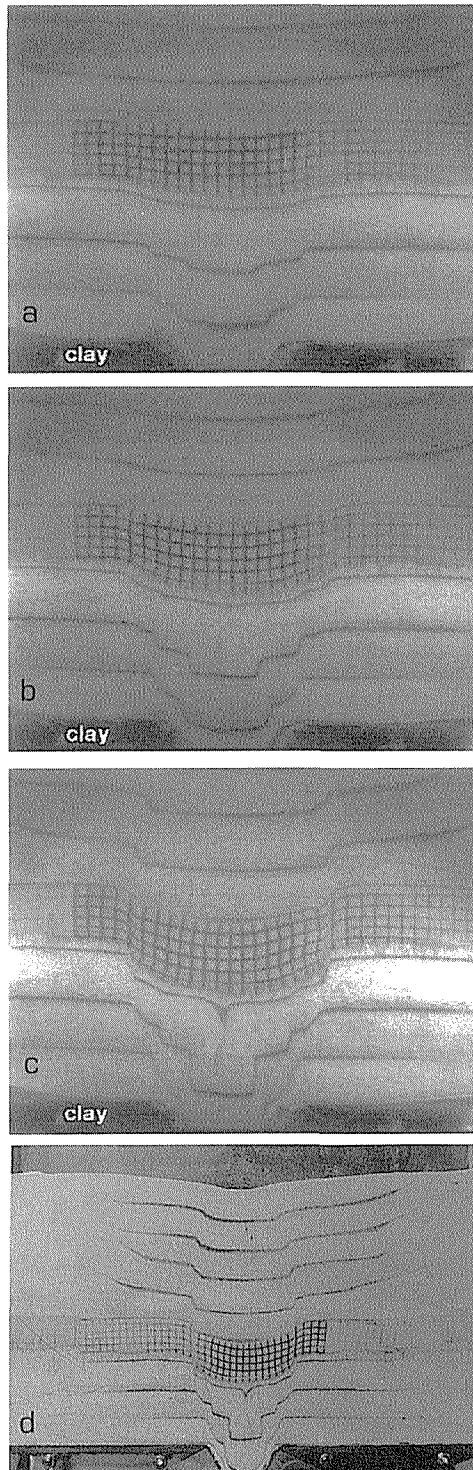


Fig. 5 Test at 100g; the simulated height of the soil layer is 35 m, the thickness of the clay is 2 m at a depth of 20 m.

clay was approximately 25 kPa. A dense sand bed with a height of 35 m was simulated, where the clay layer simulates a thickness of 3 m. The depth of the clay layer was approximately 20 m. The different stages show how the sand punches sharply through the clay layer. Typical is the very little influence of the clay layer on the failure mechanism in the sand. In Fig. 5(d) a photograph of the whole sample is shown. It can be seen that even at the surface of the sample large gradients in the vertical displacement are visible. The discontinuous transitions in the sand are almost the same as in tests without a clay layer. A similar picture is obtained if the clay layer is made thicker. Large displacements are required to develop strong shear zones into the clay.

In Fig. 6 a clay layer with a simulated thickness of 5 m was located on a sand layer with a thickness of 30 m. Also in this test strong gradients in the vertical displacement can be observed close to the surface of the sand layer. However, the deformation in the clay layer is more smooth in this case. The surface of the clay layer is subjected to bending, which can cause tensile and compression forces at the clay surface. It seems that the active zone in the sand is concentrated to a more narrow area at larger distance

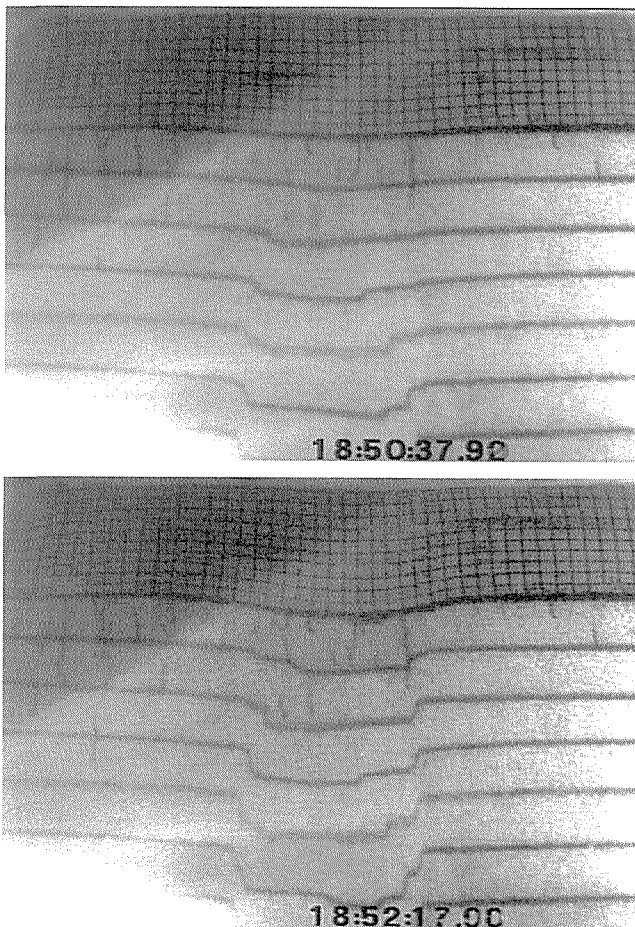


Fig. 6 Test at 100g; the simulated height of the sand is 30 m with a cover of 5 m clay.

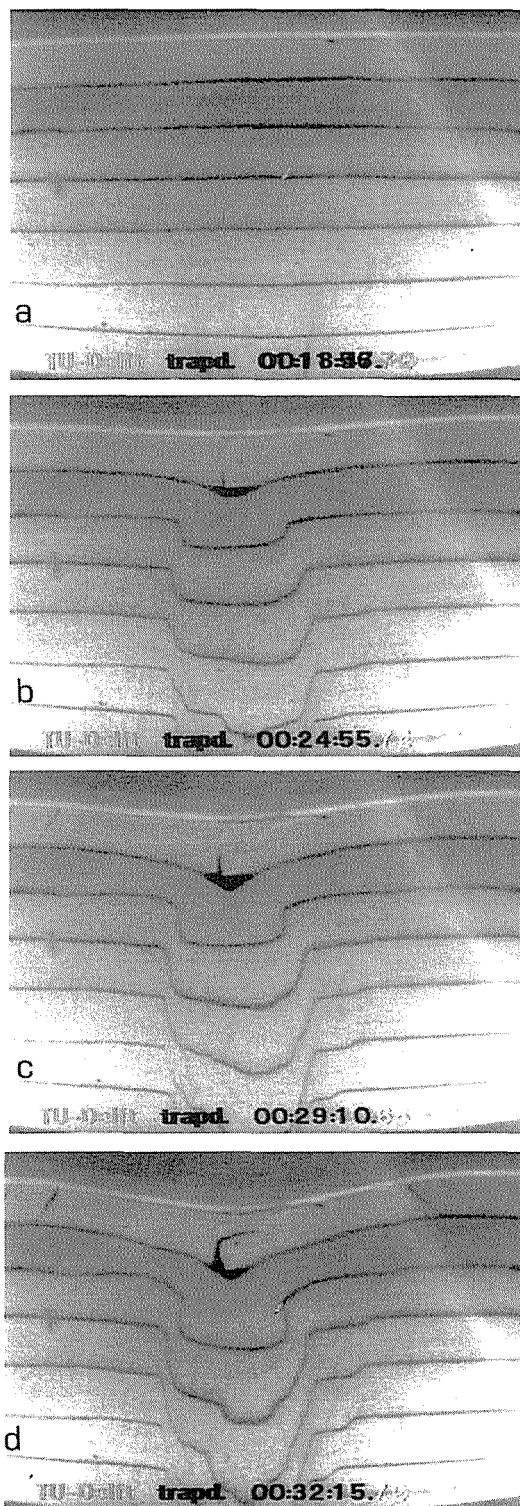


Fig. 7 Simulation of a rocky layer of soft material (plaster).

from the source. Furthermore it can be observed that the volume of the sand increases due to dilation.

Sand with rocky material

In Fig. 7 a soil layer with a thickness of 40 m and a layer of rocky material with a thickness of 1.5 m is simulated. In this test, soft rock was simulated by a layer of plaster

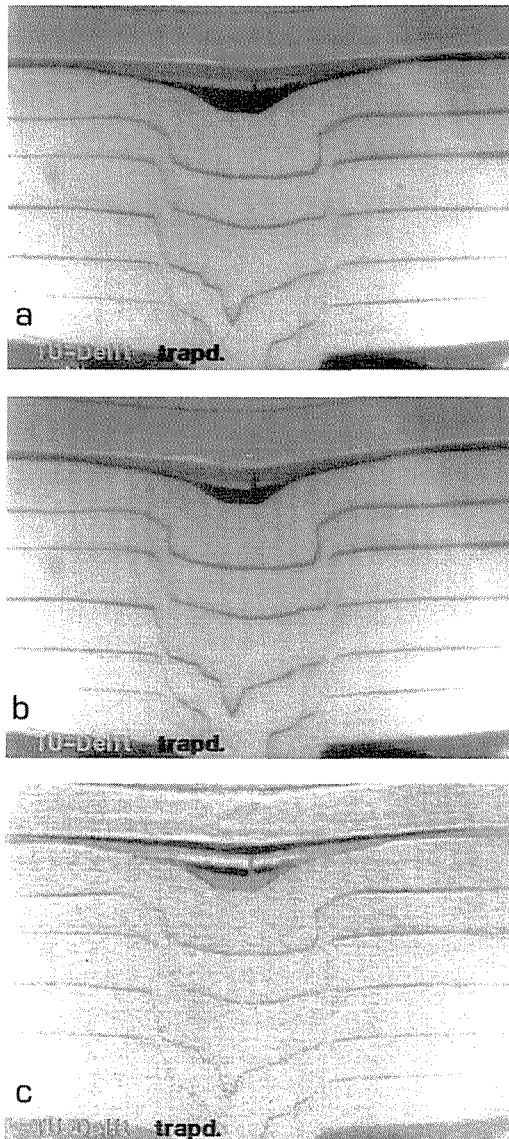


Fig. 8 The moment of cracking of a rocky layer of stronger material (tile of backed clay).

of 15 mm. During the course of the test the first crack could be observed in the centre. At a later stage, two cracks are formed in the plaster, approximately half way the centre and the boundary. Because plaster is quite soft the process proceeds rather gently. A stronger rock layer was simulated in Fig. 8 by means of a tile of backed clay with a thickness of 10 mm (1 m prototype). Also in this case a first crack is observed in the centre of the layer. At a later stage, when the support of the rock layer decreases, two cracks are formed at the same locations as in the test with soft rock.

However, in this test the formation of the cracks was accompanied by a sudden vertical displacement of the sand layer. The situation before and after cracking is shown in Fig. 8(a) and (b) respectively. The moment of the jump has been made visible in more detail by subtracting the images before and after the jump respectively. In Fig. 8(c) only the rock layer is displaced, where only very slight displacements can be observed in the sand below the rock layer. Perhaps this mechanism could be responsible for light earthquake shocks, i.e. due to gas extraction from deep layers.

In contrast to the clay layer, the rock material causes a more smooth vertical settlement of the sand which is located above the rocky layer.

CONCLUSIONS

It is shown that localized settlements at deep layers can be simulated very well by centrifuge tests. It appeared that the stress level has a great influence on the failure mechanism. However, there are indications that above some stress level the behaviour remains constant, so that the simulated depth is perhaps also representative for larger depths.

If the behaviour of cohesive materials has to be investigated centrifuge tests are the only way to perform useful small scale tests.

It seemed that a clay layer at some depth has little influence on the failure mechanism of the sand. However, a clay layer located at the surface of a sand bed makes that the vertical displacements at the surface became more smooth.

If rocky material is included in the sand layer, the formation of cracks can be observed during the test. At the moment of cracking a sudden displacement of the soil layer has been observed. This phenomenon could be a simulation of a light earthquake shock.

The major aim of the reported test program was to demonstrate the possibilities of centrifuge research in this area. It is believed that these types of tests are very valuable to examine subsidence phenomena and to validate calculation methods.

An interesting item for further research is to investigate in how far soil layers with a simulated thickness of i.e. 60 m are representative for soil behaviour in layers of more than 1000 m. This comparison can be made by means of special equipment.

REFERENCES

- Allersma, H. G. B. (1990) On line measurement of soil deformation in centrifuge tests by image processing. In: *Proc. Int. Conf. on Experimental Mechanics* (Copenhagen), 1739-1748.
- Allersma, H. G. B. (1991) Using image processing in centrifuge research. In: *Proc. Int. Conf. Centrifuge 91* (Boulder), 551-558. Balkema, Rotterdam.

- Allersma, H. G. B. (1994a) Development of miniature equipment for a small geotechnical centrifuge. *Transportation Research Record no. 1432*, 99-105. Innovation in Instrumentation and Data Acquisition Systems, National Academy Press, Washington, DC.
- Allersma, H. G. B. (1994b) The University of Delft geotechnical centrifuge. In: *Proc. Int. Conf. Centrifuge 94*, 47-52. Balkema, Rotterdam.
- Horsfield, W. T. (1977) An experimental approach to basement-controlled faulting. *Geologie en Mijnbouw* (Geology and Mining) **56**(4), 363-370.
- Terzaghi, K. (1936) Stress distribution in dry and saturated sand above a yielding trap-door. In: *Proc. Int. Conf. Soil Mech.* (Cambridge), 307-311.
- Vardoulakis, I., Graf, B. & Gudehus, G. (1981) Trap-door problem with dry sand: A statistical approach based upon model test kinematics. *J. Num. and Anal. Meth. in Geom.* **5**, 57-78.

Subsidence studies in Indian coalfields by a semi-empirical approach

P. P. BAHUGUNA

Department of Mining Engineering, Indian School of Mines, Dhanbad 826004, India

Abstract Partial norms based on an empirical approach have been developed for prediction of subsidence in Indian coalfields but these have resulted in overestimation of subsidence values. So a hybrid approach of studying the subsidence behaviour by numerical modelling and fitting in the field data in the results to develop a semi-empirical model has been followed in the present studies. Effects of each of subsidence contributing factors on maximum possible subsidence S_{\max} has been evaluated by varying the value of that factor in the model and keeping other factors constant. The assessment of S_{\max} takes account of the effects of seam thickness, depth of workings, goaf support, extraction ratio, other working seams, overburden rockmass and dip of the seam. A profile function has been suggested for Indian coalfields. The comparison with other methods showed that the predicted values of the subsidence, slope and strain profiles were the close to the field measurements.

INTRODUCTION

Partial norms developed for subsidence prediction based on empirical approach could not yield satisfactory results because of the lack of adequate database covering a variety of situations for such predictions. Subsidence studies using two dimensional material model and those using numerical modelling (Shankar & Dhar, 1989) though helped in understanding the mechanism of mine subsidence in Indian coalfields, could not result in the development of a subsidence prediction model because of the limitations of these approaches. This paper presents a hybrid approach of carrying out the parametric studies by numerical modelling of subsidence and using these qualitative results to the available field database in order to develop a semi-empirical method of prediction of subsidence in Indian coalfields.

DATA

Numerical modelling

Numerical modelling was carried out by using the Displacement Discontinuity Method (Sinha, 1979) which is a subvariation of the Boundary Element Method. Two models were used for numerical modelling. The first is two dimensional, assuming the overburden rockmass as homogeneous, linearly elastic and transversely anisotropic medium.

The second is three dimensional, also assuming a homogeneous, linearly elastic and isotropic medium. The coal seam is assumed to be a thin crack in this overburden rockmass. The mechanical characteristics of the host rockmass above and below the mine workings are highly anisotropic and complex; therefore it has not been possible to accurately simulate the rock behaviour and predict the subsidence deformations caused by underground excavations (Bahuguna *et al.*, 1991). Therefore the simple Boundary Element Method analysis, based on the above assumptions, was used only for the qualitative assessment of the effect of each subsidence contributing factor by varying its value in the model and keeping other factors constant. These qualitative results gave the insight and helped in developing a semi-empirical method by using the field data base.

PARAMETRIC STUDIES

The analysis of parametric studies by numerical modelling showed the following effects of individual subsidence influencing factors:

- (a) Parametric studies confirmed that maximum possible subsidence S_{\max} or maximum subsidence S_0 was directly proportional to the extracted thickness of the seam.
- (b) The effect of partial extraction in board and pillar mines was found to be depending upon the geometry of extraction, mining induced stressed and stiffness of coal seam, or yielding capacity and size of the remnant pillars. The stiffer the coal seam, the lesser is the magnitude of subsidence on the surface.
- (c) The subsidence was also found to be depending on the strength and condition of overburden rockmass. Presence of more hard-rock layers in the overburden results in less subsidence at the surface. On the other hand, the discontinuities or planes of weakness make the overburden weaker and result in increased subsidence.
- (d) The nature of overburden rockmass was found to be affecting not only the magnitude of the subsidence but also the shape and extent of the subsidence profile. The more fragmented the rockmass is, the larger is the angle of draw, the smaller is the subsidence over ribside and closer to the centre of panel is the point of inflection of subsidence profile curve. This implies that for weaker overburden rockmass the extent of subsidence trough extends to remoter areas and is deeper in the central portion.
- (e) The magnitude of subsidence, and the extent and shape of subsidence trough are also found to be dependent upon the width-depth ratio (w/d) of the panel. The magnitude of maximum subsidence is found to be increasing with increasing width-depth ratio until critical width is reached, beyond which it stabilizes. Similar effect is observed on the shape of the subsidence trough. For smaller w/d ratios the subsidence trough is found to be shallower than for larger w/d ratios and beyond the critical width the shape of the sides of the trough remains unchanged.
- (f) The magnitude of the maximum subsidence is found to be increasing with the depth of the working. This increase gradually decreases with larger depths.
- (g) The effect of sand stowing is found to be dependent on the degree of stowing. The higher the degree of stowing, the smaller is the subsidence, whereas in case of caving the magnitude of subsidence is found to be maximal for the given mining and geological condition.
- (h) The effect of the dip of the seam is reduction of magnitude of subsidence in dipping seams whereas the shape of the subsidence profile also changed.

Semi-empirical method

The results of the above parametric studies have been incorporated in a field data base to develop a semi-empirical method. The prediction of maximum possible subsidence (S_{\max}) and maximum subsidence (S_o) have been discussed elsewhere (Bahuguna *et al.*, 1993) and is based on the following formula:

$$S_{\max} = m g_f e R_f d_f d' t \quad (1)$$

where m is the extracted thickness of the seam; g_f = goaf treatment factor [0.95 for caving, 0.07-0.1 for sand stowing]; e is the extraction factor; R_f is the rock factor for effect of composition and strength of overburden rock mass (Fig. 1); d_f is the factor for the effect of depth of the workings [0.87 for depths up to 400 m and 1.0 for more than 400 m], d' is the factor for effect of dip of the seam [= $\cos \alpha$, where α is the angle of dip]; t is the time factor [to be taken as 1 for finished subsidence]. The maximum subsidence is given by:

$$S_o = S_{\max} [l - e^{n(1/d)^2}] [l - e^{n(w/d)^2}] \quad (2)$$

where l , w and d are the length, width and depth of the panel and n is an empirical constant whose average value may be taken equal to 3.0.

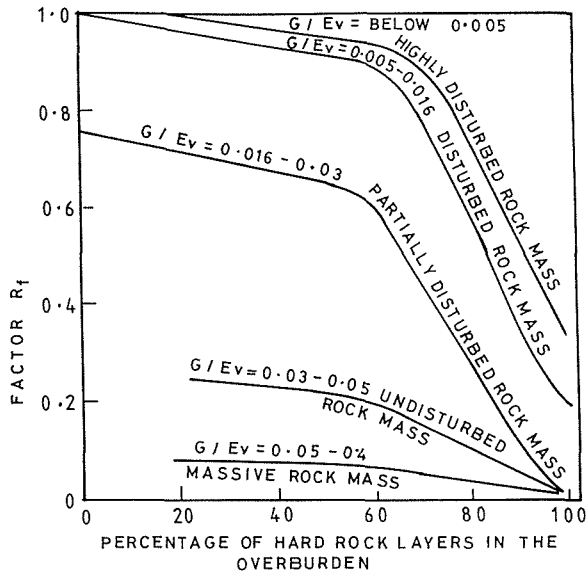


Fig. 1 Rock factor for various types of overburden rockmass.

Prediction of subsidence profile

A profile function was developed for Indian coal mines to predict subsidence along a given line. The point undergoing maximum subsidence S_o or maximum possible subsidence S_{\max} lies in the centre of a rectangular panel. The extent of subsidence trough along a profile line passing through the centre stretches outwards up to a distance $r =$

$d \tan \zeta$ from the ribside where d is the depth of seam on the ribside and ζ is the angle of draw. For dipping seams d will be different on both ribsidess. Similarly the angle of draw will be different on static and dynamic end so the total length of the subsidence profile will be $d_1 \tan \zeta_1 + w + d_2 \tan \zeta_2$ where w is the width of the excavation. The critical diameter r is given by

$$\begin{aligned} r &= r_1 + r_2 \\ r &= d_1 \tan \zeta_1 + d_2 \tan \zeta_2 \end{aligned} \quad (3)$$

The subsidence s_i at a point i at a distance x_i from a point undergoing maximum subsidence S_{\max} or S_0 has been found to be given by the following expressions:

for subcritical widths:

$$S_i = S_0 [e^{-M(x_i/(r+x_i/2))^2}] \quad (4)$$

for critical and supercritical widths:

$$S_i = S_{\max} [e^{-M(x_i/(r+x_i/2))^2}] \quad (5)$$

where x_i is the distance of the given point from the nearest point on the profile line undergoing maximum subsidence. In the equations above M is a profile constant and is dependent upon the nature of overburden rockmass. This constant governs the shape of the subsidence profile. Nomograms (Fig. 2) have been developed to find the values of ζ_1 , ζ_2 and M for different w/d ratios and different type of overburden (Bahuguna, 1993).

Prediction of slope, horizontal displacements and horizontal strains

The slope between two consecutive points, say i and $(i - 1)$, of the panel centre can geometrically be obtained as:

$$g_i = \frac{ds}{dx} = \frac{S_i - S_{i-1}}{dx} \quad (6)$$

where S_i and S_{i-1} are the subsidence of the i th and $(i - 1)$ th point and dx is the distance between these two points.

The profile of horizontal displacements is similar in nature to the profile curve of slopes. Therefore a linear proportionality may be established between the two curves which suggests that horizontal displacement u_i at the i th point from the panel centre may be given by:

$$u_i = B g_i \quad (7)$$

where B is the proportionality constant and g_i is the slope of the ground at the i th point. The proportionality constant has been found to be dependent on the nature of the overburden rockmass and the w/d ratio of the extracted panel. The value of B (Fig. 2) may be found out for a given w/d ratio from the developed nomograms (Bahuguna, 1993). Once the horizontal displacements are known, the horizontal strains may be found from the following equation:

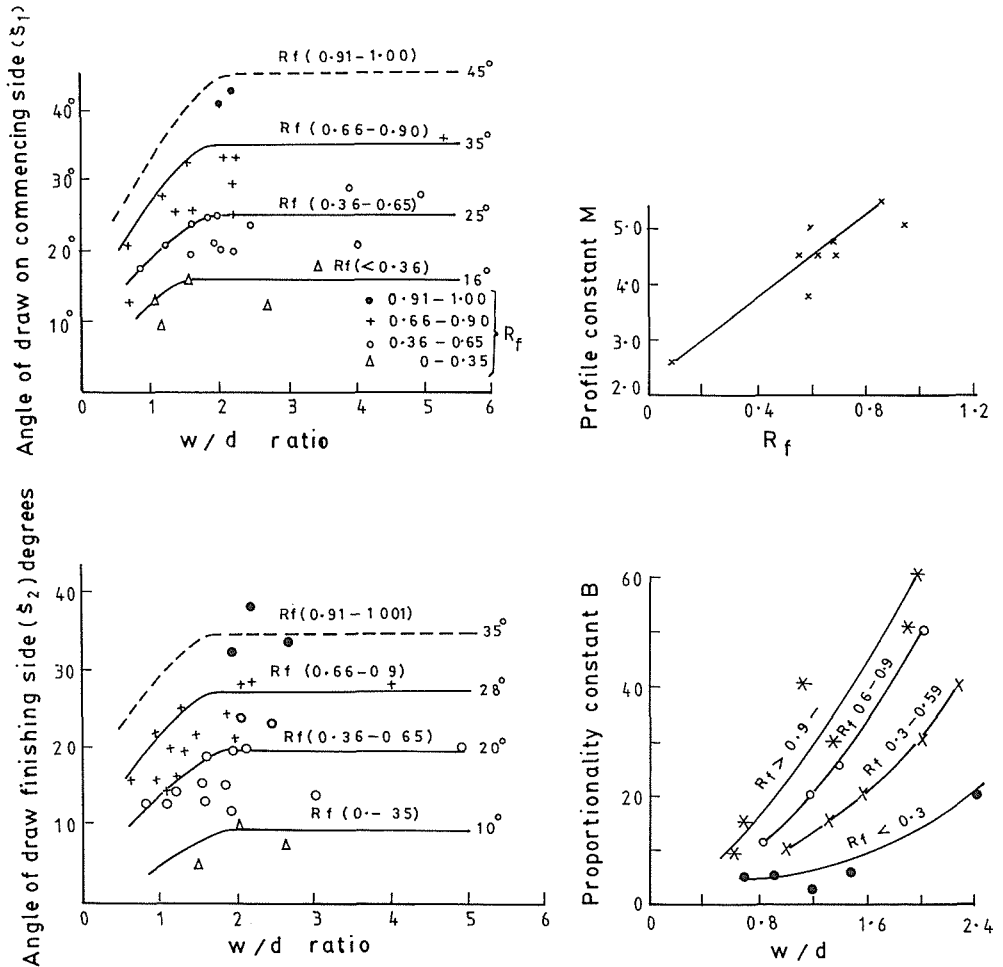


Fig. 2 Nomograms for the values of ζ_1 , ζ_2 , M and B .

$$e_i = \frac{du_i}{dx} \tag{8}$$

where e_i is the horizontal strain between the i th and the $(i - 1)$ th point situated at a distance dx apart and du_i is the difference in horizontal displacement of these two points.

RESULTS

The results of prediction of S_{max} by this approach have been described elsewhere (Bahuguna, 1993). Normalized subsidence, slope and horizontal strains were obtained from the developed model based on the Profile Function Method for 15 mine workings from Indian coalfields and were compared with those profiles obtained from other methods. Comparison of the profile obtained from one mine working only is being given

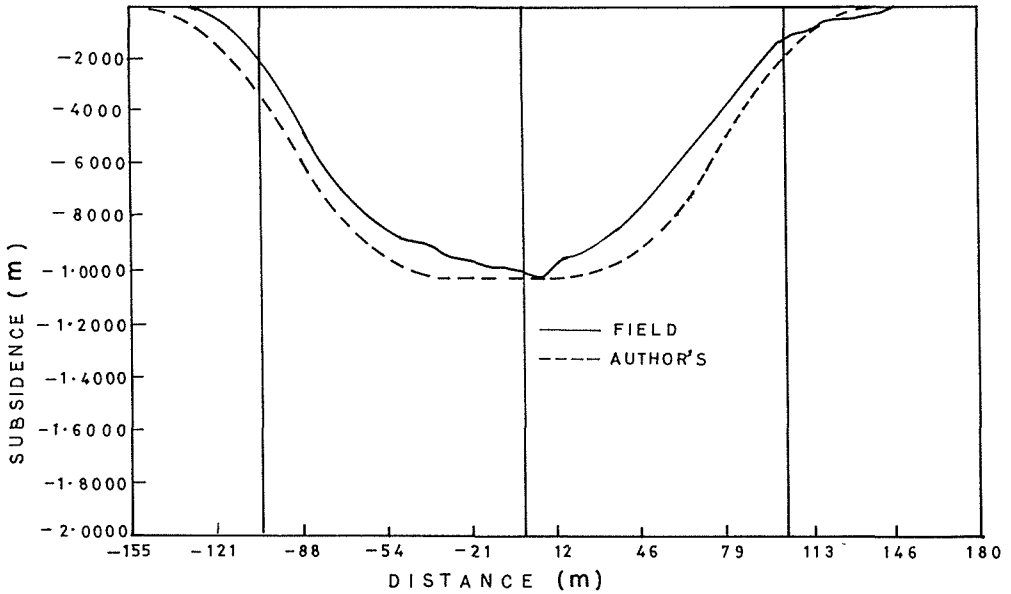


Fig. 3 Comparison of subsidence profiles.

here for lack of space. Figure 3 shows the subsidence profiles as obtained from the field measurements and predictions from the present method. Similarly Figs 4 and 5 show the profiles of slope and horizontal strains.

The comparison shows a good agreement of the subsidence, slope and strains profiles obtained from the present method with those obtained from field measurements.

In other cases also generally the predictions from the method given here were close to the measured values. Nomograms for the values of R_f , ζ_1 , ζ_2 , M and B may be found

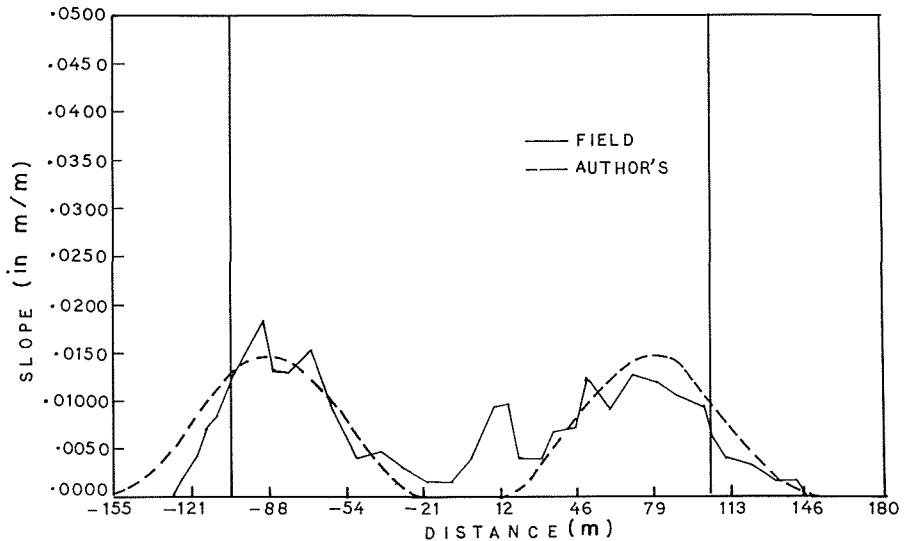


Fig. 4 Comparison of slope profiles.

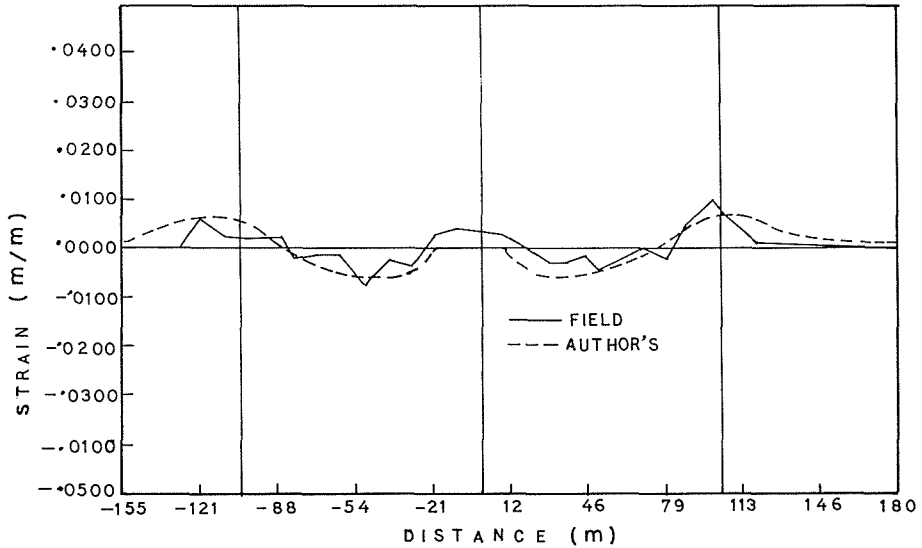


Fig. 5 Comparison of strain profiles.

for other coalfields also, to develop a suitable prediction model on the same lines. The method is simple and easy to use in the field.

REFERENCES

- Bahuguna, P. P., Srivastava A. M. C. & Saxena, N. C. (1991) A critical review of mine subsidence prediction methods. *Mining Science and Technol.* **13**, 369-382.
- Bahuguna, P. P., Bhawani Singh, Srivastava, A. M. C. & Saxena, N. C. (1993) A semi-empirical method for calculation of maximum subsidence in coal mines. *Geotechnical & Geological Engng* **11**, 249-261.
- Bahuguna, P. P. (1993) Development of mine subsidence prediction model for Indian coalfields. PhD Thesis, Dept of Civil Engng, University of Roorkee, India.
- Shankar, K. V. & Dhar, B. B. (1989) Subsidence prediction based on numerical modelling techniques. In: *Proc. Int. Symposium on Land Subsidence* (Dhanbad, India), 41-47.
- Sinha, K. P. (1979) Displacement discontinuity technique for analyzing stresses and displacements due to mining in seam deposits. PhD Thesis, Univ. of Minnesota, USA.

Consolidation settlements caused by a shield tunnel for the Taipei Mass Rapid Transit System

**JERRY JWO-RAN CHEN, TAI-YUAN HO, FU-SHENG CHEN
& CHI-SHENG CHAO**

*CECI, Department of Geotechnical Engineering, 20FL., 185 Hsin-Hai Road,
Sec. 2, Taipei, Taiwan*

Abstract This paper describes the use of elasto-plastic finite element modelling to predict the ground surface settlements due to a shield driven tunnel. Settlement readings of a case study are used to be compared with the numerical results. The predictions are mainly concerned with the consolidation settlement. The modified Cam-clay model, coupled with pore water pressure estimated using Biot's equation, is adopted to analysis the consolidation behaviour. Comparisons are presented between measured and predicted behaviour. Generally it appears that the prediction of consolidation settlement, is in acceptable agreement with the actual value.

INTRODUCTION

It is a basic requirement of tunnelling in the downtown of the city that the construction should not cause damages to any surrounding or overlying structure. In order to satisfy this requirement, the method of shield tunnelling is adopted in the construction of the Taipei Mass Rapid Transit System. In general, the ground settlement due to the construction of the shield tunnel can be divided into two stages:

- (a) *Ground (or immediate) loss*: The immediate settlement occurs as the tunnelling face is advanced under the settlement point, and the transverse array has the form of an error function curve (Peck, 1969; Schmidt, 1974; Chen, 1993). The ground loss takes place in a short time. In general, the closure of tail void is the main cause of the immediate settlement.
- (b) *Consolidation settlements*: The consolidated settlements are often associated with the removal of compressed air from a tunnel. The soil at the top of the tunnel face is compressed during the removal of compressed air from a tunnel and excess pore pressure is generated. The dissipation of the excess pore pressure leads to the consolidation settlements. The completed time of the consolidation depends on the permeability constant of the soil stratum.

Peck's approach is usually followed to evaluate the ground settlement. In consideration of the geological condition for the Taipei basin, Chen (1993) presents another approach to assess the ground loss. However, both do not reflect the consolidation settlement which can usually take a long time.

Many causes may induce the pore pressure. The immediate gap of a tunnel lining within the tailpiece of protective shield is the vital factor to result in the excess pore pressure generated and it is of major concern in this paper. A modified Cam-clay model

coupled with pore water pressure, estimated using Biot's equation (Biot, 1941), is adopted to analyse the deformation and consolidation behaviour due to the shield tunnelling. Numerical predictions of consolidation settlement are compared with the measured behaviour. Also, the possible reasons are given for the differences found.

DATA

Gap parameter

In accordance with foregoing studies (Peck, 1969; Schmidt, 1974; Chen *et al.*, 1993), the ground surface subsidence is strongly related to the buried depth, the diameter of the shield tunnel and the gap parameter (Rowe & Lo, 1983; Rowe & Kack, 1983). With the advance of the tunnelling machine, soil in front of the heading will move both radially and axially towards the face. In the shield driven tunnel, the installation of a new lining within the protective tail results in the conditions shown in (Fig. 1(a)). The annular void is equal to the difference between the diameter of the excavated surface and the lining. As the shield driven advances, the weight of lining will cause it to rest on the excavated surface as shown in (Fig. 1(b)). If the invert of the tunnel lining rests on the underlying soil then the gap parameter g is the vertical distance between the crown of the tunnel lining and the crown of the excavated surface prior to removal of the tunnel traction. It is also equal to the difference between the diameter of excavated surface (D_m) and the tunnel lining (D_l), (Rowe *et al.*, 1983), the so-called gap parameter: $g = D_m - D_l$.

Construction effects can be approximately incorporated in terms of the gap parameter. For instance, the effect of the grouting may be expected to be decrease settlements. It is equivalent to the decrease of the gap parameter which would be employed in the finite element analysis.

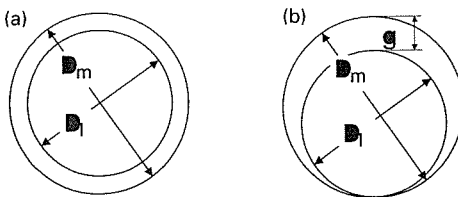


Fig. 1 Definition of gap parameter (Rowe, 1983).

Geotechnical data

The geotechnical characteristics of soils in Taipei basin have been studied for more than 25 years. A comprehensive collection of geotechnical data has been conducted by MAA in 1987 and the results of study have been published (Huang *et al.*, 1987; Cheng, 1987, 1988). In general, the Taipei basin is a tectonic basin covered with more than 200 m of Quaternary sedimentary deposits overlying the Tertiary bedrock. The Quaternary deposits can be classified into three major formations in which the Sungshan Formation is generally located at the town centre of Taipei City. Hung (1966) proposed that Sungshan Formation can be subdivided into six layers. The thickness of each sub layer

Table 1 Geotechnical properties of the Taipei basin.

Layer	Thickness (m)	E (MPa)	c (MPa)	ϕ ($^{\circ}$)	μ Poisson ratio
VI	4.5	13.2	0.0	33.6	0.35
V	10.1	29.0	-	32.5	0.3
IV	10.0	18.0	0.0	32.3	0.32
III	10.6	29.0	-	33.3	0.3
II	8.4	-	0.0	35.5	0.3
I	4.5	-	-	33.3	0.3

may vary from area to area in the basin. The site is located at the T_2 zone of Taipei basin. Typical soil properties of the T_2 zone are given in Table 1.

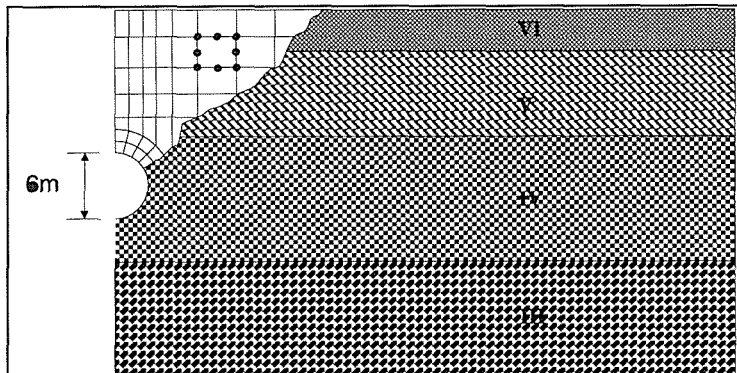
Implementation of finite element analyses

The actual behaviour of the subsoil is very complex. A simplified soil profile of Taipei basin and a typical finite element mesh used to model the behaviour of the shield driven tunnel is shown in (Fig. 2). The modified Cam-clay model coupled with Biot's equation, provide a set of equations. The finite element method will be applied to equations (1) and (2), using displacements and pore pressure as the basic parameters.

$$[K]\{u\} - [Q]\{p_w\} = \{F_1\} \quad (1)$$

$$[Q]^T\{u\} + [S]\{p_w\} + [H]\{p_w\} = \{F_2\} \quad (2)$$

$[K]$, $[Q]$, $[S]$ and $[H]$ are the matrices of stiffness, coupling, compressibility and seepage, respectively. In which,

**Fig. 2** Finite element mesh for shield driven tunnel in the Taipei basin.

$$[K] = \int_{\Omega} [B]^T [D] [B] d\Omega$$

the constitutive matrix of modified Camclay $[D]$ is employed in the analysis. $\{F_1\}$ and $\{F_2\}$ are the nodal force and flow vector, respectively; $\{u\}$ is the displacement vector and $\{p_w\}$ is the pore water pressure. The complete set of equations is used in the time-stepping procedure outlined above to determine the value $\{u\}$ and $\{p_w\}$ at any point in the time relating to their initial values. In the nonlinear cases some or all matrices $[K]$, $[Q]$, $[S]$ and $\{F_1\}$ and $\{F_2\}$ are dependent on the values of unknown, $\{u\}$ and $\{p_w\}$, so that theoretically iterations within each time step are required.

Comparisons between predicted and measured behaviour

A case study of the Taipei Rapid System was conducted by Moh & Associates Inc. (Hwang et al., 1995). Settlement readings obtained at the centre of the shield tunnel are

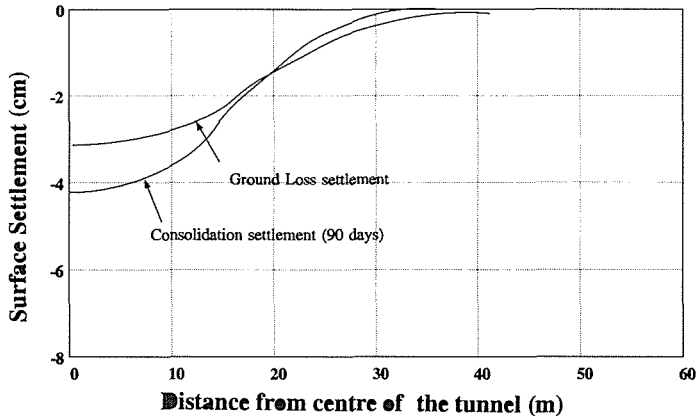


Fig. 3 Ground surface settlements in the cross-section of the tunnel against time.

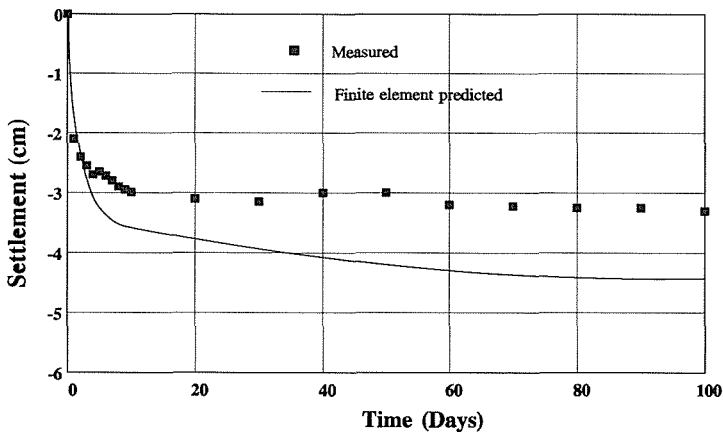


Fig. 4 Ground surface settlements in the longitudinal direction of the tunnel against time.

shown in Fig. 4. It can be seen that a 20 mm surface settlement suddenly took place as the tail passed. The prediction of the ground surface settlement in the finite element analysis is strongly related to the gap parameter, which can be obtained from the difference between the excavated surface and the tunnel. The outer diameter of the shield is 605 cm and that of the lined tunnel is 590 cm. In consideration of the condition for grouting, the gap parameter 10 cm is employed in FEM analysis. The soil parameters were chosen primarily from available published literature of Taipei basin. The effective Young's modulus E and Poisson's ratio of the various soil types for the effective finite element analysis are shown in Table 1. The coefficient of permeability for vertical flow is around $k_v = 1.0 \times 10^{-6} \text{ m s}^{-1}$. The horizontal coefficient of permeability values were assumed to be 1.5 times higher than the vertical value. Figure 3 shows the predicted settlement profile beneath the ground surface. Figure 4 compares the predicted and observed surface settlement at centre of the shield driven tunnel. The general shape of the settlement profile is predicted reasonably, but at the ground (immediate) loss, the predicted surface settlements exceed the measured values. The larger predicted values of the ground loss reflect a too big gap parameter value used in the analysis. It is also likely that the values of Young's modulus adopted in the predictions were too low. However, the amount of the consolidation deformation lies around 30% of the total settlement and shows a reasonable agreement with the measured data.

Acknowledgement The authors would like to express their sincere thanks to Dr C. C. Liang for his explanation of settlement readings and for invaluable instructions.

REFERENCES

- Biot, M. A. (1941) General theory of three-dimensional consolidation. *J. Appl. Physics* **12**, 155-164.
- Chen, J., Chao, G. & Chen, F. (1993) Ground loss caused by tunnelling for Taipei Mass Rapid Transit System. In: *Proc. 2nd Asian-Pacific Conf. on Computational Mechanics* (Sydney, Australia), 349-354.
- Cheng, T. Y. (1987) Geotechnical characteristics of Sungshan Formation within Taipei City. M.Eng. Thesis, Asian Institute of Technology, Bangkok.
- Hung, Y. J., Chin, C. T., Wong, Y. L. & Chen, M. S. (1987) Geotechnical engineering mapping of Taipei basin. In: *Proc. 9th Southeast Asian Geotechnical Conf.* (Bangkok, Thailand), vol. 1, 3-109 to 3-120.
- Hwang, R. N., Fan, C. B. & Yang, G. R. (1995) Consolidation settlement due to tunnelling. In: *South East Asian Symposium on Underground Space Development*, 79-86. Japan Tunnelling Association, Bangkok.
- Moh & Associates, Inc. (1987) Engineering properties of the soil deposits in Taipei Basin (in Chinese). *Report no. 85043, submitted to Ret-Ser Engineering Agency/Taipei, Public Works Dept., Taipei, Taiwan.*
- Peck, R. B. (1969) Deep excavations and tunnelling in soft ground. In: *Proc. 7th Int. Conf. on Soil Mechanics and Foundation Engng* (Mexico City).
- Rowe, P. K. & Lo, K. Y. (1983) A method of estimating surface settlement above tunnels constructed in soft ground. *Canad. Geotech. J.* **20**, 11-22.
- Rowe, P. K. & Kack, G. J. (1983) A theoretical examination of settlements induced by tunnelling four case histories. *Canad. Geotech. J.* **20**, 299-314.
- Schmidt, B. (1974) Prediction of settlements due to tunnelling in soil: three case histories. *RETC Proc.*
- Wu, W. T. (1979) Geotechnical characteristics of index and mechanical properties of soils in Taipei basin (in Chinese). *J. Civ. & Hydraul. Engng* **5**(4), 53-64.
- Wu, W. T. (1988) Geotechnical engineering characteristics of soils in relation to horizontal zoning in Taipei basin. *Sino-Geotechnics* **22**, 5-27.

The influence of mining induced subsidence on groundwater resources

DEREK ELSWORTH & JISHAN LIU

*Department of Mineral Engineering, Pennsylvania State University,
University Park, Pennsylvania 16802-5000, USA*

Abstract An approach is developed to quantify the impact of longwall mining on the potential disruption of groundwater resources. The underlying premise of the method is to assume that the primary mechanism causing dewatering is the development of new fractures or the dilation of existing fractures, as a result of mining induced displacements. From this assumption it is possible to evaluate the potential influence on groundwater resources by; (1) evaluating the anticipated distribution of strain that will accompany mining advance; (2) from this strain distribution, quantify the magnitude and spatial distribution of modified permeabilities; and (3) use this modified hydraulic conductivity field to define changes in the hydrologic budget, thereby defining the potential for, and extent of, any dewatering. Numerical simulation, using the finite element method, is used to both determine the mining induced distribution in strain and to complete hydrologic budget calculations with the revised conductivity field. This approach is applied to mining geometries representative of the eastern United States to define the anticipated sensitivity of these systems to changes in overburden thickness and topography. Results indicate that observed trends in dewatering behaviour may be explained on the basis of zones of contiguous extensile strain, induced within the overburden as a result of mining.

INTRODUCTION

High productivity longwall mining is becoming increasingly popular for uninterrupted mining and near horizontal coal seams. A single panel removes the entire height of the seam that is typically of the order of 1-2 m, and may reach dimensions of 300 x 3000 m in plan. The exposed seam at the face is removed by a shearer that cuts parallel to the short axis of the panel and is protected by roof supports that move with the migrating face. Despite high productivity, further development of longwall mining is hampered by the adverse environmental impact of this high recovery technique (Hasenfus *et al.*, 1990; Leavitt & Gibbens, 1992).

Surface subsidence, curvature and fracturing damages on- and in-ground structures and disrupts surface drainage. In the Appalachian Mountains, and elsewhere, underground mining by longwall (full extraction) methods commonly affects groundwater resources, but the severity of impact remains difficult to determine *a priori*. Consequently, accurately determining the probable hydrologic consequences of mining

on groundwater resources is a critical issue in both courting public acceptance of proposed mining ventures, and in meeting legal requirements.

Subsidence induced ground displacements modify the hydrologic regime, may drain proximal water supplies (Ciffeli & Rauch, 1986; Walker, 1986) and affect water quality through accelerated pyrite oxidation, acidification and associated heavy metal uptake. Determining the potential for any of these mechanisms to evolve is of clear practical importance. Rationalization of this problem, however, has been made difficult by the seemingly random and highly variable responses observed in undermined aquifers. Our approach has been to develop data constrained numerical models that couple the effects of deformation into anticipated changes in hydraulic conductivity (Elsworth *et al.*, 1994; Liu *et al.*, 1995; Matetic *et al.*, 1995), that in turn prescribe the effect on the groundwater budget and the potential for acidification. Results are promising in that the full variability of observed responses are explicable purely in terms of deterministic physical models.

DATA

Physical representation

The potential impact of longwall mining on groundwater resources may be evaluated through application of a straightforward procedure. This entails defining the magnitude and distribution of the mining-induced strain field throughout the surrounding strata. This evaluation must incorporate the failure characteristics of the material when subjected to large strains, and may be accommodated through finite element modelling that incorporates strain softening in tension. This enables observed subsidence profiles to be closely replicated. With the strain field determined, the change in hydraulic conductivity field may be evaluated if the pre-mining distribution is also known, together with some rudimentary knowledge of fracture spacing and mechanical properties. These data are typically the most difficult to obtain (Girrens & Anderson, 1981), but may be estimated within reasonable tolerances. The post-mining hydraulic conductivity field may be determined directly from the evaluated strain field through the relation (Ouyang & Elsworth, 1993):

$$\frac{K_x}{K_{x_0}} = \left[1 + \frac{b + s(1 - R_m)}{b} \Delta \varepsilon_y \right]^3 \quad (1)$$

where K_x and K_{x_0} are the pre- and post-mining hydraulic conductivity magnitudes in the x direction, b is the initial fracture aperture (determined from the pre-mining hydraulic conductivity), s is the fracture spacing, R_m is an equivalent mechanical modulus reduction factor, and the mining-induced strain in the y direction is defined as $\Delta \varepsilon_y$. A similar relation exists for conductivities in the y and z directions. The modulus reduction factor, R_m , effectively partitions the induced strain field between the dilation of fractures and that of the intact rock. The induced conductivity change is largest for $R_m = 0$ where the body strain is applied exclusively in dilating or compressing the fractures.

This representation of changes in hydraulic conductivities is the critical link in the analysis since it enables the influence of subsidence on the groundwater flow system to

be quantified. With the revised conductivity field determined, any modification to the flow system may be quantified through a forward analysis, again using a finite element model. The solid deformation and flow models are coupled through the influence of the strain field in defining the changed conductivity field. In defining the form of the induced strain field, care must be taken to correctly represent the potential for failure in the overlying strata. Correspondingly, a nonlinear stress-strain relation is used to represent the weakness of the material in tension.

Evaluation of groundwater effect

The methodology described in the preceding has been applied to a study of the potential for dewatering around longwall panels (Liu, 1993). A simple sectional geometry is assumed (Fig. 1) and the influence of mining beneath plateau, hilltop and valley base environments is examined. For the geometries the long axis of the 200 m wide panel strikes, parallel to the slope and depth of the 1.5 m thick seam, is varied between 100 and 300 m. Pre-mining hydraulic conductivities of $3 \times 10^{-5} \text{ m s}^{-1}$ are assumed, together with a mean fracture spacing of 0.3 m.

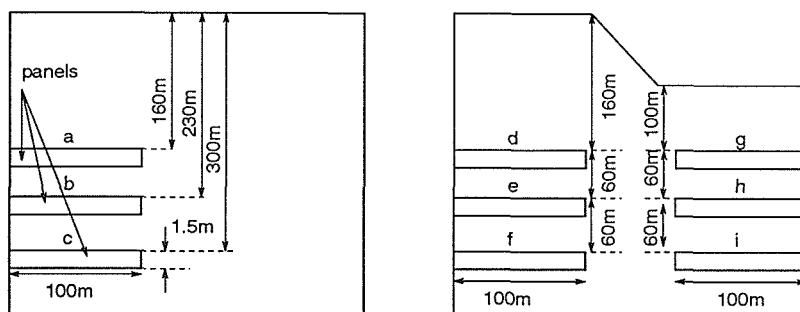


Fig. 1 Selected two-dimensional geometry to represent (a) sub-plateau and (b) sub-hilltop and sub-valley settings. Long axis of panel strikes parallel to strike of slope.

From the prescribed geometric information, the influence of subsidence on the groundwater system may be evaluated for these specific conditions. The relative changes in the conductivity ratio, K/K_0 , will vary with the choice of parameters, however the location of the null influence contour, $K/K_0 = 1$, is invariant. Correspondingly, it is the location and extent of the zones of conductivity enhancement ($K/K_0 > 1$) that controls the potential for aquifer dewatering.

Definition of hydraulic effect

The changes in hydraulic conductivities defined by the strain field induced within the overburden are evaluated. Since change in water supply will be most influenced where conductivities are increased, the most obvious index to define zones of potential hydraulic impact is the ratio of post-mining to pre-mining hydraulic conductivity (K/K_0).

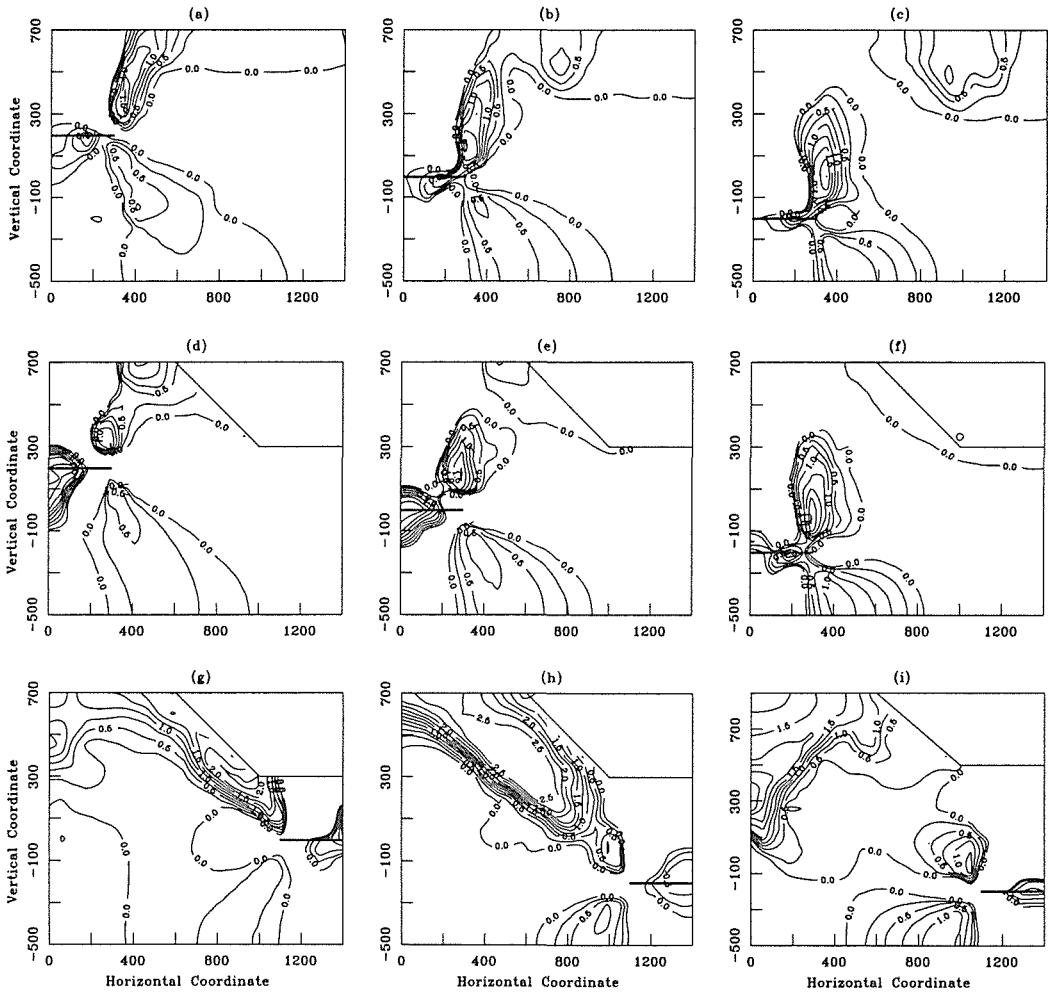


Fig. 2 Contours of ratio of post-mining vertical hydraulic conductivity to pre-mining conductivity ($\log(K_y/K_0)$). The null influence contour is represented as a log ratio of zero.

These ratios are reported for changes in vertical and horizontal conductivities in the nine distinct mining geometries in Figs 2 and 3, respectively.

Apparent from these figures is that the main influence on the hydraulic conductivity is both close to the panel and at the ground surface. Three distinct zones develop, namely gravitational detachment above the panel, shear failure in the abutment region and in the near surface zone. The zones of conductivity change are predominantly above panel elevation, but also penetrate to displacements induced below the panel. These sub-panel displacements are manifest as floor heave in the panel and as abutment shear failure. Changes in conductivity resulting from elastic (rather than failure *per se*) displacements diminish rapidly with depth and away from the panel. Based on these parametric results, the conceptualized representations of overburden hydraulic response to longwall mining in these three mining environments are presented in the following.

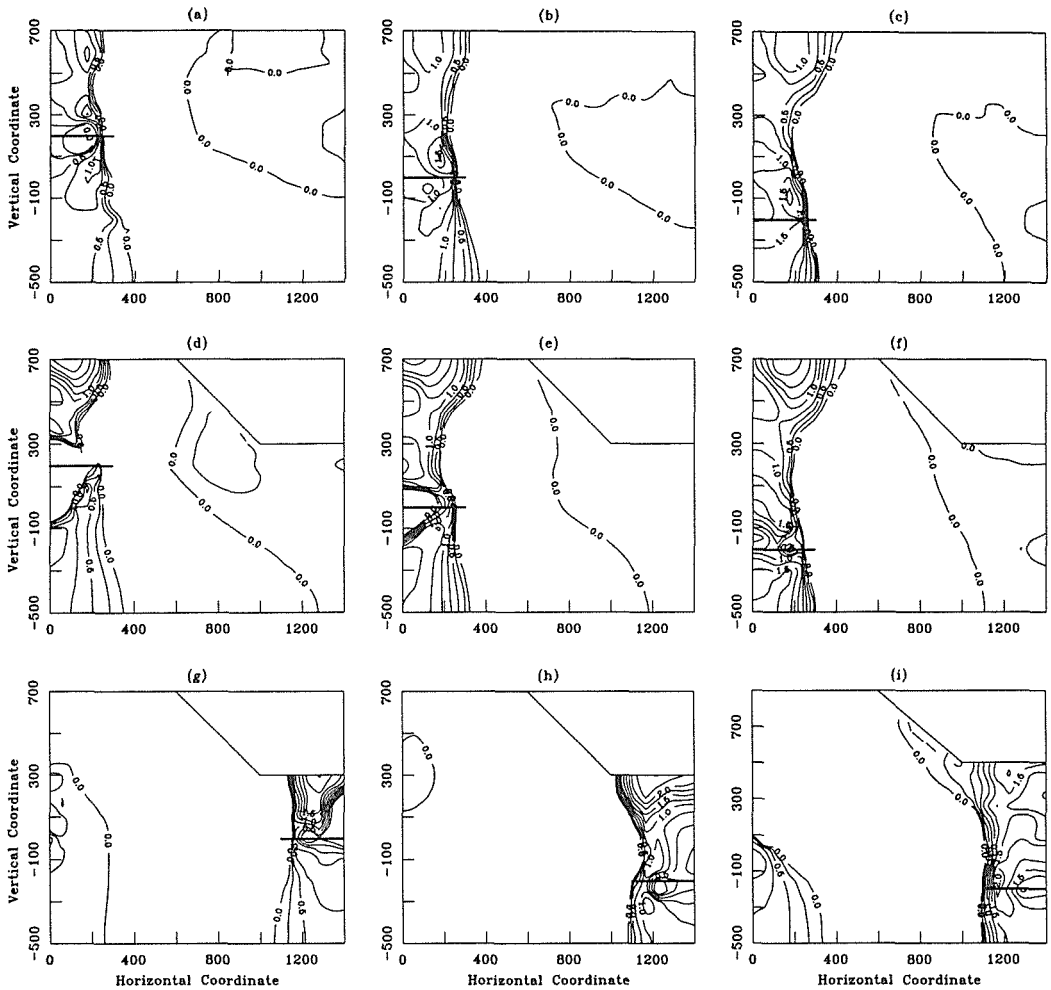


Fig. 3 Contours of ratio of post-mining horizontal hydraulic conductivity to pre-mining conductivity ($\log(K_x/K_0)$). The null influence contour is represented as a log ratio of zero.

Conceptual models representing idealized overburden hydraulic response to longwall mining are illustrated in Figs 4(a) through (c) describing zones of increased conductivity. The enhancement of overburden hydraulic conductivity can be represented by three distinct zones, namely, Zone 1: the supra-panel zone, suffering gravitational detachment, Zone 2: the abutment shear zone, and Zone 3: the surface zone, as illustrated in Fig. 4. The responses of these zones are quite differently in the three different mining settings. The conceptual models of the overburden hydraulic response to longwall mining in the three mining environments are presented in detail as follows.

The extent of the zones of potential hydraulic impact within the overburden is controlled both by mining geometry and by topography. In evaluating the true hydraulic effect, groundwater recharge and transmissive characteristics must be considered together to give a definitive evaluation of dewatering potential. However, in the absence

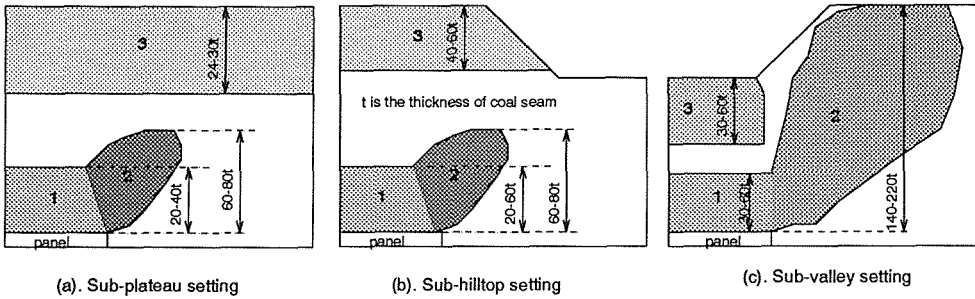


Fig. 4 Conceptual models of overburden hydraulic response to longwall mining. Zone 1 is the supra-panel gravitational detachment zone, Zone 2 is the abutment zone of shear failure and Zone 3 is the surface zone. All zones register conductivity enhancement. Sub-panel enhancements are neglected in this depiction.

of this information, some qualified evaluation of dewatering potential may be estimated. For the same geometric setting, the impacts of longwall mining on water supplies are mainly controlled by topography.

Sub-plateau mining environment

The conceptual model of the overburden hydraulic response to longwall mining in the sub-plateau mining environment is illustrated in Fig. 4(a). The average heights of Zone 1, Zone 2, and Zone 3 of hydraulic conductivity enhancement are $28t$, $73t$, and $33t$ (t is the thickness of coal seam, taken as 1.5 m in this example), respectively. The enhancement of the hydraulic conductivity in Zone 1 is in the horizontal direction (as a result of vertical strains) as shown in Figs 3(a) through (c). The enhancement of the hydraulic conductivity in Zone 2 is predominantly in the vertical direction as shown in Figs 2(a) through (c). The enhancement of the hydraulic conductivity in Zone 3 is predominantly in the horizontal direction as shown in Figs 3(a) through (c).

Sub-hilltop mining environment

The conceptual model of the overburden hydraulic response to longwall mining in the sub-hilltop mining environment is illustrated in Fig. 4(b). The average heights of Zone 1, Zone 2, and Zone 3 of the hydraulic conductivity enhancement are $35t$, $73t$, and $50t$, respectively. The enhancement of the hydraulic conductivity in Zone 1 is both in the vertical and horizontal directions as shown in Figs 2(d) through (f) and Figs 3(d) through (f). The enhancement of the hydraulic conductivity in Zone 2 is predominantly in the vertical direction as shown in Figs 2(d) through (f). The enhancement of the hydraulic conductivity in Zone 3 is predominantly in the horizontal direction as shown in Figs 3(d) through (f).

Sub-valley mining environment

The conceptual model of the overburden hydraulic response to longwall mining in the sub-valley mining environment is illustrated in Fig. 4(c). In this case Zone 2, the lateral

zone of hydraulic conductivity enhancement spreads directly into the upland area. The average heights of Zone 1, Zone 2, and Zone 3 of hydraulic conductivity enhancement are $60t$, $180t$, and $60t$, respectively. The enhancement of hydraulic conductivity in Zone 1 is both in the horizontal and vertical directions as shown in Figs 2(g) through 2(i) and Figs 3(g) through (i). The enhancement of hydraulic conductivity in Zone 2 is predominantly in the vertical direction as shown in Figs 2(g) through 2(i). The enhancement of the hydraulic conductivity in Zone 3 is predominantly in the horizontal direction as shown in Figs 3(g) through (i).

CONCLUSIONS

Application of this approach is beginning to separate the most important variables from the maze of factors that may influence dewatering potential. For instance, the topographic setting has been shown to be important in defining both the hydraulic base level of the groundwater system and in defining the potential presence of existing fracture zones that will aid dewatering. Perhaps as important, however, topography has been shown to play a pivotal role in determining the strain field that evolves around a mined panel, and consequently indexes the severity of impact. Correspondingly, groundwater resources located in valley bases remain the most secure, and hilltop resources the least, with potential safe mining depths being potentially defined.

Results indicate that observed trends in dewatering behaviour may be explained on the basis of zones of contiguous extensile strain, induced within the overburden as a result of mining. The systems are more sensitive to the sense of mining induced strain (extensile versus compressional) rather than the absolute magnitude. This is due to the extreme sensitivity of hydraulic conductivity to even relatively modest changes in extensile strain. Correspondingly, observational rules developed to predict the extent and location of potential aquifer dewatering are confirmed and may be extended to evaluate the potential long term influence of mining on the groundwater system.

Acknowledgement This work has been supported by the National Science Foundation under Grant no. MSS-9209059 and by the National Mine Land Reclamation Center under Grant no. CO 388026. This support is gratefully acknowledged.

REFERENCES

- Ciffeli, R. C. & Rauch, H. W. (1986) Dewatering effects from selected underground coal mines in North-central West Virginia. In: *Proc. 2nd Workshop on Surface Subsidence due to Underground Mining* (ed. by S. S. Peng) (June 1986), 249-263.
- Elsworth, D., Liu, J. & Ouyang, Z. (1994) Some approaches to determine the influence of long wall mining on groundwater resources. In: *Int. Mine Drainage Conf.* (Pittsburgh, Pennsylvania, April 1994), 172-179.
- Girrens, S. P. & Anderson, C. A. (1981) Numerical prediction of subsidence with coupled geomechanical – hydrological modelling. In: *Proc. Workshop on Surface Subsidence due to Underground Mining* (ed. by S. S. Peng) (Morgantown, West Virginia, November-December 1981), vol. 2, 63-72.
- Hasenfus, G. J., Johnson, K. L. & Su, D. H. W. (1990) A hydrogeomechanical study of overburden aquifer response to longwall mining. In: *Proc. 7th International Conference on Ground Control in Mining* (ed. by S. S. Peng), 149-162.
- Leavitt, B. R. & Gibbens, J. F. (1992) Effects of longwall coal mining on rural water supplies and stress relief fracture flow systems. In: *Proc. of 3rd Subsidence Workshop due to Underground Mining* (June 1992), 228-236.
- Liu, J. (1993) Topographic influence of longwall mining on groundwater supplies. MS thesis, Department of Mineral Engineering, The Pennsylvania State University, University Park, Pennsylvania.

- Liu, J., Elsworth, D. & Matetic, R. J. (1995) Evaluation of the post-mining groundwater regime following longwall mining. *Wat. Resour. Res.*, submitted for publication.
- Matetic, R. J., Liu, J. & Elsworth, D. (1995) Modelling the effects of longwall mining on the groundwater system. *US Bureau of Mines, R.I. 9516*.
- National Coal Board (UK) (1966) *Subsidence Engineer's Handbook*. National Coal Board, UK.
- Ouyang, Z. & Elsworth, D. (1993) Evaluation of groundwater flow into mined panels. *Int. J. Rock Mech. Min. Sci. & Geomech. Abstr.* 30(2), 71-79.
- Walker, J. S. (1988) Case study of the effects of longwall mining induced subsidence on shallow ground water sources in the Northern Appalachian Coalfield. R19198, *US Bureau of Mines, US Dept of the Interior*, 17.

Ground and building settlement due to tunnelling in Hong Kong

R. A. FORTH

University of Newcastle upon Tyne, Department of Civil Engineering, Newcastle upon Tyne NE1 7RU, UK

C. B. B. THORLEY

Gutteridge Haskins and Davey Pty Ltd, 15 Astor Terrace, Brisbane, Queensland 4000, Australia

Abstract Extensive monitoring of the ground and buildings affected by the construction of the Island Line (ISL) of the Mass Transit Railway (MTR) in Hong Kong was carried out between 1982 and 1986. Predictions were based on the Peck method (Peck, 1969) and the monitoring enabled a comparison of prediction and performance to be made. The results suggested that tunnels in completely weathered granite behaved as in Peck's sands (cohesive granular soils) whilst the shallow tunnels in colluvium, alluvium or marine clays behaved like Peck's soft clay. This paper reports the results of some of the monitoring and provides a tunnelling settlement estimate method suitable for Hong Kong.

INTRODUCTION

Between 1982 and 1986 the Island Line (ISL) of the Mass Transit Railway (MTR) was constructed along the northern part of Hong Kong Island from Chai Wan in the east to Sheung Wan in the west. The alignment followed some of the busiest roads in this densely populated city and in order to minimize disruption to normal life, a decision was made to construct the bulk of the route underground by tunnelling methods.

Twin running tunnels, 6 m in diameter, and station tunnels, 8 m in diameter, were constructed using a variety of methods, principally tunnelling shields and compressed air in soft ground, hand mining methods in mixed ground, and conventional drill and blast techniques in rock. The station tunnels were connected to 12 new station concourses by adits. The concourses were excavations up to 35 m deep, often constructed by diaphragm wall techniques.

An extensive site investigation carried out before the commencement of construction revealed a geological succession consisting of a variable thickness of reclamation fill overlying marine deposits, alluvium, colluvium and weathered granite, before encountering fresh granite. A typical geological profile is shown in Fig. 1.

BUILDING CLASSIFICATION AND MONITORING

In most cases tunnelling and concourse excavations were carried out in very close

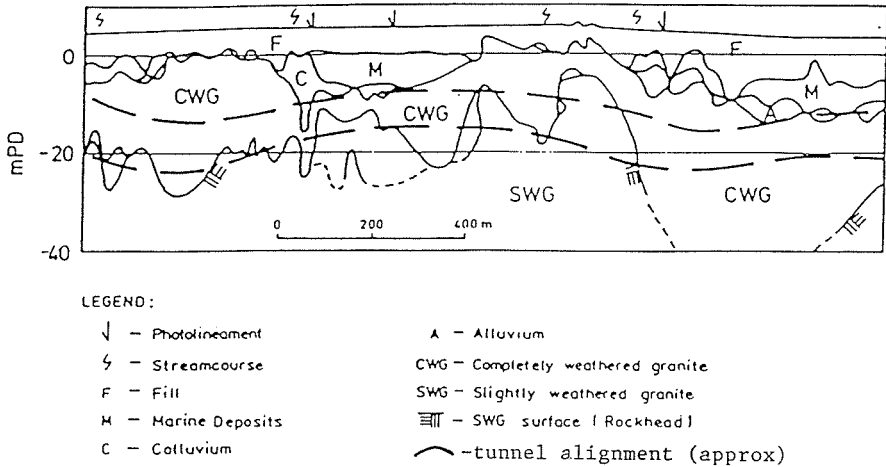


Fig. 1 Typical geological profile.

proximity to buildings. As a result a comprehensive building monitoring programme was carried out. Buildings were classified prior to construction of the ISL according to age and condition, and predictions were made of settlement and distortion, based on the Peck method (Peck, 1969), and hence structural damage. In a few cases buildings likely to have been severely damaged were demolished, although this was only carried out in exceptional circumstances on very old buildings on shallow footings.

The building classification adopted by the MTR Corporation is shown at Table 1. The condition of each structure was also noted on a four point scale.

Table 1 Building classification adopted by the MTR Corporation.

Type	Age	Size	Foundations	Structure
A	pre World War II	<4 storeys	Spread footings or wooden piles?	Mainly brick or masonry load bearing walls
B	late 1940s to early 1960s	4-6 storeys	Spread footings or timber piles?	Often built in terraces using cross-wall infill to a r.c. frame.
C	early 1950s to mid 1960s	>6 storeys	Usually concrete piles founded in or on weathered granite	r.c. framed buildings
D	since mid 1960s	>15 storeys	Deep concrete or driven piles to weathered or fresh rock	r.c. framed buildings

TUNNELLING EFFECTS

Settlement data

Figures 2 and 3 present the ground and building settlements recorded above the centreline of a 5.8 m diameter tunnel constructed using a shield and compressed air. The

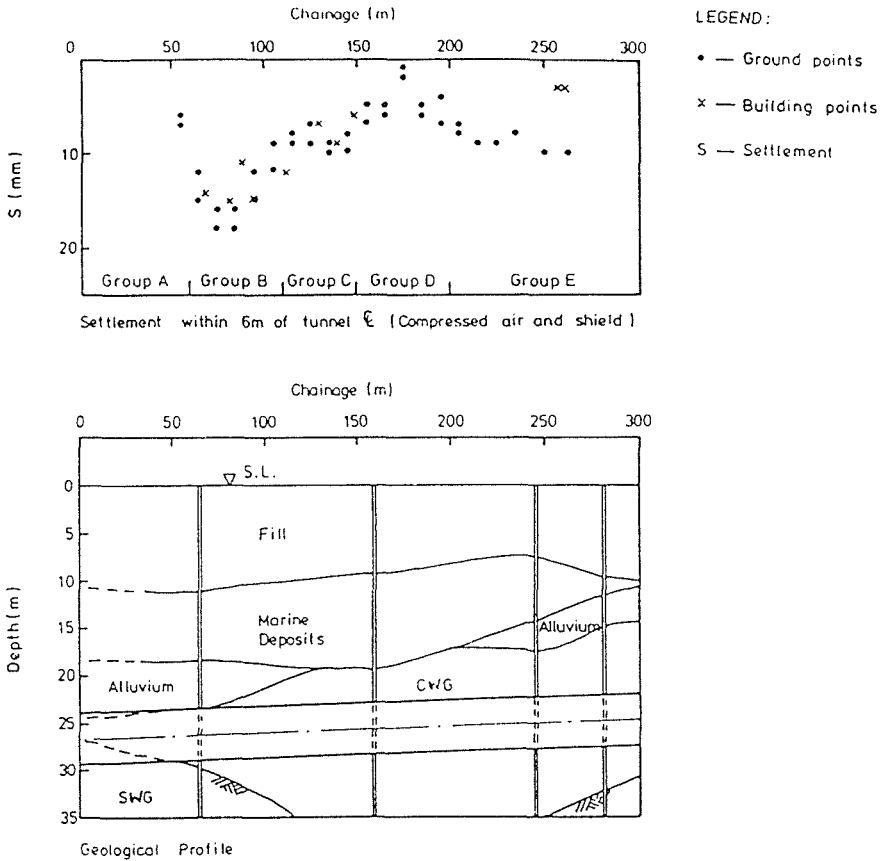


Fig. 2 Settlement and geological profile vs. shield drive.

settlements are due to tunnelling only and were measured prior to decompression of the drive. A geological profile determined from site investigation boreholes is also shown in Fig. 2. The data are related where possible to site investigation information as it is on this that the original designs and estimates are based. Noticeably from the chainage-settlement plot in Fig. 2, the settlements appear to follow a definite trend which is dependent on their location. Accordingly the settlements have been separated into Groups A to E according to their relative magnitudes and location. These five locations are shown as cross-sections in Fig. 3 with all building and ground points included for each group. The curves shown in Fig. 3 represent gaussian curves of best fit calculated by the method of least squares.

Figure 4 shows for a 5.8 m diameter tunnel (shield and compressed air) the building and adjacent ground settlement resulting from the driving of the tunnel below the buildings central piles. The excavation of the tunnel involved cutting off several of the pile-tips below the central raft. The settlement shown is prior to decompression. Preventive works to the building foundation included grouting of the fill strata below the central pile cap and structural extension of the cap itself.

Figure 5 presents a time-settlement plot of three ground points above the centreline of a 6.3 m wide horseshoe-shaped tunnel constructed using NATM methods. Support

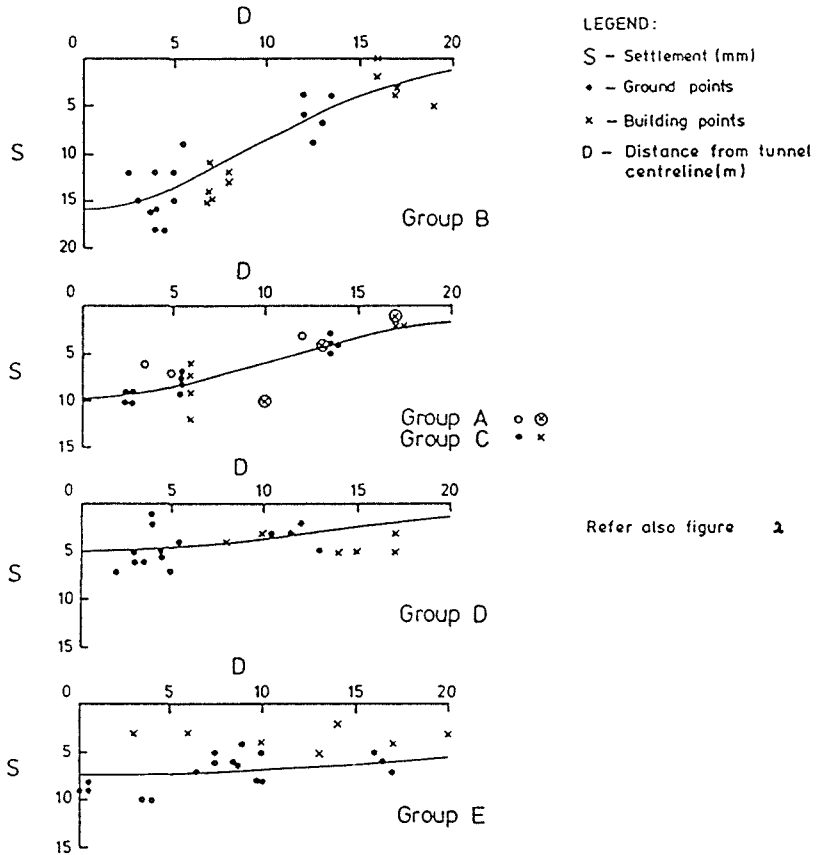
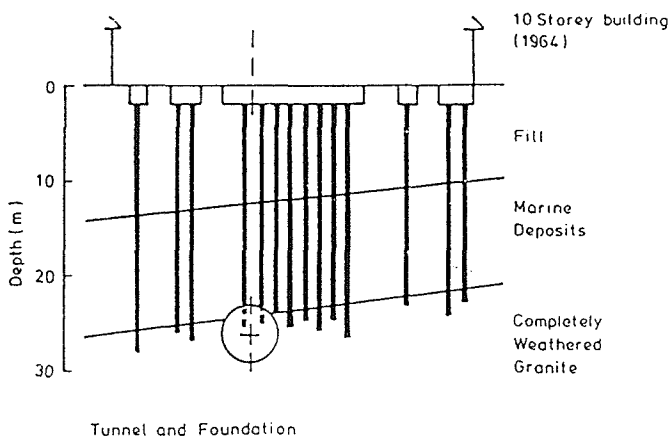
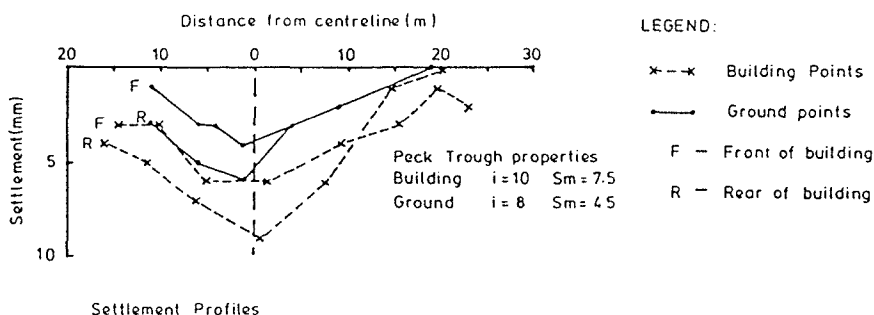


Fig. 3 Settlement profiles vs. shield drive.

to the tunnel was steel-arch ribs and shotcrete and the drive was advanced using a top ring cut and bench. The geology of the face ranged from marine deposits overlying rock. The excavation was undertaken in free air through an annulus of grouted ground. Cross-sections showing settlement and distance from the tunnel centreline for each of the three locations are also included in Fig. 5. The best fit gaussian curves are shown for the data points at each section. Figure 6 shows a summary of the settlement data from the same drive with plots of chainage against maximum settlement (S_m), crown settlement measured at a point on the crown of the arch ribs after installation (c), and percentage equivalent face loss (shown as $A\%$). The calculated i values expressed as a function of tunnel depth and "diameter" are also shown in Fig. 6 plotted in the form proposed by Peck (1969).

Percentage equivalent face loss is the area of the surface trough expressed as a percentage of the tunnel cross-sectional area. This parameter is more aptly called the tunnel settlement ratio by Cater *et al.* (1984) as it represents a relative area rather than a specific loss into the tunnel. For the purpose of this paper, however, it is referred to as the percentage face loss (EFL) for reasons of consistency.

The tunnelling settlement and decompression settlement due to two 5.8 m diameter tunnels constructed by hand mining under compressed air is presented in Fig. 7. Both



Note - Fill strata grouted and pile cap above tunnel extended

Fig. 4 Building settlement profile vs. shield drive.

ground and building data are included although no ground settlement data due to tunnelling alone were available. The best fit gaussian curve for the building points is included and in addition a best fit logarithmic curve for the decompression settlements. Published data to date (Cater *et al.*, 1984) have suggested that decompression settlement, due to the migration of pore water back towards the tunnel on the release of the air pressures, forms a wider trough than the pure tunnelling settlement trough. No theory has been published to indicate a means of estimating the likely magnitudes or width of this trough in Hong Kong conditions. The reason for this is that all piezometers are backfilled prior to compressed air work to prevent water ingress to, and air escape from, the tunnel and consequently the behaviour of the groundwater during compressed air tunnelling is unknown. It would seem logical, however, that the settlement on decompression is due to groundwater movement towards the tunnel and therefore it may take the form of a classic dewatering curve which is generally a logarithmic function relating distance to head. Obviously the air pressure behaviour and consequent pore water migration is dependent on the specific geology and soil permeability of the tunnel alignment as shown in the data presented by Cater *et al.* (1984). However, the logarithmic curves in Fig. 7 show a reasonable agreement with the data. (The two curves

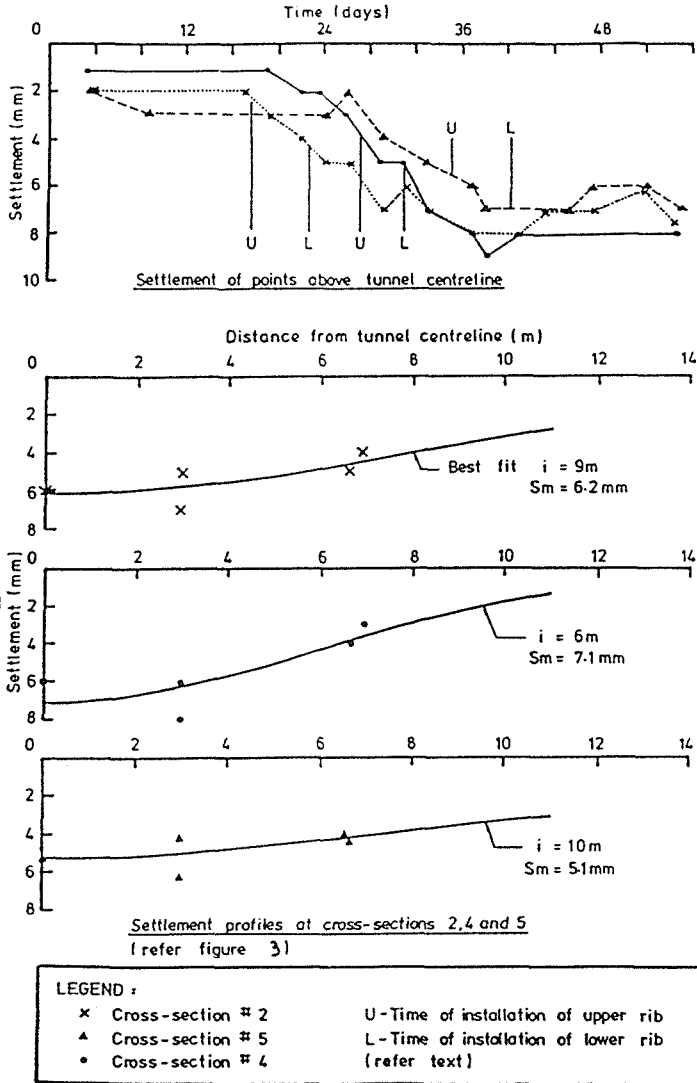


Fig. 5 Settlement development vs. NATM drive.

for each of the tunnels have been visually aligned at the centre-lines, as is the case with a normal symmetric dewatering profile.)

ANALYSIS OF GROUND SETTLEMENT DATA

Forms of magnitude of settlement

The data presented in Figs 2 to 7 represent the measured effects of various types of tunnelling on both ground and buildings. The estimates of settlement for these tunnels were originally based on the methods proposed by Peck (1969) with the parameters

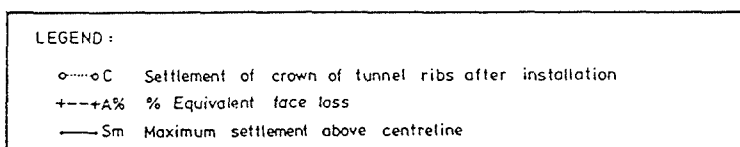
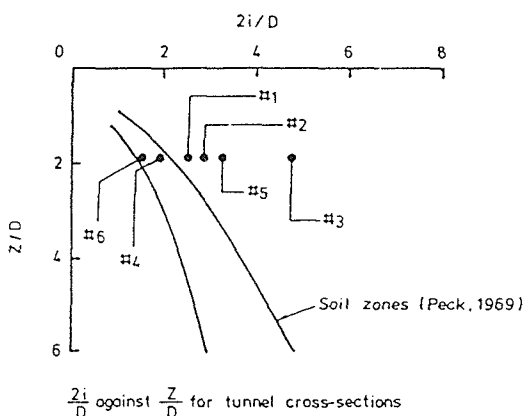
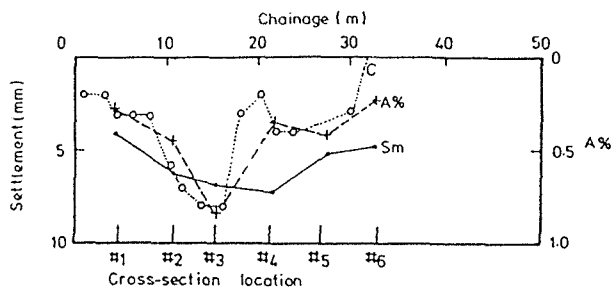


Fig. 6 Settlement summary vs. NATM drive.

assumed for Hong Kong conditions based on the previous experience of the MTRC and their consultants. Cater *et al.* (1984) have updated and refined these methods of estimation and proposed values of tunnelling settlement ratio (equivalent face loss) and values of i based on the tunnelling undertaken on the ISL. The relevant findings presented in their paper are:

- the proposal of values of "EFL" or "settlement ratio" which are related to the face conditions (degree of support to a face and crown is dependent on both the overall tunnelling method and the face geology and then surface trough area is suggested by Peck to be governed by this);
- the proposal of a value of i for Hong Kong to be equal to the tunnel depth divided by 2;
- highlighting of the phenomena of decompression settlement as distinct from tunnelling settlement and the provision of data to show the shape of the trough after each stage.

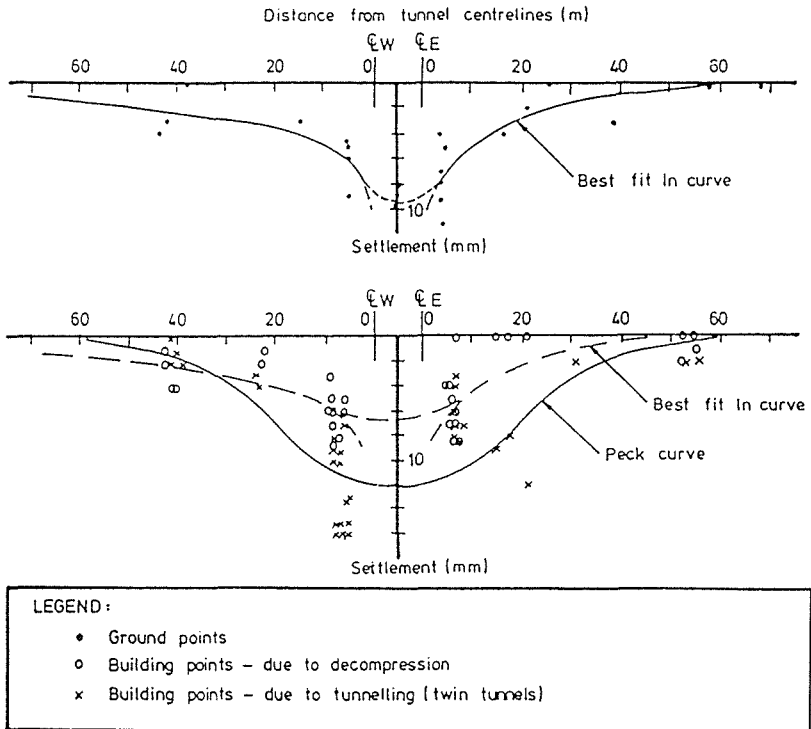


Fig. 7 Decompression data – ground and buildings.

Considering the data in Figs 2 to 7, the initial conclusion is that the Peck method is indeed applicable to soft-ground tunnelling in Hong Kong. Figures 3 and 5 show reasonable agreement between the settlement data and a curve of best fit based on Peck's gaussian error curve. (In Fig. 3 the Group E curve is appreciably wider than for the other groups and this often indicates some dewatering effects during tunnelling or possibly the effects of outside sites.) Also the cross-sectional areas of the troughs presented agree with the values reported by Cater and also those used for estimating to date. The curves in Fig. 3 represent equivalent face losses (EFL) of 0.6% to 1.9% which agree with the range of 0% to 3.2% proposed by Cater for shield tunnels in both alluvium and CWG. Similarly, the curves in Fig. 5 represent EFLs of 0.2% to 0.8% compared to the range of 0 to 1% reported (although for compressed air). The twin-tunnel data in Fig. 7 has an EFL of 1.8, or 0.9% per tunnel, compared to the published range for a NATM driven tunnel under air of 0 to 1% or a shield driven tunnel under air of 0 to 3.2%. Therefore it would seem reasonable to assume that Peck curve describes the form of the settlement trough above tunnels in Hong Kong soils and that the area of this trough can be related to the data published to date.

Surface trough parameters

To obtain a surface trough's shape, given its area, two parameters need to be defined; maximum settlement (S_m) and width (i). As previously described, Peck proposes the

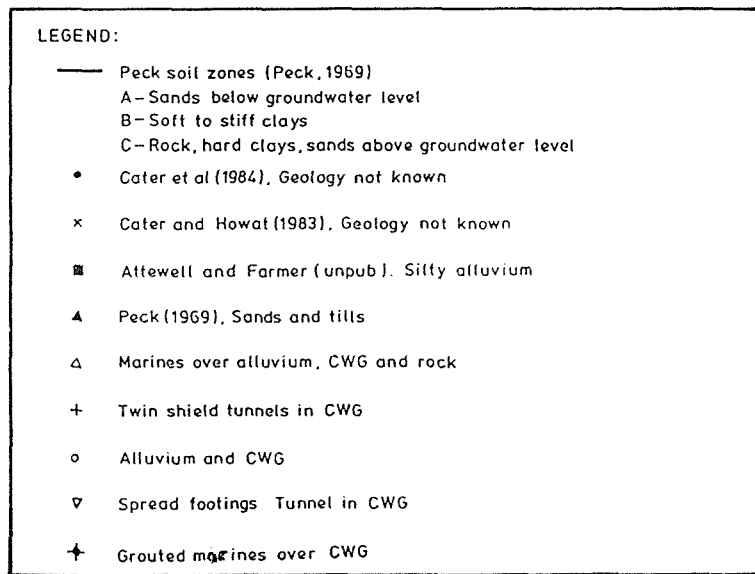
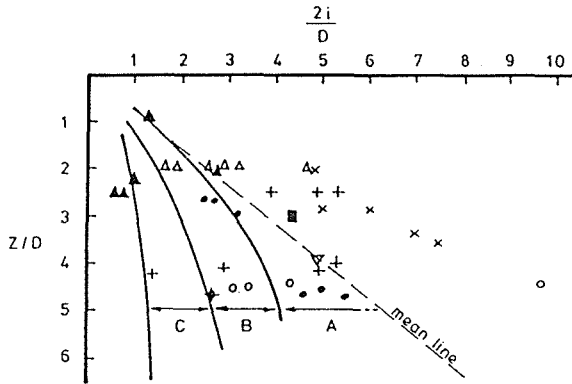


Fig. 8 *i* values for Hong Kong conditions.

parameter *i* to be dependent on soil conditions and tunnel size and depth. Given this relationship, the maximum settlement is therefore interrelated to trough area and is dependent on tunnelling methods and the degree of support. This relationship of equivalent face loss or trough area to tunnelling methods is described above and appears to be now reasonably well defined for Hong Kong conditions (Cater *et al.*, 1984). However along any tunnel drive the likely EFL will change with changing face conditions, as is evidenced by the chainage-settlement plots in Figs 2 and 6. The EFL of Group B points in Fig. 2 (refer also to Fig. 3) is 1.4% where the face intersects both alluvial and CWG material. In the group C and D areas, however, the EFL is 0.6% to 0.9% (Fig. 3) as the tunnel progresses through CWG only. Similarly, in Fig. 6 the plot of trough area (shown as A%) follows the crown settlement plot (C) along the tunnel drive but only approximately follows the maximum settlement trend (*Sm*). This is significant in that a direct measure of tunnel crown movement (albeit only after the support measure is installed) can be related to EFL. The variation compared to the

maximum settlement is because of the variation in i values at each cross section as shown in the $2i$ vs. Z plot, also in Fig. 6.

Width of surface trough

The determination of the value of i for Hong Kong conditions is less well documented. Cater *et al.* (1984) have proposed that i is equal to half the tunnel depth (Z). An earlier proposal (Howat & Cater, 1983) was that i was equal to depth Z , although in the latter paper by Cater *et al.* (1984) they note that changing geology and possibly dewatering effects may have contributed to the wider troughs. Until now it has been generally considered that Hong Kong conditions approximated to the Peck "sands below groundwater level" zone (Peck, 1969). The i equal to half the depth line described above partly follows this Peck limit. A set relationship, however, between i and Z assumes that the stress-strain relationship causing the location of the troughs point of inflexion is the same for all soil types encountered in Hong Kong. It is thought that the location of the point of inflexion i (Mair, 1983) and therefore the development of this strain pattern depends on the soil properties and stress distributions around the tunnel face and crown. It is possible therefore that for any given depth Z , the i value should be chosen depending on the face properties and their classification according to Peck's general soil types. To address this point Fig. 2 shows a plot of data from Figs 2 to 7 and also published data relating depth Z to width i . The Peck soil zones are included for reference. The mean line represents a line of best fit for all the points derived in Hong Kong. This line corresponds to an i value equal to 0.6 tunnel depth and in that respect compares well with previously published data (Rankin, 1988; Mair *et al.*, 1993). However, for individual drives there appears to be a spread as evidenced by the plot in Fig. 6. This tunnel was of a constant depth and the gaussian curves of best fit showed varying i values along its length. Similarly, i values at specific sections of the drive represented by Fig. 3, and i values from a drive of twin tunnels in CWG all show a spread at a constant tunnel depth (Fig. 7). This spread may be attributed to the spread of the original settlement data or it may indicate that, because of soil properties, there is a variation in i for a constant depth tunnel. In this latter case Hong Kong soils will not exhibit a single i , Z relationship but a band of values more in keeping with Peck's bands for differing soil types. The data in Fig. 7 do not readily group themselves into classifications such as Marine soils and weathered granite soils. However, in many instances this is because of mixed soil conditions at the face. Furthermore, for a typical Hong Kong reclaimed land profile in CWG, whereas shallower tunnels will in many areas be located in the fill/marines/colluvium/ alluvium strata (Fig. 1). Therefore a shallow tunnel, say Z/D less than 2 or 3, and with i equal to half the depth, will have an i value of 4 to 9. This places the points right on the limit between Peck's submerged sands and soft clays. A deeper tunnel, however, with Z/D equal to say 5 or more, will have for i equal to half the depth, an i value of 15, which is well within the submerged sands zone defined by Peck. A unique relationship for Hong Kong may, therefore, be a result of the stratigraphy in that for the deeper CWG tunnels the settlement behaviour is more like Peck's sands (also described as cohesive granular soils) and for the shallow depositional strata tunnels the settlement behaviour is closer to Peck's soft clays behaviour. Without additional well-documented case histories it is difficult to further

determine the relationships for Hong Kong soils. The relationship by Cater *et al.* (1984) and the mean relationship shown in Fig. 7 agree reasonably well, however, keeping in mind the usual scatter of settlement points above a tunnel (Fig. 3), this line of i equal to half the tunnel depth should be considered reasonable for estimating purposes in Hong Kong soils. Data do indicate however that the limits could be from i equal to $0.4Z$ to i equal to Z .

Building settlement

The previous sections consider mainly the ground settlement above a tunnel. Settlement of buildings is influenced not only by ground surface movement but also by ground movement at the location of the foundations, be they piles or footings. Building data are shown in Figs 3, 4 and 7. From Fig. 3 it is evident that generally building settlements follow ground settlements. The exception is for the wider trough shown as Group E. In all cases the buildings shown are on piles founded above or close to the tunnel level. No relationship appears to exist between foundation depth and settlement for this drive except that for all buildings the magnitude and form of settlement can be said to approximate to ground settlement. It is possible that the lower building settlements recorded for Group E may be due to a larger i value at this location. If this is due to dewatering effects the stresses causing settlement may have less effect on a piled building than on the ground, especially if the dewatering was less at the pile founding level.

Figure 4 shows building and ground settlement due to a shield tunnel intersecting the buildings piles. It is of interest that building settlement and ground settlement troughs are approximately the same width but with the building suffering approximately 70% greater settlement at the centre-line. This suggests that the ground movement at tunnel level and just above may be greater than indicated by surface movement and therefore the downward force extended on the piles, or the pile-tip movement, results in a larger settlement. The similar width troughs may be a result of similar development of strain patterns close to the tunnel as at the surface, which suggests that the bands of maximum strain achieve their maximum width in the area just above the tunnel, or alternatively the building has redistributed some load across its width. Figure 7 shows ground and building settlements due to decompression. No ground data due to tunnelling were available for this drive so this aspect cannot be studied. On decompression, however, it is noted that generally, within the limits of the data, the building movement approximated to ground movement. There again appears no definite relationship to foundation level for these data. The several points showing zero decompression adjacent the E tunnel axis (Fig. 7) were in a zone where annulus grouting had been carried out around the tunnel and therefore decompression or dewatering effects were possibly prevented.

CONCLUSIONS

From the data analysed, and the information and proposed methods available from other publications, a tunnelling settlement estimate method that appears suitable for Hong Kong conditions is as follows:

- For a given tunnelling method and likely face conditions, choose an equivalent percentage face loss (EFL) or tunnel settlement ratio (refer to Cater *et al.*, 1984).
- Using the above value and the tunnel cross-sectional area (A_t), calculate the area of surface trough (A_s) from:

$$\text{EFL} = \frac{A_s}{A_t} \% \quad (1)$$

Assume a value of i , say equal to half the tunnel depth (Z), and calculate maximum settlement (Sm) as follows:

$$i = \frac{Z}{2} \quad (2)$$

$$A_s = 2.5i Sm \quad (3)$$

Obtain surface settlements (S) at any distance (X) from the tunnel centreline according to equation (4):

$$S = Sm \exp \left[-\frac{X^2}{2i^2} \right] \quad (4)$$

This method applies to ground settlements. For building settlements, considering the maximum values likely of only 5 to 15 mm, it seems reasonable to assume that they can be approximated in magnitude and form to ground settlements.

Acknowledgements The authors wish to acknowledge their former colleagues of the Geotechnical Engineering Office (GEO) of the Hong Kong Government for their contributions to this paper.

REFERENCES

- Cater, R. W., Shirlaw, J. N., Sullivan, C. A. & Chan, W. T. (1984) Tunnels constructed for the Hong Kong Mass Transit Railway. *Hong Kong Engr* 12(10), 37-49.
- Howat, M. D. & Cater, R. W. (1983) Ground settlement due to tunnelling in weathered granite. In: *Proc. of the International Symp. on Engineering Geology and Underground Construction* (Lisbon), vol. 1, 1.257 to 1.276.
- Mair, R. J. (1983) Geotechnical aspects of soft-ground tunnelling. *Proc. Conf. on Construction Problems in Soft Soils*. N.T.I., Singapore.
- Mair, R. J., Taylor, R. N. & Bracegirdle, A. (1993) Subsurface settlement profiles above tunnels in clay. *Geotechnique* 43(2), 315-320.
- Peck, R. B. (1969) Deep excavations and tunnelling in soft ground. In: *Proc. Seventh International Conf. on Soil Mechanics and Foundation Engineering* (Mexico City), State-of-the-Art Vol., 266-290.
- Rankin, W. J. (1988) Ground movements resulting from urban tunnelling. In: *Proc. Conf. on the Engineering Geology of Underground Movements* (Nottingham, UK), 79-92. London Geological Society.

Dynamic subsidence prediction over longwall mining in Abu-Tartur mines, Egypt

SAID S. IMBABY

Assiut University, Mining & Metallurgy Engineering Department, Faculty of Engineering, Assiut, Egypt

Abstract The ultimate goal of surface subsidence studies is to use the acquired knowledge of surface subsidence in structural and environmental protection against subsidence damage and disturbance. For this purpose, the accurate prediction of dynamic subsidence plays a much more important role than that of final subsidence. Based on the subsidence data collected through a subsidence monitoring programme conducted over two longwall panels in Abu-Tartur phosphate mines, a mathematical model has been proposed for predicting the final subsidence. In this paper a physical model study is carried out on the limestone specimens to determine the strain rate. The rate of subsidence for the limestone layer which is the upper one in the geological succession at Abu-Tartur area, is calculated and equals $0.797 \text{ m year}^{-1}$. The percentage error between the *in situ* final subsidence and the predicted one from physical model after 2 years from the beginning of working is 7.29%, while this error is 1.81% after 14 years stoppage of the face.

INTRODUCTION

Prediction of ground subsidence associated with underground mining based on the shape of final settlement trough of ground surface could be insufficient. Surface subsidence due to mining is a dynamic process which obeys mechanical principles. Several methods for the investigation of the subsidence process related to elasticity, FEM and BEM have been studied for many years (Berry & Sales, 1961, 1962; Crouch & Starfield, 1983; and Eissa, 1990). However, a marked progress has not been achieved in describing the dynamic subsidence. Applying the principles of rheology, the nature of the process of subsidence can be revealed more effectively in time and space domains. Hence, the results will greatly improve the protection of undermined surface structures. Viscoelasticity was applied to study the time dependent surface subsidence caused by underground mining (Zhuoqiao & Xinjian, 1992). The presented viscoelastic analyses have been given a clear physical interpretation of the time factor C , which is a measure of the rock strain rate. Its value can be expressed and defined either by means of laboratory tests on rock specimen or from mine subsidence surveys (Xia & Zhong, 1988).

Konthe (1959) made the well-known assumption, investigating the mine subsidence process, which assumed that the surface will subside when an underlying body of ore is exploited,

$$\frac{dW_{(t)}}{dt} = C[W_k - W_{(t)}] \quad (1)$$

where W_k is the final subsidence of a surface point, $W_{(t)}$ is the subsidence of a point at time t and C is the subsidence velocity factor, or time factor.

The above relationship was used to describe mining subsidence phenomena, and notable successes have been achieved. It must be mentioned that the time factor C , in Konthe's approach could be determined by mine subsidence surveys.

Based on the collected data through the subsidence monitoring programme conducted over two longwall panels in an Illinois coal mine, empirical models have been proposed for predicting final and dynamic subsidence for that region (Peng & Luo, 1991). At Abu-Tartur experimental mine the vertical components of surface movement are measured over two longwall panels separated by rib pillars of width 30 m. A mathematical model to predict the final subsidence is developed (Gomma *et al.*, 1994).

In this paper a simple loading frame is designed to give a static load to the beam shaped rock specimen. A physical model from limestone rock is tested by the loading frame under the action of distributed load (75% of bending strength). The strain is measured at different positions located on the specimen by means of electric wire strain gauges connected to data logger. By means of geometrical similarity the measured strains in the laboratory are transformed to the prototype.

Subsidence monitoring at the Abu-Tartur area

Surface subsidence over two longwall panels at the experimental phosphate mine 150 m below the surface have been monitored during the period from February 1980 to December 1981. The two panels shown in Fig. 1 were 500 m long and 60 m wide. The mining height was about 2.3 m and the rate of face advance was 0.63 m/shift (Technical Report, 1983). The measured values of vertical components of surface subsidence are shown in Fig. 1. A mathematical model to predict the final surface subsidence in this

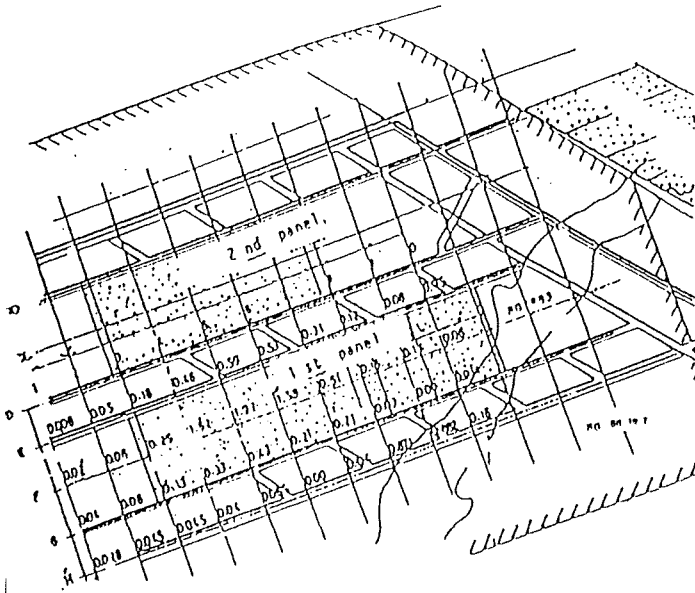


Fig. 1 Network of the subsidence measurements.

area was developed. From the proposed model the tilt and curvature were obtained (Gomma *et al.*, 1994).

Method of obtaining time factor C from mine subsidence surveys

When a surface point P is undermined by a subcritical, critical or supercritical excavation, the subsidence development curve can be obtained by levelling measurements once per week or per month. Figure 2 shows a typical subsidence development curve. The abscissa represents time t , the ordinate is the subsidence value. From a given point A on the excavation existing far beyond the critical area which means that W_k is unchanged hereafter. Below point A , this curve can be represented by equation (1), with W_k constant. At any point B below A , the slope of the tangent to the curve at point B ($\tan \alpha$) is $dW_{(t)}/dt$ as follows:

$$\tan \alpha = \frac{dW_{(t)}}{dt} = C[W_k - W_{(t)}] \tag{2}$$

then

$$C = \frac{\tan \alpha}{W_k - W_{(t)}} \text{ l year}^{-1} \tag{3}$$

By measuring $W_{(t)}$ and $\tan \alpha$, the time factor C can be obtained graphically or analytically. With C known, the subsidence at a surface point at any time can be calculated.

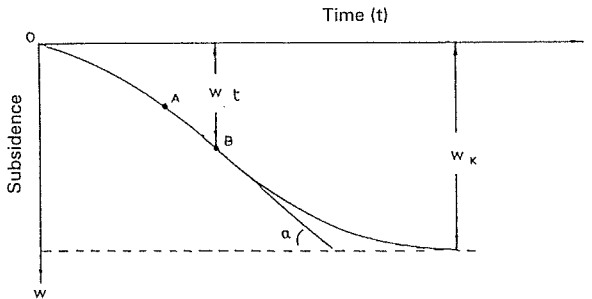


Fig. 2 Typical subsidence development curve.

Determination of subsidence rate from Konthe's hypothesis

From equation (1) the subsidence rate can be calculated as follows:

$$\frac{dW_{(t)}}{dt} = C[W_k - W_{(t)}]$$

because W_k is constant,

$$\int \frac{dW_{(t)}}{W_k - W_t} = \int c dt$$

$$-\ln(W_k - W_t) = Ct + C_1$$

From the boundary conditions the constant C_1 is obtained, at $t = 0$, $W_t = 0$ then:

$$\begin{aligned} C_1 &= -\ln W_k \\ \ln(W_k - W_t) - \ln W_k &= -Ct \\ \ln \frac{W_k - W_t}{W_k} &= -Ct \\ W_k - W_t &= W_k e^{-Ct} \\ W_t &= W_k(1 - e^{-Ct}) \end{aligned} \quad (4)$$

By substitution from equation (4) in equation (1)

$$\frac{dW(t)}{dt} = CW_k e^{-Ct} \text{ m year}^{-1} \quad (5)$$

It is obvious that equation (4) gives the subsidence at any time t and equation (5) gives the subsidence rate.

Experimental work and results

The upper layer at Abu-Tartur geological succession consists of limestone of average thickness 70 m. which bends due to phosphate ore exploitation. Rock specimens from limestone deposit are tested to determine the bending strength (2.22 kN cm^{-1}). A rock specimen of size $3 \times 3 \times 10 \text{ cm}^3$ is taken as a physical model and tested by the loading frame shown in Fig. 3 under the action of distributed load which achieves 75% of the bending strength. The strains are measured at different positions on the specimen by means of electric wire strain gauges connected with data logger which has an accuracy of $0.0005 \text{ mm cm}^{-1}$.

The measured strains during four months at the point P located at the centre of the specimen are shown in Table 1. These strains are transformed to the prototype (vertical subsidence) by means of geometrical similarity. The vertical subsidence versus time is shown in Fig. 4. From this figure the following dynamic subsidence parameters are

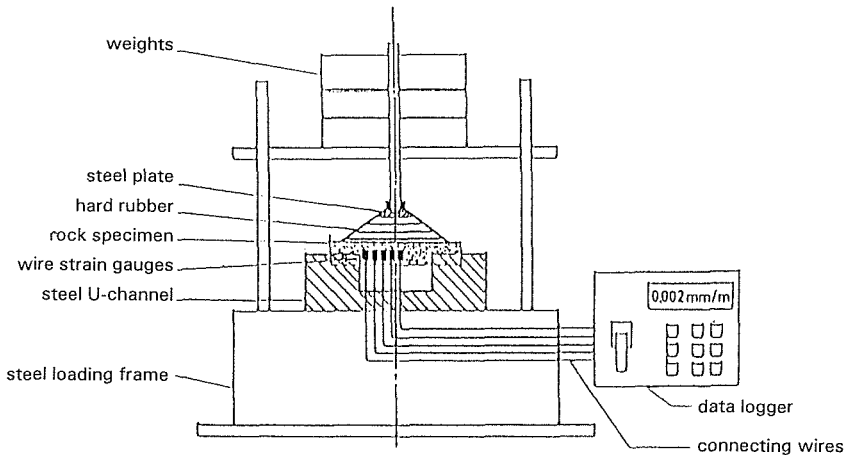


Fig. 3 Loading frame and data logger for creep test.

Table 1 The values of strains at point P at the centre of limestone specimen and the equivalent vertical subsidence at different times.

Time	Strain in the model (mm m ⁻¹)	Vertical subsidence in the prototype (m)
1st week	0.0030	0.49
2nd week	0.0040	0.65
3rd week	0.0060	0.89
1st month	0.0090	1.47
2nd month	0.0100	1.63
3rd month	0.0110	1.80
4th month	0.0135	2.21

obtained: $\alpha = 30^\circ$, $W_k = 2.21$ m, $W_t = 1.5$ m at $t = 1$ month. The time factor C from equation (3) is:

$$C = \frac{\tan 30}{2.21 - 1.5} = 0.813 \quad 1 \text{ year}^{-1}$$

From equation (5) the rate of subsidence will be:

$$\frac{dW(t)}{dt} = 2.21 * 0.813 e^{-0.813 * 1} = 0.797 \quad \text{m year}^{-1}$$

The maximum and final vertical subsidence at station F₅, (Fig. 1) over the longwall panel is measured by levelling and its value was found to be 1.92 m. Applying equation (4), W_t after about 2 years from the beginning of working is given as follows:

$$W_t = 2.21(1 - e^{0.813 * 2}) = 1.78 \text{ m}$$

The percentage error between *in situ* vertical subsidence and the predicted one from the physical model is 7.29%. After 14 years stoppage of the face, the subsidence over the longwall panel at station F₅ is measured and its value equals 2.17 m. From equation (4), W at $t = 14$ years will be:

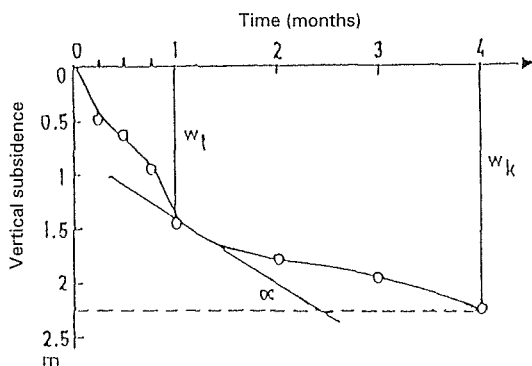


Fig. 4 Vertical subsidence vs. time for limestone specimen at point P.

$$W_{(t)} = 2.21(1 - e^{0.813 * 14}) = 2.20 \text{ m}$$

The percentage error between the measured subsidence and the predicted one at station F₅ is 1.81%.

CONCLUSIONS

The collected data of vertical subsidence over two longwall panels in Abu-Tartur mines have provided us with an excellent opportunity to acquire a better understanding of the nature of surface subsidence process in this area. Accurate prediction of dynamic subsidence plays a much more important role than that of final subsidence. Important relationships between the time factor C , final subsidence W_k , and the subsidence velocity are obtained. From the physical model study on limestone specimens, the values of time factor C and the rate of subsidence or subsidence velocity, dW_t/dt are $0.813 \text{ l year}^{-1}$ and $0.797 \text{ m year}^{-1}$ respectively. After 2 years from the beginning of working, the percentage error between the *in situ* final subsidence and the predicted one is 7.29%. After 14 years from the face stoppage the percentage error is 1.81% which indicates that the suggested model can be used for accurate prediction of dynamic subsidence at Abu-Tartur area.

REFERENCES

- Berry, D. S. & Sales, I. W. (1961) An elastic treatment of ground movement due to mining. II – Transversely isotropic ground. *J. Mech. Phys. Solids* **9**, 52-62.
- Berry, D. S. & Sales, I. W. (1962) An elastic treatment of ground movement due to mining. III – Three dimensional problem, transversely isotropic ground. *J. Mech. Phys. Solids* **10**(1).
- Crouch, S. L. & Starfield, A. M. (1983) *Boundary Element Methods in Soil Mechanics*. George Allen & Unwin, London.
- Eissa, E. A. (1990) Prediction of trough subsidence associated with mining of seam type deposit. *Bull. Faculty of Engng, Assiut Univ.* **18**, part 2.
- Gomma, W. A., Ibrahim, A. R., Imbaby, S. S. & Yousef, W. M. (1994) Prediction of surface subsidence over longwall mining in Abu-Tartur area. *The Fourth Mining, Petroleum & Metall. Conf.* (Faculty of Engineering, Assiut Univ., Assiut, Egypt).
- Konthe, S. (1959) Observation of surface movement under influence of mining and their theoretical interpretation. *Proc. European Congr. on Ground Movement* (Leeds, UK).
- Peng, S. S. & Luo, Y. (1991) Subsidence prediction in Illinois coal basin. In: *Proc. 10th Int. Conf. on Ground Control in Mining* (West Virginia Univ., Morgantown, West Virginia), 212-219.
- Technical Report (1983) *Vertical subsidence over longwall panels*. Surveying Section in Abu-Tartur Mines.
- Xia, C. C. & Zhong, S. Y. (1988) A discussion about the scale effects of rheological deformability of rock. *J. Central-South Inst. Min. Metall.*, 128-136.
- Zhuoqiao, Z. & Xinjian, K. (1992) Application of viscoelasticity to study the time dependent surface subsidence by underground mining. *Engng Geol.* **32**, 279-284.

Prediction of subsoil subsidence caused by opencast mining

HALINA KONDERLA & MACIEJ HAWRYSZ

*Institute of Geotechnics and Hydrotechnics, Technical University of Wrocław,
Wybrzeże Wyspiańskiego 27, 50-370 Wrocław, Poland*

Abstract Attempts were made to formulate the correlation between the subsidence of the soil mass exposed to opencast mining and the parameters characterizing the development of the depression and the geological structure of the seam. The process of soil surface subsidence was analysed, making use of the results from geodetic and piezometric measurements carried out in one of Poland's brown-coal mines. A simple model was proposed for the prediction of superficial displacements produced by the dewatering of the soil mass. The subsidence and rise of the soil surface, recorded in the course of geodetic measurements, reflect both the effect of seam dewatering and the effect of mining operations. A future verification of the model should include the effect of soil mass decompression concomitant with the stripping of the overburden, the working of the seam, and the construction of the external dumping ground.

INTRODUCTION

Opencast mining is associated with soil deformations which are primarily due to the dewatering and decompression of the soil mass, and vary with its geological structure. Theoretically, decompression reaches a significant depth on the soil mass, thus accounting for an increase in the rock volume, for the movement of the entire excavation, and for vertical displacements in the adjacent soils. It is difficult to distinguish the displacements produced by decompression alone, because they add to some other movements, such as subsidence due to dewatering, and displacement due to creeping (mostly clays). Thus, the problem of how to predict subsoil subsidence resulting from opencast mining is, in fact, very complex.

So far, any attempts to represent the process in terms of conventional soil mechanics have failed to be reliable, because the subsidence predicted *via* the above route varied from several tens to several hundred percent, as compared to the measured values. Another method of solving the problem in question consists in establishing the correlation between real subsidence and some factors that affect the course of the process. The objective of the present paper was to construct a model describing such relationships, with the assumption that the relations are site-specific. Analysed were the measured displacements of the vertical benchmarks situated in one of Poland's brown-coal mines (Fig. 1). The variations of the water table position, produced by the dewatering of the excavated seam, were assumed to be the main factor contributing to subsoil subsidence. Making use of the results from piezometric measurements, water

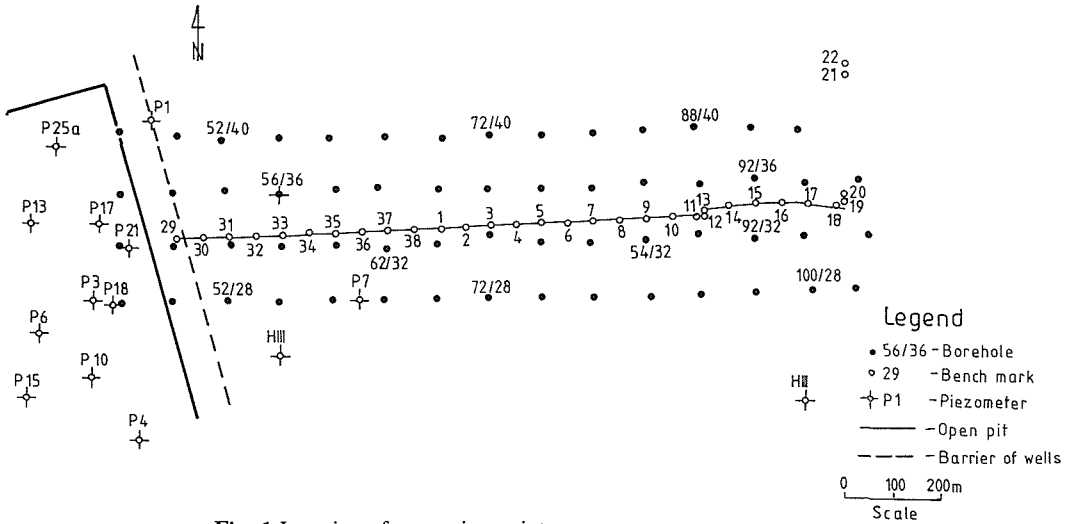


Fig. 1 Location of measuring points.

level variations in the soil mass were related to the benchmark positions and to the surveying time (Przedsiębiorstwo Geologiczne, 1966). The non-cohesive soil thickness and the dewatered layer thickness were adopted as the parameter characterizing the geological structure of the soil mass. Considering the random distribution of the boreholes and piezometers with respect to the benchmark line, use was made of the SURFER programme packet (Tanski, 1991).

GEOLOGICAL STRUCTURE

The hydrogeological structure of the opencast mine under study is shown by the cross section of the benchmark line (Fig. 2). The deposit consists of three stratigraphic formations – Upper Cretaceous, Tertiary and Quaternary. The Upper Cretaceous sediments are built of marls displaying fissured zones. Those sediments underlie the Tertiary formation in which the following series can be distinguished: seam-underlying series, brown-coal seam and seam-overlying series. The seam-underlying series is formed of a fine Miocene sand layer with numerous lenticular silty or (less frequently) clayey interbeddings. In the central part of the seam, the thickness of the underlying sand-silt series amounts up to 25 m, decreasing towards the edge part, and these forms are predominantly subject to thinning away before they reach the coal boundary. Coals in the form of a single stratum occur flat at the depth of 30 to 55 m, generally with no disturbances. The seam-overlying series (made of Poznan clays) covers the coal stratum with a thin layer of a thickness ranging approximately between 5 and 15 m. The Quaternary forms overlie the Tertiary ones; they consist of overburden sands (central), boulder clays, and near-surface sands. The central sands (from several to about 19 m thick) show a considerable variability (not only in the vertical profile, but also in the horizontal distribution), and are characterized by the occurrence of gravel agglomerates. The sands are overlain by boulder clays in the form of a continuous layer with a

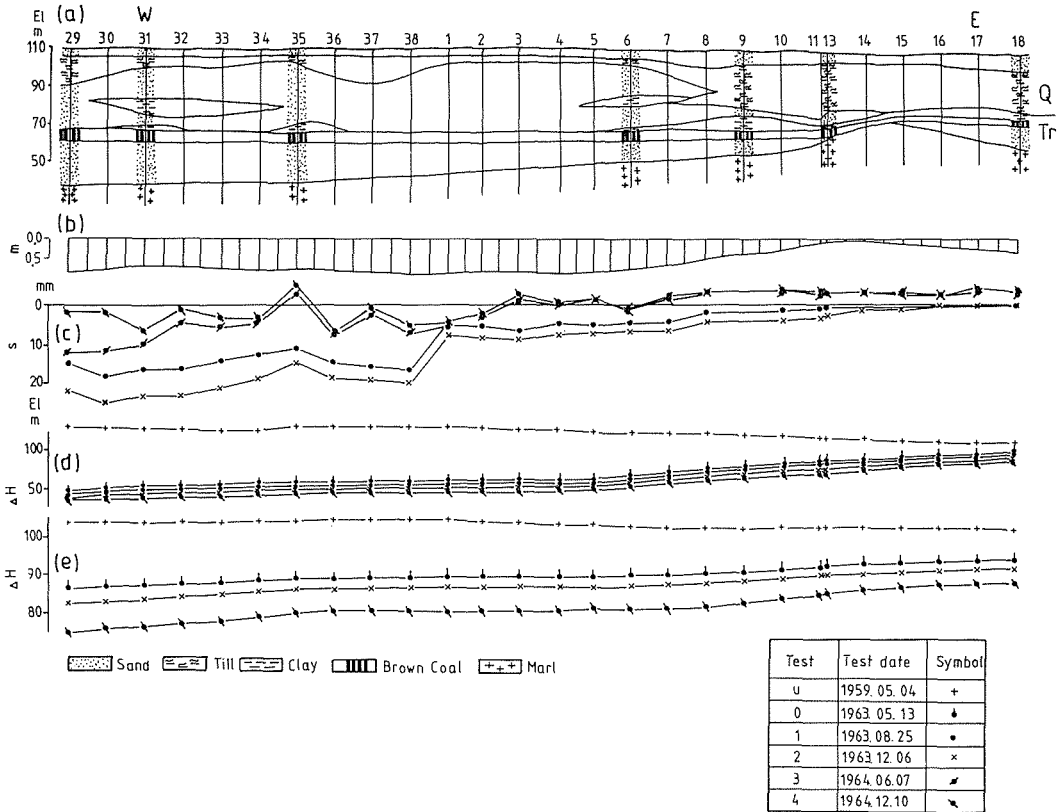


Fig. 2 Readings from superficial benchmarks measuring surface displacements and water surface: (a) geological cross section, (b) factor m , (c) displacements of benchmarks, (d) of water surface N II, (e) variations of water surface N III.

thickness varying between several and approximately 16 m. The roof part of the Quaternary forms is built of a layer of near-surface sands which differ in thickness.

Two major aquifers were distinguished in the seam under study:

- (a) *In coal-overlying sands*: the roof and floor being built of boulder clays, respectively (referred to as N II).
- (b) *In coal-underlying sands*: separated from the roof by the brown-coal seam (referred to as N III).

SUGGESTED FORM OF CORRELATION

The following form was postulated:

$$s_i = \Phi(\Delta H_i, m_i) \tag{1}$$

where s_i is vertical displacement of soil surface; ΔH_i denotes variation of piezometric groundwater table, and m_i indicates geological structure of the soil mass which is to be dewatered.

Soil surface deformation was predicted by making use of the proposed correlation, and taking into account the results of geodetic survey and piezometric measurements carried out in the opencast mine under study. The geodetic line comprised 28 surface benchmarks placed along the west-east direction. The situation of the measuring points is shown in Fig. 1. From 13 May 1963 to 10 December 1964 five geodetic observations were carried out to determine the relative displacements of the benchmarks, without controlling their heights with respect to the benchmark network outside the open pit-mined area. In the first version of the equation (1) subsidence was related solely to the soil-mass dewatering which, in that particular case, was expressed in terms of the total depression of the coal-overlying and coal-underlying groundwater tables (ΔH_i).

To determine the form of the correlation function it is necessary to establish sets of ΔH_i and m_i values at the points which correspond with the location of the benches observed. Not only geological boreholes for the determination of the seam structure, but also hydrogeological wells for the measurement of water horizon positions were located at other points than those of the observation network. Thus it was necessary to make use of approximating procedures so as to find the values of ΔH_i and m_i . The application of the SURFER packet made it possible to draw three-dimensional maps of the values to be found (e.g. Fig. 3(a)) and two-dimensional maps for the inclusion of isolines and measuring points (Fig. 3(b)).

ANALYSIS OF MEASURED DATA

The geological structure of the soil mass corresponding to the geodetic observation line is shown in Fig. 2(a). Figures 2(d) and 2(e) present the varying positions of the coal-overlying water table (N II) and coal-underlying water table (N III), respectively. The same figures also include undisturbed water table positions, as they were prior to the dewatering of the excavation (symbol u). The dewatering of the excavation (which began in August 1959) was carried out through drilled wells which drew water from overburden sands and coal-underlying sands. The results of geodetic observations are plotted in Fig. 2(c). In addition, Fig. 2 incorporates the plot of parameter m . Its value corresponds with the ratio of non-cohesive soil thickness to total thickness of the active layer. The term "active layer" has been adopted to denote the total thickness of the layers occurring between the actual piezometric level of the groundwater table and the roof of non-deformable strata. The actual piezometric level is defined by the values of N II and N III (which are similar). The depth of active layer occurrence is limited by the roof of the Cretaceous stratum which has a stress-strain characteristics differing considerably from that of the overlying soil series. The relative displacements of the benchmarks (s) were related to measurement 0, carried out in May 1963. Successive measurements were performed in August 1963, December 1963, June 1964 and December 1964 (and are denoted as 1, 2, 3 and 4 respectively). On analysing the variations of the benchmark positions, we noticed two distinct stages of the subsidence process. Thus, stage one consisted of subsidence alone (measurements 1 and 2 of Fig. 2(c)) and stage two was characterized by the commencement of the soil surface rise (measurements 3 and 4). In the course of geodetic observations, both groundwater levels decreased at constant average rates. Thus, N II had a subsidence rate of about 2 m year^{-1} and 1 m year^{-1} in the time interval between measurement 0 and 2 and in the time interval

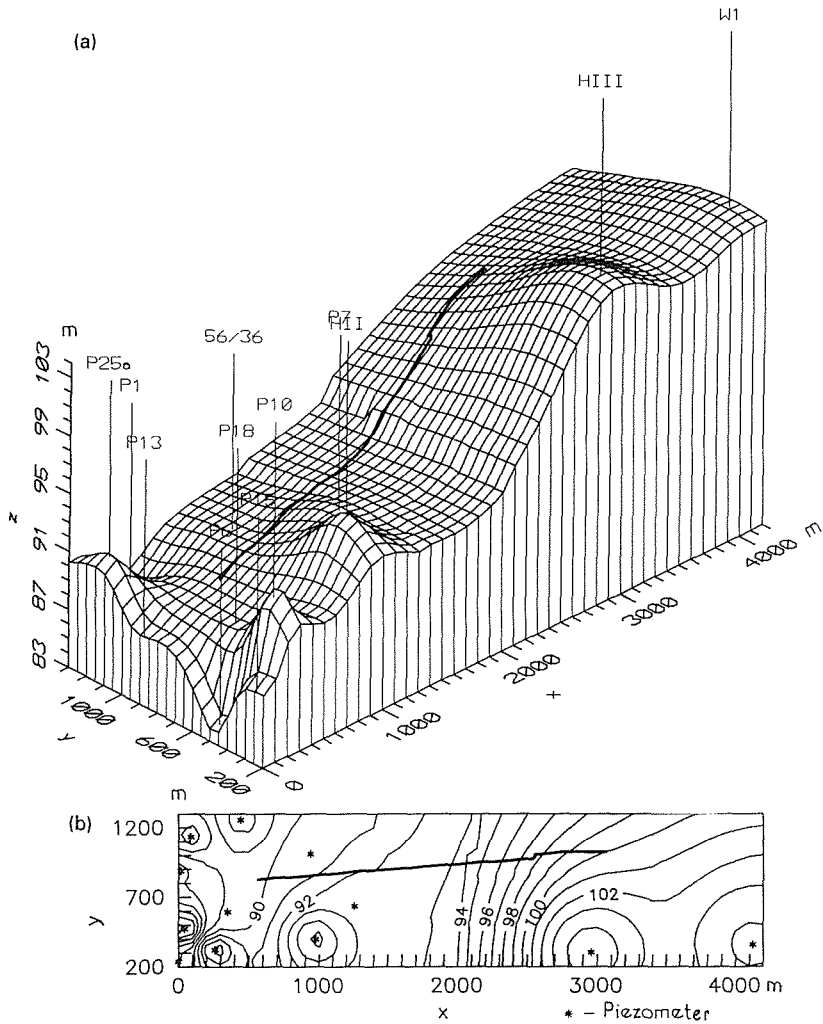


Fig. 3 Plots of factor m : (a) 3D view, (b) contour map.

between measurement 2 and 4, respectively. The subsidence rate of N III amounted to 5 m year^{-1} for the entire period under study. The rise of the soil surface recorded during measurements 3 and 4 should be attributed to the decompression of the soil mass induced by the stripping of the overburden which began on 1 September 1961.

Figure 4 shows the varying positions of the working fronts which correspond with geodetic measurements 2 and 4. The cross section of the open pit is an extension of the observation line in the west-direction. From the data of Fig. 4 it is clearly seen that the overburden volume stripped in the time interval between measurements 2 and 4 was substantially greater than the one removed between measurements 0 and 2. It should be noted that the vertical soil displacements recorded in this study reflect the contribution of both dewatering and decompression.

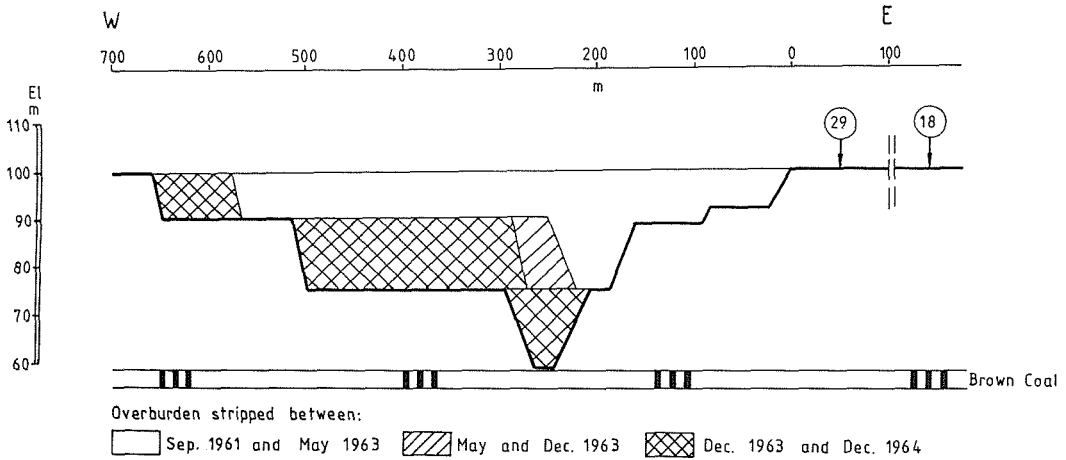


Fig. 4 Mining operations in the timespan from 1961 to 1964.

PRELIMINARY MODEL FOR THE PREDICTION OF LAND SURFACE SUBSIDENCE

Analysis of soil displacement measurements, exemplified by the observation of the aforementioned measuring line, allows only preliminary interpretation of the subsidence process by making use of an increment model. A very simple form of the correlation (1) was adopted:

$$\Delta s_i = A m_i \Delta H_i \quad (2)$$

where Δs_i denotes height variation of the i th point on the soil surface ((-) and (+) being subsidence and rise, respectively); m_i indicates the geological structure coefficient (defined in an earlier Section) at the i th point; ΔH_i describes total change of groundwater table at the i th point ((-) standing for depression of water tables, and (+) representing rise of water tables), and A is scale coefficient determined by approximation.

The subsidence process was found to run at two distinct stages:

- Stage I (subsidence) corresponding with the time interval between measurements 0 and 2.
- Stage II (rise) corresponding with the time interval between measurements 2 and 4.

Assuming that the scale coefficient A is constant, its value was assessed by the least-square method. Thus,

for Stage I: $A = 4.1$, and correlation coefficient $R = 0.79$

for Stage II: $A = 2.9$, and correlation coefficient $R = 0.88$

The procedure for the assessment of the A -values, and the justification for the low correlation coefficient values are found in Fig. 5. In this way it has been possible to describe the deformation of the soil surface along the analysed measuring line.

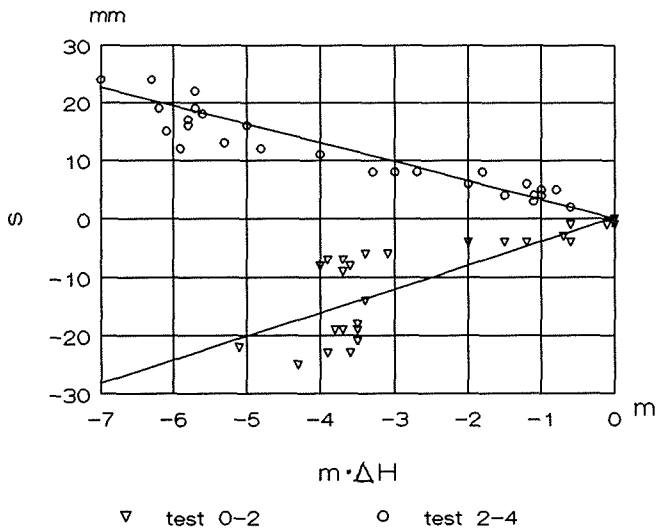


Fig. 5 Evaluation of scale coefficient.

CONCLUSIONS

Provided is an example of how to interpret the results from the measurements of vertical soil displacements recorded in the vicinity of a brown-coal mine in Poland. Taking into account the insufficiency of the data base, as well as the complex nature of the process, the correlation obtained has a local meaning and should therefore be regarded as a preliminary approach to the construction of a feasible model which would predict the deformation of the soil surface exposed to opencast mining. Further verification of the model is recommended. A major postulate for the model is that it should incorporate the decompression induced by the removal of the overburden, by the working of the seam and by the construction of the dumping ground.

REFERENCES

- Przedsiębiorstwo Geologiczne (1966) *Kompleksowa aktualizacja dokumentacji geologicznej* (Follow-up of geological specification). Przedsiębiorstwo Geologiczne, Wrocław.
- Tanski, T. (1991) *Surfer*. PLJ, Warszawa.

Subsidence prediction and management in the Collie coalfields (Western Australia)

IAN MISICH

Department of Minerals and Energy Western Australia, East Perth, Western Australia 6004, Australia

ALBERT EVANS

Collie Campus, Curtin University, Bentley, Western Australia, Australia

ODWYN JONES

Brodie Hall Research and Consultancy Centre, Curtin University, Western Australia, Australia

Abstract Extensive field monitoring from 1985 to 1994 has enabled the researchers to establish a sound database from which empirical models have been developed for predicting surface and subsurface subsidence in the Collie coalfields. These predictive procedures have been successfully used to efficiently design coal extraction panels and thereby manage ground subsidence with respect to subsidence tolerance of specific superimposed features both on the surface and subsurface.

INTRODUCTION

There are basically two forms of mining induced subsidence in the Collie basin:

- (a) Discontinuous or stepped surface subsidence (at typically <40 m cover) resulting from all forms of coal extraction. This form of subsidence has been discussed in detail by Misich *et al.* (1993) and is not discussed in this paper.
- (b) Continuous trough-shaped subsidence (at typically >40 m cover), caused by extensive pillar collapse in board and pillar mining or one of many "total" extraction systems.

Continuous trough-shaped subsidence can be manifested in a number of ways (as illustrated in Fig. 1). and can have significant effects on superimposed features and can, in some cases, preclude the use of certain coal extraction techniques. It is therefore essential to be able to predict and manage ground subsidence for any mining scenario. This paper describes the prediction methods and mine design techniques used following research of the subsidence characteristics of the Collie coalfields sediments in Western Australia.

SUBSIDENCE MONITORING RESULTS AND EMPIRICAL MODELLING

As mentioned previously, an extensive subsidence monitoring programme has been underway since 1985 to establish a sound database for the development of empirical predictive subsidence models. The subsidence monitoring techniques involve the use of

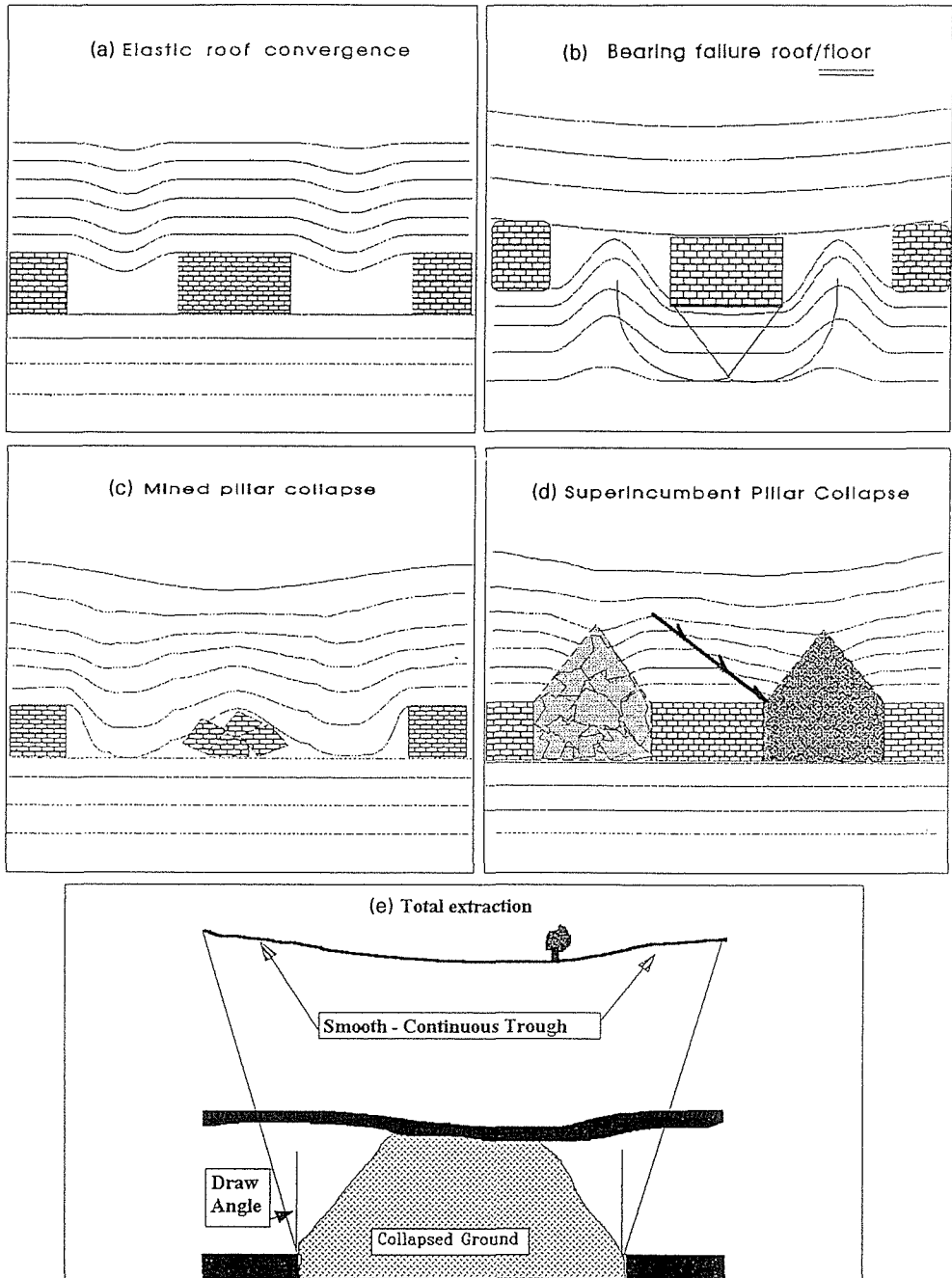


Fig. 1 Illustration of the basic modes of mine subsidence development. (a) Elastic mine roof convergence. (b) Foundation-type bearing failure of roof or floor materials. Floor "punching" illustrated. (c) Mined pillar collapse resulting from excessive vertical/tributary load. (d) Superincumbent strata pillar collapse. Caving on either side of a mine pillar can form an irregular shaped column of material which is susceptible to failure from excessive loads. (e) Total extraction. Many mining methods can be grouped into this classification. Some methods can leave up to 20% of mineable resource unmined.

various survey methods to record the movement of specific survey stations; borehole extensometers (using mechanically installed wire-line anchors) for detecting subsurface subsidence; and borehole piezometers, V-notch weirs, and mine-water flow meters for monitoring groundwater movements.

These monitoring techniques were used successfully in all panels and enabled the development of empirical charts and procedures which could be used to predict the complete surface subsidence profile in the Collie basin for any range of mining width, height and depth. These predictive models, based on curve fitting equations for ease of calculation, are well described by Misich *et al.* (1993). These equations can be used to predict tilts, curvature and strains at any point along the subsidence trough (Misich *et al.*, 1994). In turn, the predicted subsidence parameters can then be used to predict the likely damage to specific surface features. Some of the more accepted models for surface subsidence damage classification are listed in the National Coal Board (1975) publication, and by Peng (1992).

Subsurface subsidence at any height above the excavation can in turn be estimated using the nomogram illustrated in Fig. 2 which relates the surface subsidence to subsurface subsidence at aquitard layers, at any height above the mine workings. Subsurface subsidence profiles derived from this nomogram can then be used to predict the aquitard strains and the potential for aquitard rupture and likely groundwater inflow to the mine workings (Misich *et al.*, 1991). This nomogram is only suitable for extraction panel widths (W) greater than 0.25 times cover depth (H). For narrower extraction panels (when $W/H < 0.25$); where surface subsidence cannot be distinguished from survey error or natural ground movements, aquitard rupture/cracking begins when the "unsupported span" (as illustrated in Fig. 3) of the aquitard typically exceeds 5 m. The length of the unsupported span is calculated by plotting the angle of break from both

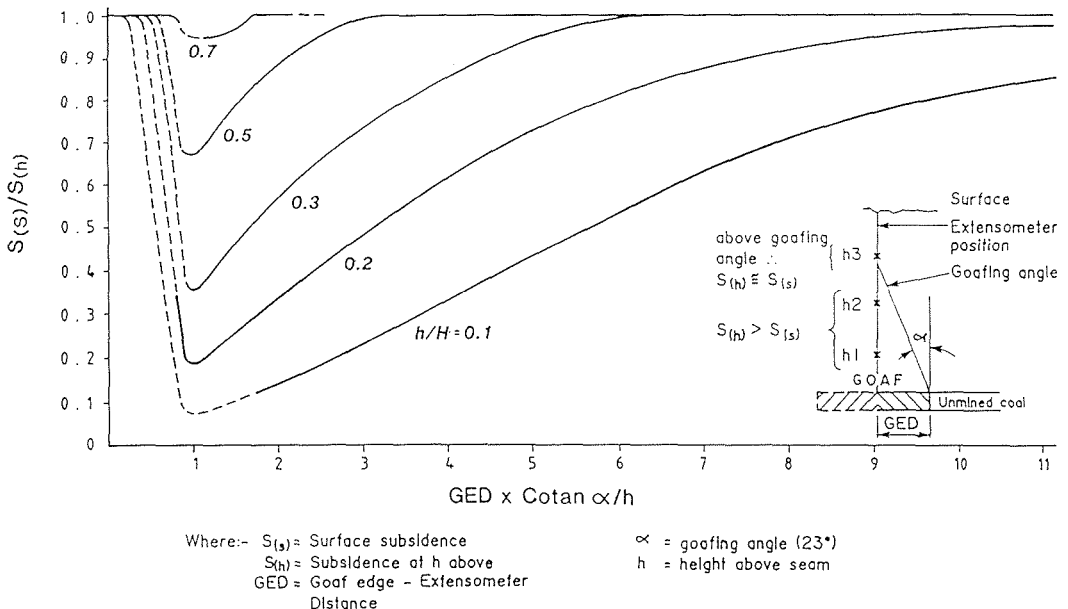


Fig. 2 Subsurface subsidence prediction nomogram. (To be used for panel widths $> 1/4$ mining depth.)

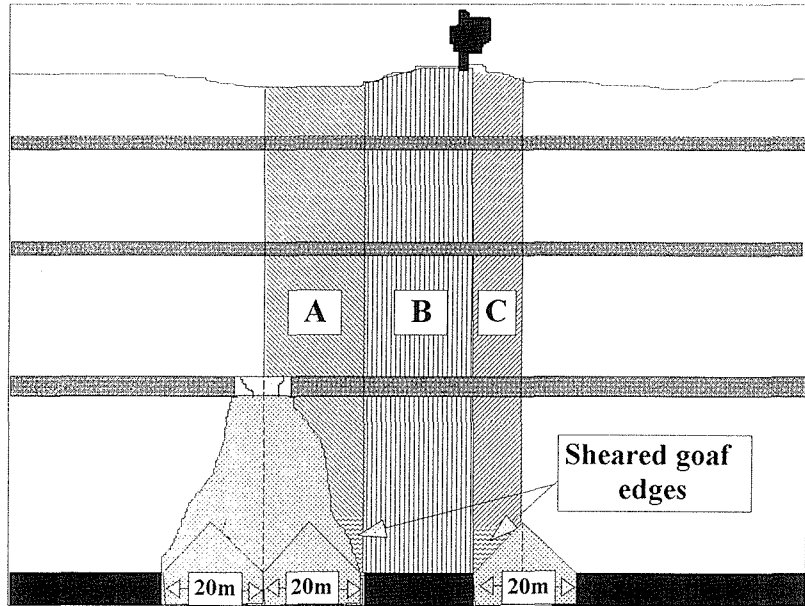


Fig. 3 Unsupported aquitard span concept. (To be used for extraction panel widths $< 1/4$ cover depth.)

panel edges to the position of the aquitard and calculating the distance between the intercepts.

The effect of various "unsupported aquitard spans" on aquitard integrity depends on the geomechanical properties of, and large scale geological discontinuities in the superimposed strata and in particular the aquitard itself. For example:

- (a) massive, strong sandstones can span very large distances (however it is likely that these lithologies will only significantly affect the subsidence profile near the caving zone) and minimize subsidence magnitudes and effects, and
- (b) very soft, plastic strata – usually weak clays – can absorb large strain energy and have the capacity to "re-knit" with minimal confining pressure, thereby maintaining the integrity of the aquitard;
- (c) weak overburden material forming the caved overhang which supports the base of bridging aquitards can crush; thereby increasing the unsupported span. In this case the panel width is limited by not allowing the projected caving angles to intersect at or above the position of the aquitard. The design width for panels located below these weaker sediments (as in Collie) is 10 m less than the maximum allowable width for stronger sediments.

Assuming that aquitards are usually composed of interbedded coals, shales, siltstones and sandstones it is reasonable to assume that some other mining areas will experience similar conditions to those prevailing in the Collie basin.

Concurrent with subsidence monitoring and modelling, the researchers investigated various mining and mine design methods for controlling subsidence and developed criteria for the design of extraction panels. This research is summarized below.

SUBSIDENCE MANAGEMENT – MINING METHODS

Subsidence damage to surface and subsurface features most commonly results from a change in ground curvature and corresponding strain. It therefore follows that if this curvature (and indirectly the maximum slope of the subsidence trough – Misich, 1996) can be controlled, then concomitant ground effects will also be managed. Two basic methods have been identified which can be used to reduce the curvature of subsidence troughs:

- (a) reducing maximum subsidence (S_{max}) and/or
- (b) softening the "sharp" subsidence profile above the edge of extraction panels (e.g. by leaving "yield" pillars immediately adjacent to the extraction panel, or in thick seams – by mining successive strips of coal with vertically and inwardly staggered edges).

The design and application of each of these techniques will vary according to the geological and geotechnical characteristics of the strata in each particular mining area. In the Collie basin, the most appropriate method for managing subsidence was to reduce the maximum subsidence with the adoption of the panel/pillar "Wongawilli" extraction method as illustrated in Fig. 4.

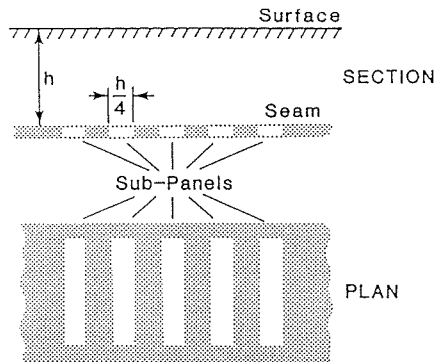


Fig. 4 Panel/pillar mining concept (adapted from Brauner, 1973).

SUBSIDENCE MANAGEMENT

After identifying that panel/pillar mining was the best suited mining method for subsidence management, it was decided to set up a trial panel/pillar extraction panel in the NWB3 area of Western Collieries' WD6 mine. The following (successful) stepped approach illustrates the design methodology used for this panel.

- (a) Establish the maximum extraction width according to superimposed features. The first task is to obtain all relevant information about the superincumbent strata and superimposed surface features and establish subsidence tolerance limits for anything needing to be safeguarded against subsidence damage. For example, the trial panel had a requirement to protect both a sealed open-pit haulroad sited 145 m directly above the panel and the aquitard immediately below aquifer 3 (35 m above the mine workings – see Fig. 5). (Aquifers 1 and 2 were largely depressurized by previous

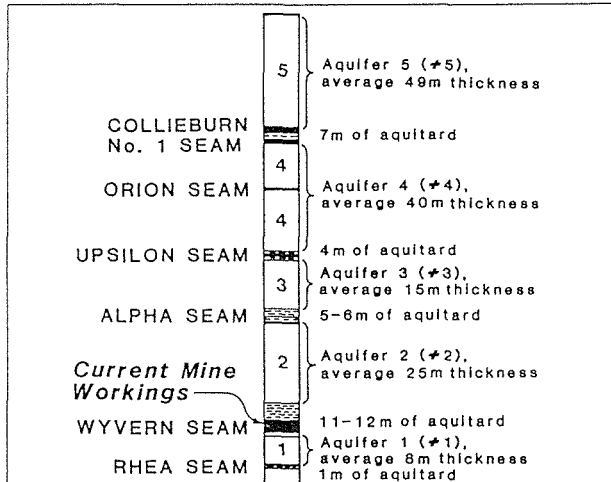


Fig. 5 Typical hydrostratigraphy above trial extraction panel – NWB3 WD6 Mine.

mining activity around the panel.) Thus the first issue needing consideration was the safe upper limit of surface subsidence for the protection of the haulroad and its drainage features (selected to be 100 mm). Using the S_{\max} prediction "Growth Curve" as developed by Misich *et al.* (1994), the maximum panel width allowable to limit S_{\max} to less than 100 mm is 55 m.

The second issue of importance was the need to protect the mine workings from water inundation from aquifer 3 by restricting the panel width so that the unsupported span of the protective aquitard does not exceed a critical width. (Historical evidence indicated that an unsupported aquitard span in excess of 5 m began to develop open cracks along cleavage planes and that a 10 m span always led to failure of similar aquitards.)

Therefore, using the unsupported span/fracture angle concept (Fig. 3) described previously, the maximum allowable extraction panel width (W_{ext}) is calculated by:

$$W_{\text{ext}} = 2h \tan \alpha \pm 5 = 25 \text{ m} \quad (1)$$

where α = angle of fracture (23°), and h = height of aquitard above the panel (35 m); +5 is used for strong interburden and -5 is used for weak interburden.. It follows therefore that the maximum width of extraction had to be designed in accordance with the need to protect the closest aquitard.

In the case study, the resultant panel design also had to take account of the imposed restrictions of previous mining in the area which effectively defined the shape and size of the extraction panel, and also the need to satisfy management's production requirements which previously were dependant on mining 6 m wide "splits" and 7 m wide "fenders", lifted on either side each split. Consequently, the final panel layout incorporated 40 m (2 x 20 m) wide sub-panels, separated by 20 m wide intra-panel pillars and included drainage and sump facilities to accommodate the expected inflow of groundwater into the workings from aquifer 3.

- (b) Establish the minimum intra-panel pillar widths to ensure (i) safe mining conditions for mine personnel and (ii) prevention of collapse of coal and/or superincumbent

strata which would result in an increase in final subsidence and, in turn, potentially damage superimposed surface and subsurface features and result in a major inflow of water into the mine. Similar increases in subsidence would result if the coal pillar abutment loads were to exceed the roof or floor bearing capacity causing the pillars to "punch" into the roof or floor strata. The intra-panel pillars must therefore be designed for long-term stability for the whole "pillar system".

Firstly, a suitable design Factor of Safety (FOS_C) had to be adopted for the design of the intra-panel coal pillars which ensures the required long term stability of the complete pillar support system. The FOS_C of mine pillars being given by:

$$FOS_C = \frac{\text{pillar strength}}{\text{pillar load}} \tag{2}$$

This approach is supported by the comprehensive investigation into design coal pillars in the South African coalfields by Salamon & Oravec (1967) which led to the conclusions that a design FOS_C of 1.6 is acceptable in most situations but that a FOS_C of 2.0 be adopted for pillars between development entries.

In the trial case study, because pillar width was preselected to be 20 m, it was necessary to check that the corresponding FOS_C was of sufficient magnitude to take into account the potential collapse of the weak overlying sediments. Intra-panel coal pillar strength for the Collie basin was calculated using a modified Hustralid/Salamon-Munro/Wagner (Bieniawski, 1982; Wagner, 1980) pillar strength design criteria as described by Misich & Humphreys (1988). The pillar strength (PS) and pillar load (PL) are calculated by:

$$PS = k \frac{(W_{eff}/W_o)^{0.46}}{(T/T_o)^{0.66}} \text{ (MPa)} \tag{3}$$

$$PL = \frac{(A + B + C) \gamma \cdot 10^{-6}}{W_p} \text{ (MPa)} \tag{4}$$

where, $A + B + C$ are tributary load components per extraction widths (see Fig. 6); γ = unit weight of superincumbent strata, MN; $W_o, T_o = 1$ m; W_p = pillar width, m; k = compressive strength of 1 m³ of coal, which in Collie is estimated to be 6.5 MPa; T = mining height/thickness, m

$$W_{eff} \text{ (effective pillar width)} = 4 \frac{A_p}{C_p} \text{ (Wagner, 1980), m} \tag{5}$$

where, A_p = pillar area, m; C_p = pillar circumference, m.

Using this approach for the trial case study, the calculated FOS_C for the 20 m wide intra-panel pillar with 40 m sub-panels on either side was 2.2 which was accepted as being adequate for preliminary design. For situations where the mine planner has more design options for intra-panel pillars, the coal pillar width for a designated FOS_C , suitable for local conditions, can therefore be calculated by:

$$FOS_C \gamma H + FOS_C \gamma H \frac{W_{ext}}{W_p} = \frac{k}{T^{0.66}} \left[4W_p \frac{L_p}{2W_p} + 2L_p \right]^{0.46} \tag{6}$$

where, L_p = pillar length, and W_{ext} = extraction width.

The proposed design FOS_C for intra-panel coal pillars at Collie is discussed below. As mentioned previously, it is also necessary to design the coal pillar width to have sufficient bearing area so as to prevent failure of the roof and floor material. The design criteria adopted for the Collie basin sediments was a modified Terzaghi/Hansen formula (Scott, 1980; and Stacey & Page, 1986) with a design Factor of Safety against bearing failure (FOS_B) of 3.0. The FOS_B is calculated by:

$$\frac{Q_{ult}}{PL} \quad (7)$$

where:

$$Q_{ult} = cN_c + q_0N_q + \gamma 0.5 WpN_\gamma \quad (8)$$

and c = cohesive strength, kPa, and N_c , N_γ and N_q are functions dependent on frictional properties of the roof or floor material.

In the case study, with floor material properties (being the weakest), of $c = 200$ kPa and $\phi = 30^\circ$, the resultant (FOS_B) for a 20 m wide intra-panel pillar is well in excess of the design limit of 3.0 for bearing failure; which further supported the use of 20 m wide intra-panel pillars.

FURTHER STUDIES

Due to the concern for rupture of the "undisturbed" weak column of sandstone above the designed coal pillars, it was decided to conduct two geotechnical centrifuge tests on scaled models of the extraction system to examine the potential for such an event occurring. Centrifuge modelling is an effective and versatile method of producing realistic small scale model tests which can be related directly to a prototype situation. This is due to the fact that the behaviour of geotechnical materials such as soil and rock is largely dependent on stress levels. In a conventional model test, performed in the earth's gravitational field, it is not possible to maintain similarity with prototype situations whilst ensuring that the stress levels in areas of interest reach prototype values. A geotechnical centrifuge can subject small scale models to centripetal accelerations which are many times the earth's gravitational acceleration. This makes it possible to better represent full scale stress levels and thus ground response in the small scale model, and in particular the goafed material which is an important part of the subsidence processes.

The first model (run immediately prior to extraction of the trial panel; to further test the proposed use of 20 m wide intra-panel pillars) was scaled directly to 1/300 of the dimensions of the prototype extraction panel given earlier. The results from this test largely supported previous design assumptions that relatively small strains occurred in all aquitards, with the exception of the first aquitard where horizontal strains approached the ultimate failure strain of these materials ($1.6 \rightarrow 2.0$ mm m⁻¹ as established from laboratory testing). This centrifuge test also proved that no measurable subsidence developed, and that no interaction between the separate goafs on either side of the pillar occurred. This evidence gave the researchers greater confidence in the proposed design for the trial panel/pillar extraction panel.

The second geotechnical centrifuge test modelled a 13 m wide intra-panel pillar with two 40 m sub-panels on either side at 104 m depth of cover. The mining height adopted for this model was artificially high – 4.3 m. This model demonstrated emphatically that a large scale collapse of the "undisturbed" superincumbent sandstone column was possible and should be taken into account for coal pillar design. This collapse resulted in an increase in overall subsidence from very little to greater than 60% mining height at 50% cover depth above the intra-panel pillar. This test demonstrated that a major collapse occurred immediately after "extraction" of the first of the two 20 m wide "lifts" in the second of the 40 m wide sub-panels. It is thought that the timing of the collapse is critical to this event occurring and has been attributed to the point in time when minimal confinement is provided by first caving at the newly goafed edge of the intra-panel pillar. This lack of confinement thereby allows the superincumbent sandstone column to shear toward this, initially, unconsolidated goaf.

It is proposed that the stability of this "undisturbed" column is also influenced by the height of first caving and the rock mass strength of the superincumbent column of strata between the two areas of collapsed ground. However, at this stage, neither of these variables can be defined well enough to be used for design purposes in all mining conditions.

TENTATIVE DESIGN FOS_C

It has already been established that a design FOS_C of 2.2 is adequate to maintain stability of the entire pillar support system between the two fully goafed 40 m wide sub-panels

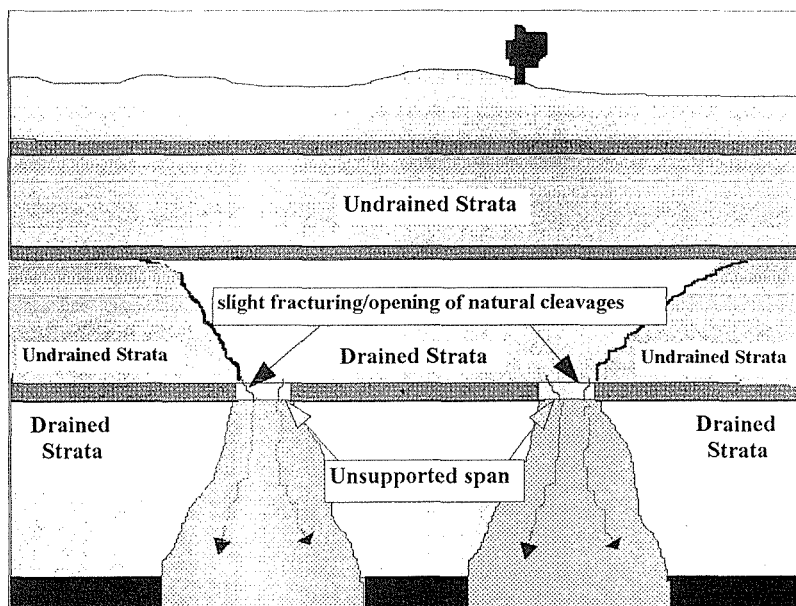


Fig. 6 Illustration of shearing of triangular wedge at the goaf edge and tributary load. This momentarily results in a rectangular shaped pillar which is useful for calculation of required pillar dimensions.

however the precise lower limit for the design FOS_C has yet to be determined. In order to assist the definition of a design FOS_C for the intra-panel coal pillars for narrower or wider panels, in ground conditions similar to those existing at Collie, the following points are listed:

- (a) It has been demonstrated that major failure can occur with limited extraction on one side of the pillar and large scale extraction on the other. It follows therefore that the pillar design FOS_C must be calculated for this worst case scenario.
- (b) It is postulated that in cases where large goafed areas exist on both sides of intra-panel pillars – in this case 40 m or more each side – the constraining pressure provided to both the superincumbent sandstone column and coal pillar by the goaf material will increase the apparent strength of the pillar.
- (c) Through back-analysis of the trial panel, the resultant FOS_C with a fully collapsed goaf on one side and first caving on the other side of the pillar is 2.6. After back-analysis of the failure of the 13 m wide superincumbent sandstone column with a 4.2 m mining height, in the second centrifuge test (when failure occurred with a 40 m goaf on one side and a 20 m goaf on the other side of the intra-panel pillar – see Fig. 6); the resultant FOS_C of the coal pillar was 1.2.

Therefore, taking these points into consideration, and in the absence of further testing, it is suggested that a design FOS_C of 2.5 be used when designing for the long-term stability of intra-panel coal pillars below weak sediments of similar nature to those existing in the test panel.

CONCLUSIONS

Mining subsidence mechanisms and characteristics of the unique, weak and water saturated coal bearing sediments in the Collie basin have been investigated both in the field, and laboratory. Empirical predictive subsidence "models" have been established from these investigations and design criteria established which have been successfully used for subsidence management through panel/pillar mining. It has been established that in conjunction with the need to limit mining widths to control subsidence, it is also essential to maintain the permanent stability of the supporting column of strata between the sub-panels. Failure to keep this supportive strata intact will result in the large scale collapse of this material and therefore the development of significantly more subsidence than is desired.

Acknowledgements The authors wish to thank Western Collieries Ltd and the Minerals and Energy Research Institute of Western Australia for their support and encouragement for this project. The views expressed in this report represent those of the authors and are not necessarily the same as those of the Company.

REFERENCES

- Bieniawski, Z. T. (1982) New design approach for room and pillar coal mines in the USA. Source unknown.
- Brauner, G. (1973) *Subsidence Due to Underground Mining*. US Dept of the Interior, Washington USA.
- Misich, I. (1995) *Underground mine planning and subsidence prediction in the Collie coalfields*. Forthcoming PhD dissertation, Curtin University, Perth, Western Australia.

- Misich, I. & Humphreys, D. (1988) Internal memorandum to Western Collieries Ltd. Collie, W. A., Misich, I., Evans, A. & Jones, O. (1993) Subsidence prediction and management in Collie (Western Australia). *Proc. Conf. in Mining Subsidence in Urban Areas* (Rock Springs, Wyoming, September 1993).
- Misich, I. Evans, A. & Jones, O. (1991) Control and strata investigations to allow total extraction of coal by underground methods in the Collie basin (Western Australia). *Proc. 4th Int. Mine Water Congress* (Ljubljana, Slovenia, September 1991).
- Misich, I. Evans, A. & Jones, O. (1994) Subsidence prediction and management in the Collie coalfields (Western Australia). *Proc. Third International Conference on Environmental Issues and Waste Management in Energy and Mineral Production* (Perth, Western Australia).
- National Coal Board (1975) *Subsidence Engineers Handbook*. Braun Brumfield Inc., Ann Arbor, Michigan.
- Peng, S. (1992) *Surface Subsidence Engineering*. Braun Brumfield Inc., Ann Arbor Michigan.
- Salamon, M. D. G. & Oravec, K. I. (1967) Rock mechanics in coal mining. *Contract Report to the Coal Mining Research Controlling Council*. Chamber of Mines, South Africa.
- Scott, C. R. (1980) *Soil Mechanics and Foundations*. Applied Science Publishers, London.
- Stacey, T. R. & Page, C. H. (1986) *Practical Handbook for Underground Rock Mechanics*. Trans Tech Publications, Clausthal, Germany.
- Wagner, H. (1980) Pillar design in coal mine. *J. S. Afr. Inst. Min. Metall.* **80**, 37-45.

Origin, diagnostics, and mitigation of a salt dissolution sinkhole at the US Strategic Petroleum Reserve storage site, Weeks Island, Louisiana

JAMES T. NEAL

Sandia National Laboratories, Albuquerque, New Mexico 87185-0706, USA

ROBERT E. MYERS

US Department of Energy, 900 E. Commerce Road, New Orleans, Louisiana 70123, USA

Abstract A sinkhole was first observed in May 1992 over the edge of the two-level former salt mine that was converted for oil storage by the US Strategic Petroleum Reserve (SPR). Diagnostic studies that included geophysical, geochemical, drilling, and hydrological methods suggest a direct connection exists between the surface collapse area and the underground mine as shown by correlative measurements of sediment slump rates and probable brine influx into the mine. The dissolution of salt below the sinkhole that initiated the leak into the mine was likely caused by several confluent geologic processes, and exacerbated by mining-induced stresses that created fractures which served as hydrologic flowpaths. Modelling studies of mine stresses show that years may be required before tensional cracking begins to occur, but once begun can continue to develop, and relieve the stress in that specific regime. The crack regime creates the avenue for incursion of groundwater, very slowly initially, but gradually enlarging as undersaturated groundwater dissolves salt on the sides of the crack. Mitigation measures include increasing the mine pressure, slowing the dissolution by injecting brine into the sinkhole throat, and construction of a freeze curtain to restrict hydrologic flowpaths.

INTRODUCTION

A sinkhole measuring 11 m (36 ft) across and 9 m (30 ft) deep was first noted in the sediments that overlie the Weeks Island, Louisiana, salt dome in May 1992, but appeared to be about a year old, based on initial surface appearance and later reverse extrapolation of growth rates. Its position directly over the edge of the SPR oil storage chamber, a former room-and-pillar salt mine, caused immediate concern. The association of sinkholes over mines is well established and this occurrence suggested that groundwater influx was probably causing salt dissolution at depth, with associated collapse of soil at the surface. Leaks of groundwater into other salt mines in Louisiana have sometimes led to flooding and eventual abandonment. Consequently, much attention has been and continues to be given to characterizing this occurrence, and to possible mitigation. This paper summarizes current knowledge, and describes diagnostic

and risk mitigation efforts being conducted by the US Department of Energy, operator of the Strategic Petroleum Reserve (Bauer *et al.*, 1994).

LOCATION, OCCURRENCE, AND CHARACTERISTICS

The Weeks Island salt dome is located 23 km (14 miles) south of New Iberia, Louisiana, and is the central dome in the Five Islands chain, along with Belle Isle, and Cote Blanche, Avery, and Jefferson Islands. All five have been mined because of their near-surface salt, and their logistical advantage near the Gulf of Mexico and the Intracoastal Waterway. Belle Isle and Jefferson Island are now closed to mining because of deliberate and inadvertent flooding, respectively.

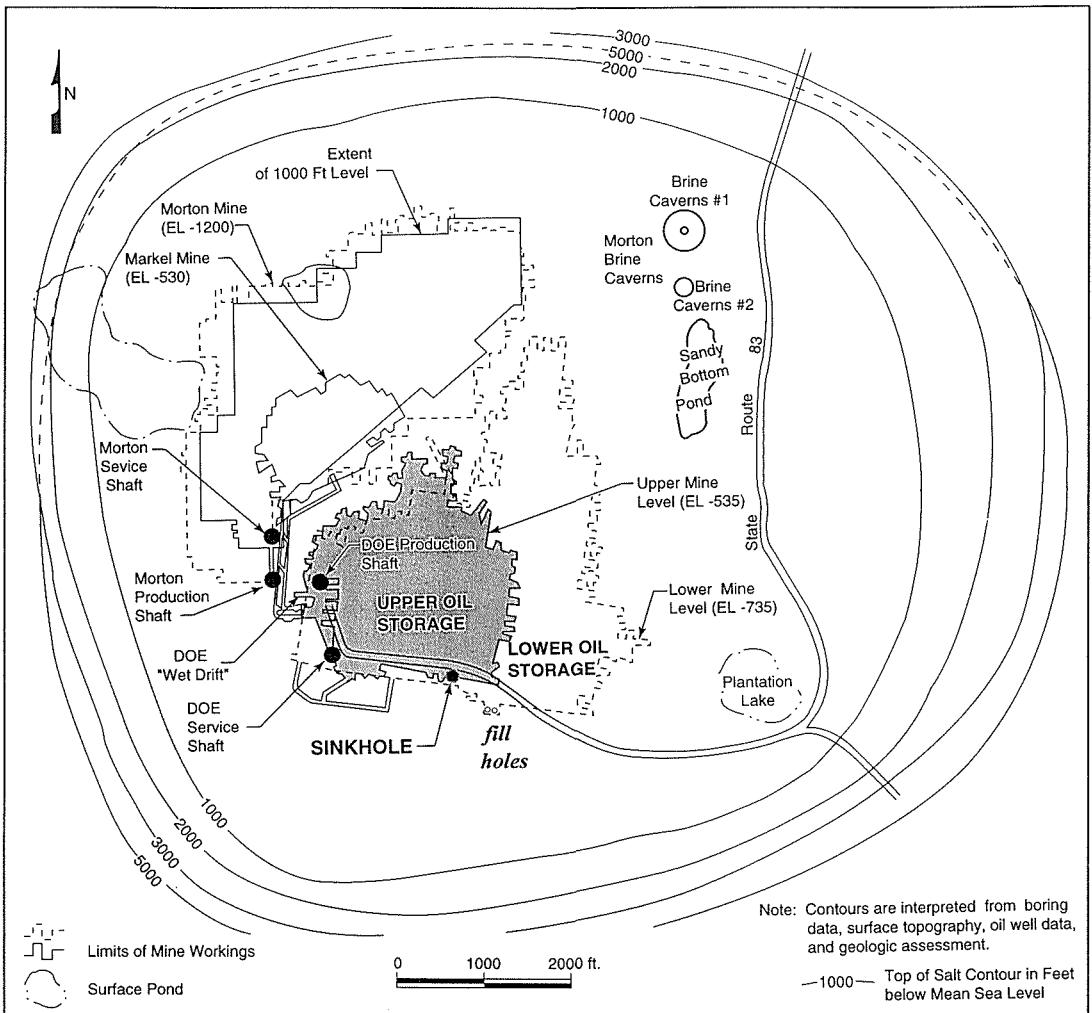


Fig. 1 Weeks Island salt dome, Louisiana, showing location of the sinkhole, fill holes, mined areas, and contours atop the salt stock (below mean sea level).

The Weeks Island sinkhole occurs over the southern perimeter of the Upper Level of the two-level SPR mine (Figs 1, 2), which has held 73 million barrels of crude oil since 1981. The mine was originally opened in 1902 and salt was extracted commercially until 1977, at which time Morton Salt developed a new mine immediately adjacent to the northwest while the older workings were converted for oil storage. Minor leaks of water had been noted at various times during the 75 years of active mining, but in-mine grouting was able to control inflow (Acres International Corporation, 1987).

The nearly vertical sidewalls in the surface sediments surrounding the sinkhole caused some perplexity initially, but were readily explained geologically as typical of Pleistocene loess deposits which cap the island. The sinkhole was also directly beneath a former residence of the now dismantled Morton town site, but appears unrelated to the sinkhole origin.

The sediment cover, consisting of deltaic alluvium of the ancestral Mississippi River, is about 56 m (185 ft) thick over the top of salt, which is 30 m (100 ft) below sea level at the sinkhole. The water table conforms generally with sea level over the dome but fluctuates with topography and frequent torrential rains.

The relatively small size of the sinkhole and lack of diagnostic evidence linking it with the SPR mine caused little concern initially. The location near both the edge of the

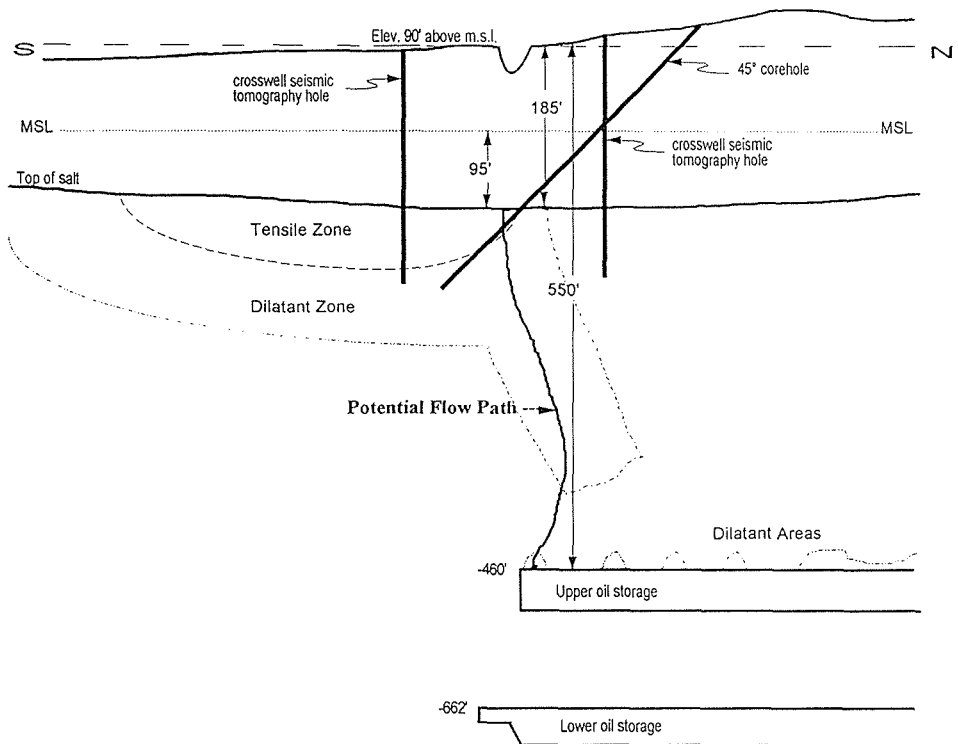


Fig. 2 Geomechanical modelling by Ehgartner (1993) showed mechanism for crack development in tension zone that would develop over mined openings after a number of years, and progressing through weakened dilatant zone. Based largely on these modelling results, crosswell tomography was conducted and angled boreholes were planned to intersect such features.

dome and anomalous features in the salt stock suggested the possibility of an entirely natural origin (Neal *et al.*, 1993), although Martinez (1992) insisted that mine-induced factors were likely involved. A watch and wait position was adopted, and in March 1993 fluoroscein dye was placed in the sinkhole as a means of detecting connections with the underground mine, or to the surface down dip of the sinkhole. But by mid-1993 it was apparent that the sinkhole was deepening, and there was monitoring data suggesting that the brine influx into the mine was increasing. Calculations of long-term geomechanical behaviour showed that salt cracks would be predicted at peripheral positions over mined openings, thus providing a mechanism for eventual incursion of groundwater (Fig. 2).

Sinkholes also had formed under very similar conditions at other mines in domal salt (Neal, 1994). Thoms (1994) suggested that the salt under the sinkhole may have been geologically susceptible in addition to being stressed by mine deformation, as evidenced by several anomalous conditions that were noted during the original mining, including black salt, blowouts, and minor seeps. Collectively the evidence suggested ongoing dissolution was increasing and that further study was required, in addition to engineering planning to address actions for decreasing the risk of continued oil storage and/or relocating the inventory.

DIAGNOSTIC EFFORTS

Unlike other mines where leaks can be observed underground, the SPR mine is sealed and must rely on indirect evidence such as changes in the oil/water interface, increased pressure, or changed isotopic composition of the contained water ($\sim 750\,000$ barrels or $1.19 \times 10^5 \text{ m}^3$), about one percent of the total volume. The diagnostics are complicated by salt creep closure, which is gradually reducing the storage volume by one-fifth of one percent per year ($\sim 160\,000$ barrels, $2.54 \times 10^4 \text{ m}^3$), a very small amount overall, but a *very large* amount with respect to the few gallons per minute leaks which could explain the sinkhole.

Water inflow into the mine was suggested by increasing amounts of brine that was observable in the fill hole sump used for injecting oil during initial fill operations. While not a precise measurement, in early 1994 the inflow trend increased from one to nearly three gallons per minute. This increase was noticed immediately following filling of the sinkhole with sand; the decision to fill was made because it had deepened to more than 12 m (40 ft) and its location 15 m (50 ft) from the main access road was hazardous. As soon as the fill was placed, continued deepening of the sinkhole began occurring, at a rate of about 1.5 m^3 (2 yards³) per day, requiring new fill weekly. This suggested that dissolution was ongoing, and there appeared to be a correlation with the amount of increasing brine that was observed in the fill holes and the increasing sinkhole volume.

Brine hydrochemistry is frequently analyzed in salt mines to distinguish meteoric water from connate water. At Weeks Island a decided change in isotopic composition was evident in comparing 1993 water from the fillhole sump with that obtained in late 1991, about the same time postulated for the sinkhole origin (Knauth, 1994). Although inconclusive, earlier data suggested that the leak may have existed as early as 1987.

Rock mechanics modelling by Ehgartner (1993) showed that the areas near the mine perimeter would be in tension and that fractures in salt could have formed as early as 1970 (Fig. 3). Such a crack could be exposed to undersaturated groundwater and

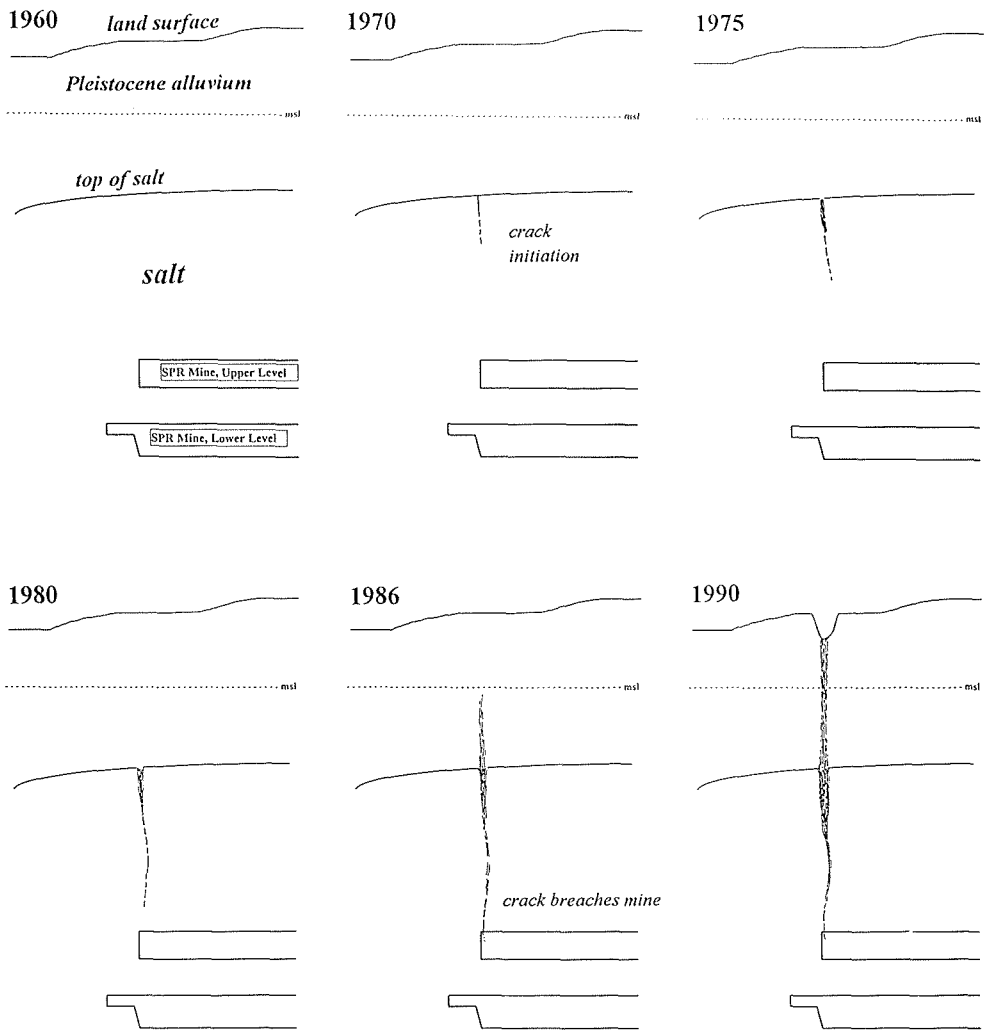


Fig. 3 Conceptual development of Weeks Island, Louisiana, sinkhole, based on geomechanical modelling and presumed hydrologic connection with undersaturated groundwater. The sinkhole was first observed in 1992, but likely took years to develop. Progressive enlargement of the dissolution channel was initiated following formation of tension crack(s) ca. 1970, but not manifesting as a sinkhole until about 1990-1991.

gradually enlarge at the same time the crack was extending. The modelling results are validated by actual survey data showing subsidence over the mine, which is in close agreement with Ehgartner's modelling

Seismic reflection profiling was conducted in the area of the sinkhole in early 1994, being an expedient way to obtain subsurface information (Miller *et al.*, 1994). A prominent reflector, first thought to be top-of-salt, was noted throughout the area at shallow depth. Subsequent drilling, coring, and geophysics showed that the reflector was essentially coincident with the piezometric surface, and that a localized 4 m (13 ft) deflection at the sinkhole was a possible drawdown created by the inflow of groundwater

into the presumed point of leakage. Secondary anomalous step deflections were noted north of the main sinkhole and caused some concern initially, realizing that sinkholes often progress and occur in multiples. However, these secondary features disappeared with refined velocity corrections. Permeabilities of the surrounding sediments were later found to be very high; thus there is insufficient information to identify the specific source of the seismic reflector as it most likely cannot be the water table. The deflection of the reflector at the sinkhole may be an expression of the sediment collapse into the dissolution void below the sinkhole.

Crosswell seismic tomography was conducted by placing sources and receivers in four boreholes on diagonals of the sinkhole. The boreholes also provided direct information on sediment and salt geometry, and the hydrologic environment. The tomograms showed clear evidence of low-velocity material below the top of salt, verifying that a sediment-filled void(s), possibly interconnected, occurred between the much higher velocity salt on either side (Harding, 1994). However, the combination of drilling and tomography showed that the area of dissolution below the sinkhole is laterally limited, and with a strongly-vertical dimension.

Slanthole drilling directly into and below the sinkhole provided the most direct confirmation of dissolution geometry as evidenced by the drilling of boreholes BH-7A and BH-9 (Fig. 4). *Slanthole BH-9*, adjacent to the sinkhole, was drilled at a high-angle approach directly over the top of the subsurface extension of the surface expression. It extended below the top-of-salt elevation encountered in the tomography holes. This wellbore provided the opportunity in July 1994 for injection of rhodamine dye into the apparent throat of the sinkhole. The dye, if detected in the fill hole sump, would provide unequivocal evidence of hydrologic connection with the mine. After seven months of

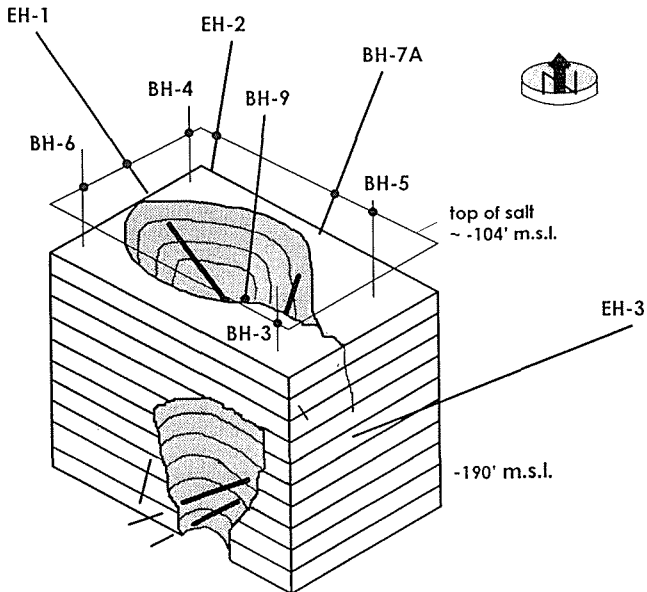


Fig. 4 Diagrammatic representation of exploratory drilling and geometry of sinkhole throat. Boreholes BH-3, 4, 5, and 6 were drilled for crosswell seismic tomography; slantholes BH-7A and 9 were drilled for throat definition. EH-1, 2, 3 further defined the throat and provided decisive information regarding grouting potential. Accentuated portions of boreholes define throat penetrations.

monitoring, dye had not yet been detected in the mine. Dye dispersion calculations predicted that it could take a year or more to reach the sampling point (Linn & Hinkebein, 1994).

Slanthole BH-7A started at 60° inclination and was aimed at the sinkhole at depth. It penetrated the top-of-salt at the normal depth of 185 feet (~56 m) and then continued on through salt into a major sand-filled void at least 22 m (72 ft) deep and 2 m (7 ft) wide. A 3-D hydrologic flowmeter was installed in the void and operated for two weeks (Bauer *et al.*, 1994; Ballard, 1995a,b). The data indicated essentially vertical flow down the throat, diminishing to 0.3 m/day. The 3 cm (~1 in) per day downward movement of the flowmeter itself also indicated that sediment was moving down the throat, presumably in response to dissolution of salt by undersaturated groundwater at some point below. This borehole also enabled the injection of more dye.

Slanthole EH-1, at 90° to BH-7A, transected a 5.5 m (18 ft) sand-filled void at about the same depth, further defining an elongated cross-section. *Slanthole EH-2* between EH-1 and 7A did not enter the void, even after several offset attempts. *Slanthole EH-3* intersected the void from the opposite (east) side, with lateral dimensions of 15 and 10 ft at two different depths. The drilling indicated a very irregular dissolution feature, but with strong vertical dimensions directly below the sinkhole. Throat sand samples recovered in EH-1 and BH-7A showed strong rhodamine dye saturation. Even though throat sand samples recovered from EH-3 and EH-3 sidetrack #1 showed no dye saturation, it was determined to be hydraulically connected based on flowmeter response in BH-9, 90 ft (27.5 m) above, during attempts to place a flowmeter below in BH-3.

Near-surface gas mapping (hydrogen, methane, others) in the vicinity of the sinkhole was conducted, as this method has been employed in identifying leaking hydrocarbon sources elsewhere, as well as for oil exploration. The surveys did find localized areas of high hydrogen, but not in the sinkhole. High methane levels were found in the sinkhole, which alone without ethane would not confirm crude oil vapour (LSU, 1994). This study has not yet provided conclusive interpretations based on limited data but should not imply that the method was unsuccessful, as other anomalies were consistently measured. Gas mapping of petrogenic methane may be useful in delineating salt stock features, e.g. anomalous zones, elsewhere.

Self Potential (SP) surveys were successful at one other sinkhole at another mine by virtue of mapping streaming potential caused by groundwater flow; thus the method was tested at Weeks Island (Bauer *et al.*, 1994). As anomalous drawdown was believed to occur near the sinkhole, it was thought that this method might reveal other indications, and possibly more about secondary areas of leakage, hinted at by apparent anomalous seismic reflections northeast of the main sinkhole. The data did show anomalies near the sinkhole, but also contained ambiguities. The anomalous streaming potentials were interpreted to result from vertical fluid flow along near-vertical planar surfaces.

Piezometric monitoring and permeability testing was initiated in late 1994, as a means of observing the groundwater environment more directly. Permeability measurement was a high priority for determining grouting approaches, and for estimating other hydrologic conditions involving the water inflow. Permeabilities in the 35-90 Darcy range (averaging ~60 Darcies) were measured for the 30 m (100 ft)-thick saturated alluvial sediment sections during several pump tests (ViroGroup, 1994; Ostensen, 1994). These high permeabilities showed the difficulty of measuring any fluctuations in water levels, especially those associated with a very small flow rate into the sinkhole leak area.

Progression of the sinkhole, including new occurrences, is anticipated but with unknown timing, based on similar experience elsewhere, and the continuing development of causative factors that produce the salt dissolution. In addition to monitoring subsidence annually over the entire mined areas, the surface over the perimeter of the mine has been visually observed for telltale changes. Because of the anticipated progression, several mitigation approaches were considered.

MITIGATION EFFORTS

Once the geometry of a deep void or crevasse was identified, with direct measurement of downward flow of water, the suggestion was made by Diamond & Mills (1994) to *feed saturated brine* directly into the throat through Borehole 7A. Beginning in August 1994 and continuing at present, approximately three gallons per minute are being gravity fed into the throat 22 m (72 ft) below the top of salt. The encouraging result was that subsidence at the sinkhole was arrested, and virtually no additional downward movement of fillsand was measurable. In addition, the apparent groundwater depression at the sinkhole no longer was observable. The brine introduction evidently had stopped the dissolution of salt, but whether this could be a longer-term fix was problematic; a decision was then made to relocate the SPR oil inventory at an early date and by the safest means.

Raising the internal mine pressure from 4.8×10^4 to 1.7×10^5 Pa (7 to 25 psi) was instituted in mid-1994 as a means of reducing inflow of brine. Although this increase was only a small amount, raising the pressure has the effect of reducing the external pressure gradient, as well as slowing salt creep closure (Bauer *et al.*, 1994).

Grouting was considered early but not yet instituted by late 1994 because of the effectiveness of introducing brine to control dissolution, combined with the uncertainty about the hydrologic environment and how and where to place grout, and the fear of doing more harm than good. In early 1995, following the completion of the diagnostics effort and mapping of the "plumbing," a decision was made that permeation grouting would be ineffective and that groundwater control could better be achieved by the installation of a freeze curtain; plans were underway to begin construction in 1995, followed by removal of oil from the mine and relocation to other SPR sites.

CONCLUSIONS

The sinkhole at Weeks Island formed over the edge of the mine as a result of geological, hydrological, and mine-induced factors. The location near the edge of the dome, astride a probable geologically anomalous zone, set the stage for the mine configuration and boundaries. Mine geometry and excavation-induced stresses placed the mine periphery in tension, probably favouring crack development as early as 1970. Eventual incursion of undersaturated groundwater traversed the 107 m (350 ft) salt back over the mine, allowing entry of brine into the SPR mine. Gradually increasing dissolution enlarged a void at the top of salt, creating the collapse environment for the sinkhole which formed circa 1990-1991. Exploratory drilling and geophysics defined the void or crevasse beneath the sinkhole, enabling the introduction of saturated brine directly into the throat.

The brine arrested the continuing subsidence at the sinkhole, apparently as a result of controlling ongoing dissolution. Additional drilling diagnostics and hydrologic analyses determined that mitigation could best be achieved by constructing a freeze wall around the sinkhole to control groundwater, prior to removing oil from the mine.

Acknowledgements This paper summarizes the collective efforts of literally dozens of people at Sandia National Laboratories, DynMcDermott Petroleum Operations Company, and the US Department of Energy. This work was performed at Sandia National Laboratories and supported by the US Department of Energy under Contract DE-ACO4-94AL85000.

REFERENCES

- Acres International Corporation (1987) Weeks Island Strategic Petroleum Reserve geological site characterization report, Albuquerque, New Mexico. *Sandia National Laboratories Report SAND87-7111*.
- Ballard, S. (1995a) The in situ permeable flow sensor: a groundwater flow velocity meter. *J. Groundwater*, in press.
- Ballard, S. (1995b) Groundwater flow velocity measurements in a sinkhole at the Weeks Island Strategic Petroleum Reserve Facility, Louisiana. *Symp. on Appl. of Geophysics to Environmental and Engineering Problems* (Orlando, Florida).
- Bauer, S. J. *et al.* (1994) Update of assessment of geotechnical risks, Strategic Petroleum Reserve, Weeks Island Site, Albuquerque, New Mexico. *Sandia National Laboratories Report SAND94-2969*.
- Diamond, W. & Mills, K. E. (1994) Informal communication at a meeting of SPR participants and Morton Salt Company, July, 1994. The idea of injecting brine evidently was a collective, spontaneous decision arrived at by several individuals, most conspicuously Diamond & Mills.
- Ehgartner, B. L. (1993) Weeks Island stress prediction and relationship to sinkhole formation. Internal memorandum, 18 October 1993, Sandia National Laboratories Dept 6113, Albuquerque, New Mexico.
- Harding, R. S. Jr (1994) Borehole seismic survey, Weeks Island Sinkhole. Internal memorandum with attachments, Sandia National Laboratories Dept 6114, Albuquerque, New Mexico.
- Knauth, L. P. (1994) Stable isotope constraints on the origin of brine in the Weeks Island Strategic Petroleum Reserve. *Arizona State University Contract Report to DynMcDermott Petroleum Operations Company, New Orleans, Louisiana*.
- Linn, J. K. & Hinkebein, T. E. (1994) Modelling estimates of dye detection in fill holes. Internal memorandum, Sandia National Laboratories Dept 6113, Albuquerque, New Mexico.
- LSU (1994) Contract report from Institute for Environmental Studies, Louisiana State University to Sandia National Laboratories, Albuquerque, New Mexico, 29 July, and October 1994.
- Martinez, J. D. (1992) Personal communication with Dr Martinez established that natural causes probably were less likely than mine-induced factors. Professor Emeritus, Louisiana State University, Baton Rouge, Louisiana.
- Miller, R. D. *et al.* (1994) High resolution seismic survey near SPR surface collapse feature at Weeks Island, Louisiana. Contract report, Kansas Geological Survey to Sandia National Laboratories, Albuquerque, New Mexico.
- Neal, J. T. *et al.* (1993) Anomalous zones in Gulf Coast salt domes, with special reference to Big Hill, Texas, and Weeks Island, Louisiana, Albuquerque, New Mexico. *Sandia National Laboratories Report SAND92-2283*.
- Neal, J. T. (1994) Surface features indicative of subsurface evaporite dissolution: implications for storage and mining. *Solution Mining Research Institute Spring Meeting* (Houston, Texas, 25-27 April 1994).
- Ostensen, R. W. (1994) Permeability inferred from Weeks Island well tests. Internal memorandum, Sandia National Laboratories Dept 6113, Albuquerque, New Mexico.
- Thoms, R. L. (1994) Weeks Island sinkhole. Draft report submitted to Sandia National Laboratories, Department 6113 internal contract with AGM Inc., February 1994.
- ViroGroup (1994) Weeks Island SPR site aquifer evaluation. Contract Report to Dillingham/Foundation.

Prediction of land subsidence caused by mine dewatering

HAMID REZA NIKRAZ, MARTIN PRESS

School of Civil Engineering, Curtin University of Technology, Kent Street, GPO Box U 1987, Perth 6001, Western Australia

ALBERT EVANS

Collie Federated School of Mines, Curtin University of Technology, Kent Street, Perth, Western Australia

Abstract This paper describes the research carried out to evaluate the compaction associated with dewatering as an aid to surface subsidence prediction in the Collie Coal basin. A triaxial test technique has been adapted to evaluate the compaction characteristics of the sandstone aquifer in the Collie basin. The technique, which allows the strata stress regime to be reproduced by triaxial loading with zero lateral strain, also provides a precise evaluation of lateral stresses and consequently Poisson's ratio under *in situ* conditions. The paper contains a description of equipment commission, test techniques, results, and the analysis and interpretation of derived data obtained. The testing and evaluation techniques are general in nature and are applicable to field situations in locations where similar weak sandstones occur.

INTRODUCTION

The Collie basin lies nearly 200 km south-southeast of Perth in Western Australia and is 27 km long by 13 km wide, covering an area of approximately 230 km². It contains extensive reserves of good steaming coal which is currently being mined by both open cut and underground methods.

The Collie Coalfield has a long history of strata control problems. They manifest themselves in the form of localized poor roof control, surface subsidence, slope instability and mine abandonment (due to a sand-slurry inrush). Major sources of these problems include the very extensive, weak, saturated, sandstone aquifers. As a result, underground operations have been limited to room and pillar extraction, presently carried out by continuous miners and road-heading machines. Approximately 30-40% recovery by volume is being achieved by this method.

In order to increase the recovery to approximately 70%, the Wongawilli method of shortwall mining has been introduced. With this method, extensive aquifer dewatering is carried out prior to caving of the immediate roof. However, due to the porous and weak nature of the aquifers, dewatering has the potential to cause subsidence, with a significant risk of environmental instability on a large scale. This is particularly critical adjacent to townsites and industrial complexes. For safe operations and limits to surface subsidence, an engineering design was needed which would control strata deformation

with a high degree of confidence. A better understanding of strata mechanics was needed to achieve this.

The roof dewatering/depressurization procedure involved a combination of in-mine vertical roof drainage holes and conventional dewatering bores constructed from the ground surface above the mining area. A full account of the dewatering strategy may be found elsewhere (Humphreys & Hebblewhite, 1988; Dundon *et al.*, 1988). Of prime concern is the effect of pore pressure reduction upon strata compaction. To simulate those effects it is necessary to perform tests under triaxial conditions of the same order as experienced *in situ*.

The pore pressure effect phenomenon is not a new concept. However, investigation of the effect under triaxial conditions is relatively new. Although rock bulk compressibility figures are generally larger for high porosities, simple compressibility porosity correlations do not exist. Furthermore, compressibility data reported for poorly-consolidated sandstone differ greatly. This paper describes the equipment and the techniques and procedures used in carrying out deformation characteristics of poorly-consolidated sandstone in Collie Coal basin.

ROCK MOVEMENTS CAUSED BY DE-WATERING IN POORLY CONSOLIDATED SANDSTONE

Land subsidence is caused by a number of mechanisms including withdrawal of fluid and the collapse of underground openings. This study is concerned with the former.

Deformations resulting from equilibrium disturbance of the aquifer rock due to water pressure decline, are either elastic or non-elastic. Elastic deformations are mostly of a negligible extent with respect to both the involved surface subsidence and the reserve of the stored water, being only of importance in respect to the variation of the rate of flow.

The extent of the non-elastic deformation are due to compaction or migration of the rock material. The former, depends on the geotechnical characteristics of the rock, and on the extent of the pore pressure reduction. The extent of migration, on the other hand, depends on the pressure gradient (the flow velocity). The compaction may cause regional subsidence, while the migration of the rock particles causes local displacement, both phenomena being dependent upon the characteristics of the aquifer rock and the extent of dewatering.

Several techniques are available for predicting subsidence due to fluid withdrawal, classed by Poland (1984) into three broad categories: empirical, semi-theoretical and theoretical. Empirical methods essentially plot past subsidence *vs.* time and extrapolate into the future based on a selected curve fitting technique. They suffer from a lack of well documented examples to establish their validity. Semi-theoretical methods link on-going induced subsidence to some other measurable phenomenon in the field. Theoretical techniques require knowledge of the mechanical rock properties, which are either obtained from laboratory tests on core samples or deduced from field observations. Essentially, however, theoretical techniques use equations derived from fundamental laws of physics, such as mass balance.

Geertsma (1966, 1973) has shown in a theoretical analysis that reservoirs deform mainly in the vertical direction and that lateral variations may be discarded if the lateral

dimensions of the reservoir are large compared with its thickness. For the one-dimensional compaction approximation, the vertical deformation of a prism of the aquifer material can be computed by:

$$\Delta h = C_m h \delta P \quad (1)$$

where Δh is the change in the prism height, C_m is the one-dimensional compaction coefficient, h is the prism height, and δP is the change in pore fluid pressure.

This approach was adapted by Martin & Serdengecti (1984). They suggest that the best way to obtain values of C_m , which in most cases is the most difficult of the three one-dimensional compaction parameters to determine, is to measure it on core samples in the laboratory.

The one-dimensional compaction coefficient " C_m " of friable sandstones can be measured by different methods:

- indirect measurement by measuring rock compressibility " C_b " under hydrostatic load and estimating Poisson's ratio of the rock;
- direct measurement by equipment which simulates the aquifer boundary condition of zero lateral displacement (such as, Oedometer cell test, or a modified triaxial cell test).

Although the triaxial test method is laborious and time consuming, its unique experimental conditions make it essential as they reproduce aquifer stress quite well. In addition, the triaxial set-up has the advantage that the circumferential pressure needed to prevent lateral strain is measurable. The Poisson's ratio of the rock sample can therefore be determined independently from the ratio of lateral to vertical stress.

LABORATORY-DETERMINED COMPRESSIBILITIES

The cores taken from Collie basin vary markedly in both porosity and grain correlation. Medium to high porosities are found in consolidated and semi-consolidated sections. In addition, the nonhomogeneous appearance of the cores suggest that rock properties vary over short distances. Consequently, compaction is expected to vary considerably with depth, implying that the cores must be sampled systematically at short intervals to obtain a reliable compaction profile. As this involves compaction measurements on a large scale, a simple, rapid, but nevertheless reliable measuring technique must be developed.

The earlier studies by Grassman (1951), Biot (1941), Geertsma (1957) and Van der Knaap (1959) resulted in the theory of pore elasticity. They demonstrated that compaction behaviour depends only on effective frame stress, i.e. the difference between external and internal stresses. Nikraz (1991) has confirmed that the effective stress theory is applicable to Collie sandstone. Therefore, to stimulate aquifer compaction in a laboratory experiment requires application of the stress difference instead of the actual stresses. Experimentally the most attractive approach is to load the samples externally, keeping the pore water pressure constant and atmospheric.

The triaxial technique which was developed in accordance with this reasoning predicts the compaction behaviour of strata due to dewatering in particular for the weakly cemented Collie sandstone. The technique allows the strata stress regime to be reproduced by triaxial loading with zero lateral strain, and also provides a precise evaluation of lateral stresses and consequently Poisson's ratio under *in situ* stress

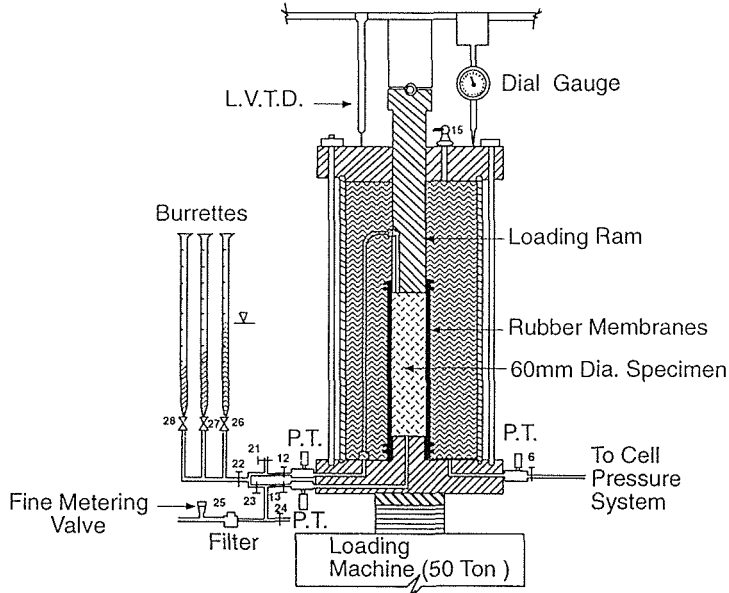


Fig. 1 Arrangement of apparatus for compaction test.

conditions. The condition of zero lateral strain during triaxial compaction test is achieved by both preventing any volume change in the cell-water system surrounding the specimen and by using the modified piston and top cap (Fig. 1). This piston is of the same diameter as the sample, therefore induced the triaxial stress in the sample, not the deviator stress. Because bulk volume change was detected from pore volume changes, the pores of the specimens had to be completely saturated. For full detail of the equipment design see Nikraz (1991). The experimental procedure had two stages:

- the preparatory stage, in which the specimen was brought into an "initial" loading state prior to the test;
- the test itself, which further compacted the specimen.

In order to eliminate possible membrane penetration effects during the test and thereby cause errors in test results, the specimens were first loaded hydrostatically to a pressure of 1.25 MPa. The volume change related to this pressure was assumed as a reference point. The axial stress was then measured continuously at a constant rate until the desired axial stress was achieved. The cell pressure was adjusted simultaneously to prevent any lateral strain. However, the maximum axial stress level was confined within cell pressure limitation (maximum cell pressure limited to 12 MPa).

To check the zero lateral strain, the following relationship had to be satisfied:

$$\Delta V = \frac{A X}{1000} \quad (\text{ml}) \quad (2)$$

where ΔV is the volume change (ml), A is the cross sectional area of the specimen (mm^2) and X is the axial deflection (mm).

To determine the effect of loading history on compaction, the axial stress was released incrementally to approximately 1.5 MPa. Consequently, the confining pressure was adjusted to satisfy equation (2). The loading and unloading were repeated for

another two cycles. A total of six tests were made on specimens at strain rate of $2 \times 10^{-4} \text{ min}^{-1}$.

RESULTS, ANALYSIS AND INTERPRETATION

Typical axial stress/uniaxial compaction and lateral stress/uniaxial compaction are shown in Figs 2 and 3 respectively. Similar behaviour was observed in the other five specimens.

The problem of choice of loading cycle for field application has been studied by Knutson & Bohor (1963), van Kesteren (1973), Mattax *et al.* (1975) and Mess (1978).

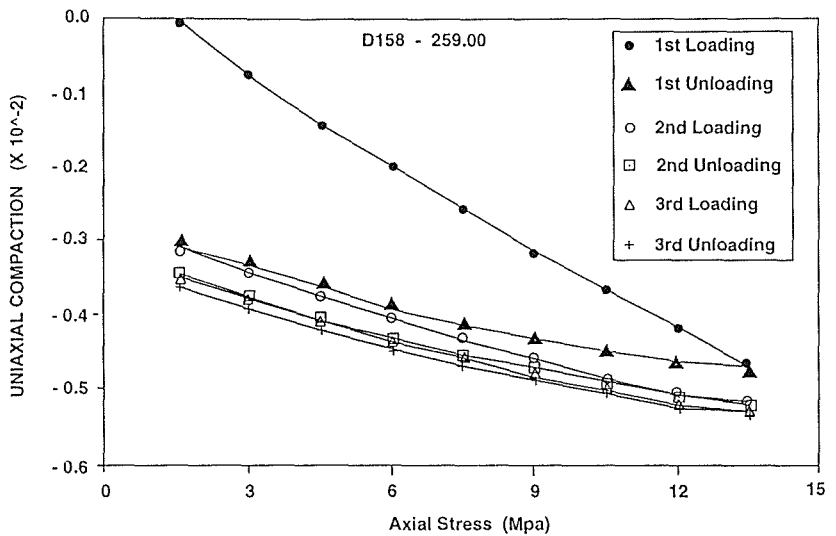


Fig. 2 Typical axial stress-strain compaction relationship with three loading cycles.

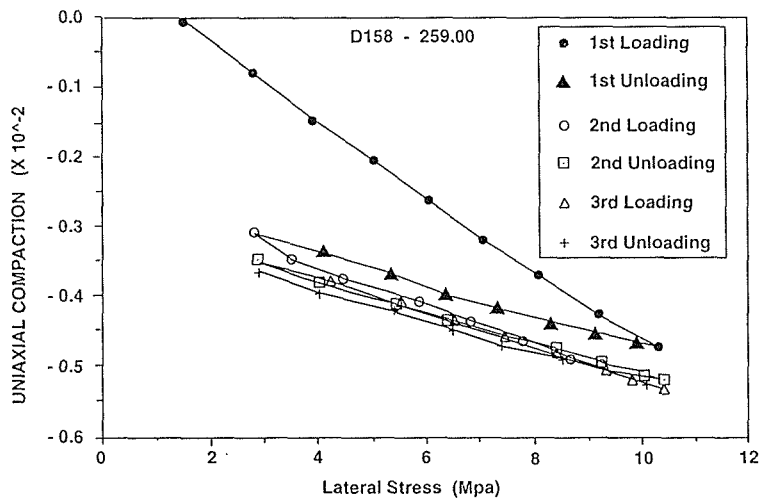


Fig. 3 Typical lateral stress-strain compaction relationship with three loading cycles.

For fully undisturbed unloaded core material, compressibility values derived in laboratory tests should be lower than *in situ* values for reservoirs that are not over-consolidated. For over-consolidated reservoirs they could be either too low or too high for *in situ* application, depending on the degree of over-consolidation of the reservoir rock.

Knutson & Bohor (1963) suggest that a reasonable compressibility value may be obtained by averaging values from the first and subsequent cycle. However, from extensive laboratory and *in situ* tests on relatively soft rock, Mattax *et al.* (1975) suggest that the first cycle compressibility is the most realistic measure of *in situ* response to changes in effective pressure that occur during reservoir depletion. However, erroneously high values of first cycle compressibility were obtained in the laboratory tests on unconsolidated sands because of systematic experimental error (caused by freezing and thawing of the sample, and some grain crushing). It was therefore recommended that about two thirds of the first cycle compressibility be taken as representative of *in situ* compaction. The uniaxial compaction curves representing the six samples tested are plotted in Fig. 4 for the first loading cycles. The graph shows an almost linear compaction/stress relationship for higher stresses, so that average compaction per unit stress can be calculated for this range. Further, the compaction curves are parabolic thus there is an observed relationship:

$$\varepsilon_1 \propto \sqrt{\sigma_1'} \tag{3}$$

where ε_1 is the axial strain and σ_1' is the axial effective stress.

To demonstrate the observed relationship the axial strains have been replotted against $\sqrt{\sigma_1'}$ (Fig. 5). This plot provides straight lines, although it is noted that some points deviate slightly from linearity. By using the linear relationship as shown in Fig. 5, the uniaxial compaction coefficient C_m may be calculated over the relevant stress interval.

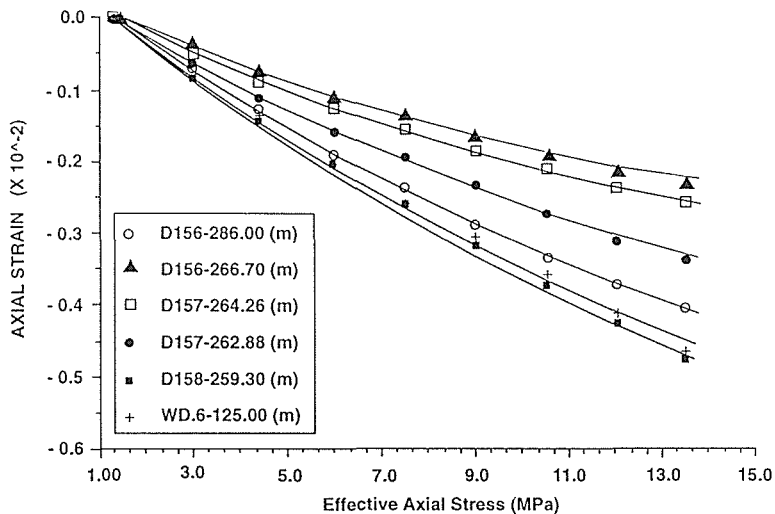


Fig. 4 Relationship between axial strain and effective axial stress for first loading.

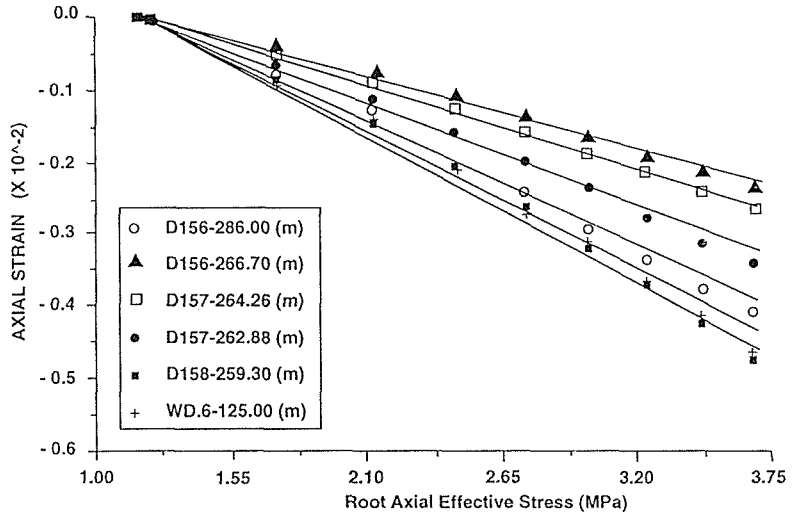


Fig. 5 Relationship between axial strain and root of effective axial stress for first loading.

Consider the simulation of dewatering operations for a typical specimen such as D156-286. Assuming an average overburden density of 2.5 t m^{-3} , the initial *in situ* hydrostatic effective stress 7 MPa would increase to 9 MPa to simulate the effects of dewatering. Hence the uniaxial compaction can be calculated by:

$$C_m = \frac{(\varepsilon_1)_9 - (\varepsilon_1)_7}{9 - 7} \tag{4}$$

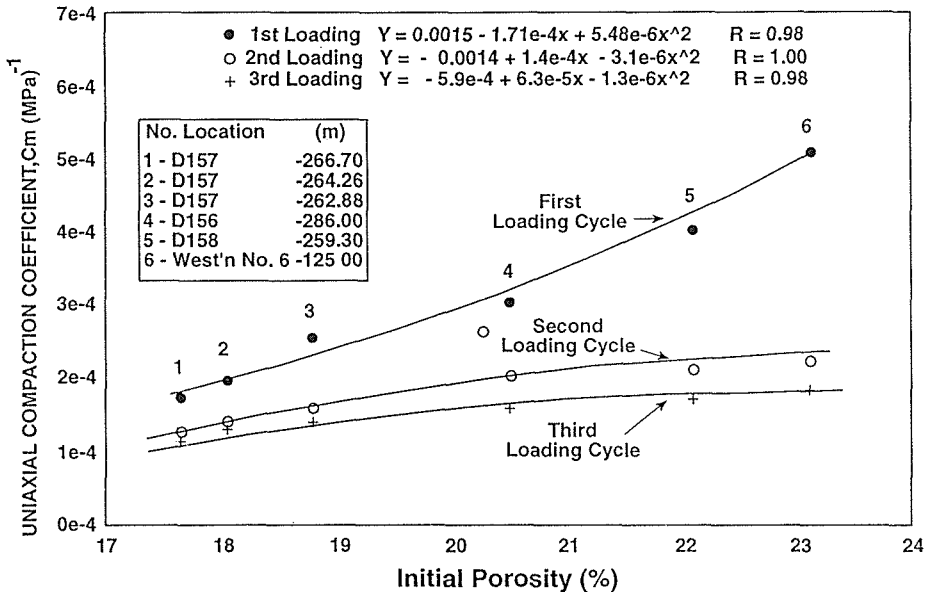


Fig. 6 Relationship between uniaxial compaction coefficient and initial porosity for first, second, and third loading.

where $(\varepsilon_1)_7$ and $(\varepsilon_1)_9$ are axial strain at hydrostatic effective stresses of 7 and 9 MPa respectively, giving:

$$C_m = \frac{(0.288 - 0.277) * 10^{-2}}{2} \quad (5)$$

The uniaxial compaction coefficient data corresponding to first, second and third loading cycles are plotted as a function of initial porosity in Fig. 6. It appears that compaction is greater for the first loading, indicating loading history influences on compaction. However, those correlations serve to assess a reliable average field value of the uniaxial compaction coefficient, which is required for a prediction of field compaction.

In an early study (Nikraz, 1991), the average porosity obtained from 105 samples tested as 20.77% of bulk volume. Variation in porosity between holes was considered to be minor. This, and the near linear relationship between uniaxial compaction and porosity prompted the acceptance of 20.77% porosity for the determination of an average value of the uniaxial compaction coefficient.

Based on the first loading cycle, Fig. 6 indicates a uniaxial compaction coefficient of $3.124 \times 10^{-4} \text{ (MPa)}^{-1}$. The effects of stress relief upon sampling are accommodated within this value. However, the second and third loading cycles exhibit elastic compaction characteristics and provide an average value of uniaxial compaction coefficient for the second and subsequent loading cycles of $1.6409 \times 10^{-4} \text{ (MPa)}^{-1}$.

The difference between the two values indicates the elastic component of compaction. Considering the strain-hardening and core disturbance arguments one may expect the true compaction to be somewhere in between. In view of the quite small difference between maximum and minimum values, the most practical approach seems to be to take the average as a working value, thus reducing the uncertainty to an acceptable limit. Thus, a mean value of $2.382 \times 10^{-4} \text{ (Mpa)}^{-1}$ was used to represent the *in situ* compaction coefficient.

Applying these results to a 12.5 m thick aquifer above the Collieburn No. 2, with an ultimate reduction in pore water pressure of 2.0 MPa could produce a vertical compaction of:

$$\begin{aligned} \Delta h &= -C_m h \Delta P \\ &= 2.382 * 10^{-4} * 12.5 * 10^3 * 2 \\ &= 5.96 \text{ mm} \end{aligned} \quad (6)$$

The Poisson ratio of the specimens tested can be determined independently using the ratio of lateral to vertical stresses. The ratio of lateral to vertical stresses under isotropic conditions suggested by Teeuw (1971) is:

$$\frac{\sigma_h}{\sigma_v} = \left[\frac{\nu}{1-\nu} \right]^{1/n} \quad (7)$$

where ν is Poisson's ratio and n is the exponent in relationship of the uniaxial compaction/axial pressure in Fig. 6. The exponent reflects the deformation of the contact points and/or contact areas between grains (Brandt, 1955). According to Hertz's theory (Timoshenko & Goodier, 1951) for perfect spheres $n = 2.3$, while for linear elastic media such as non-porous quartz and steel, $n = 1$ reducing equation (7) to the well known equation:

$$\frac{\sigma_h}{\sigma_v} = \frac{\nu}{1-\nu} \quad (8)$$

Thus, for ideally elastic materials, a variation in n reflects a change in grain sphericity at the point of contact between adjoining grains. The values of n for the specimen tested range from 0.869 to 0.982. This range is higher than the value of 0.677 for spheres and indicates flatter contact surfaces.

CONCLUSION

Special purpose-designed triaxial testing equipment has been designed, tested and commissioned. A series of uniaxial compaction tests were performed for laboratory determination of compressibilities and *in situ* behaviour of the Collie sandstone. The following conclusions are drawn.

Whilst recognizing the early stages of development of subsidence prediction, some deformation has been postulated based on laboratory observations. *In situ* monitoring of strata deformation will be required for verification of the actual deformation mechanisms at work. It has been observed that the uniaxial compression of Collie sandstone is characterized by significant nonlinearity, hysteresis and an irrecoverable strain on unloading.

Uniaxial compaction curves have been presented for the sandstone aquifer in the Collie basin. It was found that the uniaxial compaction curves were parabolic over the major part of the stress range. This yielded the expression:

$$\varepsilon_1 \propto \sqrt{\sigma_1'} \quad (9)$$

A good correlation was found to exist between the uniaxial compaction coefficient and porosity. The correlation was quantified by regression analysis. Considering the different compaction behaviour of the specimens in the first and subsequent loading cycles, an average value for uniaxial compaction coefficient equal to $2.382 \times 10^{-4} \text{ (MPa)}^{-1}$ was obtained for an average porosity of 20.77%.

REFERENCES

- Boit, M. A. (1941) General theory of three-dimensional consolidation. *J. Appl. Phys.* **12**(2), 155-162.
- Brandt, H. (1955) A study on the speed of sound in porous granular media. *J. Appl. Phys.* **22**(3), 479.
- Dundon, P. J., Humphreys, D. & Hebblewhite, B. (1988) Roof depressurisation for total extraction mining trials, Collie basin, Western Australia. *3rd International Mine Water Congress* (Melbourne, Australia), 743-752.
- Geertsma, J. (1957) The effect of fluid pressure decline on volumetric changes of porous rock. *Trans. AIME* **210**, 331-430.
- Geertsma, J. (1966) Problems of rock mechanics in petroleum production engineering. *Proc. First Congress of the International Society of Rock Mechanics* (Lisbon), vol. 1, 584-594.
- Geertsma, J. (1973) Land subsidence above compacting oil and gas reservoirs. *J. Petrol. Technol.* **25**, 734-744.
- Grassman, F. (1951) Uber die Elastizitat Poroser Medien. *Vierteljahrsschrift der Naturforschenden Gesellschaft in Zurich* **96**(1), Sec. 1-51.
- Humphreys, D. & Hebblewhite, B. K. (1988) Introduction of total extraction mining in conjunction with strata dewatering at Collie, Western Australia. *The Coal Journal, Austral. J. Coal Mining Technol. Res.* no. 19, 45-56.
- Knutson, C. F. & Bohor, B. F. (1963) Reservoir rock behaviour under moderate confining pressure. In: *Rock Mechanics* (Proc. 5th Rock Mechanics Symp., University of Minnesota). Macmillan, New York.
- Martin, J. C. & Serdengecti, S. (1984) Subsidence over oil and gas fields. In: *Man-induced Land Subsidence* (ed. by T. L. Holzer), *Rev. Engng Geology* **VI**, 23-34. The Geological Soc. of America.

- Mattax, C. C., McKinley, R. M. & Clothier, A. T. (1975) Core analysis of unconsolidated and friable sands. *J. Petrol. Technol.* **27**, 14-23.
- Mess, K. W. (1978) On the interpretation of core compaction behaviour. In: *Evaluation and Prediction of Subsidence* (ed. by K. S. Surendra), 76-91. American Society of Civil Engineers.
- Nikraz, H. R. (1991) Laboratory evaluation of the geotechnical design characteristics of the sandstone aquifer in the Collie basin. PhD Thesis, Curtin University of Technology.
- Poland, J. F. (1984) *Guide to the Study of Land Subsidence due to Groundwater Withdrawal*. UNESCO, Paris.
- Teeuw, D. (1971) Prediction of formation compaction from laboratory compressibility data. *Soc. Petrol. Engrs J.* **1193**, 263-271.
- Timoshenko, S. & Goodier, J. N. (1951) *Theory of Elasticity*. McGraw-Hill Book Co., New York.
- Van der Knaap, W. (1959) Non-linear behaviour of elastic porous media. *Trans. AIME* **216**, 179-187.
- Van Kesteren, J. (1973) Estimate of compaction data representative of the Groningen field. *Verhandelingen Mijnbouwkundig Genootschap* **28**, 33-42.

Subsidence due to coal mining in India

R. P. SINGH & R. N. YADAV

Indian Institute of Technology, Department of Civil Engineering, Kanpur 208016, India

Abstract In India, every year loss of life occurs due to subsidence of land in coal mining areas. Subsidence is very prevalent in the Raniganj coal field which is a major coal producing area. The occurrence of thick coal seam at shallow depth is the main reason for the subsidence and as a result collapses have occurred in many coal mines in recent years. In the present paper, a review of coal mining subsidence in India will be presented. The Indian scientists have made efforts to predict the subsidence using empirical relations but it was not found to be successful since the geology of the coal mining area is found to be quite variable. We have made efforts to predict the subsidence occurring in the Indian coal fields in general and in particular in the Raniganj coal field using a visco-elastic model. Computed subsidence profiles of Ratibati and Shivadanga coal mines of the Raniganj coal field have been compared. The results show a reasonable match of the predicted and observed subsidence in the case of the Ratibati coal mine. In the case of the Shivadanga coal mine the predicted subsidence profile is found to be larger than the observed profile. However, the bottom of the observed troughs is found to match with the predicted troughs. Detailed analyses have been carried out to investigate the effect of mine parameters on the subsidence.

INTRODUCTION

Subsidence is an inevitable phenomenon of ground movement caused by various manmade and natural activities. The economic prosperity by the exploitation of the hidden resources in the earth is always accompanied by the adverse impacts of subsidence. Subsidence due to underground coal mining has been reported from almost all parts of the world and India being a major coal producer has been facing very severe problems of subsidence in some of its coal fields.

In the present work, we have made efforts to predict subsidence using a visco-elastic model. This model incorporates both continuous and discontinuous profiles. Detailed analyses have been carried out to predict subsidence due to underground coal mining. The validation of the model has been done by taking parameters and observed values from Ratibati and Shivadanga coal mines of the Raniganj coal field. The subsidence profiles for these coal mines have been predicted. We have found a reasonably good match between the observed and predicted subsidence profiles.

COAL MINING IN INDIA

Coal mining in India has a history of over 200 years starting from Raniganj (West Bengal) in 1774. Coal is a prime source of energy, indispensable input in steel and chemical industries. About 60% of the national commercial power requirements are fulfilled by coal. Coal production in India has rapidly increased in the last four decades. The largest reserve of coal is found in Bihar state which covers about 33.53% of the total coal reserve in India, and the second largest coal producing state Orissa covers about 23.57% of the total coal reserves in India. About 90.3% of coal is found in the states of Bihar, Orissa, West Bengal and Madhya Pradesh. The major coalfields in India are: Raniganj, Jharia, East Bokaro and West Bokaro, Panch-Kanhan and Tawa valley, Singrauli, Talcher, Chanda-Wardha, Godavari valley, and Karnapura (Fig. 1).



Fig. 1 Location map showing coal reserves in India.

SUBSIDENCE PROBLEM

Jharia (JCF) and Raniganj (RCF) coal fields are facing significant subsidence problem due to underground coal mining. Extraction of thick seams at shallow depths has damaged the ground surface in the form of subsidence and formation of cracks reaching up to the surface, enhancing the chances of spontaneous heating of coal seams leading to mine fires. The JCF has experienced over 70 mine fire spread over an area of 17.32 km². In JCF, the coal mining started in the beginning of the twentieth century and is still practised. The board and pillar method of underground mining is very common, this method is used in more than 90% of Indian coal fields. In JCF, about 57% of the area is affected by subsidence, fire areas, overburden dumps and abandoned quarries; and subsidence affects 33% of the area. Mining activities in RCF have degraded a sizable land area and have endangered about 42 localities (townships, villages and other residential areas). The subsided area in the Raniganj coalfield covers about 43.43 km² (CMRS, 1991).

SUBSIDENCE PREDICTION

Various efforts have been made by scientists from the UK, USA, China, Australia and other countries to predict the subsidence of coal mines using numerous methods such as the profile function methods (Kumar *et al.*, 1983), the influence function methods (Ren *et al.*, 1989) and the void diffusion method (Hao & Ma, 1990). Apart from these methods, many theoretical studies have been carried out using stochastic (Litwiniszyn, 1964), elastic (Salamon, 1977; and Berry, 1977), and visco-elastic (Zeng & Kou, 1992) methods. Recent efforts include the use of finite element methods (Reddish, 1984; Jones & Kohli, 1985; Siriwardne & Amanat, 1985, 1988) and distinct element method (Calthard & Dutton, 1988) in the prediction of subsidence. In India, numerical modelling for the prediction of subsidence caused by ground water withdrawal (Mishra *et al.*, 1993) has been carried out. Efforts have been made by the Indian scientists to use the best known empirical method developed by the National Coal Board (NCB) in the UK, however, it was not applicable in the Indian coal field areas, since the NCB method are applicable for the longwall coal mines whereas in India most of the coal mines use the board and pillar method. Generally, Indian scientists have made efforts to predict subsidence based on empirical methods which are restricted only to continuous subsidence profiles and are highly dependent on local conditions. In India, coal is found at numerous places, the geology of these coal fields is highly variable from one field to another. A theoretical model based on physical concepts and an understanding of the mechanism of subsidence are needed in order to anticipate continuous as well as discontinuous subsidence profiles in Indian coal fields.

SUBSIDENCE MODEL

The coal mine subsidence model considered is shown in Fig. 2(a), which is representative of continuous as well as discontinuous subsidence profiles. In this model, a coal mine is considered as a beam or plate (coal layer), resting on a visco-elastic

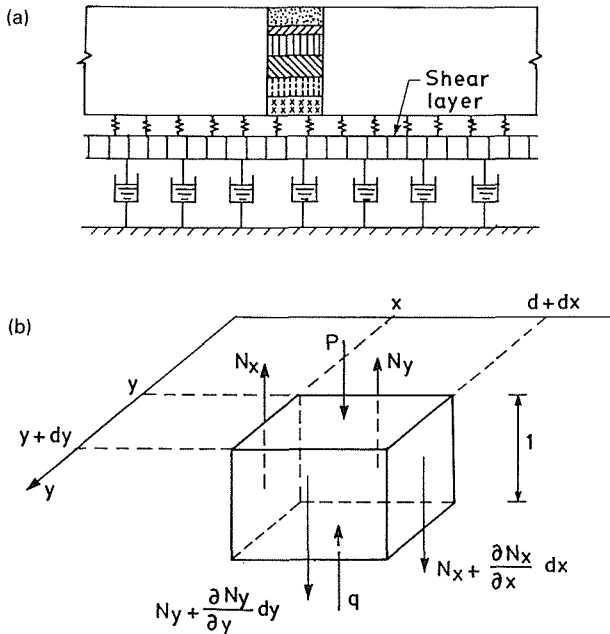


Fig. 2 (a) Schematic diagram of visco-elastic model. (b) The distribution of forces acting on shear layer element.

medium (the overburden and the rock strata underlying the coal seam) which deforms only due to transverse shear due to the excavation of the coal. Thus, the layers of a coal mine model are represented by a semi-infinite medium. Various components of the coal mine (Fig. 3(a)) model are:

- (a) dashpot – represents the time-dependent property of infilled material,
- (b) shear layer – ensures inter-dependence of springs and dashpots,
- (c) spring – represents the time-independent property of infilled material,
- (d) overburden – depicts rock strata over excavated underground mine.

If we consider the displacement of the ground surface w due to a line load P (Fig. 2(b)), μ is viscosity coefficient related to the shear deformation of infilled material, and η is an visco-compressibility coefficient of infilled material, the governing equation for subsidence of the earth's surface is written as (Singh & Yadav, 1995):

$$\frac{\delta^2}{\delta t^2} (\nabla - \lambda^2) w = 0 \tag{1}$$

where $\lambda^2 = \eta/\mu$. The vertical displacement of the ground surface is given by equation (1).

FLEXIBLE OVERBURDEN

The subsidence outside (w_o) the loaded region $|x| \geq b$ and inside (w_i) the loaded region $-b \leq x \leq b$ is given by the following equations (Singh & Yadav, 1995):

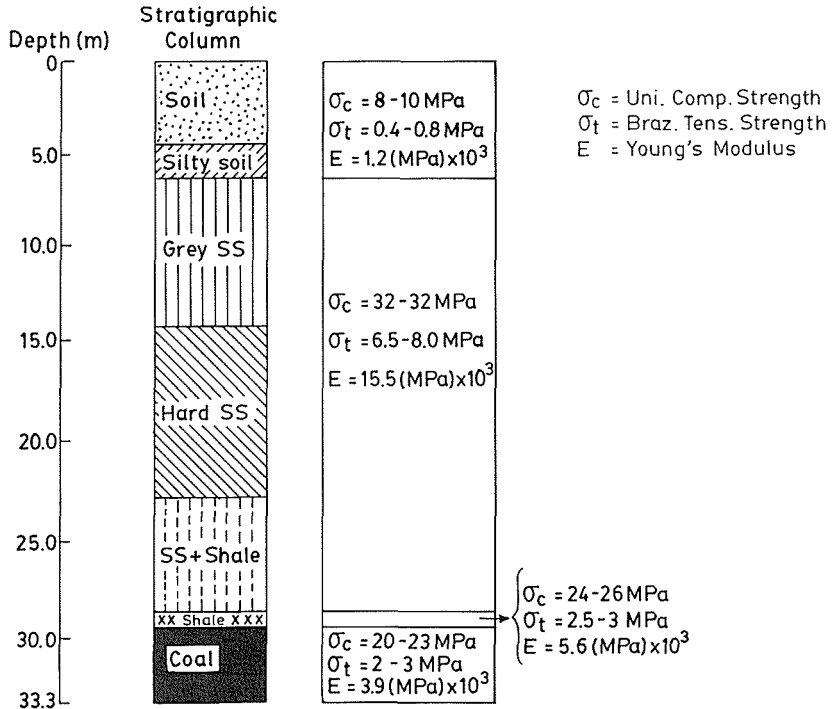


Fig. 3 Borehole strata with physical parameters from the Raniganj coal field.

$$w_0 + Pt\eta^{-1} \sinh(\lambda b) e^{-\lambda x} \quad x \geq b \quad (\text{outside the loaded region}) \quad (2)$$

$$w_i = Pt\eta^{-1} [1 - e^{-\lambda b} \cosh(\lambda x)] \quad -b \geq x \geq b \quad (\text{inside the loaded region}) \quad (3)$$

RIGID OVERBURDEN

The subsidence outside the overburden $x \geq b$ is written as (Singh & Yadav, 1995):

$$w_i(x, t) = w_0 e^{-\lambda(x-b)} \quad x \geq b \quad (4)$$

and the subsidence inside the overburden region $-b \leq x \leq b$ is written as (Singh & Yadav, 1995):

$$w_0(t) = \lambda\eta^{-1} \frac{Pbt}{(\lambda b + 1)} \quad (5)$$

The ground surface will subside similar to a stepped subsidence profile.

MODEL PARAMETERS

The average value of the above parameters are easily available from the two coal mines (Ratibati and Shivadanga) in the Raniganj coal field, however it was very difficult to get

actual parameters for the two coal mines. In the present work the above parameters used for the prediction of subsidence profiles for two coal mines are taken from the literature (Venkateshwarlu, 1986; and CMRS, 1991). Apart from these parameters, the calculation of subsidence also requires the viscosity coefficient related to the shear deformation of the infilled material (μ), and the visco-compressibility coefficient (η) of infilled materials which have been taken from Venkateshwarlu (1986). The borehole strata chart along with the average parameters of the layers are shown in Fig. 3.

RESULTS AND DISCUSSION

The actual observed subsidence profiles at Ratibati and Shivadanga coal mines are shown by star (*) symbol, respectively in Figs 4(a) and 4(b). The maximum subsidence occurs at the centre of each mine, and the observed subsidence is found to be up to 1 m at Ratibati and up to about 1.5 m at the Shivadanga coal mines. The effect of subsidence on the surface is seen up to about 120 m in the case of Ratibati and up to about 240 m in the case of Shivadanga. The nature of the observed subsidence profiles in the two mines is very similar with little difference in the bottom of the subsidence troughs (Figs 4(a) and (b)).

We have taken a generalized coal mine model representative of coal mines of the Raniganj coal field and carried out numerical studies to predict the subsidence profiles at the Ratibati and Shivadanga coal mines. The coal mine parameters used for the two mines are given in Table 1. The average strength of the rock strata given in Fig. 3 is taken for the two coal mines. From our detailed analyses, we have found a reasonably close match between predicted and observed profiles in the case of subsidence with rigid overburden for the Ratibati coal mine and the case of subsidence with flexible overburden for the Shivadanga coal mine. However, the values of the elastic parameters of the overburden in the two mines are taken as equal. We have shown the computed

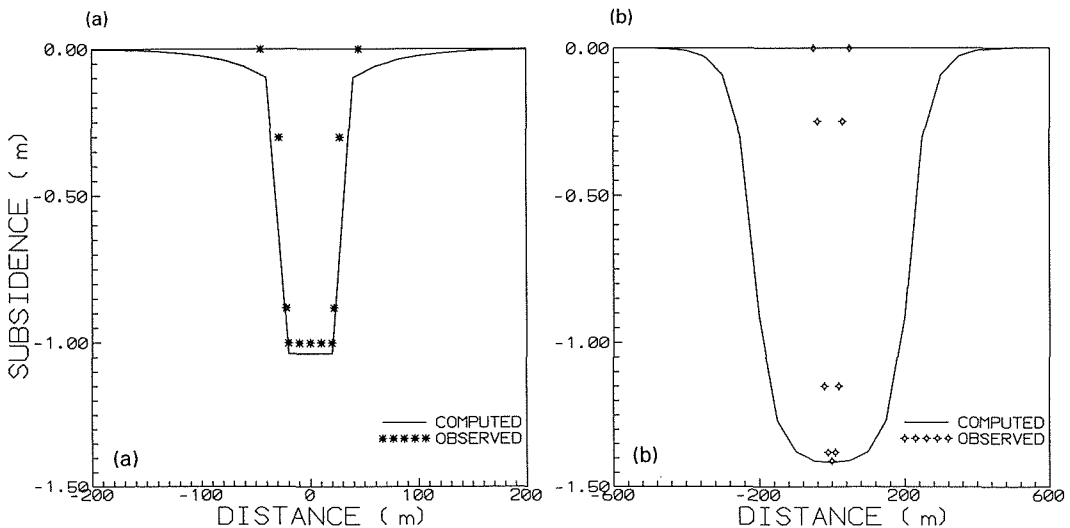


Fig. 4 Observed and predicted subsidence profile at (a) the Ratibati coal mine, and (b) the Shivadanga coal mine.

Table 1 Coal mine parameters used for the Ratibati coal mine and Shivadanga coal mine.

Parameters	Ratibati coal mine	Shivadanga coal mine
Extraction width (w)	122 m	214 m
Overburden thickness (H)	42.5 m	104 m
Extraction thickness	3.8 m	2.4 m
Extraction length	189 m	220 m

subsidence up to 200 m from the centre of the Ratibati coal mine with the solid line in Fig. 4(a). The predicted (computed) subsidence profile is found to be stepped and quite similar to the observed profile (Fig. 4(a)) for the Ratibati coal mine. The predicted subsidence in the case of the Shivadanga coal mine is shown in Fig. 4(b) (solid curve) which is found to be smooth in the case of Shivadanga (flexible overburden) coal mine, the bottom of the computed and predicted subsidence troughs are similar, however the nature of the subsidence profile is quite different (Fig. 4(b)). This may be attributed to the difference between the parameters used for calculation and the real data. The value of the physical parameters used are only average and do not account for any change with time and other factors and also various inhomogeneities present in the overburden.

The strength of a rock mass changes with time, therefore the subsidence in a coal mine is also time dependent. From Fig. 5(a), it is found that the subsidence increases with time, however the subsidence attains a maximum value which remains almost constant with the increase in time. It is clearly seen that the subsidence changes only at the initial period of two years and afterwards it becomes stabilized (Fig. 5(a)). The subsidence is found to increase with the decrease of overburden thickness for a particular width of coal seam (Fig. 5(b)). For a particular overburden thickness of coal mine, the subsidence is found to increase with the increase of extraction width (Fig. 5(b)).

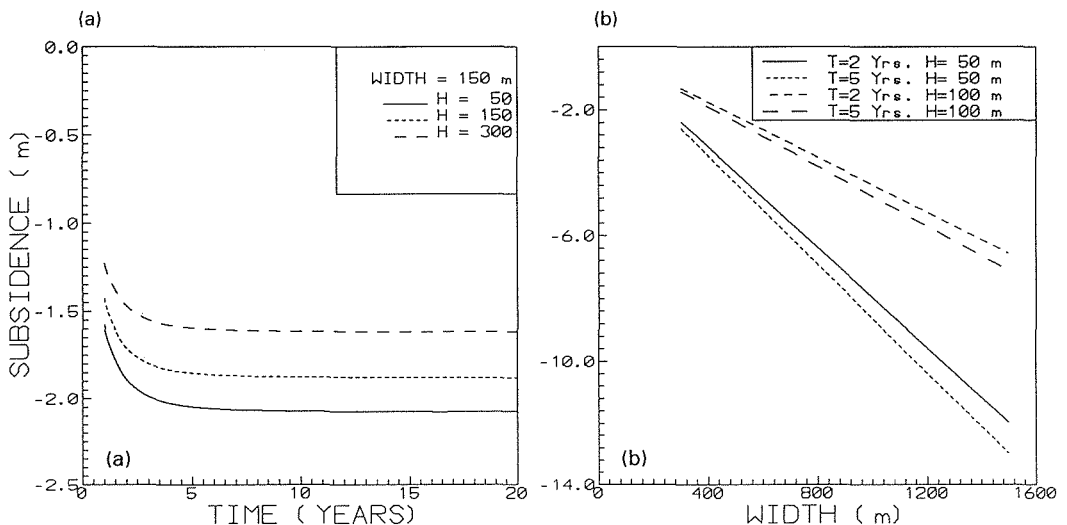


Fig. 5 (a) Variation of subsidence with time. (b) Effect of overburden thickness and extraction width on subsidence.

CONCLUSIONS

The present study was carried out to predict the subsidence profiles due to underground coal mining in Indian coal fields. For the validation of the proposed visco-elastic model for Indian coal mines, the subsidence has been investigated in the Ratibati and Shivadanga coal mines. In both the mines, the nature of the predicted subsidence profiles has been found quite similar to that observed in the field. The maximum computed subsidence has also been found to be in good agreement with the observed data in both areas. In the case of the Shivadanga coal mine, the overall nature of the subsidence is similar, however, the predicted subsidence profile is spread over a larger area compared to that observed. The present results also show the pronounced effect of the width of the extraction and the overburden thickness on subsidence. The results discussed in the present paper will be very useful for coal mining planning in India.

Acknowledgements The part of the work is supported through a research project sponsored by the All India Council of Technical Education (AICTE), New Delhi.

REFERENCES

- Berry, D. S. (1977) Progress in the analysis of ground movement due to mining. In: *Proc. Conference on Large Ground Movement and Structures* (ed. by J. D. Geddes) (Cardiff), 781-810. Pentech Press.
- Calthard, M. A. & Dutton, A. J. (1988) Numerical modelling of subsidence induced by underground coal mining. In: *Key Questions in Rock Mechanics* (Proc. US Symp. on Rock Mechanics), vol. 29, 529-536.
- CMRS (1991) Surface subsidence in mining areas. *Project Report 1964-1 1990, Central Mining Research Station (Council of Scientific and Industrial Research), Barwa Road, Dhanbad, India.*
- Hao, Q. W. & Ma, W. M. (1990) Void diffusion models for analysis and prediction of mine subsidence. In: *Rock Mechanics Contributions and Challenges* (Proc. US Symp. on Rock Mechanics), vol. 31, 203-210.
- Jones, T. J. & Kohli, K. K. (1985) Subsidence over a room and pillar mine in the Appalachian coal province and the use of subsidence predictive methods – a comparative analysis. In: *Proc. US Symp. Rock Mechanics*, 26, 179-187.
- Kumar, B., Saxena, N. C. & Singh, B. (1983) A new hypothesis for subsidence prediction. *J. Mines, Metals and Fuels* 31, 459-465.
- Litwiniszyn, J. (1964) On certain linear and non linear strata theoretical models. In: *Proc. Int. Conf. on Strata Control* (New York), 83-394.
- Mishra, S. K., Singh, R. P. & Chandra, S. (1993) Prediction of subsidence in Indo-Gangetic basin due to ground water withdrawal. *Engng Geol.* 33, 227-239.
- Reddish, D. J. (1984) Study of ground strain in relation to mining subsidence. PhD Thesis, University of Nottingham, UK.
- Ren, G., Whittaker, B. N. & Reddish, D. J. (1989) Mining subsidence and displacement prediction using influence function methods for steep seams. *Min. Sci. and Technol.* 8, 235-252.
- Salamon, M. D. G. (1977) The role of linear models in the estimation of surface ground movements induced by mining tabular deposits. In: *Proc. Conf. on Large Ground Movement and Structures* (ed. by J. D. Geddes) (Cardiff), 187-208. Pentech Press.
- Singh, R. P. & Yadav, R. N. (1995) Prediction of subsidence due to coal mining in Raniganj coalfield, West Bengal, India. *Engng Geol.* 39, 103-111.
- Siriwardane, H. J. & Amanat (1985) Numerical modeling of the behavior of overburden rock mass associated with longwall mining. In: *Proc. US Symp. Rock Mechanics*, 26, 171-177.
- Siriwardane, H. J. & Amanat (1988) Modelling of subsidence caused by longwall mining using finite difference and displacement discontinuity methods. In: *Proc. Int. Conf. Numerical Methods in Geomechanics* 6, 1901-1910.
- Venkateshwarlu, V. (1986) Geomechanics classification of coal measure rocks vis-a-vis roof supports. PhD thesis, Indian School of Mines, Dhanbad.
- Zeng, Z & Kou, X. (1992) Application of visco-elasticity to study the time dependent surface subsidence caused by underground mining. *Engng Geol.* 32, 297-284.

Etude expérimentale des tassements provoqués lors du creusement par la méthode de prédécoupage mécanique

ABDELHAQ SKIKER & PIERRE CHAMBON

Laboratoire de Génie Civil, Ecole Centrale de Nantes, 1 Rue de la Noé, F-44072 Nantes, France

JACQUES GARNIER

Laboratoire Central des Ponts et Chaussées, BP 19, F-44340 Bouguenais, France

Abstract During recent years many cases of local subsidence have been observed during the boring of shallow tunnels in soft ground. In order to better fit with settlements limitations and to reduce various risks attached to tunnels boring, new techniques have been developed. The main originality of the precutting method compared to NATM consists of a concrete vault which is built within the soil in front of the tunnel face. The present paper, on the basis of several tests series performed on the LCPC centrifuge (Nantes, France), focuses on surface settlements with or without a vault. It is pointed out that a vault can reduce settlements due to bad face conditions especially when water flows through the face. But tests have also shown that the settlement trough is still very sensitive to face conditions, even if movements are of small magnitude and that it extends twice the diameter from both sides of the tunnel axis.

INTRODUCTION

Creusement sans tranchée et tassements

La construction des tunnels en terrain meuble donne lieu à des désordres géotechniques dont l'importance dépend de nombreux facteurs plus ou moins bien maîtrisés (la méthode de creusement, la profondeur, les conditions hydrauliques et géotechniques, ...). Si le souci primordial de l'ingénieur en charge de ce type de projet s'est longtemps limité à assurer des conditions de stabilité globale à terme de l'ouvrage, il n'en est plus de même dans une période où les villes, domaines sensibles par excellence, sont le lieu privilégié des ouvrages souterrains, dont le creusement doit se faire vite, avec le minimum de nuisances sur l'environnement, selon des contraintes de forme strictes et pour un coût optimisé. C'est ainsi que le creusement sans tranchée, au bouclier ou selon des méthodes plus traditionnelles (NATM) a très nettement pris le pas sur les méthodes en tranchées couvertes. En ce qui concerne les méthodes au bouclier, qui ont pris leur essor dans les années 1980 en Europe, les principales sources de tassement en surface sont connues (Hanya, 1977):

- perte de sol: le volume de sol convoyé vers l'extérieur est supérieur au volume excavé;

- surcreusement de trajectoire: inscription dans une courbe, cabrage;
- surcreusement de conicité du tunnelier;
- surcreusement d'épaisseur de la jupe: le vide annulaire est en principe injecté;
- remaniement des terrains traversés, suivi de consolidation ou de gonflement.

Profils de tassements typiques

En un point de la surface du sol au droit du profil en long d'un chantier, le tassement évolue avec l'avancement du front de taille. Il s'amorce à l'approche du front, augmente rapidement à son passage et se stabilise progressivement comme l'illustre la Fig. 1. Pour rendre compte de l'influence de la proximité du front sur la cuvette de tassements du point de vue de l'approche numérique, on utilise couramment la notion de taux de déconfinement selon laquelle dans une coupe $y = \text{constante}$, le tassement résulte de l'application sur les parois de la galerie d'une fraction des vecteurs contraintes calculés à l'état géostatique avant creusement.

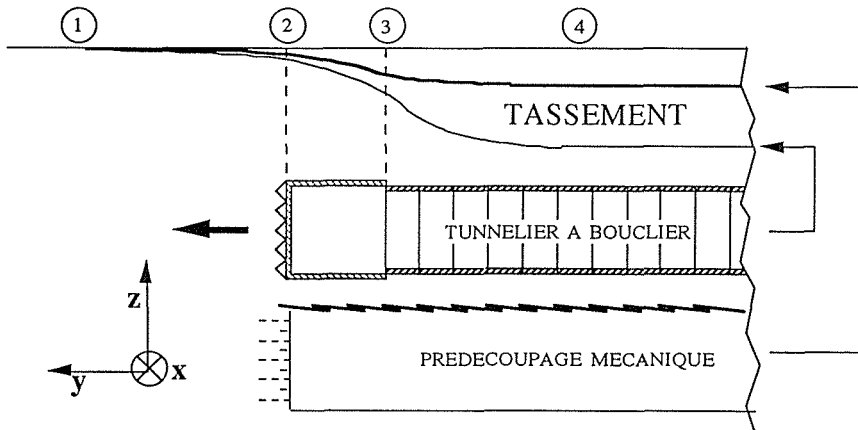


Fig. 1 Evolution qualitative des tassements en fonction de l'avancement et orientation des axes. 1 – Début du tassement antérieur. 2 – Arrivée du bouclier. 3 – Passage de la queue du tunnelier. 4 – Fin des tassements différés.

On admet qu'en coupe transversale, le profil de la cuvette de tassements, à une distance y du front, a la forme d'une courbe de Gauss ainsi que l'illustre la Fig. 2:

$$S_y(X) = S_{y\max} \exp \left[-\frac{x^2}{2i^2} \right] \quad (1)$$

S_y étant le tassement, à une distance donnée du front " y " en fonction de la distance " x " à l'axe, du tunnel, $S_{y\max}$ le tassement maximal et i le point d'inflexion de la courbe, c'est à dire la position de gradient maximal qui est naturellement lié à la profondeur de l'ouvrage. Les dommages subis par les structures environnantes sont plus liées au tassement différentiel, donc à i , qu'au tassement maximal, ce qui souligne la nécessité de pouvoir évaluer, à différentes étapes d'avancement et pour des conditions de creusement données, les caractéristiques de la cuvette de tassement prévisible pour être

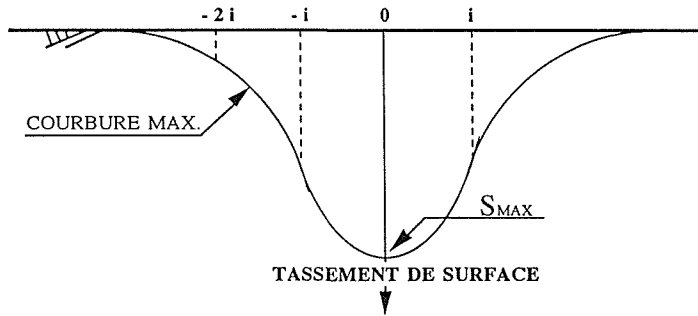


Fig. 2 Profil de la cuvette de tassement.

en mesure de modifier les paramètres de pilotage du bouclier (pression au front, vitesse, pression d'injection à l'arrière de la jupe...).

Le prédécoupage mécanique

La technique de prédécoupage mécanique, initialement développée pour le creusement dans les roches, a été récemment adaptée au creusement des tunnels en terrain meuble (Bougard *et al.*, 1977). Elle consiste à haver le sol à l'avancement sur une partie de la circonférence et sur une profondeur de quelques mètres, à injecter au béton projeté la saillie ainsi réalisée (ce qui forme la prévoûte), puis à excaver le sol à l'abri de ladite prévoûte (Fig. 3). La présence d'une prévoûte a notamment pour ambition de limiter les tassements en surface. Faute de disposer d'un nombre important de sites où cette méthode a été mise en oeuvre, un projet européen associant plusieurs partenaires a été monté dans le but d'évaluer les potentialités de la méthode. Dans ce cadre un certain nombre d'essais sur la centrifugeuse du LCPC (Nantes, France) ont été réalisés. Nous présentons dans ce qui suit les résultats de cette campagne d'essais en cours, du point de vue des tassements observés en surface en fonction des conditions au front de taille.

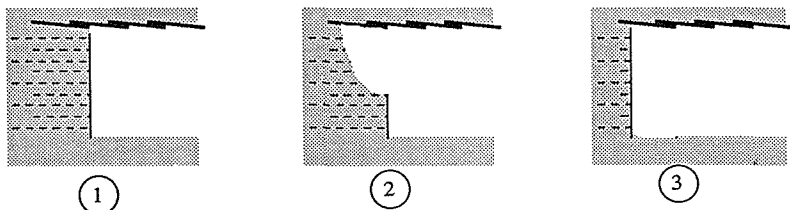


Fig. 3 Méthode de prédécoupage mécanique. 1 – Exécution de la prévoûte par havage, boulonnage du front et des piédroits. 2 – Abattage et marinage. 3 – Béton projeté au front.

DEMARCHE EXPERIMENTALE

Principes de l'expérience

Dans une configuration réelle, la tenue du front est assurée par clouage. Dans cette étude, nous nous proposons d'évaluer la tenue du front de taille en l'absence de ce

clouage. Les résultats obtenus devant permettre d'une part de caler les modèles numériques et d'autre part d'estimer la densité de clouage pour obtenir une marge de sécurité donnée. Aussi la démarche de l'essai a-t-elle été d'appliquer au front une pression de soutien qui devait être réduite progressivement jusqu'à rupture.

On connaît le phénomène de fontis, brusque affaissement apparaissant à la surface à la suite d'un mauvais conditionnement au front et d'un effondrement de celui-ci. Le fontis ne survient qu'accidentellement, ce qui le distingue fondamentalement du tassement qui est dû à un déséquilibre entre les pressions au front et l'état de contraintes dans le sol en place et qui apparaît de façon plus ou moins marqué sur tous les chantiers. Pour chaque étude expérimentale, il a ainsi été possible de mettre en évidence une pression limite de rupture σ_{TC} et un profil d'évolution des tassements jusqu'à rupture du front. On introduit alors le facteur de charge LF , analogue au taux de déconfinement, défini par:

$$LF = \frac{\sigma_v - \sigma_T}{\sigma_v - \sigma_{TC}} \quad (2)$$

σ_T étant la pression appliquée sur le front de taille du tunnel et σ_v étant la contrainte verticale géostatique à l'axe du tunnel. Il est initialement nul et tend vers 1 lorsqu'on tend vers la rupture du front.

Nous envisageons le cas d'un tunnel prototype d'un diamètre $D = 5$ m sous une couverture $C = 10$ m représenté par un modèle réduit ($Dm = 100$ mm, $Cm = 200$ mm) pour lequel les conditions de similitude sont remplies lorsque l'accélération subie vaut cinquante fois la gravité terrestre. La partie représentant le revêtement de la galerie et la jupe du bouclier est rigide.

Le but de l'essai, en terme de tassements, est alors d'évaluer les mouvements de surface lorsque les conditions au front sont modifiées. Trois cas de figure sont envisagés en présence ou non de prévoûte: lorsque le tunnel se trouve dans un sable sec, lorsqu'il est sous nappe statique (front imperméable), et lorsque le front est perméable et siège d'écoulement. Pour chaque configuration, un nombre d'essais suffisant a été réalisé pour s'assurer que la dispersion des mesures n'affectait pas les conclusions de l'étude.

Dans toutes les expérimentations effectuées nous avons utilisé le même type de sol, le sable de Fontainebleau, qui est un sable siliceux fin propre et homogène (Garnier *et al.*, 1994). Ce matériau est mis en place par pluviation dans un conteneur, ce qui lui confère un poids volumique connu de $16 \text{ kN m}^{-3} \pm 0.05$ ($\text{Id} = 81\%$).

Le modèle représenté sur la Fig. 4 est constitué d'un tube rigide et le front de taille est matérialisé par une membrane souple. Différents dispositifs permettent la mise en place d'une prévoûte, le drainage au front, le contrôle d'une nappe. La prévoûte est une coque métallique foncée dans le massif avant centrifugation. Le drainage au front doit être assuré en même temps que la mesure de la pression de soutien. Pour rendre cela possible, une galette de géotextile est posée sur le front pour rediriger le drainage de face vers un réseau de tubes répartis sur la circonférence qui évacuent l'eau. Le contrôle de la stabilité de la nappe est faite par l'opérateur qui tire parti des mesures de pression interstitielle dans les cloisons du conteneur. Les choix géométriques concernant la prévoûte ont été faits pour correspondre aux longueurs usuelles. Elle est supposée s'étendre à 1.50 m en avant du front.

Les essais se déroulent suivant un protocole strict qui leur garantissent une répétitivité optimale:

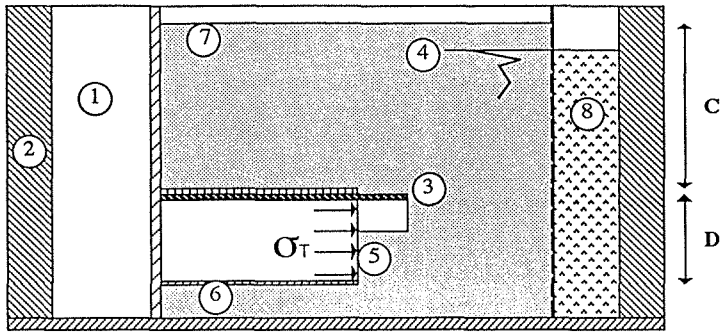


Fig. 4 Modèle réduit dans son conteneur, en présence de nappe et de prévoûte. 1 – Partie technique du conteneur (alimentation, fonçage de la prévoûte). 2 – Conteneur en acier. 3 – Prévoûte. 4 – Position de la nappe. 5 – Interface souple sol/tunnel. 6 – Revêtement rigide. 7 – Surface du sol. 8 – Cloison d'alimentation de la nappe.

- Constitution du massif en salle de pluviation. Mise en centrifugeuse. Mise sous nappe éventuelle (suivant essais). Raccordements.
- Mise en pression du front et montée en accélération en assurant une pression égale à la contrainte géostatique verticale à l'axe σ_v . Le facteur de charge LF est alors nul.
- Ouverture éventuelle du drainage au front et alimentation simultanée de la nappe pour maintenir son niveau constant sur les bords du conteneur.
- Déconfinement lent du front jusqu'à initialisation de la rupture. Le facteur de charge est alors égal à 1.
- Arrêt de la centrifugeuse, essorage du massif et découpe en plans verticaux pour identification des processus de rupture.

Les mesures sont effectuées par des rampes de capteurs de tassement disposées à la surface du massif.

RESULTATS EXPERIMENTAUX

Dans l'analyse qui suit les résultats sont donnés autant que possible en grandeurs adimensionnelles. Lorsque ce n'est pas le cas les valeurs sont données pour l'ouvrage en grandeur réelle (prototype).

Evolution des tassements en fonction de la pression au front

Quelque soit la position à laquelle on s'intéresse, l'amplitude des tassements reste relativement faible. Ils progressent régulièrement jusqu'à des valeurs de l'ordre de 3 à 5 mm soit environ 0.1% du diamètre, puis à l'approche immédiate de la rupture, ils s'accroissent brutalement. Ce comportement s'apparente à celui que l'on observe pour l'enfoncement du front. Toutefois, le tassement maximal mesuré reste toujours nettement inférieur à l'enfoncement du front et l'écart s'accroît significativement au voisinage de la rupture ainsi qu'en témoigne la Fig. 5 ou apparaissent deux étapes. Au tout début du déconfinement une progression identique des deux mouvements de très faible amplitude. Ce déplacement de quelques mm pourrait correspondre à la

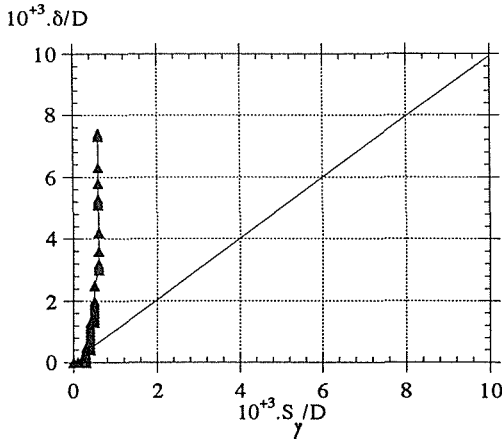


Fig. 5 Corrélation entre tassement en surface S_y et déplacement du front δD , diamètre du tunnel.

mobilisation de l'effet de voûte. Puis, lorsque la voûte est activée, le front semble pouvoir se déplacer sans affecter significativement la surface. Enfin, à la rupture (qui n'est pas représentée sur la figure) l'apparition brutale du fontis se traduit par progression soudaine des deux mouvements (front et face).

De façon plus globale, il est possible d'estimer pour chaque facteur de charge, à partir des résultats des différents capteurs, le volume de la cuvette ainsi que celui de la partie de sol ayant dépassé le plan du front. La différence – négative – entre ces deux valeurs atteste que sur ce chemin de sollicitation, de type relaxation, le sol se décomprime. Sous l'effet de chargements en surface, le sol est alors susceptible d'accuser des tassements de reconsolidation.

En sable sec, si l'on se réfère aux résultats donnés par Chambon & Corté (1994) pour une profondeur relative $C/D = 1$, la présence d'une prévoûte ne semble pas modifier significativement l'évolution et l'amplitude des tassements au droit du front. Si l'on s'intéresse à l'effet de l'eau, on peut conclure que dans le cas d'une nappe statique, c'est à dire dans les hypothèses d'un front imperméable, la présence d'une prévoûte diminue environ d'un facteur 2 les tassements maximaux avant rupture.

Les conclusions sont plus nettes encore lorsque le front de taille est considéré comme perméable. Plusieurs débits au front ainsi que plusieurs niveaux de nappe ont été testés. Trois types de tassement sont à distinguer:

- (a) tassement de consolidation lors de la montée en g ;
- (b) tassement de consolidation dû au drainage;
- (c) le tassement qui est la conséquence directe d'une baisse de pression au front de taille.

Ce sont les tassements cumulés (b) et (c) qui sont pris en compte dans cette étude puisqu'ils correspondent à une réalité physique du site.

On observe dans tous les cas (Fig. 7) des tassements plus faibles en présence d'une prévoûte (0.3% du diamètre sans prévoûte contre 0.1 à 0.2% du diamètre lorsqu'une prévoûte couvrant les trois quarts de la circonférence du front est mise en place). Néanmoins les tassements se développent avec le déconfinement avec les mêmes tendances et restent mesurables, même sur un modèle réduit, ce qui les rend non négligeables à l'échelle de l'ouvrage (quelques mm).

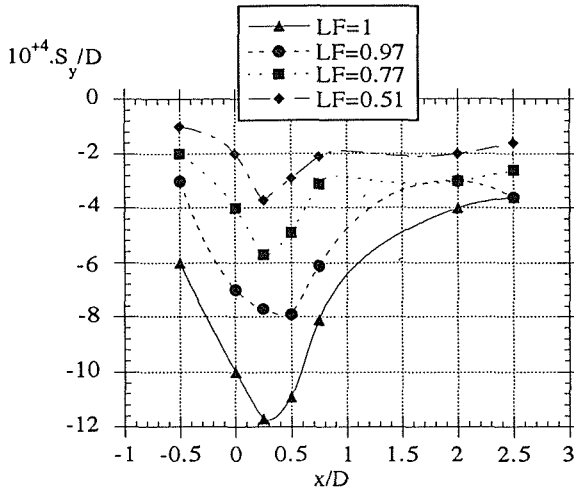


Fig. 6 Profil de tassements en surface pour différents facteurs de charge LF . x distance à l'axe du tunnel, S_y tassement au droit du front.

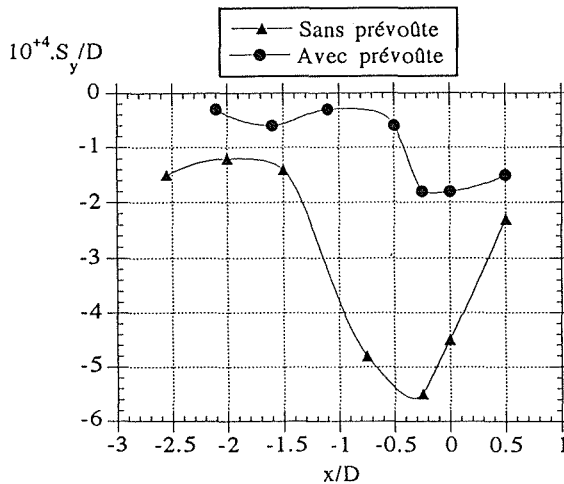


Fig. 7 Comparaison des profils de tassement transversaux en présence d'écoulement: effet de la prévoûte. x distance à l'axe du tunnel, S_y tassement au droit du front.

Enfin l'influence de l'étendue de la couverture de la prévoûte, c'est à dire la portion de circonférence du front sur laquelle elle va être réalisée, a été étudiée. Les essais avec prévoûte très fermée ne montrent pas d'amélioration sur la prévention des tassements: une prévoûte couvrant une demie-circonférence, c'est à dire s'arrêtant aux piédroits, conduit sensiblement aux mêmes résultats.

Cuvettes de tassement

La Fig. 6 montre, dans le cas d'un sable sec, la distribution transversale du tassement vertical en surface pour différents facteurs de charge. Les profils expérimentaux

s'apparentent effectivement aux courbes de Gauss pour les facteurs de charge importants (la dispersion des mesures est importante pour les faibles facteurs de charge, du fait de la résolution des capteurs). L'abscisse du point d'inflexion i permettant de mettre dans la meilleure coïncidence les points expérimentaux et la courbe de Gauss est obtenue en ajustant la corrélation linéaire entre $\ln(S)$ (où S est le tassement) et x^2 (où x est la distance à l'axe) compte tenu du passage au logarithme dans l'équation de Gauss. Il apparaît ainsi pour le cas étudié que i/D est de l'ordre de 1.8 au voisinage immédiat du front et diminue sensiblement à mesure que l'on s'en éloigne ($i/D = 1.7$ à $0.4 D$ en avant du front). Dans un sable sec la prévoûte ne semble jouer de rôle important ni sur la forme de la cuvette ni sur l'évolution des tassements en fonction de la pression au front. Pour les essais effectués en présence d'une nappe phréatique statique, les valeurs de i/D sont plus faibles (de l'ordre de 1), traduisant une cuvette légèrement plus localisée. La prévoûte n'a pas non plus de rôle significatif. On retrouve pour les cuvettes l'influence sensible des gradients hydrauliques. Plus le niveau de la nappe est bas et moins la cuvette de tassement est profonde.

La Fig. 7 illustre d'autre part le profil comparatif de tassement transversal pour un essai sans prévoûte et avec prévoûte. On constate que la présence d'une prévoûte contribue à diminuer les tassements en surface. On note dans tous les cas qu'à l'approche de la rupture ($LF = 1$) la cuvette expérimentale s'étend transversalement à plus de deux diamètres de l'axe. En ce qui concerne le profil longitudinal, la Fig. 8 montre qu'il prend naissance derrière le front, qu'il accuse un maximum d'amplitude au droit de la prévoûte et qu'il retrouve le niveau initial de la surface devant le front à une distance n'excédant pas 2 diamètres.

On sait, de par les études expérimentales et théoriques, que les processus de rupture localisés concernent la partie de sol située sous la prévoûte (Skiker *et al.*, 1994) et sont, pour les milieux pulvérulents, peu influencés par la profondeur. On voit donc qu'il n'en est pas de même pour le volume de sol qui subit une déformation ou un tassement à la suite du déconfinement (et donc à l'excavation dans une configuration réelle).

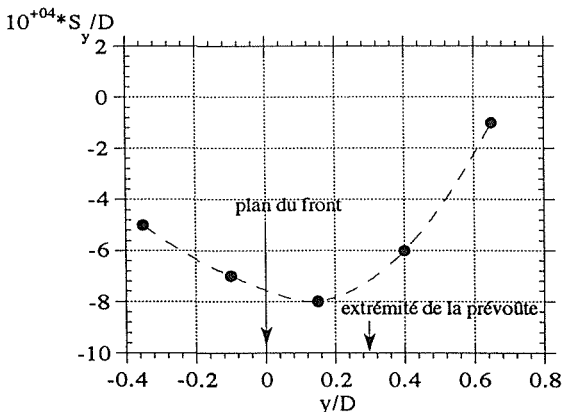


Fig. 8 Profil longitudinal des tassements dans le plan de l'axe du tunnel. y distance au front du tunnel, S_y tassement au droit du front.

CONCLUSIONS

Ainsi que nous l'avons dit, lors de la construction d'un ouvrage réel, la pratique du prédécoupage diffère sensiblement de l'approche modèle qui est faite. De plus, il est clair que l'approche du constructeur visera à assurer le meilleur soutien du front et non, comme nous le faisons, à le décompresser. Aussi, il est difficile de donner une comparaison quantitative entre tassements sur ouvrage et tassement observés sur modèle. On peut en revanche conclure d'une part que l'ordre de grandeur des tassements maximaux observés est respecté (de l'ordre de 1 cm) et d'autre part que l'évolution de la cuvette de tassement en fonction du facteur de charge est analogue aux observations sur sites pour les taux de déconfinement usuellement employés pour la méthode (0.35 à 0.5).

De plus, la campagne d'essais en cours montre que si les tassements provoqués par un déséquilibre de pression au front de taille demeurent faibles (inférieurs à 1% du diamètre de l'ouvrage), ils restent cependant mesurables et fortement liés à ce déséquilibre même en présence de prévoûte. Malgré une certaine dispersion des mesures, due essentiellement à la faible amplitude des mouvements mesurés, certaines tendances nettes ont pu être déduites des résultats des essais:

- Le sol décompacté par une pression insuffisante au front peut paraître sain (peu de tassements) mais cacher une certaine fragilité et donner lieu à des désordres différés.
- Les flux liquides à travers le front donnent lieu à des désordres plus importants qu'en sable sec. C'est un cas où la prévoûte apporte un gain significatif puisqu'elle permet de diviser les tassements environ par deux.
- Même en l'absence de surcreusement, il est établi qu'un mauvais conditionnement au front provoque une cuvette de tassement tridimensionnelle avec une partie importante à l'avant du front.

Remerciements Les auteurs remercient l'entreprise Perforex de leur avoir permis de s'associer aux travaux sur le prédécoupage mécanique et d'avoir pu mener à bien une campagne d'essais conséquente sur centrifugeuse.

REFERENCES

- Bougard, J.-F., François, R. & Longelin, R. (1977) Le prédécoupage mécanique, un procédé nouveau pour le creusement des tunnels. *Tunnels et Ouvrages Souterrains* **22**, **23**, **24**.
- Chambon, P. & Corté, J.-F. (1994) Shallow tunnels in cohesionless soil: stability of tunnel face. *J. Geotech. Engng Div. ASCE* **120**(7), 1148-1165.
- Garnier J., Canepa, Y., Corté, J.-F. & Bakir, N. E. (1994) Etude de la portance des fondations en bord de talus. In: *XIII ICSMFE* (New Delhi), 705-708.
- Hanya, T. (1977) Ground movements due to construction of shield-driven tunnels. In: *IXth ICSMFE* (Tokyo), 759-790.
- Skiker, A., Chambon, P., Leca, E. & Garnier, J. (1994) Face stability of tunnels constructed using the mechanical precutting method. In: *Proc. Centrifuge 94* (Singapore), 713-718. Balkema, Rotterdam.

Subsidence of underground quarries in Ohya district, Japan

YUKIMITSU YOKOYAMA, KATSUTOSHI UENO & TAKAE MIZUNUMA

Utsunomiya University, Department of Civil Engineering, 2753, Ishii, Utsunomiya, Tochigi 321, Japan

Abstract A collapse of an underground Ohya quarry in Ohya district, a northern part of Kanto area in Japan, caused a large scale subsidence about 3300 m² wide. Unfortunately, subsequent large scale subsidence has occurred in the same district. In order to clarify the reason why such large scale subsidence occurred, the authors have investigated strength characteristics of Ohya stone, especially strength deterioration and creep characteristics, since 1988. The specimens used in this study were strictly maintained in their saturation condition. A drying history caused a 50% deterioration of strength. Long term loading also led to a creep failure phenomenon in Ohya stone. Both the dimensions and loads acting on *in situ* residual columns supporting the roof of the underground quarry were tentatively estimated. Consequently, values of 100 m² for the cross section area and 6 MPa for the shared stress were obtained for the threshold values that dominate the occurrence of subsidence.

INTRODUCTION

On 10 February 1989, a large scale subsidence with dimensions of 3300 m² in area and about 30 m in depth occurred at Sakamoto, Ohya district, located 7 km northwest of the centre of Utsunomiya city. (This subsidence will be called the 1st Sakamoto subsidence, hereafter.) Unfortunately, the occurrence of such subsidence incidents has not yet been brought to an end. Consequent large scale subsidence occurred in Ohya district on 29 March 1990 (called 2nd Sakamoto subsidence) and 29 April 1991 (also called Kawarasaki subsidence). These were caused by the collapse of underground cavities created by quarrying Ohya stone. Ohya stone, which is used as a building material, has been produced since the period of ancient burial mounds. Currently the estimated annual production is at least 300 kt and the quarrying has supported an important industry in Ohya district.

In order to clarify the mechanism of the subsidence in Ohya, since 1988 the authors have investigated the characteristics of Ohya stone, and have discussed the subsidence mechanisms. Noteworthy research projects on the mechanical properties of sedimentary soft rock in Japan have been reported by Akai *et al.* (1978) who studied the elasto-plastic behaviour of sedimentary soft rock, and Adachi & Ogawa (1980), who studies the mechanical properties and failure criterion of sedimentary soft rock. Both of the studies dealt with Ohya stone as a typical sedimentary soft rock, and successfully constructed a constitutive law and a failure criterion for sedimentary soft rock, respectively. Samples

used in these studies were, however, subjected to drying during transportation and preparation, so that it was feared that the physical test results reported by the researchers did not properly estimate the strength and deformation characteristics of *in situ* Ohya stone.

The study presented in this paper is based on *in situ* Ohya stone. The authors investigate the deterioration of strength due to dry-wet histories and creep failure of virgin Ohya stone, and point out that these factors severely affect the occurrence of subsidence. The subsidence mechanism at Ohya quarries is also discussed in this paper.

OHYA QUARRY

Ohya district shown in Fig. 1 is located about 7 km northwest of the centre of Utsunomiya city and about 100 km north of Tokyo. Locations of the sites at which subsidence has occurred are shown by hatched circles on this figure. The scale and the date of the recorded subsidence occurrences are listed in Table 1. There were 15 large scale occurrences of subsidence in the last 50 years.

Ohya stone is a kind of green tuff composed of pyroclastic sea deposits during the Miocene epoch, spreading about 100 km² wide and 200 m deep under the northern Kanto area, and widely used as a building material in this area. After World War II,

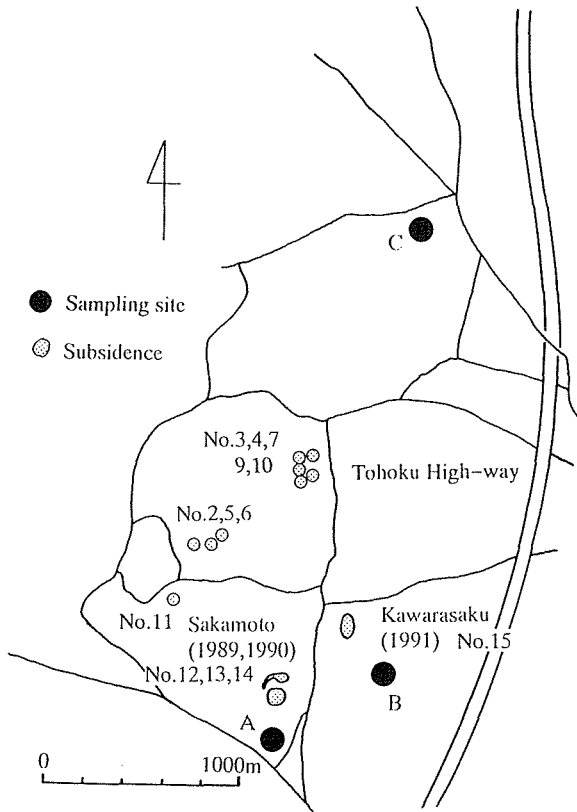


Fig. 1 Location of subsidence and sampling sites.

Table 1 Subsidence in recent 50 years.

No.	Date	Region	Area(m ²)
1	30 Oct. 1946	East Tanga	3000
2	27 Feb. 1954	Tanga	2000
3	5 Jun. 1955	Tateiwa	1980
4	11 Jul. 1955	"	20000
5	6 Jul. 1958	Benten	4620
6	5 May 1959	"	1000
7	10 May 1960	Tateiwa	3900
8	20 Apr. 1962	Iwamoto	1470
9	30 Jul. 1962	Tateiwa	3306
10	11 Dec. 1973	"	3000
11	6 Feb. 1981	Tanga	3000
12	10 Feb. 1989	Sakamoto	3300
13 ¹	6 Mar. 1989	"	6700
14	29 Mar. 1990	"	7500
15	29 Apr. 1991	Kawarasaku	17500

¹Enlarging of No. 12

machine quarrying techniques which were rapidly introduced throughout the Ohya district, allowed deep quarrying, and drastically increased the annual production volume of Ohya stone. Consequently this has led to the frequent occurrence of large scale subsidence during the last 50 years. Although since it began, quarrying of Ohya stone has produced many underground cavities, except for recent quarrying, few geographic records have been officially maintained. Therefore, in Ohya district, it is a fact that there are many underground cavities the scale and structure of which have not yet been identified satisfactorily.

ENGINEERING CHARACTERISTICS OF OHYA STONE

Physical properties

The properties of Ohya stone evaluated by means of procedures specified by Japanese Society of Soil Mechanics and Foundation Engineering (1990) are given in Table.2. Specimens were sampled from three different sites shown in Fig. 1: site A was located about 150 m south of the 1st Sakamoto subsidence; site B, about 200 m south of the Kawarasaku subsidence site; and site C, from Takaragi-honcho located the northern part of Ohya district where subsidence has not occurred.

Endo *et al.* (1973) investigated the degree of saturation of filed Ohya stone, and verified that the values were spread over 94.4%. Since water tables exist several meters under the ground surface at these sites and humidities in quarries were quite high, the specimens sampled were almost saturated. In order to keep *in situ* moisture condition and to prevent oxidation, the specimens were immediately immersed in containers filled with groundwater pumped at each of the sites, then transferred to our laboratory. The value of 2.40 for the specific density of Ohya stone, as listed in Table 2, is similar to serpentine or attapulgite, rather than ordinary soils and rocks. Ohya stone, which is a

Table 2 Physical properties of Ohya stone.

Site/Sample		A	B-1	B-2	B-3	B-4	C
Class		fine	fine	fine	fine	fine	coarse
Depth	(m)	80	90	100	110	110	110
Wet density	ρ_w (g/cm ³)	1.85	1.86	1.84	1.84	1.89	1.89
Dry density	ρ_d (g/cm ³)	1.50	1.47	1.44	1.43	1.52	1.50
Water content	w (%)	24.2	27.0	27.8	28.0	24.9	25.4
Specific density	ρ_s (g/cm ³)	2.45	2.40	2.40	2.46	2.34	2.41
Void ratio	e	0.640	0.636	0.667	0.718	0.590	0.603
Deg. of sat.	Sr (%)	92.2	100	100	96.1	100	100
Unconfined compressive strength	q_u (MPa)	13.5	9.49	8.11	8.71	9.82	8.09
Internal friction	ϕ (deg.)	64	31				

kind of tuff, consists of crynptillolite having a pipe-shaped void structure with about 0.3 nm diameter. Because the diameter of the pipe-shaped void is so small, water cannot percolate the void to saturate it. According to Tohgo (1989), the specific density of Ohya stone, therefore, tends to be smaller than that of ordinary soils and rocks. The specific surface defined by surface area per gram ranges from 30 to 150 m² g⁻¹. This indicates that the particles comprising Ohya stone have a large number of micro void structures. The void ratio ranges from 0.6 to 0.7, which is similar to that for Miocene sedimentary rocks as well as alluvial sands.

Strength characteristics

In order to investigate deformation behaviour and strength characteristics of Ohya stone, a series of conventional triaxial compression tests (CD tests) with B-1 specimens having a dimension of 100 mm in diameter and 200 mm in height, under effective confining stresses of from 198 kPa to 4.41 MPa were performed. The results of these test are shown in Figs 2-4.

The deviator stress vs. axial strain curves plotted in Fig. 2 rise to a sharp peak, then drop suddenly to a residual state. The curves indicate the remarkable strain softening phenomenon of Ohya stone. Relationships between volumetric strain and axial strain presented in Fig. 3 illustrate dilative characteristics of Ohya stone, except for the tests performed under confining pressures larger than 2.94 MPa.

Deviator stresses ($q = \sigma_1 - \sigma_3$) are plotted against effective mean stresses $p' = (\sigma'_1 + 2\sigma'_3)/3$ in Fig. 4. Both the Hvorslev surface having a slope of $H = 0.42$ and a critical state line associated with 1.36 of M -value are also presented in Fig. 4. Arrows in this figure indicate peak and residual values. After having reached the Hvorslev surface at their peak value, all the stress paths go back to critical state line. Since the Hvorslev surface was intercepted by the critical state line at the point $(\sigma'_1 + 2\sigma'_3)/3 = 9.8$ MPa, it can be expected that about a 10 MPa of an isotropic pre-stressed histories had been provided for the *in situ* Ohya stone, at a depth of 90 m under the site B. Because of a huge degree of overconsolidation, it can be understood that the reason why the remarkable dilative behaviour, as seen in Fig. 3, was observed under relatively low confining pressures.

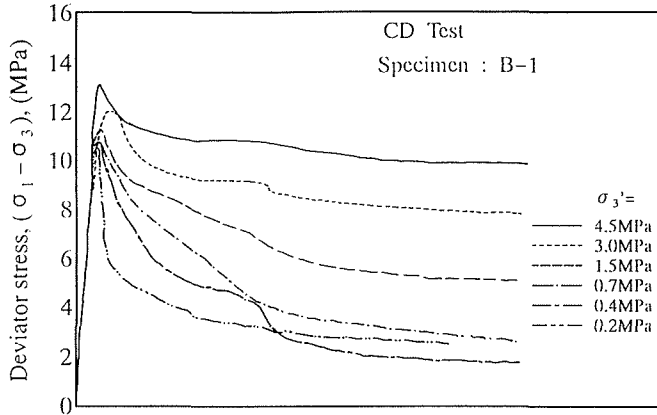


Fig. 2 Stress strain relationships for B-1 specimens observed with conventional CD triaxial test.

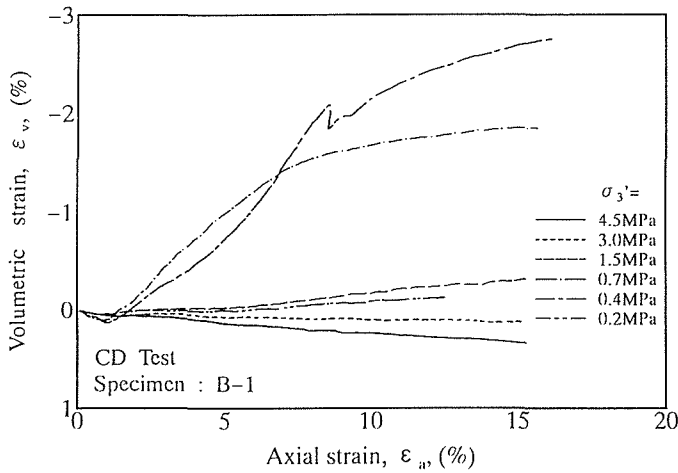


Fig. 3 Volume changes for B-1 specimens in conventional CD triaxial test results.

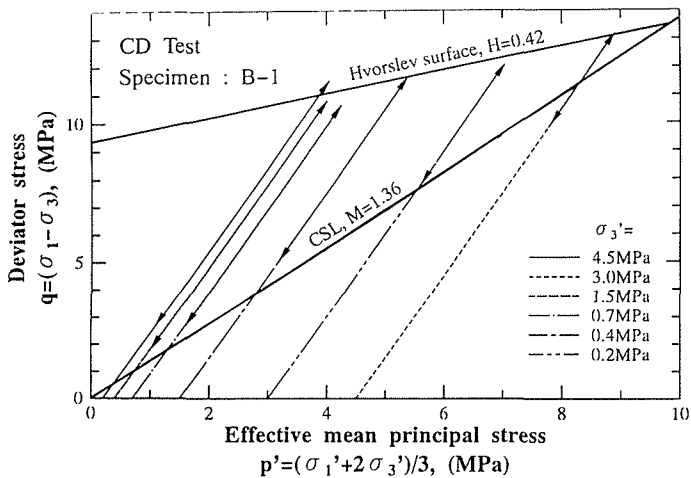


Fig. 4 Stress paths for B-1 specimens.

Note that the deformation behaviour and strength characteristics of Ohya stone were quite similar to those of heavily overconsolidated clays, rather than those characteristically observed for intact hard rocks. Therefore, it can be concluded that soil mechanical approaches usually employed for overconsolidated clay can potentially be applied to the problem of determining the mechanical characteristics of tuff rocks.

Strength deterioration due to wet-dry-wet history

It is well known that for certain kinds of sedimentary soft rocks, slaking phenomena cause a deterioration in strength. The authors, therefore, investigated the influence of wet-dry-wet histories on the strength of Ohya stone, and conducted the following two series of unconfined compression tests.

WDW tests Two types of completely saturated specimens with 50 mm diameter and 100 mm height were used in the wet-dry-wet (WDW) tests. Both B-3 specimens and C specimens were used. After having been dried in an oven at 110°C, for from 1 h to three days, B-3 specimens were soaked for up to 72 h in groundwater pumped from a depth of 110 m at site B. After C specimens had been dried for up to 25 days in the air, the specimens were then soaked in groundwater, exactly the same as for specimens B-3. After subjecting the specimens to the above mentioned wet-dry-wet regime, a series of unconfined compression tests was conducted.

Changes in the degree of saturation obtained from WDW tests are plotted against time in Fig. 5. In this figure, the solid and dashed lines represent measured data and symbols indicate the stages at which compression tests were performed. The specimens once dried never became saturated even after soaking for three days.

The symbols in Fig. 6 show the relationships between unconfined compressive strength q_u and degree of saturation S_r . For both B-3 and C of specimens, although values of q_u around $S_r = 30-40\%$ became slightly smaller than the values for completely saturated virgin specimens, the values for more dried specimens increased with decreasing degrees of saturation toward the values of about 40% larger than for virgin specimens. On the other hand, noticeable deterioration of strength were observed in wetting sequences. The values of q_u significantly decreased at $S_r \cong 85\%$ and became 50-80% smaller than the values for virgin specimens.

WDWC tests After being subjected to a few wet-dry-wet cycles (WDWC) with three days oven drying and three days wetting, virgin B-3 specimens were used for unconfined compression tests. Unconfined compressive strength q_u obtained from WDWC tests are plotted against the number of the wet-dry-wet histories, as shown in Fig. 7. The values of q_u sharply decreased after the first cycle, but kept constant for successive cycles.

Note that the above-mentioned test results imply that mechanical investigations of the strength of *in situ* Ohya stone, such as unconfined compression tests, should be conducted using virgin specimens that have never been subjected to wet-dry-wet cycles.

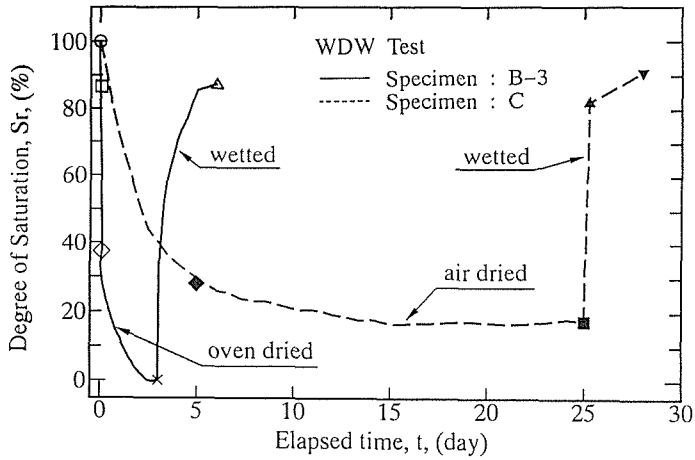


Fig. 5 Changes in degree of saturation obtained from WDW tests.

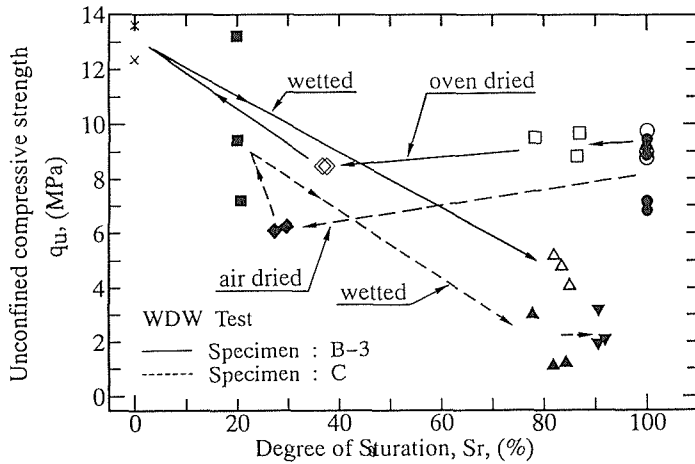


Fig. 6 Influence of wet-dry-wet histories on q_u obtained from WDW tests.

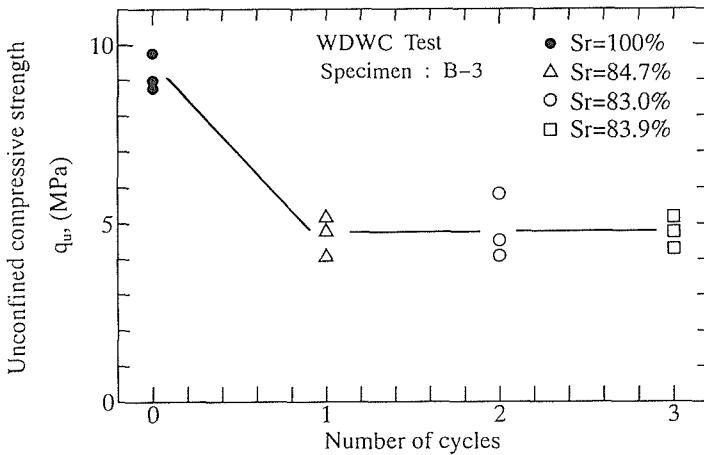


Fig. 7 Influence of the number of wet-dry-wet cycles on q_u .

Creep characteristics

As well known for visco-elastic materials, such as concrete, continuous loading with an intensity larger than 70% of the strength of the materials results in the creep failure phenomenon. The authors, therefore, developed two sets of brief creep test apparatus to evaluate the creep strength of Ohya stone.

The test apparatus is shown in Fig. 8. An air cylinder installed on the top of a strong steel frame, having a capacity of 30 kN, generates a continuous axial load for the creep test. The deformation and loading intensity were measured by using a LVDT and a load cell, and recorded by a personal computer equipped with 12 bits eight channels AD converter with four channels DA converter through two signal conditioners. Loading sequences and data processing were also intelligently controlled by the personal computer. In order to maintain *in situ* moisture conditions during the creep tests, a specimen was placed in an acrylic bottom-closed cylinder filled with temperature regulated groundwater. After the instruments and specimen were prepared, the creep tests were, thus, performed.

The relationship between the failure time t_f and the stress ratio η , defined as $\eta = \sigma_a/q_u$, for specimens B-2, B-3 and C, are presented in Fig. 9 together with similar test results conducted by Shimizu Co. (1990). These test results clearly show that the relationship between t_f and η can be represented by a power function, i.e.:

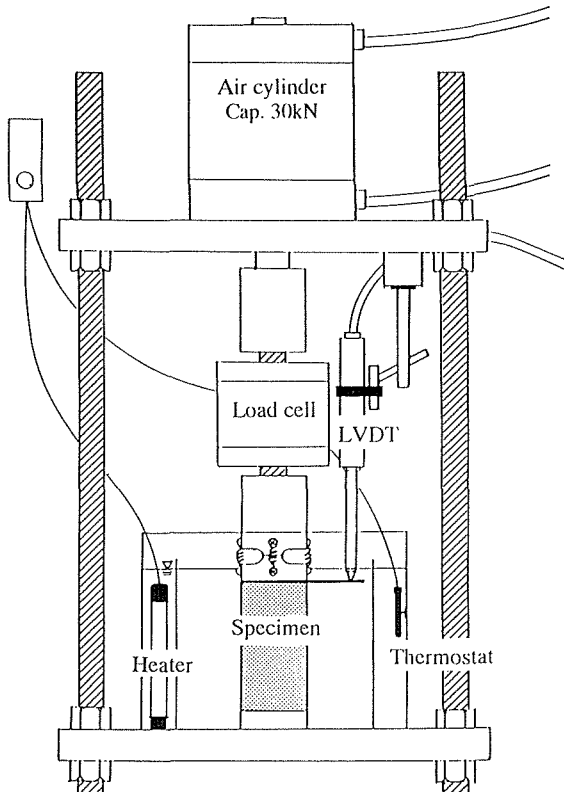


Fig. 8 The set-up for creep tests.

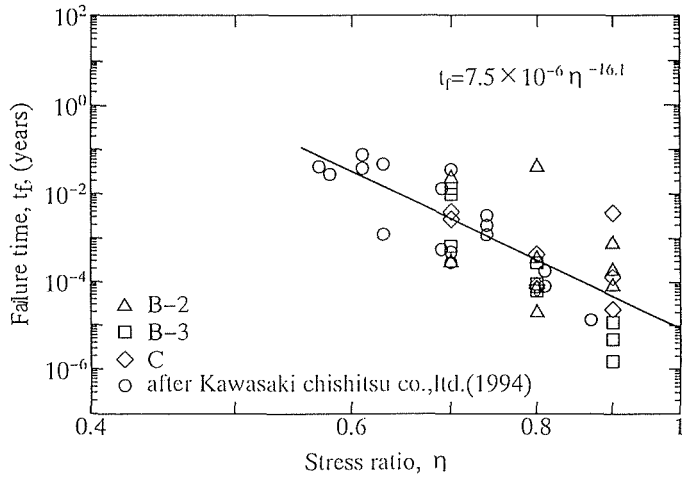


Fig. 9 Creep test results.

$$t_f = 7.5 \times 10^{-6} \eta^{-16.1} \quad (0.57 < \eta < 1.0)$$

where t_f is the failure time in years; η , the stress ratio; σ_a , the applied axial stress; q_u , the unconfined compressive strength.

DISCUSSION

Figure 10 illustrates an assignment of residual columns and the subsidence zones for the first Sakamoto subsidence. Rectangles are residual columns, while hatched zones represent the zones of subsidence.

Axial loads acting on residual columns in this site were approximately estimated. Figure 11 demonstrates how the axial loads were estimated. First, the authors connected gravity centres of two adjacent residual columns each other, and made quadrilaterals, as shown with dashed lines in Fig. 11. Second, the quadrilaterals were divided into four

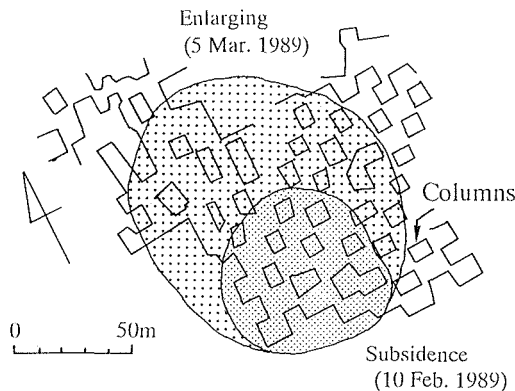


Fig. 10 Residual column assignment in the primary subsided quarry at Sakamoto.

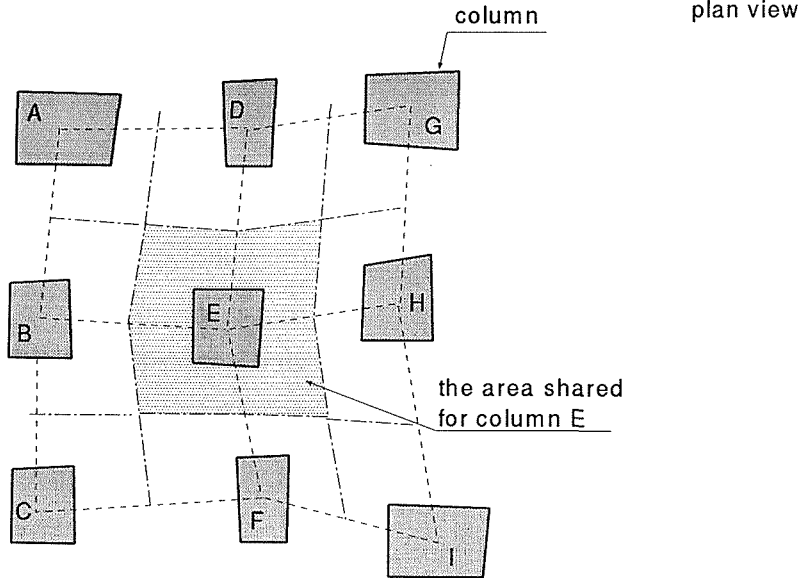


Fig. 11 Load sharing method.

small quadrilaterals by two intermediate lines drawn with chained lines. Third, multiplying the area shared for columns by the associated overburden pressures and dividing by the cross sectional area of the columns, the authors calculated axial stresses acting on residual columns.

Figure 12 shows the distributions of the estimated axial stress vs. the cross sectional area of the columns in the quarry at Sakamoto that collapsed on 10 February 1989 and enlarged on 5 March 1989. Hollow triangles show such distributions for columns in a concave pit, while hollow circles show those in a healthy pit.

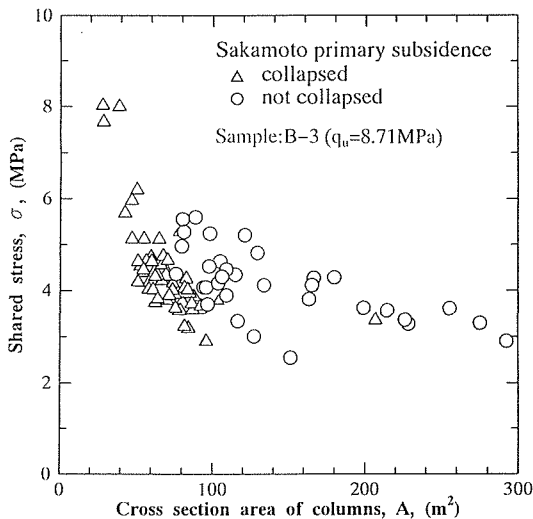


Fig. 12 Distributions of the estimated axial stress vs. the area of columns in the subsided quarry at Sakamoto.

For most of the columns in the concave pit, their cross section areas were smaller than 100 m^2 . Consequently, they had to bear comparatively larger axial loads than the columns in the healthy pit. Furthermore, three columns in the concave pit were subjected to shared stresses of over 80% of their unconfined compressive strengths q_u . Remember that such a high degree of axial stress caused creep failure in Ohya stone, as shown in Fig. 9. Therefore, what probably happened is that firstly, creep failure occurred in the three columns; secondly, the overburden load was redistributed to other adjacent columns and axial stresses acting on each column increased; thirdly, certain new creep failures successively occurred among the columns having a cross section area smaller than 100 m^2 ; and finally, the roof which had been supported by the collapsed columns could not bear the bending induced by the overburden load, and large scale subsidence occurred. Residents in Ohya report that they have frequently heard loud noises and felt shocks prior to the occurrence of subsidence. The successive creep failure of the columns might generate the loud noises and shock.

On the other, in the healthy pit, the areas of about 75% of the columns were larger than 100 m^2 and the shared stresses were less than 6 MPa. It seems that the columns having large cross section areas prevented the propagation of the successive failures into the healthy pit. Note that the values of 100 m^2 in the cross section area and 6 MPa of the shared stress should be the threshold values that dominated the occurrence of subsidence. Therefore, it is necessary for subsidence control to investigate assignments and dimensions of the residual columns in Ohya quarries.

CONCLUDING REMARKS

In order to clarify the subsidence mechanism at the Ohya quarries, three kinds of physical tests, conventional consolidated drained triaxial tests, unconfined compression tests and creep tests, have been carried out. The following conclusions were drawn from these results:

- (a) Deformation behaviour and strength characteristics of Ohya stone were quite similar to that of heavily overconsolidated clays that have been subjected to an isotropic pressure of about 10 MPa. Therefore, soil mechanical approaches usually employed for overconsolidated clay are may also be considered for investigating the mechanical characteristics of tuff rocks.
- (b) A 50% of strength deterioration due to fluctuating dry-wet conditions was observed in this study. This implied that physical tests for evaluating the *in situ* strength of Ohya stone should be conducted with specimens which have never been subjected to dry-wet histories. In addition, this also suggested it is significant for maintenance of underground cavities to keep the residual columns in the cavities completely saturated.
- (c) If the value of axial stress acting on a specimen become larger than 0.57 of their unconfined compression strength, it is likely to lead to creep failure. The authors estimated shared stresses acting on *in situ* residual columns in both a collapsed pit and a healthy pit and indicated that the values of 100 m^2 in the cross section area and 6 MPa of the shared stress should be the threshold values dominating the occurrence of subsidence, in this case.

Acknowledgements The study presented here is financially supported by a Japanese Government Grant for Scientific Research (Type B 04452223). The authors are grateful to Professor H. Ishii in Tokyo University, Professor M. Ohtake and Mr H. Tsuruoka, in Tohoku University for their advice.

REFERENCES

- Adachi, T. & Ogawa, T. (1980) Mechanical properties and failure criterion of soft sedimentary rock (in Japanese). *Proc. Japanese Soc. Civ. Engng* **295**, 51-63.
- Akai, K., Adachi, T. & Nishi, K. (1978) Elasto-plastic behaviour of soft sedimentary rock (porous tuff) (in Japanese). *Proc. Japanese Soc. Civ. Engng* **271**, 83-95.
- Endo, G., Tanaka, K. & Kusunoki, K. (1973) The basic research for setting up the standard of mining Ohya stone – field experiments on material quality of Ohya stone (in Japanese). *Technical Report 2, Science and Engineering Research Laboratory, Waseda University*.
- Japanese Society of Soil Mechanics and Foundation Engineering (1990) *Procedures and Interpretations of Soil Testing* (in Japanese). Japanese Society of Soil Mechanics and Foundation Engineering.
- Shimizu Co. (1990) Private communication to authors (in Japanese).
- Tohgo, S. (1989) Estimation of absorption performance by means of liquid phase absorption method – especially Ohya stone and volcanic ash (in Japanese). PhD thesis, Waseda University.

Horizontal ground movements due to water abstraction and formation of earth fissures

LEO ROTHENBURG

University of Waterloo, Department of Civil Engineering, Waterloo, Ontario, Canada N2L 3G1

AHMED OBAH, SOLEIMAN EL BARUNI

General Water Authority, PO Box 5332, Tripoli, Libya

Abstract The paper presents analytical developments for calculation of horizontal ground displacements and strains resulting from water table decline in unconsolidated sediments. The theory is based on a nucleus of volumetric strain solution for poro-elastic half-space. Horizontal ground displacements are computed for specific patterns of water level decline corresponding to regional drawdown and drawdown around pumped wells. A numerical technique for calculation of ground movements and strains for an arbitrary pattern of water table decline is presented. The theory is applied to postulate a mechanism of fissure formation and to explain the occurrence and locations of fissures due to water abstraction in the Sarir agricultural area in the Libyan desert.

INTRODUCTION

Ground movements leading to formation of tension cracks ranging from small fissures to surface faults is a well known phenomenon invariably associated with ground water abstraction from unconsolidated aquifers. Many areas where earth fissures were found are also affected by subsidence. Although the areal association of both phenomena with water level decline is evident, the link between subsidence and earth fissures is not obvious. In many instances earth fissures have been observed at modest levels of groundwater decline and low subsidence (Holtzer, 1984).

Although precise mechanisms of fissure formation are not known in details there is little doubt that formation of fissures involves some form of tensile ground strain. In some cases tension can be justifiably associated with bending of the subsiding ground over the upward-concave bedrock surface. In other situations the source of tension may be linked with localized differential subsidence or bending of the ground surface as a result of subsidence. When subsidence is clearly small an attempt can be made to attribute surface tension to ground contraction possibly related to capillary stress similar to the one that leads to desiccation cracks. Only the last mechanism explicitly refers to horizontal ground strain. Other mechanisms are not easily quantifiable as they address the cause of fissures indirectly, through vertical movements.

Any reduction in pore pressure at a point will have a tendency to create contraction that involves both vertical and horizontal components of displacement. When ground movements due to consolidation of a thin clay layer are taken as purely vertical it implies that the media around the consolidating layer completely restrains horizontal

deformations. This is certainly correct when the surrounding media is much stiffer than the consolidating layer. It is not difficult to imagine, however, a set of conditions when the stiffness contrast is insufficient to prevent horizontal contraction. One frequent example is sandy clay/silty sand combination of layers. Elastic compression of sediments due to water level decrease is another example of this type.

The primary reason for carrying out analyses assuming strictly vertical deformations is the simplicity of calculations. From a physical point of view this is an extreme assumption as it neglects horizontal ground movements and strains altogether. An almost impossible rigorous alternative would require the knowledge of stiffness properties for all sediments. There is, however, another extreme case that lends itself to simple calculations: it involves neglecting the stiffness contrast between various sediments in the aquifer. The main objective of the present paper is to pursue this avenue by developing relationships for horizontal and vertical ground displacements and strains. These relationships are further applied to explain formation of fissures as a result of a large scale water abstraction in the Sarir agricultural area in the Libyan desert.

THE NUCLEUS OF STRAIN SOLUTION

An estimate of ground movements caused by pore pressure decline can be made based on the solution for the displacement field caused by volumetric strain concentrated in an infinitesimal volume of a homogeneous elastic half-space (Mindlin & Chang, 1950). Geertsma (1973) applied this solution to calculate subsidence from pressure decline in deep oil reservoirs.

When the pore pressure change $\Delta p(x,y,z)$ is non-homogeneous and affects some finite volume V , the gross effect can be obtained by integrating over the entire volume the elementary effects of pressure change at a point (x,y,z) :

$$\begin{aligned} u_z(X, Y) &= \frac{1-\nu}{\pi} \int \frac{c_m \Delta p(x, y, z) z \, dx \, dy \, dz}{[(X-x)^2 + (Y-y)^2 + z^2]^{3/2}} \\ u_x(X, Y) &= \frac{1-\nu}{\pi} \int \frac{c_m \Delta p(x, y, z) (X-x) \, dx \, dy \, dz}{[(X-x)^2 + (Y-y)^2 + z^2]^{3/2}} \end{aligned} \quad (1)$$

where c_m is the coefficient of uniaxial compaction and ν is Poisson's ratio. In an important special case when the pressure decline has a radial symmetry, i.e. $\Delta p = \Delta p(r)$, integrals (1) can be evaluated in polar coordinates and integration with respect to the polar angle performed to obtain ground surface displacements resulting from pressure decline in a horizontal slice of small thickness δh located at depth D in the aquifer:

$$\delta u_z(R) = 2 \frac{1-\nu}{\pi} c_m \delta h \int_0^{\infty} \frac{D}{[(R-r)^2 + D^2]} E \left[\sqrt{\frac{4rR}{(R+r)^2 + D^2}} \right] \frac{r \Delta p(r) dr}{\sqrt{(R+r)^2 + D^2}} \quad (2)$$

$$\delta u_r(R) = 2 \frac{1-\nu}{\pi} c_m \delta h \int_0^\infty \left[K \left[\sqrt{\frac{4rR}{(R+r)^2 + D^2}} \right] - \frac{R^2 + D^2 - r^2}{(R-r)^2 + D^2} E \left[\sqrt{\frac{4rR}{(R+r)^2 + D^2}} \right] \right] \times \frac{r \Delta p(r) dr}{R \sqrt{(R+r)^2 + D^2}} \quad (3)$$

where K and E are complete elliptic integrals of the first and second kind respectively.

Effect of horizontal strains on subsidence

In order to examine the influence of lateral strain on vertical ground movement it is convenient to consider a simple case of a uniform pressure decline $\overline{\Delta p}$ within a cylindrical volume of small thickness δh and radius R . Geertsma (1957) integrated (2) to obtain subsidence above the centre of a circular area as follows:

$$\delta u_z(0) = \delta_\nu 2(1-\nu) \left[1 - \frac{D/R}{\sqrt{1+(D/R)^2}} \right] \quad (\delta_\nu = c_m \overline{\Delta p} \delta h) \quad (4)$$

An important feature of the above expression is that for $D/R \ll 1$ (a very shallow or a very wide area of pore pressure decline) the subsidence in the centre is $\delta_\nu 2(1-\nu)$. This is a factor of $2(1-\nu)$ greater compared to the value of $\delta_\nu = c_m \overline{\Delta p} \delta h$ that corresponds to subsidence computed neglecting horizontal strains. This phenomenon was explained by Geertsma (1957) who showed that the horizontal contraction of a layer results in a contraction of the surrounding media in such a way that the base and the top of a shallow aquifer are both subsiding.

Calculation of ground movement in conditions of non-homogeneous pore pressure decline

If an attempt is made to calculate integrals of the type (1) by approximating them with integral sums, a very fine subdivision of the area of integration is required to achieve an acceptable accuracy. This is due to the singularity of the integrand in (1) at $D = 0$. In order to avoid this difficulty the volume contributing to ground movements has to be subdivided into thin horizontal slices of thickness δh and located at depth D . Further, the spatial extent of each slice must be subdivided into elementary rectangles of the size chosen in such a way that the variation of pressure decline can be neglected on the scale of an elementary area. In this case Δp within each such area i can be considered constant and replaced by a value Δp^i at the centre of the area. The contribution of each elementary area A_i is proportional to its vertical thickness and ground movements can be represented as sums of contributions from each area:

$$\delta u_z(X, Y) = \sum_i \delta_\nu^i \frac{1-\nu}{\pi} \int_{A_i} \frac{D dx dy}{[(X-x)^2 + (Y-y)^2 + D^2]^{3/2}} \quad (5)$$

$$\delta u_x(X, Y) = \sum_i \delta_\nu^i \frac{1-\nu}{\pi} \int_{A_i} \frac{(X-x) dx dy}{[(X-x)^2 + (Y-y)^2 + D^2]^{3/2}}$$

where $\delta^i_\nu = c_m \Delta p^i \delta h$ is the vertical compression assuming the condition of no lateral strain.

The above integrals can be evaluated analytically. The results are presented in the next section.

Ground movements due to specific patterns of water table decline

It appears that the only analytically tractable case for which ground movements can be evaluated in closed form corresponds to a uniform pattern of pressure decline over a rectangular area. Integrals (2-3) describing subsidence and horizontal movements resulting from radially symmetric patterns can only be evaluated numerically. Numerical and analytical results are presented below and compared with each other for the following patterns:

- (a) Uniform pressure decline of magnitude $\overline{\Delta p}$ within rectangular and circular areas.
- (b) "Bell"-shaped pattern simulating regional drawdown: $\Delta p(r) = \overline{\Delta p} 3e^{-3(r/R)^2}$.
- (c) Transient cone of depression around a well: $\Delta p(r) = \overline{\Delta p} \int_{(r/R)^2}^{\infty} e^{-u} \frac{du}{u} \left[R = \sqrt{\frac{tT}{4S}} \right] \dots$

The above equations are written in a scalable form and parameters are selected in such a way that $\overline{\Delta p}$ can always be interpreted as the average pressure decline in the drainage area of radius R . This is because

$$\int_{-\infty}^{\infty} \int \Delta p(x, y) dx dy = \overline{\Delta p} A$$

where $A = \pi R^2$. The parameter R can be legitimately interpreted as an effective drainage radius because 97% of the area under $\Delta p(r)$ for the "bell"-shaped and 95% for the Theis function are within the drainage radius defined above.

Ground displacements corresponding to uniform pressure decline in a rectangular slice of a small thickness δh , dimensions $2L_x, 2L_y$ and centred at $x = 0, y = 0$ at depth D can be obtained by evaluating the area integrals in (5):

$$\delta u_z(X, Y) = \overline{\delta}_\nu \frac{1-\nu}{\pi} \operatorname{atan} \left(\frac{xy}{D\sqrt{x^2+y^2+D^2}} \right) \left\| \begin{matrix} X+L_x, Y+L_y \\ X-L_x, Y-L_y \end{matrix} \right. \tag{6}$$

$$\delta u_x(X, Y) = \overline{\delta}_\nu \frac{1-\nu}{\pi} \log \left(\frac{y + \sqrt{x^2+y^2+D^2}}{D} \right) \left\| \begin{matrix} X+L_x, Y+L_y \\ X-L_x, Y-L_y \end{matrix} \right. \tag{7}$$

where $\overline{\delta}_\nu = c_m \overline{\Delta p} \delta h$ and the above operation of double substitution means the following:

$$U(x,y) \left\| \begin{matrix} X+L_x, Y+L_y \\ X-L_x, Y-L_y \end{matrix} \right. = U(X+L_x, Y+L_y) - U(X-L_x, Y+L_y) - U(X-L_x, Y-L_y) + U(X+L_x, Y-L_y)$$

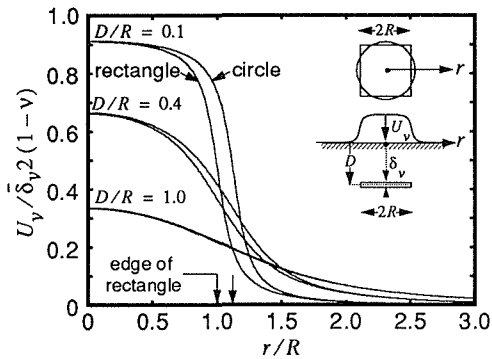


Fig. 1 Vertical displacements due to uniform pressure decline within rectangular and circular areas.

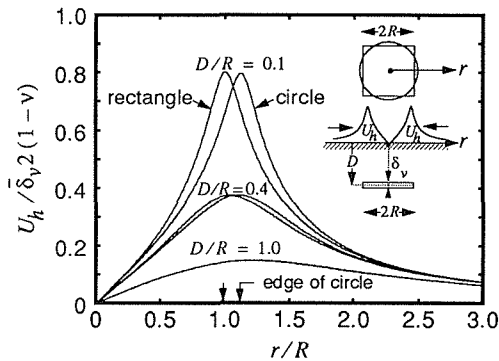


Fig. 2 Horizontal displacements due to uniform pressure decline within rectangular and circular areas.

Figure 1 illustrates patterns of vertical displacements according to (6) and compares them with numerically calculated displacements according to (2) for a uniform drawdown within a circular region of the same area. Figure 2 presents the same comparison for horizontal displacements that are of about the same magnitude as vertical.

Ground movements computed for the bell-shaped pressure decline pattern and for a pumped wells are illustrated in Figs 3 and 4.

Horizontal displacements can be differentiated numerically to obtain horizontal ground strains to identify locations of tension zones and peak ground strains. These strains are compared qualitatively with bending strains resulting from vertical subsidence. The latter are proportional to the curvature of the subsidence profile and are depicted qualitatively in Fig. 5. It is important to observe that the peak horizontal strain occurs very close to the point of maximum curvature. Figure 6 illustrates the same comparison for horizontal strains around a pumped well.

The above relationships will be now applied to a case history described in the next section.

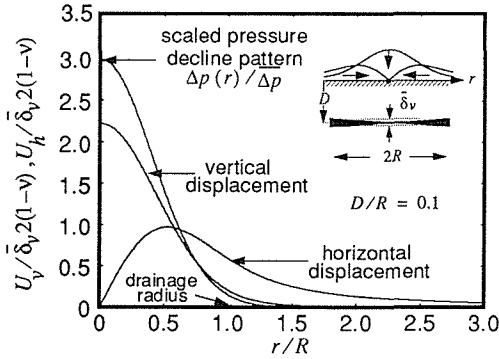


Fig. 3 Vertical and horizontal ground displacements due to bell-shaped pressure pattern.

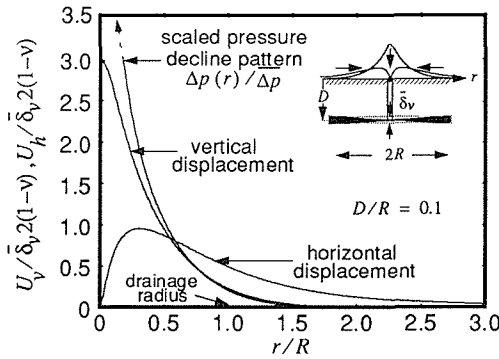


Fig. 4 Vertical and horizontal ground displacements due to pressure decline near a well.

THE SARIR AGRICULTURAL PROJECT

The Sarir agricultural area is located approximately 600 km south of Benghazi deep in the Libyan desert where extensive fresh water aquifers occur within sediments of post Eocene age. The agricultural production in the Sarir area is supported by irrigation from two well fields about 50 km apart. The Sarir South field is the largest of the two with 157 wells on the area of about 2200 km². The wells are approximately 300 m deep and are arranged in double rows running east to west. The well spacing is 2.5 km. The layout of both fields is shown in Fig. 7.

Ground water at Sarir is drawn from two aquifers that are hydraulically separated over a considerable part of the area. The shallow aquifer consists of unconsolidated sediments of post-Middle Miocene age. Unconsolidated and semi-consolidated sediments of the deep aquifer are of Lower Middle Miocene age. This main aquifer is multi-layered and includes sequences of unconsolidated and semiconsolidated sands, silts, shales clays and siltstones.

The sediments separating the two aquifers are only clearly defined in the Sarir North area where the static head is about 3 m higher in the deep aquifer. This aquifer behaves as confined during long-term pumping. In the Sarir South area the static head difference between the two aquifers is only 10 cm on average and the deep aquifer behaves as a

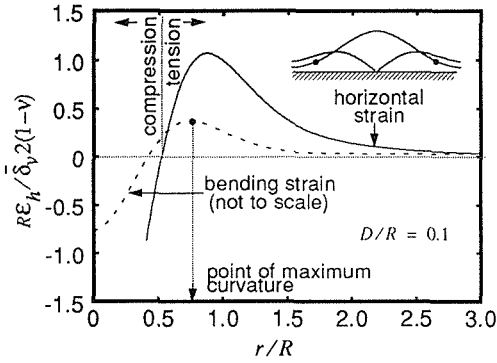


Fig. 5 Comparison of horizontal strain pattern and curvature of regional subsidence profile.

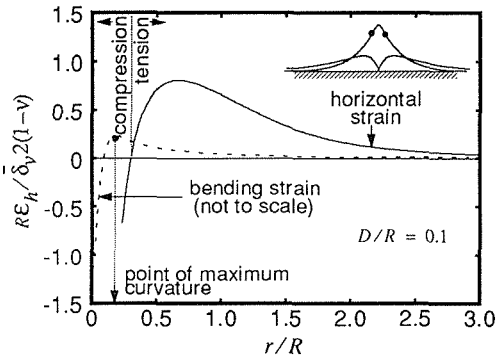


Fig. 6 Comparison of horizontal strain pattern and curvature of subsidence profile near a well.

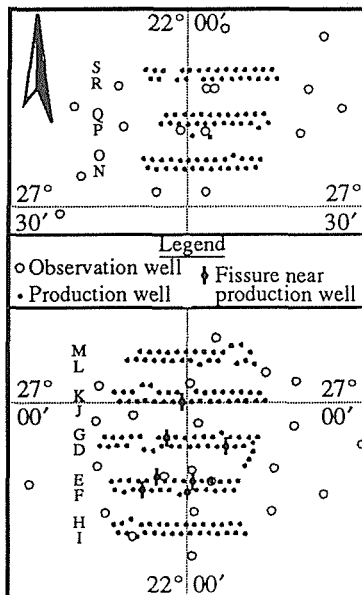


Fig. 7 The Sarir well fields.

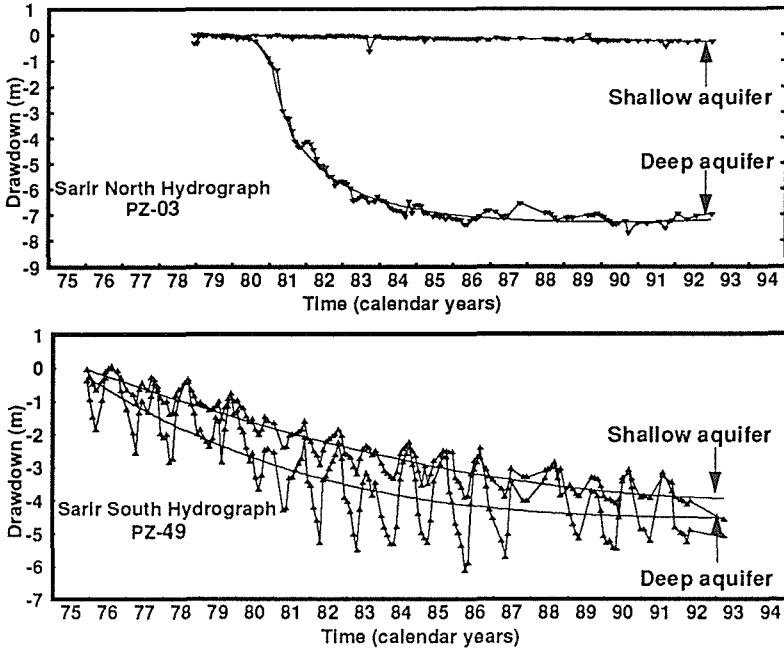


Fig. 8 Typical drawdown patterns in observation wells.

leaky aquifer in a long run. Typical drawdown patterns in Fig. 8 for observation wells completed as dual shallow/deep piezometers illustrate differences in performance of the deep aquifer in the two fields.

Groundwater pumping in the Sarir South field began in 1975 with only several production wells. The gross production rate was growing steadily up to 1983 when it reached about 135 million cubic metres per year and remained approximately steady afterwards.

Earth fissures in the Sarir area

The first earth fissure in the Sarir area was noticed in 1982 in the vicinity of the production well D3, about 1.2 km to the north. A year later new fissures were visible near wells in rows E and F and by 1987 fissures progressed further south towards the row H, Fig. 7. Fissures first appear as narrow and shallow cracks 1 cm to 2 cm wide and with no vertical offset. They are initially formed from aligned tiny sand craters and sink-like depressions. Fully developed fissures range in length from several metres to over 1 km and are up to 1 m wide.

When the first fissure was discovered in 1982 the maximum regional piezometric level decline was 3.5 m in the deep aquifer. This figure reflects the average water level over a year and excludes seasonal variations that could add another 2 m during pumping periods (Fig. 8).

Compressible sediments in the area are mainly sandy and silty clays and silts. Their aggregate thickness is about 50 m out of approximately 250 m depth affected by

drawdown. Clay units are generally 1 to 2.5 m thick and are of limited spatial extent. Such sediments are expected to consolidate rapidly. A review of geotechnical properties based on well logs and geologic history of sediments gave a subsidence estimate of 9 cm for 1982 when the first fissure was discovered. This includes 2 cm to account for elastic compression of coarse-grained sediments. The estimated subsidence corresponds to a unit compressibility of about $1 \times 10^{-4} \text{ m m}^{-1} \text{ m}^{-1}$.

Ground strains

Horizontal ground strains assuming *isotropic* compaction of sediments were calculated based on regional drawdown data from observations wells. Results are presented in Fig. 9.

Despite that very low strains were computed as a result of a regional drawdown, the distribution of tension zones in the Sarir South field is quite revealing (Fig. 9). For drawdown contours corresponding to 1982 the boundary of the tension zone makes a peculiar twist and passes in the vicinity of the well D3 where the first fissure was discovered. The reason for such an unusual shape of the tensile zone is the existence of two separate drawdown areas as indicated in Fig. 9 by head loss contours in the deep aquifer. Later on, in 1987, the computed tension zone is entirely on the margins of the field, as shown in Fig. 9. Nevertheless, most of the fissures that were formed between 1982 and 1987 are within the area most significantly affected by drawdown.

In order to address this apparent contradiction it is important to note that most fissures have been observed not far from wells. During pumping periods drawdowns in wells can reach 20-40 m creating a possibility of horizontal differential ground movements that occur in concentrated areas between wells. With hydraulic properties for all well and pumping rates known (transmissivity of $1240 \text{ m}^2 \text{ day}^{-1}$; storage

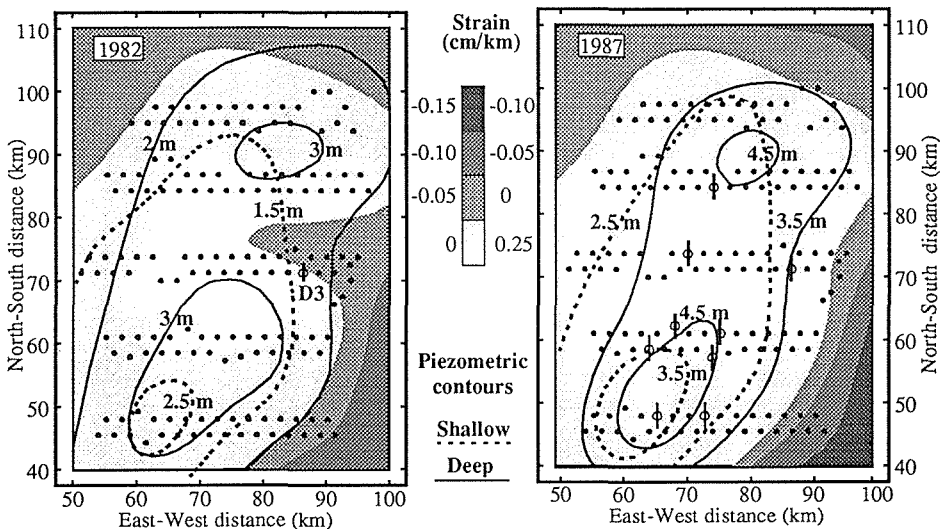


Fig. 9 Regional water table decline contours in shallow and deep aquifers and computed zones of ground tension due to regional drawdown.

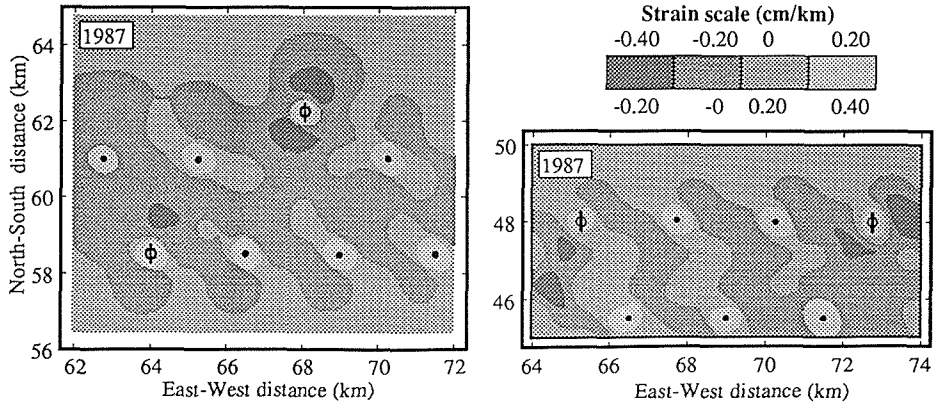


Fig. 10 Tension zones due to drawdown in wells and regional water level decline.

coefficient in the shallow aquifer 0.05; pumping rate $6,500 \text{ m}^3 \text{ day}^{-1}$ on average for all wells), horizontal ground movements around wells can be estimated. The maximum tensile strain between two wells can be about 1.2 cm km^{-1} . The gross horizontal differential movement is sufficient to overcome compression from the regional drawdown and to create islands of tensile strain between wells (Fig. 10).

Mechanism of fissure formation

It is clear that tensile strains of the order of 1 cm per 1 km would not be able to open a fissure that is 1 m wide. Nevertheless, it is not inconceivable that inhomogeneities on the ground surface would cause strain concentration initiating fissures in some areas. An important observation from the Sarir South field is that all fissures occur on an uncultivated land 40-50 m from crop areas. The same was reported by Contaldo & Mueller (1991) for the Mimbres basin in New Mexico. It is therefore likely that stiffer cultivated areas at Sarir South are not deforming in a relative sense and make it possible for strains to concentrate in between fields. If this is true, opening small fissures about a centimetre wide becomes feasible. The islands of tensile strain in Fig. 10 are about 2 km wide and the differential movement induced across this area is close 1 cm. It should be noted that no fissures were observed in the Sarir North field where there is very little water table decline in the shallow aquifer. Strains resulting from well-related drawdowns in the confined aquifer are not sufficient to overcome compression from the regional drawdown.

In order to address the issue of large fissures it is worth noting that the above solutions for horizontal deformations resulting from isotropic contraction take into account a restraining action of the surrounding media. If this media is unable to provide the restraint because of weakening by vertical fissures, for example, the magnitude of horizontal movements is expected to increase. The following estimate is instructive. Assume, for example, a large shallow aquifer such that because of vertical fissures on its margins the surrounding media completely loses its ability to provide resistance to horizontal contraction. If the radius of the aquifer is, say, 20 km, as roughly the case of the Sarir South field, a volumetric contraction of 1×10^{-4} per metre of head loss and per

meter of a linear dimension will create a horizontal contraction of 2 m m^{-1} of head loss. This example indicates an enormous potential of large areas affected by drawdown to develop significant horizontal movements.

The presented theory of fissure formation gives reasonable estimates of fissure locations for the Sarir South well field based on identification of tension zones. It predicts no fissures in the Sarir North field. The theory also qualitatively explains locations of fissures on boundaries of crop areas and points out on a possibility of significant horizontal ground movements when large areas are affected by even a modest water level decline.

Acknowledgements The study outlined in this paper is part of the UNDP project "Water Resources Development and Soil Studies (LIB/88/002)". The authors are indebted to the staff of the General Water Authority, Tripoli, Libya, for their effort in collecting and interpreting the Sarir hydrogeological data and for permission to publish this paper.

REFERENCES

- Geertsma, J. (1957) The effect of fluid-pressure decline on volumetric changes in porous rocks. *Trans Am. Inst. Mech. Engng* **210**, 331-343.
- Contaldo, G. J. & Mueller, J. E. (1991) Earth fissures and land subsidence in the Mimbres basin, southwestern New Mexico, USA. In: *Land Subsidence* (ed. by A. I. Johnson) (Proc. Fourth Int. Symp. on Land Subsidence, Houston, May 1991), 301-310. IAHS Publ. no. 200.
- Holzer, T. L. (1984) Ground failure induced by groundwater withdrawal from unconsolidated sediments. In: *Man-Induced Land Subsidence* (ed. by T. L. Holtzer), *Reviews in Engineering Geology*, vol. VI, 67-101. The Geological Society of America.
- Mindlin, R. D. & Chang, D. (1950) Thermoelastic stress in the semi-infinite solid. *J. Appl. Phys.* **21**, 931-942.

A method to predict final subsidence basins by means of a finite difference computer code

**LEANDRO R. ALEJANO MONGE,
PEDRO RAMÍREZ OYANGUREN &
RODRÍGUEZ DE LA FUENTE**

*Department of Mining Engineering, Polytechnic University of Madrid,
Ríos Rosas 21, E-28003 Madrid, Spain*

Abstract In this paper a method to predict subsidence due to total extraction of flat coal seams is presented. The method is based on the adequate characterization and the correct definition of the constitutive model of behaviour of rock masses, and is implemented in a finite difference numerical code. Due to the existence of an enormous quantity of data related to material properties as well as to subsidence measurements in the UK, the method is validated with acceptable results for standard British carboniferous coal measures rock masses.

INTRODUCTION

During the last decades many researches have been devoted to understand and adequately predict the phenomenon of subsidence due to total extraction of coal seams. In the recent years, research has been focused not only on the surface effects, but on the actual behaviour of cover rock. The main aim of our work has been to model correctly the behaviour of rock masses in such a way that displacements at the surface and plastification of the overburden could be predicted and compared with measured data.

In order to reach this objective, it has been decided to model standard English coalfields rock masses. The main reasons are on the one hand the many data about the features and properties of materials present in English coalfields (Coal Measures) and on the other hand the existing sufficiently accurate empirical prediction methods to check the results.

The prediction method to compare our results to, has been an empirical graphical method produced by the National Coal Board from subsidence measurements taken in more than one hundred collieries in different British coalfields for fifteen years. This prediction system was first published in the so called *Subsidence Engineer's Handbook* (SEH) in 1965 and updated 10 years later (National Coal Board, 1965, 1975). This method presents a series of formulae and graphs which can be used to predict future subsidence effects. Thus, it applies only to mining and ground conditions similar to those where the measurements were taken, i.e. to an overburden consisting predominantly of mudstone and siltstone, for which cases the model can predict the subsidence with an accuracy better than 10% of the extraction height.

When a wide enough longwall coal panel is mined, the cover rocks suffer different degrees of deformation and damage. Peng (1992) differentiates four zones in the overburden:

- *Caved Zone*: The immediate roof caves irregularly, filling the void. The strata lose their continuity and bedding planes disappear.
- *Fractured Zone*: Located over the caved zone, its main feature is the loss of continuity and breaking or yielding of materials but some bedding planes may remain.
- *Continuous Bending Zone*: In which strata bend downwards without breaking. Only occasional tension cracks can be observed.
- *Soil Zone*: The surface layer, whose behaviour is very site-dependent.

The first two zones can be considered plastified, that's to say their forming materials yield, so they can be simulated by means of an elasto-plastic constitutive behaviour model. According to Peng (1992) the combined height of these two zones is in general 20 to 30 times the extraction height, being bigger for hard strata and vice versa. The two upper zones do not suffer yield, they just deform elastically, so they can be considered elastic.

Following Farmer (1983) and Hoek & Brown (1980), and after some numerical validation studies, it was decided to use an elasto-plastic model with the following features:

- Elastic transversely isotropic behaviour before yield, as was used by Yao *et al.* (1993), in a similar finite element analysis.
- Anisotropic rock strength due to the presence of weakness planes, as it was observed in slates by Jaeger & Cook (1976). This can be modelled by the "ubiquitous joint model" provided in the used code, in which the Hoek-Brown failure criterion is used for the material, while the strength of the planes of weakness is expressed by means of the Mohr-Coulomb parameters.
- Isotropic elastic post-failure behaviour, because it is considered that the rock mass loses its anisotropy after yielding.

COALFIELD ROCK MASS CHARACTERIZATION

A typical English coalfield, as those where the SEH measurements were taken, is basically formed by mudstone and siltstone. Although sandstone and underclay may exist in small amounts, they are not going to be taken into account in this analysis.

To characterize a rock mass in order to define its mechanical behaviour, Hoek (1994) defined the Geological Strength Index (GSI). The calculation of the GSI of the British Coal Measures containing 50% mudstone and 50% siltstone is presented in Table 1.

Strength properties

Hassani & Scoble (1981) present the following data of uniaxial compressive strength (UCS) and triaxial failure behaviour of mudstone and siltstone, according to Bieniawski's yield criterion:

$$\text{mudstone: UCS} = 39 \text{ MPa} \quad \frac{\tau_m}{\sigma_c} - 0.05 = 0.888 \cdot \left(\frac{\sigma_m}{\sigma_c} \right)^{0.767} \quad (1)$$

Table 1 Estimation of the GSI of a Coal Measures rock mass.

	Mudstone		Siltstone		Average rock mass
	Values	Rating	Value	Rating	Rating
UCS	30 MPa *	4	53.9 MPa *	7	5.5
R.Q.D.***	58% **	12	90% **	19	15.5
Joint spacing	250 mm	13	300 mm	14	13.5
Conditions joints	rough-hard	20	rough-hard	20	20
Groundwater	-	10	-	10	10
GSI		59		70	64.5

* Data estimated from Hassani & Scoble (1981).

** Data obtained from Spears & Taylor (1972).

*** R.Q.D. = Rock Quality Designation.

The rest of the data are estimates.

Table 2 Strength properties of the rock masses.

Material	Mudstone	Siltstone	Rock mass (average)
GSI	59	70	64.5
Hoek-Brown parameters of rock	UCS = 30 MPa $m = 12.14$	UCS = 53.86 MPa $m = 16.39$	UCS = 41.92 MPa $m = 14.26$
Hoek-Brown parameters of "rock mass"	$m(i) = 2.8077$ $m(b) = 0.6492$ $s(i) = 0.0105$ $s(b) = 0.00107$ U.T.S. = 0.112 MPa	$m(i) = 5.6139$ $m(b) = 1.9228$ $s(i) = 0.0356$ $s(b) = 0.00674$ U.T.S. = 0.341 MPa	$m(i) = 4.014$ $m(b) = 1.13$ $s(i) = 0.0194$ $s(b) = 0.00269$ U.T.S. = 0.2019 MPa

Table 3 Strength properties of the discontinuities of the rock mass.

		Mudstone	Siltstone	Average rock mass
		Cohesion (kPa)	Range	0-200
	Mean	100	200	150
Friction (°)	Range	21-33	28-33	21-33
	Mean	27	30.5	28.75

$$\text{siltstone: } UCS = 63 \text{ MPa } \frac{\tau_m}{\sigma_c} - 0.06 = 0.944 \cdot \left[\frac{\sigma_m}{\sigma_c} \right]^{0.813} \quad (2)$$

With these data and the previously obtained GSI, the values "m" and "s" of intact and broken rock mass for mudstone, siltstone and average rock, as shown in Table 2, can be deduced from the equations of Hoek (1994). The Mohr-Coulomb parameters, namely cohesion and friction angle, at the natural interfaces obtained by Hassani & Scoble (1981) are presented in Table 3.

Deformability properties

The deformability parameters have a great influence on the final shape of the subsidence basin, that's why they have been extensively studied. Hassani & Scoble (1981) in his laboratory studies obtained a Young's modulus of elasticity of 5000 MPa and 6000 MPa for mudstone and siltstone rocks respectively. The data of deformability of the rock mass estimated after several sources are presented in Table 4.

Table 4 Deformability properties of the rock mass.

Intact rock mass (transversely isotropic elastic model)	Broken rock mass (elastic isotropic model)
$E_x = 980 \text{ MPa}^*$ $E_x/E_y \approx 1.72^{**}$ $G_{xy} = 33.02 \text{ MPa}^{**}$ $\nu_x = 0.2^{**}$ $\nu_y = 0.2^{**}$	$E = 300 \text{ MPa}^*$ $\nu = 0.275^{***}$

* Data obtained by means of a benchmarking procedure with computer code analysis.

** Data estimated from Yao *et al.* (1993).

*** Datum extrapolated from Hoek (1994).

One relation has been found in literature (Afrouz, 1992) giving more or less the same ratio between the Young's modulus of rock and rock mass obtained in this study. This equation is:

$$E_{\text{rock mass}} = E_{\text{rock}} \cdot \exp(0.564 \cdot RMR - 5.64) \quad (3)$$

The Young's modulus of the broken rock mass may be stress dependent, as it usually happens with backfill materials.

NUMERICAL SIMULATION

The main goal of the simulation is to assess the mechanical behaviour of the Coal Measures rock mass, by comparing the results obtained from the computer model to the ones provided by the SEH, taking also into account the plastified zone height.

The code FLAC version 3.22 (Itasca, 1993) has been used to carry out the simulation. This is a two dimensional explicit finite difference code which simulates the mechanical behaviour of rocks, as a continuum, which may undergo plastic flow.

Assumptions, initial conditions, mesh and model restrain

Since FLAC is a bidimensional code, the simulation has to be performed in plane-strain. As far as the coal seam is flat, a vertical symmetry axis exists in its centre, and so only half of the model has to be simulated, saving computer time.

The natural stress field in the area of the mine has proved to be a fairly important and very site-specific issue in subsidence. According to different types of stress measurements carried out in several British coalfields (British Coal Corporation, 1994) it can be concluded that the average horizontal and vertical stresses are very much alike

(usually σ_v is a little bigger than σ_h) in most of the deposits studied. Therefore it has been decided to use as initial condition:

$$\sigma_h = \sigma_v = \rho \cdot g \cdot h \tag{4}$$

To make a first approach to the problem a specific mining situation has been selected ($W =$ width = 600 m, $h =$ depth = 300 m and $M =$ extraction height = 2 m). After several tentative runs it has been decided to use an area of discretization of 850 m wide and 600 m deep. The mesh size is big enough to ensure that the influence of the boundaries is not important in the model behaviour. The zone size is variable, being smaller in zones where important gradients of stress or displacement will occur (around the excavation) and wider close to the boundaries. The mesh is restrained in the horizontal direction at the symmetry line (right border) and at the left boundary, and in the vertical direction at the bottom boundary. The model and its restraints are shown in Fig. 1.

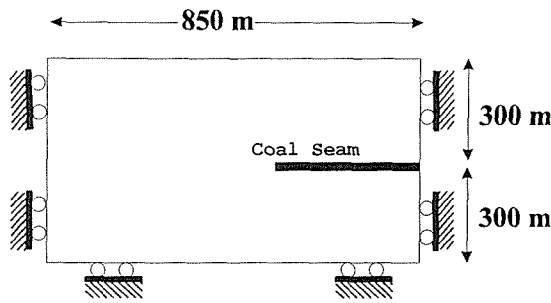


Fig. 1 Area of discretization and boundary conditions.

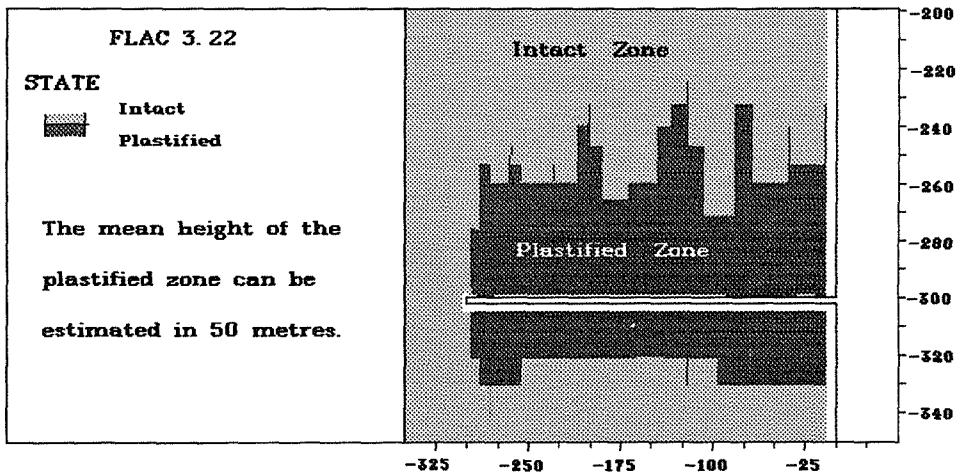


Fig. 2 Plastification zone after the first run of the case with $W = 600$ m, $h = 300$ m and $M = 2$ m, by means of the ubiquitous joint model. The height of the plastified zone over the longwall coincides with Peng's observations.

Implementation of the predefined constitutive model

The predefined constitutive model cannot be directly implemented in FLAC. To adequately simulate the behaviour of the rock mass the following strategy has been implemented. First, the whole material is modelled as an ubiquitous joint model with isotropic elastic softened post-failure behaviour (this involves isotropic elastic pre-failure behaviour, too). This first run shows up to what height over the seam the plastification reaches (this should accord with Peng’s results). Then, a second and definitive model is run, in which the material up to the height previously obtained is modelled as before and the rest of the rock mass is considered to behave according to be elastic. In Fig. 2 the area that has suffered plastification after the first run is presented.

In this way the caved and fractured zones are simulated by the ubiquitous joint model, because plastification is the most important aspect in the mechanical response of these zones; while the continuous deformation and soil zones are simulated by the transversely isotropic model, since the anisotropic deformation is the basic behavioral phenomenon in this upper part of the model.

RESULTS

The above mentioned supercritical case has been run in order to test up to what extent the subsidence profile calculated resembles the one predicted by SEH. In Fig. 3 both profiles are shown and it can be seen that the maximum subsidences (S) are very similar. All the subsidences obtained are within 10% M of the values predicted by the SEH, but over the ribsides the difference is a little bigger. This is probably due to the fact that FLAC models a continuum, where as in reality the presence of strata originates a "bridging effect" making subsidence smaller over the ribsides. The code is not capable to simulate this effect.

If the limit angle is defined like the angle formed by a vertical line on the ribsides and a line passing through the ribsides point and the closest surface point with no subsidence

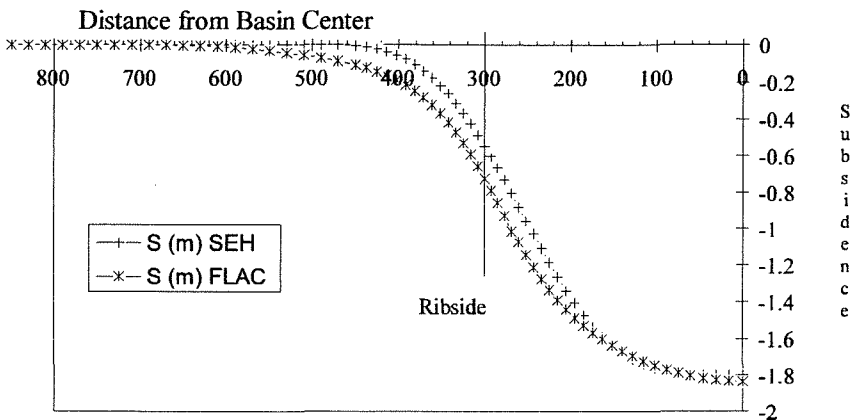


Fig. 3 Subsidence profiles for the case with $W = 600$ m, $h = 300$ m, and $M = 2$ m, obtained by the proposed method and SEH.

at all; then the limit angle obtained by the proposed method would be more than 45° , while according to SEH this limit angle has to be 35° . Nevertheless, if a second line is defined as passing through the ribside and the ground point where subsidence is not null but very small ($0.025 S = 45 \text{ mm}$), then the limit angle predicted by the proposed method will be 36° . Taking into account that it is actually impossible to locate precisely the first point with no movement, the above mentioned divergency is meaningless.

The surface horizontal displacements predicted by both methods are shown in Fig. 4. In this case the proposed method overestimates the values of this parameter.

In order to extrapolate the results to different W/h ratios, more cases have been run, varying the extraction height and depth as well. The results of S/M against W/h obtained have been plotted together with the standard SEH curve in Fig. 5. According to this figure the results of S/M , foreseen by FLAC for each W/h ratio, are always within 10% of the SEH predictions. So, the method can be considered acceptable.

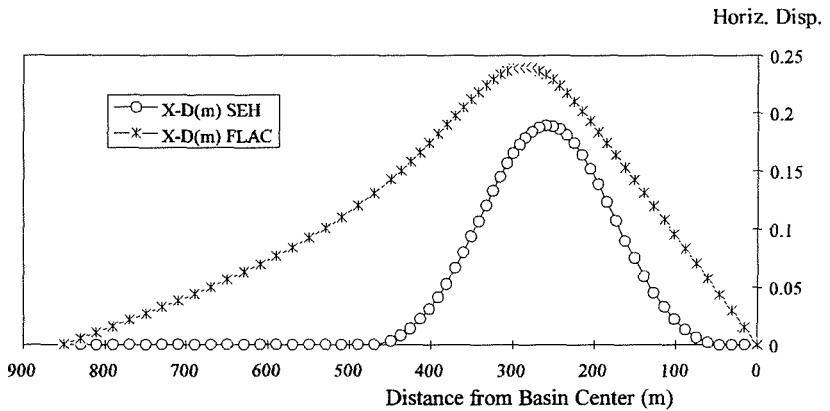


Fig. 4 Horizontal displacement profiles for the case with $W = 600 \text{ m}$, $h = 300 \text{ m}$, and $M = 2 \text{ m}$, obtained by the proposed method and SEH.

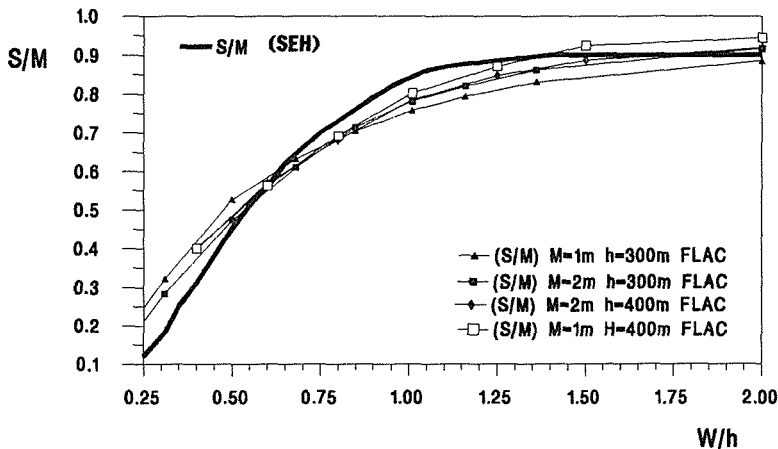


Fig. 5 Subsidence/extraction height at various width/depth ratios. Standard SEH curve and different values obtained by the proposed method for different mining geometries.

CONCLUSIONS AND FUTURE WORK

The characterization data of the English Coal Measures and the subsidence prediction method SEH have been successfully used to define a new subsidence prediction numerical method. Although very time-consuming and heavily dependent on the quality of the characterization of the overburden, this method could help not only to deepen the understanding of the phenomenon of mining subsidence due to longwall extraction, but to assess the influence of the overburden mass behavioral properties and to study more complicated mining geometries like inclined seam and multiple-seam mining.

Among the topics on the subsidence phenomenon, found to be definitely important, the natural stress field and the deformability properties of rock masses ought to be highlighted. Specially, this last aspect is of primordial interest and more research should be focused on the estimation of Young's modulus and Poisson's ratio of rock masses.

Starting from the results obtained so far, future work will be oriented to the extrapolation of the method to inclined seams and to the realization of some site-specific case studies.

Acknowledgement The authors thank the Mineral Resources Engineering Department of the University of Nottingham and especially Dr D. J. Reddish for the permission of scientific use of subsidence prediction programs.

REFERENCES

- Afrouz, A. A. (1992) *Practical Handbook of Rock Mass Classification Systems and Modes of Ground Failure*. CRC Press Inc.
- British Coal Corporation (1994) The effect of in-situ stress on mining conditions. *European Commission on Technical Coal Research, Report EUR 14528 EN*.
- Farmer, I. W. (1983) *Engineering Behaviour of Rocks*, second edn. Chapman and Hall, London.
- Itasca (1993) *User Manual for FLAC*, Version 3.22. Itasca Consulting Group Inc., Min., USA.
- Hassani, F. P. & Scoble, M. J. (1981) Properties of weak rocks, with special reference to the shear strength of their discontinuities, as encountered in British surface coal mining. In: *Proc. Int. Symposium on Weak Rock* (Tokyo). Balkema.
- Hoek, E. & Brown, E. T. (1980) *Underground Excavations in Rock*. IMM.
- Hoek, E. (1994) Strength of rock and rock masses. Extract from book: *Support of Underground Excavations in Hard Rock*. Balkema.
- Jaeger, J. C. & Cook, N. G. (1976) *Fundamentals of Rock Mechanics*. Chapman and Hall, London.
- National Coal Board (1965, 1975) *Subsidence Engineer's Handbook*. National Coal Board, London.
- Peng, S. S. (1992) *Surface Subsidence Engineering*. SME.
- Spears, D. A. & Taylor, R. K. (1972) The influence of weathering on the composition and engineering properties of in-situ Coal Measures Rocks. *Int. J. Rock Mech. Sci. & Geomech. Abstr.* 9(6).
- Yao, X. L., Reddish, D. J. & Whittaker, B. N. (1993) Non-linear finite element analysis of surface subsidence arising from inclined seam extraction. *Int. J. Rock Mech. Sci. & Geomech. Abstr.* 30(4).

On the necessity to consider varying parameters in land subsidence computations

ALAIN DASSARGUES

Laboratoires de Géologie de l'Ingénieur, d'Hydrogéologie et de Prospection Géophysique (LGIH), University of Liège, Bâtiment B19, B-4000 Liège, Belgium

Abstract Geotechnical scientists have long been aware that during consolidation of compressible layers, changes in porosity due to a rearrangement of the soil skeleton may lead to decrease of both the permeability and the compressibility of the porous medium. The variation of these two parameters influences strongly the further consolidation processes. These variations must be taken into account in the land subsidence models. These variable and highly interdependent geotechnical parameters introduce nonlinearities and coupling in the numerical procedure to simulate the consolidation process. A fully nonlinear approach is proposed to compute with accuracy the land subsidence due to groundwater withdrawal in loose sediments. Of course, field and laboratory data are needed to implement the additional constitutive laws describing the variations of the hydraulic conductivity and of the compressibility (coupled to the specific storage coefficient). Comparisons between computations with constant parameters and with varying parameters have been performed. The computed pore pressures are strongly affected, inducing automatically the main differences in the calculated subsidences. Moreover, it is demonstrated that with identical pore pressure distribution and initial parameters, the subsidence computed with constant parameters will be systematically overestimated when compared with those computed with varying parameters. These developments are illustrated by some linear and nonlinear computations, realized on the case study of Shanghai.

INDUCED LAND SUBSIDENCE

Young unconsolidated or semi-consolidated sediments of high porosity, laid down in alluvial or shallow marine environments, form a succession of layers which can often be characterized (from an hydrogeological point of view) as semiconfined or confined aquifer systems (Poland, 1984). They consist of silty sand and sand aquifers of high permeability (hydraulic conductivity) and low compressibility, interbedded with clayey aquitards characterized by low vertical permeability and high compressibility. According to Terzaghi (1943), the geostatic pressure or total stress (σ) that any point undergoes in the soil is considered as the result of two additional components: the fluid pore pressure and the effective stress (σ'). The global soil compressibility is a factor 20 to 1000 larger than grain compressibility, so that it would be useless to choose another principle based on, for example, Biot's theory (1956). Applying Terzaghi's principle, the lowering of

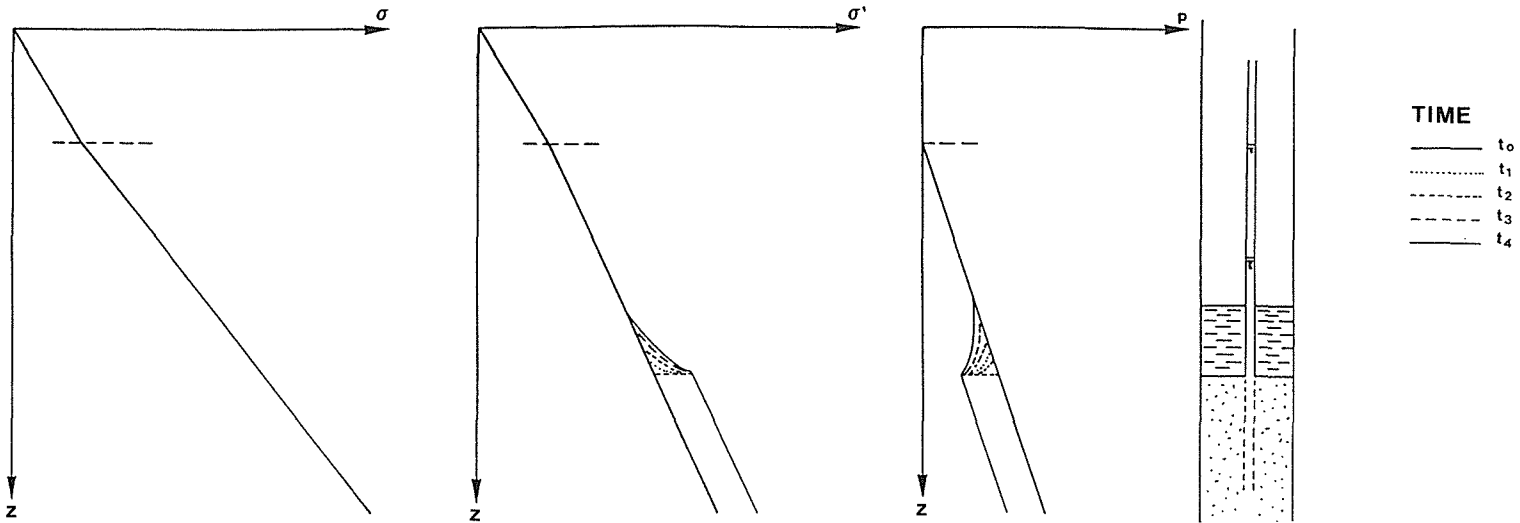


Fig. 1 Evolution of the total stress, pore pressure and effective stress as a function of depth when lowering the piezometric head in a confined aquifer. First stage: the pore pressure decrease has not yet propagated above the confining layer.

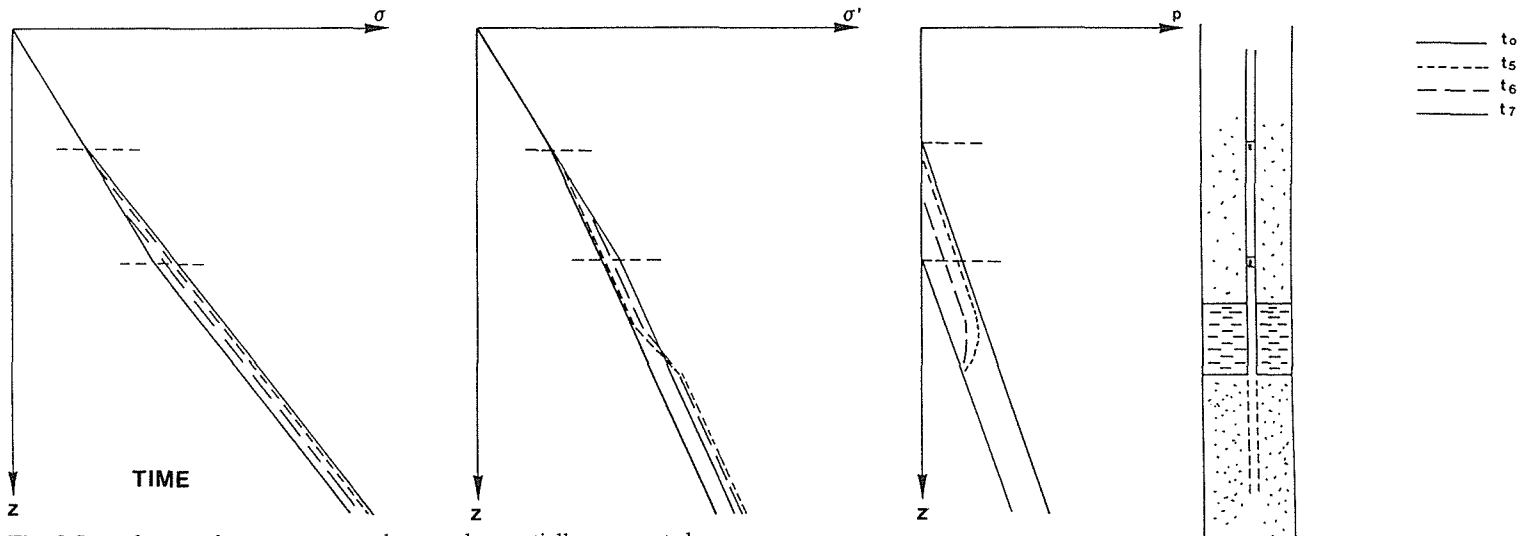


Fig. 2 Second stage: the pore pressure decrease has partially propagated.

the piezometric head in a confined aquifer (Fig. 1) induces additional effective stresses in the layers. If an initial hydrostatic pore pressure is assumed, the pore pressure is decreased in the aquifer and partially decreased in the underlying/overlying aquitards. During this stage, the total stress can be assumed constant as the pressure decrease propagation through the aquitards is very slow. Moreover, the upper layers can be saturated by the recharge. The slow propagation of the pore pressure variation in semi-permeable layers induces automatically an equivalent increase in effective stress in these compressible layers and a drained consolidation process is started. After a very long period (Fig. 2), the pore pressure decrease can reach the top of the confining layer and then, as for unconfined situations, a decrease of the thickness of saturated soils is recorded. In this case, the total stress can begin to vary (except if there is an important infiltration or recharge). There is a strong transient behaviour of the process due to the fact that the main consolidation (usually called primary consolidation) is activated by the decrease of pore pressure as long as hydrostatic equilibrium is not restored.

Physically, the structural evolution of clays during the consolidation process is dominated by the reduction of the pore dimensions, so that the whole porosity is decreasing. Many authors have observed that clay minerals tend to orient their plates orthogonally to the direction of the main applied stress developing a kind of structural anisotropy (Delage & Lefebvre, 1984; and Rieke & Chilingarian, 1974).

RHEOLOGY OF THE LOOSE SEDIMENTS

The geomechanical behaviour of the soils can be idealized in terms of rheological models. The skeleton deformation under increasing effective stress is supposed to follow elastic, plastic or visco-elastic laws or any combination of these. For example, an elasto-plastic material can be represented by a Hookean spring and a Saint-Venant resistance placed in series, a visco-elastic model describing the creep of clayey soils consists in a spring and a dashpot taken in parallel (Kelvin model). Many other models can be imagined by combination in parallel or in series of these global or individual units, trying to reproduce the real behaviour of loose soils and recently deposited sediments. Clayey soils and loose sediments have a geomechanical behaviour qualified often as nonlinear elasticity with progressive plasticity and viscosity. This particular behaviour leads, in practice, to choose models based on experimental laws rather than on combinations of theoretical models. Elasto-visco-plastic laws in one or three dimensions can be established from experimental results. Different loading steps, more or less elaborated, can be applied to samples in order to find the parameters of an experimental law. These experimental constitutive laws allow a more simple introduction of nonlinear and interaction effects of the parameters.

HYDROGEOLOGICAL AND GEOTECHNICAL PROPERTIES

For modelling purposes, space integration is realized on a Representative Elementary Volume (REV) to obtain macroscopic values for porosity and permeability (hydraulic conductivity) of this porous medium. The porosity describes the reservoir property to release a fluid quantity; the permeability describes the reservoir ability to convey the fluid flow.

The hydraulic conductivity or permeability coefficient (K) may be expressed as:

$$K = \frac{k \cdot \rho \cdot g}{\mu} \quad (1)$$

where k is the intrinsic permeability of the porous medium, ρ the density of water, g is the constant of gravity and μ the viscosity of the water. The generalized Darcy's law, in three dimensions can be written as:

$$\underline{v} = \frac{k}{\mu} (\underline{\nabla}p + \rho \cdot g \underline{\nabla}z) = -\underline{K} \underline{\nabla}h \quad (2)$$

where \underline{v} is the Darcy velocity vector and \underline{K} is the permeability coefficient tensor. For silty and clayey semi-pervious formations, the permeability is often measured during consolidation tests (oedometer and triaxial tests). The values are obtained at different stages of effective stress, leading to the relation: $K = f(\sigma')$. The groundwater flow in a saturated porous medium can be expressed by the continuity equation:

$$\text{div}(\rho \cdot \underline{v}) + \rho \cdot q = -\frac{\partial}{\partial t}(\rho \cdot n) \quad (3)$$

where n is the porosity and q is flow rate (per volume unit) exchanged by the REV with the outside environment (positive if flow is entering into the system). The right-hand side of equation (3) characterizes the aquifer capacity to store or release a volume of water in function of the pore pressure prevailing in the formation. Seven important assumptions are needed to define the specific storage coefficient of a saturated porous medium:

- the REV concept is applied,
- isothermal conditions,
- the fluid is homogeneous, so that $\rho = \rho(p)$,
- the Darcy's velocity is a relative filtration velocity,
- the solid density (ρ_s) is constant, so that the compressibility of the solid grains is negligible,
- Terzaghi's effective stress principle holds,
- the total stress is constant.

In these conditions:

$$\frac{\partial}{\partial t}(\rho \cdot n) = \rho \cdot S_s \cdot \frac{\partial h}{\partial t} \quad \text{with} \quad S_s = \rho \cdot g \cdot (\alpha + n\beta) \quad (4)$$

where S_s is the specific storage coefficient of a saturated porous medium, α the volume compressibility coefficient of the porous medium, and β the water compressibility coefficient. Equation (4) shows the direct coupling between the transient groundwater flow and the consolidation processes, as the specific storage coefficient (S_s) is expressed in function of the compressibility coefficients of the porous medium and water.

The specific storage coefficient is determined on basis of oedometer tests realized with the following assumptions:

- the total stress is constant (drained test),
- lateral deformations are prevented and neglected,
- uniaxial state of stress and strain.

Moreover, fluid and solid grains compressibilities are neglected in regard to α so that:

$$S_y = \rho \cdot g \alpha \tag{5}$$

Generally, the S_y values obtained by pumping tests are larger than those obtained on samples by consolidation tests (Domenico & Mifflin, 1965). In loose sedimentary layers, it is really difficult to make such comparisons as undisturbed sampling is difficult in silty to sandy aquifer layers, and moreover the piezometric levels are hard to measure with accuracy in clayey aquitards.

PERMEABILITY AND COMPRESSIBILITY VARIATIONS

During consolidation of highly compressible clays, changes in porosity due to a rearrangement of the soil skeleton may lead to decreases in both the permeability and the compressibility of the porous medium. For example, Lambe & Whitman (1969) have presented data indicating that permeability values can change by orders of magnitude and compressibility can decrease significantly as void ratio is decreased. Neither of these variations is linear with void ratio.

Nonlinearity of the specific storage coefficient linked to the compressibility

Assuming a constant total stress and a negligible compressibility of water, the equation (5) can be used. By definition, the volumetric coefficient (α) is written:

$$\alpha = \frac{d\varepsilon_v}{d\sigma'} \tag{6}$$

where ε_v is the relative volumetric strain and σ' is the effective stress. We obtain:

$$\alpha = -\frac{dV}{V \cdot d\sigma'} \quad \alpha = -\frac{dn}{(1-n) \cdot d\sigma'} \quad \alpha = -\frac{de}{(1+e) \cdot d\sigma'} \tag{7}$$

where n and e are respectively the porosity and the void ratio at the beginning of the effective stress variation ($d\sigma'$).

The oedometer tests are the common one dimensional consolidation tests. The results are usually plotted on (σ' , ε_v) diagrams, allowing to determine α for each effective stress level (Fig. 3).

The compressibility coefficient for sandy to clayey materials depends on effective stress and on the effective preconsolidation stress value (σ'_p). In order to linearize

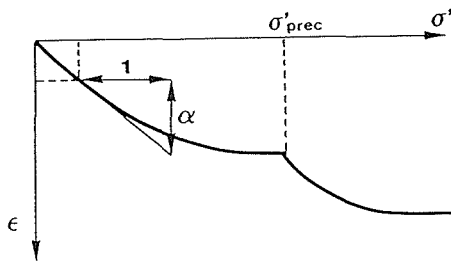


Fig. 3 Results of an oedometer test.

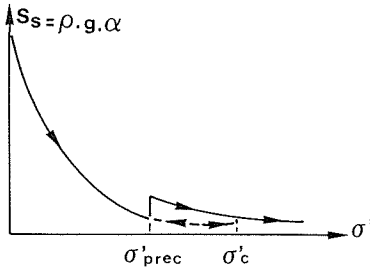


Fig. 4 Variation of the specific storage coefficient (S_s) in function of the effective stress σ' .

oedometer curves ($\varepsilon_v - \ln(\sigma')$ or $(e - \ln(\sigma'))$ diagrams can be used, and the compressibility coefficient can be expressed by:

$$\alpha(\sigma') = \frac{1}{A \cdot \sigma'} \quad \sigma' < \sigma'_p \quad (8)$$

$$\alpha(\sigma') = \frac{1}{C \cdot \sigma'} \quad \sigma' \geq \sigma'_p$$

One can remark that the specific storage coefficient is expressed as a function of $1/\sigma'$ values (Fig. 4). A more general relation linking the void ratio (e) to the effective stress, can be proposed as follows (Feldkamp, 1989):

$$e = \frac{a}{\sigma'^b} \quad (9)$$

where a and b are experimentally determined for each material. The compressibility coefficient can then be expressed as a function of the void ratio only:

$$\alpha(e) = c \cdot \frac{e^d}{1+e} \quad (10)$$

where c and d are experimentally determined for each material.

Nonlinearity of the permeability

To interpret porosity logs in terms of reservoir permeability, many relations linking the permeability coefficient K to total porosity or void ratio are used in reservoir engineering. However, these relations are not applicable for consolidation and subsidence computations in loose sediments as they are derived for hardened rocks. In our case, we are looking for empirical (experimentally found) relations linking permeability to void ratio or porosity, in layers characterized generally by high clay and peat contents, high compressibilities and low permeabilities. Many factors influence the permeability values:

- lithology,
- grain size,
- shapes, orientations and specific surface of the grains,
- spatial distribution of pores.

As mentioned above, the micro-structural evolution of clays during consolidation, orienting the plates more orthogonally to the direction of the vertical applied effective stress, develops an increasing structural anisotropy. This evolution increases the tortuosity of the flow channels when the groundwater flow is parallel to the vertical effective stress. This statement does not rule out the decrease in K by a decrease of the total void ratio. For practical purposes, it could be convenient to establish a relation $K = f(e)$ in a similar form to the formalism of the $(\log \sigma', e)$ oedometer relations (Fig. 5):

$$\begin{aligned}
 e &= C_{K_1} \log K + cst & K > K_p \\
 e &= C_{K_2} \log K + cst & K \leq K_p
 \end{aligned}
 \tag{11}$$

where K_p is the permeability coefficient corresponding to the effective preconsolidation stress (σ'_p), C_{K_1} and C_{K_2} are defined respectively as the elastic and plastic rate of K -variation during the consolidation. The constant being determined experimentally, the relation could be generalized:

$$K = \frac{C}{\sigma'^a}
 \tag{12}$$

However it could be difficult to determine α or C_{K_1} and C_{K_2} in practice. Many other relations can be experimentally fitted to the test results (Terzaghi, 1943; Rieke & Chilingarian, 1974; Barends, 1990; Safai & Pinder, 1980; Lambe & Whitman, 1969). For example, Nishida & Nakagawa (1970) have presented an equation linking K to e , taking into account the plasticity index (I_p) as an additional parameter. This last relation has been generalized and applied successfully for the computation of the subsidence in the Shanghai area (Dassargues *et al.*, 1991) with the form:

$$K = e^{a \cdot e + b} \quad \text{where } a = \frac{2.3}{c \cdot I_p + d}
 \tag{13}$$

b, c, d are experimentally determined. Therefore, many relations are known, more or less well adapted to each studied case. It is important to choose a relation and to fit the parameters, constants or exponents using the maximum of available data.

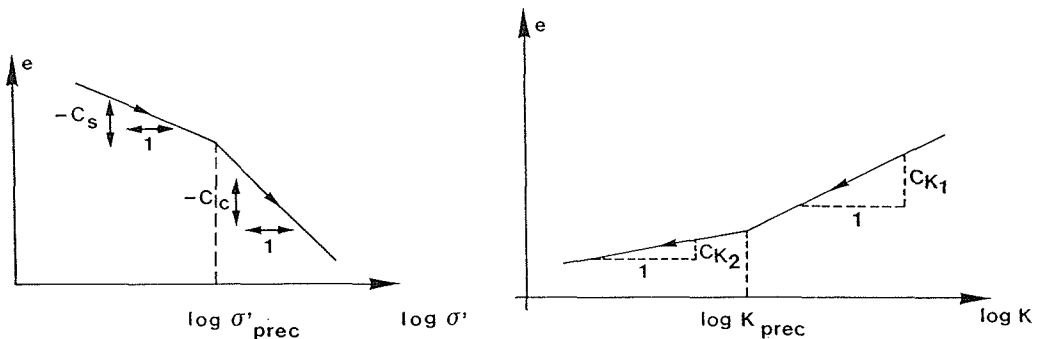


Fig. 5 $(\log K, e)$ diagram very similar to the $(\log \sigma' - e)$ diagram describing the oedometer test results.

INFLUENCE ON COMPUTED CONSOLIDATIONS

Rudolph & Frind (1991) have shown that for a pore pressure variation imposed at the bottom of a clayey column, it takes more time to reach permanent flow conditions with varying parameters than with constant parameters. These conclusions are always verified if K and S_s values are taken identical at the beginning of both computations. Differences in the calculated pore pressure spatial distributions induce automatically (by the Terzaghi principle) the main differences in calculated subsidences. Moreover, if pore pressures are taken rigorously identical, the subsidence computed by the simulation with constant parameters will be systematically overestimated when compared to the subsidence calculated with varying parameters (if the initial parameters are taken identical). From equations (5) and (6), the strain of the porous medium can be expressed on a time step Δt by:

$$\int_{\epsilon(t)}^{\epsilon(t+\Delta t)} d\epsilon = \int_{\sigma'(t)}^{\sigma'(t+\Delta t)} \frac{S_s}{\rho \cdot g} d\sigma' \quad (14)$$

In the case of constant parameters (K and S_s), equation (14) becomes:

$$\int_{\epsilon(t)}^{\epsilon(t+\Delta t)} d\epsilon = \frac{S_s}{\rho \cdot g} \int_{\sigma'(t)}^{\sigma'(t+\Delta t)} d\sigma' \quad (15)$$

On the contrary, in the case where S_s may vary as a function of σ' , equation (14) becomes:

$$\int_{\epsilon(t)}^{\epsilon(t+\Delta t)} d\epsilon = \frac{1}{\rho \cdot g} \int_{\sigma'(t)}^{\sigma'(t+\Delta t)} S_s(\sigma') d\sigma' \quad (16)$$

Replacing S_s by its value in equation (8), and after integration, the right-hand sides of equations (15) and (16) are respectively:

$$\frac{1}{\sigma'_{imp}} (\sigma'(t+\Delta t) - \sigma'(t)); \quad \ln \left[\frac{\sigma'(t+\Delta t)}{\sigma'(t)} \right]$$

where σ'_{imp} is a constant implicitly chosen when working with a constant value of S_s (in each layer). At the first time step of the computation, the first value of S_s for the non linear simulation is: $S_s = 1/(C \cdot \sigma'_{imp}(t))$ because the initial value of S_s is the same for both simulations. Since $\exp((a - c)/c) \geq a/c$ if $a \geq c$, we can write:

$$\frac{\sigma'(t+\Delta t)}{\sigma'_{imp}(t)} - 1 \geq \ln \left[\frac{\sigma'(t+\Delta t)}{\sigma'_{imp}(t)} \right] \quad \text{with } \sigma'(t+\Delta t) \geq \sigma'_{imp}(t) \quad (17)$$

For the next time step of the simulation, we can write:

$$\frac{1}{\sigma'_{imp}(t)} [\sigma'(t+\Delta t) - \sigma'(t)] \geq \ln \left[\frac{\sigma'(t+\Delta t)}{\sigma'(t)} \right] \quad \text{with } \sigma'(t+\Delta t) \geq \sigma'(t) \geq \sigma'_{imp}(t) \quad (18)$$

because $\exp((a - b)/c) \geq a/b$ if $a \geq b \geq c$. These inequalities (17) and (18) (Dassargues, 1991) prove that if the initial parameters are taken identical, the subsidence

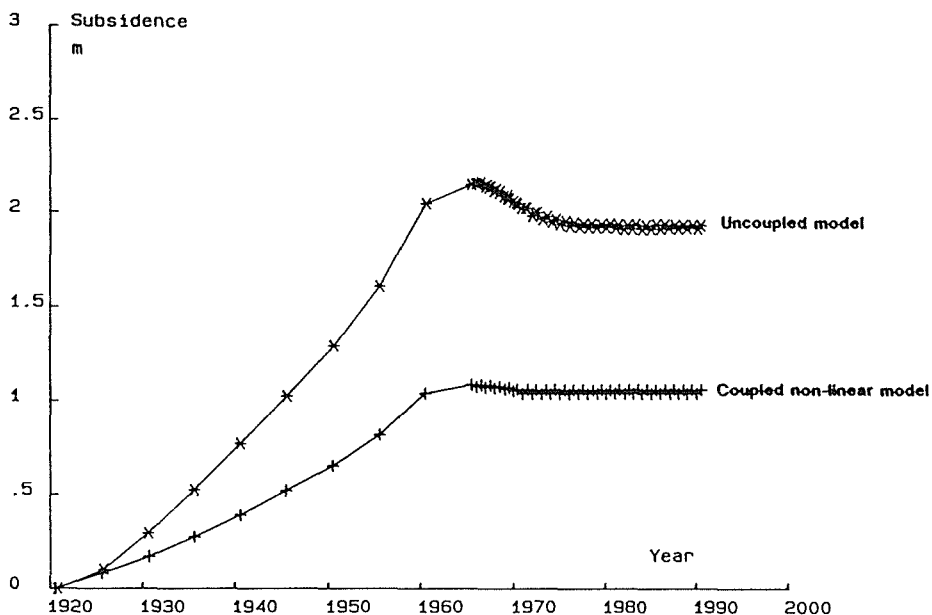


Fig. 6 Total computed subsidence since 1920 for one column of the case study of Shanghai; the computation neglecting the variation of K and S_v during the consolidation process leads to an overestimation of the subsidence of nearly 100% at this place (from Dassargues, 1991).

computed by the simulation with constant parameters will be systematically overestimated when compared to the subsidence calculated with varying parameters.

CONCLUSIONS AND EXAMPLE

For the case study of Shanghai, coupled and nonlinear models, taking into account the variation of the permeability and of the compressibility, have been applied. An example of results is given in Fig. 6 showing how inaccurate a model can be, when the variation of parameters in flow-compaction computations is neglected. For more details about this case history, see Dassargues *et al.* (1991) about the preparation of the hydrogeological and geotechnical data, and Dassargues & Li (1991) for a summary of the computational aspects. Moreover the Bulletin of the International Association of Engineering Geology (IAEG) has published recently a group of papers describing the whole study and the detailed data set used for the simulations: Dassargues & Zhang (1992), Schroeder *et al.* (1992), Dassargues *et al.* (1993a,b). Using the Finite Element Method (FEM), the computations are based on a detailed three dimensional flow model of the whole area. This flow model has been coupled to 32 nonlinear one dimensional flow-compaction models, located where accurate measured data were available (32 boreholes). Careful calibrations of both hydrogeological and geotechnical parameters have been made in the 32 detailed flow-compaction models. Then, future subsidence may be computed until the year 2000, with global pumping = 1.3 x recharge in the aquifers.

REFERENCES

- Barends, F. B. J. (1990) The role of pore water in geological and geotechnical engineering. *Proc. 6th IAEG Congress* (Rotterdam). Balkema.
- Biot, M. A. (1956) General solutions of the equations of elasticity and consolidation for a porous material. *J. Appl. Mech.*, Trans. ASME, **23**, 91-96.
- Dassargues, A. (1991) Paramétrisation et simulation des réservoirs souterrains: couplages et non linéarités. PhD Thesis, Faculty of Applied Sciences, *Collection des publications, no. 34, University of Liège*.
- Dassargues, A., Biver, P. & Monjoie, A. (1991) Geotechnical properties of the Quaternary sediments in Shanghai. *Engng Geol.* **31**, 71-90.
- Dassargues, A. & Li, X. L. (1991) Computing the land subsidence of Shanghai by finite element method. In: *Land Subsidence* (ed. by A. I. Johnson) (Proc. 4th Int. Symp. on Land Subsidence, Houston, May 1991), 613-624. IAHS Publ. no. 200.
- Dassargues, A. & Zhang, J. (1992) Land subsidence in Shanghai: hydrogeological conditions and subsidence measurements, *Bull. IAEG* **46**, 27-36, Paris.
- Dassargues, A., Schroeder, Ch. & Li, X. L. (1993a) Applying the Lagamine model to compute land subsidence in Shanghai, *Bull. IAEG* **47**, 13-26, Paris.
- Dassargues, A., Radu, J. P., Charlier, R., Li, X. L. & Li, Q. F. (1993b) Computed subsidence in the central area of Shanghai. *Bull. IAEG* **47**, 27-50, Paris.
- Delage, P. & Lefebvre, G. (1984) Study of the structure of a sensitive Champlain clay and of its evolution during consolidation. *Can. Geotech. J.* **21**, 21-35.
- Domenico, P. A. & Mifflin, M. D. (1965) Water from low-permeability sediments and land subsidence. *Wat. Resour. Res.* **1**(4), 563-576.
- Feldkamp, J. R. (1989) Numerical analysis of one-dimensional nonlinear large-strain consolidation by the Finite Element Method. *Transport in Porous Media* **4**, 239-257.
- Lambe, T. W. & Whitman, R. V. (1969) *Soil Mechanics*. John Wiley, New York.
- Nishida, Y. & Nakagawa, S. (1970) Water permeability and plastic index of soils. In: *Land Subsidence* (Proc. Tokyo Symp., 1969), 573-578. IAHS Publ. no. 89.
- Poland, J. F. (1984) *Guidebook to Studies of Land Subsidence Due to Groundwater Withdrawal*. Studies and Reports in Hydrology no. 40, UNESCO, Paris.
- Rieke, H. H. & Chilingarian, G. V. (1974) *Compaction of Argillaceous Sediments*. Elsevier, Amsterdam.
- Rudolph, D. L. & Frind, E. O. (1991) Hydraulic response of highly compressible aquitards during consolidation. *Wat. Resour. Res.* **27**(1), 17-30.
- Safai, N. M. & Pinder, G. F. (1980) Vertical and horizontal land deformation due to fluid withdrawal. *J. Numer. Anal. Meth. Geomech.* **4**, 131-142.
- Schroeder, Ch., Dassargues, A. & Li, X. L. (1992) Engineering geological conditions in the central area of Shanghai. *Bull. IAEG* **46**, 37-43, Paris.
- Terzaghi, K. (1943) *Theoretical Soil Mechanics*. Chapman and Hall, London.

Some direct and inverse problems in land subsidence theory

VESELINA DIMOVA

Department of Theoretical and Applied Mechanics, University of Mining and Geology, 1100 Sofia, Bulgaria

Abstract One of the effects of the underground human activities (geotechnological or civil engineering works) is the occurrence of land subsidence. The latter creates unfavourable conditions for the functioning of surface items (buildings, equipment, bands, etc.). In connection with this, the following two problems are considered and solved in this paper. (a) Direct problem – the mining system is given; determine the equation of the land subsidence. This problem is reduced to the Dirichlet problem for Fourier's equation. (b) Inverse problem – the equation of the mining subsidence is given, determine the underground operations from which the given subsidence is realized. This problem is of extreme importance in the cases when mining has to be done under built-up areas. In these cases the building standards dictate the land subsidence equation. This necessitates a more rigorous formulation of a new inverse problem in the land subsidence theory. The problem is reduced to an inverse Dirichlet problem for Fourier's equation. This is an incorrectly posed problem of mathematical physics in the sense of Hadamard. Its solution is obtained by Lions' quasi-inversion method. Some generalizations of the posed problems are discussed. The posing and solving of the unique inverse problem in the applied geosciences allows to speak about laying the foundations of a modern land protection geo-engineering field.

INTRODUCTION

One of the effects of underground mining or civil engineering works is the occurrence of land subsidence. In connection with this phenomenon the following two problems arise (Fig. 1):

- *Prediction problem* (direct problem) – given the subsidence of the immediate roof, i.e. the mining system, determine the mining subsidence equation.
- *Protection problem* (inverse problem) – given the equation of the mining subsidence, dictated by the building norms for protection of the surface items, determine the underground operations which guarantee the required subsidence appearance.

Data assignment in the direct and indirect problems

In the direct problem the subsidence of the immediate roof $w^o(x,0) = \varphi(x)$ (w^o = the vertical displacement of the rock mass points) is constructed either on the base of the

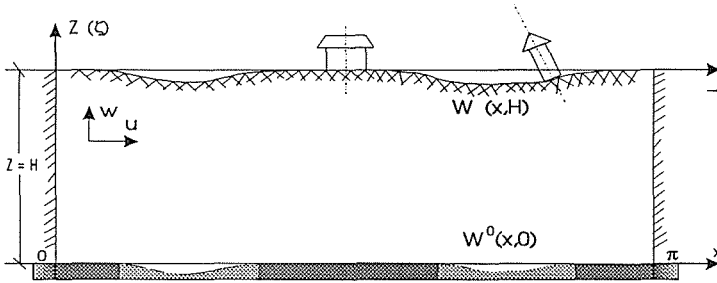


Fig. 1 An illustrative scheme.

observations results or by the following procedure: above the mined area it is accepted that $w^0 = m\eta$, where m is the thickness of the seam, η is a coefficient which depends on the mining method (e.g. for back filling method $\eta = 0.55 \pm 0.05$), and above the unmined area it is accepted that $w^0 = 0$. The experience shows that this formulation of the "initial" conditions does work (Dimova, 1990; Litwiniszyn, 1974).

In the inverse problem the equation of the desired subsidence, as we noted already is constructed on the basis of the building norms for the surface sites preservation ("from...to..."). Consequently this equation is approximately given. Let us immediately emphasize that even if the equation were given exactly, errors would still exist. The reason is in the use of computers in solving these problems. Errors occur as a result of using numerical methods and rounding errors. The most important conclusion which follows here is that the subsidence equation is given approximately.

PREDICTION PROBLEM

The rock mass that is not influenced by openings can be separated from the rock mass that is influenced. Thereby the answer to the direct problem posed in the previous item (for convenience the plane problem is considered), gives the solution, for an appropriate scale, to the Dirichlet problem for Fourier's equation (Fig. 1):

$$\zeta = \int_0^z B(\lambda) d\lambda, \quad \frac{\partial^2 w}{\partial x^2} = \frac{\partial w}{\partial \zeta}, \quad 0 \leq x \leq \pi, \quad 0 \leq \zeta \leq \zeta_H = \zeta_{z=H} \quad (1)$$

$$w^0(x,0) = \varphi(x), \quad 0 \leq x \leq \pi, \quad \zeta = 0 \quad (2)$$

$$w(0,\zeta) = w(\pi,\zeta) = 0, \quad 0 \leq \zeta \leq \zeta_H = \zeta_{z=H} \quad (3)$$

where $B = B(z)$ is a rock mass characteristic (Lattes & Lions, 1967; Dimova, 1990).

Problem (1)-(3) is correctly posed, because it satisfies all Hadamard's requirements (Tikhonov & Arsenin, 1977; Dimova, 1990b):

- existence of a solution,
- uniqueness of the solution,
- stability of the solution, i.e. small changes in the initial data should lead to small changes in the solution.

When solving the prediction problem we are not faced with any difficulties.

PROTECTION PROBLEM

When mining operations takes place under built-up areas, the problem, as we mentioned above, is inverse (Dimov & Dimova, 1994b; 1987; Dimova, 1990b): given the subsidence equation $w(x, \zeta_H) = \psi(x)$, determine the subsidence of the immediate roof (i.e. sequence of mining) $w(x, 0) = \varphi(x)$.

This problem can be formulated as follows:

$$\zeta = \int_0^z B(\lambda) d\lambda, \quad \frac{\partial^2 w}{\partial x^2} = \frac{\partial w}{\partial \zeta}, \quad 0 \leq x \leq \pi, \quad 0 \leq \zeta \leq \zeta_H \quad (4)$$

$$w(x, \zeta_H) = \psi(x), \quad 0 \leq x \leq \pi, \quad \zeta = \zeta_H \quad (5)$$

$$w(0, \zeta) = w(\pi, \zeta) = 0, \quad 0 \leq \zeta \leq \zeta_H \quad (6)$$

where the function $\psi = \psi(x)$ is initially given and the function searched is $w = w(x, 0)$.

Now we will prove that problem (4)-(6) is incorrect in Hadamard's sense and therefore requires a careful treatment.

Let us suppose that function $w(x, \zeta)$ is a solution to problem (4)-(6) and let us introduce function $w(x, 0) = \chi(x)$, $0 \leq x \leq \pi$. It is clear that function $w(x, \zeta)$ can be considered as a solution to Dirichlet's problem for equation (4) with boundary conditions:

$$w(x, 0) = \chi(x), \quad w(0, \zeta) = w(\pi, \zeta) = 0 \quad (7)$$

and consequently (Genchev, 1988) the function $\psi(x) = w(x, \zeta_H)$ proves to be limitless times differentiable. If this property is not available, problem (4)-(6) is unsolvable. It is not difficult to prove that this problem is incorrect even in the class of the infinitely smooth functions. In order to make sure that this is true, it is sufficient to add the following function to one solution of problem (4)-(6):

$$v_n(x, \zeta) = \frac{\epsilon}{n^k} \exp\{-n^2(\zeta - \zeta_H)\} \sin nx \quad (8)$$

which satisfies both equation (4) and conditions $v(0, \zeta) = v(\pi, \zeta) = 0$. Although we obviously have:

$$\left| \frac{\partial^v}{\partial x^v} v_n(x, \zeta_H) \right| \leq \epsilon \quad \text{for } v = 0, 1, \dots, k \quad (9)$$

the sequence $\{v_n(x, 0), n = 1, 2, \dots\}$ is not limited. In this way the statement is proved. This shows that we cannot "restore" the subsidence of the immediate roof (the initial conditions; the cause for the phenomenon) provided we know the earth's subsidence equation (the result). It follows directly from the fact that equation (4) describes also the phenomenon "heat conductivity" (Fourier), i.e. an irreversible process and is not invariant with respect to the change $\tau = -\zeta$. Generally speaking, John's problem for the heat conductivity equation with "back time" is an incorrect problem (in (4) ζ is a "timelike" variable) (John, 1955).

There are a number of methods for solving incorrect problems (Tikhonov & Arsenin, 1977; Dimova, 1990). Here we will discuss the method proposed by Lions (Lattes & Lions, 1967; Tikhonov & Arsenin, 1977; Dimova, 1990). According to this method, instead of a concrete incorrect problem, a correct one similar to the incorrect one (in the sense of defined measure for similarity π) is considered. Thus in place of equation (4), the enhanced equation is considered (Babenko, 1986):

$$\frac{\partial w}{\partial \zeta} = \frac{\partial^2 w}{\partial x^2} + \epsilon \frac{\partial^4 w}{\partial x^4}, \quad \epsilon > 0, \quad 0 \leq x \leq \pi, \quad 0 \leq \zeta \leq \zeta_H \quad (10)$$

with boundary and initial conditions:

$$w(x, \zeta_H) = \psi(x), \quad 0 \leq x \leq \pi, \quad \zeta = \zeta_H \quad (11)$$

$$w(0, \zeta) = \frac{\partial^2 w(0, \zeta)}{\partial x^2} = 0, \quad w(\pi, \zeta) = \frac{\partial^2 w(\pi, \zeta)}{\partial x^2} = 0 \quad (12)$$

Problem (10)-(12) is correctly posed and its solution has the form:

$$w(x, \zeta) = \sum_{k=1}^{+\infty} a_k \exp\{\lambda_k \zeta\} \sin kx \quad (13)$$

where $\lambda_k = -k^2 + \epsilon k^4$.

If $\psi(x) = \sum_{k=1}^{+\infty} a_k \sin kx$, then

$$w(x, \zeta) = \sum_{k=1}^{+\infty} a_k \exp\{\lambda_k(\zeta - \zeta_H)\} \sin kx \quad (14)$$

the function:

$$w(x, 0) = \sum_{k=1}^{+\infty} a_k \exp\{-\lambda_k \zeta_H\} \sin kx \quad (15)$$

is the sought approximate solution of the incorrect problem (4)-(6) (Babenko, 1986). If we now solve problem (1)-(3) with the "initial" data (15), we will obtain:

$$v(x, \zeta_H) = \sum_{k=1}^{+\infty} a_k \exp\{-\epsilon k^2 \zeta_H\} \sin kx \quad (16)$$

a function which can be considered as an element of some compact Y , similar to the initial function $\psi(x)$.

We propose that for a determined measure for similarity η , ϵ should be determined from the equation (Babenko, 1986):

$$\sum_{k=1}^{+\infty} a_k^2 (1 - \exp\{-\epsilon k^2 \zeta_H\})^2 = \pi^2 \sum_{k=1}^{+\infty} a_k^2 \quad (17)$$

We have applied Lions's method many times successfully. The results are encouraging.

SOME GENERALIZATIONS

Let us point out, that here we considered two basic problems in a bounded domain:

- prediction problem, also called direct problem,
- protection problem, also called inverse problem.

Now let us draw our attention to the following: If we are based on the integro-geometrical theory (influence function) for mining subsidence (Whittaker & Reddish, 1989), then the solution to the prediction problem, i.e. the problem for determining function $w(x, \zeta_H) = \psi(x)$ is reduced to the solution of the integral:

$$\int_a^b K(x - \zeta) \varphi(\zeta), \quad c < x < \pi \quad (18)$$

for a given function $\varphi(\zeta)$ and $K(x - \zeta)$ – influence function, which according to different authors (King, Bals, Knothe, etc.) and for different regions, takes different forms (Whittaker & Reddish, 1989); a and b are the boundaries of the mined-out area, c and d are the boundaries within which the solution is searched.

The protection problem consists in seeking a solution to Fredholm's integral equation of the first kind (18), i.e. for a given function $K(x - \zeta)$ and $\varphi(x)$, let us determine the function $w(x, 0) = \varphi(\zeta)$. This problem has an instable solution, hence it is incorrect in J. Hadamard's sense (Kolmogoroff & Fomin, 1981). When searching for the solution to equation (18), we apply Tikhonov's regularization method (Tikhonov & Arsenin, 1977; Lavrentiev *et al.*, 1980). We considered both the 3-D case, and the case with an inaccurately given kernel $K(x - \zeta)$ (Dimova, 1994b and Dimova & Dimov, 1994_a). Let us stress here that the kernel is constructed on the basis of the results from the survey measurements. This is what causes the errors in setting $K(x - \zeta)$.

If we consider the treated problems in the light of the functional analysis, we can say that the protection problem is reduced to seeking a solution to the operator equation:

$$A\varphi = \psi, \quad \varphi \in \Phi, \quad \psi \in \Psi \quad (19)$$

where Φ and Ψ are some functional spaces and A is a completely continuous linear operator (the operator is such in (18) (Kolmogoroff & Fomin, 1981; Lavrentiev *et al.*, 1980)) which acts from Φ to Ψ . It is known that this problem is incorrectly posed, because operator A^{-1} , inverse to operator A , exists and is not continuous (Lavrentiev *et al.*, 1980; Tikhonov & Arsenin, 1977; Dimova, 1995). It is also known that if spaces Φ and Ψ are properly selected, problem (19) can be transformed into a correctly posed problem (Lavrentiev *et al.*, 1980; Kalitkin, 1978). However this method is not constructive because of the inaccurate setting of the right part in (19) (Lavrentiev *et al.*, 1980; Kalitkin, 1978).

CONCLUSION

Finally let us summarize:

- The protection problem is incorrectly posed in Hadamard's sense and in solving it, special methods have to be used. The classical mathematical methods do not work here (Tikhonov & Arsenin, 1977; Lattes & Lions, 1967; Dimova, 1990).

The primitive "selection method", applied in mining practice, i.e. the inverse problem solved by numerous direct problems and comparing the result with the "desired" result, has a limited sphere of influence here. It can be applied only for the protection of one or two objects in the case of the plane problem. For more objects and the 3-D problem, the application of the "selection method" is impossible.

- In summary we should note that we were the first to formulate the original protection problem, to introduce the terms "inverse problem" and "protection problem" and to show the way of solving it in 1985 (Dimov & Dimova, 1985). Our claims have been confirmed by an independent source (Review Journal, 1988). The monograph (Dimova, 1990) devoted to the inverse problems in the mine subsidence theory is unique in the world mining literature and reflects our results until 1990. The new results obtained after 1990 are described in the other references given here (Dimov & Dimova, 1994a; Dimova & Dimov, 1994b; Dimova, 1994a,b, 1993). Our studies lay the foundations of the modern theory of protection of surface sites in mine areas.

Note: The theory presented here can be applied in studying subsidence arising from groundwater withdrawal, oil and gas field activities and underground coal gasification (see also (Whittaker & Reddish, 1989)). About some other applications of the subsidence theory see (Dimova, 1995).

REFERENCES

- Babenko, K. I. (1986) *Osnovy Chislennogo Analiza* (Numerical analysis foundations) (in Russian). Nauka, Moscow.
- Dimov, I. V. & Dimova, V. I. (1985) Nekorektni zadachi v geomehanikata (Incorrect problems in geomechanics) (in Bulgarian). *NIPRORUDA*, no. 4. Sofia, Bulgaria.
- Dimov, I. V. & Dimova, V. I. (1987) Some new problems in geomechanics. *C. R. Acad. bul. des Sci.* **40**(10). Sofia, Bulgaria.
- Dimov, I. V. & Dimova, V. I. (1994a) Some 2D inverse problems arising in strata mechanics. In: *World Mining Congress* (Proc. 16th World Mining Congr., September 1994, Sofia, Bulgaria), vol. 5.
- Dimov, I. V. & Dimova, V. I. (1994b) Some incorrect problems of mathematical physics arising in strata mechanics. In: *Zeszyty Nauk. Politech. Slanskej*, s. Gornictwo, **221** (Proc. 6th Int. Symp. on Mining at Great Depth, October 1994, Ustron-Zawodzie, Poland).
- Dimova, V. I. (1990a) *Some Direct and Inverse Problems in Applied Geomechanics*. Univ. of Mining and Geology Press, Sofia, Bulgaria.
- Dimova, V. I. (1990b) Influence of surface load on the equation of mining subsidence. In: *Proceedings Sixth International Congress International Association of Engineering Geology* (ed. by D. G. Price) (August 1990, Amsterdam, The Netherlands).
- Dimova, V. I. (1993) Subsidence as a modern theory of environmental protection. In: *Safety and Environmental Issues in Rock Engineering, EUROCK'93* (Proc. ISRM Int. Symp., June 1993, Lisbon, Portugal).
- Dimova, V. I. (1994a) Some incorrect problems in ground movement theory. In: *The impact of Mining on the Environment – Problems and Solution* (Proc. Int. Symp., January 1994, Nagpur, India).
- Dimova, V. I. (1994b) Numerical solution of the 3D basic inverse and incorrect problems in theory of Earth surface protection in mining areas. In: *Computer Methods and Advances in Geomechanics* (ed. by H. J. Siriwardane & M. M. Zaman) (Proc. Eighth Int. Conf. on Computer Methods and Advances in Geomechanics, May 1994, Morgantown, USA).
- Dimova, V. I. (1995) Some direct and inverse problems in folding theory. In: *Proc. Second Int. Conf. on Mechanics of Jointed and Faulted Rock* (April 1995, Vienna).
- Dimova, V. I. & Dimov, I. V. (1994a) Inverse problems of land subsidence due to longwall mining. In: *Proc. 1994 ISRM Int. Symp.* (May 1994, Santiago, Chile).
- Dimova, V. I. & Dimov, I. V. (1994b) Basic inverse problems in ground movement theory. In: *Proc. 7th Congr. of the Int. Assoc. of Engineering Geology* (September 1994, Lisbon, Portugal).
- Genchev, T. (1988) *Chastni Diferentsialni Uraveniya* (Partial differential equations) (in Bulgarian). Nauka i Izkustvo, Sofia, Bulgaria.

- John, F. (1955) Numerical solution of the equation of heat conduction for proceeding times. *Ann. Mat. Pure and Appl.* **40**.
- Kalitkin, N. N. (1978) *Chislennye Metody (Computational methods)* (in Russian). Nauka, Moscow.
- Kolmogoroff, A. N. & Fomin, S. V. (1981) *Elementy Teorii Funktsiy i Funktsionalnogo Analiza* (Elements of functional theory and functional analysis (in Russian). Nauka, Moscow.
- Lattes, R. & Lions, J. P. (1967) *Méthode de Quasi-Reversibilité et Applications*. Dunod, Paris.
- Lavrentiev, M. M., Romanov, V. G. & Sishanskiy, S. P. (1980) *Nekorrektnye Zadachi Matematicheskoy Fiziki i Analiza* (Incorrect problems of mathematical physics and analysis (in Russian). Nauka, Moscow.
- Litwinişzyn, J. (1974) *Stochastic Methods in Mechanics of Granular Bodies*. Springer-Verlag, Vienna.
- Referativnyy Zhurnal "Gornoe delo"* - referat 12B82 (*Review Journal of Mining, reference 12B82*) (in Russian) (1988) Moscow.
- Tikhonov, A. N. & Arsenin, V. Y. (1977) *Solution of Ill-Posed Problems*. V. H. Winston & Sons, Washington, DC, USA.
- Whittaker, B. N. & Reddish, D. J. (1989) *Subsidence*. Elsevier, Amsterdam-Oxford-New York-Tokyo.

Creep related subsidence caused by oil and gas extraction

GUDMUND EIKSUND, GEIR SVANØ

SINTEF Geotechnical Engineering, N-7034 Trondheim, Norway

NEAL B. NAGEL

Phillips Petroleum Company Norway, N-4056 Tananger, Norway

Abstract The paper presents results from a project in which the contribution from creep on compaction of the Ekofisk oil and gas reservoir is studied. Creep parameters are derived from long-term uniaxial strain tests on the formation rock for specific porosity classes. The accumulated thickness within each porosity class is used to establish a one-dimensional model of the reservoir. Laboratory tests with sea water injections (SWI) are used to model the effect of SWI on creep. The pore pressure depletion history for the reservoir in combination with arching effects, is used to estimate the effective stress history in the reservoir. The role of creep to date is addressed and future compaction predictions for different pore pressure scenarios are presented.

METHOD OF ANALYSIS

The Ekofisk reservoir consists of the Ekofisk formation overlaying the Tor formation with about 3 km of overburden rock. The thickness of the reservoir is about 300 m and its width varies from 5 to 8 km. The reservoir is under increasing effective stresses during most of the production period except during short periods with a high rate of sea water injection, in which the pore pressure actually may increase at some locations. For the purposes of this paper, the entire production life of the reservoir is modelled using a fully coupled stress-strain-time model. The primary objective is to identify the role of creep.

Conceptual creep model

The rheological behaviour of the Ekofisk Chalk has been interpreted within the framework of a stress-strain-time model for soils presented by Svanø *et al.* (1991). This model is based on fundamental concepts from Bjerrum (1967), Janbu (1969), Šuklje (1969, 1978) and Nowacki (1973). The model, which can handle vertical deformation under confined lateral conditions ("uniaxial strain"), is based on the assumption that the creep strain rate is a function of the total developed compaction strain and the effective stress:

$$\dot{\epsilon}_c = f(\sigma', \epsilon) \quad (1)$$

The creep strain rate is characterized by its inverse, the "Time resistance" R , where $R = 1/\dot{\epsilon}_c$.

A conceptual drawing is included in Fig. 1. The figure represents one load step in an incremental loading test, with a strain-time plot at constant load shown in the upper portion and a typical R - t plot shown in the lower portion. After a time t_0 , the time resistance plot may become linear, so that "time resistance" may be modelled by a linear function of time:

$$R = R_0 + r(t - t_0) \tag{2}$$

where R_0 is the initial time resistance, r is the "time resistance number", and t is time. The creep strain $\Delta\epsilon_c$ from $t = t_0$ to $t = t$ is found by integration:

$$\Delta\epsilon_c = \int_{t_0}^t \frac{1}{R} dt = \frac{1}{r} \ln \left[\frac{R_0 + r(t - t_0)}{R_0} \right] \tag{3}$$

Letting ϵ_0 represent the strain at $t = t_0$, and replacing the numerator within the brackets with R according to equation (2), it is easily verified that at the considered load step, the "Time resistance" R may be written as a function of strain as follows:

$$R = R_0 \exp[r\Delta\epsilon_c] = R_0 \exp[r(\epsilon - \epsilon_0)] \tag{4}$$

Here ϵ is the actual compaction strain at some point in time. With this formulation time is not an implicit part of the time resistance, which is a precondition to be able to model a creep process where the stress changes with time. In Fig. 2, the time resistance function in equation (4) is illustrated in a 3D σ' - ϵ - R plot for three subsequent load steps. Between these loadsteps, interpolations are made on the parameters r , R_0 and ϵ_0 , so that at any stress σ' , equation (4) can be applied directly. Hence, the creep strain rate at constant effective stress is given as a function of actual strain ϵ :

$$\dot{\epsilon}_c = \frac{1}{R} = \frac{1}{R_0} \exp[-r(\epsilon - \epsilon_0)] \tag{5}$$

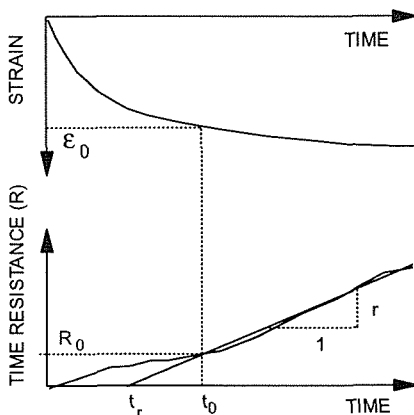


Fig. 1 Time resistance – principle drawing.

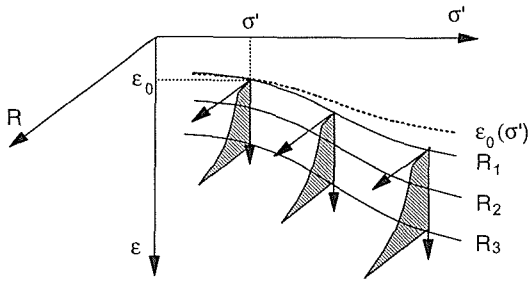


Fig. 2 Time resistance in "3D" plot and with "iso-time resistance" curves.

In general, ε_0 , R_0 and r are found to be functions of the effective stress σ' . The "Time resistance function" may then be written as:

$$R = R(\sigma', \varepsilon) = R_0(\sigma') \cdot \exp[r(\sigma')(\varepsilon - \varepsilon_0(\sigma'))] \quad (6)$$

For a given set of data, *iso-R* curves may be constructed in the σ' - ε space. These curves will connect points with equal "Time resistance" (R_1 , R_2 or R_3 in Fig. 2). All points on a given curve have the same R -value, and therefore the same creep strain rate. An increase in effective stress brings the sample to an "iso-R" curve with a lower time resistance (R). The creep strain rate will therefore increase due to the increased stress.

Creep test interpretations

Creep parameters were interpreted from a large number of incremental uniaxial strain tests performed by Phillips on a Chalk reservoir. In general, the axial stress was increased in steps of 3.45 MPa and each load step was maintained for about 24 h. At 27.6 and 41.4 MPa the load was maintained for up to several hundred hours, and the time resistance number (r) was always interpreted at these load levels. In some of the tests creep data were also obtained at 18.8 MPa.

The behaviour of the reservoir material was found to be strongly dependent on the initial porosity. We have grouped the material into porosity classes. A representative set of parameters was determined for each porosity class. In addition, the laboratory tests were used to determine the unloading/reloading stiffness modulus M_{RE} .

Most of the tests showed a steady increase in strains from zero effective stress. As the initial effective stress in the reservoir was about 14 MPa, we have chosen to interpret the strains at stresses lower than 14 MPa in the incremental loading tests as rebound strains. The strains developed after 24 h at the 14 MPa stress level were therefore subtracted from ε_0 - σ relations. The parameters are summarized in Table 1.

The complete computational scheme for one time step may be described as follows: At time t_{old} , the strain is ε_{old} and the effective vertical stress is σ'_{old} . During the time increment Δt , the effective stress change is $\Delta\sigma'$, and the new stress is $\sigma'_{new} = \sigma'_{old} + \Delta\sigma'$. The immediate change in strain is computed as $\Delta\varepsilon_{EL} = \Delta\sigma'/M_{RE}$. Before any creep is included at the new effective stress level, the strain is therefore $\varepsilon_{EL} = \varepsilon_{old} + \Delta\varepsilon_{EL}$. Values for $\varepsilon_{0,new}$, $R_{0,new}$ and r_{new} are then found for the new stress level σ'_{new} by interpolation in Table 1. The initial "Time resistance" R_i at the new effective stress may then be computed by inserting ε_{EL} into equation (4):

Table 1 Interpreted input for the creep model.

Porosity	Stress (MPa)	R_0 (year)	r	ε_0 (%)	M_{RE} (GPa)
$n > 42\%$	13.8	1.25	500	0	6
	27.6	0.61	157	3.9	
	41.4	0.84	106	7.9	
40%-42%	13.8	2.51	740	0	17
	27.6	1.0	161	1.7	
	41.4	0.8	154	4.2	
38%-40%	13.8	2.12	489	0	17
	27.6	1.88	329	1.6	
	41.4	1.46	187	3.8	
35%-38%	13.8	3.69	1100	0	35
	27.6	3.61	226	0.75	
	41.4	1.32	154	2.2	
30%-35%	13.8	3.69	1500	0	52
	27.6	3.61	600	0.4	
	41.4	1.32	300	1.2	
$n < 30\%$	13.8	3.69	2000	0	200
	27.6	3.61	1000	0.14	
	41.4	1.32	400	0.275	

$$R_i = R_{0,new} \exp[r_{new}(\varepsilon_{EL} - \varepsilon_{0,new})] \quad (7)$$

The creep strain developed over the time increment Δt is found from equation (3), replacing R_0 with R_i . The resulting total strain after the time increment will hence come out as follows:

$$\varepsilon = \varepsilon_{old} + \Delta \varepsilon_{EL} + \Delta \varepsilon_C = \varepsilon_{old} + \frac{\sigma'_{new} - \sigma'_{old}}{M_{RE}} + \frac{1}{r_{new}} \ln \left[\frac{R_i + r_{new} \Delta t}{R_i} \right] \quad (8)$$

Effect of sea water injection

The laboratory tests show that sea water injection (SWI) causes an increased creep rate in test specimens from the Ekofisk formation while test specimens from the Tor formation show little or no response. Consequently, the effect of SWI was interpreted as a reduction in the creep resistance $R(\sigma, \varepsilon)$ at the time of injection by a factor f_r ; $R_{SWI} = f_r \cdot R_I$. In order to model the SWI effect, a reference strain increment $\Delta \varepsilon_s$ corresponding to the reduction in time resistance is computed, so that after SWI, the following equation is used to compute the time resistance:

$$R = R_0(\sigma') \cdot \exp[r(\sigma')(\varepsilon - (\Delta \varepsilon_s + \varepsilon_0(\sigma')))] \quad (9)$$

For the upper Ekofisk formation $f_r = 0.5$ is chosen to represent typical behaviour. In the lower Ekofisk formation (layer EC and ED), sea water was injected both in 1991 and 1993, but at different locations. In order to "model" this distributed injection in the 1D-model, $f_r = 0.7$ is applied at two separate times in these layers.

RESERVOIR MODEL

A distribution of the porosity at the reservoir centre is shown in Table 2. The porosity distribution is determined from porosity-logs for a number of wells supplied by Phillips. Each layer is treated separately in order to model the effect of sea water injections and pore pressure depletion. A simulated pore pressure development for each layer in the reservoir from mid 1971 to 1994 is shown in Fig. 3. Layers EA and EB are, however, treated as one unit. A "corrected" column for layer ED is included to the right in the table. In this column, each porosity class has been shifted up one place, i.e. more material with high porosity is modelled. This was done for the following two reasons: (1) the observed strain in the reservoir was much higher than first modelled in layer ED; and (2) the two creep tests on material specifically from the ED layer were comparable with results from one porosity class higher as compared to the other layers. In the calculations, the "corrected" porosity distribution is used for the ED layer.

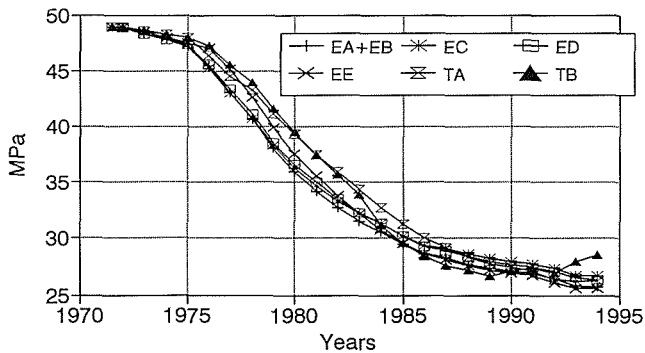


Fig. 3 Pore pressure histories for the different layers.

Table 2 Porosity distribution for detailed modelling of reservoir centre.

Porosity (%)	Equivalent thickness (m) for each porosity class						
	EA+EB	EC	ED	EE	TA	TB	ED corr
>42	0.48	1.63	11.24	0	0.85	0	20.33
40-42	5.61	2.51	9.09	0	3.15	0	2.66
38-40	11.52	3.77	2.66	0	4.57	0	10.08
35-38	11.2	5.95	10.08	0	27.83	0	13.26
30-35	21.71	9.25	13.26	3.33	22.24	5.8	1.11
<30	11.15	5.28	1.11	14.85	8.83	55.11	0
Thickness of layer (m)	40.49	28.39	47.44	18.19	67.46	60.91	47.44

FINITE ELEMENT ANALYSIS

Finite element modelling of the overburden was performed to study the arching effect. During compaction of the reservoir, the arching effect of the overburden causes a reduction in total vertical stress. Two sets of stiffness parameters were used for the overburden. The "high" stiffness values were interpreted directly from measured stress wave velocities in the overburden and are only valid at low shear mobilization of the material. The "low" stiffness values correspond to what we expect triaxial tests would give for the actual material. The analysis gave a compaction induced vertical stress reduction of 0.15 MPa m^{-1} reservoir compaction for the low stiffness or "Soft" overburden, and 0.87 MPa m^{-1} for high stiffness or "Stiff" overburden. The value for the "Stiff" overburden compares with a similar study reported by Boade *et al.* (1988). Their analysis gave about 1.17 MPa m^{-1} in compaction induced reduction of the total vertical stress. The finite element analysis also gave an estimate of the relation between reservoir compaction and seabed subsidence (C/S-ratio) of 1.65. The C/S-ratio is used to estimate the surface subsidence corresponding to a calculated reservoir compaction.

SUBSIDENCE AND COMPACTION SIMULATIONS

The total vertical stress (initially 63 MPa) used in the simulation is reduced during reservoir compaction according to the arching effects found in the FEM analysis. The effective stress for each layer is then found by subtracting the corresponding pore pressure history. In the simulation, a 1000-year initial time increment is applied at initial effective stress conditions in order to achieve a realistic initial condition, before simulation of pore pressure depletion is started. Figure 4 shows the calculated seabed subsidence for a C/S ratio of 1.65 for three different stress reduction histories due to arching; one case with a constant total vertical stress of 63 MPa, and two cases with the arching effect for low and high stiffness of the overburden. The analysis shows that the arching effect in the overburden has a clear influence on total reservoir compaction. As compared to the measured subsidence, the simulation also gives a too high subsidence rate before 1982 and too low later on. After 1985, the subsidence rate is only to a small

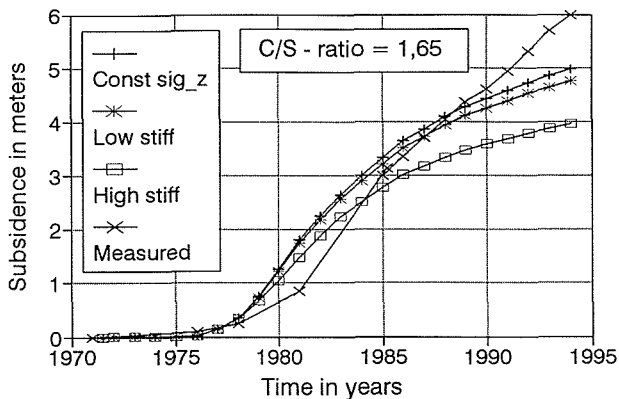


Fig. 4 Simulated seabed subsidence with three cases of overburden stiffness compared with measured subsidence.

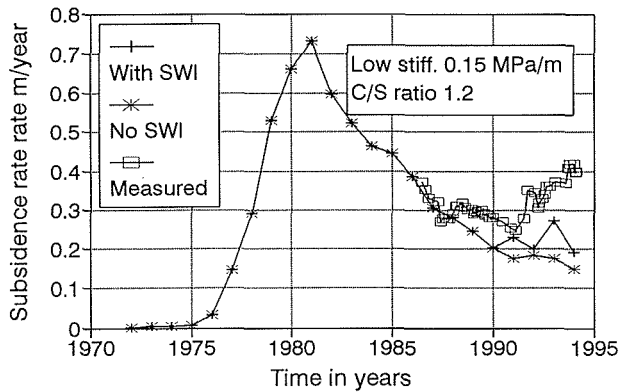


Fig. 5 Simulated subsidence rate including the effect of sea water injection.

degree influenced by the different overburden stiffness assumptions. However, a change from high to low stiffness during the simulated time period would give an increase in calculated compaction rate. Such a shift in stiffness could be related to a number of mechanisms, such as nonlinear stress-strain response in the overburden rock, or activation of old faults and slip planes.

The simulated effect of SWI on the subsidence rate is shown in Fig. 5. The arching effect due to low overburden stiffness and a C/S ratio of 1.2 is here assumed. When compared to actual field measurements, the simulation without modelling SWI-effect predicts far too low subsidence and compaction rates after 1985. A decreasing rate is calculated (Fig. 5), whereas the observed subsidence had a higher gradient at 1991-1993 (Fig. 4). The inclusion of the SWI-effect improves the model predictions as compared to the field observations, but the agreement between the two, however, is still poor.

The effect of creep on reservoir compaction is studied in the period from 1988 to 1994. The low overburden stiffness case is used as the basis for the analysis. The simulated reservoir compaction with creep is 1.33 m compared to 0.5 m without creep. This gives an average compaction of 0.22 m year^{-1} with creep and 0.08 m year^{-1} without creep in the period. From this a "creep contribution" of $0.22 - 0.08 = 0.14 \text{ m year}^{-1}$ can be estimated. The influence of creep is also studied by keeping the 1994 pore pressure constant for one year. In such a case, the reservoir would compact due to creep alone. This simulation gave a creep compaction of 0.15 m over one year.

Future reservoir compaction is calculated for the period from 1994 to 2011 for two different pore pressure scenarios not including SWI effects. Low stiffness in overburden is used as the basis for the analysis. In the first pore pressure scenario, constant pore pressure is assumed in the period, while in the second, the pore pressure is increased linearly from 1994 to 2011 by 5.52 MPa. The result of the analysis is shown in Fig. 6. The increase in pore pressure reduces the compaction developing in the 1994-2011 period by 0.89 m. Figure 7 shows the simulated stress-strain paths for the porosity class $n > 42\%$ in layer EA for the increased pore pressure scenario. *Iso-R* curves, or equal creep strain rate curves, are also shown on the figure. In the figure one can see that creep strains are predicted to develop also for the case of decreasing effective stress and increasing pore pressure.

The calculations generally overestimate the subsidence and compaction rate before 1983-1985, and underestimate the rate after. Other mechanisms contributing to the

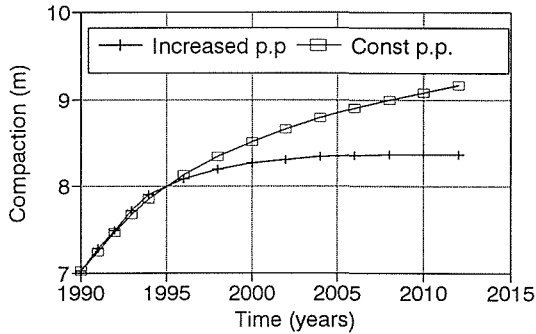


Fig. 6 Future compaction for two different pore pressure scenarios.

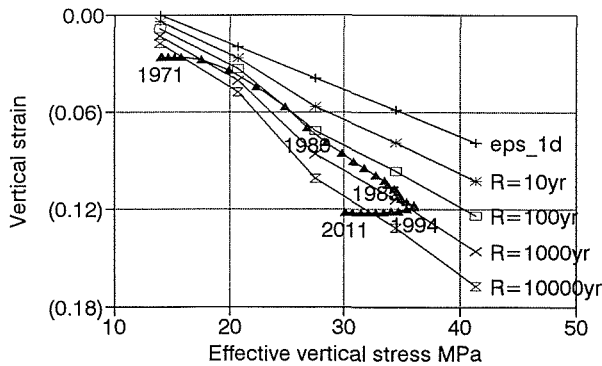


Fig. 7 Time resistance contours for porosity class $n > 42\%$ in layer EA. Increased pore pressure scenario.

discrepancy between observed and calculated subsidence may therefore be present. One such mechanism may be core sample disturbance, leading to overestimated strains at moderate stress increments, and therefore a too high stiffness at higher stresses. Furthermore, long term deformations in the overburden may reduce the C/S ratio, and shed more weight onto the reservoir. Both of these effects would lead to an increased calculated seabed subsidence, but only the latter to an increased reservoir compaction rate.

CONCLUSIONS

This paper demonstrates that a creep model originally developed for soft soils may be used to illustrate creep effects on the compaction of a Chalk reservoir during oil and gas extraction. It is also shown that the effect of sea water injection on compaction rate may be incorporated in the model. The calculations indicate that creep has contributed and still contributes to the reservoir compaction. However, the simulations show that creep effects alone can not explain the measured subsidence rate after 1985. Simulations of future subsidence show that the subsidence can be reduced by increasing the pore pressure in the reservoir, however, some creep strain will still develop even at reduced vertical effective stress.

Acknowledgement The authors wish to express thanks to Douglas Rhett, Phillips Petroleum Company for conducting the laboratory experiments which provided the laboratory data used in the paper and to Frode Ramstad, Phillips Petroleum Company Norway for collecting and collating all the laboratory and field data used in the paper. Further, the authors wish to express thanks to Phillips Petroleum Company Norway and its partners in the Ekofisk field including Fina Exploration Norway S.C.A, Norsk Agip A.S., Elf Petroleum Norge A.S, Norsk Hydro A.S, Den norske stats oljeselskap A.S, Total Norge A.S., Elf Rex Norge A.S. and Norminol A.S. for granting permission to publish this paper, and for supplying the tests results on the formation rock, background material, and pore pressure development from the reservoir model. The opinions expressed in the paper are those of the authors and do not necessarily represent those of the Phillips Norway Group.

REFERENCES

- Bjerrum, L. (1967) Engineering geology of Norwegian normally-consolidated marine clays as related to settlement of buildings (7th Rankine lecture). *Géotechnique* **18**, 81-118.
- Boade, R. R, Chin, L. Y. & Siemers, W. T. (1988) Forecasting of Ekofisk reservoir compaction and subsidence by numerical simulation. *OTC* 5622.
- Janbu, N. (1969) The resistance concept applied to the deformation of soils. *Proc 7th ICSFME* (Mexico City).
- Svanø, G., Christensen, S. & Nordal, S. (1991) A soil model for consolidation and creep. In: *Proc. 10th ECSFME* (Firenze), vol. 1, 269-272. Balkema, Rotterdam.
- Nowacki, F. (1973) Endimensjonal konsolidering med spennings- og tidsavhengige material egenskaper. Dr.ing thesis, NTH, Trondheim.
- Suklje, L. (1969) *Rheological Aspects of Soil Mechanics*. John Wiley & Sons Ltd.
- Suklje, L. (1978) Stresses and strains in non-linear viscous soils. *Int. J. Num. and Anal. Meth. in Geot. Engng* **2**, 129-158.

Analytical system assisting underground development with prediction and confinement of changes in the subterranean environment

TETSURO ESAKI, GUOYUN ZHOU

Kyushu University, Institute of Environmental Systems, Hakozaki 6-10-1, Higashiku, Fukuoka 812-81, Japan

KOICHI SHIKATA

Kyushu Tokai University, Department of Civil Engineering, Kumamoto 862, Japan

Abstract In the designing of rational development projects, it is very important to predict and confine changes in the subterranean environment due to underground development, such as groundwater pumping, natural gas extraction and coal mining. This paper at first discusses the factors which should be considered in analytical systems for evaluating subterranean environmental problems. It is concluded that the system must consider the following: (a) three-dimensional propagation of ground movement, (b) progress of the development, (c) time delay effect, (d) the modification of the model by field data and (e) coupling phenomena such as groundwater flow-subsidence coupling. Then, two sorts of analytical assisting systems applied to two case studies are presented: a natural gas field and a groundwater pumping site. The two systems were established by creative analytical methods which include the necessary factors mentioned above. These systems give useful information on future conditions and have contributed to some development projects without environment hindrance over a long time.

INTRODUCTION

In the recent years, underground development, defined not only as underground natural resource development, but also as underground space development, has attracted considerable attention in Japan. With underground development, a series of environmental problems might be expected, for example, land subsidence, cave-in of cavities and sea-water intrusion. Special consideration must be taken for the solution of the problems since the problems are linked not only with the damage in surface affairs, but also with various aspects of the society. In this paper, the general characteristics of problems and corresponding analytical system will be discussed from an environmental view of point and two practical analytical systems assisting underground development are introduced.

ANALYTICAL SYSTEM ASSISTING UNDERGROUND DEVELOPMENT

Environmental problems due to underground development, especially underground natural resource development, such as coal mining, oil and gas extraction, groundwater

pumping, are mainly appearing as land subsidence. Land subsidence due to natural gas and groundwater extraction has occurred in many places in Japan, and much researches on the problem has been made in different places. A comprehensive survey of the research and data by Esaki (1987, 1991) and Zhou (1986), concluded that land subsidence should be treated as an environmental system. The effect of land subsidence is complicated, not only limited in the change of land elevation, it should comprise a prediction and control system, social factor, economical factor, policy-making in order to reach a better harmony between development and environment.

In general, an analytical system assisting underground development should consider the following factors:

- *Three-dimensional propagation of the movement*: For a long time many studies on land subsidence have been done at different water withdrawal sites, and evaluating aquifer system deformation at the sites was the objective of most of the studies. However land subsidence will occur as a result of three-dimensional propagation of the aquifer system deformation at depth, characterized by an influence factor within a limit angle. It is necessary to consider multidimensional propagation of the movement.
- *Progress of the development*: Land subsidence is decided by underground development with different stages. The past development history, future plan and intensity in the stages should be considered in the analytical system.
- *The modification of the model by field measurements*: Special attention should be paid to this factor. In the case of land subsidence, the mechanism of subsidence is not so simple so that it can be represented by an ideal model, and in the geological structure and parameter determination there are some unavoidable unknown quantities, therefore feedback (back analysis) is an important step in model modification. In fact, modification by field data is served as a field scale in situ experiment.
- *The effect of time delay*: On account of propagation of the deformation the dissipation of pore water pressure, land subsidence shows a certain time lag compared with the fluctuation of water level. On the other hand, the groundwater level will also show a certain time delay compared with groundwater pumping. This factor also should be included in the analysis.
- *Coupling phenomena*: To clarify the interrelationship between each element in the system, coupling phenomena should be also considered. Coupling has a multiple meaning, for example, groundwater flow-subsidence coupling, subsidence-economical loss evaluation coupling and subsidence-economy-policy-making coupling.

It is natural that based on the local characteristics of land subsidence, some factors mentioned above will be emphasized, and some can be neglected.

ANALYTICAL SYSTEM 1: LAND SUBSIDENCE IN NATURAL GAS FIELD

The Miyazaki gas field is located in southern Japan as shown in Fig. 1(a). The groundwater containing water-soluble natural gas is extracted from two aquifer systems at depth from 300 to 600 m and from 1100 to 1500 m respectively (Fig. 1(b)). At present 47 wells are in operation at intervals of about 500 m in an area of 40 km² and

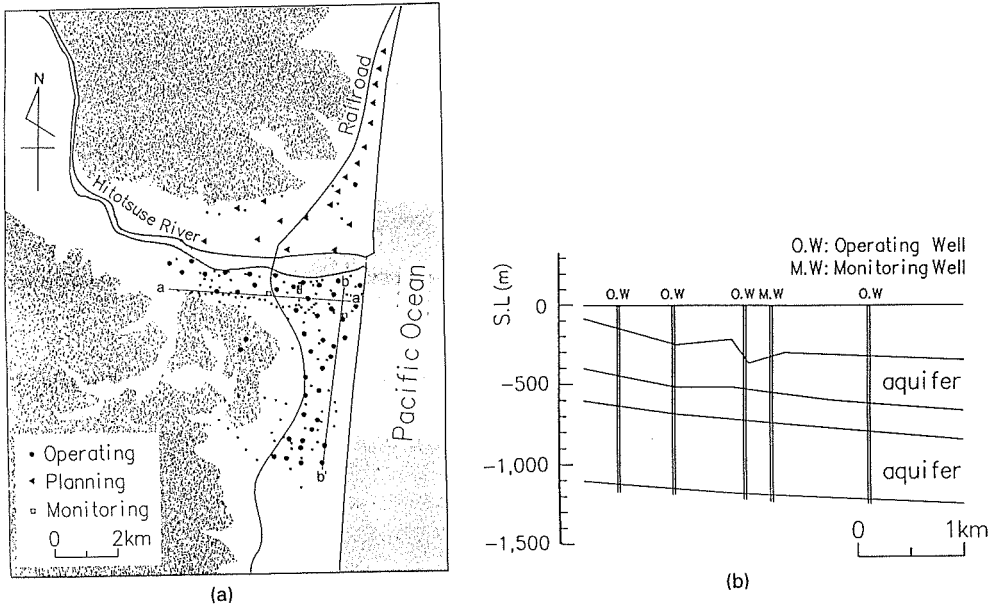


Fig. 1 Plain view and geological cross-section (section a-a') of the natural gas field.

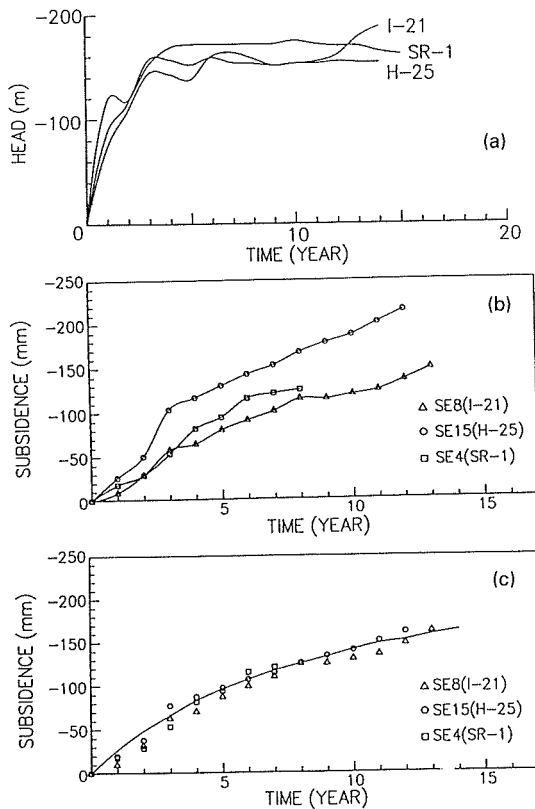


Fig. 2 Time factor with a mechanical model.

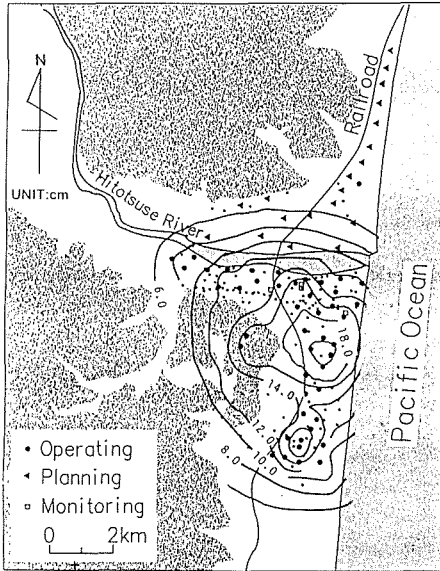


Fig. 3 Contour map of calculated land subsidence in 1990.

20 wells will be developed in the northern area in the next decade. Land subsidence has occurred since 1975 and has been researched by the authors of this paper as members of a local subsidence prevention technical committee. The two aquifers are confined beds and have no natural recharge. The physical properties of aquitards indicate that the aquitards are overconsolidated soil with low compressibility and subsidence in this field is attributed to the deformation of the two aquifers and the propagation of the deformation three-dimensionally with time. A coupling analytical system towards land subsidence control is established and is mainly composed of a underground water unsteady flow FEM model and a land subsidence prediction model. The analytical system has following characteristics:

- Though most analytical methods to predict land subsidence are based on the Terzaghi's consolidation theory which is suitable for relatively shallow and/or unconsolidated strata such as soft clay, our method is based on the generalized Hook's law because elastic behaviour dominates the relatively deep and/or compact strata(aquifers) in this gas field.

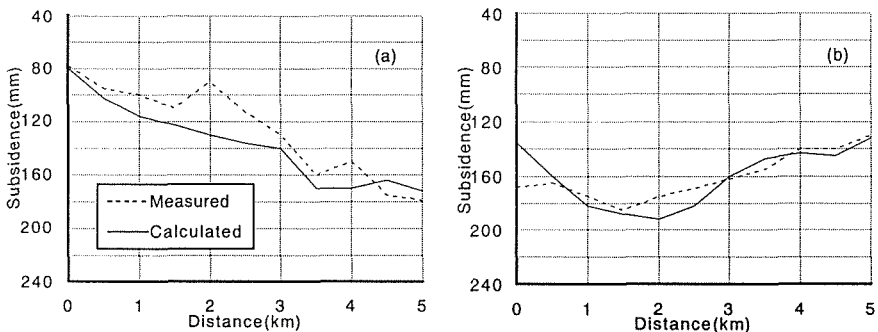


Fig. 4 Profiles of land subsidence corresponding to section a-a' and b-b' in Fig. 1.

- In this area land subsidence is not proportional to the decline of water level. As shown in Fig. 2(a) and Fig. 2(b), subsidence continues to increase over a long period, while the changes in water level were small except for the initial steep loss. This is because the seam deformation at a depth propagates three-dimensionally with a time lag. The subsidence with time delay phenomena in the area is simulated by the influence function method where the Voight model has been used to deal with the time delay. The influence function method is a quasi-three-dimensional method that can obtain displacement at a large number of points and distribution of subsidence both accurately and efficiently (Esaki *et al.*, 1987). The time delay factor is determined according to the local variation of geological formation as shown in Fig. 2(c).

By using the analytical system a series of subsidence calculation contour maps have been obtained. Figure 3 gives a subsidence calculation contour map, and along the two profiles corresponding to a-a' and b-b' in Fig. 1 the calculated subsidence and observed subsidence are shown in Fig. 4(a) and Fig. 4(b). The shape of the two curves is close. During the 19 years the model and parameters have been modified several times by the latest field data. Based on the calculation results and predictions, many suggestions have been put forward to the technical committee. Up to now, the subsidence in the field has been restricted within 30 mm year^{-1} and the decline in water level has also been limited within S.L. – 200 m. The analytical system mentioned above will also be useful for the development of the northern part of the field.

ANALYTICAL SYSTEM 2: LAND SUBSIDENCE IN SAGA AREA, JAPAN

Saga plain, located in the southwest Japan islands, has almost 35 year's history of land subsidence. The land elevation of almost the whole area is under high tide position classified as lowlands. At present land subsidence has decreased in Saga city area, but in the southwest part of Saga plain, land subsidence is still serious with average subsidence of $3050 \text{ mm year}^{-1}$ and subsidence area covers 250 km^2 . In 1994 because of a severe lack of precipitation, large amounts of groundwater were pumped and the maximum land subsidence reached 200 mm. The Japanese Government has been greatly concerned by this land subsidence and a special committee has been established to organize research and make policy.

Saga area is underlain by continually distributed sediments with average thickness of 200 m, which can be divided into two layers:

- The saturated soil layer (aquitard), which has a high water content and high compressibility with thickness from 10 to 25 m.
- Sand predominant layer (confined bed) with thickness from 180 to 220 m. In this area the subsidence is mainly caused by the soil consolidation (aquitard) and residual deformation of the sand predominant layer (aquifer).

The established analytical system is composed of two parts:

- groundwater flow simulation FEM model with back analysis function (parameter optimization);
- land subsidence prediction model with feed back function and parameter optimization function.

Groundwater simulation is based on the well-known unsteady flow differential equation which has been solved by the FEM technique.

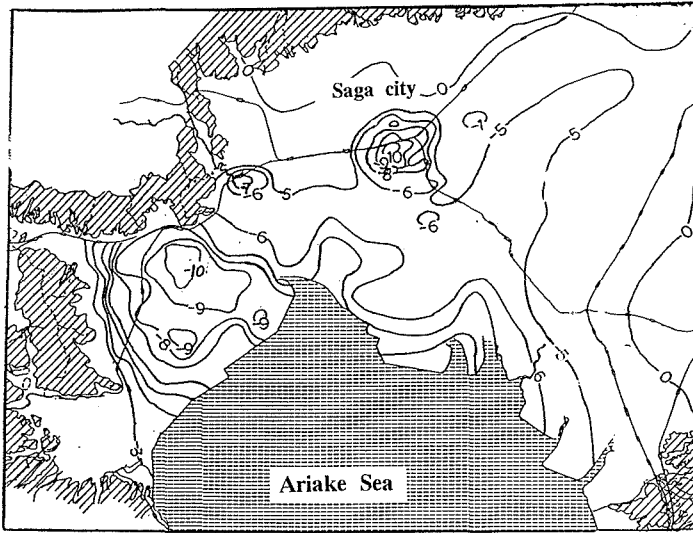


Fig. 5 Observation water level contour map in September 1979 (unit: m).

The research area is about 750 km² and has been divided into 923 pumping elements each with an area of 1 km², and four parameter sub-zones (transmissibility and storativity). The optimization method (Powell method) is employed to conduct model modification. 13 year's water level has been simulated successfully. Figures 5 and 6 show the calculated and observed water levels as an example. A satisfactory agreement between the two maps can be seen.

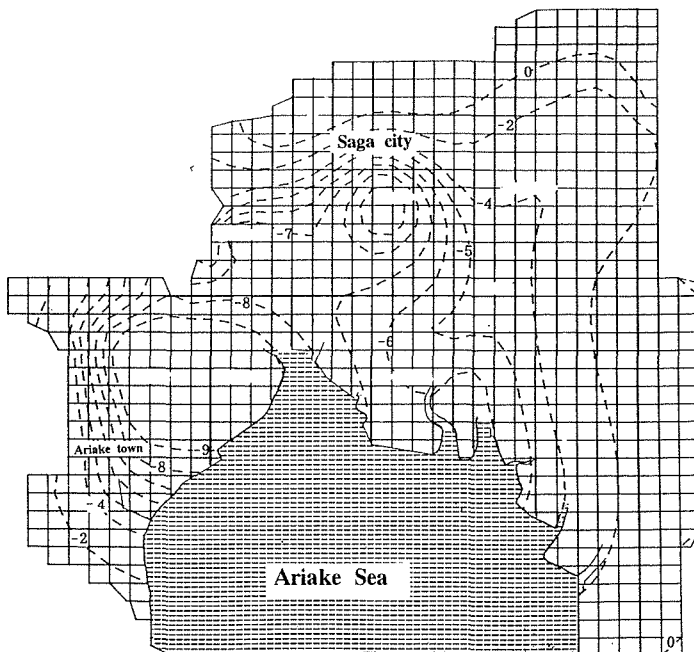


Fig. 6 Calculation water level contour map in September 1979 (unit: m).

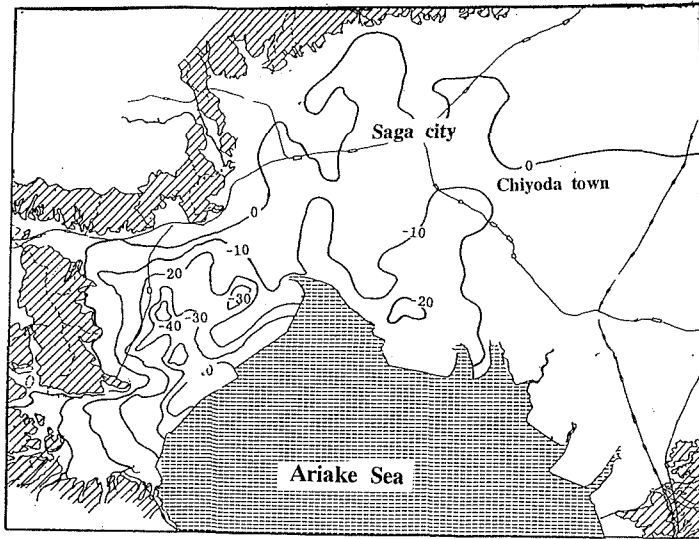


Fig. 7 Accumulative land subsidence (observed) in Saga area in 1992 (unit: cm).

The land subsidence calculation model is based on the Terzaghi's one-dimensional consolidation theory, while the deformation of the aquifer is calculated by elastic theory. By using the Laplace transform and residue theorem Terzaghi's one-dimensional consolidation partial differential equation can be solved and the time-dependent

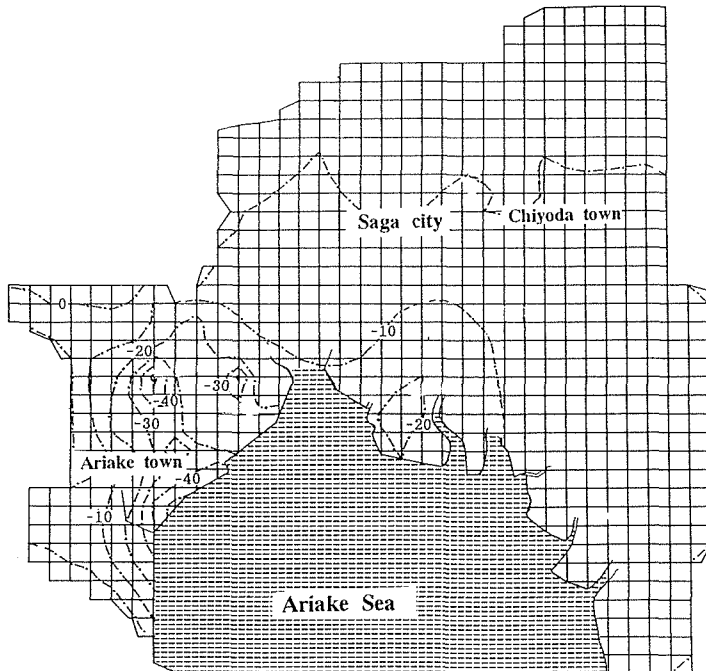


Fig. 8 Accumulative land subsidence(calculated) in Saga area in 1992 (unit: cm).

subsidence can be expressed as follows:

$$S(t) = \frac{4K}{H} \Delta h \sum_{n=1}^{\infty} \frac{1}{N} (1 - \exp(-Nt)) \quad (1)$$

where: $N = C_v(2n + 1)^2 \pi^2 / H^2$, $S(t)$ is time-dependent subsidence (cm), t is time (days), K is permeability of aquitard (cm day^{-1}), C_v the soil consolidation coefficient ($\text{cm}^2 \text{day}^{-1}$), H is thickness of aquitard (m), Δh the groundwater level fluctuation (m).

The parameters K and C_v (compression period) and K_{vs} C_{vs} (expansion period) are determined based on back analysing the observed time-dependent subsidence. As the final results: $K = 0.0064 \text{ cm day}^{-1}$; $C_v = 86 \text{ cm}^2 \text{day}^{-1}$ and $K/K_{vs} = 1.15$, $C_v/C_{vs} = 1.25$, E (Young's modulus for the aquifer) = 6100 kg cm^{-2} ; E/E_{vs} (E_{vs} : expansion period) = 0.65. The monitoring data can be input to the model periodically and the latest modification of the parameters can be made automatically. Based on the simulation results of groundwater level and using the subsidence model the land subsidence in the whole area has been calculated. Figures 7 and 8 give the comparison of the calculated and the observed subsidence. The results appears to be satisfactory. The prediction is made based on the future pumping scenarios determined by local government. Some suggestions on the optimal pumping scenarios according to the calculation results have been proposed to the local government. The above analytical systems have become a useful tool used for land subsidence control in the Saga area.

CONCLUSION

From the overall discussion on analytical systems assisting underground development and two specific system applications, the following main conclusions can be drawn:

- An analytical system towards the land subsidence control should comprises some indispensable factors discussed in the paper.
- Coupling technique and feedback are very important procedures in the practice of land subsidence modelling in order to make the analytical system become reliable and practical.
- The analytical systems established by the authors enable the prediction of land subsidence with high accuracy in each area, and, thus they have become a powerful tool in policy-making for local government.

REFERENCES

- Esaki, T. (1986) Theory and practice in predicting subsidence. Chapter 5.1 in: *Course Notes for Group Training Course in Coal Science and Technology*, 1-40. Kyushu University, Japan.
- Esaki, T. et al. (1987) Subsidence analysis for complex irregular tabular extraction by use of personal computer. *Proc. 7th Japan Symp. on Rock Mechanics*, 413-418.
- Esaki, T. et al. (1991) Environmental systems for subsidence engineering. In: *Land Subsidence* (ed. by A. I. Johnson) (Proc. Fourth Int. Symp. on Land Subsidence, Houston, May 1991), 163-172. IAHS Publ. no. 200.
- Zhou, G. Y. (1986) Mathematical model and prediction of land subsidence by optimization method in Ningbo city, China. Master thesis, China University of Geosciences.

A computing model based on cyclic consolidation tests

GU XIAO-YUN, XU DA-NENG & DENG WEI

Institute of Mechanics, Chinese Academy of Sciences, Beijing 100080, China

Abstract The primary and secondary consolidation tests under cyclic loading are carried out to simulate the yearly periodical fluctuation of groundwater levels in Shanghai. The computing model is verified by the experimental data, and the soil parameters are obtained. The computation by using finite differential method is conducted, and the results prove the validity of the model.

NOTATION

B	empirical constant
c_v	average coefficient of consolidation
c_{vc}	coefficient of consolidation during loading
c_{vs}	coefficient of consolidation during unloading
c_α	secondary consolidation coefficient
e	void ratio
e_0	initial void ratio
e_1	void ratio at P_o
H	thickness of soil layer
k	coefficient of permeability
m_{vc}	coefficient of volume compression
m_{vs}	coefficient of volume rebound
N	number of cycles
OCR	overconsolidation ratio
P'	effective stress
P_c	preconsolidation pressure
P_o	overburden pressure
ΔP	increment of cyclic loading
S	soil deformation
S_c	accumulated deformation
S_α	secondary deformation
t	time
u	excess pore pressure
z	depth
α	empirical constant
γ_w	unit weight of water

INTRODUCTION

Land subsidence due to pumpage of groundwater in Shanghai is already a well-known

phenomenon. In spite of the acceptance of computation method based on primary consolidation (Gu *et al.*, 1991), some divergency between the computation results and measured data has appeared in 1980s and continuously minor subsidence has been obtained, especially in the third engineering geological zone described in Gu *et al.* (1990), e.g. at Bus Station No. 2, where the rheological property of the compressible layers is obvious. Therefore, the effect of secondary consolidation on the land subsidence must be taken into account. Two categories of computing models considering rheological properties do exist. One are models consisting of different kinds of rheological elements, the other are models considering primary and secondary consolidation. For the former one, it is often difficult to determine the parameters of the rheological elements. The authors prefer the latter one, and this is the reason to conduct the experimental study.

Since the groundwater level change, which causes land subsidence in Shanghai, has the character of yearly periodical fluctuation (see Fig. 1), the consolidation tests observing both primary and secondary consolidation under cyclic loading are carried out. The test results provide the basis for the computing model and the soil parameters for computation. The validity of the model is proved by the computation.

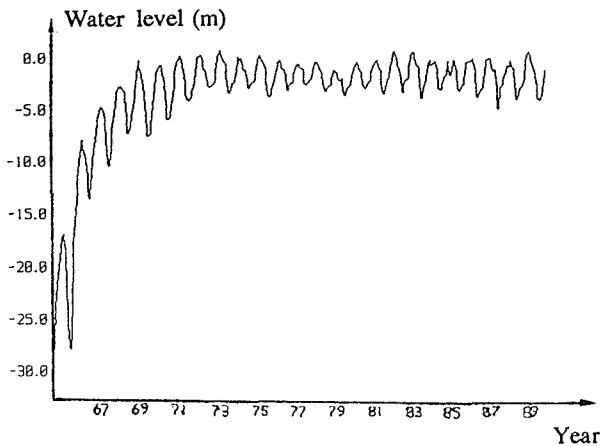


Fig. 1 Water level change curve.

ACTUAL STRESS CONDITION

From the curve of water level change (Fig. 1) the stress-strain diagram (Fig. 2) can be drawn. The drawdown of the boundary water level till 1965 produces the effective stress P_c . During the lowest water level soil deformation is AB. From 1965 to 1970 the groundwater level rose due to recharging, the stress-strain change can be described by BC. Since 1970 the yearly periodical fluctuation with basically unchangeable central line causes cyclic loading with increment ΔP . N cycles of loading lead to deformation CD. Consequently, the secondary consolidation under P_o will be DE.

From Fig. 2 it can be seen that:

- (a) Before 1970 the drawdown or uprising of water level is significant in comparison with the fluctuation.

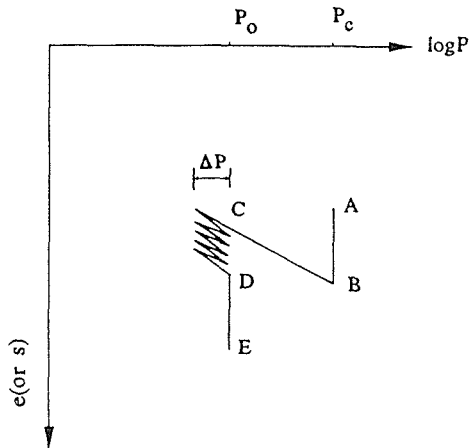


Fig. 2 Stress-strain diagram.

- (b) After 1970 the cyclic loading is dominant. The loading direction appears like unloading-loading rather than loading-unloading.
- (c) Due to recharging, the compressible soil layer, especially the second compressible layer which locates close to the aquifer, is in the overconsolidated state.
- (d) The relationship between secondary consolidation and the accumulated deformation caused by cyclic loading should be found.

TESTING

Because the assumption of one-dimensional seepage and deformation in the compressible layer is reasonable (Tsien & Gu, 1981), oedometers are used. The period of cyclic loading is determined by the equivalent time factor, e.g. from 1 minute to 4 minutes, depending on the thickness of the soil layer. After the preceding tests showing the agreement between the results of sinusoidal and rectangular loading patterns (Gu & Xu, 1994), the rectangular loading pattern is applied. The factors such as order of loading and unloading, effect of consolidation state, as well as relationships between accumulated deformation and secondary consolidation are studied in the experiments. In order to clarify whether the primary and secondary consolidation take place simultaneously or separately, the pore pressure is measured. All the tests are conducted under constant temperature.

Figures 3 and 4 show typical S-N curves. From the test data m_{vc} and m_{vs} are obtained. m_{vs} can be considered as a constant value. For loading-unloading condition,

$$m_{vc} = B[N^\alpha - (N-1)^\alpha] + m_{vs} \quad \text{as } N \leq 10 \quad (1)$$

As $N > 10$, m_{vc} are different constants at different intervals of N . For unloading-loading condition, m_{vc} can be expressed by several constants in dependence of N .

Figures 5 and 6 are the whole consolidation curves, including the static loading stage, cyclic loading stage and pure secondary consolidation stage, for the unloading-loading and loading-unloading conditions respectively. From Fig. 5, c_α does not change

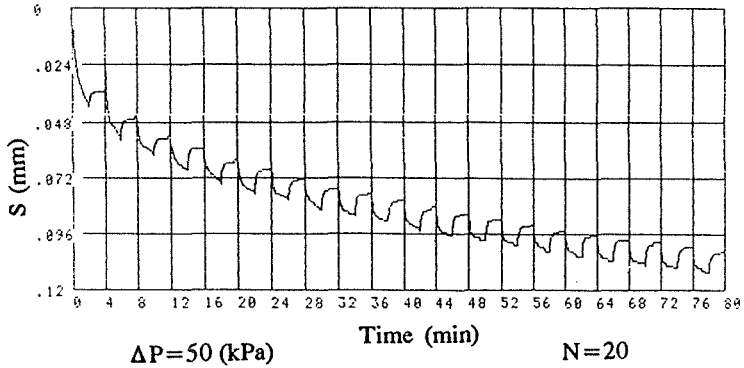


Fig. 3 S - N curve for loading-unloading condition.

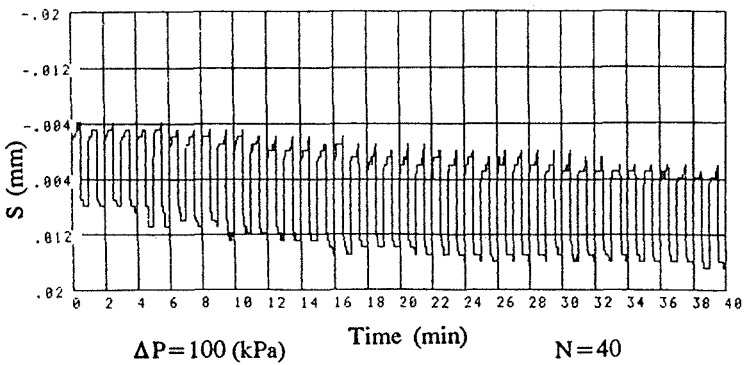


Fig. 4 S - N curve for unloading-loading condition.

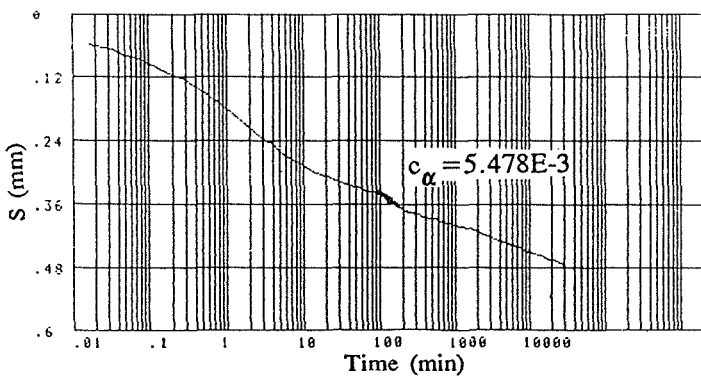


Fig. 5 Whole consolidation curve for unloading-loading condition.

basically before and after the cyclic loading. For loading-unloading condition, c_{α} after cyclic loading could be less than that before cyclic loading. The decreasing extent of c_{α} depends on the amount of S_c . The above results together with some other round the clock tests (Gu & Xu, 1994) show S_c and S_{α} are mutual compensated, and also verify the superposition theorem between S_c and S_{α} .

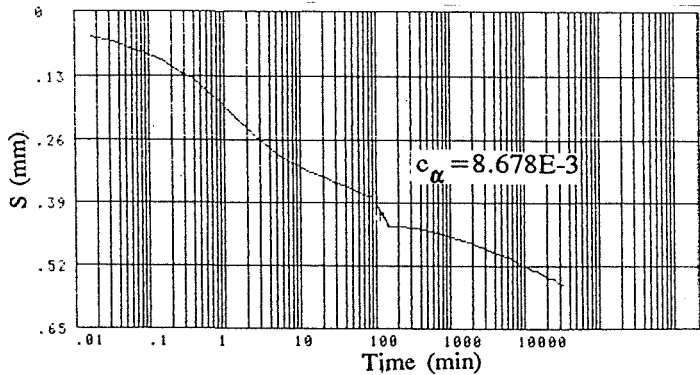


Fig. 6 Whole consolidation curve for loading-unloading condition.

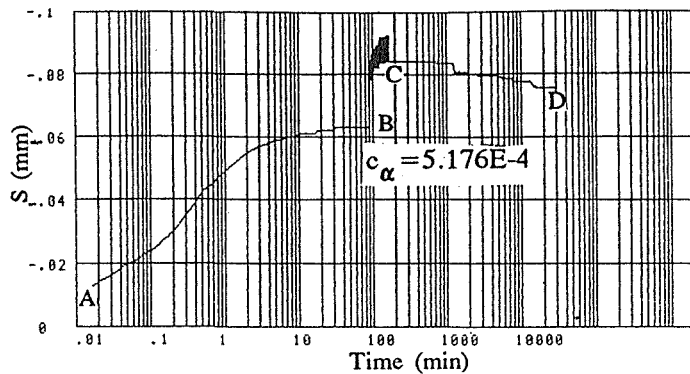


Fig. 7 Whole consolidation curve for overconsolidated sample.

The whole consolidation curve for overconsolidated sample is shown in Fig. 7. The cyclic loading can cause some rebound, and c_α becomes smaller. Table 1 shows c_α for different OCR.

Figures 8 and 9 present the relationships between pore pressure and soil deformation under static and cyclic loading respectively. The straight line in Fig. 8 indicates the one-to-one correspondence during the primary consolidation. The divergent part implies the development of secondary consolidation at the later stage of primary consolidation. Figure 9 has the same law as Fig. 8.

Table 1 Secondary consolidation coefficients for different OCR.

Sample no.	OCR	$c_\alpha (\times 10^{-3})$
Q22	2.0	0.5
	1.0	5.1
W31	1.5	1.3
	1.0	4.2

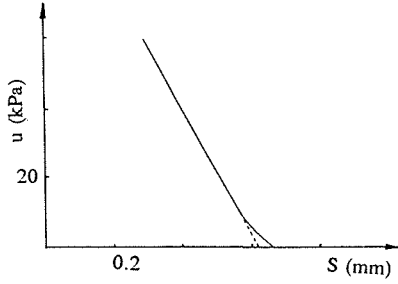


Fig. 8 *S-u* relationship for static loading.

COMPUTING MODEL AND SOIL PARAMETERS

Figures 8 and 9 verify that creep has taken place in the course of the dissipation of excess pore pressure. Thus the void ratio change should include the change caused by the effective stress change and the change with constant effective stress. The equation is expressed as follows:

$$\frac{\partial e}{\partial t} = \frac{\partial e}{\partial P'} \frac{\partial P'}{\partial t} + \left[\frac{\partial e}{\partial t} \right]_c \tag{2}$$

where $\partial e/\partial P'$ is compressibility, and $(\partial e/\partial t)_c$ creep rate. This is just Bjerrum's concept about instant and delay compression (Bjerrum, 1967).

Then the equations governing the consolidation of a saturated clay undergoing one-dimensional compression and drainage are:

$$\left\{ \begin{aligned} \frac{\partial e}{\partial t} &= \frac{k(1+e_0)}{\gamma_w} \frac{\partial^2 u}{\partial z^2} \\ \frac{\partial P'}{\partial t} &= \frac{\partial u}{\partial t} \\ \frac{\partial e}{\partial t} &= \frac{\partial e}{\partial P'} \frac{\partial P'}{\partial t} + \left[\frac{\partial e}{\partial t} \right]_c \end{aligned} \right. \tag{3}$$

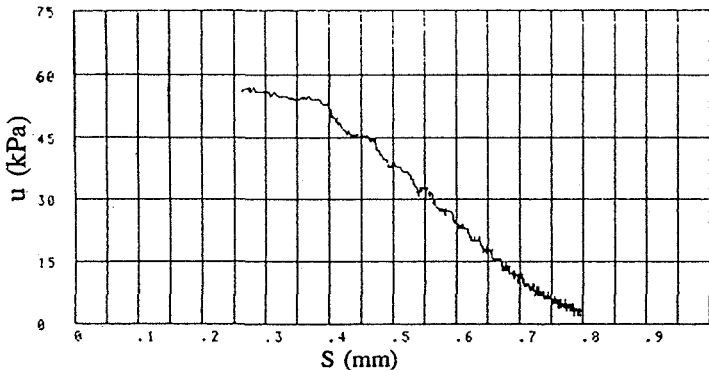


Fig. 9 *S-u* relationship for cyclic loading.

Nevertheless, Bjerrum did not consider the cyclic loading. In our case, the validity of superposition theorem implies the accumulated and secondary deformation are uncoupled. Similarity of c_α before and after cyclic loading indicates the cyclic loading does not further disturb the soil structure, thus S_c and S_α are mutual compensated. Therefore, Bjerrum's concept can still be used.

Referring to Garlanger (1972), $\partial e/\partial P'$ and $\partial e/\partial t$ are determined by the equations:

$$\left\{ \begin{array}{l} -\frac{\partial e}{\partial P'} = \frac{ae}{P'} \quad (P_o \leq P \leq P_c) \\ -\frac{\partial e}{\partial P'} = \frac{be}{P'} \quad (P' > P_c) \\ -\left[\frac{\partial e}{\partial t}\right]_c = \frac{ce}{t_1} \left[\frac{e}{e_c}\right]^{1/c} \left[\frac{P'}{P_c}\right]^{b/c} \end{array} \right. \quad (4)$$

where: $e_c = e_0(P'/P_c)^{-a}$, $a = m_{vs}(1 + e_0)P'/e_1$, $b = m_{vc}(1 + e_0)P'/e_1$, $c = 0.434c_\alpha/e_1$, $t_1 = H^2/c_v$.

Another character of the computing model consists of the nonlinearity of soil parameters. Corresponding to the water level change, the selected parameters are different in different periods. Due to the effect of the boundary water level, OCR of the compressible layer with different depth differs. All these factors should be considered in selecting soil parameters. The soil parameters used in the computation at Bus Station No. 2 are listed in Table 2.

Table 2 Soil parameters used in computation.

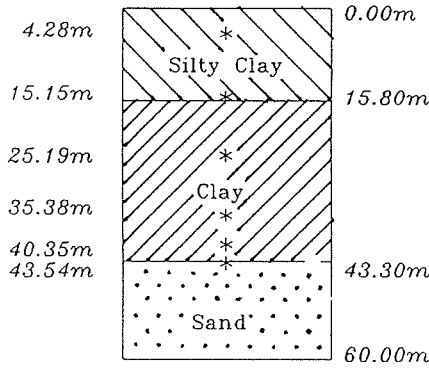
	I compressible layer		II compressible layer	
γ (kN m ⁻³)	17.1		18.4	
e_0	1.2		0.85	
k (10 ⁻⁷ cm s ⁻¹)	1.24		2.3	
c_{vc} (10 ⁻³ cm ² s ⁻¹)	3.0	(1)	20.0	(1)
	32.0	(2)	120.0	(2)
c_{vs} (10 ⁻³ cm ² s ⁻¹)	7.3	(1)	65.0	(1)
	32.0	(2)	120.0	(2)
m_{vc} (10 ⁻⁴ kPa ⁻¹)	3.8[(N + 1) ^{0.45} - N ^{0.45}] + 0.52		1.06[(N + 3) ^{0.36} - (N + 2) ^{0.36}] + 0.14	
		(1)		(1)
	0.06[(N + 1) ^{0.45} - N ^{0.45}] + 0.15		0.1	(3)
		(3)		
	0.155	(4)	0.097	(4)
m_{vs} (10 ⁻⁴ kPa ⁻¹)	0.52	(1)	0.14	(1)
	0.15	(2)	0.065	(2)
$c_{\alpha c}$	0.011		0.005	
$c_{\alpha s}$			0.0005	
OCR	1.0		1.0 (H < 27.5 m)	
			1.5 (H > 27.5 m)	

(1) Before 1970

(2) After 1970

(3) From 1970 to 1980

(4) After 1980



* Pore pressure probe

Fig. 10 Geological profile at Bus Station No. 2.

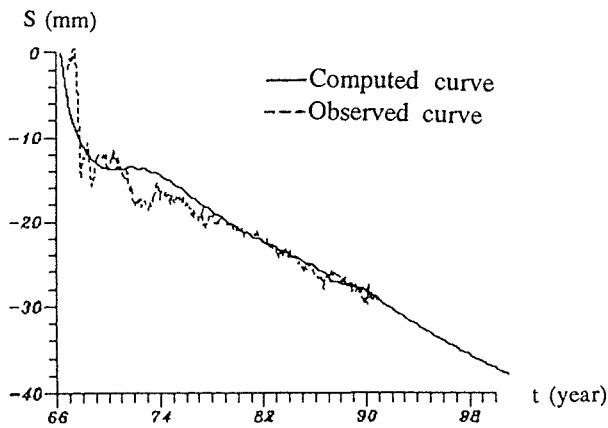


Fig. 11 Subsidence curves of the first layer.

COMPUTATION, RESULTS AND CONCLUSIONS

Because of the consideration of the creep rate, the nonlinearity of soil parameters, as well as the complex of engineering conditions of the studied subject, such as the irregularity of the boundary water level and the randomness to some extent in initial conditions, it is convenient to use finite differential method for computation (Gu *et al.*, 1993).

For the example at Bus Station No. 2, where the geological profile is shown in Fig. 10, the subsidence curves for the first silty clay layer and the second clay layer are presented in Figs 11 and 12 respectively. The good agreement between the computation results and observed data proves the validity of the model and its obvious advantage of the primary consolidation theory.

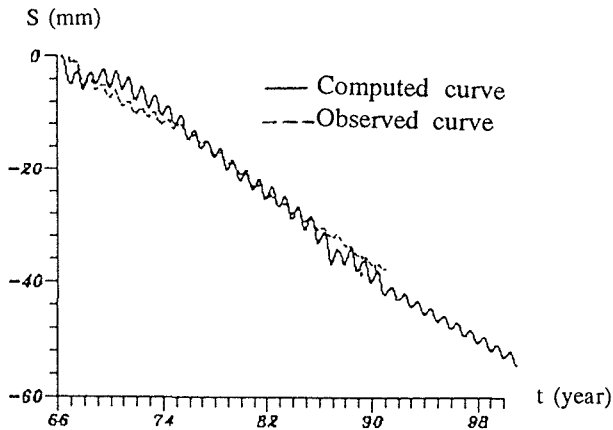


Fig. 12 Subsidence curves of the second layer.

Moreover, on the basis of the presented model, some suggestions for more effective recharging programme, such as selecting the recharging time, frequency and intensity, have been made

Acknowledgement The authors thank Dr K.H. Andersen from NGI for beneficial discussion during the time of testing.

REFERENCES

- Bjerrum, L. (1967) Engineering geology of Norwegian normally consolidated marine clays as related to settlements of buildings. *Geotechnique* **17**, 81-118.
- Garlanger, J. E. (1972) The consolidation of soil exhibiting creep under constant effective stress. *Geotechnique* **22**, 71-78.
- Gu, X. Y., Gong, S. L., Huang, H. C. & Liu, Y. (1990) Quantitative study of land subsidence in Shanghai. In: *Proc. 6th International Congress of IAEG* (Amsterdam), vol. 2, 1363-1370.
- Gu, X. Y., Tsien, S. I., Huang, H. C. & Liu, Y. (1991) Analysis of Shanghai land subsidence. In: *Land Subsidence* (ed. by A. I. Johnson) (Proc. Fourth Int. Symp. on Land Subsidence, Houston, May 1991), 603-612. IAHS Publ. no. 200.
- Gu, X. Y., Deng, W., Xu, D. N. & Liu, Y. (1993) Computation of land subsidence in Shanghai with secondary consolidation effect. In: *Recent Advances in Soft Soil Engineering* (Proc. ICSSSE), 98-103. Science Press, Beijing.
- Gu, X. Y. & Xu, D. N. (1994) Primary and secondary consolidation of Shanghai clay related to land subsidence (in Chinese). *Report IMCAS CR-91029*.
- Tsien, S. I. & Gu, X. Y. (1981) Computation of land subsidence in Shanghai, China. In: *Proc. IX ICSMFE* (Stockholm), vol. 1, 251-254.

Entropy approach – an alternative for effective prediction of land subsidence from mining

ROSSEN HALATCHEV, GEORGE ANDREEV

Higher Institute of Mining and Geology, Sofia-1156, Bulgaria

DELIANA GABEVA

Geological Institute, Bulgarian Academy of Sciences, Sofia-1113, Bulgaria

Abstract A new approach for thermodynamic modelling of the rock mass is developed, which is intended for predicting the land subsidence due to underground mining activity. It is based on the postulates of Non-Equilibrium Thermodynamics and the rock mass is treated as a dissipative system being in a mechanical non-equilibrium state as a result of receiving and dissipating mechanical energy. The natural system is identified as a viscous-elastic medium, for which is inherent the phenomenon of creep. The influence of the temperature field on the stress-strain state of the rock mass is also taken into account. The thermodynamic criterion for assessing the land subsidence state is the entropy variation.

INTRODUCTION

To be able to predict the land subsidence phenomena is vital for man to be able live in harmony with the environment. In this context the investigations made till the present mark a rich history of the engagement of scientific thought and considerable success at the solution of the problem.

Without launching out into a detailed review of the existed approaches we will summarize only their more considerable shortcomings as:

- predomination of the static approach ignoring time as a factor;
- emphasis mainly on modelling the subsidence form through displacements and/or strains and ignoring the variety of chemical-physical processes occurring in the rock mass;
- using criteria for assessing the subsidence state which are characteristic of the different mechanical processes then ones of the state of a given system;
- neglecting the importance of the fact that the exchange of energy (including thermal energy) between the structural elements of the rock mass determines its real state.

In the present paper a new approach is suggested which aims to solve the above shortcomings. The new approach uses Non-Equilibrium Thermodynamics (Glansdorff & Prigogine, 1973; Nicolis & Prigogine, 1979) which open wide possibilities for adequate modelling of land subsidence. The specific feature of the approach is the inclusion of the dynamic characteristics of the rock mass state in the thermodynamic model (TDM) for assessing the viscosity of the medium which can be determined *in situ* with geophysical monitoring.

MODEL FORMULATION

The development of TDM needs to be defined some terms in the context of the Non-Equilibrium Thermodynamics. In this connection a question arises about the concrete thermodynamic system that should be modelled. From logical considerations such a system can be identified with a zone of the rock mass with a border Γ_2 as shown in Fig. 1, in which land subsidence is expected from underground mining. We adopt this system as a common system. It also can be classified as a closed continuous thermodynamic system that exchanges thermal energy at the external border Γ_1 through solar radiation and at the internal border Γ_2 through thermal conduction due to the geothermal gradient. The common system is divided into two subsystems A and B with the border Γ_s determined by the spatial location of the probable subsidence border. The subsystem A represents the zone of subsidence and it behaves dynamically. Its location is changed in time and space due to the variation of the physical properties of the rock mass and mostly to the influence of the gravitational (and sometimes tectonic) field. This subsystem also represents a closed system exchanging a thermal energy at the borders Γ_1 and Γ_s . The subsystem B is identified with the rest part of the common system. This division allows the prediction land subsidence in time and within the framework of the common system. In this way every irreversible process can be localized at the border Γ_s with the exception of processes dealing with the chemical reactions (Westerhoff & Van Dam, 1992).

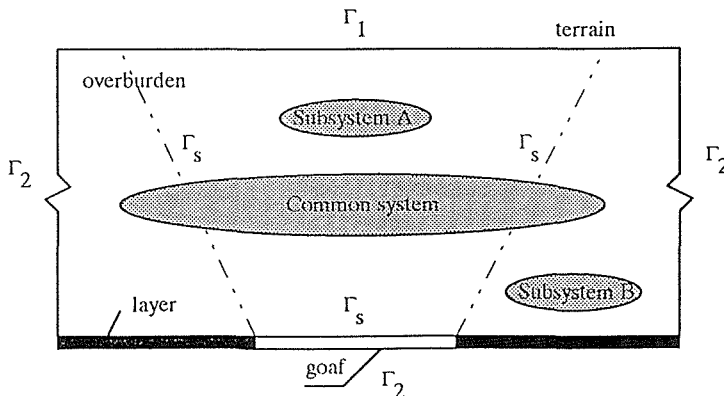


Fig. 1 Scheme of the thermodynamic model of land subsidence.

The state of the common system can be described in accordance with the postulates of linear Non-Equilibrium Thermodynamics only if the requirement for a local equilibrium at every small element of the rock mass is satisfied (Glansdorff & Prigogine, 1973). Here local equilibrium means that the local entropy has to be the same function of the local macroscopical variables as for the system in an equilibrium state. The admission, however, for a local equilibrium does not contradict the fact that the common system as a whole is in a non-equilibrium state, because irreversible processes can take place in it. Such a kind of admission can be acceptable for the present investigation because a similar approach was already used successfully by Sokolovski (Turchaninov et al., 1989), although in a pure mechanical aspect, applying the conception for a local limit equilibrium at every point of the critical zone affected by engineering work.

Entropy of the system

For the subsidence zone identified with a closed thermodynamic system the following expression of the entropy variation is valid (Nicolis & Prigogine, 1979):

$$dS = dS^{(i)} + dS^{(e)} \quad (1)$$

where $dS^{(i)}$ is the entropy production in subsystem A, $dS^{(e)}$ is the entropy flow to the subsystem A at the borders Γ_1 and Γ_s (Fig. 1).

The division of the entropy into production (source) and flow aims to be assessed the state of the thermodynamic equilibrium in the case that the entropy production does not exist. Equation (1) can be presented also for an element of the common system as follows:

$$\sigma[S] = \partial_t(\rho s) + \text{div}\Phi[S] \geq 0 \quad (2)$$

where $\sigma[S]$ and $\Phi[S]$ have the meaning of $dS^{(i)}$ and $dS^{(e)}$ respectively; ρ is density; s is specific entropy.

Having used the equation of the entropy balance (Glansdorff & Prigogine, 1973) and ignoring its terms which reflect the exchange of substance and passing of chemical reactions, we obtain the equation of the entropy production for an element of the common system:

$$\sigma[S] = \frac{1}{T^2} \sum_{j=1}^3 w_j \frac{\partial T}{\partial x_j} - \frac{1}{T} \sum_{i=1}^3 \sum_{j=1}^3 \sigma_{ij}^d \frac{\partial v_i}{\partial x_j} \quad (3)$$

where T is temperature; w_j is heat flow; $\partial T/\partial x_j$ is the j th component of the temperature gradient; σ_{ij}^d is tensor of the dissipative (inelastic) stresses; $\partial v_i/\partial x_j$ is the j th gradient of velocity in i th direction.

In the context of Non-Equilibrium Thermodynamics equation (3) for the 3-D case can be expressed as follows:

$$\sigma[S] = \sum_{\alpha=1}^3 J_{\alpha} X_{\alpha} + \sum_{\alpha=4}^{12} J_{\alpha} X_{\alpha} = \sum_{\alpha=1}^{12} J_{\alpha} X_{\alpha} \quad (4)$$

where $J_{\alpha_{(\alpha=1,3)}}$, $X_{\alpha_{(\alpha=1,3)}}$ are the flows and forces of the thermal conduction:

$$J_{\alpha} = w_j \quad (5)$$

$$X_{\alpha} = -\frac{1}{T^2} \frac{\partial T}{\partial x_j} \quad (6)$$

$J_{\alpha_{(\alpha=4,12)}}$, $X_{\alpha_{(\alpha=4,12)}}$ are the flows and forces of the viscous deformation:

$$J_{\alpha} = \sigma_{ij}^d \quad (7)$$

$$X_{\alpha} = -\frac{1}{T} \frac{\partial v_i}{\partial x_j} \quad (8)$$

The flows and forces in equation (4) indicate the passing of two basic processes in the subsidence zone – thermal conduction and viscous deformation. The first process is a vector process while the second is a tensor process. The difference in the character of these processes does not allow them to be combined as it is stated in Glansdorff &

Prigogine (1973) with the aim to be applied the Onsager's relationship and hence, every flow and force can have its own contribution to the entropy production.

The acceptance of the tensor of the dissipative stresses as a group of flows, respectively the strain rates as forces, is debatable. For example, an attempt was already made for classifying the strains and stresses as flows and forces respectively (Chelidze, 1987). In our case, however, we took into account the conclusion of Glansdorff & Prigogine (1973) that the dissipative stresses represent flows because they correspond to carrying an impulse into the system.

We note also that the entropy production describes the dissipative irreversible processes in the subsidence zone, for which the requirement $\sigma[S] > 0$ is always satisfied. In this case the entropy production represents a thermodynamic quantity due to forces X_α and a kinetic quantity due to flows J_α . When a state of thermodynamic equilibrium is reached the entropy production becomes $\sigma[S] = 0$.

The full entropy of the subsidence zone with a volume V and for time t can be evaluated using the expression:

$$S = -\frac{1}{T^2} \int_0^t \int_V \sum_{j=1}^3 w_j \frac{\partial T}{\partial x_j} dV dt - \frac{1}{T} \int_0^t \int_V \sum_{i=1}^3 \sum_{j=1}^3 \sigma_{ij} d \frac{\partial v_i}{\partial x_j} dV dt + \int_0^t \int_{\Gamma_1} w_{\Gamma_1} d\Gamma_1 dt + \int_0^t \int_{\Gamma_s} w_{\Gamma_s} d\Gamma_s dt \quad (9)$$

where W_{Γ_1} and W_{Γ_s} are the heat flows to the subsystem A at the borders Γ_1 and Γ_s , respectively.

The evaluation of the entropy production for every element of the discretization (if a numerical approach is used for stress-strain modelling of the system) and for the common system allows conclusions to be made about the state of the land subsidence. For example, one of the possible states is the thermodynamic equilibrium ($\sigma[S] = 0$), which definition has a disparate meaning regarding the limit equilibrium of the system in a purely mechanical sense. Also, a non-equilibrium stationary state can take place ($\Phi[S] = -\sigma[S] < 0$), for which is inherent the equality of the quantity of the flow of the energy and the dissipating energy. Hence, the thermodynamic approach suggests wider possibilities for differentiating the state of land subsidence than the pure mechanical approach, predominant in mining practice, which explores only the criterion of the limit equilibrium.

Stress-strain state

The mathematical description of the stress-strain state of the land subsidence zone identified with a continuous medium, which is subordinated to the laws of the linear theory of the viscous-elasticity, is reached with the solution of the following system of differential equations:

(a) Equations of the medium movement:

$$\sigma_{ij,j} + \rho F_i = 0 \quad 1 \leq j, i \leq 3 \quad (10)$$

where $\sigma_{ij} = \sigma_{ij}^e + \sigma_{ij}^d$ is the tensor of the stresses presented by the tensors of the elastic (σ_{ij}^e) and dissipative (σ_{ij}^d) stresses; F_i is mass force.

The right part of equation (10) does not include inertial forces because the non-equilibrium process of deformation being discussed from the positions of the

Thermodynamics is realized indeed very slowly and for every discretization in time the movement of the rock mass due to the action of the viscous forces satisfies the requirement for static equilibrium, i.e. the right-hand part should be equal zero. The elastic stresses satisfy Hooke's law while the dissipative stresses are described with an integral equation which can be presented in the following way:

$$\sigma_{ij}^d = f(c_p, c_s, Q_p, Q_s, \nu, t) \quad (11)$$

where c_p , c_s are velocities of the longitudinal and transverse seismic waves; Q_p , Q_s are quality factors regarding c_p , c_s ; ν is a strain rate; and t is time.

The model (11) is suggested by Gubkin (1984) and solves successfully the problem for assessing the dissipation of the energy in a solid. It uses the conception that the dissipative stresses are determined by the loading history. The dissipative stresses are proportional to the rate of strains and they relax continuously in time. The action of these stresses leads to a dissipation of a mechanical energy that is reduced into a heat.

- (b) Cauchy's equations describing the relationship between the tensor of strains and the vector of the displacements.
- (c) Saint Venant's equations for the medium continuity before and after the deformation.

The solution of the above system of equations is made with the Finite Element Method using fixed initial and boundary conditions (Zienkiewicz, 1971; Hematian & Porter, 1993).

The identification of the rock mass within the zone of land subsidence as a viscous-elastic medium is motivated by the fact that the process of deformation in time is a consequence of the creep phenomenon, which is inherent for that kind of medium. The approach suggested for modelling stress-strain has a specific feature due to the inclusion of Gubkin's model. This solution replaces the classical approach involving the use of the well-known Kelvin-Voigt and Maxwell units (Pytel & Chugh, 1992). Also, Gubkin's model allows the organization of a geophysical monitoring of the land subsidence and realization of an automated control of its state. Namely this circumstance that is in unison with the new tendencies in the Rock Mechanics applications for mining purposes (Bawden, 1993; Ferrero *et al.*, 1993; Mendecki, 1993; Halatchev *et al.*, 1993) determines the actuality of the model and approach as a whole.

Temperature field

The modelling of the temperature field of the zone of land subsidence in this investigation has a methodological character because of the fact that every concrete mining object has own specific features exceeding the bounds of the standard. From this point of view we treat the case of a stationary process of the thermal conduction which is described with Laplace's equation (Dmitriev & Gontcharov, 1983). The solution of this equation is made with the Boundary Integral Equations Method using fixed boundary conditions at the borders Γ_1 and Γ_2 (Gabeva, 1992).

From a thermodynamic point of view Laplace's equation describes a fixed non-equilibrium thermal process in the rock mass that means an invariability of the

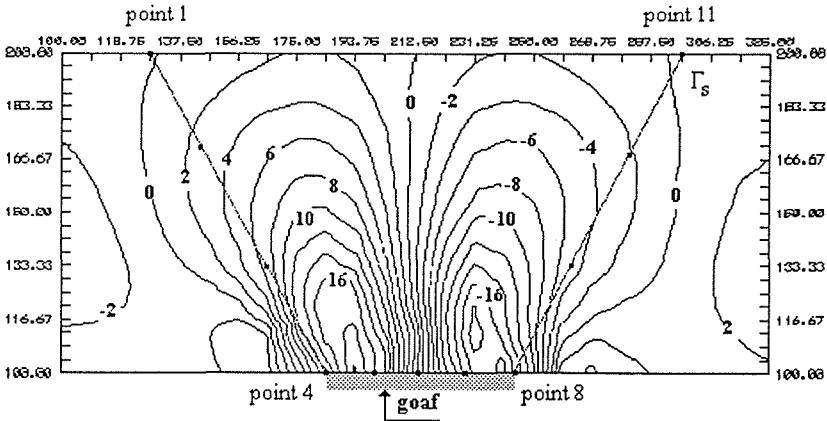


Fig. 2 Distribution of the shear stresses $(\tau_{xy}, 10^4 \text{ Pa})$.

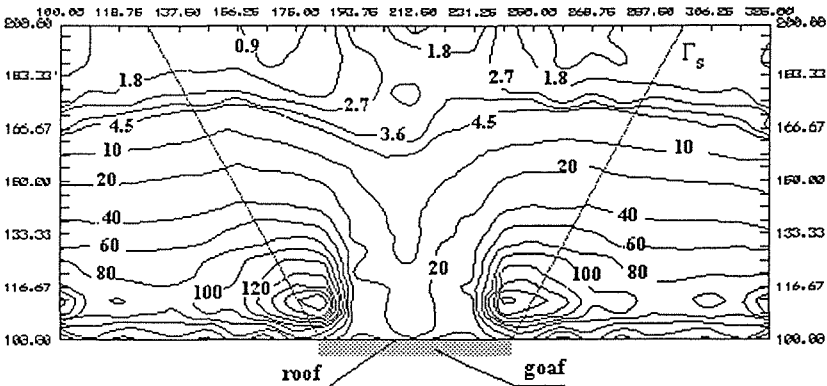


Fig. 3 Distribution of the local specific entropy $(s, \text{kJ m}^{-3} \text{K}^{-1})$.

temperature in time for every point of the medium but with different assessments at the different points. The support of the thermal process is due to the geothermal gradient.

The evaluation of the heat flow (w) in the TDM is made with the use of Fourier's law.

EXAMPLE SOLUTION

A computer program TFEM written in QuickBASIC-4.5 version of Microsoft Corp is created for the practical realization of the thermodynamic approach. The program is developed on a module principle and includes also the codes FEM and BIEMH written in FORTRAN 77 and intended for calculation procedures with the Finite Element Method and Boundary Integral Equations Method for the 2-D case (Halatchev, 1993).

A hypothetical land subsidence is investigated with a height of 100 m. The length of the goaf in the rock mass is 65 m. The homogeneous strata are characterized with: $\rho = 20 \text{ kN m}^{-3}$, $c_p = 1950 \text{ m s}^{-1}$, $c_s = 800 \text{ m s}^{-1}$, $Q_s = 30$. The time of the subsidence

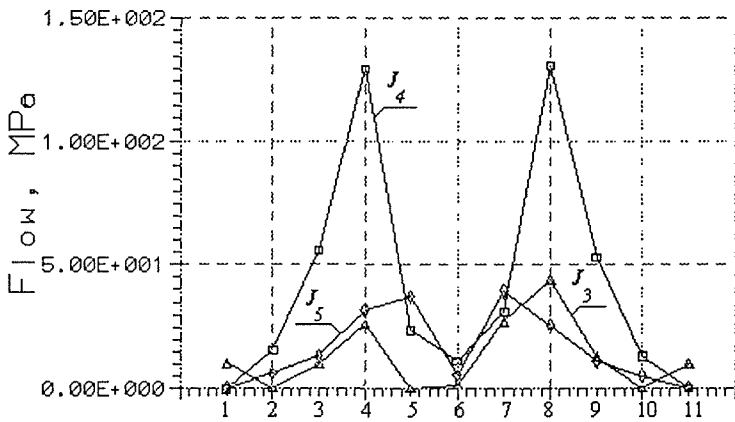


Fig. 4 Flows of the viscous deformation at points of the border Γ_s .

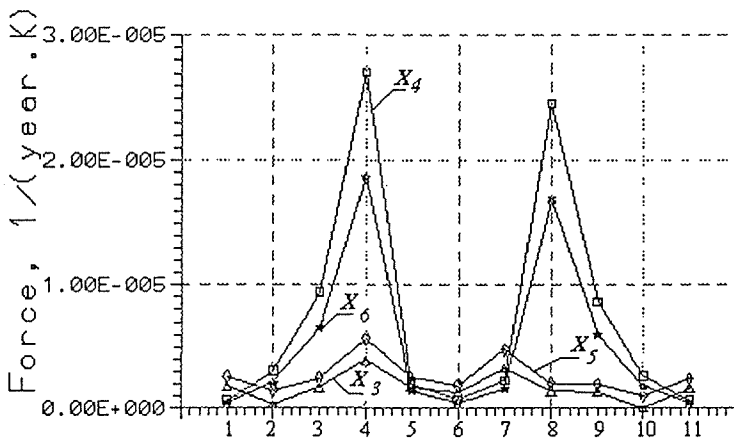


Fig. 5 Forces of the viscous deformation at points of the border Γ_s .

prediction is 6 years. The results about the shear stress distribution obtained by the FEM program are illustrated in Fig. 2. The distribution of the local specific entropy is given in Fig. 3 and its analysis shows an increase of the degree of the dissipation of a mechanical energy in close proximity to the goaf. In the upper central zone of the subsidence the entropy is minimum which means the rock mass subsides with a preservation of the medium continuity, i.e. with minimum deformations. Figures 4 and 5 show the distributions of the forces and flows at points of the probable border Γ_s fixed in the Fig. 2. The assessment of the subsidence entropy for the border Γ_s is 29.91 MJ K^{-1} .

Acknowledgement The authors thank the Management of the Bulgarian National Foundation for Scientific Investigations for financial support for this investigation under Grant no. TN-170/91.

REFERENCES

- Bawden, W. F. (1993) Some ideas on the use of mine induced seismic monitoring to characterize a fractured rock mass based on a conceptual stress-velocity-seismicity-geomechanical model. In: *Geotechnical Instrumentation & Monitoring in Open Pit & Underground Mining* (ed. by T. Szwedzicki) (Proc. Int. Conf., Kalgoorlie, Western Australia, June 1993), 15-31. Balkema, Rotterdam.
- Chelidze, T. L. (1987) *Methods of the Theory of Flow in the Mechanics of Geomaterials* (in Russian). Nedra Publishers, Moscow.
- Dmitriev, A. P. & Gontcharov, S. A. (1983) *Thermodynamic Processes in Rock Masses* (in Russian). Nedra Publishers, Moscow.
- Ferrero, L., Godio, A. & Sambuelli, L. (1993) Geophysical monitoring in a room and pillars talc mine in Italy. In: *Geotechnical Instrumentation and Monitoring in Open Pit and Underground Mining* (ed. by T. Szwedzicki) (Proc. Int. Conf., Kalgoorlie, Western Australia, June 1993), 161-167. Balkema, Rotterdam.
- Gabeva, D. A. (1992) Application of the Boundary Integral Equations Method for modelling a steady-state two-dimensional flow of underground water (in Bulgarian). In: *Third Int. Colloquium in Differential Equations* (18-22 August, Plovdiv, Bulgaria).
- Glandsdorff, P. & Prigogine, I. (1973) *Thermodynamic Theory of Structure, Stability and Fluctuations* (in Russian). Mir Publishers, Moscow.
- Gubkin, K. E. (1984) On the absorption of the elastic waves in solid media (in Russian). *Trans. AN USSR, Physics of Earth*, 3, 26-34.
- Halatchev, R. A. (1993) Thermodynamic model of rock slope stability in deep open-pit mines (in Bulgarian). *Research Report no. TH-170/1991, National Research Foundation at the Ministry of Science and Education of Bulgaria*.
- Halatchev, R. A., Stephanov, P. S. & Gabeva-Halatcheva, D. A. (1993) An approach for back slope stability analysis. In: *Geotechnical Instrumentation and Monitoring in Open Pit and Underground Mining* (ed. by T. Szwedzicki) (Proc. Int. Conf., Kalgoorlie, Western Australia, June 1993), 195-200. Balkema, Rotterdam.
- Hematian, J. & Porter, I. (1993) Consideration of the post-failure behaviour of rocks during finite element analysis of underground structures. In: *Applications of Computers in The Mineral Industry* (ed. by E. Baafi) (Proc. Austral. Conf., Wollongong, NSW, Australia, October 1993), 176-180. University of Wollongong Printery Services, Australia.
- Mendecki, A. J. (1993) Monitoring rock mass response to mining. In: *Geotechnical Instrumentation and Monitoring in Open Pit and Underground Mining, Kalgoorlie* (ed. by T. Szwedzicki) (Proc. Int. Conf., Kalgoorlie, Western Australia, June 1993), 357-364. Balkema, Rotterdam.
- Nicolis, G. & Prigogine, I. (1979) *Self-Organization in Non-Equilibrium Systems. From Dissipative Structures to Order through Fluctuations* (in Russian). Mir Publishers, Moscow.
- Pytel, W. M. & Chugh, Y. P. (1992) Application of a simplified 3-D roof-pillar-floor interaction analysis model for subsidence prediction. In: *Ground Control in Mining, Wollongong* (ed. by N. Aziz & S. Peng) (Proc. 11th Int. Conf., Wollongong, NSW, Australia, July 1992), 526-533. University of Wollongong Printery Services, Australia.
- Turchaninov, I. A., Iofis, M. A. & Kasparyan, E. V. (1989) *Fundamentals of Rock Mechanics* (in Russian). Nedra Publishers, Moscow.
- Westerhoff, H. & Van Dam, K. (1992) *Thermodynamics and Control of Biological Free-Energy Transduction* (in Russian). Mir Publishers, Moscow.
- Zienkiewicz, O. C. (1971) *The Finite Element Method in Engineering Science*. McGraw-Hill, London.

The step-loading model of subsidence induced by groundwater level changes with time

LAY SENG YAW & SHIEH MING JYH

Institute of Harbour and Marine Technology Wuchi, Taichung, Taiwan

Abstract This paper tries to develop a step-loading model for simulating the complex stress of soil deposits, and utilizes the Biot consolidation theory and superposition concept to analyse subsidence phenomena induced by changes in groundwater level with time. Finally, the *in situ* investigation data of Wang-Kon, which is located in the coastal region of Chang-Hwa, Taiwan, will be checked in order to prove the usefulness of this model.

INTRODUCTION

The most serious subsidence problems at Taiwan coastal areas is due to overpumping groundwater. The groundwater levels fluctuate repeatedly, because of fluctuations in the amount of groundwater withdrawal, and fluctuations in rainfall. This study looks at the temporal effects on subsidence of the repeated processes of loading, unloading, reloading on soil deposits and the cyclic changes in groundwater levels.

Studies of surface consolidation settlement induced by groundwater pumping can be divided into two categories, one is the decoupled approach method based on Terzaghi's (Terzaghi, 1943; Taylor, 1948) consolidation theory, the other is the coupled approach method based on Biot's (Biot, 1941, 1955) consolidation theory. The former first looks at the pore water pressure distribution, then calculates the strain of the soil deposits and total settlement of the ground surface by applying the concept of effective stress. The latter is a couple theory by adopting the displacement of porous media and the pore water pressure as the basic variables, which is based on the interaction of pore water and porous media. This couple consolidation theory is generally recognized to be more reasonable.

Therefore, this paper not only uses the couple consolidation theory of Biot to study the subsidence problem, but also develops a step-loading model to simulate the complex stress behaviour of soil deposits due to changing water levels, in order to analyse the effects on land subsidence with time.

BIOT COUPLE CONSOLIDATION THEORY

The analytical model of land subsidence in this paper is based on the soil couple consolidation theory. The couple consolidation theory concerning soil was firstly presented by Biot (1941), then Verruijt (1969), Bear & Corapcioglu (1981) and Corapcioglu & Bear (1983) etc. studied this theory and derived consolidation models from the viewpoint of flowing groundwater. Their basic assumptions:

- (a) fully saturated,
 - (b) pore water is compressible,
 - (c) solid grain is incompressible,
 - (d) follows Darcy's law,
 - (e) isotropic and homogeneous,
 - (f) small strains,
 - (g) linearity of stress-strain relations,
 - (h) the main factor to affect porosity is the effective stress of medium.
- According to the above assumptions, the basic equation of this coupled consolidation theory can be expressed as follows:

$$\begin{aligned}
 G\nabla^2 u_x + \frac{G}{1-2\nu} \frac{\partial \varepsilon}{\partial x} - \frac{\partial p}{\partial x} &= 0 \\
 G\nabla^2 u_y + \frac{G}{1-2\nu} \frac{\partial \varepsilon}{\partial y} - \frac{\partial p}{\partial y} &= 0 \\
 G\nabla^2 u_z + \frac{G}{1-2\nu} \frac{\partial \varepsilon}{\partial z} - \frac{\partial p}{\partial z} &= 0 \\
 -k\nabla^2 p + \frac{\partial \varepsilon}{\partial t} + n\beta \frac{\partial p}{\partial t} &= 0
 \end{aligned} \tag{1}$$

in these relations, $\nabla^2 = \partial^2/\partial x^2 + \partial^2/\partial y^2 + \partial^2/\partial z^2$, u_x , u_y , and u_z may be interpreted respectively as the displacement of the soil medium in the x , y , and z direction, $\varepsilon = \varepsilon_{xx} + \varepsilon_{yy} + \varepsilon_{zz}$ represents strain amount of medium volume, p represents the excess pore water pressure, E , ν , and G may be interpreted respectively as Young's modulus, Poisson's ratio and shear modulus, where $G = E/2(1 + \nu)$, and the other constants k , n and β may be interpreted, respectively, as permeability, porosity and compressibility of pore water.

If we only consider one-dimension consolidation i.e. $u_x = u_y = 0$, $\varepsilon = \partial u_z/\partial z$, $\partial u_x/\partial x = \partial u_y/\partial y = 0$, then the basic equation may be simplified as follows:

$$\begin{aligned}
 2\eta G \frac{\partial^2 u_z}{\partial z^2} - \frac{\partial p}{\partial z} &= 0 \\
 -k \frac{\partial^2 p}{\partial z^2} + \frac{\partial^2 u_z}{\partial z \partial t} + n\beta \frac{\partial p}{\partial t} &= 0
 \end{aligned} \tag{2}$$

in which $\eta = (1 - \nu)/(1 - 2\nu)$. In this equation, soil displacement u_z and pore water pressure p appear simultaneously so that it is a one-dimensional couple consolidation model.

If we consider that a soil deposit, with thickness H , suffers an instant loading p_o , then by analysing equation (2) its consolidation settlement could be expressed as equation (3):

$$u_z = \frac{4p_o H}{\Pi^2 \eta G} \sum_{n=0}^{\infty} \frac{1}{(2n+1)^2} \times \left\{ 1 - \exp \left[- \left[\frac{(2n+1)\Pi}{2H_d} \right]^2 C_v t \right] \right\} \tag{3}$$

in which vertical consolidation coefficient $C_v = k/(n\beta + 1/(2\eta G))$, H_d is the length of drainage, $H_d = H$ when the drainage condition is one-dimensional, but $H_d = H/2$ when the drainage condition is two-dimensional.

STEP-LOADING MODEL

Owing to the soil consolidation behaviour (Taiwan Inst. of Harbor and Marine Tech., 1993) can be divided into two parts: one is permutative deformation of soil particles, the other is elastic deformation of soil particles and pore water. The former is the main part of soil deformation, which is not reversible, and the later is reversible and represents a very small amount of deformation.

In this model, the major consolidation of subsidence analysis is the loading deformation by the increment of soil effective pressure during the process of lowering the water level, and the small changes of unloading and reloading deformation are neglected.

The analysis procedure of the step-loading model could be described as follows:

Transfer the groundwater level curve to consolidation water level curve
Although the groundwater level curve, shown in Fig. 1, includes the complex processes of water level lowering, rising and relowering etc., this model does not consider the tiny deformation induced by the rising and relowering effects of groundwater level, therefore, it just only reserves the lowering stages of water level and deletes the other meaningless factors. It means that this model only selects the lowest water level of each stage to form a consolidation water level curve, shown as Fig. 2, and this curve looks like a step-loading process constituted by several consolidation stages.

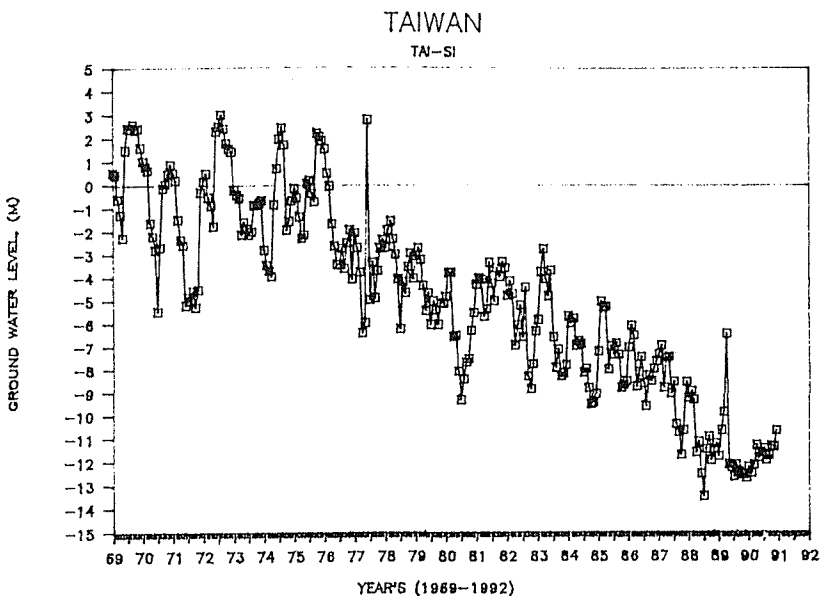


Fig. 1 The free water level variety with time.

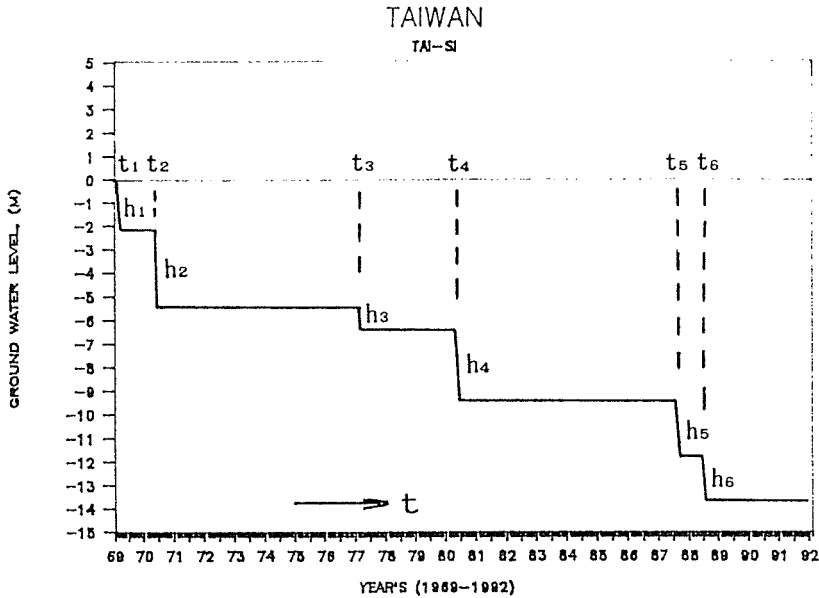


Fig. 2 The consolidation water level variety with time.

Analysing the settlement curve of each consolidation stage Owing to measured data of water level from an observation well which represent the changes in water level in nearby areas, this subsidence type belongs to regional subsidence. Therefore, we utilized equation (3) which derived from one-dimensional Biot couple consolidation theory to approach the subsidence variety. If the thickness of the soil deposit is H , the water unit weight is r_w , the lowering amount of consolidation water level is h , which means the effective stress adds an amount $r_w h$, then the settlement variety with time in each consolidated stage can be calculated by the following formula:

$$u_z = \frac{4r_w h H_i}{\Pi^2 \eta_i G_i} \sum_{n=0}^{\infty} \frac{1}{(2n+1)^2} \times \left\{ 1 - \exp \left[- \left(\frac{(2n+1)\Pi}{2H_{di}} \right)^2 C_{vi} t \right] \right\} \quad (4)$$

in which $H_p, H_{di}, \eta_i, G_i, C_{vi}$ may be interpreted, respectively, as soil thickness, drain path length, Poisson ratio function, shear modulus and consolidation coefficient of No. I soil deposit. According to the analysis of equation (4), the settlement with time at each consolidation stage is showed in Fig. 3.

Calculating the settlement curve for a single soil stratum If there are k consolidation stages in the No. I soil stratum, we can use superposition theory to calculate the settlement variety with time $S_i(t)$ by the following formula:

$$S_i(t) = \frac{4H_i}{\Pi^2 \eta_i G_i} \sum_{j=1}^k \left\{ r_w h_j \sum_{n=0}^{\infty} \frac{1}{(2n+1)^2} \times \left[1 - \exp \left[- \left(\frac{(2n+1)\Pi}{2H_{di}} \right)^2 C_{vi} (t-t_j) \right] \right] u(t-t_j) \right\} \quad (5)$$

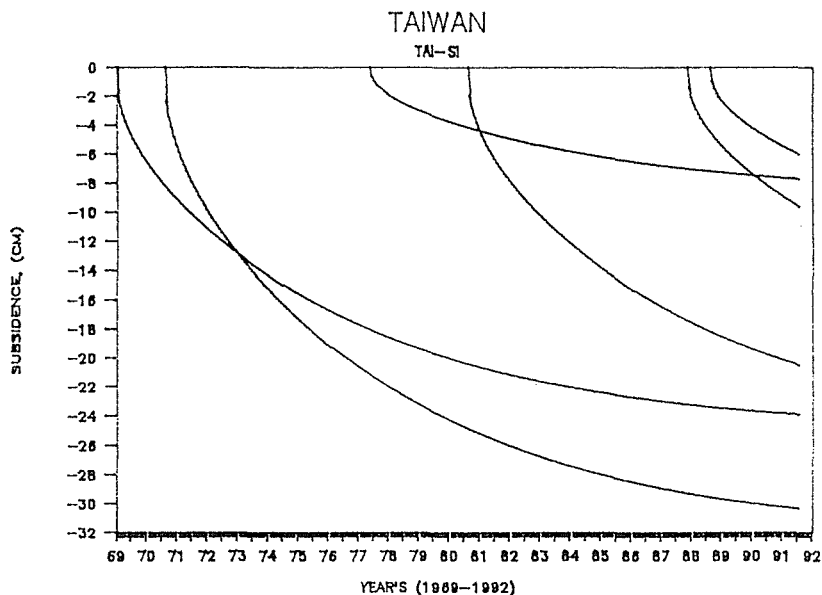


Fig. 3 The settlement of each consolidation stage.

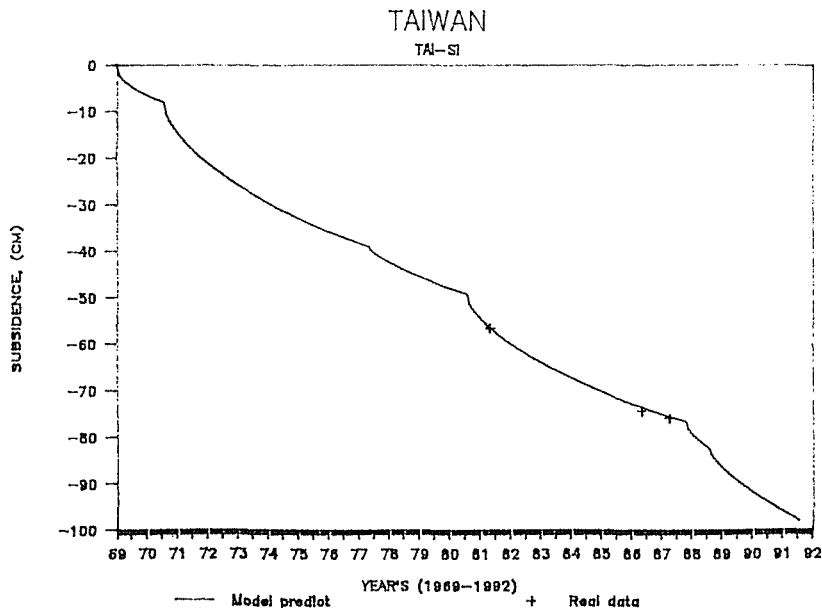


Fig. 4 The settlement changes with time in Tai-si.

in which t_j , h_j represent respectively the initial time and the lowering amount of consolidation water level in the No. J consolidation stage, the $u(t - t_j)$ is the Heaviside step function, $u(t - t_j) = 0$ when $t < t_j$, $u(t - t_j) = 1$ when $t \geq t_j$, Fig. 3 is the settlement curve in each consolidation stage. By equation (5), we can obtain the settlement changes with time of the No. I soil stratum. This result is shown in Fig. 4.

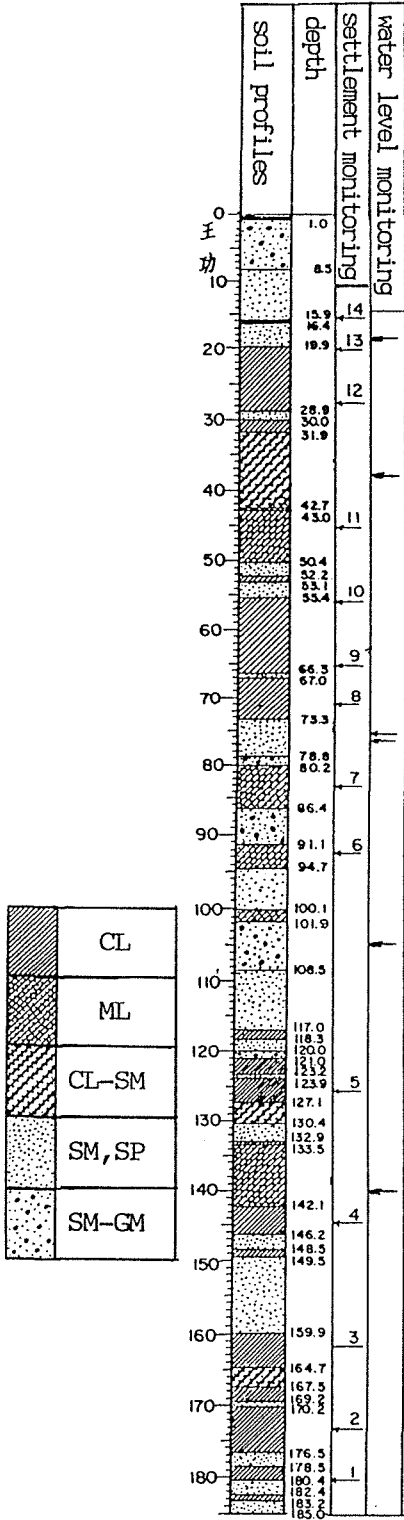


Fig. 5 Soil profiles and monitoring depth in Wang-Kon.

Calculating the subsidence curve for the whole soil deposits If there are m soil strata, we can use superposition theory again to calculate the total subsidence $S_T(t)$ by the following formula:

$$S_T(t) = \sum_{i=1}^m S_i(t) \quad (6)$$

EXAMPLE ANALYSIS

The application of the model is illustrated by the *in situ* observed data of Wang-Kon, which is situated on the Chang-Hwa coast of Taiwan. Here an investigation station of groundwater level and settlement was established for each separated soil stratum by the Water Conservancy Bureau in May 1989 (Taiwan Water Conservancy Bureau, 1993).

According to the observed data, the soil profiles, the groundwater level and the settlement of each stratum are shown in Figs 5, 6 and 7, respectively. From the groundwater level changes of each stratum in Fig. 6, we can find that the change in free water level in the shallow stratum is so small that the settlement of shallow stratum is tiny, that can also be explained from the settlements of No. 11-No.14 in Fig. 7. Additionally, we can find that the major settlement range is located at No. 5-No. 11, which means that the major settlement is distributed at depths of 44.5-125.5 m. Therefore, the subsidence analysis in this paper aims mainly at the range of depth 44.5-125.5 m.

From Fig. 6, we can find that the changes of confined water level at depth 76 m, 82 m, 106 m are almost the same, therefore, our subsidence analysis is based on the variety of water level at depth 106 m. Through the trial and error method, we find the Preconsolidation Head is -8.2 m, and the initial water level in May 1989 is -9.3 m. Because the stratum at depth 44.5-50.4 m is a part of the upper confining bed and the stratum at depth 123.9-125.5 m is a part of the lower confining bed, their settlement when calculated by equation (5), had to be reduced appropriately. As the other parts at

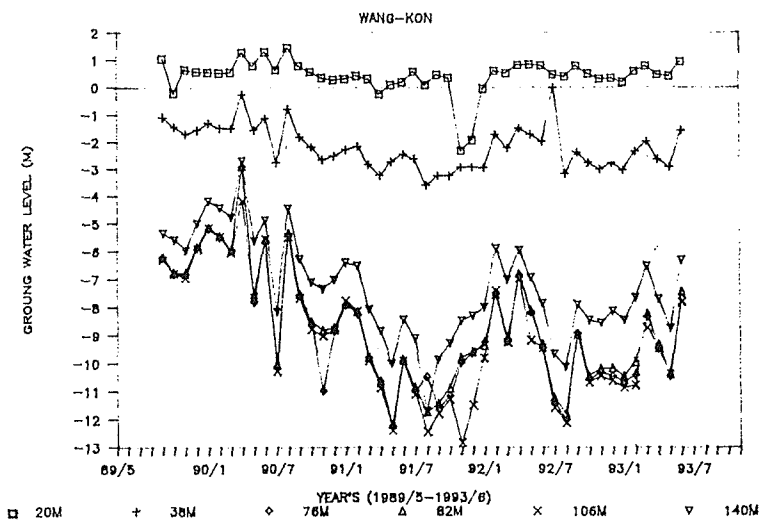


Fig. 6 The water level changes of each stratum in Wang-Kon.

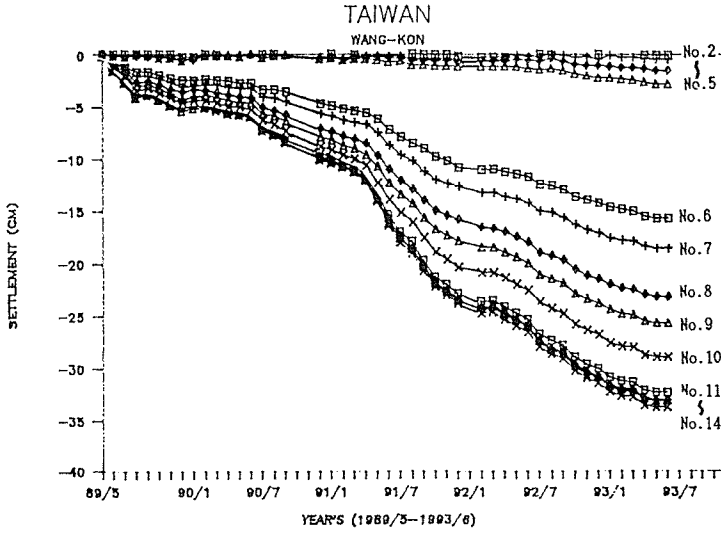


Fig. 7 The settlement changes of each stratum in Wang-Kon.

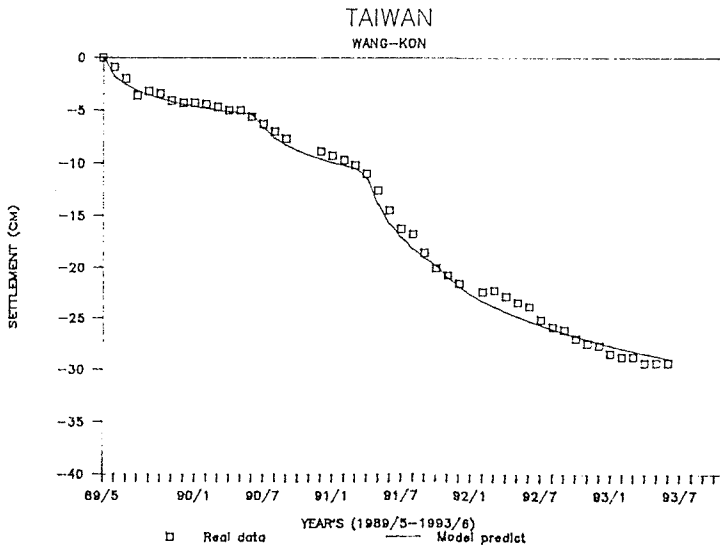


Fig. 8 Total settlement at 44.5-125.5 m depth in Wang-Kon.

Table 1 Soil characteristics in Wang-Kon.

Soil class.	E ($t\ m^{-2}$)	ν	C_v ($m^2\ year^{-1}$)
CL	450	0.35	8
ML	700	0.35	15
CL-SM	600	0.35	10
SM,SP	1000	0.30	30
SM-GM	1300	0.30	40

depth 50.4-123.9 m belong to the confined aquifer or interbed, their settlement when calculated by equation (5) need not be reduced.

Owing to the above considerations and the subsidence analysis of step-loading model, after inputting the data of Table 1 we can obtain the total settlement variety with time at the depth of 44.5-125.5 m (Fig. 8), and these results match the *in situ* observed data very well.

CONCLUSION

- (a) This paper uses Biot couple consolidation theory, a step-loading model and the superposition concept to analyse the subsidence induced by changes in groundwater level. The analytical results correspond to the data observed *in situ*.
- (b) It is very important to distinguish between confined aquifer, confining bed and interbed for making a reasonable analysis, and the parameters of settlement characteristics in each stratum are also the key of reliability of analytical results. Additionally, the supposition of preconsolidation head and initial groundwater level also affect the analysis result of subsidence.

REFERENCES

- Bear, J. & Corapcioglu, M. J. (1981) Land subsidence due to pumping, 1. Integrated aquifer subsidence equation based on vertical displacement only. *Wat. Resour. Res.* **17**(4), 937-946.
- Biot, M. A. (1941) General theory of three-dimensional consolidation. *J. Appl. Phys.* **12**(2), 155-164.
- Biot, M. A. (1955) Theory of elasticity and consolidation for a porous anisotropic solid. *J. Appl. Phys.* **26**(2), 182-185.
- Corapcioglu, M. J. & Bear, J. (1983) A mathematical model for regional land subsidence due to pumping, 3. Integrated equation for a phreatic aquifer. *Wat. Resour. Res.* **19**(4), 895-908.
- Terzaghi, K. (1943) *Theoretical Soil Mechanics*. John Wiley & Sons, New York.
- Taylor, D. W. (1948) *Fundamental of Soil Mechanics*. John Wiley & Sons, New York.
- Taiwan Inst. of Harbor and Marine Tech. (1993) The behavior and prediction of land subsidence at Taiwan coast.
- Taiwan Water Conservancy Bureau (1993) The study of monitor groundwater level and settlement for each separated soil stratum in the Wang-Kon of Taiwan.
- Verruijt, A. (1969) Elastic storage of aquifers. In: *Flow Through Porous Media* (ed. by R. J. M. de Weist), 331-376. Academic Press, New York.

A general formulation for saturated aquifer deformation under dynamic and viscous conditions

JIANG LI & DONALD HELM

Nevada Bureau of Mines and Geology, University of Nevada-Reno, Mail Stop 178, Reno, Nevada 89557-0088, USA

Abstract A general formulation is presented for dynamic and viscous deformation of saturated sedimentary material. Based on first principles (such as conservation of momentum and mass), constitutive laws (for both pore fluid and the solid matrix) and the effective stress principle, a complete mathematical description is developed for aquifer movement. The governing equation derived in this paper not only generalizes the dynamic governing equations derived by Fukuo (1970) and Zienkiewicz & Bettess (1982), but can be further reduced to various quasi-dynamic equations (consolidation or subsidence equations) including those of Terzaghi (1925), Biot (1941), Mikasa (1965) and Helm (1987). The new formulation unifies multiple physical processes such as wave, diffusion and creep into a single powerful governing equation with surprisingly few parameters. Self-contradictions of physical assumptions introduced by Fukuo and Zienkiewicz & Bettess are discussed.

INTRODUCTION

The dynamic behaviour of saturated porous material interests investigators in many fields such as earthquake engineering and geotechnical engineering. Biot (1962) investigated acoustic propagation through deformable and saturated porous media. Zienkiewicz & Bettess (1982) generalized Biot's formulation and gave a more general mathematical description that is widely applied to problems investigated by earthquake and geotechnical engineers. Fukuo (1970) in a paper presented in the first international symposium on land subsidence in Tokyo formulated the governing equation for movement of saturated soil under dynamic conditions. In all these previous investigations, the significance of relative acceleration a_r between the solid and fluid phases and the physical constraints required for correctly applying Darcy-Gersevanov's law are ignored. As a result, some self-contradictions become intermixed in the theory. In this paper, a new formulation is developed.

FUNDAMENTAL RELATIONS

Mass conservation

Assuming that no mass is destroyed or created within a control volume of interest in space and that mass conservation holds for each individual phase (water or soil phase)

gives the following equations:

$$\frac{\partial \rho_s}{\partial t} + \nabla \cdot (\rho_s \mathbf{v}^s) = 0 \quad (1)$$

$$\frac{\partial \rho_w}{\partial t} + \nabla \cdot (\rho_w \mathbf{v}^w) = 0 \quad (2)$$

where $\partial/\partial t$ is the partial derivative with respect to time, superscripts "s" and "w" denote soil and water, ρ_s and ρ_w are water and soil densities respectively, \mathbf{v}^s and \mathbf{v}^w denote phase velocities (bold means vector or tensor everywhere in this paper). If one multiplies each term in (1) by $(1 - n)$ and in (2) by n and then sum, by noting the definition of the bulk flux $\mathbf{q}^b (= n\mathbf{v}^w + (1 - n)\mathbf{v}^s)$ introduced by Helm (1987), one has an alternative mass conservation expression for bulk flow (Helm, 1987):

$$\nabla \cdot \mathbf{q}^b = - \left[\frac{1 - n}{\rho_s} \right] \frac{d\rho_s}{dt} - \left[\frac{n}{\rho_w} \right] \frac{d\rho_w}{dt} \quad (3)$$

where n is porosity, d/dt denotes the material derivative with respect to time t . When the density of each phase is constant (or all constituents are incompressible), the right-hand side of (3) equals zero, namely $\nabla \cdot \mathbf{q}^b = 0$ which represents an incompressibility condition.

Momentum conservation

Momentum equation for a two phase mixture Momentum conservation for saturated porous material (namely, soil and water, a two phase mixture) is given (Li, 1994) by:

$$\nabla \sigma^{ts} + \nabla \sigma^{tw} + \rho^b \mathbf{b} = \rho^s \mathbf{a}^s + \rho^w \mathbf{a}^w \quad (4)$$

where bulk density ρ^b can be expressed as $\rho^b = (1 - n)\rho_s + n\rho_w$ and equals the sum of the phase densities $\rho^s (= (1 - n)\rho_s)$ and $\rho^w (= n\rho_w)$ that are weighted by the volume ratio occupied by the each phase, \mathbf{a}^s is the acceleration of the skeletal matrix, \mathbf{a}^w of interstitial water, and σ^{tw} is a second order tensor that represents the total stress on water defined by:

$$\nabla \sigma^{tw} = n \nabla (p \delta) - n \nabla \tau^w \quad (5)$$

δ (or δ_{ij}) is the Kronecker delta, p is water pressure, τ^w represents the viscous stress on the cutting surface of the element of interest including through water (fluid-fluid viscous stress) and the water-soil interface (fluid-solid viscous stress). A total stress σ^{ts} gradient on the solid skeleton is given by:

$$\nabla \sigma^{ts} = \nabla \sigma' + (1 - n) \nabla p \delta + n \nabla \tau^s \quad (6)$$

where σ' is effective stress (Terzaghi, 1925), and τ^s denotes stress on the solid-water interface.

In this paper, it is assumed for simplicity that the component of fluid-fluid viscous stress is negligibly small when compared to the fluid-solid viscous stress component (namely, assuming $\tau^s = \tau^w = \tau$).

Following the solution for viscous force on the surface of a single sphere (Landau & Lifshitz, 1975) and introducing the concept of average drag force per unit volume $F^{drag} (= \nabla \tau)$ on a control element of interest in space (Li, 1994) give:

$$F^{drag} = \left[\frac{\rho_w}{2e} \right] m^{-1} a^r + \left[3\rho_w \left[\frac{ng}{2eK\pi} \right]^{0.5} \right] m^{-1} \int_{-\infty}^t \frac{dv^r/d\tau}{\sqrt{t-\tau}} d\tau + \gamma_w K^{-1} q \quad (7)$$

where e is the void ratio and m ($=K/K$ where K and K are hydraulic conductivity in forms of a matrix and a scalar) is a second order directional tensor that accounts for anisotropic material (Li, 1994). For isotropic material, m reduces to δ . In (7), laminar Newtonian flow of water relative to the skeleton is assumed. The term a^r ($=a^w - a^s$) is relative acceleration, v^r ($=v^w - v^s$) is relative velocity, q ($=nv^r$) is specific discharge, g is gravitational acceleration, γ_w is the unit weight of water.

Governing equation for solid matrix movement

Based on momentum conservation, a governing equation of aquifer movement is now developed. If momentum is conserved individually for each phase (see (4)), one can reach an expression derived by Li (1994):

$$\left[1 + \frac{1}{eG} \right] a^s - \frac{\nabla \sigma}{\rho^s} - \frac{\nabla \tau}{\rho^s} - \left[1 - \frac{1}{G} \right] b - \frac{a^b}{nG} = 0 \quad (8)$$

where G ($=\rho_s/\rho_w$) is the specific weight of the solid phase, a^b ($=n a^w + (1 - n) a^s$) is defined as bulk acceleration.

Introducing (7) into (8) by eliminating $\nabla \tau$ ($=F^{drag}$) gives the governing equation for the movement of the skeletal matrix, namely:

$$c_1 a^s - c_2 v^s - c_3 \nabla \sigma' - c_4 b + c_5 \dot{q}^b + c_2 q^b + c_6 = 0 \quad (9)$$

where \dot{q}^b is the time derivative of q^b and coefficients c_1 through c_6 are given by:

$$c_1 = \delta(1 + /eG) - m^{-1}/2n^2G \quad (10)$$

$$c_2 = \left\{ \frac{d(\ln m)}{dt} (\delta/Gn - m^{-1}/2n^2G) + \gamma_w K^{-1}/\rho^s \right\} \quad (11)$$

$$c_3 = \frac{1}{\rho^s} \quad (12)$$

$$c_4 = n \frac{1}{G-1} \quad (13)$$

$$c_5 = \frac{m^{-1}}{2n^2G} - \frac{\delta}{nG} \quad (14)$$

$$c_6 = 3\rho_w \sqrt{ng/2eK\pi} \frac{m^{-1}f(t)}{\rho^s} \quad (15)$$

One of the advantages of (9) is that if q^b is written in explicit terms, one can conveniently apply the incompressibility condition. Equation (9) is a new governing equation and describes solid matrix movement under dynamic and viscous conditions.

General relation of drag and driving forces for viscous laminar flow By combining momentum conservation for the fluid only and an average drag force on the solid matrix (7), one obtains a general relation between drag and driving forces (Li, 1994) by:

$$K^{-1}f^d = -J \tag{16}$$

where the right-hand term J denotes a dimensionless driving force and the left-hand product is a dimensionless drag force. f^d and J are given by:

$$f^d = \left\{ \frac{K}{2eg} a^r + \left[n \frac{K/cg\pi^{0.5}}{2} \right] \left[\int_{-\infty}^t \frac{dv^r/d\tau}{\sqrt{t-\tau}} d\tau \right] + q \right\} \tag{17}$$

$$J = \left[\frac{\partial v_w}{\partial t} + (v^p \cdot \nabla) v_w \right] / g + (\nabla p \delta) / \gamma_w + \nabla z(t) \tag{18}$$

where $z(t)$ is the elevation of an arbitrarily selected point of interest (usually fixed in the solid phase) whose velocity is v^p . When the first and second terms in (17) are negligibly small when compared to the third term q due to small relative acceleration a^r , drag force f^d defined by (17) reduces to specific discharge q . Correspondingly, when the first two terms in (18) are negligibly small (for example, if a^w/g is small when compared to the last two terms in (18)), then the driving force defined by (18) can be reduced to the gradient of hydraulic head. Accordingly, equation (18) simplifies to Darcy-Gersevanov's law and eventually to Darcy's law when $v^w \gg v^s$ (Li, 1994). It is important to emphasize that equation (16) is a general relation of drag and driving force which is derived from momentum conservation of flowing pore fluid. *Darcy-Gersevanov's law and Darcy's law are simply special cases of (16).*

Constitutive law for skeletal matrix Following Helm's (1992) conceptual lead, the soil skeleton (solid phase) is considered in the present paper to be a very viscous non-Newtonian fluid. The general constitutive relationship defined for non-Newtonian material with nonlinear viscosity is given by:

$$\sigma' = D\dot{\varepsilon} \tag{19}$$

where ε denotes the structural infinitesimal strain tensor which is a symmetric second order tensor that can be defined as $L\mathbf{u}^s$ where L is a matrix for definition of strain and \mathbf{u}^s is the displacement field of the solid phase. The dot represents a total derivative with respect to time. D is a fourth order tensor of viscosity for the constitutive law. For isotropic and isothermal material, D has only two independent parameters and can be expressed in the form with indices:

$$D_{ijkl} = (\kappa - 2\mu/3)\delta_{ij}\delta_{kl} + \mu(\delta_{ik}\delta_{jk} + \delta_{il}\delta_{jl}) \tag{20}$$

where κ and μ are nonlinear viscous parameters. Li (1994) further defines, the bulk viscous parameter κ as a function of both the first strain invariant $J_1 (=tr\varepsilon$ which denotes

the trace of strain tensor ε and the second deviatoric strain invariant J_2^D ($=0.5\varepsilon^D\varepsilon^D$ where ε^D is the deviatoric strain), and the shear viscous parameter μ is expressed by the second deviatoric invariant J_2^D of strain in the forms:

$$\kappa = \kappa_0 \exp[(1 + \alpha^D)(J_1 - J_{10})/A_1] \tag{21}$$

$$\mu = \mu_0 \exp[2(\sqrt{J_2^D} - \sqrt{J_{20}^D})/A_2] \tag{22}$$

where subscript "0" represents the initial state at time $t = 0$, A_i ($i = 1, 2$) denotes the constitutive parameters that are assumed to be constants in this paper, α^D is defined as the dilatant coefficient that is a function of J_2^D and J_1 . When $i = j$ is assumed for a spherical stress-strain relationship only, then (19) and (21) reduce to Helm's (1995) earlier development.

It is important to discuss the term $\nu\sigma'$ that plays such an important part in governing equation (9). From (19), one has the form:

$$\nabla \sigma' = (\nabla D)\dot{\varepsilon} + D(\nabla \dot{\varepsilon}) \tag{23}$$

Taking the derivative operator delta to (20) with assumptions (21 and (22) and substituting the result into the first term on the right-hand side of (23) give the expression as an alternative to equation (23):

$$\nabla \sigma' = D\nabla \dot{\varepsilon} + \dot{D}\nabla \varepsilon + R^\alpha \tag{24}$$

where:

$$R^\alpha = (\kappa \Delta \text{tr} \varepsilon / A_1) [\text{tr} \dot{\varepsilon} \nabla \alpha^D - \dot{\alpha}^D \nabla \cdot \text{tr} \varepsilon] \delta \tag{25}$$

In a later section, equation (24) plays a key role in the governing equation for multiple processes.

Complete mathematical description In order to show a complete mathematical description, it is worthwhile to summarize all the fundamental equations involved in the derivation of governing equation (9).

Effective stress

$$\sigma' = \sigma' + p\delta$$

Infinitesimal strain definition

$$\varepsilon = Lu^s$$

Constitutive law

$$\sigma' = D\dot{\varepsilon}$$

Momentum conservation for a two-phase mixture

$$\nabla \sigma' + \rho^b b = \rho^s a^s + \rho^w a^w$$

Momentum conservation for interstitial fluid

$$\rho^w a^w - n \nabla(p\delta) + n F^{drag} - \rho^w b = 0$$

Incompressibility condition

$$\nabla \cdot \mathbf{q}^b = \nabla \cdot [n\mathbf{v}_w + (1-n)\mathbf{v}^s] = 0$$

Average drag force per volume

$$\mathbf{F}_{drag} = \{(\rho_w/2e)\mathbf{m}^{-1}\mathbf{a}^r + [3\rho_w(n g/2e \mathbf{K} \pi)^{0.5}]\mathbf{m}^{-1}f(a^r) + \gamma_w \mathbf{K}^{-1} \mathbf{q}\}$$

There are a total of 28 equations and 28 unknowns (\mathbf{u}^s , \mathbf{u}^w , σ^t , σ^s , ε , p , \mathbf{F}^{drag}), thereby constituting a complete mathematical description.

DISCUSSION AND COMPARISON TO PREVIOUS INVESTIGATIONS

Discussion of the mass conservation

If the following equations of state are assumed for water and individual solid grains:

$$\rho_w = \rho_{w0} \exp(\beta_w p) \quad (26)$$

and

$$\rho_s = \rho_{s0} \beta_s \sigma_v^{ts} \quad (27)$$

then (3) can be simplified to:

$$\nabla \cdot \mathbf{q} = -\nabla \cdot \mathbf{v}^s - n\beta_w dp/dt - [(1-n)\rho_{s0}\beta_s/\rho_s]d\sigma_v^{ts}/dt \quad (28)$$

where β_s and β_w are compressibility of an individual soil grain and water respectively and σ_v^{ts} is the total spherical stress on each grain. If one further assumes small strain for the individual solid grain and if σ_v^{ts} is decomposed into water pressure p and a resultant stress $\sigma_v'^s$, equation (28) becomes

$$\nabla \cdot [n(\mathbf{v}^w - \mathbf{v}^s)] = -\nabla \cdot \mathbf{v}^s - n\beta_w dp/dt - (1-n)(\beta_s d\sigma_v'^s/dt + \beta_s dp/dt) \quad (29)$$

where the definition of \mathbf{q} has been included in the left-hand side of (29).

Mass balance equation (29) is now contrasted to Zienkiewicz & Bettess' (1982) equation which can be expressed:

$$\nabla \cdot [n(\mathbf{v}^w - \mathbf{v}^s) + \dot{n}(\mathbf{u}^w - \mathbf{u}^s)] = -\nabla \cdot \mathbf{v}^s - n\beta_w dp/dt - (1-n)\beta_s dp/dt - \beta_s d\sigma_v'/dt \quad (30)$$

where \mathbf{u}^s and \mathbf{u}^w represent the displacement fields respectively of the aquifer's skeletal matrix and interstitial water, whereby $\mathbf{v}^s = \dot{\mathbf{u}}^s$ and $\mathbf{v}^w = \dot{\mathbf{u}}^w$. Whereas Zienkiewicz & Bettess' effective stress term $d\sigma_v'/dt$ in (30) can easily be perceived as representing our $(1-n)d\sigma_v'^s/dt$ in (31), the second term $\nabla \cdot d(\mathbf{u}^r n)/dt$ in the left-hand side of (30) can not be so easily explained. This term appears also in Zienkiewicz & Bettess' expression of Darcy's law, namely:

$$n(\mathbf{v}^w - \mathbf{v}^s) + \dot{n}(\mathbf{u}^w - \mathbf{u}^s) = -\mathbf{K} \nabla h \quad (31)$$

which contrasts to Gersevanov's (1934), Biot's (1941), Fukuo's (1970), and Helm's (1987) expressions of Darcy's law. All others omit the term that includes the porosity

time derivative. It appears this term is extraneous and should be omitted both from (30) and (31).

Fukuo (1970) employed a simplified form of (3) in which only the first term remains on the right-hand side. That is, he requires $\nabla \cdot \mathbf{q} = -\nabla \cdot \mathbf{v}^s$ which actually is identical to the incompressibility condition $\nabla \cdot \mathbf{q}^b = 0$.

Discussion of the general momentum equation

Assuming that the third term on the right-hand side of (24) is negligibly small when compared to other two terms and inserting (24) into the third term of (9) give an expression of soil displacement:

$$c_1 \ddot{\mathbf{u}}^s + c_2 \dot{\mathbf{u}}^s + c_3 [D\nabla(L\dot{\mathbf{u}}^s) + \dot{D}\nabla(L\mathbf{u}^s)] = \mathbf{R} \tag{32}$$

where two dots indicate the second derivative with respect to time ($\mathbf{a}^s = \ddot{\mathbf{u}}^s$). Vector \mathbf{R} is defined by:

$$\mathbf{R} = c_4 \mathbf{b} + c_5 \dot{\mathbf{q}}^b + c_2 \mathbf{q}^b + c_6 \tag{33}$$

Equation (32) is an informative governing equation describing solid matrix (aquifer) movement in multiple physical processes. The first term on the left-hand side is the inertial force, the second is the viscous force caused by viscous drag of pore water flow on the skeletal matrix, the third represents a viscous resistant force (friction) of the skeletal matrix on itself and the last is an apparent structural elastic force on the solid matrix. The third and the fourth terms together behave as a "Kelvin model" due to non-Newtonian behaviour. A Kelvin model has a spring and dashpot linked together in parallel. The first term and the fourth dominate wave propagation of the displacement field \mathbf{u}^s ; the first and third dominate diffusion of the velocity field \mathbf{v}^s ; the second and the fourth control diffusion of the displacement field \mathbf{u}^s . The right-hand vector \mathbf{R} has several components which include changes in body force, drag force and other forces caused by the bulk flux \mathbf{q}^b and $\dot{\mathbf{q}}^b$ whose divergence can be reduced by invoking incompressibility conditions.

It is interesting to compare equation (4) to the momentum equation given by Zienkiewicz & Bettess (1982):

$$\nabla \sigma' + \rho^b \mathbf{b} = \rho^b \mathbf{a}^s + \rho^w \frac{d^2(n\mathbf{u})/dt^2}{n} \tag{34}$$

where \mathbf{u}^r is the relative displacement. For the sake of the comparison, equation (4) is alternatively expressed by:

$$\nabla \sigma' + \rho^b \mathbf{b} = \rho^b \mathbf{a}^s + \rho^w \mathbf{a}^r \tag{35}$$

Comparing equation (34) to (35) shows that the difference is between the second terms on the right-hand side. One is written in terms of $d^2(n\mathbf{u}^r)/dt^2$, the other in terms of relative acceleration \mathbf{a}^r . Recalling the definition $\mathbf{a}^r (= \mathbf{a}^w - \mathbf{a}^s)$ and \mathbf{u}^r allows one to derive the following relation:

$$\mathbf{a}^r \triangleq \ddot{\mathbf{u}}^r = \frac{d^2(n\mathbf{u}^r)/dt - \ddot{n}\mathbf{u}^r - 2\dot{n}\dot{\mathbf{u}}^r}{n} \tag{36}$$

Equation (34) can not equal (35) unless porosity n is not a function of time. Alternatively, any porosity rates that occur in the final term in equation (34) are based on an error, similar to what was discussed in the previous section. It should be emphasized from a physical point of view, the validity of the final term on the right-hand side of (34) is questionable. The time derivatives of weighted average displacement, originally defined by Biot (1962), may not be physically meaningful for momentum conservation (34). In other words, equation (34) is an incorrect expression of momentum conservation.

Similarly, the fluid momentum equation given by Zienkiewicz & Bettess (1982) reflects an emphasis on porosity derivatives:

$$-\nabla p - \rho_w \mathbf{b} = \gamma_w \mathbf{K}^{-1} + \rho_w \frac{d^2(n\mathbf{u}^r)/dt^2}{n} + \rho_w \mathbf{a}^s \quad (37)$$

Only when \mathbf{a}^r equals $(d^2(n\mathbf{u}^r)/dt^2)/n$ in (37) does the sum of the second and third terms on the right-hand side of (37) become $\rho_w \mathbf{a}^w$ which is required in order to reach the following correct form:

$$-\mathbf{J} = - \left[\frac{\mathbf{a}^w}{g} + \frac{\nabla p}{\gamma_w} + \frac{\mathbf{b}}{\rho_w} \right] = -\mathbf{K}^{-1} \mathbf{q} \quad (38)$$

Based on the above discussion of (34), equation (37) with derivatives of porosity with respect to time is a questionable description of momentum balance of pore fluid. Another important point is the following. According to (16)-(18), (38) is a simplified form of (16) and requires $\mathbf{a}^r = 0$. Because (37) does not require \mathbf{a}^r to be zero valued, there is a self-contradiction for (37) to reach (38). An editorial comment can also be made. The term γ_w is missing in Zienkiewicz & Bettess' (1982) equation.

In brief, the following points are important. Firstly, Darcy-Gersevanov's law should not be introduced into the general momentum equation as if it is an independent formula as was done by Zienkiewicz & Bettess (1982). Darcy-Gersevanov's law is a special case of momentum conservation of water flowing in porous material. Secondly, as a special case, Darcy-Gersevanov's law requires all acceleration terms to be negligibly small when compared to velocity terms. Otherwise, application of this law into momentum balance considerations introduce self-contradictions. Thirdly, to be physically meaningful, derivatives are either material or local derivatives of physical properties. When a mixture is occupying a bulk volume, these derivatives can be weighted by the volume fraction and summed, for example \mathbf{a}^b . These material derivatives and their volume fraction sums are substantially distinct in concept from simply taking the derivative of a physically meaningful vector sum, $\dot{\mathbf{q}}^b$ vs. \mathbf{a}^b . Unfortunately, the term $(d^2(n\mathbf{u}^r)/dt^2)/n$, which represents time derivatives of the normalized relative displacement field $n\mathbf{u}^s$ introduced by Biot (1962), are employed in (34) and (37) in place of physical meaningful relative forces per unit mass, \mathbf{a}^r .

Discussion of the momentum equation with small relative acceleration

If the relative acceleration \mathbf{a}^r is very small when compared to phase inertial terms, (9) reduces to:

$$\rho_s^* a^s - \gamma_w K^{-1} v^s - \nabla \sigma' - \rho_s^* b + \gamma_w K^{-1} q^b = 0 \tag{39}$$

where ρ_s^* ($= (1 - n)(\rho_s - \rho_w)$) denotes the submerged density of a solid (or effective density). If one takes the divergence of each term in (39) with the assumptions of homogeneous, isotropic skeletal material, the bulk incompressibility condition ($\nabla \cdot q^b = 0$), negligibly small change in body force ($\nabla \cdot b = 0$) and negligibly small change of porosity in space ($\nabla n = 0$), then one can rewrite (39) in terms of volume strain ε_v and effective stress without invoking a constitutive law:

$$\rho_s^* \ddot{\varepsilon}_v - \gamma_w K^{-1} \dot{\varepsilon}_v - \nabla \cdot \nabla \sigma' = 0 \tag{40}$$

The coefficient for the first term in (40) is different from the one that appears in Fukuo's (1970) equation, which is:

$$\left(\rho_s^* + \frac{\rho_w}{e} \right) \frac{\partial^2 \varepsilon_v}{\partial t^2} + \gamma_w K^{-1} \frac{\partial \varepsilon_v}{\partial t} - \nabla \cdot \nabla \sigma' = 0 \tag{41}$$

in which phase densities (ρ_s and ρ_w) and hydraulic conductivity K are assumed to be constant. Relative acceleration and effective body force are also tacitly assumed to be negligibly small. Note that the signs of the first and second terms in (40) and (41) are different. The difference of signs is caused by different sign convention. The following discussion will centre on the coefficients that occur first terms. For convenience of comparison, one can rewrite (39) as:

$$\left(\rho_s^* + \frac{\rho_w}{e} \right) a^s - \gamma_w K^{-1} v^s - \nabla \sigma' - \rho_s^* b + \gamma_w K^{-1} q^b - \left(\frac{\rho^s}{nG} \right) a^b = 0 \tag{42}$$

Taking the divergence of each term in (42) and making the same assumptions as Fukuo in (41), namely, that phase densities (or incompressibility condition), hydraulic conductivity and porosity are constant and that the effective body force is negligibly small, one has:

$$\left(\rho_s^* + \frac{\rho_w}{e} \right) \ddot{\varepsilon}_v - \gamma_w K^{-1} \dot{\varepsilon}_v - \nabla \cdot \nabla \sigma' - \left(\frac{\rho^s}{nG} \right) a^b = 0 \tag{43}$$

It is evident that the necessary condition for (43) to reach Fukuo's form (41) requires the divergence of the last term in (43) to be zero, namely the term $\nabla \cdot a^b = 0$. It can be shown that Fukuo tacitly makes this assumption during his derivation. However, we shall demonstrate that this term can not be zero. In general, bulk acceleration a^b equals $na^f + a^s$. The assumption of $a^f = 0$ in (41) requires therefore that $a^b = a^s$. Taking the divergence of a^b , one has the expression for the present case:

$$\nabla \cdot a^b = \nabla \cdot a^s = \ddot{\varepsilon}_v \tag{44}$$

Observing (41), one knows that $\nabla \cdot a^b$ in (44) can not equal zero, otherwise the first term in (41) disappears and the dynamic description reduces to quasi-dynamic one inherently without an inertial term. A self-contradiction is imbedded in Fukuo's governing equation for dynamic motion.

Discussion of the momentum equation with small absolute acceleration

Consider the case when slow movement of the solid frame \mathbf{v}^s only gradually approaches zero. Laminar pore water flow relative to the solid frame \mathbf{q} is not necessarily small and correspondingly viscous forces are assumed to dominate inertial forces. Acceleration terms on the left-hand side of (39) can be assumed to be much smaller than the velocity terms, $(\mathbf{K}\rho^*/\gamma_w)\mathbf{a}^s \ll \mathbf{v}^s$. Also \mathbf{a}^w tacitly equals \mathbf{a}^s due to the previous assumption that relative acceleration \mathbf{a}^r is small compared to \mathbf{a}^s . Then (39) reduces to:

$$\mathbf{v}^s + \gamma_w^{-1} \mathbf{K} \nabla \sigma' = \mathbf{q}^b - \gamma_w^{-1} \mathbf{K} \rho_s^* \mathbf{b} \quad (45)$$

or

$$\mathbf{q} = \gamma_w^{-1} \mathbf{K} [\nabla \sigma' + \rho_s^* \mathbf{b}] \quad (46)$$

as an alternative expression of the Darcy-Gersevanov law. Furthermore, if one takes the divergence of each term of (46), one gets:

$$\dot{\epsilon}_v = -\nabla \cdot [\gamma_w^{-1} \mathbf{K} (\nabla \sigma' + \rho_s^* \mathbf{b})] \quad (47)$$

Equation (47) becomes a diffusion equation in terms of volume strain if elastic skeletal material is assumed and $\nabla \cdot \rho_s^* \mathbf{b}$ is small. The resulting poroelastic diffusion equation is essentially Biot's (1941) and Mikasa's (1965) equations of consolidation. These strain-based or Terzaghi's (1925) pressure-based or Helm's (1987) displacement-based diffusion equations can be used to model subsidence.

Acknowledgement This research was supported by the Las Vegas Valley Water District, the Nevada Bureau of Mines and Geology, and the Nevada State Water Research Institute Program. The writing of this paper was supported by the US Department of Energy under contract DEFCO8-93NV11359.

REFERENCES

- Biot, M. A. (1941) General theory of three-dimensional consolidation. *J. Appl. Phys.* **12**(2), 155-164.
- Biot, M. A. (1962) Mechanics of deformation and acoustic propagation in porous media. *J. Appl. Phys.* **33**(4), 1483-1498.
- Fukuo, Y. (1970) Visco-elastic theory of the deformation of a confined aquifer. In: *Land Subsidence* (Proc. Tokyo Symp., September 1969), vol. 2, 547-562. IAHS Publ. no. 89.
- Gersevanov, N. M. (1934) *The Foundations of Dynamics of Soils* (in Russian). Stroiizdat, Leningrad.
- Helm, D. C. (1987) Three-dimensional consolidation theory in terms of the velocity of solids. *Geotechnique* **37**(3), 369-392.
- Helm, D. C. (1995) Poroviscosity. In: *Diversity in Engineering Geology and Groundwater Resources* (Proc. 1995 Annual Meeting of the Association of Engineering Geologists, Sacramento, October 1995), 54-55.
- Landau, L. D. & Lifshitz, E. M. (1975) *Fluid Mechanics* (translated from the Russian by J. B. Sykes & W. H. Reid). Pergamon Press.
- Li, J. (1994) Fundamentals of aquifer multiphase flow in response to inertial forces. PhD Dissertation, University of Nevada, Reno, UMI Dissertation Services, a Bell & Howell Company.
- Mikasa, M. (1965) The consolidation of soft clay—a new consolidation theory and its application. *Civ. Engng in Japan*, 21-26. Japan Society of Civil Engineering, Tokyo.
- Terzaghi, K. (1925) Principles of soil mechanics. IV, Settlement and consolidation of clay. *Engng News-Records* **3**, 204.
- Zienkiewicz, O. C. & Bettess, P. (1982) Soil and other saturated media under transient, dynamic conditions; general formulation and the validity of various simplifying assumptions. In: *Soil Mechanics-Transient and Cyclic Loads, Constitutive Relation and Numerical Treatment* (ed. by G. N. Pande & O. C. Zienkiewicz), 1-8. John Wiley & Sons.

A geotechnical model of mining subsidence in the Comanesti coalfield

CRISTIAN MARUNTEANU

University of Bucharest, Faculty of Geology and Geophysics, 6 Traian Vuia St., Bucharest, Romania

Abstract A complex geological and geotechnical model is proposed, regarding the mining subsidence phenomena in the case of stratified coal deposits. The qualitative and quantitative analysis of geological, structural, geotechnical and mining factors were used in a forecasting model for estimating subsidence displacements, the angles of limit of subsidence and the subsidence trough characteristics of the ground surface in a new coalfield. Finally, forecasting subsidence maps and ground deformation parameters enable the assessment of building stability level induced by the evolution of the ground surface subsidence in the Vermesti area of the Comanesti coalfield.

GEOLOGICAL AND MINING FACTORS

Mechanical properties of the rocks

Mechanical properties of the rocks vary from brittle sandstone to plastic marly-shale. The proportion of shale in the roof strata ranges from 25 to 56% of the total volume. Although the thickness and the continuity of the shale beds are variable, physical tests and granulometric analysis of the marly-shale rocks show uniform properties (Table 1). Their compressive strength are rather weak and isotropic (Table 2), however higher than the strength of the coal (Table 3).

Swelling of shales can cause the heaving of the floor with 25-50 cm in mining works. In laboratory investigations, uniaxial swelling of clay-shale rocks could swell 1-5% for coaly shales and over 24% for grey shales within 24 h.

The sandstones are often sandy or even silty, clay and carbonate cemented. Their weak cohesion and strength are responsible of their breaking up into small pieces.

These properties of the rocks determine subsidence by collapse of the immediate roof, followed by slow settlement, without fracturing the roof strata to the surface. The clayey rocks will deform as plastic material while the sandstones will suffer small displacements accompanied by joint closing and opening in areas affected by compression and extension, respectively. Superficial deposits, sometimes 20 m thick, reduce also the influence of subsidence on the ground surface, amortising the displacement and limiting fracture propagation.

Tectonic factors

Monoclinial geological structure and lack of faults (see Fig. 1) prevent severe

Table 1 Physical properties of the shales (mean values).

Location	Specific weight γ_s (kN m ⁻³)	Unit weight γ (kN m ⁻³)	Moisture w (%)	Porosity n (%)	Pore index e	Saturation degree S_r
Seam 1 floor	27.19	25.07	7.4	15.0	0.18	0.88
roof	26.45	23.95	6.6	15.6	0.18	0.91
Seam 2 floor	25.57	21.60	8.2	21.7	0.27	0.76
roof	27.02	23.74	6.2	17.5	0.21	0.80

Table 2 Mechanical properties of the shales.

Location	$\sigma_c \parallel$ (daN cm ⁻²):			$\sigma_c \perp$ (daN cm ⁻²):		
	max.	mean	min.	max.	mean	min.
Seam 1 floor	57.40	35.88	19.60	49.00	30.20	37.77
roof	57.60	39.52	24.50	65.10	40.07	30.60
Seam 2 floor	32.70	16.49	6.70	31.90	15.59	6.30
roof	56.40	43.56	25.00	68.30	53.17	38.80

Table 3 Mechanical properties of the coal.

Location	$\sigma_c \parallel$ (daN cm ⁻²):			$\sigma_c \perp$ (daN cm ⁻²):		
	max.	mean	min.	max.	mean	min.
Seam 1	35.8	28.60	15.7	32.6	29.50	20.8
Seam 2	38.4	26.00	17.5	44.6	29.77	18.4

differential subsidence being induced at the surface in the zone of influence of the fault.

Hydrogeological factors

The presence of two aquifers in the roof strata of the coal seams requires preliminary underground dewatering below a protective layer.

Seam thickness

An important factor governing the amount of subsidence is the seam thickness. Maximum vertical subsidence may equal 90% of the thickness of the coal seam extracted. In the Vermesti area two coal seams are worked and then the subsidence effect will be cumulative. The resulting isopach map (Fig. 2) shows two maxima in the central part (2.42 m) and in the northern part (1.78 m) of the coalfield, respectively.

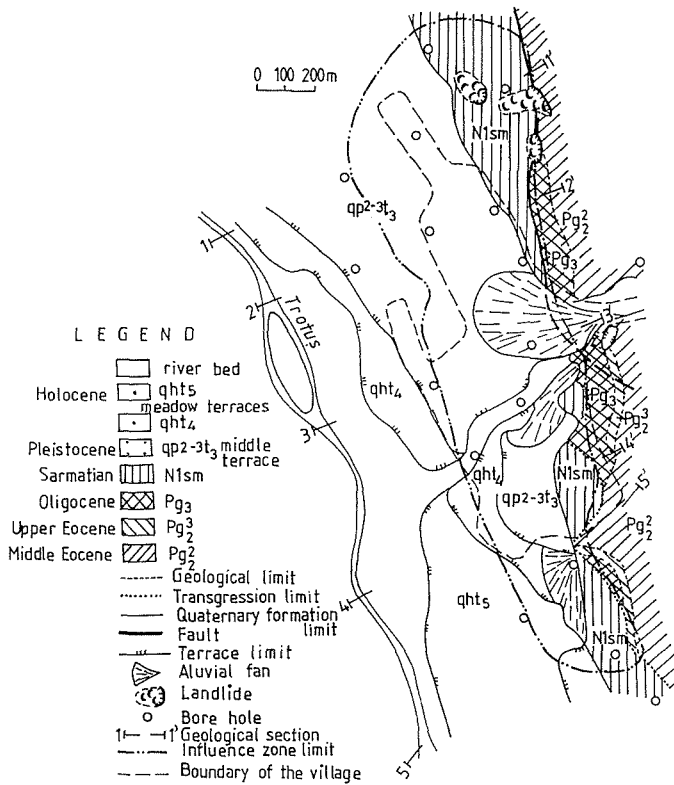


Fig. 1 Geology of the Vermesti area (after Micu, 1982).

Seam inclination

For inclined seams, the surface subsidence trough is displaced towards the less deep edge of the opening (Bomboe & Marunteanu, 1993), maximum subsidence increasing with the seam inclination. The isobath map at the bed level of the two seams (Fig. 3) shows a monoclinial structure constant along the direction. The seams inclination vary from 20-30° in the deeper part to 30-35° in the upper edge of the structure.

Width and depth of the opening

The width and depth of the underground opening determine together both the amplitude of the subsidence and the "critical area" or "area of influence". For a given point P on the surface the lines inclined with angles equal to the angles of limit of subsidence up dip and down dip drawn from P intersect the coal seam at points A and B (Fig. 4). The length AB is called the critical width. In relation to the critical area, a given working will be subcritical or supercritical. The maximum possible subsidence is only achieved when the width of working is either critical or greater than critical. On the map of the ratio width/depth built in the studied coalfield (Fig. 5) and

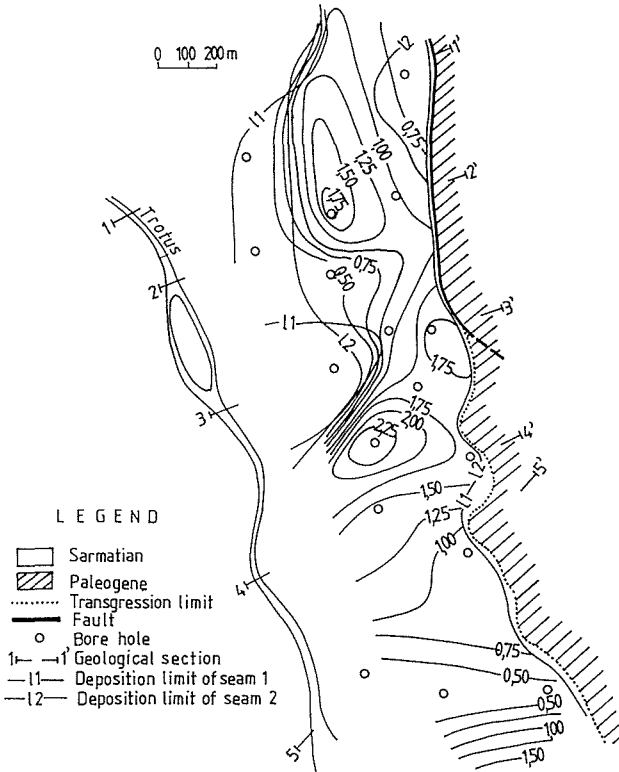


Fig. 2 Isopach map (cumulative thickness).

considering descending mining, the critical area is a bend varying from 50-75 m wide in the northern part to 250 m wide in the southern part. This bend is limited to the east by the natural limit of the coal seam and to the west by the calculated limit of the critical area. Knowing also that the maximum possible subsidence corresponds to a ratio of width to depth greater than 1.4 independent of the type of support used (Orchard, 1964 and others), the subsidence will be maximum in the supercritical area with values of width/depth ratio greater than 1.4 (Fig. 5).

Type of support

Under the conditions of the Comanesti coalfield, the only efficient extraction method is the longwall method with caving of the roof, the maximum possible subsidence attaining in this case 80-90% of the cumulative seam thickness.

THE INFLUENCE ZONE AT THE SURFACE

Limit of influence

The angle of limit of subsidence is the angle between the horizontal to the edge of the

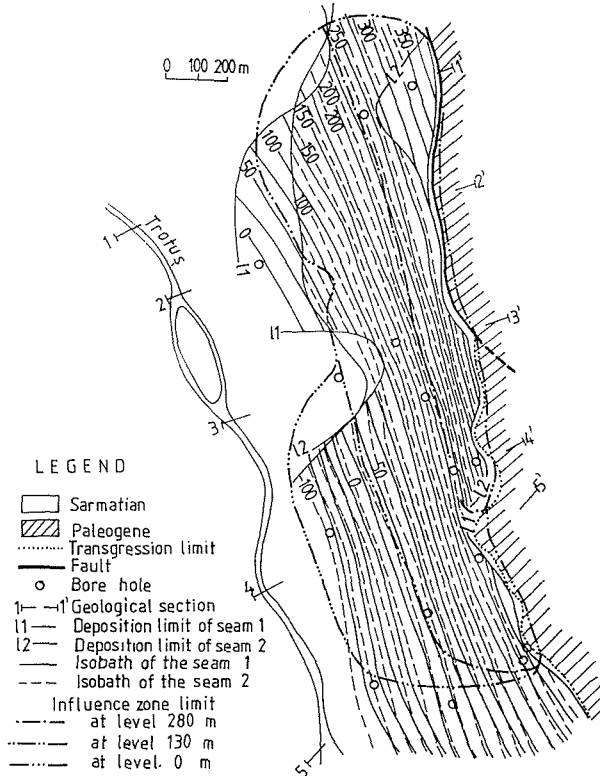


Fig. 3 Isobath map at the bed level of seam 1 and seam 2.

opening and a line connecting the edge of the opening and a point at the surface where subsidence diminishes to zero. The surface directly above excavated openings subsides in a trough, the limit of which is defined by the angles of limit of subsidence up dip (γ), down dip (β) and along the strike (δ). Angles of limit of subsidence or angles of influence ranges from 45° to 90° depending on coalfield and local factors. Table 4 shows some cited angles of limit of subsidence in different countries.

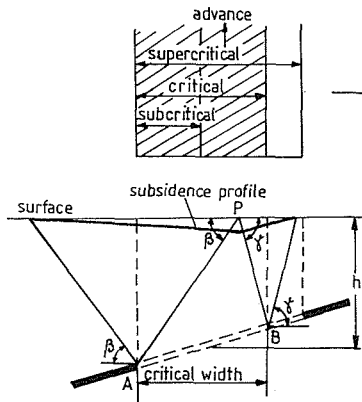


Fig. 4 Critical width of an underground opening.

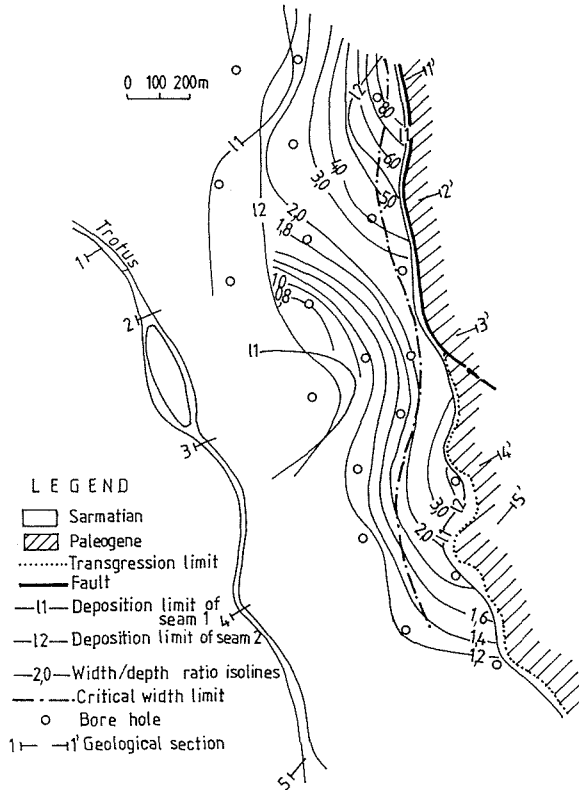


Fig. 5 Width/depth ratio isoline map and the supercritical area.

Table 4 Commonly cited angles of limit of subsidence (after Peng, 1978).

Country	Angle of limit of subsidence (°)
Netherlands	45-55
Germany	45-60
Northern France	55
Soviet Union	60
Great Britain	55-65
USA - Eastern	63-75
USA - Central	81.5-90
USA - Western	84-88

The angles of influence in the Comanesti coalfield were defined by Mining Board Instructions as a function of mechanical properties ($\sigma_c = 60-200 \text{ daN cm}^{-2}$) seam thickness (0.4-4.0 m) and seam inclination (10-70°) (Table 5). In the coarse superficial deposits the considered angle of influence is 40°. The angles of influence are shown in the geological sections (Fig. 6) and the limits of the subsidence trough at different levels of extraction are drawn on the isobath map (Fig. 3).

Table 5 Angles of limit of subsidence in the Comanesti coalfield.

Angle of dip (°)	15	20	25	30	35	40	45	50	55
Angle of influence:									
down dip β	70	68	63	58	56	52	49	45	42
up dip γ						73*			
along the strike δ						75*			

*Constant value for any angle of dip.

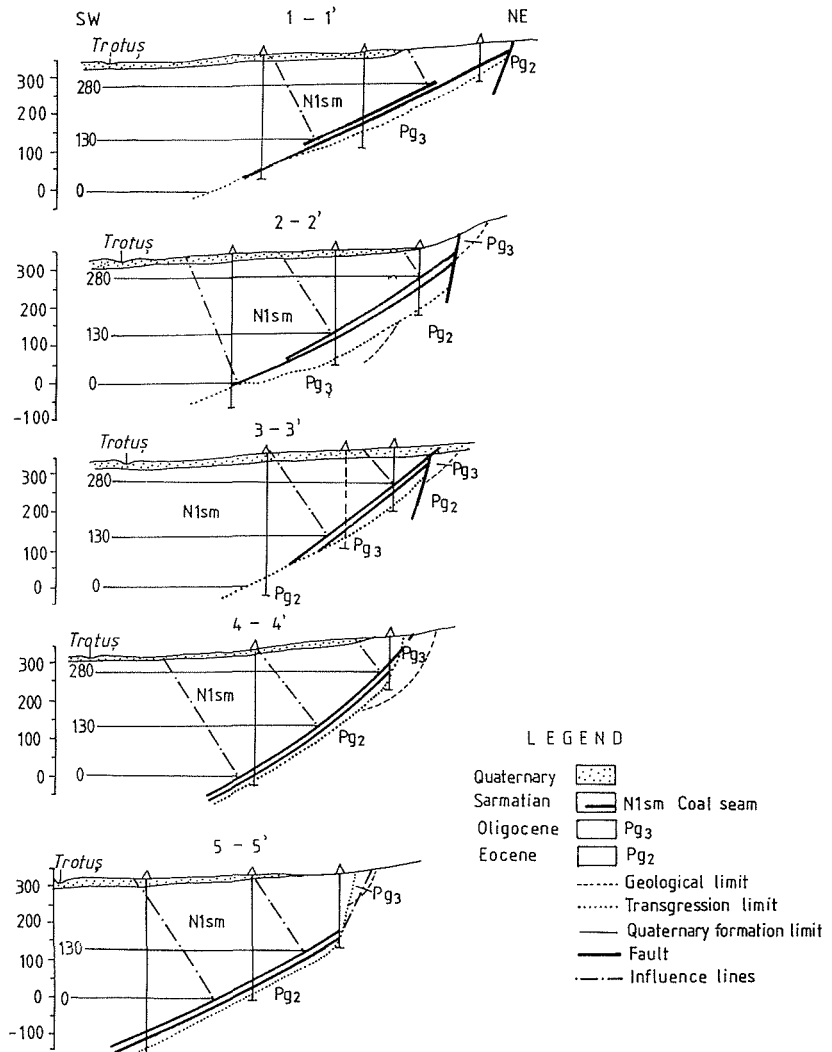


Fig. 6 Geological sections and the influence lines for different extraction levels.

Profile and parameters of subsidence

Maximum subsidence The maximum subsidence can be evaluated as a function of the workable cumulative thickness of the coal seams and of the ratio of extraction width to the depth of the longwall face. The resulting subsidence isoline map and the limit of the subsidence trough are shown in Fig. 7, assuming complete extraction by caving to the depth of the level 130 m. The maximum subsidence area is situated in the middle of the coalfield. The isoline values represent however the maximum possible subsidence, without considering loosing coefficient of the rocks, floor swelling or other working factors that would reduce the values of theoretical subsidence by 20-30%.

Ground tilt The tilt or slope of a subsidence profile is found by dividing the difference in subsidence (or in level) by the distance between two points:

$$i_{1-2} = \frac{s_1 - s_2}{l_{1-2}} \quad (\text{mm m}^{-1}) \tag{1}$$

Maximum ground tilts are developed about the limits of the area of subsidence, occurring at the point of inflection, at one-half maximum subsidence.

For the forecasted subsidence trough, the calculated values of the maximum tilt vary from 1×10^{-3} to 5×10^{-3} , but in the central maximum subsidence area would be 16×10^{-3} .

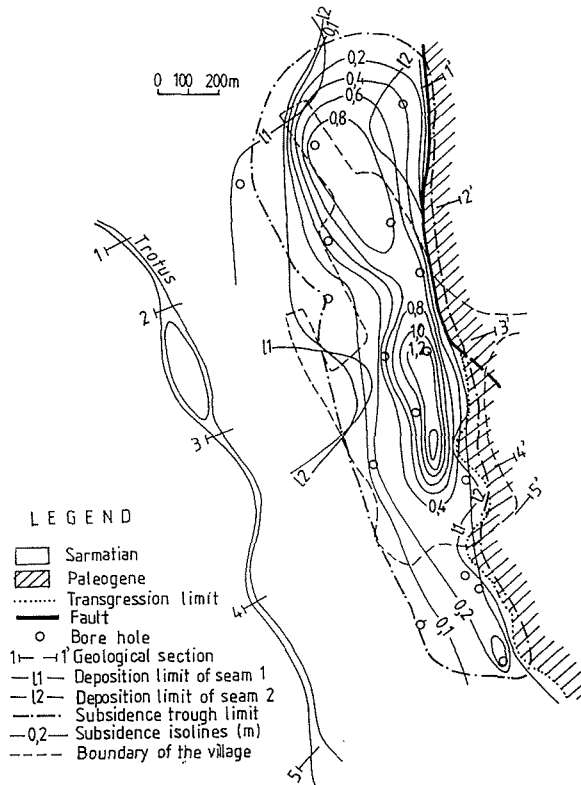


Fig. 7 Maximum possible subsidence map.

Curvature Curvature can be expressed by the difference in slope of the two neighbouring intervals divided by half the sum of their length:

$$K = \frac{2(i_{1-2} - i_{2-3})}{l_{1-2} + l_{2-3}} = \frac{1}{R} \quad (2)$$

where R = radius of curvature.

Strain can also be predicted from curvature. Most structural damages in a subsidence trough are caused by tensile strain that occurs in the convex portion of a profile. Calculated radii of curvature are generally greater than 20 km, but about the maximum subsidence zone the radius of curvature would decrease to 12 km.

The subsidence trough can be classified by the possible surface deformation (see Table 6). According to this classification, the subsidence trough predicted in Comanesti coalfield (Vermesti area) can be defined by category IV and partially III.

Table 6 Classification of subsidence trough (after Fota, 1981).

Subsidence trough (category)	Possible deformation of the surface:		
	Strain ϵ (10^{-3} mm m^{-1})	Radius of curvature R (km)	Tilt i (10^{-3} mm m^{-1})
I	12-8	1-3	20-10
II	8-5	3-7	10-7
III	5-3	7-12	7-5
IV	3-1	12-20	5-3

SURFACE DAMAGE

Surface damage is in relation to the intensity of ground strain (or differential movement) and to the sensitivity of the structures.

The prognosis of the surface structural damage can be achieved by the coefficient of building damage, Δl (after Fota, 1981):

$$\Delta l = \sqrt{(m_\epsilon \epsilon)^2 + \left[m_k \frac{h_c}{R} \right]^2} \quad (\text{mm}) \quad (3)$$

where:

l = length of the structure,

h_c = height of the structure,

$m_\epsilon m_k$ = coefficients in relation to the length of the structure (see Table 7),

ϵ = surface strain,

R = curvature radius of the surface.

Most of buildings in the village of Plopu are one floor buildings with maximum length of 12 m and maximum height of 6 m, or two floor buildings with maximum length of 20 m and maximum height of 10 m, calculated damage coefficients of which

Table 7 Coefficients depending on the length of the structure.

l	<15 m	15-30 m	> 30 m
m_ϵ	1.0	0.85	0.70
m_k	1.0	0.70	0.55

Table 8 Classification of the possible damage in the Vermesti area (extract only).

Group	Category of building	Category of damage	Cracks opening in walls (mm)	Coefficient of damage Δl (mm)
C	Apartments and public buildings (1-2 floors)	I: Very slight or negligible; preventive works not necessary; repairs to decoration probably	0-3	80

are 36 mm and 52 mm, respectively. Strain (ϵ) and radius of curvature (R) considered were $3 \times 10^{-3} \text{ mm m}^{-1}$ and 12 km, respectively, corresponding to a category IV subsidence trough.

Classification of damage categories is based on the relationship of damage to coefficient of building damage and category of building. According to this classification, partially presented in Table 8, the possible damage to the buildings in the subsidence area are classified in category I.

CONCLUSIONS

The assessment of a subsidence model considering geological, geotechnical and mining factors allowed the forecasting of the displacement parameters of the subsidence trough and the damage of the surface structures in a new coalfield. The results of the research have demonstrated the availability of turning the coal reserves into the category of geological reserves that could be exploited without major damage to the locality.

REFERENCES

- Bomboe, P. & Marunteanu, C. (1993) Mining subsidence forecasting by structural and geomechanical analysis. *Bull. Int. Assoc. Engng Geol.* **47**, 71-77.
- Fota, D. (1981) The influence of the underground works on the stability of surface structures (in Romanian). In: *Engineering Geology* (ed. by I. Băncilă *et al.*), vol. II, 393-422. published by Tehnica, Bucurest.
- Micu, M. (1982) Geology of Comanesti basin (in Romanian). *C. R. Inst. Géol. et Géophys.* **LXIX**, 187-208.
- Orchard, R. J. (1964) Partial extraction and subsidence. *Mining Engineer* **123**, 417-427.
- Peng, S. S. (1978) *Coal Mine Ground Control*. John Wiley & Sons, New York.

Modelling deformations in land subsidence developments at the Slovak coalfields

VLADIMIR SEDLAK

Department of Geodesy and Geophysics, Technical University of Kosice, Letna 9, SK-04200, Slovakia

Abstract The modelling of subsidence development is presented as a convenient subsidence prediction technique. The proposed prediction method of mining induced subsidence development applied at the Slovak Handlova coalfield which has longwall mining operations is based on a prediction method by Knothe. Theoretical calculations by modelling were verified using surface monitoring data from which the appropriate site-specific parameters were obtained. The results with accuracy analysis in subsidence development modelling have confirmed the applicability of this method in deformation surveying practice.

INTRODUCTION

The dynamic nature of mining subsidence of the hanging walls on the earth surface is dependent on a mining technology and the time of its activity. The determination of subsidence development over time being the final phase of the related deformation analysis as a convenient subsidence prediction technique is a basis of the subsidence models. Many methods for determining the nature of subsidence can be used to simulate in advance the final and continuous state of the subsidence process.

The theory of modelling subsidence development follows from a method proposed by Knothe. The method is based on the Gauss distribution of effects. The method determining the time dependence of subsidence is verified by several studies of the undermined area in the Slovak brown coal deposit at Handlova (Sedlak, 1992).

The main methods of simulating the movement of the earth surface caused by mining activity are generally oriented to the final asymptotic strain state. The process of development of subsidence with time does not make it possible to carry out detailed calculation of the deformation parameters in the individual intermediate stages of its development, during subsidence. Even the most efficient mining projects, such as planning of deformation measurements to prevent or minimize the damage caused by mining activity in the earth's surface, requires a suitable method for determining the development of subsidence and a method enabling prediction of the procedure of formation of the process of subsidence in relation to the time factor.

The currently available solution of the time dependence of the formation of subsidence often disregard many important subsidence data in the stage from monitoring subsidence up to scientific analysis. The development of the methods of the time dependence makes it possible to use data which support the formation of several reliable and convincing technologies which can be used in predicting the nature of the subsidence process.

In this paper, the existing method defining the gradual development of subsidence in relation to time is described, mainly for mining coalfields by the longwall mining operations. This method is analysed and suitably applied to the specific mining and geological conditions of the Handlova brown coalfield in Slovakia.

Computer modelling of subsidence development is very important from a mining surveying view. The periodic monitoring of subsidence data at each observed measurement point of the monitoring station must be adjusted and saved. A process of computer modelling subsidence development can be simplified and speeded up by some integrated measurement systems – the total geodetic stations, hardware and software (for example MicroStation). The MicroStation Development Language (MDL) can be used for modelling mine subsidence (Sedlak & Havlice, 1994).

DATA

Modelling subsidence development – theoretical principles

The effect of time during subsidence can be expressed by the function (Knothe, 1953):

$$z(t) = 1 - \exp(-ct) \quad (1)$$

and, considering that $c(t)$ is constant, the subsidence rate $s(t)$ can be expressed by means of the difference (Knothe, 1953, 1957):

$$s(t) = c[s_f(t) - s(t)] \quad (2)$$

where $s_f(t)$ is the final subsidence at time t , $s(t)$ is the actual subsidence at time t , $[s_f(t) - s(t)]$ is the subsidence potential at time t , c is the time coefficient.

Solving this relation the actual subsidence $s(t)$ at time t is:

$$s(t) = s_f(t) - \exp(-ct) \int_0^t s_f(g) \exp(cg) dg \quad (3)$$

where $s_f(g)$ is the rate of the final subsidence development, g is a coefficient which takes into account the geometrical parameters of the mined coalfield and the influence radius.

If the most simple example of the rectangular block mining operations with a single moving wall representing longwall operation is taken into account (Fig. 1), the final subsidence can be expressed by using the method of the function of the effect using the normal distribution of subsidence (Knothe, 1957, 1984):

$$s_f(x_t, x_0, y_1, z) = \frac{s_{max}}{r_h^2} \int_{x_0}^{x_t} \int_{y_1}^{y_2} \exp \left[-\pi \frac{x^2 y^2}{r_h^2} \right] dx dy \quad (4)$$

where s_{max} is the maximum subsidence ($s_{max} = -am$, a is the subsidence factor, m is the thickness of the mined layer); r_h is the influence radius on the horizon h .

The origin of the coordinate system is placed at the point A(0,0) at which subsidence is examined, with the mining advancing at a constant rate v on the x -axis (Fig. 1).

The time development of subsidence of the longwall layers over the mined layers which can be indicated by periodic monitoring of the observed point network on the

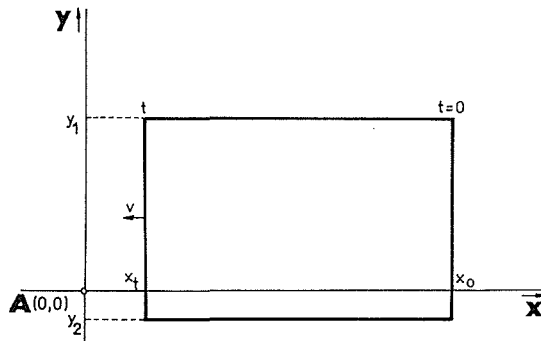


Fig. 1 Geometry of the longwall mining operation with a single moving wall.

earth surface, has three main subsidence phases. All phases are conditional on mining excavation technology and its time working schedule. The first subsidence phase is the initial phase and begins from the start of mining activity up to the moment when the face wall moves below the observed point in the earth surface. The second phase is defined by the time period t conditioned by the mining rate v , time coefficient c and influence radius r . The time period of this main subsidence part can be expressed by the simple equation (Karmis *et al.*, 1990):

$$t = (r/v + 1/c) \quad (5)$$

The third phase presenting the final subsidence is limited by the end of the second phase and the time at which the observed point acquires the final subsidence value. The second main phase of subsidence development in time participates on the maximum rate of subsidence which is approximated by the following equation:

$$s_{\max} = \frac{s_f v}{r + (v/c)} \quad (6)$$

where s_f is the final subsidence value.

In the case in which subsidence is continuous without interruption ($c = \infty$), the maximum rate of subsidence will be

$$s_{\max} = (s_f/r)v \quad (7)$$

Then modelling subsidence development can be possible for each observed point of a monitoring station in the earth surface or some mine horizon as the maximum rate of subsidence in any time of mining activity.

Application of the method in modelling to the Handlova brown coalfield

The Handlova brown coalfield belongs to the largest and the most economically significant coalfield in Slovakia. The longwall mine method is the typical extraction method for this coalfield. Two coal flat technically faulted seams with an extraction thickness of 2 m are found at a depth of 300–400 m.

On the basis of long-term examination of deformation changes in the earth surface of the Handlova brown coalfield we collected and analysed subsidence data of three main

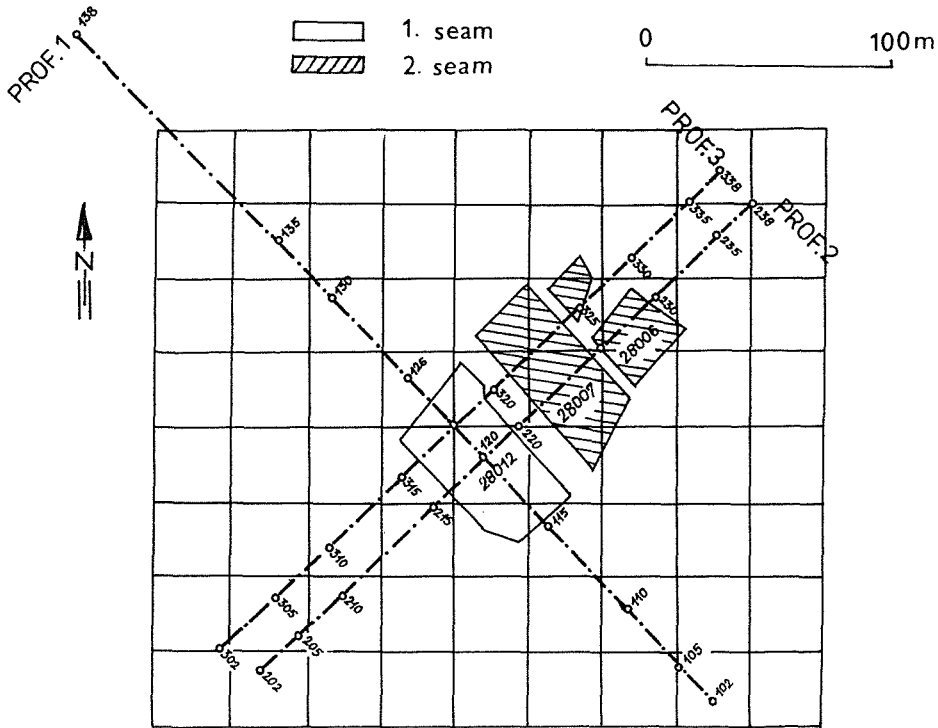


Fig. 2 Monitoring station at Handlova-Nova Lehota.

subsidence lines from more than 90 measurement points in the monitoring station (Fig. 2). In all cases of the subsidence examination we selected, from the final subsidence curves, characteristic parameters for the functional method of the subsidence effect with respect to time, such as (Sedlak, 1992):

- the influence radius r ($170 \div 200$ m);
- the final subsidence s_f ($0.2 \div 2.5$ m);
- the distance of the so-called "edge effect" d , i.e. the distance by which the wall must advance to ensure that the rock on the undermined region comes to assume a regular form $d = (1/4 \div 1/5)$ of the mined depth h , (theoretical calculated distance d and the actual distance d , of the "edge effect" were taken into account in the modelling);
- the mined depth h ($300 \div 400$ m);
- the mining rate v ($0.9 \div 1.2$ m day⁻¹);
- the phase of main subsidence t ($60 \div 80$ days);
- the content of hard rock in hanging wall layers TH ($35 \div 40$ %);
- the time coefficient c (0.036 day⁻¹, i.e. 1.3 year⁻¹).

Table 1 shows the comparison of the maximum subsidence development rate values $s_{max,G}$ from periodic geodetic measurements and calculated (modelling) ones $s_{max,M}$ from equation (6). Figure 3 demonstrates cases of the single function approximating the time dependence of subsidence development for two chosen observation points at the monitoring station.

The modelling subsidence development of each observation point at the monitoring station at the Handlova brown coalfield can be made out from the presented theory about

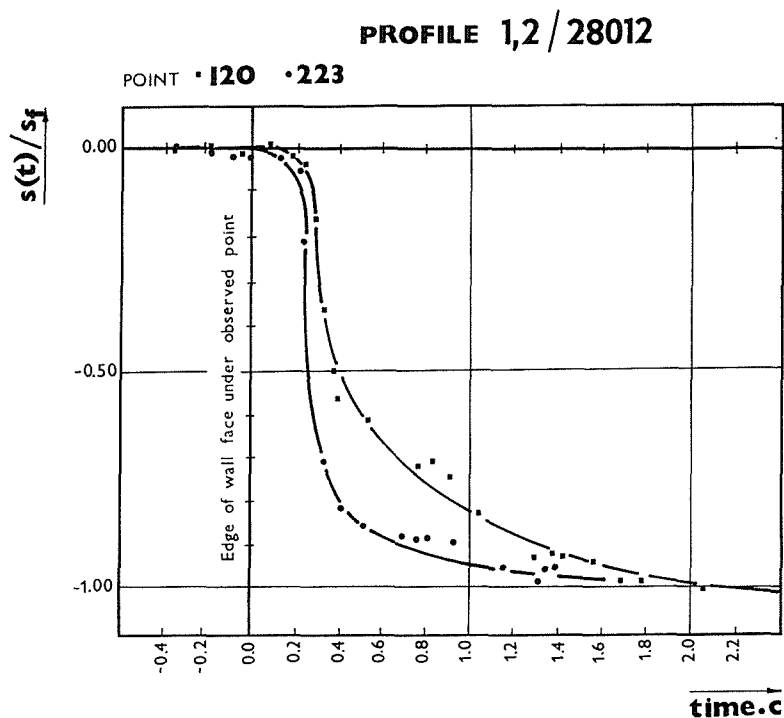
Table 1 Subsidence development rate values.

Profile	Point	H (m)	v (m day ⁻¹)	s_f (m)	$s_{max,G}$ (10 ⁻³ m day ⁻¹)	$s_{max,M}$ (10 ⁻² m day ⁻¹)
1/28012	120	346	0.9	1.775	1.8	1.8
1/28012	123	337	0.8	2.281	2.8	2.9
2/28012	220	370	1.2	1.530	2.5	2.3
2/28012	223	340	1.2	0.967	2.5	2.2
3/28012	312	392	1.1	0.996	2.4	2.2
3/28012	320	313	1.1	1.324	2.0	2.1

the time dependence of the subsidence development for a various moment of mining activity. In this way the predicted subsidence development of the earth surface over a mined space can be obtained. Comparison of the measured subsidence development and calculated one at the profile No. 1/28012 of the Handlova monitoring station is shown in Fig. 4.

Analysis of subsidence accuracy

The accuracy of the investigated subsidence is determined by comparing the subsidence at monitoring station observation points, which were experimentally determined using a geodetic method, with those determined by modelling.

**Fig. 3** Time dependence of subsidence for chosen points.

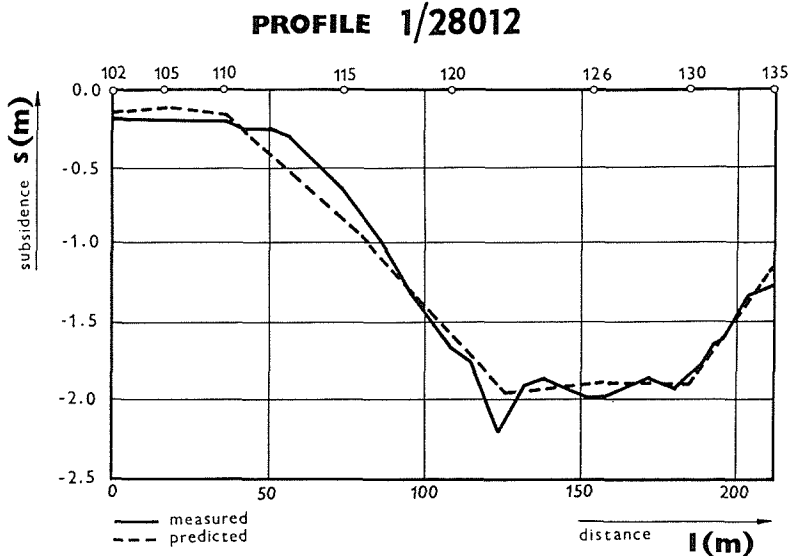


Fig. 4 Graphical comparison of measured and predicted subsidence development – PROFILE 1/28012.

Note: For the purpose of simplification of the following symbols are introduced:

– geodetic subsidence:

$$\begin{aligned}
 s_{geod} &= S_{120-120'}G = S_{G1}; S_{123-123'}G = S_{G2}; \dots \\
 \dots S_{(320-320')G} &= S_{Gn} = S_{ijG} = S_G
 \end{aligned}
 \tag{8}$$

– modelling subsidence:

$$\begin{aligned}
 s_{model} &= S_{120-120'}M = S_{M1}; S_{123-123'}M = S_{M2}; \dots \\
 \dots S_{(320-320')M} &= S_{Mn} = S_{ijM} = S_M
 \end{aligned}
 \tag{9}$$

Every space distance S_{ij} ; $i, j < 1, n >$ (subsiding point makes a space distance from its start, for example point 120, to final subsidence value, point 120) is defined by two points B_i, B_j whose coordinates X, Y, Z are determined in a Cartesian three-dimensional rectangular system by convenient geodetic method. For these subsidences hold:

$$\begin{aligned}
 S_{120-120'} &= (X_{120'} - X_{120})^2 + (Y_{120'} - Y_{120})^2 + (Z_{120'} - Z_{120})^2 \\
 &\vdots \\
 &\vdots \\
 S_{i,j} &= (S_j - X_i)^2 + (Y_j - Y_i)^2 + (Z_j - Z_i)^2 \\
 &\vdots \\
 &\vdots
 \end{aligned}
 \tag{10}$$

$$S = f(C_1, \dots, C_i, C_j, \dots)$$

mining rate v , phase of main subsidence t , content of hard rock in hanging wall layers TH , time coefficient c , etc.). However, in mining damage the 3% accuracy in subsidence development predicted by modelling is very exact.

RESULTS

The results of modelling subsidence developments obtained in this paper confirm the close correlation between measured and predicted subsidence data. This approximation can be efficiently used for the mining and geological conditions in the Handlova brown coalfield. An analysis of the results indicates that for mined depths of approximately 300 ÷ 400 m with the wall heading advance of the face front from 0.9 ÷ 1.2 m day⁻¹ and the content of hard rock in the hanging wall layers in the range from 35 to 40%, the time coefficient c is 0.036 day⁻¹, i.e. 1.3 year⁻¹. Theoretical examination of the problem of subsidence with time, described in this paper, and comparison of the calculated and measured results for the given examples of the Handlova brown coalfield confirm and validate the efficiency of the modelling method of characterization of the time dependence of subsidence. To determine more accurately the time coefficient c , it is necessary to analyse some further deformation parameters, for example tilting, tensile and compressive strains, horizontal movements, etc. It will form a part of the future research into this problem.

REFERENCES

- Karmis, M., Agioutantis, Z. & Jarosz, A. (1990) Subsidence techniques in the United States: a state-of-the-art review. *Mining Res. Engng* 3(3), 197-210.
- Knothe, S. (1953) Wplyw czasu na kasztalowanie sie niecki osiadenia. *Archiwum Górnictwa i Hutnictwa* 1(1).
- Knothe, S. (1957) Observations of surface movements under influence of mining and the theoretical interpretation. In: *Ground Movement* (Proc. European Congr., Leeds, April 1957), 210-215. University of Leeds, UK.
- Knothe, S. (1984) *Prognozowanie Wplywów Eksploatacji Górniczej*.
- Sedlak, V. (1992) Casovy faktor pri vytvarani poklesov v handlovskom hnedouholnom lozisku. *Uhli/Rudy* 11(1), 398-401.
- Sedlak, V. & Havlice, K. (1994) Time coefficient in modelling subsidence development at the Slovak coalfields. In: *IXth Intern. Congress and Exhibition ISM* (Proc. ISM Congr., Prague, April 1994), 104-107. Leica.

A new three-dimensional nonlinear model of the subsidence at Venice

PIETRO TEATINI, GIUSEPPE GAMBOLATI

Dipartimento di Metodi e Modelli Matematici per le Scienze Applicate, Università di Padova, via Belzoni 7, I-35131 Padua, Italy

LUIGI TOSI

Istituto per lo Studio della Dinamica delle Grandi Masse, CNR, S. Polo 1364, I-30125 Venice, Italy

Abstract A new quasi 3-D nonlinear finite element model is developed for the simulation and prediction of land subsidence due to groundwater withdrawal in the Venice Lagoon. The nonlinearity is accounted for by the use of aquitard hydraulic conductivity and specific storage related to the effective intergranular stress and solved by a block successive over-relaxation (SOR) procedure with the optimal block SOR factor. The hydrologic response is then fed into a nonlinear 1-D vertical compaction model. The overall modelling approach is applied to the regional multi-aquifer system underlying the Venetian Lagoon where extensive groundwater pumping from the upper aquifers has caused an alarming land subsidence at Venice over the period 1950-1970 and a more modest settlement in the southern and northern lagoon areas thereafter. The 3-D nonlinear flow and 1-D compaction models have been calibrated against the past available piezometric and settlement records and reproduce very satisfactorily the event as was observed from the inception of pumping until the early seventy when the cone of depression achieved the largest extent. The simulations for later years up to the present time are currently under way.

INTRODUCTION

A study of land subsidence at Venice has pointed out that the event is related to the aquitard compaction due to the extensive groundwater withdrawal that occurred from the upper 300 m of the unconsolidated Quaternary sediments underlying the lagoon during the period 1950-1970 (Gambolati *et al.*, 1974).

In the 1970s several analyses were performed to reconstruct the lagoon subsurface system (Carbognin *et al.*, 1974; Gatto, 1974; Ricceri & Butterfield, 1974), locate the artesian wells (Serandrei-Barbero, 1972), and evaluate the drawdown in the pumped aquifers (Mozzi *et al.*, 1975; Volpi *et al.*, 1979).

The collected data were fed into an axi-symmetrical finite element model (Gambolati & Freeze, 1973) for the first historical analysis and prediction of land subsidence in the Venice area (Gambolati *et al.*, 1974; Carbognin *et al.*, 1977).

The limitations of the Gambolati & Freeze model, i.e. linear aquitard behaviour in compression and simplified aquifer system geometry, are removed by developing a new

quasi 3-D nonlinear finite element approach (Gambolati & Teatini, 1994), in which the resulting nonlinear equations are solved by a block SOR procedure with the *a priori* assessment of the optimal block over-relaxation factor (Gambolati & Teatini, 1995).

The model is based on the assumption of quasi-three-dimensional flow and one dimensional compaction, and allows for a complete 3-D geologic representation of the multi-aquifer system. A fully numerical method is used to solve the nonlinear aquitard equations, where the hydraulic conductivity is taken to be related to porosity and the specific storage to both porosity and effective intergranular stress.

After a short description of the new 3-D geologic representation, and corresponding mathematical model, of the regional Venice nonlinear multi-aquifer system, some simulation results from 1930 to 1973 are shown and discussed.

3-D GEOLOGIC RECONSTRUCTION OF THE VENICE MULTI-AQUIFER SYSTEM

The interconnected Venetian aquifer-aquitard system has its recharge area in the thick coarse deposits that extend from the Alps to the alignment Cittadella-Castelfranco-Treviso (Fig. 1). From this area the aquifer system becomes well developed downstream down to the coastline. The natural boundaries of the system eastward and southward can be identified in the Piave River and the Brenta, Bacchiglione, and Adige Rivers, respectively (Fig. 1).

A regional geologic reconstruction of the six pumped aquifers and the intervening aquitards has been made on the basis of a number of available stratigraphic sections (Fig. 1) obtained from many artesian wells scattered over the area (Carbognin *et al.*,

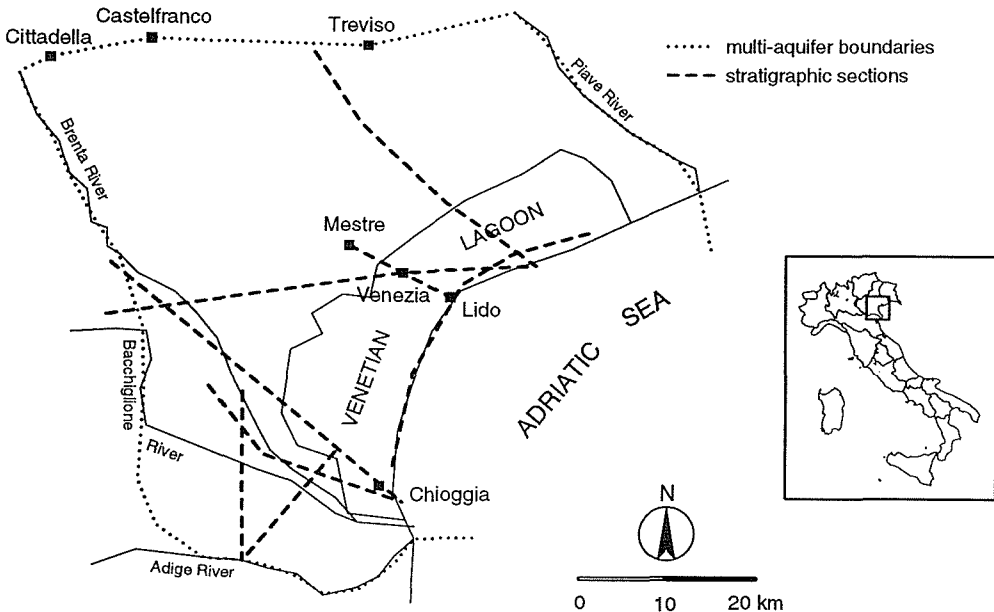


Fig. 1 Map of the Venice Lagoon and inland area with the natural boundaries of the Venice multi-aquifer system and the trace of the available stratigraphic cross-sectional profiles.

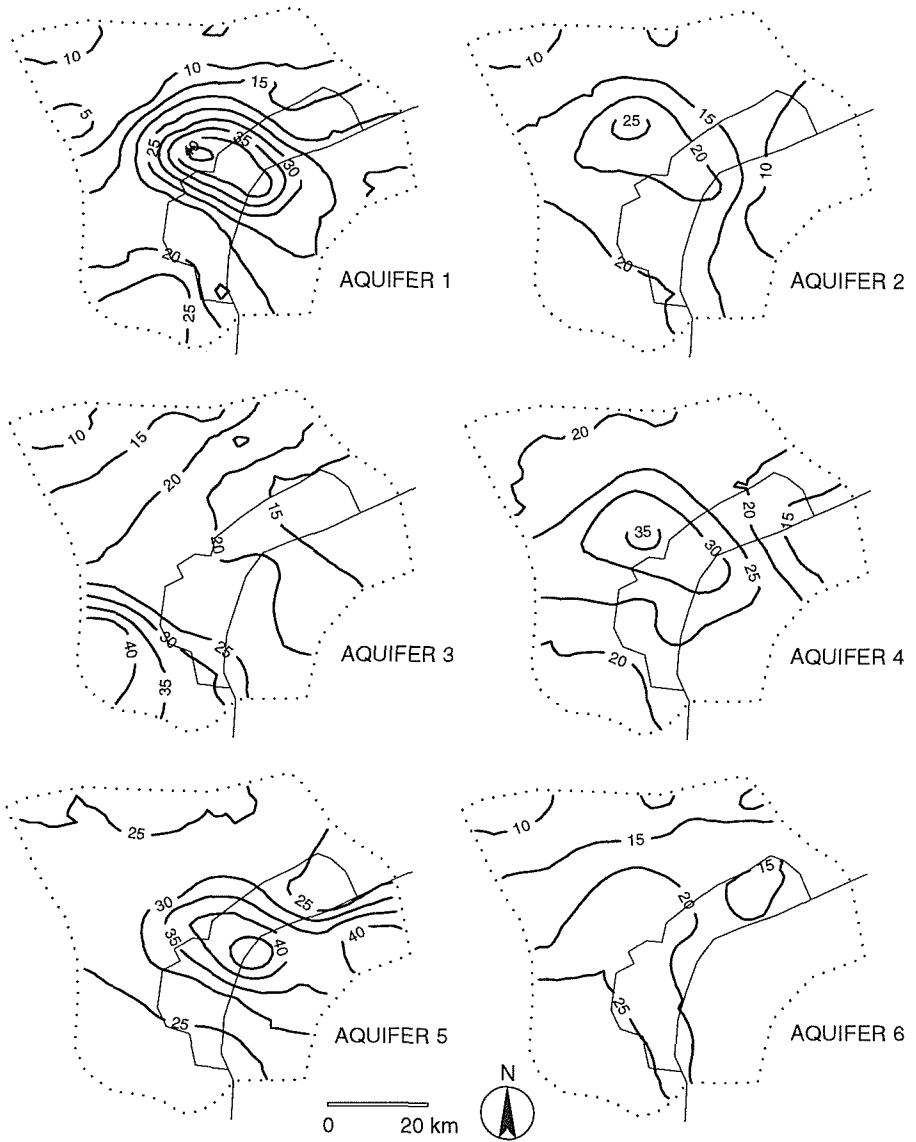


Fig. 2 Contour lines of equal thickness (m) for the main pumped aquifers underlying the Venice Lagoon.

1974; Gatto, 1974; Regione Veneto, 1984) and from the accurate lithologic profile of a deep test hole drilled in Venice at Tronchetto (CNR, 1971). Unfortunately, these cross-sectional profiles are not always equally reliable or detailed, and in particular close to the recharge area an accurate characterization of the layering proves rather difficult. However, on the basis of these data it is possible to obtain a working 3-D geologic configuration at a regional scale. Using a bilinear interpolation procedure, maps of thickness and top and bottom depth of each formation have been drawn and used in the simulations. As an example, Fig. 2 shows the contour lines of equal thickness for the six pumped aquifers.

As far as the physical properties of the formations are concerned, the data are rather sparse. If some new data on aquifer hydraulic transmissivity T are provided by recent pumping tests performed in 1994 in the lagoon area (Di Molfetta, 1992; Tosi, 1994), values of the bulk specific weight γ , the aquitard hydraulic conductivity K_z and the porosity n are taken from the laboratory tests executed in the early 1970s on the core samples from the Tronchetto bore hole and used already in the model of Gambolati *et al.* (1974). A recent analysis of consolidation results performed on the aquitard clay samples provides new indications on the compression and re-compression indices (C_c and C_s , respectively) needed for the nonlinear simulation of the aquitard behaviour.

NONLINEAR FINITE ELEMENT MODELS

The mathematical model presented in this communication to simulate groundwater flow, sediment compaction and land subsidence at a regional scale is based on a quasi-three-dimensional approach for flow and makes use of a one dimensional vertical consolidation model, combining Terzaghi's effective stress concept and empirical constitutive relationships for soil behaviour.

Quasi 3-D nonlinear flow model

The hydrologic response of a multi-aquifer system to pumping is highly dependent on the difference between the physical parameter values of sandy and clayey layers. When a high contrast in hydraulic conductivity exists, water flow can be assumed essentially horizontal in the aquifers and vertical in the aquitards. Quasi-three-dimensional models rely on the assumption that flow conforms with this pattern.

Neglecting point and distributed sources, the governing flow equation in the i th aquifer confined between aquitards j and $j + 1$ can be written as:

$$\frac{\partial}{\partial x} \left[T_{xi} \frac{\partial h_i}{\partial x} \right] + \frac{\partial}{\partial y} \left[T_{yi} \frac{\partial h_i}{\partial y} \right] = S_i \frac{\partial h_i}{\partial t} + q_j - q_{j+1} \quad (1)$$

where T_{xi} , T_{yi} , S_i indicate the components of the anisotropic transmissivity and the elastic storage coefficient, respectively, h_i is the hydraulic potential head, t is time, and q_j , q_{j+1} represent distributed sources accounting for leakage from the overlying and underlying aquitards.

Vertical flow in the aquitard j is governed by the diffusion equation:

$$\frac{\partial}{\partial z} \left[K_{zj}(n) \frac{\partial h_j}{\partial z} \right] = S_{sj}(n, \sigma') \frac{\partial h_j}{\partial t} \quad (2)$$

where $K_{zj}(n)$ is the vertical permeability given as a function of porosity n , $S_{sj}(n, \sigma')$ is the specific elastic storage related to n and to effective intergranular stress σ' .

Equations (1) and (2) are solved numerically by the finite element method upon discretization of the aquifers into triangles and the aquitards into one-dimensional elements. Figure 3 shows the 3-D grid of the Venetian multi-aquifer system used in the simulations. Each aquifer is composed of 1158 triangles with 608 nodes and each

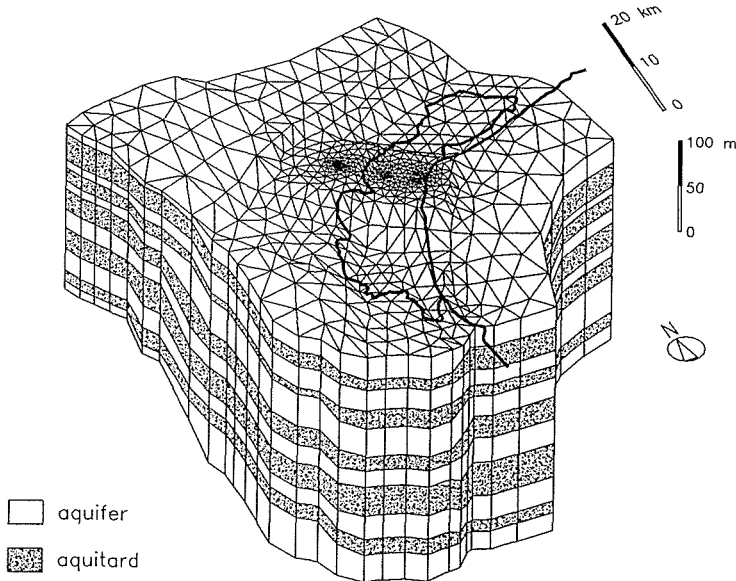


Fig. 3 Perspective three-dimensional view of the regional finite element model used to simulate the groundwater flow in the Venice multi-aquifer system.

aquitard column is discretized into six linear elements. The total number of nodes is 18 848.

Coupling together equations (1) and (2) by the continuity requirement of hydraulic head and water flux at the aquifer-aquitard interface, and applying the Crank-Nicolson scheme for the integration in time, yields a large sparse system of nonlinear equations, as K_{zj} and S_{sj} are both dependent on hydraulic head h_j . Given the initial permeability value, K_{z0} , and the initial porosity, n_0 , and evaluated the effective intergranular stress at the point of interest by Terzaghi's law, the empirical nonlinear relationships relating the hydrogeological parameters to σ' ($> \sigma'_{pre}$), are (Rivera *et al.*, 1991):

$$n = n_0 - 0.434C_c(1 - n)^2 \frac{d\sigma'}{\sigma'} \tag{3}$$

$$K_z(n) = K_{z0} \left[\frac{n(1 - n_0)}{n_0(1 - n)} \right]^m \tag{4}$$

$$S_s(n, \sigma') = \gamma_w \left[0.434C_c \frac{1 - n}{\sigma'} + n\beta_w \right] \tag{5}$$

where m is a material-dependent coefficient, γ_w and β_w are the specific weight and the compressibility of water and C_c must be replaced by C_s whenever in expansion $\sigma' < \sigma'_{pre}$.

The nonlinearity of equations (1) and (2) is solved by an original solution strategy developed by Gambolati & Teatini (1994, 1995). The procedure, as naturally suggested by the structure of the multi-aquifer system that yields a block-tridiagonal coefficient matrix, can be shown to be equivalent to a block iterative Gauss-Seidel procedure and

hence generalized into a block SOR scheme with the numerical assessment of an optimal over-relaxation factor ω_{opt} .

1-D nonlinear compaction model

When the head changes Δh occurred in the time step Δt have been computed, land sinking during Δt can be evaluated as the sum of the compaction of the individual elemental layers using the equation ($\sigma' > \sigma'_{pre}$) (Gambolati, 1973):

$$\eta(\Delta t) = \sum_{j=1}^N \sum_{k=1}^M 0.434 \gamma_w (1-n) \frac{C_c}{\sigma'} \Delta h_{k,j} \Delta b_{k,j} \quad (6)$$

where N is the number of aquitards and M the number of vertical elements into which each aquitard is discretized, while $\Delta b_{k,j}$ is the thickness of the k th finite element of the j th aquitard.

MODEL CALIBRATION

The calibration of the nonlinear model has been performed against the past available records of hydraulic head and land subsidence from 1930 to 1973.

Assuming that top and bottom of the multi-aquifer system are impervious, and boundary conditions of principal type (mean sea level along the seaward boundary, ground elevation along the recharge boundary and average water level along the stream boundaries), and adjusting by a trial and error procedure the parameter estimates obtained from the in situ and laboratory measurements, the flow model has been

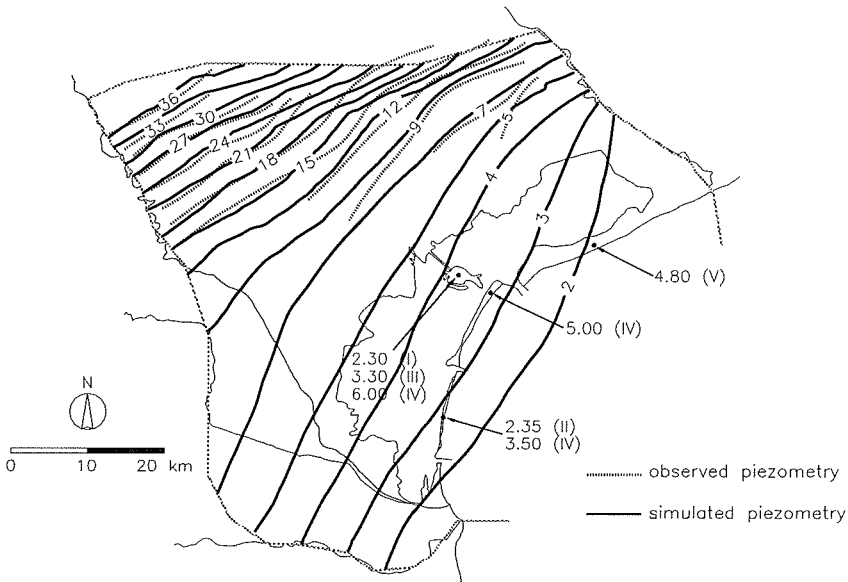


Fig. 4 Average hydraulic head (m a.m.s.l.) in the Venice system in 1930 before pumping as reconstructed on the basis of the observed piezometry (Mozzi *et al.*, 1975; Serandrei-Barbero, 1972) and provided by the flow model.

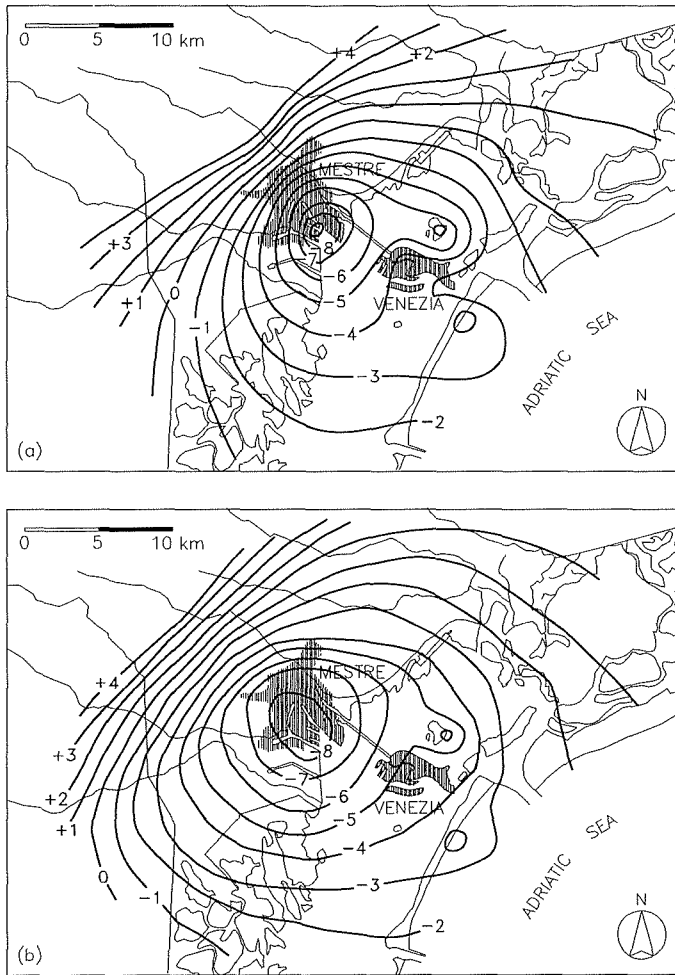


Fig. 5 Contour lines of equal hydraulic head (m a.m.s.l.) in the 4th Venetian aquifer in 1973 (a) as reconstructed on the basis of the observed piezometry (Volpi *et al.*, 1979) and (b) as provided by the flow model.

validated so as to reproduce the piezometric head before the inception of water production (Fig. 4) and the historical piezometric decline in 1973 in each aquifer unit. As an example, Fig. 5 shows the groundwater contour lines in the 4th aquifer in 1973 as reconstructed by stochastic interpolation of the observed data (Volpi *et al.*, 1976) and as provided by the model. The match is considered to be very satisfactory.

Concerning the nonlinear simulation of land subsidence, only some preliminary results are shown using in each aquitard the same spatial discretization as the flow model (six vertical elements) and making use of equation (6).

The validation of the compaction model has been made for the period 1952-1973, since the periodic geodetic surveys started in 1952. Figure 6(a) shows the outcome of the model presented as contour lines of equal subsidence in the region of interest. Figure 6(b) shows the comparison of the simulated and observed land sinking along the levelling profile which connects Mestre-Venice-Lido. The agreement between the model

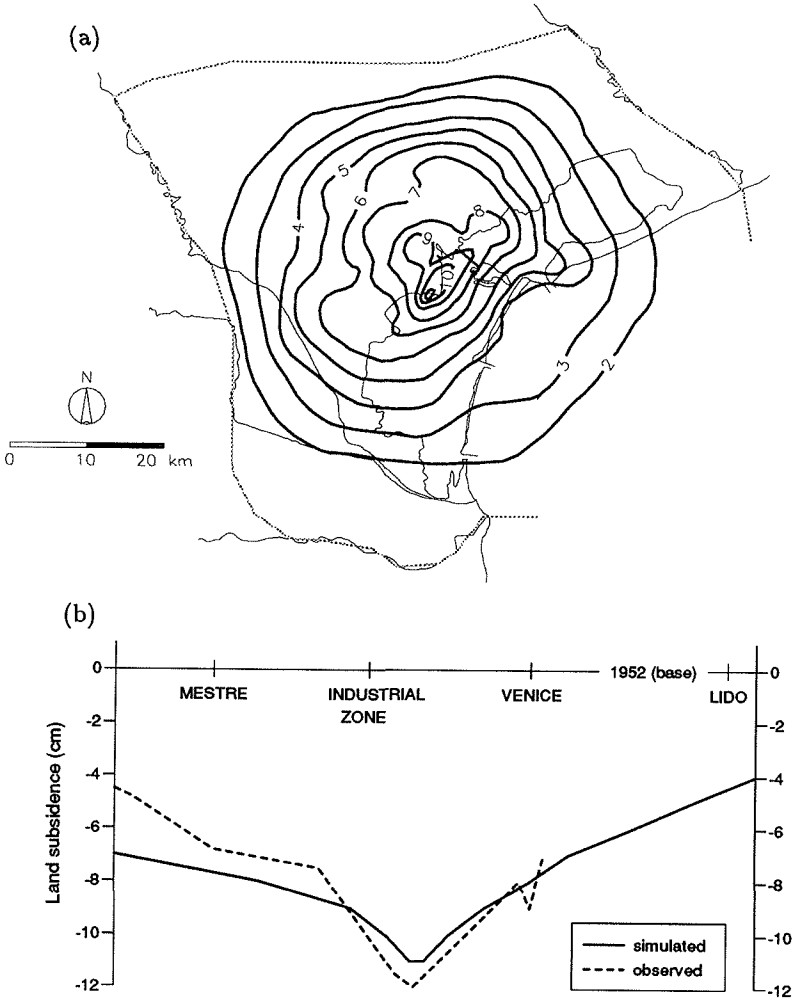


Fig. 6 (a) Contour lines of equal land sinking (cm) in the Venice area between 1952-1973 as provided by the numerical model, and (b) comparison between the simulated and the observed subsidence along the leveling profile which connects Mestre-Venice-Lido for the same period.

results and the measured values is considered to be quite good in the lagoon area, while in the inland zone some difference results which is related to the fact that the compression indices obtained from the softer Venice clay units have been extended to the mainland area.

CONCLUSION

A new quasi 3-D flow model has been developed for the multi-aquifer system underlying the Venice Lagoon. The model implements an updated reconstruction of the geology with variable thickness for the pumped aquifers and a nonlinear relationship for the

hydraulic as well as the mechanical behaviour of the aquitard formations. The solution is obtained using finite elements and an accelerated block over-relaxation procedure. The calibration of the model, which is performed over the period 1930-1973, shows a good agreement between the simulated and the observed piezometry before the inception of pumping, and the drawdown and land subsidence over the lagoon area in 1973 when the cone of depression achieved the maximal extent.

Acknowledgement This work was developed in the CNR project "Sistema Lagunare Veneziano", Linea di Ricerca 2-7, U.O. 1-2.

REFERENCES

- Carbognin, L., Gatto, P. & Mozzi, G. (1974) Situazione idrogeologica del sottosuolo di Venezia – ricostruzione degli acquiferi soggetti a sfruttamento sulla base dei dati relativi ai pozzi artesiani (Hydrogeologic configuration of Venice subsurface system – pumped aquifer reconstruction based on the artesian wells) (in Italian). *Tech. Report no. 32, CNR, ISDGM, Venezia*.
- Carbognin, L., Gatto, P., Mozzi, G., Gambolati, G. & Ricceri, G. (1977) New trend in the subsidence of Venice. In: *Land Subsidence* (Proc. 2nd Int. Symp. on Land Subsidence, Anaheim, December 1976), 65-81. IAHS Publ. no. 121.
- CNR (1971), Relazione sul pozzo VE1 CNR (Report on the VE1 CNR bore hole) (in Italian). *Tech. Reports no. 14-21, CNR, ISDGM, Venezia*.
- Di Molfetta, A. (1992) Determinazione della trasmissività degli acquiferi mediante correlazione con la portata specifica (Aquifer transmissivity determination by correlation with specific pumping rate) (in Italian). *Ingegneria e Geologia degli Acquiferi* **1**, 81-86.
- Gambolati, G. (1973) Equation for one-dimensional vertical flow of groundwater. 2. Validity range of the diffusion equation. *Wat. Resour. Res.* **9**, 1385-1395.
- Gambolati, G. & Freeze, R. A. (1973) Mathematical simulation of the subsidence of Venice. 1. Theory. *Wat. Resour. Res.* **9**, 721-733.
- Gambolati, G., Gatto, P. & Freeze, R. A. (1974) Mathematical simulation of the subsidence of Venice. 2. Results. *Wat. Resour. Res.* **10**, 563-577.
- Gambolati, G. & Teatini, P. (1994) Block iterative strategies for multiaquifer flow model. In: *Proc. Symp. on Advanced Methods for Groundwater Pollution Control* (Udine, Italy). Springer-Verlag. In press.
- Gambolati, G. & Teatini, P. (1995) A block iterative finite element model for non-linear aquifer systems. Accepted for publication in *Wat. Resour. Res.*
- Gatto, P. (1974) Ricostruzione litostratigrafica del sottosuolo della zona di Venezia sulla base della documentazione delle 120 serie stratigrafiche (Lithostratigraphic reconstruction of the Venice subsurface system on the basis of 120 selected lithostratigraphies) (in Italian). *Tech. Report no. 33, CNR, ISDGM, Venezia*.
- Mozzi, G., Benini, G., Carbognin, L., Gatto, P. & Masutti, M. (1975) Situazione idrogeologica del comune di Venezia – Evoluzione delle pressioni di strato negli acquiferi artesiani (Hydrogeologic configuration in the Venice area – piezometric head behavior of the artesian aquifers) (in Italian). *Tech. Report no. 66, CNR, ISDGM, Venezia*.
- Regione Veneto (1984) *Carta Regionale delle Acque* (Regional map of groundwater) (in Italian). Giunta Regionale, Segreteria Regionale del Territorio, Venezia.
- Ricceri, G. & Butterfield, R. (1974) An analysis of compressibility data from a deep bore hole in Venice. *Geotechnique* **24**(2), 175-192.
- Rivera, A., Ledoux, E. & de Marsily, G. (1991) Non-linear modeling of groundwater flow and total land subsidence of Mexico-City aquifer-aquitard system. In: *Land Subsidence* (ed. by A. I. Johnson) (Proc. 4th Int. Symp. on Land Subsidence, Houston, May 1991), 45-58. IAHS Publ. no. 200.
- Serandrei-Barbero, R. (1972) Indagine sullo sfruttamento artesiano nel comune di Venezia, 1846-1970 (Research on the artesian exploitation in the Venice area, 1846-1970) (in Italian). *Tech. Report no. 31, CNR, ISDGM, Venezia*.
- Tosi, L. (1994) Caratteristiche idrogeologiche degli acquiferi sfruttati nel comprensorio lagunare. Valutazione sperimentale delle caratteristiche di trasmissività. (Hydrogeologic features of the lagoon pumped aquifers. Experimental estimation of transmissivity) (in Italian). *Tech. Report no. 189, CNR, ISDGM, Venezia*.
- Volpi, G., Gambolati, G., Carbognin, L., Gatto, P. & Mozzi, G. (1979) Groundwater contour mapping in Venice by stochastic interpolators. 2. Results. *Wat. Resour. Res.* **15**(2), 291-297.

Prediction of future land subsidence in Kerman, Iran, due to groundwater withdrawal

**MOHAMMAD MOHSEN TOUFIGH &
BEHNAM SHAFIEI SABET**

University of Kerman, Department of Civil Engineering, Iran

Abstract The relationship between land subsidence and water level decline caused by groundwater withdrawal in Kerman province, Iran, due to pistachio farming has been investigated by many researchers since 1992. The scope of this work is to examine the previous subsidence and predict the future subsidence. A detailed mathematical model of the actual land subsidence in Kerman is constructed for analysis. This fully coupled finite element consolidation model simulates the subsidence and the continuous piezometric decline of the area. The simulation is comprised of a 3-D flow model for resulting water pressure distribution at each time step. There is good correspondence between the finite element analysis and the actual field data.

INTRODUCTION

Land subsidence in Kerman province in Iran has become a major problem for pistachio farmers. The earth fissures and differential settlement causes them huge water losses. This land subsidence is due to consolidation of soil layers caused by extensive groundwater withdrawal. Subsidence in Kerman was first reported by Kerman Regional Water Board in 1980. A semi-complete field investigation was first undertaken by Rahmanian (1986). His results shows that in the Rafsanjan region subsidence and earth fissures were related only to the heavy pumping of groundwater and subsequent continuous decline in the water table. Up to now no one studied the prediction and simulation of settlement in the region. In order to simulate and predict such phenomenon in a given aquifer, the authors used an axisymmetric fully coupled finite element model based on Biot's three-dimensional consolidation theory. This model is capable of predicting the settlement as the water table continues to decline.

FINITE ELEMENT FORMULATION

The basic formulation presented here is based on Biot's consolidation theory. In Biot's consolidation theory the soil skeleton is assumed to be a porous elastic solid and the laminar pore fluid is coupled to the solid by the conditions of compressibility and continuity. While water is pumping from the aquifer through wells, both radial and axial flows are symmetric in term of longitudinal direction. Thus Biot's governing equation is given by:

$$c_r \left[\frac{\partial^2 u_e}{\partial r^2} + \frac{1}{r} \frac{\partial u_e}{\partial r} \right] + c_z \frac{\partial^2 u_e}{\partial z^2} = \frac{\partial u_e}{\partial t} - \frac{\partial p}{\partial t} \tag{1}$$

where u_e is the excess pore water pressure, p is the mean total stress, z and r are the longitudinal and radial directions, t is the time and c_r, c_z are the coefficient of consolidation in the radial and longitudinal directions, respectively (Smith & Griffiths, 1992).

When discretization and the Galerkin process are completed, equations of equilibrium, stress-strain and continuity lead to (Lewis & Schrefler, 1987):

$$\begin{aligned} KM r + C u_e &= F \\ C^T \frac{dr}{dt} - K P u_e &= 0 \end{aligned} \tag{2}$$

where, for an element with four nodes:

$$r = \{u_1, v_1, u_2, v_2, u_3, v_3, u_4, v_4\}^T, \quad u_e = \{u_{e1}, u_{e2}, u_{e3}, u_{e4}\}^T \tag{3}$$

and u, v are the displacement in r and z direction, respectively. KM is the elastic matrix and is:

$$KM = \int \int B^T D B r dr dz \tag{4}$$

where, $B = AN$ and N is the vector of shape function, and

$$A = \begin{pmatrix} \frac{\partial}{\partial r} & 0 \\ 0 & \frac{\partial}{\partial z} \\ \frac{\partial}{\partial z} & \frac{\partial}{\partial r} \\ \frac{1}{r} & 0 \end{pmatrix} \tag{5}$$

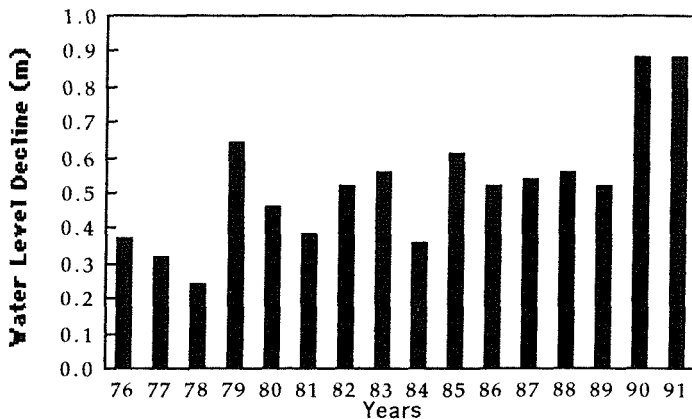


Fig. 1 Histogram of mean water table decline in Rafsanjan.

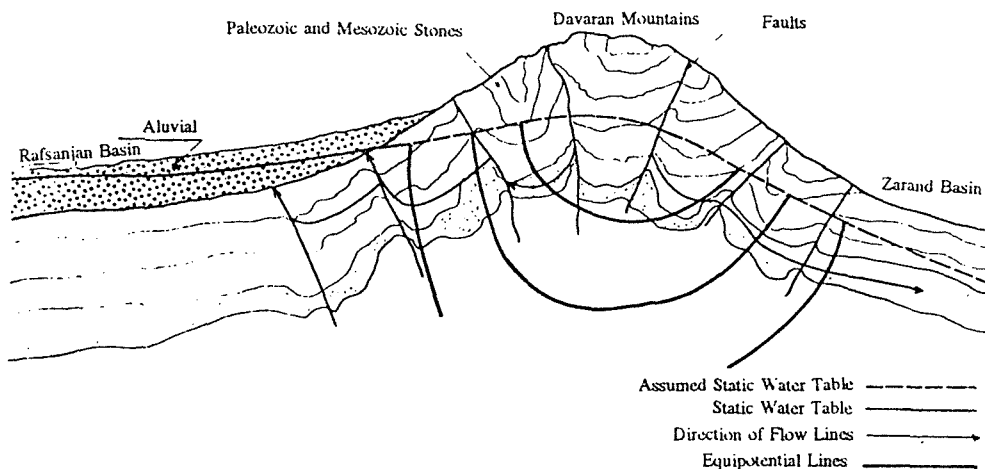


Fig. 2 Geological section of Rafsanjan basin.

and KP is the fluid stiffness matrix, which is:

$$KP = \int \int (c_r \frac{\partial N_i}{\partial r} \frac{\partial N_j}{\partial r} + c_z \frac{\partial N_i}{\partial z} \frac{\partial N_j}{\partial z}) r dr dz \quad (6)$$

and C is a rectangular coupling matrix, and F is the external loading vector.

There are many methods available to integrate equation (2) with respect to time, but the simplest linear interpolation with respect to time using finite differences was considered here.

FIELD DATA

Data that have been used for this study were collected and interpolated from Kavab (1992) & Rahmanian (1986) for Rafsanjan basin. The recorded decline of water table level from piezometric wells in the whole of the Rafsanjan basin are shown in Fig. 1.

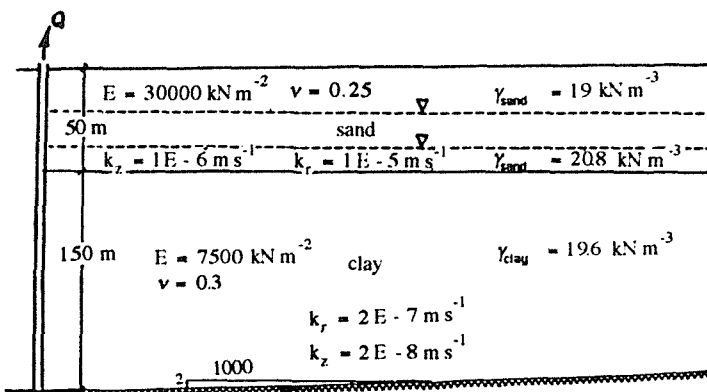


Fig. 3 Typical Rafsanjan soil profile and soil properties.

It can be seen that water decline in 1991 was about 0.88 m. These piezometric wells are at locations where the soil thickness is not maximum. But in the centre of the basin the recorded water table decline is about 22 m for the 21-year period; which is more than one metre per year. Figure 2 shows a typical geological section of the Rafsanjan basin. The settlement of the ground surface recorded at the centre of the basin was about 10 cm (Rahmanian, 1994). The method of measuring was based on well casing growth and field observations at several locations. The soil profile properties such as layer thickness, saturated density, elasticity parameters, and axial and radial permeability are summarized in Fig. 3. Since there are more than one thousand wells which are continuously pumping in the region, for modelling it is assumed that the water table is declining at a rate of 105 cm year⁻¹ just next to each well, and 95 cm year⁻¹ at a distance of 1 km from each well with hydraulic gradient of 0.0001.

NUMERICAL RESULTS

Based on finite element formulation, a computer program was developed to predict and examine various soil behaviours and conditions. Different ways of water table decline can be analysed by this program. Figure 4 shows finite element discretization used for mathematical modelling of the soil profile. Computer analysis results of land subsidence *vs.* time at different distances from the pumping station is shown in Fig. 5. Since the water table is dropping continuously, this can create additional load every time step in computation which is affecting the future consolidation of the layers. It can be clearly seen in this figure that the rate of settlement increases with time. This differential settlement caused earth fissures and shear failure zones in the basin. It should be noted that this conclusion can only be drawn by using Biot's three-dimensional consolidation theory. Figure 6 shows the results of subsidence rate *vs.* time at different distances from the well. It can be seen that the settlement rate near the pumping station is higher than at other locations. This is mainly due to faster drainage near the well casing which causes more settlement. This analysis can be confirmed by field data that after 20 years of pumping, the measured rate of settlement at the well is about 10 cm which equivalent to numerical analysis as shown in Fig. 6 for the year 1995. By using these analyses it is possible to predict the total settlement and rate of settlement for the next 10 years. In

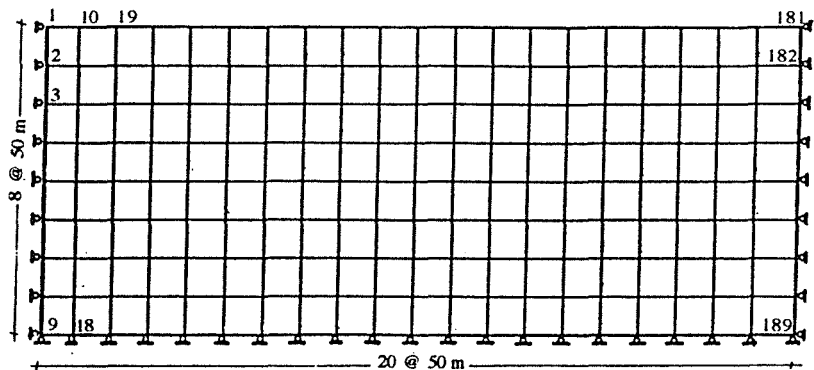


Fig. 4 Finite element discretization.

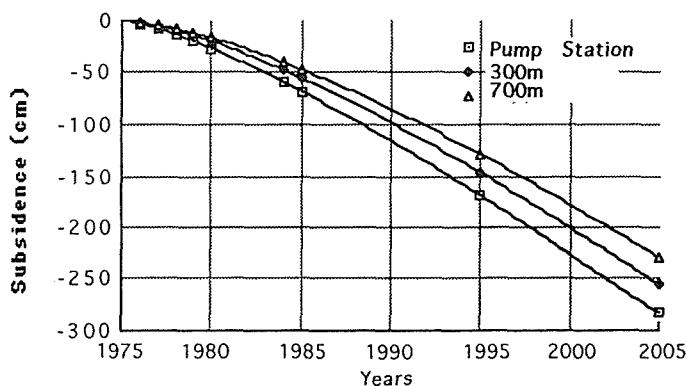


Fig. 5 Subsidence vs. time at a pumping station, 300 and 700 m from the centre of the model.

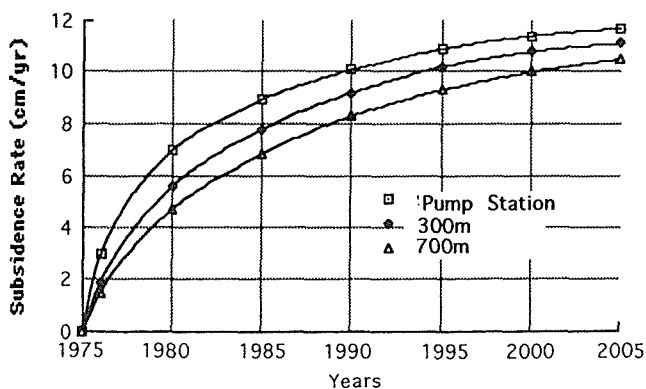


Fig. 6 Subsidence rate vs. time at a pumping station, 300 and 700 m from the centre of the model.

the year 2005 if the water table keeps dropping at the current rate, the total settlement will be about 260 cm and the rate of settlement will be around 12 cm year^{-1} (Shafiei, 1995).

REFERENCES

- Kavab (1992) *Optimum Usage of Rafsanjan Groundwater*, vol. 2. Kerman Regional Water Board.
- Lewis, R. W. & Schrefler, B. A. (1987) *The Finite Element Method in the Deformation and Consolidation of Porous Media*. John Wiley, Chichester, UK.
- Rahmanian, D. (1994) Land subsidence in Kerman due to pumping of groundwater. *Mahab Ghods Consulting Company Report*.
- Rahmanian, D. (1986) Land subsidence and earth fissures due to groundwater withdrawal in Kerman. *J. Water* 6.
- Reddy, J. N. (1984) *An Introduction to the Finite Element Method*. McGraw-Hill, New York.
- Shafiei, B. (1995) Modelling of land subsidence due to lowering of the groundwater level. Master's Degree Thesis Submitted to Dept. of Civil Engng, Univ. of Kerman.
- Smith, I. M. & Griffiths, D. V. (1992) *Programming the Finite Element*, 2nd edn. John Wiley, Chichester, UK.

Predicting land subsidence with a constant-parameter coupled model for groundwater flow and aquitard compaction: the Markerwaard case

TIANFU XU

Universidad de La Coruña, Escuela Técnica Superior de Ingenieros de Caminos, Canales y Puertos, Campus de Elviña s/n, E-15192 La Coruña, Spain

JAC A. M. VAN DER GUN

TNO Institute of Applied Geoscience, PO Box 6012, 2600 JA Delft, The Netherlands

Abstract A constant-parameter coupled model for groundwater flow and aquitard compaction, based on MODFLOW and a special compaction-related IBS module, is used in this paper to predict land subsidence that would occur as a consequence of reclaiming the Markerwaard Polder in The Netherlands. The same case has been analyzed previously in an uncoupled approach, but taking into account stress-dependency of geotechnical parameters. Comparing the new model output with the previous results enables conclusions to be drawn for this particular case regarding the importance of a coupled modelling approach, and regarding the errors made when using constant geotechnical parameters instead of stress-dependent ones. Analysing the performance of the MODFLOW-IBS modelling approach in this case may help appreciate the advantages of a coupled modelling approach and understand under which conditions it is still acceptable to use constant parameters, given a certain accuracy required.

NOTATION

C	compression coefficient, dimensionless
C_c	compression index, dimensionless
C_r	recompression index, dimensionless
e	void ratio, dimensionless
e_0	initial void ratio, dimensionless
g	gravitational acceleration, m s^{-2}
K_{xx}, K_{yy}, K_{zz}	hydraulic conductivity, m s^{-1}
n	porosity, dimensionless
N	source or sink term, s^{-1}
p	hydraulic pressure, Pa
S_s	specific storage coefficient of aquifer, m^{-1}
S_{sk}	specific storage coefficient of interbeds or confining bed, m^{-1}
S_{ske}	elastic S_{sk} , m^{-1}
S_{skv}	inelastic S_{sk} , m^{-1}
t	time, s

x,y,z	spatial coordinates, m
α	volume compressibility, Pa ⁻¹
γ	specific weight, kN m ⁻³
ϕ	hydraulic head, m
ρ	density of water, kg m ⁻³
σ	geostatic pressure, Pa
σ_s	effective stress, Pa
σ_{s0}	initial effective stress, Pa
σ_{s1}	terminal effective stress, Pa
$\Delta\sigma_s$	increment of effective stress, Pa

INTRODUCTION

During the twentieth century considerable parts of Lake Yssel (the former Zuiderzee) in The Netherlands were reclaimed and converted to "new" polderlands, with surface levels a few metres below mean sea level. These projects had a significant impact on the groundwater flow regimes in the adjacent "old land" zones, because keeping the polders dry means a permanent change of boundary conditions to the regional groundwater flow systems. The idea of a possible reclamation of part of the remaining smaller Lake Yssel – which would create the Markerwaard Polder – was studied during the 1980s. Among the studies carried out was a prediction of the land subsidence to be expected in the westward bordering land in the province of Noord-Holland. This prediction was done by first running a groundwater model to predict the changes in hydraulic head (Hebbink & Schultz, 1983), and afterwards using these outputs as an input to a compression model (Delft Geotechnics, 1983).

The flow of groundwater and the compression of layers of peat, clays and silts in response to changing hydraulic heads are coupled processes. Hence, it seems to be preferable to simulate them in a coupled model, rather than simulating flow/piezometry and compression sequentially as mentioned above. In an attempt to obtain a more clear idea of the possible merits of a coupled model, the model prediction done in the past was repeated with an extended version of the well-known groundwater model code MODFLOW, incorporating a so-called Inter Bed Storage Module (IBS) to take care of partly irreversible sediment compression and associated groundwater fluxes. The IBS module used has the limitation that it considers only stress-independent geotechnical parameters ("constant parameters").

The Interbed Storage Package used (IBS1) was originally developed to account for compaction of "interbeds" or lenticular compressive intercalations inside aquifers (Leake & Prudic, 1988). In this paper it is used to simulate compaction of a continuous confining bed. The flow equation as ordinarily used by MODFLOW (McDonald & Harbaugh, 1988):

$$\frac{\partial}{\partial x}(K_{xx} \frac{\partial \phi}{\partial x}) + \frac{\partial}{\partial y}(K_{yy} \frac{\partial \phi}{\partial y}) + \frac{\partial}{\partial z}(K_{zz} \frac{\partial \phi}{\partial z}) + N = S_s \frac{\partial \phi}{\partial t} \quad (1)$$

assumes specific storativity (S_s) to be constant in time, except for the case where a confined aquifer becomes unconfined (or *vice versa*). To account for changes in storage caused by compaction of interbeds or confining beds, an additional term has to be added to the right-hand side of the equation. This term can be expressed as:

$$q_i = S_{sk} \frac{\partial \phi}{\partial t} \quad (2)$$

Equation (2) represents an average flow into or out of storage per unit volume of interbed or confining bed and per unit of time. The specific storage value S_{sk} in Equation (2) varies between an "elastic" and an "inelastic" value depending on the relation of the current hydraulic head to the preconsolidation head. The preconsolidation head can also change during the simulation as the model updates it.

Comparing the output of the new model with the previous results allows conclusions to be drawn for this particular case regarding the importance of a coupled modelling approach, and regarding the errors made when using constant geotechnical parameters instead of stress-dependent ones.

Prediction of land subsidence is confined to part of the province of Noord-Holland, in a belt along the western boundary of the projected Markerwaard polder, because it is there where this new polder is expected to produce significant impacts in terms of land subsidence.

GEOHYDROLOGICAL SETTING AND MODEL SCHEMATIZATION

The study area is underlain by a thick sequence of Quaternary unconsolidated deposits, in an alternation of highly permeable aquifer beds and less permeable aquitards. One of the aquitards forms the top of the system; it is continuous and consists of Holocene sediments. Two semi-continuous aquitards divide the sandy Pleistocene sediments below this Holocene cover into three separate aquifer units. Geometric and hydraulic characteristics of the individual layers are summarized in Fig. 1.

Figure 1 shows the MODFLOW schematization as well: it distinguishes five model layers. The two aquitards dividing the Pleistocene sands into three aquifers are assumed to be able to transmit water, but their capacity to store or release water is considered negligible. For the second model layer (Holocene deposits), on the contrary, change of storage is explicitly taken into account in the model, for reasons mentioned below.

Polder water levels form an upper boundary condition to the system. In the projected Markerwaard zone they are assumed to drop from some 0.25 m below N.A.P. initially (before reclamation) to 6.5-4.5 m below N.A.P. after the polder reclamation would have taken place (see Figs 2 and 3). For simplicity, it is assumed that this drop will take place instantaneously. The drop in polder level will influence the piezometric levels in the Quaternary sediments below, and the effect will spread laterally from the Markerwaard zone towards the surrounding areas (under which the Noord-Holland zone considered). The Pleistocene aquifer complex is underlain by clay, which in the model is assumed to be impervious. The model area chosen is large enough to assume constant-head lateral boundary conditions. It measures 60 km from east to west and 54 km from north to south. The number of model cells used is 2208.

GEOTECHNICAL FEATURES AND SCHEMATIZATION

Preliminary investigations have made plausible that more than 90% of the sediment compaction to be expected in Noord-Holland as a result of polder reclamation will take

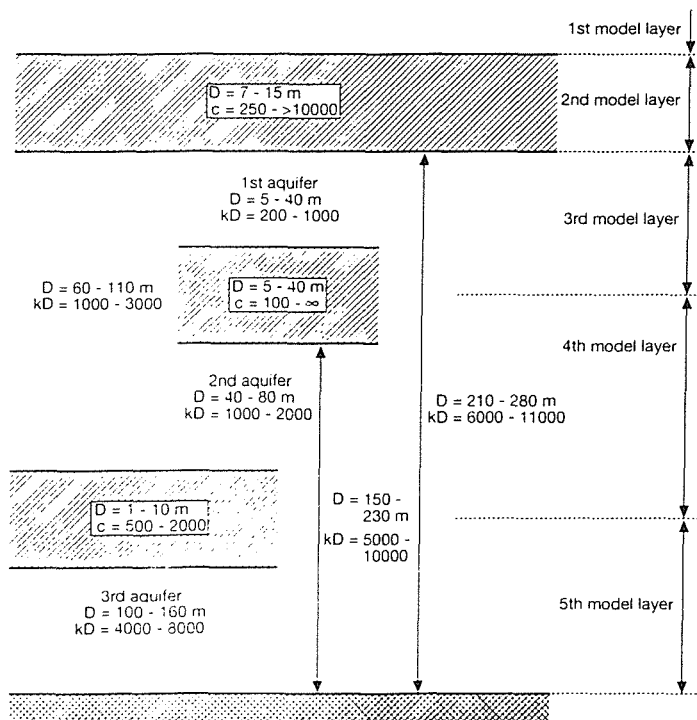


Fig. 1 Sketch of the geohydrological framework and model schematization.

place in the Holocene cover (model layer 2). This is because this layer contains highly compressible clays and peat, and the anticipated relative changes in effective stress are much greater there than at greater depths. The compression of the other aquitards is expected to be insignificant compared to that of the Holocene layer. Hence, the model developed focuses on deformation of the confining Holocene layer only, in the before-mentioned zone in the province of Noord-Holland.

The Holocene deposits belong all to the Westland Formation, which includes from bottom to top the following genetically and lithologically distinct sublayers:

- layer 1: base peat: a thin layer of compact peat;
- layer 2: a sand deposit ("sand"), with intercalated clay lenses;
- layer 3: a clay deposit with little silt and gravel ("middle clay");
- layer 4: "Holland peat", a thick compressible peat layer;
- layer 5: a clay cover ("top clay").

The lateral variation of the Holocene series is great, with variable occurrence and thickness of the different sublayers, which makes the Holocene cover with respect to hydraulic and mechanical properties a highly heterogeneous complex.

Data on the lithology and mechanical characteristics of the Holocene cover, as compiled by Xu (1993), are summarized in Table 1. The observed ranges of depths and of present-day pressures and stresses are presented in Table 2.

The deformation of an aquitard can be simulated in the IBS1 package on the basis of a specific storage coefficient S_{sk} . This coefficient obtains an inelastic value (S_{skv}) or an elastic value (S_{ske}) depending on whether the current effective stress is smaller or

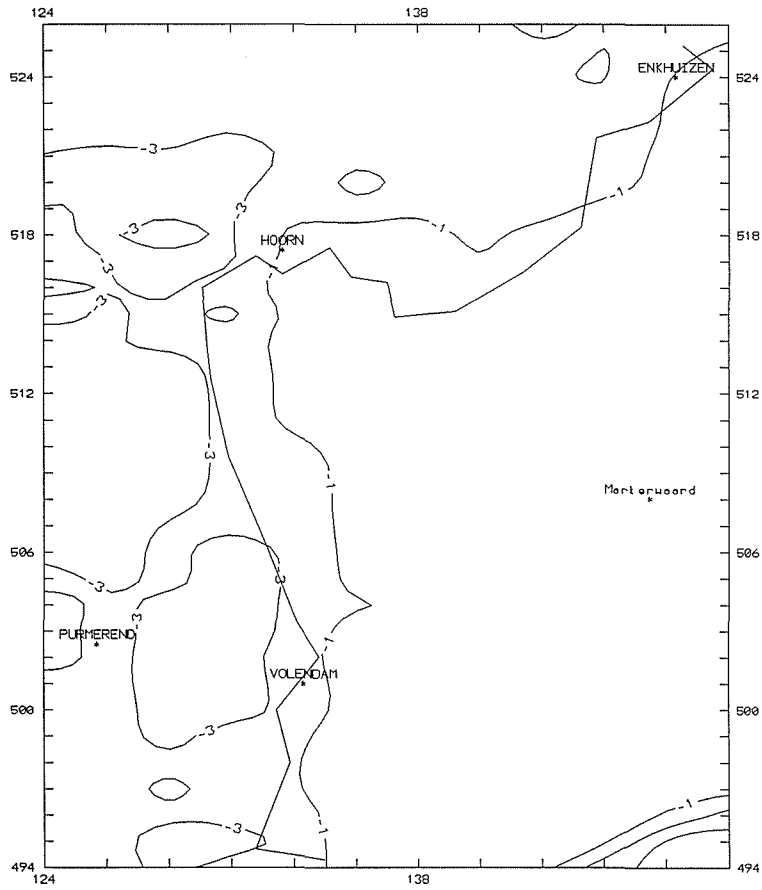


Fig. 2 Polder water level before reclamation.

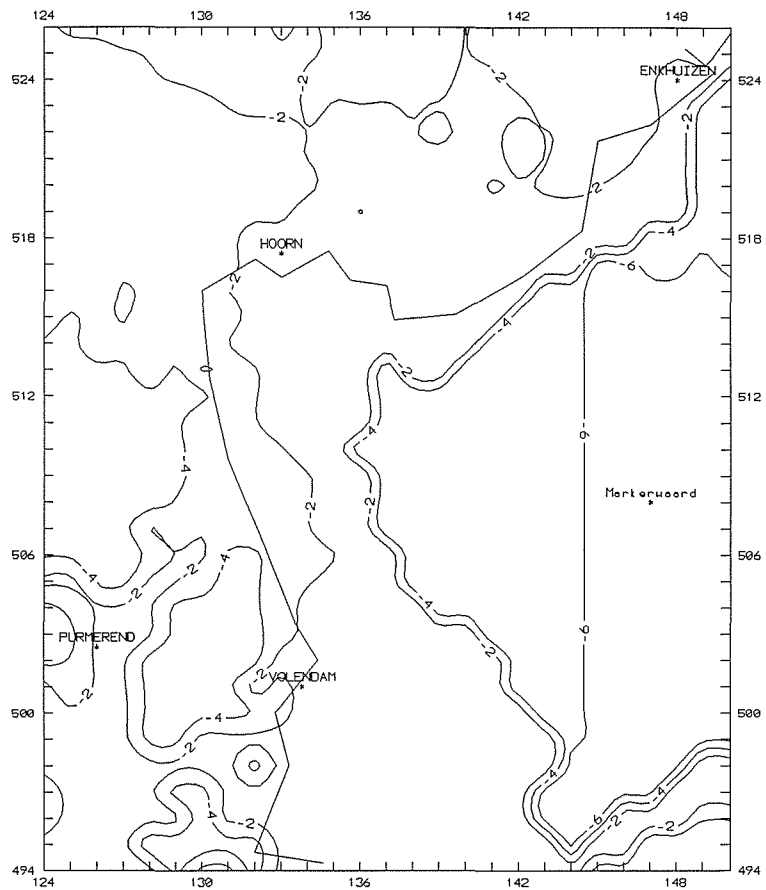


Fig. 3 Polder water level after reclamation.

Table 1 Basic mechanical data of the Holocene sublayers.

Layer	Lithology	ρ (kN m ⁻³)	n	e	Mean e
5	top clay	13-14	0.74-0.80	2.85-4.00	3.42
4	Holland peat	10.6	0.85	5.67	5.67
3	middle clay	14-16	0.62-0.74	1.63-2.85	2.24
2	sand	18-19	0.43-0.50	0.75-1.0	0.88
1	base peat	11.0	0.75	3.00	3.00

Table 2 Ranges of initial geostatic pressure, water pressure and effective stress in the Holocene cover.

Layer	Depth (m - surface)	σ (kPa)	p (kPa)	σ_s (kPa)	Mean σ_s (kPa)
5	0.7-7.8	15-110	0-60	15-50	33
4	0.7-10.4	10-130	0-80	10-50	30
3	1.5-16.2	20-240	0-140	20-100	60
2	4.2-17.1	60-290	20-160	40-130	85
1	8.7-16.3	130-270	75-155	65-115	90

greater than the preconsolidation stress. The specific storage coefficient is related to effective stress as follows (Neuman & Preller, 1982; Leake, 1991):

$$S_{skv} = \frac{C_c \rho g}{2.3(1 + e_0)\sigma_s} \tag{3}$$

$$S_{ske} = \frac{C_r \rho g}{2.3(1 + e_0)\sigma_s} \tag{4}$$

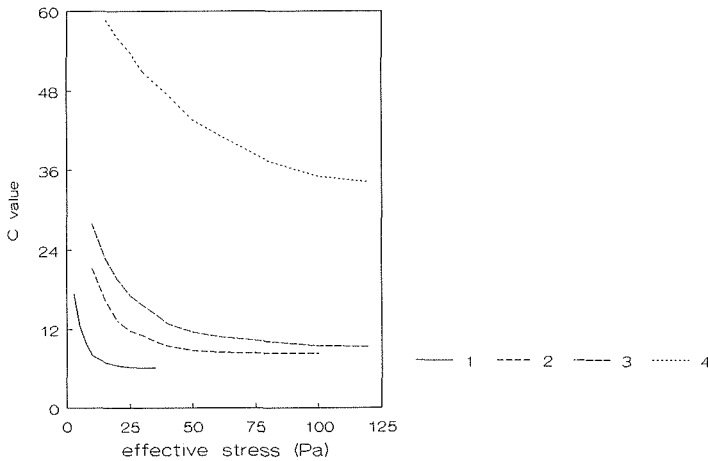


Fig. 4 Compression coefficient vs. effective stress for Holocene cover in North Holland:

1. peat, $\gamma = 10-11$ kN m⁻³; 2. clay, $\gamma = 13-14$ kN m⁻³; 3. clay, $\gamma = 14-16$ kN m⁻³;
4. sand, $\gamma = 18-19$ kN m⁻³ (Delft Geotechnics, 1983).

Table 3 Specific storage coefficient of the sublayers of the Holocene cover (present situation).

Layer	Lithology	σ_s (kPa)	C	α (Pa ⁻¹)	S_{skv} (m ⁻¹)
5	top clay	33	13.5	0.0224E-4	0.0224
4	Holland peat	30	7.0	0.0476E-4	0.0476
3	middle clay	60	14.5	0.0115E-4	0.0115
2	sand	85	38.0	0.0031E-4	0.0031
1	base peat	90	6.0	0.0185E-4	0.0185

Following general practice in soil mechanics in The Netherlands, we use here a compression coefficient C (Koppejan, 1948), which is related to the compression index C_c in the following way:

$$C = \frac{2.3(1 + e_0)}{C_c} \tag{5}$$

A plot of the compression coefficient vs. effective stress determined for samples of Holocene sediments in Noord-Holland (Delft Geotechnics, 1983) is shown in Fig. 4. In combination with Table 2, this figure allows an average value of S_{skv} to be estimated for

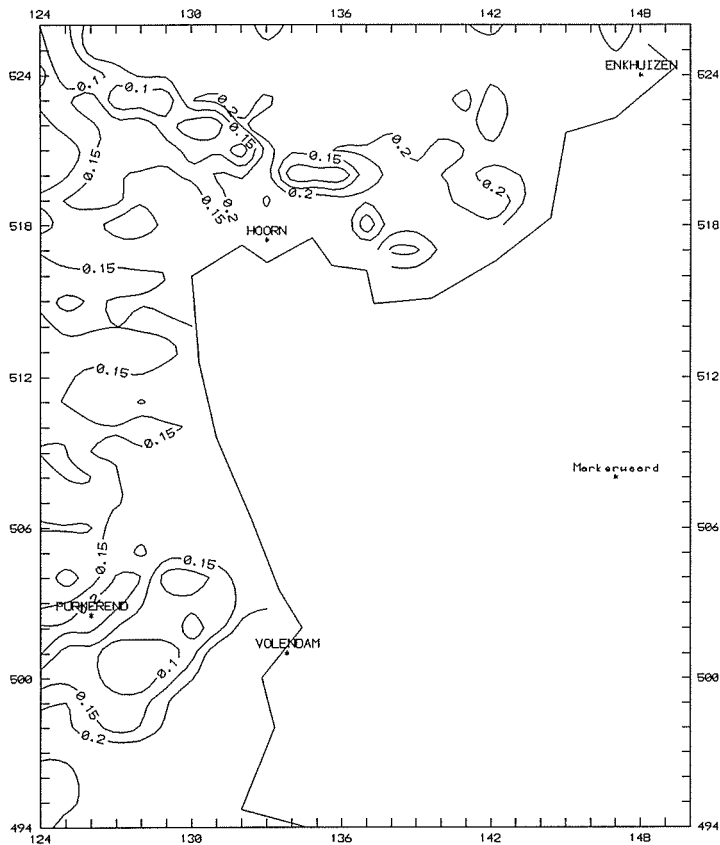


Fig. 5 Inelastic storage coefficient of the Holocene layer in the study area.

each of the lithological sublayers within the Holocene cover in Noord-Holland. These estimates are presented in Table 3. By summing the products of specific storage coefficient and thickness for each sublayer, inelastic storage coefficients were obtained for 497 grid points (Xu, 1993). A map of this storage coefficient of the Holocene cover (model-layer 2) is shown in Fig. 5.

SIMULATION RESULTS

According to expectation, the simulation results show that the declines of the piezometric levels in the second and third aquifer are much smaller than those in the first one. The final (i.e. steady state) drawdown in the first aquifer after polder reclamation is presented in Fig. 6. The final subsidence in the zone adjacent to the polder is presented in Fig. 7. The general trend is a greater subsidence at smaller distance to the polder; the maximum simulated value is 13.1 cm.

At most locations it takes about 30 years for the compaction process to be completed. Approximately 25% of the final compaction is reached within one year after reclamation, 60% at 5 years, 80% after 10 years, and more than 90% after 20 years.

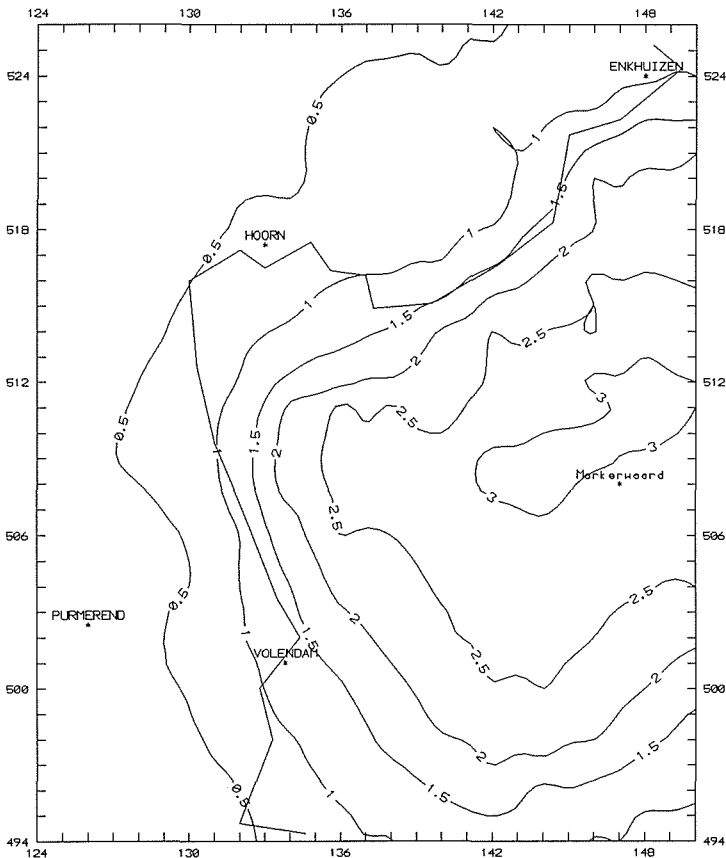


Fig. 6 Final drawdown in first aquifer (in m).

The simulation results agree very closely with the ones obtained in the earlier study (Delft Geotechnics, 1983). This is clear by comparing the predicted land subsidence according to both studies (Figs 7 and 8); the simulated piezometry of the aquifers shows little difference either (Xu, 1993). Careful analysis indicates that the land subsidence predicted in the current study is slightly larger than that of the previous study. The local maximum of subsidence predicted in the previous study is 12.0 cm.

Given the fact that both studies basically have used the same field data, it is concluded that the two different methodologies (uncoupled/stress-dependent parameters vs. coupled/constant parameters) produce in this case results that are almost identical.

ERRORS DUE TO THE USE OF CONSTANT PARAMETERS

Compressibility and specific storage coefficients decrease with progressing compaction. Hence, applying constant storage coefficients estimated for initial conditions may lead to overestimating land subsidence. By integrating equation (3) over effective stress and

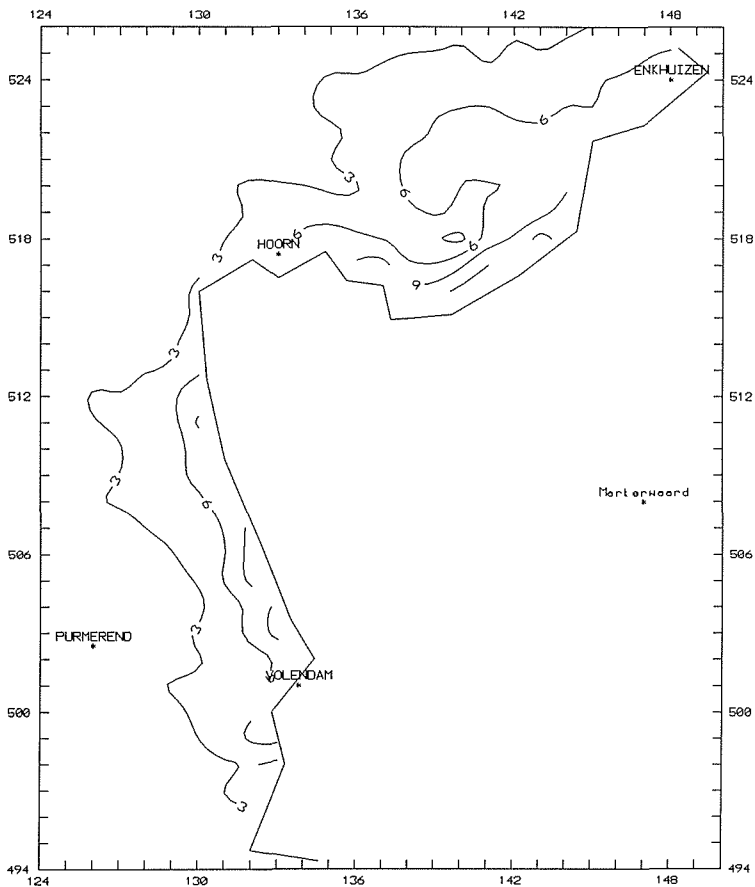


Fig. 7 Final land subsidence after reclamation (in cm).

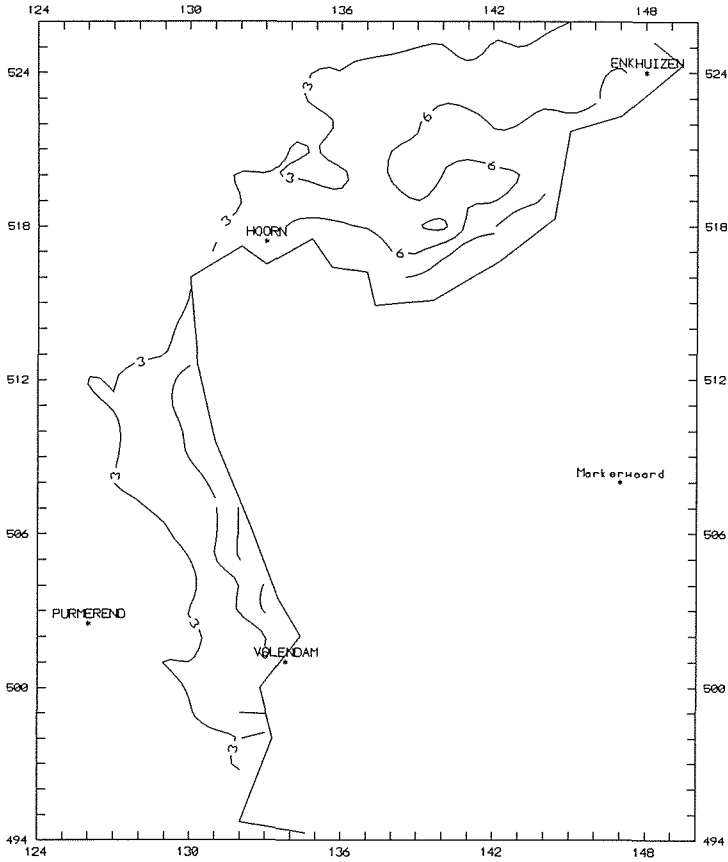


Fig. 8 Land subsidence predicted in the previous study.

dividing by the increment of effective stress, a time-averaged specific storage coefficient during the compacting process can be derived:

$$\bar{S}_{skv} = \frac{C_c \rho g \ln(\sigma_{s1}/\sigma_{s0})}{2.3(1 + e_0)\Delta\sigma_s} \quad (6)$$

which allows the errors due to assuming a constant storage coefficient to be assessed. Differences between initial and time-averaged storage coefficients for each of the

Table 4 Comparison of the average specific storage coefficient with the initial one.

Layer	σ_{s0} (kPa)	$\Delta\sigma_s$ (kPa)	Initial S_{skv} (m^{-1})	Average S_{skv} (m^{-1})	Percentage error
top clay	33	5	0.0224	0.0209	7.40
Holland peat	30	5	0.0476	0.0440	8.12
middle clay	60	5	0.0115	0.0110	4.11
sand	85	5	0.0031	0.0030	2.91
base peat	90	5	0.0185	0.0180	2.75
Average					5.05

Holocene sublayers, expressed as percentages of the former, are listed in Table 4 for a 5 kPa increment in effective stress (which corresponds to the average predicted piezometric drop). These percentages indicate the percentage of error in the predicted land subsidence, as far as caused by using a constant storage coefficient. Note that the error decreases with increasing depth. Taking into account these errors explains most of the already slight differences between Figs 7 and 8.

CONCLUSIONS

MODFLOW in combination with the ISB1 package is an adequate tool for simulating land subsidence in the case presented. The coupled approach offers significant practical advantages over an uncoupled approach. In principle, it also calculates groundwater fluxes more accurately, because of taking into account the additional fluxes due to change of storage in the compacting layer; but the effect appears insignificant in the current case. The error due to assumed constant storage coefficients is small in the case studied: this is because the relative changes in effective stress were only small. To judge whether the MODFLOW-IBS1 modelling approach would be satisfactory for any other case as well, an error assessment like the one shown above may provide guidance.

Acknowledgements The authors express special thanks to Dr E. Schultz and Mr A. Hebbink (Ministry of Public Works) and to Mr M. Viergever (Delft Geotechnics) for providing the data on the case study; to Mr S. Leake (USGS) for useful comments on the IBS1 package; and to our colleague Dr W. Zijl (TNO) for his appreciated contribution to the investigation.

REFERENCES

- Delft Geotechnics (1983) *Report No.CO-242060/300*, Invloed aanleg Markerwaard: Grondparameters en Zettingsberekeningen.
- Hebbink, A. J. & Schultz, E. (1983) *Geohydrologie van het Noord-Hollandse randgebied van de Markerwaard. Flevovericht, no. 238, Ministerie van Verkeer en Waterstaat.*
- Koppejan, A. W. (1948) A formula combining the Terzaghi load-compression relationship and the Buisman secular time effect. *Proc. 2nd Int. Conf. Soil Mech. Found. Engng* (21-30 June 1948).
- Leake, S. A. (1991) Simulation of vertical compaction in models of regional groundwater flow. In: *Land Subsidence* (ed. by A. I. Johnson) (Proc. Fourth Int. Symp. on Land Subsidence, Houston, May 1991), 565-574. IAHS Publ. no. 200.
- Leake, S. A. & Prudic, D. E. (1988) Documentation of a computer program to simulate aquifer-system computation using the modular finite-difference ground-water flow model. *US Geol. Survey Open-File Report 88-482.*
- McDonald, M. G. & Harbaugh, A. W. (1988) A modular three-dimensional finite-difference ground-water flow model. *US Geol. Survey Open-File Report 83-875.*
- Neuman, S. P. & Preller, C. (1982) Adaptive explicit-implicit quasi three-dimensional finite element model of flow and subsidence in multi-aquifer systems. *Wat. Resour. Res.* **18**(5), 1551-1561.
- Xu, Tianfu (1993) A study on land subsidence due to regional groundwater withdrawal in multiple aquifer-aquitard systems. MSc Thesis H.H. no. 144, IHE, Delft, The Netherlands.

Conceptual models for earth fissuring in Las Vegas Valley, Nevada, USA

ZHUPING SHENG & DONALD C. HELM

Nevada Bureau of Mines and Geology, University of Nevada-Reno, Mail Stop 178, Reno, Nevada 89557-0088, USA

Abstract Earth fissures due to groundwater withdrawal always coexist with land subsidence, but earth fissures are not necessarily caused by land subsidence. Both land subsidence and earth fissures are closely related to aquifer movement. The direct relationship between earth fissures and aquifer movement is the key for understanding the mechanism of fissuring. According to the relationship between fissuring and aquifer movement, ground failure can be classified into two overlapping groups: failure related primarily to vertical movement and primarily to horizontal movement. In this paper the authors present several basic conceptual models for earth fissuring, which are based on Helm's hypothesis of a general hydraulic force. Effects of the general hydraulic force and pre-existing geologic structures are emphasized.

INTRODUCTION

Ground failures due to groundwater withdrawal cause damage to utilities, structures, and buildings. Such damage results in difficulties for urban planning and construction. Therefore their occurrence and migration are investigated by hydrologists, engineering geologists, and engineers. Several mechanisms of ground failures, namely earth fissures and surface faults associated with groundwater withdrawal, have been suggested (Lofgren, 1978; Holzer, 1984; Carpenter, 1993; Helm, 1994). However, previous studies on ground failures have generally focused on land subsidence because earth fissures coexist with land subsidence. In fact, ground failure is not necessarily a result of land subsidence, at least land subsidence is not an essential cause for ground failure. They coexist and occur contemporaneously only because they have the same cause, namely aquifer movement. The key to solving the land subsidence and fissuring problem will lie in correctly characterizing the behaviour of aquifer movement.

According to the relationship between fissuring and aquifer movement, ground failure can be classified into two overlapping groups: failure related primarily to vertical movement and primarily to horizontal movement. Therefore, the ground failure is a result of at least two possible failure mechanisms. One is related to land surface bending moment which results primarily from regional vertical movement of the aquifer, the other is the surface expression of a subsurface crack which is mainly related to horizontal movement of aquifer material or localized differential displacements (vertical or horizontal) along some weakness planes at depth. For earth fissures induced by ground water withdrawal, the transient flow of water plays an important role (Helm, 1991). Weakness planes, such as joints, faults and interfaces between heterogeneous

material seem to control where critical areas of intergranular extension occur. A double key for understanding the mechanism of fissuring is to know how aquifer movement occurs at depth and eventually migrates to the land surface and how weakness planes affect this aquifer movement. In order to predict and control ground failure, it is necessary to develop conceptual models for the initiation and growth of fissures in response to aquifer movement. In this paper the authors present several basic conceptual models for earth fissuring, which are based on Helm's hypothesis of a general hydraulic force (Helm, 1994).

EARTH FISSURES IN LAS VEGAS VALLEY, NEVADA

Earth fissures are known to have been observed in Las Vegas Valley, Nevada, since 1925 (Ted Gilcrease, 1977 personal commun. to Ralph Patt; Bell & Price, 1993). They were first recognized as effects of groundwater withdrawal in the late 1950s (Domenico & Maxey, 1964; Malmberg, 1964). Earth fissures occur in two forms in Las Vegas Valley: those open to the land surface and those concealed beneath the surface (Bell, 1981). Most fissures occur as groups of short, discontinuous, frequently branching cracks. They appear at land surface initially as hairlines which are then eroded into potholes or small sinks and finally into long trench-like features. In areas of high-yield wells, the fissures typically occur as concentric and radial features centred around wells. Most of fissures express themselves at land surface during or after a rain storm. Earth fissures tend to be controlled by preexisting geologic features. Bell & Price (1993) examined the spatial relation between earth fissures and preexisting faults in Las Vegas Valley and concluded that the geologic structures that control the location of fissures induced by groundwater withdrawal are the vertical fault zones within Las Vegas Valley.

CONCEPTUAL MODELS

An aquifer system is a complex combination of fluid flow and the geologic framework. The conceptual model approach is an appropriate procedure. A conceptual model is a pictorial representation of the aquifer system. It is a simplified way to visualize a phenomenon that cannot be directly observed microscopically, but for which macroscopic responses can be observed and measured (Bear, 1972). Conceptual models help determine the dimensions of the numerical model and the design of the grid. Several basic conceptual models will be established as follows.

Model 1: an aquifer with horizontal weakness planes

In stratified material the interfaces between beds form weakness planes. Vertical compaction of the aquifer material may induce slip along these weakness planes. Horizontal hydraulic forces may induce shear displacements and shear stresses along these weakness planes (Fig. 1). Shear failure occurs along the weakness planes when the accumulated shear stress reaches the shear strength of the weakness planes (see A in Fig. 2). However, at a certain distance shear failure stops because shear stress is lower than shear strength or the stress intensity factor is lower than the stress intensity

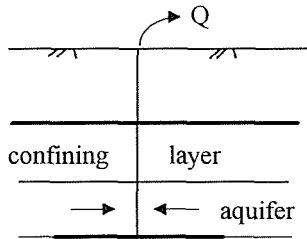


Fig. 1 Conceptual model 1.

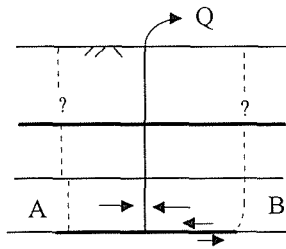


Fig. 2 Possible failure mechanisms.

resistance. At this point tensile stress may form. Once it reaches the tensile strength of the material, a potential tensile zone forms and tensile failure may occur under certain circumstances (see B in Fig. 2). Such a tensile failure may propagate upward and express itself at land surface, or be arrested or masked by other overlying weakness planes, or create a new crack in the overburden (Fig. 2).

Model 2: an aquifer intercepted by a pre-existing fault

Where an aquifer is partly truncated by a preexisting fault (Fig. 3), aquifer movement near the fault will be largely controlled by the fault (Kreitler, 1977; Holzer *et al.*, 1979; Bell & Price, 1993; Helm, 1994; Sheng & Helm, 1994). Aquifer movement may correspondingly induce differential displacement on the two walls of the fault. Such differential displacement can trigger re-shearing or opening of the fault and generate new subcracks. The opening may migrate upward and express itself at land surface as

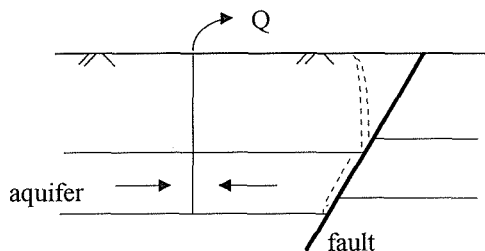


Fig. 3 Conceptual model 2.

a fissure. In Las Vegas Valley, fissuring is observed to be controlled by preexisting subvertical faults (Bell & Price, 1993).

The dip direction, dip angle, permeability of fault filling, intercepting length, distance from the well field, pumping rate and aquifer thickness are among the factors that determine the intensity of the disturbance of aquifer movements on the fault and control the effect of the fault on aquifer movement.

Model 3: an aquifer with base knobs

The disturbance of baserock knobs on aquifer movement has been observed near a number of fissures in Arizona (Bouwer, 1977; Jachens & Holzer, 1982; Larson, 1986; Carpenter, 1993). Figure 4 shows potential crack development above a bedrock ridge. The vertical subsidence away from the ridge causes the overlying slabs on each side of the ridge to rotate. The differential vertical and horizontal displacements near a stable base knob may result in a tensile zone within the aquifer and also in a draping effect. The fissures in such areas are at or above points of maximum convex-upward curvature in the topographic profiles and buried bedrock surface, respectively (Jachens & Holzer, 1982). According to Lee & Shen (1969), horizontal strains caused by differential compaction are tensile where subsidence profiles are convex-upward, and tension is greatest at points of maximum convex-upward curvature in the profiles (Fig. 4). Tensile failure would most likely occur at points of maximum tension near the land surface.

Above mechanism only accounts for the effects of vertical aquifer movement and a corresponding tensile strain at land surface. There is a possibility that horizontal movement induces tensile failure at depth. Such tensile failure could occur in the material just above the top of the ridge while aquifer material on both sides of the ridge moves away from the ridge. Such failure may extend outward and initiate a crack in overlying materials with the ongoing progress of aquifer movement. For areas where horizontal strain caused by vertical differential subsidence is insufficient to form tensile failure at land surface, the latter possibility (horizontal movement at depth) must be examined (Helm, 1994). Different geometries of the knob are expected to result in different patterns of aquifer movement around the base knob and correspondingly in different kinds of earth fissures.

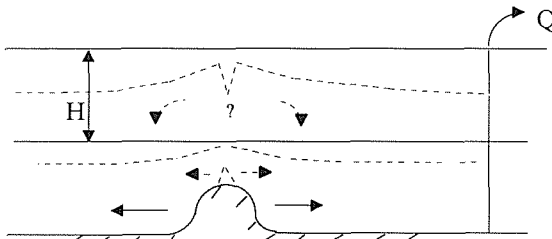


Fig. 4 Conceptual model 3 (after Jachens & Holzer, 1982).

Model 4: an aquifer with heterogeneities (a geometric abnormality)

Geometric abnormality refers to an abrupt change in thickness of an aquifer (Fig. 5) or heterogeneities. These geometric abnormalities of the aquifer may result in rotation,

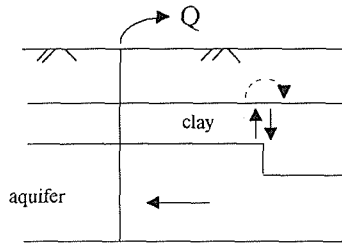


Fig. 5 Conceptual model 4.

vertical shear and even horizontal extension at depth (Helm, 1994) because of a difference of compression of material on the two sides of a geometric abnormality. Localized vertical differential displacements in the active zone (Helm, 1994) with a geometric abnormality can migrate upward into the overlying passive zone and induce tilt and shear at land surface. Localized horizontal differential displacements (Helm, 1994) may generate an extensional zone at depth and induce an opposite direction of rotation in the passive zone as well as fissures at land surface. Different types of geometric abnormalities, such as difference in interface angle, in asperity, and in the horizontal distribution of aquifer/aquitard thickness may induce distinct features of ground failures.

Model 5: further development of a fissure

This model is one of above models or a combination of them and, in addition, includes a previously induced fissure that has been observed in field. The observed fissure may cease to propagate because no more energy is accumulated to reach the critical energy release rate of the material, or be reactivated by further groundwater withdrawal and recharge or by major rain storms. The further propagation and the development of existing fissures caused by further groundwater withdrawal and recharge and by major rain storms form a potential hazard to surrounding engineering structures. As mentioned above, fissures occur in two forms in Las Vegas Valley: surface cracks and concealed cracks (Bell, 1981). Evidence suggests that in many cases tension cracks originate at depth due to groundwater withdrawal and express themselves later at land surface as earth fissures (Lofgren, 1978). Two forms of cracks in combination with two causes will be discussed as follows.

Fissure development triggered by further aquifer movement

Based on analysis of the observed correlation between horizontal movement of the fissure and water-level fluctuations, Carpenter (1993) infers that fissures will continue to move with further ground water withdrawal. Further ground-water withdrawal results in additional vertical movement, which in turn causes a surface fissure to open wider or to propagate longitudinally. It also results in further horizontal movement, which in turn triggers a subsurface crack to propagate upward and show up at land surface. It may also cause a surface fissure to open wider or to propagate longitudinally. Two simple models are shown in Fig. 6.

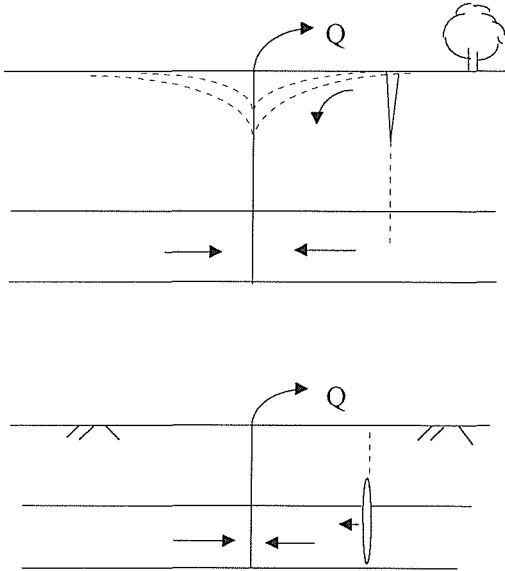
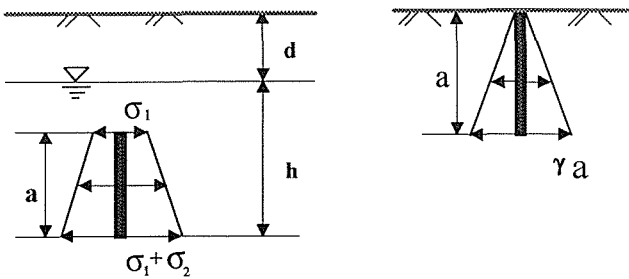


Fig. 6 Effects of the further aquifer movement on fissuring.

Fissure development triggered by localized change in pore water pressure

According to field observations (Bell, 1981; Holzer, 1984), a crack often develops into fissures at land surface during or after a rainstorm. The crack could be a pre-tensile zone or fractured zone formed under the control of preexisting structures and aquifer movement (Helm, 1994; Sheng & Helm, 1994). The driving force, which triggers crack propagation or causes the fissures to open wider, is a sudden increase of pore water pressure in the crack (Sheng, 1994). It results from the difference in hydraulic diffusivities of the crack and the surrounding material, which keeps the water pressure inside a crack from dissipating quickly into the surrounding material.

Two conceptual models are shown in Fig. 7 (Sheng, 1994). As we can see, a subsurface crack has an upward migration path from depth, while a surface crack has a downward migration path. During or after a rainstorm the local pressure head is built



Case 1: Subsurface Crack

Case 2: Surface Crack

Fig. 7 Effects of local pore water pressure on fissuring.

up quickly, which allows the stress intensity factor of the crack to reach the stress intensity resistance of material. The crack propagates upward and finally opens at land surface. The surface crack will open wider, or propagate longitudinally.

More complex models can be developed based on combination of these basic models. Future research is aimed at identifying parameters and quantifying fissure migration in accordance with these conceptual models.

Acknowledgement This research is supported by the Las Vegas Valley Water District, the Nevada Bureau of Mines and Geology, and the State Water Research Institute Program.

REFERENCES

- Bear, J. (1972) *Dynamics of Fluids in Porous Media*. Dover Publications Inc., New York.
- Bell, J. W. (1981) Subsidence in Las Vegas Valley. *Nevada Bureau of Mines and Geol. Bull. no. 95*.
- Bell, J. W. & Price, J. G. (1993) Subsidence in Las Vegas Valley, 1980-91. Final project report. *Nevada Bureau of Mines and Geol. Open-File Report 93-4*.
- Bouwer, H. (1977) Land subsidence and cracking due to ground-water depletion. *Ground Water* **15**(5), 358-364.
- Carpenter, M. C. (1993) Earth-fissure movements associated with fluctuations in ground-water levels near the Picacho Mountains, south-central Arizona, 1980-84. *US Geol. Survey Prof. Pap. 497-H*.
- Domenico, P. A. & Maxey, G. B. (1964) *An Evaluation of the Cause and Effect of Land Subsidence in Las Vegas Valley with Special Reference to Owens Avenue Area*. Desert Research Institute, University of Nevada, report to Nevada Highway Department.
- Helm, D. C. (1991) Subsidence, modelling and prediction (description of a research plan). *Report from the Nevada Bureau of Mines and Geology to the Las Vegas Valley Water District*.
- Helm, D. C. (1994) Hydraulic forces that play a role in generating fissures at depth. *Bull. AEG XXXI*(3), 293-304.
- Holzer, T. L. (1984) Ground failure induced by groundwater withdrawal from unconsolidated sediments. In: *Reviews in Engineering Geology* (ed. by T. L. Holzer), vol. VI, 67-105. Geol. Soc. Am.
- Holzer, T. L., Davis, S. N. & Lofgren, B. E. (1979) Faulting caused by groundwater extraction in south-central Arizona. *J. Geophys. Res.* **84B2**, 603-612.
- Jachens, R. C. & Holzer, T. L. (1982) Differential compaction mechanism for earth fissures near Casa Grande, Arizona. *Geol. Soc. Am. Bull.* **93**, 998-1012.
- Kreiter, R. L. (1977) Fault control of subsidence, Houston, Texas. *Ground Water* **15**(3), 203-214.
- Larson, M. K. (1986) Origin of land subsidence and earth fissuring, Northeast Phoenix, Arizona. *Bull. AEG XXIII*(2), 139-165.
- Lee, K. L. & Shen, C. K. (1969) Horizontal movements related to subsidence. *J. Soil Mech. Foundation Div. ASCE* **95**(SM1), 139-166.
- Lofgren, B. E. (1978) Hydraulic stresses cause ground movement and fissures, Picacho, Arizona? *Geol. Soc. Am. Abstract with Programs*, vol. 10, no. 3.
- Malmberg, G. T. (1964) Land subsidence in Las Vegas, Nevada 1935-63. *Nevada Department of Conservation and Natural Information Report 5*.
- Sheng, Z. (1994) The role of a sudden increase of local pore water pressure in fissuring associated with groundwater withdrawal. *Proc. of the Chinese Young Scholar Symp. on Geomechanics and Engineering Application* (Wuhan, China, December 1994), 764-769.
- Sheng, Z. & Helm, D. C. (1994) Boundary element modelling of fissures caused by groundwater withdrawal. *Proc. 8th Int. Conf. on Computer Methods and Advances in Geomechanics* (Morgantown, WV, USA, 22-28 May 1994), vol. 2, 1263-1268.

Land subsidence and degradation of the Venice littoral zone, Italy

LAURA CARBOGNIN

Istituto per lo Studio della Dinamica delle Grandi Masse-CNR, San Polo 1364, I-30125 Venice, Italy

FRANCESCO MARABINI

Istituto per la Geologia Marina, Area di Ricerca CNR, Via P. Gobetti 101, I-40129 Bologna, Italy

LUIGI TOSI

Istituto per lo Studio della Dinamica delle Grandi Masse-CNR, San Polo 1364, I-30125 Venice, Italy

Abstract The Venetian lagoon coastline is constituted by a narrow strip of land, the wholeness of which is vital for the existence of the historical city of Venice and the lagoon itself. Two processes have threatened the littoral zone: the erosive action of the sea and the land subsidence. Because of its particular setting, the fretful state of the littoral zone, is revealed by the negative evolution of the near-shore bottom slope. Five bathymetric surveys carried out in 1954, 1968, 1982, 1988 and 1992 are compared and the phenomenon of land subsidence is then analysed. Although the latter is not the primary cause of the increase in the bottom slope that has occurred, a certain correlation exists between the two processes. One may say that even a few centimetres of ground surface lowering may actually contribute to the destabilization of the littoral zone. Defence works are being undertaken.

INTRODUCTION

Land subsidence is a widespread phenomenon that may have either a natural or a man-induced origin.

Generally, geological subsidence has a slow evolution and does not arouse excessive trouble over short time periods. Subsidence induced by man's activity, on the contrary, is more frequent and has a more serious effect on the environment, mostly when induced by overexploitation of underground resources. From worldwide case histories, it appears that up to a few decades ago, the impact with the problem has in practice occurred *a posteriori*, with the direct observation of the amount and type of damage.

Environmental problems involving shallow coastal areas, often related to the erosive action of the sea and marine ingressions, are made worse by land subsidence. Damage to buildings and port structures, displacement of pipes, flooding, salt-water intrusion and decay of the vegetation, are the more common environmental impacts caused by land subsidence all over the world (Fig. 1).

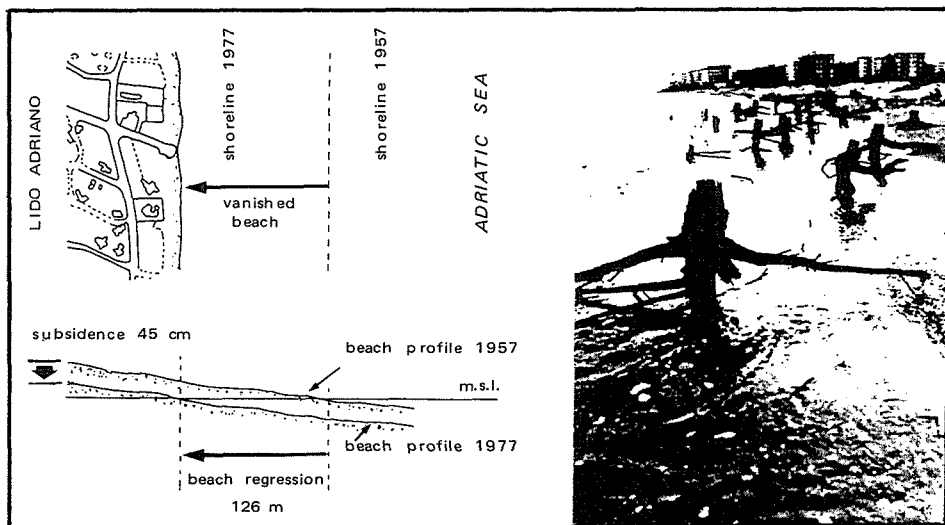


Fig. 1 Impact of land subsidence on the Ravenna coastal area, Italy, where the average beach slope is equal to 4‰. The shoreline regression which has resulted has induced the sea water ingress and the decay of the wooded pine area lying just behind.

In addition when the coastal zone belongs to a lagoon environment the existence of which is strongly connected with the completeness of the littoral zone, the problem can assume very serious proportions.

This is the case of the Venice Lagoon, Italy, whose precarious condition is made even worse by the deterioration of the littoral zone which is of tremendous importance because it is the only slender bulwark against the attacking sea.

THE VENETIAN LITTORAL ZONE

The Venetian sandy littoral zone that extends for some 40 km and separates the lagoon from the Adriatic Sea, is divided into four portions (Chioggia, Pellestrina, Lido and Cavallino) by three inlets (Chioggia, Malamocco and Lido) which also allow water to flow in and flow out of the lagoon.

The crescent shaped coastline stretches northward from Chioggia to Lido and then turns to the east along the Cavallino beach. Because of this change in direction, the littoral zone strips are attacked by the sea with a different degree of energy and also undergo different amounts of sedimentation. The Cavallino littoral zone is mostly subjected to the northeast wind (bora) sea, meanwhile those of Lido, Pellestrina and Chioggia are subjected to both sirocco (southeast) and bora wind seas (Fig. 2).

The width of the four littoral zone strips varies from several kilometres at the two extremities (close to the outflows of rivers) to a few metres in the two central parts; in some places along the Pellestrina stretch, the beach is absent and only a rubble-mound seawall – locally called "murazzi" – is present.

The coastal equilibrium is influenced by both natural events and human interventions.

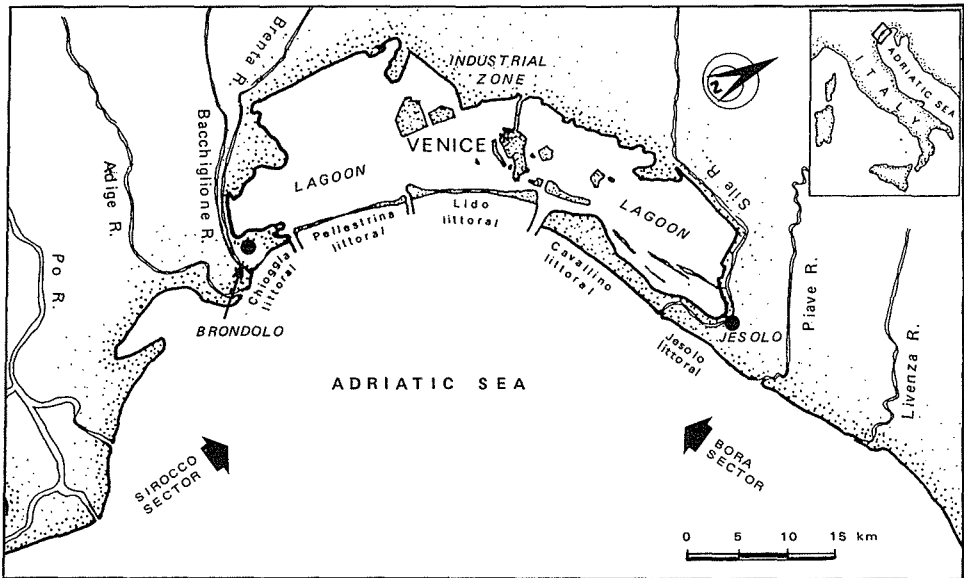


Fig. 2 Location and setting of the Venetian littoral zone strips.

Nowadays erosion is prevailing in the coastal area. The regional land subsidence which has occurred in this century, chiefly in the 1950s and the 1960s because of man's activity, has accentuated the already precarious situation of the littoral zone.

Storms and sea level rise: recent developments

It is known that a general tendency towards a climatic improvement exists in the Holocene with respect to the last glacial period. Within this phase one may distinguish climatic oscillations lasting some hundreds of years that alternate from cold-wet periods to warm and dry weather. Again, within these periods, other much shorter climatic variations with a 10-35 year (20 on average) cycle repeating the alternation of cool-damp and warm-dry periods, are recognized. These short climatic fluctuations are known as the "Brückner cycles".

Climatic changes, either short or long, occur on a global scale but their effects are detectable on a regional scale too, and they are of primary importance in the evolution of the coastal zone. Also eustatic sea level changes can play an important role.

Regarding the Venetian littoral zone (as well as the whole upper Adriatic shallow coastal area) and focusing our attention on recent developments of these phenomena, we have observed changes in the sea and weather conditions that, following the Brückner cycles, have influenced the littoral zone evolution (Marabini & Veggiani, 1991).

In particular, from the 1950s a new climatic cold/wet phase began and continued for about 20 years. An increase in rainfall, sea storms and flooding was recorded. In some places of the littoral zone, and mostly where the beach was wider and shore protection structures absent, a shoreline regression due to violent storm surges was observed (Carbognin *et al.*, 1985).

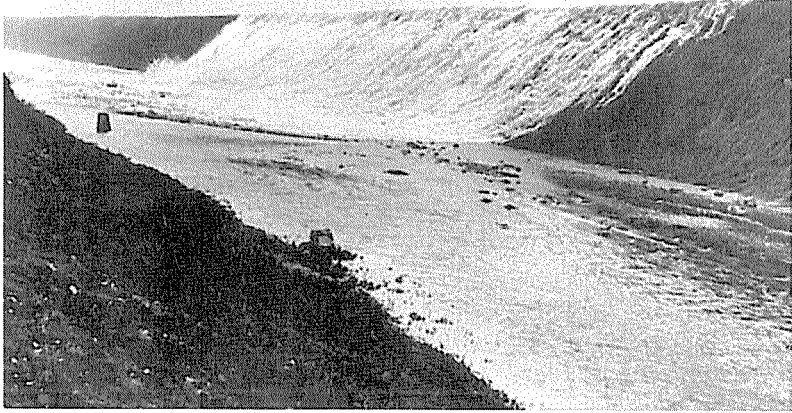


Fig. 3 Sea overtopping the littoral zone strip, 4 November 1966 (Courtesy of Cameraphoto, Venezia).



Fig. 4 Destruction of the "murazzi" at Pellestrina, after the very violent storm of 4 November 1966 (Courtesy of Cameraphoto, Venezia).

The sea and weather conditions, negative for the shore stability, culminated at the end of the 1960s with many storms, some of which were so severe that they overtopped the littoral zone strip in some places and destroyed the protection structures (Figs 3 and 4).

In this period a contribution to the deterioration of the littoral zone was also given by land subsidence as described in the next section.

A quiescent phase in the adverse meteorological-marine conditions began in the 1970s. The 1980s were characterized by a scarce rainfall and modest storm surges, typical of warm/dry periods and favourable to the coast equilibrium.

These observed climatic changes agree with the Brückner cycles.

With regard to the sea level rise (an important problem in shallow coastal areas presently under discussion at a worldwide scale), no evidence exists that this process has been felt in the Venetian lagoon in the last decades (Fig. 5).

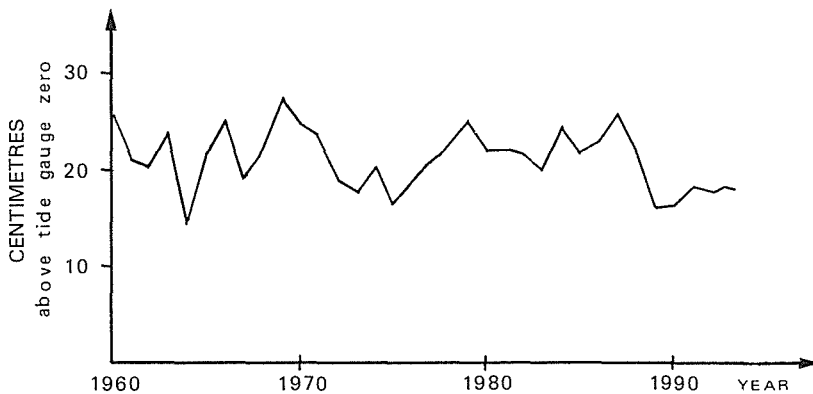


Fig. 5 Mean sea level at Venice from 1960 to 1994 (data after CNR and Comune di Venezia, 1995).

Land subsidence

The sinking of the ground surface that has affected the whole of the Venetian area has obviously also involved the littoral zone. Levels available for the littoral zone are fewer than those for the city of Venice. The subsidence of Venice in fact was investigated very carefully because of the worldwide importance of this historical city and the risk of its disappearance. Data on levels in this area have been reliably recorded since 1952 (chosen as the reference year). On the contrary only three surveys carried out in 1968, 1973 and 1993 are available for the entire littoral zone. For the Lido littoral zone it is only possible to compare five levels starting with 1961. This is not only because the levels along the Lido belong to the principal levels for the city of Venice but also because of the importance of the Lido for tourism.

On account of the studies on the origin and the evolution of the Venetian land subsidence, of the rate and magnitude of sinking (relatively small even though vital for the city of Venice), and the available measurements for the entire territory, we have attributed to the whole littoral zone the same subsidence history as that reconstructed for Venice (Bortolami *et al.*, 1985; Carbognin *et al.*, 1981, 1984). Concerning the man-induced phenomenon, the main cause of the land sinking has been the intensive exploitation of artesian water that has occurred chiefly in the industrial zone located at the edge of the lagoon (see Fig. 2) and secondly in the Lido littoral zone for tourism needs. In the other littoral zone strips, the withdrawal of groundwater has always been

of less importance and consequently it can be assumed that the induced subsidence has occurred at a smaller rate.

Regarding the subsidence of the Lido, the diagram comparing the variation in height of the benchmarks along the littoral zone in 1968, 1969 with the 1961 level is quite significant (Fig. 6). The most critical annual rate of subsidence was surveyed between 1968 and 1969, exactly as in the immediate hinterland where the subsidence "bowl" was found in the industrial zone. In the Lido area, the land subsidence touched the highest values in the lagoon basin with an average annual rate of about 1 cm year⁻¹ between 1961 and 1969 (Fig. 7(a)) (Caputo *et al.*, 1972).

From previous studies it is known that land lowering slowed down all over the region after 1970; in 1973 the subsidence came to a complete stop, and the 1975 levels even showed a significant rise equal to about 2 cm in the city of Venice (Carbognin *et al.*, 1976). The 1973 levels clearly evidenced the positive phase of the sinking process along the entire littoral strip (the ground height of this area was not measured in 1975) (Fig. 7(b)).

Since that year, one can guess that only the natural compaction of the subsoil is occurring. This process has been quantified for the whole territory to be on average 0.4 mm year⁻¹ for this century.

In 1993, twenty years after the levels were measured over the entire region, a new precise survey covering the same area (mainland, industrial zone, city of Venice, areas surrounding the lagoon, and littoral zone) was carried out (Carbognin *et al.*, 1994).

The variation of the surface height over a 20-year period indicates the actual trend of subsidence (Table 1). The comparison between the 1973 elevation (assumed as the base level) and that of 1993 is graphically presented for the whole littoral zone (Fig. 8) and for each strip (Fig. 9(a)-(d)). The coast stretching from Brondolo to Cavallino shows a land subsidence nearly similar; no significant differences appear even though the behaviour of ground elevation is pretty discontinuous. Going from the Cavallino to the Jesolo littoral zone further north, an increase in land subsidence occurs, ranging from 0.14 cm year⁻¹ (mean value of the other littoral zone strips) to 0.21 cm year⁻¹ (mean value).

In the Chioggia beach sector without erosive-geomorphological problems (Fig. 9(a)), the sinking rate (0.15 cm year⁻¹) can be considered due to the natural phenomenon of sedimentation that occurs in the deltaic zone.

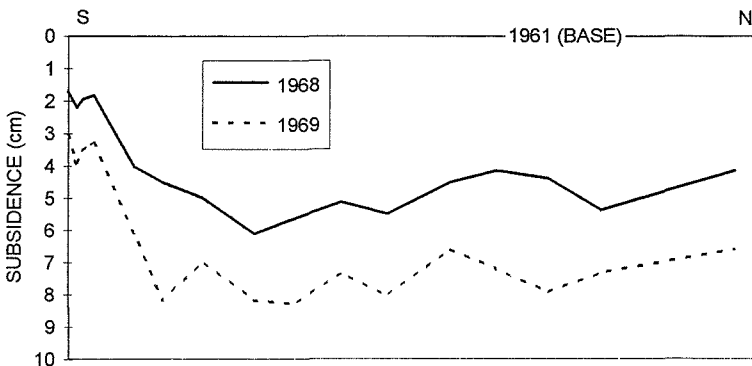


Fig. 6 Subsidence along the Lido littoral zone in the years 1968 and 1969 compared with 1961.

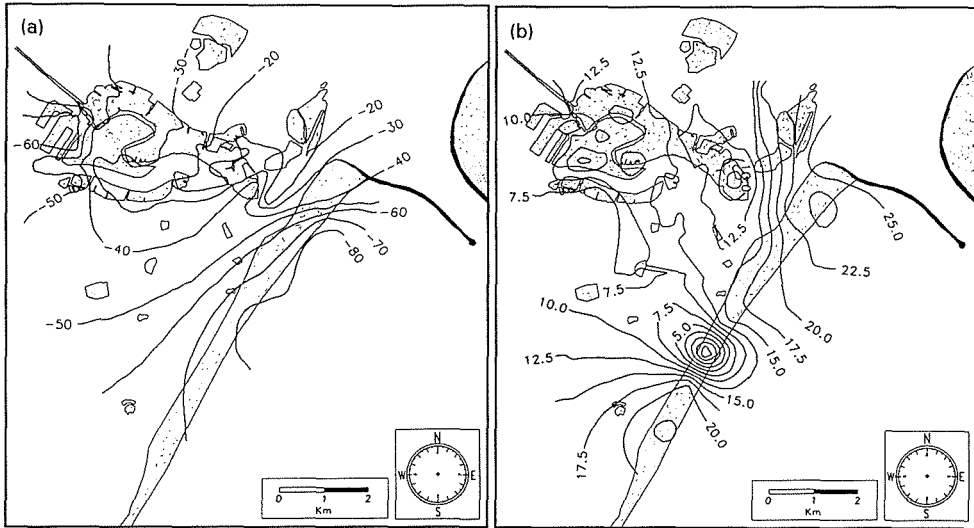


Fig. 7 Contour lines of subsidence (in mm) for the historical centre of Venice and the Lido littoral zone in the periods: (a) 1961-1969 (re-drawn after Caputo *et al.*, 1972) and (b) 1969-1973.

At Pellestrina (Fig. 9(b)), the most critical littoral zone with widespread shore protection structures, the maximum subsidence of about 5 cm in 20 years is found where the littoral zone is constituted only by the "murazzi". The negative peaks at the extremes correspond to the benchmarks established on the jetties where local structural settings have been observed (restoration work on these structures has been undertaken since 1994).

At the Lido (Fig. 9(c)) the maximum subsidence ($0.22 \text{ cm year}^{-1}$) has occurred in areas that were once agricultural before becoming residential in the 1980s. In any case, there is a notable change in the subsidence phenomenon (see also Fig. 7(b)).

The entire northern littoral zone, Cavallino-Jesolo, shows, as previously stated, the highest sinking values especially at Jesolo beach (Fig. 9(d)).

Table 1 Elementary statistics of the 1973-1993 land subsidence for the littoral zone stretches and the city of Venice.

Levelling line	Subsidence (cm) 1973-1993:			
	Mean value	Annual rate	Max. value	Min. value
Treviso-Mestre	-0.55	-0.03	-2.90	0.39
Mestre-Venice	0.27	0.01	-0.91	1.62
Venice (historical centre)	0.30	0.02	-3.58	1.64
Mestre-Brondolo	-1.51	-0.08	-10.04	1.93
Mestre-Jesolo	-2.04	-0.12	-7.97	0.30
Littoral zones	-3.26	-0.16	-9.40	-0.21
Chioggia littoral zone	-3.08	-0.15	-4.78	-1.83
Pellestrina littoral zone	-3.01	-0.15	-5.93	-0.95
Lido littoral zone	-2.49	-0.12	-4.45	-0.21
Cavallino-Jesolo littoral zone	-4.44	-0.22	-9.40	-0.10

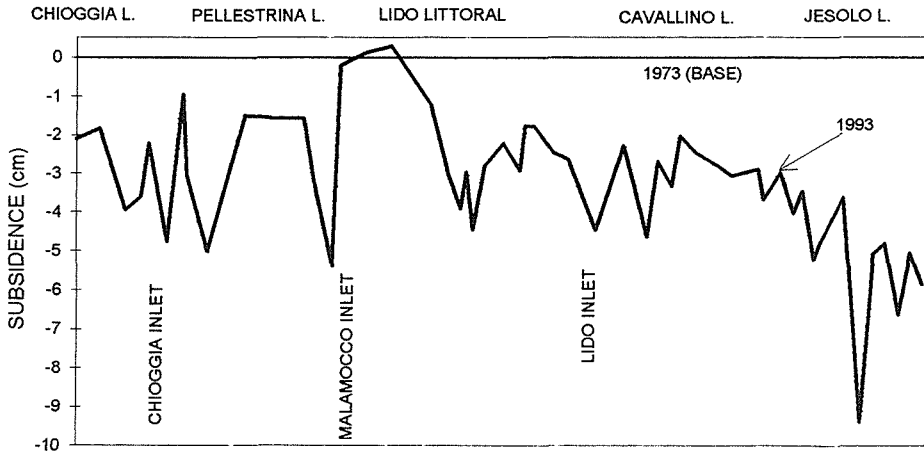


Fig. 8 Levelling profile of subsidence for the 20-year period (1973-1993) for the whole littoral zone from Brondolo to Jesolo.

In general, with respect to all areas of the Venetian region, along the littoral zone the greatest subsidence in the 20-year period was in 1993 levels. Not forgetting that the natural compaction of recent deposits is more active there than on the mainland.

The effect of land subsidence on the erosion of the littoral zone

The already precarious state of the littoral zone has been worsened by land subsidence.

Generally speaking it should be remembered that the present fluvial sediment yield to the sea is far less than in the past, and that the along-shore current moves less and less sandy material (Carbognin *et al.*, 1985; Gatto, 1984).

The actual degenerative state of the littoral zone and the role played by land subsidence, is evident by following the evolution in time of the bottom slope near the shoreline. In fact, if in general land subsidence in shallow coastal areas induces a shoreline regression, this does not happen along the Venetian littoral zone where the "murazzi" act as a fixed barrier impeding the ingression of the sea. So the destructive action of the sea develops on the submerged littoral zone.

In Fig. 10, the comparison of bathymetric surveys for 1954, 1968, 1982, 1988, and 1992 from the shoreline up to the 5 m isobath is presented. In general a notable increase of the bottom slope from 1954 to 1968 is observed along the whole coastline, followed by a steady state with the 1968 critical values up to 1992 when local negative variations are observed. In particular, the southern Chioggia beach, which is the most stable coastal strip, does not show any significant variation from the surveys available up to 1982. Pellestrina, on the contrary, experiences quite a high increase of slope especially in 1968 and 1982. The 1988 and 1992 surveys provide evidence of very modest recoveries, and also show the maintenance of the slopes greater than 1% indicating the strong environmental degrading and instability. The near-shore bottom slope of the Lido underwent the maximum increase of 0.50% or more from 1954 to 1968, and other slight negative variations in successive times as the 1982, 1988 and 1992 bathymetric surveys show. Along the northern Cavallino beach, an evident

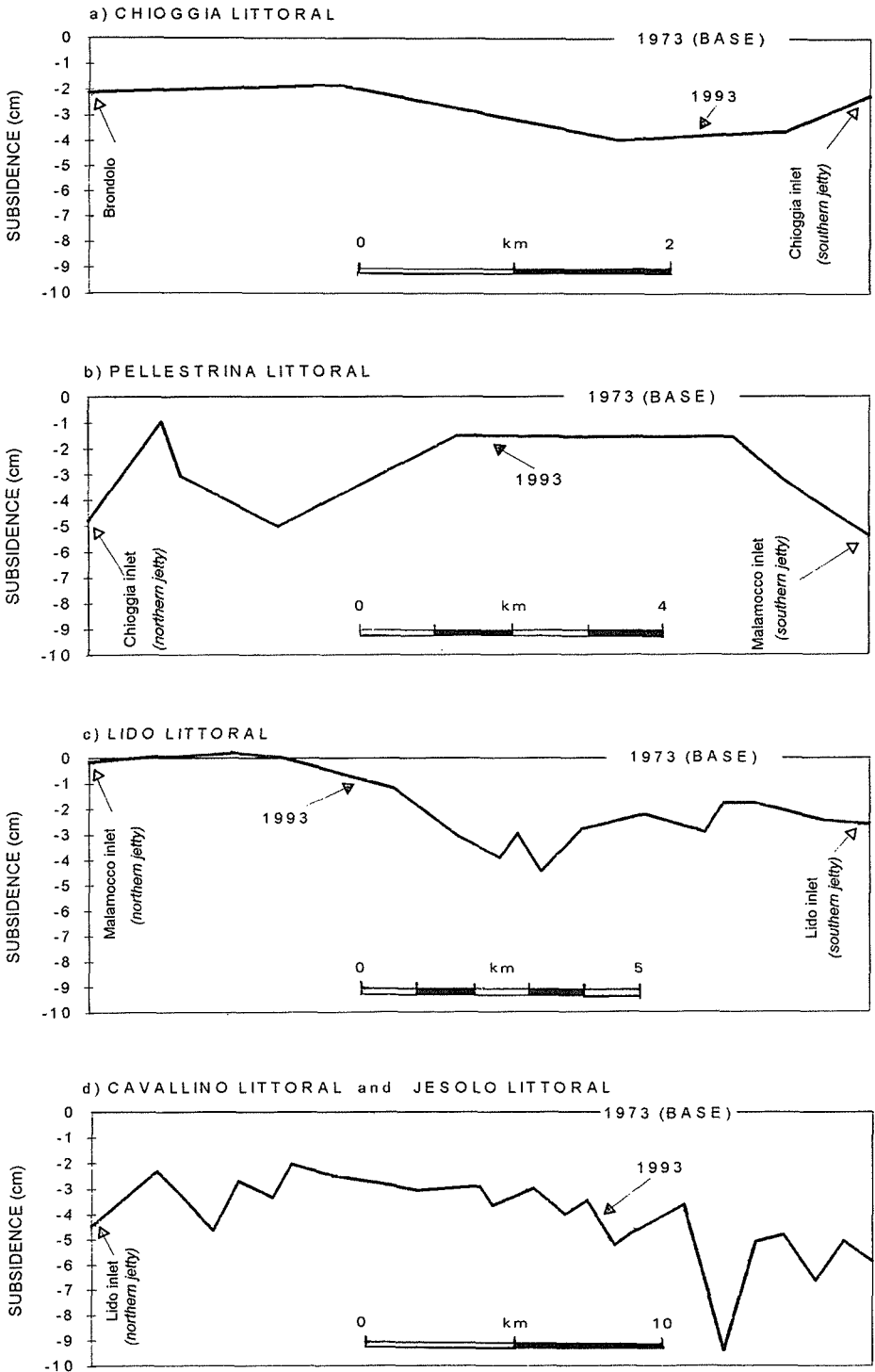


Fig. 9 The 1973-1993 subsidence profile for each littoral zone strip: (a) Chioggia, (b) Pellestrina, (c) Lido and (d) Cavallino-Jesolo.

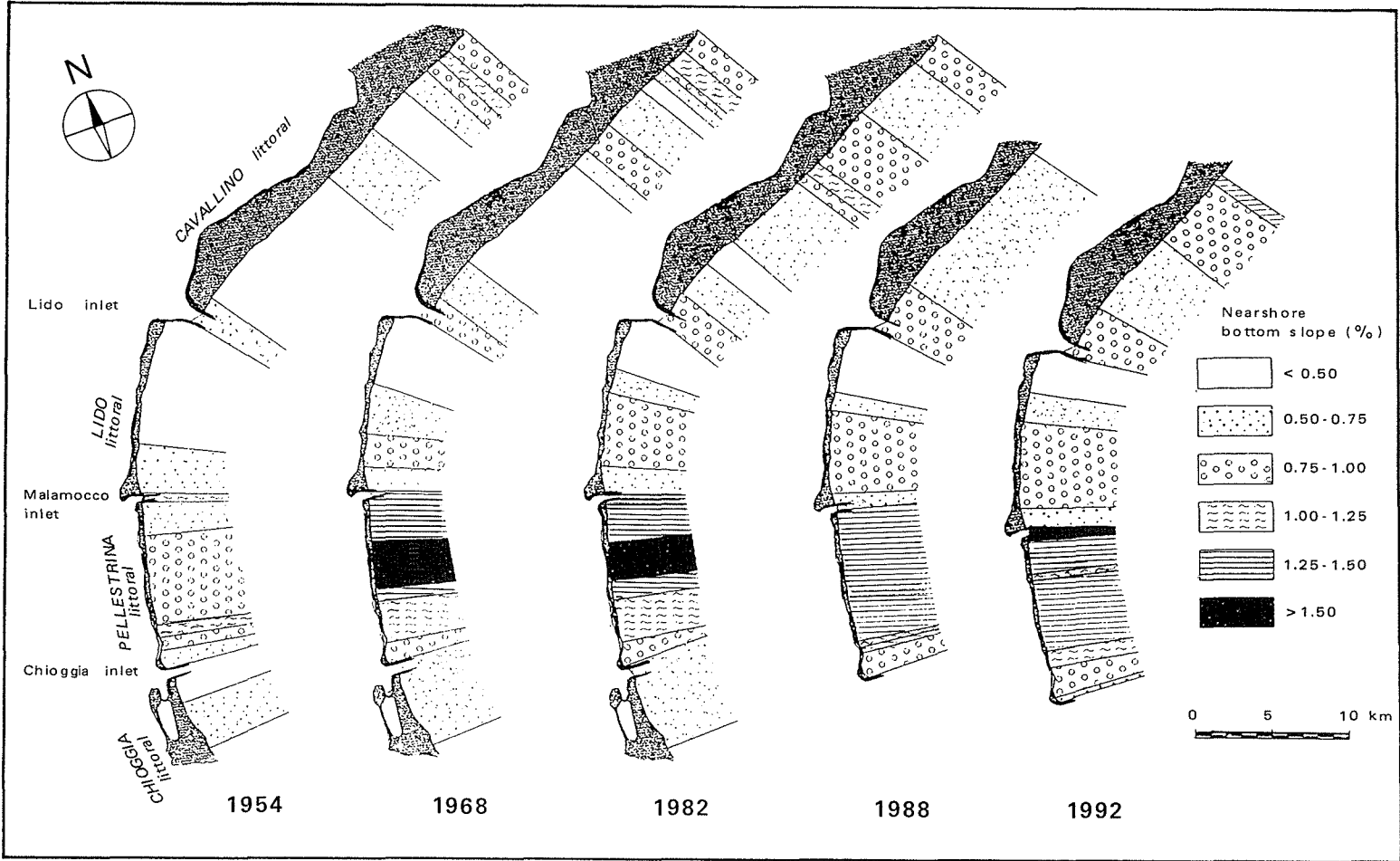


Fig. 10 Variation in the bottom slope from the shoreline to the 5 m isobath as resulting from the 1954, 1968, 1982, 1988, 1992 bathymetric surveys.

increase in sea bottom slope occurred up to 1982 followed by a slight recovery in 1988 and a new deepening in 1992.

Referring to the first span of time considered (1954-1968), the land subsidence occurred from the 1950s up to the end of the 1960s together with the high frequency of storm surges characteristic of this period, explain the deepening of near-shore bottom slope up to 1968. In the second period, 1968-1982, more favourable meteorological-marine factors, i.e. notable decrease of the southeast sea wind, and the stopping of land subsidence, occurred. The stability of the littoral zone condition has not recovered meaning that the deterioration is irrecoverable. The absence of negative climatic conditions and violent storm surges during the last 10 years do not explain the new deepening of the near-shore bottom slope surveyed in 1992 and especially along the northern littoral zone stretch. *Vice versa* one can partly justify this negative evolution considering the land subsidence at the Cavallino-Jesolo littoral zone that occurred in the 1973-1993 period. The considered values force us to think that this rather significant correlation is only qualitative.

Again, by analysing the 35 bathymetric profiles executed in 1992 (Ruol, 1994) we can see that a slight increase in near-shore bottom slope always corresponds to the subsiding points. This is true at the Cavallino littoral zone, where the phenomena are more evident, as well as along the other littoral zone strips.

CONCLUDING REMARKS

The recent land subsidence registered along the whole Venetian littoral zone, and mostly at its extremes, is in agreement with the rate of the natural compaction of recent sedimentation at the river deltas located at the north and south edges of the lagoon, and to the coastal sedimentation itself. Only locally can a partial contribution to land sinking be ascribed to human intervention (overload of new buildings and localized groundwater pumping).

Land subsidence is then occurring at a mean rate of $0.16 \text{ cm year}^{-1}$, which is not alarming with respect to the past rates of up to 1 cm year^{-1} in the 1950s and 1960s. Such a ground lowering is still considered of importance in this particular area of coast.

In fact, already in recent decades, relatively small subsidence has induced a permanent de-stabilization of the submerged littoral zone, and evidence of the correlation between the deepening of the near-shore bottom slope and land subsidence is found even today.

Moreover after the warm/dry period observed since the 1970s (according to the Brückner cycles), the situation of the Venetian littoral zone is today even more serious because in very recent times, a recommencement of heavy rainfalls and flooding has been noted. This leads us to believe that we are in the initial phase of a new cold/wet period. It is then probable that in the near future severe storm surges will attack the fragile Venetian littoral zone as in the recent past.

For these reasons some protective measures are being undertaken to reinforce the littoral zone strips. The solution chosen, after a number of expensive investigations and adequate mathematical models, is to install a number of groins opportunely spaced out.

Acknowledgements The research was financially supported by the project "Sistema Lagunare Veneziano" and developed under the research groups 2.5 and 2.7.

Particular thanks go to Mrs Jane Frankenfield Zanin for her help in the editing.

REFERENCES

- Bortolami, G., Carbognin, L. & Gatto, P. (1985) The natural subsidence in the Lagoon of Venice, Italy. In: *Land Subsidence* (ed. by A. I. Johnson, L. Carbognin & L. Ubertini) (Proc. 3rd Int. Symp. on Land Subsidence, Venice, March 1984), 777-785. IAHS Publ. no. 151.
- Caputo, M., Folloni, G., Gubellini, A., Pieri, L. & Unguendoli, M. (1972) Survey and geometric analysis of subsidence in the region of Venice and its hinterland. *Tech. Report no. 9, CNR-Lab. Studio Dinamica Grandi Masse, Venezia*.
- Carbognin, L., Gatto, P., Mozzi, G., Gambolati, G. & Ricceri, G. (1976) New trend in the subsidence of Venice. In: *Land Subsidence Symposium (Subsidence Terrestre)* (Proc. 2nd Int. Symp. on Land Subsidence, Anaheim, December 1976), 65-81. IAHS Publ. no. 121.
- Carbognin, L., Gatto, P. & Mozzi, G. (1981) La riduzione altimetrica del territorio veneziano e le sue cause (Land elevation loss in the Venetian territory and its causes). *Istituto Veneto di Lettere Scienze ed Arti, Rapporti e Studi VIII*, 55-83.
- Carbognin, L., Gatto, P. & Marabini, F. (1984) *The City and the Lagoon of Venice. A Guidebook on the Environment and Land Subsidence*. Published on the occasion of the 3rd Int. Symp. on Land Subsidence (Venice, March 1984), printed by the Ufficio Stampa, Comune di Modena.
- Carbognin, L., Gatto, P. & Marabini, F. (1985) Erosive processes in the littoral of the Venice Lagoon (Italy). In: *Coastal Zone 85* (ed. by O. T. Magoon, H. Converse, D. Miner, D. Clark & L. T. Tobin) (Proc. Fourth Symp. on Coastal and Ocean Management, Baltimore, July 1985), vol. 2, 1587-1600. ASCE.
- Carbognin, L., Marabini, F., Taroni, G., Teatini, P. & Tosi, L. (1994) Altimetria recente del comprensorio lagunare veneziano. Un'analisi critica (Recent land elevation of the Venice Lagoon and hinterland. A critical analysis). *Tech. Report no. 193, CNR-ISDGM, Venezia*.
- CNR & Comune di Venezia (1995) *Previsione delle Altezze di Marea a Venezia* (Forecasting tide height in Venice). Venezia.
- Gatto, P. (1984) Il cordone litoraneo della laguna di Venezia e le cause del suo degrado (The littoral zones of the Venice Lagoon and the causes of their degradation). *Istituto Veneto di Lettere Scienze ed Arti, Rapporti e Studi, IX*, 163-193.
- Marabini, F. & Veggiani A. (1991) Evolutional trend of the coastal zone and influence of the climatic fluctuations. *Proc. Second International Symposium on Coastal Ocean Space Utilization* (Long Beach, California, April 1991).
- Ruol, P. (1994) Batimetrie del Litorale Veneziano rilievo 1992 e confronto con il 1988 (The 1992 bathymetric survey of the Venice littoral and its comparison with the 1988 one). *Tech. Report no. 35, CNR-IGM, Bologna*.

Patterns of subsidence in landslides

R. K. BHANDARI

United Nations Centre for Human Settlements (Habitat), Nairobi, Kenya

Abstract The paper spotlights the patterns of ground subsidence in relation to landslides and related phenomena. Three fundamental mechanisms of landslides, namely: head-end interaction, tail-end interaction and the phenomenon of neighbourhood interference, are proposed and illustrated. Implications of coalescence of landslides, and the resulting damage are discussed in terms of the so-called successive, multi-tier and multi-storeyed landslides.

INTRODUCTION

Mountainous landscapes are sculptured by a bewildering variety of landslides, land subsidence and kindred phenomena, taking place over a geological time scale. By carefully mapping the change in slope morphology, especially at intervals of time, it is possible to reconstruct mechanisms causing change. Conversely, if the mechanisms are known, the ensuing changes in slope morphology could be comprehended and explained. Interplay of a multitude of factors – wide in diversity, complex in understanding, and ancient to recent on the time scale, constantly deform, distort, and mould the landslide mass. Study of the genesis, type and character of disturbance within a slope is thus important. The following points deserve consideration:

- (a) Study of location-specific case history of development of slopes and slope morphology in the overall context of the macro-geomorphology of the areas. It helps to distinguish between simple ground subsidence and an unfeigned landslide.
- (b) Once the existence of a landslide is established, the study of landslide motion at its initiation, development and decay is important. Precursory slope movements, and movement patterns throw light on the mechanism of landslide initiation. Furthermore post landslide motion and the related phases of landslide growth and development modulate slope profiles.

FIELD DATA

Land subsidence without landslides

Evidence of land subsidence alone, no matter how concrete, is not in itself a testimony to the existence of a landslide. Landslides do involve both downward and outward components of movement, although it is not untrue that in some parts, vertical subsidence dominates over the lateral movement, whereas just the opposite may prevail in some other parts.

There are notable cases of pure subsidence, associated, for example, with collapse of underground cavities due to the excessive withdrawal of water, gas and oil from the

ground. Karst topography may be construed from subsurface solution of limestone and dolomitic rocks, no matter how hard. Such can happen in chalk, gypsum, anhydride and halite terrains. "Thermokarst" topography generated by thaw of frozen ground may produce "thaw lakes" and "thaw sinks". In the case of marine erosion, presence of blow holes may cause roof collapse in the caves formed by the sea. Curious steep wall depressions, called volcanic sinks, are known to occur in some volcanoes as a consequence of the outflow of magma.

Subsidence due to leaky underground conduits, or because of water bodies causing excessive seepage and internal erosion, may also lead to predominantly vertical subsidence *without* landslides. A notable example of collapse is an about 100 m wide and nearly 30 m deep sinkhole at Winter Path, Florida, which occurred in May 1981. The collapse was partly attributed to drought (Hays, 1981).

Morphology of some first order landslides

By a first order landslide is meant a primary landslide which can be analysed individually and independently of others subsidence on a slope. Formation of features like landslide boundary shears, Riedel shears, tension cracks, ground bulge or heave, land subsidence etc., are common to most landslides. A good deal of information remains hidden in these features. For example, back-tilting of slipped masses indicates a rotational mode of failure (Fig. 1(a)). Likewise, formation of a graben usually points to a compound failure, associated with a non-circular failure surface (Fig. 1(b)). The study of deformed and broken landslide masses does provide a good idea of the intensity of the landslide activity.

A graben is one of the spectacular and easily identifiable features of some of the failed slopes. The mechanism of graben development due to the lateral spread near the

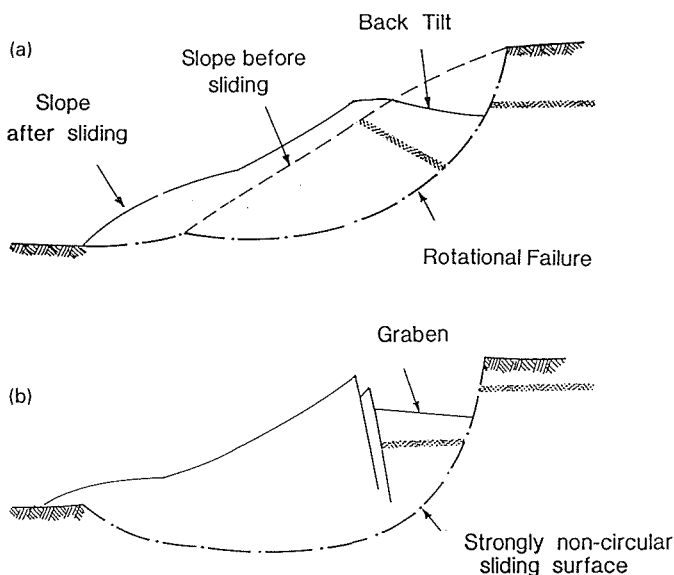


Fig. 1 Patterns of land subsidence due to some typical first order landslides.

free (outer) face of a slope is illustrated by Dobry & Baziar (1992). In the Pelton landslide it formed due to a double wedge failure on a strongly bi-linear slip surface, Cornforth & Vessely (1992). Another example of graben formation is the landslide of February 1953 in the London Clay cliffs near Herne Bay, Kent, southern England (Hutchinson, 1984).

Common landslide situations of practical significance

Some commonly encountered typical landslide situations are illustrated in Fig. 2. It is seen that when a landslide freely advances on a long and continuous sloping terrain, without interference, the landform generated is grossly different from that created when it is obstructed, or provoked. A synthesis of the documented landslide case records yield the following groupings:

- Landslides free to advance uninterruptedly on an expanse of slope continuum (Fig. 2(a)).
- Landslides which suddenly acquire the freedom to fan out and fade away (Fig. 2(b)).
- Landslides subject to toe erosion which provoke landslide motion. At times, rivers get blocked forming landslide dams (Fig. 2(c)).
- Landslides which climb up an opposite slope to come to a halt (Fig. 2(d)).
- Landslides which get obstructed at their lower end (Fig. 2(e)).

Basically all it means is that:

- (a) The force fuelling landslide motion, on an open slope, is chiefly contributed by gravity. Occasionally, an additional component of thrust is created when a landslide rapidly receives a charge of debris at its head, perhaps from another landslide on the rear slope, and also when a landslide toe rapidly gets eroded, for example, due to river or sea action.
- (b) The energy of a landslide gets dissipated chiefly by the resistance to sliding. Sudden dissipation, however, comes when the slide transits abruptly from a very steep to a flat slope. In doing so, it may fan out; strike against a barrier en route; create a landslide dam; or ride-over the opposite valley bank as the case may be.

The first point mentioned above is vital and provides the fundamental basis to explain landslide motion, later in this paper. The second point is illustrated by some examples below.

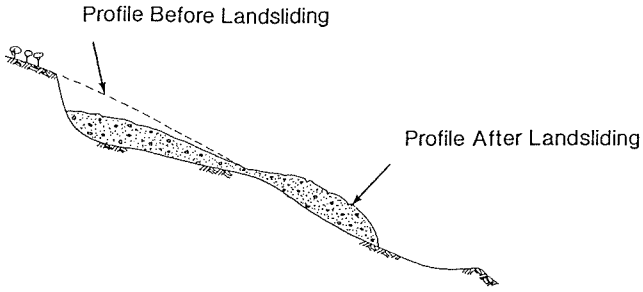
Inevitability of landslide equilibrium

All landslides eventually come to rest. In the situations described in Fig. 2, the proof is made. Time of return to equilibrium depends on a number of factors such as slope morphology, characteristics of sliding mass, velocity, volume and area involved. Sometime dominating obstacles overpower landslides and bring them to a halt.

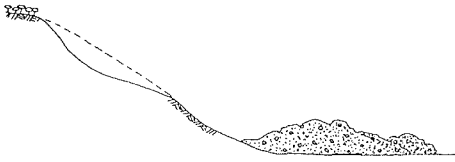
Landslide dams (Fig. 2(c))

Examples of landslides forming dams in rivers are numerous:

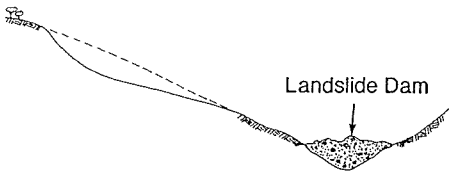
- The Gross Ventre Slide, Wyoming, of 23 June 1925, formed a dam of about 70 m



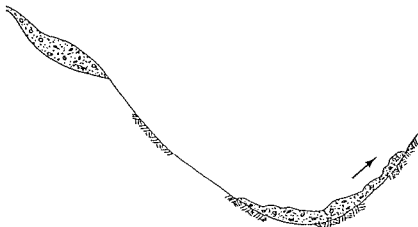
(a) Un-interrupted Motion on a Long Continuous Slope



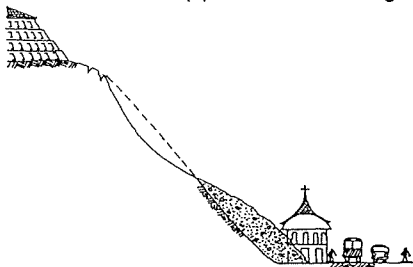
(b) Fanning out of landslide due to abrupt change of slope gradient



(c) Formation of a Landslide Dam



(d) Landslide Climbing the opposite bank



(e) Landslide blocked by a barrier on its path

Fig. 2 Some common landslide situations of practical importance.

height and 2.4 km upstream to downstream. More than 40 million cubic metres of broken limestone, sandstone, siltstone and soil broke away from the side of the steep mountain overlooking the Gross Ventre River (Sowers, 1992).

- Madison Canyon debris flow of 1959 is known to have formed a dam, impounding Hebgen Earthquake Lake. Triggered by a large earthquake (Richter magnitude 7.1), it flowed across the Madison River of western Montana, creating a dam and a lake.
- The Vong Landslide in the eastern Himalaya with a history of repetitive occurrence, blocked the nearly 40 m wide River Teesta for about 20 minutes. Every time the river flushed the debris accumulated at the landslide toe, the reactivation closely followed. Examples of major Himalayan landslide dams are provided by Bhandari (1988).
- Five major landslide dams of the western United States are described by Schuster (1985).

Landslides climbing up the opposite slopes (Fig. 2(d))

A good example of a landslide climbing up the opposite valley wall is the Madison Canyon Landslide in southwestern Montana. Rocks from the mountain top dropped about 400 m and reached the speed of about 160 km h^{-1} , before striking the valley bottom and riding up the opposite valley wall (Schuster *et al.*, 1981).

Fundamental mechanisms instigating landslide motion

The following three fundamental mechanisms of landslide motion are conspicuous because of their dramatic effect on slope morphology:

- (a) *Head-end interaction*: When a landslide gets loaded or intercepted at its head by the lower part of another landslide at the rear (Fig. 3(a)).
- (b) *Tail-end interaction*: When a landslide gets rapidly eroded at its toe by river or sea (Fig. 3(b)) or when it is influenced by another landslide lower below.
- (c) *Phenomenon of neighbourhood interference*: When three or more landslides co-exist as neighbours displaying harmony on the one hand and extreme turbulence on the other.

Head-end and tail-end interactions

The significance of the head-end and the tail-end interactions between a landslide and its external environment are seldom appreciated in full, despite their remarkable capacity to transform landscapes. The first two of the mechanisms chiefly refer to interactions between a landslide and its external environment; the following combinations of the two may occur:

- (a) Head-end loading of a landslide *without* any tail-end erosion.
- (b) Tail-end erosion of a landslide *without* any head-end loading.
- (c) Head-end loading as well as tail-end erosion, of a landslide.

Head-end undrained loading of a landslide is known to add to the activating thrust,

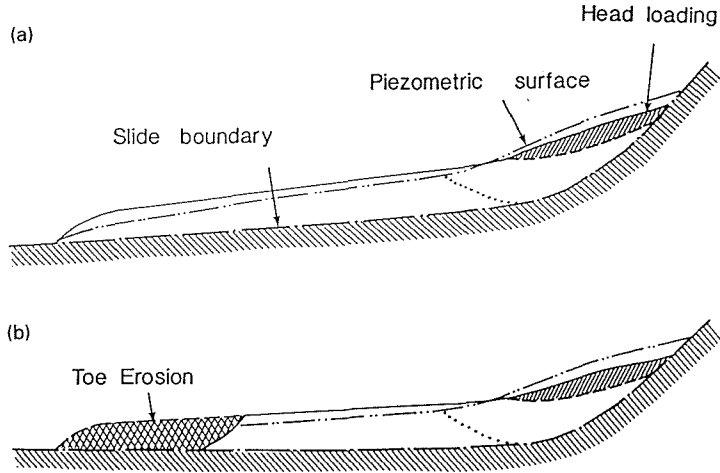


Fig. 3 Head-end and tail-end interaction.

and simultaneously bolster pore pressures in the head region of a landslide. The increase in the activating force and the decrease of the resisting force impair the slope stability (Fig. 3(a)).

The tail-end interaction involves removal of landslide tails or tongues by any means, be that due to the river action or due to the tidal action. Loss of the toe support provokes slide (Fig. 3(b)).

The fundamental mechanism of undrained loading of a landslide was suggested by Hutchinson & Bhandari (1972). They demonstrated by field measurements that rapid undrained head loading provides the necessary thrust to trigger motion of low angled mudslides in stiff, fissured clays. The validity of this mechanism has been vindicated by many researchers. For example, Sassa (1984) illustrated the mechanism of initiation of liquefied landslides and debris flows by undrained head loading. Hutchinson *et al.* (1974) explained potentially dangerous surges in an Antrim mudslide at the Minnis North of northeastern Ireland, using the very same concept.

Combined effect of interactions both at the head-end and the tail-end is illustrated by East Cucaracha slide of 13 October 1986. On the day of the landslide, basalt debris from the rear part of the Gold Hill moved 120 m on to the head of the main body of the East Cucaracha landslide. Nearly 200 000 m³ of the weathered basalt mass surcharged the active slide and provided additional thrust to it. The slide, nearly 240 m wide, 20 m deep, extended about 600 m from the canal, covered an area of 10 ha and volume of about 400 000 m³. It nearly closed a navigation canal (Berman, 1991).

Phenomenon of neighbourhood interference

By and large, all landslide cases fall into the following two categories:

- (a) Neighbouring landslides co-existing without interference or slope violence. Most successive landslides and multiple rotational landslides are the examples.
- (b) Neighbouring landslides influencing one another. Multi-storeyed landslides and certain forms of multi-tier landslides are the examples.

Successive slides

Successive slides when pitted against one another may not always interact or interfere much. An example of a triple successive landslide at Gretton Wood is cited by Hutchinson (1967). Similar slides in the Lias clay slopes in an area of the Midlands, England, are reported by Chandier (1970).

Multiple rotational landslides

Multiple rotational failures occur usually when relatively softer materials are capped by stiffer ones. For example, multiple rotational slides at the Folkestone Warren, Kent, on the south coast of England, involved a 45 m thick bed of Gault clay capped by over 120 m of chalk (Hutchinson, 1969). In the absence of a competent cap rock, the rear scarp formed by the initial slip is degraded so rapidly by shallow slips, soil falls and mudflows that unless the erosion at the slide toe is exceptionally severe, the low level of induced stresses fail to bring about a further deep seated failure. Such slides, in cliffs formed entirely of a single geological formation seem rare.

Some other examples are:

- A multi block landslide occurred in the Western Irrigation District on the Bow River in Calgary, Alberta, with the blocks moving at different rates along a common horizontal slip surface, consisting of a thin weak clay seam within the underlying bedrock (Krahan & Wymen, 1984).
- Gorshkov & Yakushova (1977) provide an example of a landslide involving series of blocks which slipped down under their own weight, but whose bedding remained undisturbed, and the surface of the beds got tilted backwards. The damage level was thus low.

Multi-storeyed landslides

By this term, Ter-Stepanian (1977) meant co-existence of several storeys of landslides, stacked one over the other. According to him "Unlike the beads-like landslides, where separate components are situated in the horizontal direction, the multi-storeyed landslides are characterized by a vertical disposition of their components. Another difference is that the components of the bead-like landslides represent the same type of sliding, e.g. earthflows, while the components of the multi-storeyed landslides belong to diverse types of sliding, distinguished by their depth and mechanism. The following groupings are proposed in this paper (Fig. 4).

- (a) Landslides in which the boundaries of various tiers do not intersect with each other – the slides may then be called single, double, triple or multi-tiered landslides.
- (b) Cases in which the higher tiered landslides are situated within the boundaries of lower tiers, and influence one another and inter slide violence is to be expected – slides may be called single, double or multi-storeyed landslides.
- (c) Cases in which boundaries of the various tiers intersect each other in a complex way and may or may not influence one another. The actual ground details should decide the classification.

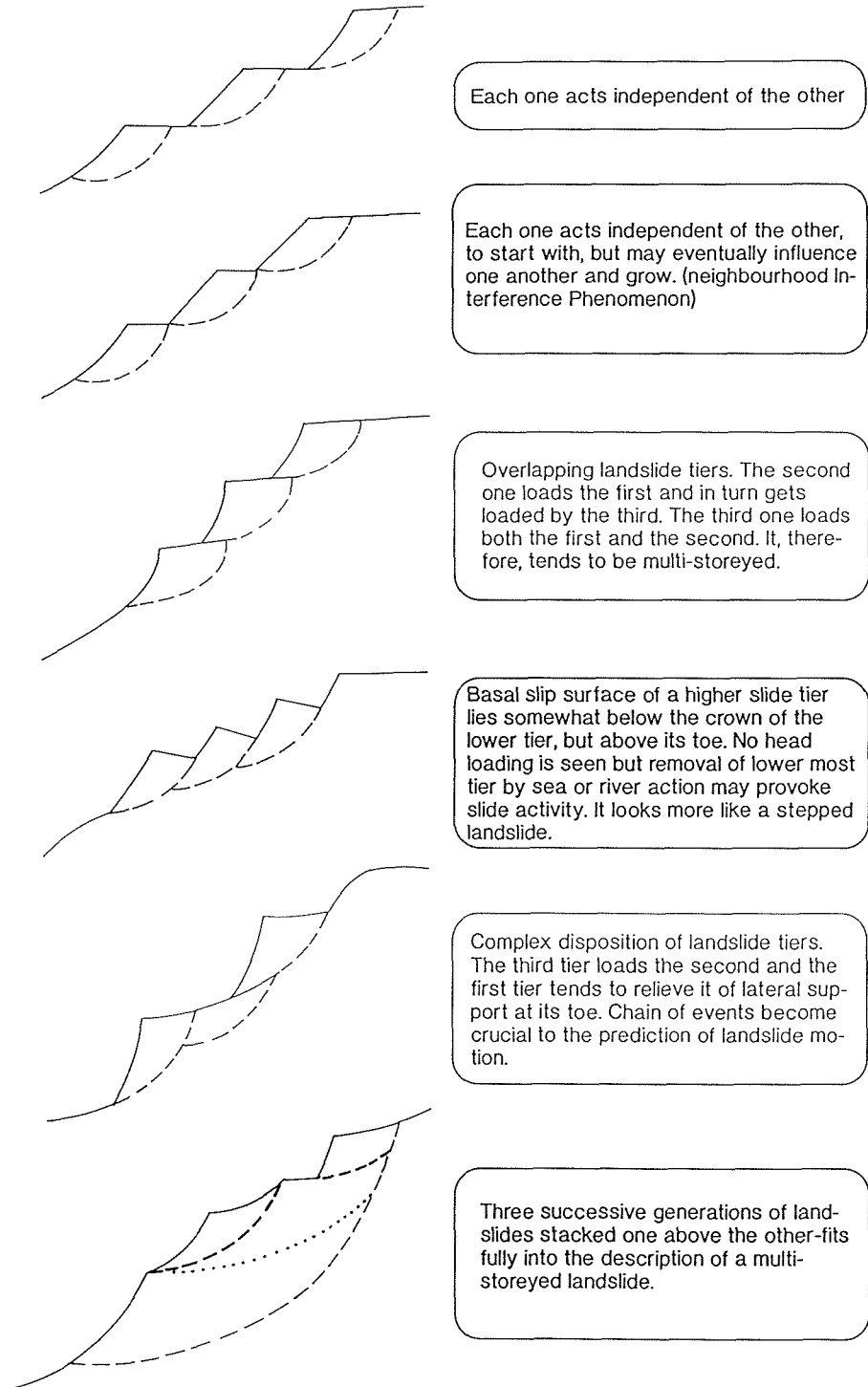


Fig. 4 Multi-tier and multi-storeyed landslides (neighbourhood interaction phenomenon).

Multi-storeyed landslides were studied for the first time on the Caucasian coast of the Black Sea in Sochi where a big three-storeyed landslide got developed. The first storey was a rotational landslide 60 m deep, involving blocks of argillites, and sandstones; the second storey was a planar sliding 20 m deep in crushed argillites, and the third storey was an earthflow 6 m deep in products of weathering of the same argillites. A revealing exposition of the concept of multi-tiered landslides is provided by Kyunttsel (1988). He distinguishes between single, double and multi-tiered landslides based on the consideration of first order slides formed and the heights of their respective displacement bases.

CONCLUDING REMARKS

Simple ground subsidence are distinguishable from unfeigned landslides on the basis of the study of slope morphology. Conversely study of slope morphology may provide important clues to the mechanism of slope dynamics. The concepts of head-end interaction, tail-end interaction and to the phenomenon of neighbourhood interaction proposed in this paper are basic. All in depth landslide studies deserve to be tuned to the ground realities, particularly when dealing with landslides other than the first order landslides, such as, for example multi-tier and multi-storeyed landslides.

Acknowledgement The paper is published with the permission of the Director General, NBRO. The views expressed in the paper are however, exclusively those of the author.

REFERENCES

- Berman, G. (1991) On East Cucaracha Slide – 1986. *Landslide News* (August 1991).
- Bhandari, R. K. (1988) Landslides in the Himalaya and protection facilities. Chapter 12 in: *UNEP/UNESCO Publication on Landslides and Mudflows*, vol. 2, 95. Moscow, USSR.
- Cornforth, D. H. & Vessely, D. A. (1992) Pelton landslide: an unusual double-wedge failure. In: *Stability and Performance of Slopes and Embankments*, vol. II. Geotech Special Publ. 31.
- Chandler, R. J. (1970) The degradation of Lias Clay Slopes in an area of Midlands. *Quart. J. Engng Geol.* 2(3), 161-181.
- Dobry, R. Baziar, M. H. (1992) Modelling of lateral spreads in silty sands by sliding soil blocks. In: *Stability and Performance of Slopes & Embankments*, vol. II, 625. Geotech Special Publ. 31.
- Gorshkov, G. & Yakushova, A. (1977) *Physical Geology* (first published 1967). Mir Publishers, Moscow.
- Hays, W. W. (1981) Facing geological and hydrological hazards. *USGS Spec. Pap. 1240-B*, B73.
- Hutchinson, J. N. (1967) The free degradation of London Clay cliffs. *Proc. Geotech. Conf.* (Oslo), vol. 1, 113-118.
- Hutchinson, J. N. (1969) A reconsideration of the coastal landslide at Folkestone Warren, Kent. *Geotechnique* 19(1), 6-38.
- Hutchinson, J. N. (1984) Landslides in Britain and their counter measures. *J. Japan. Landslide Soc.* 21-1, 4.
- Hutchinson, J. N. & Bhandari, R. K. (1972) Undrained loading, a fundamental mechanism of mudflows and other mass movements. *Geotechnique* 21(4), 353-358.
- Hutchinson, J. N., Prior, D. B. & Stephens, N. (1974) Potentially dangerous surges in an Antrim mudslide. *Quart. J. Engng Geol.* 7, 363-376.
- Krahan, J. & Wymen (1984) The WID Landslide Calgary. *37th Canadian Geotechnical Conference*, 209-217.
- Kyunttsel, V. V. (1988) Landslides and mudflows. Chapter 2 in: *Landslides*, vol. 1, 35. UNESCO and UNEP Publications.
- Sassa, K. (1984) The mechanics starting liquified landslides and debris flows. *Proc. 4th International Symposium on Landslides* (Toronto, Canada), vol. 2, 349.
- Schuster, R. L. (1985) Landslide dams in the western United States. *Proceedings of the IV Int. Conf and Field Workshop on Landslides* (Tokyo), 411-418.

- Sowers, G. F. (1992) Natural landslides. In: *Stability and Performance of Slopes and Embankments*, vol. II, 804. Geotech. Special Publ. 31.
- Ter-Stepanian, G. (1977) Types of compound and complex landslides. *Bull. IAEG*. no. 16, 72-74.

Subsidence and wetland development in the Ruhr district of Germany

PETER DRECKER

Planungsbüro Drecker, Bottroper Straße 6, D-46244 Bottrop, Germany

DIETER D. GENSKE, KLEMENS HEINRICH

Delft University of Technology, PO Box 5028, 2600 GA Delft, The Netherlands

HANS-PETER NOLL

Entwicklungsagentur Östliches Ruhrgebiet EWA GmbH, Kleiweg 10, D-59192 Bergkamen, Germany

Abstract An overview is given on subsidence in the German Ruhr district. Special attention is paid to wetland development due to the relative rise of the groundwater table. Examples of subsidence lakes and secondary biotopes are introduced.

INTRODUCTION

The Ruhr district in northwest Germany is one of the most densely populated areas in Europe. 5.3 million inhabitants share 4400 km². In urban regions the population density goes up to 2100 citizens per square kilometre (Jacobi *et al.*, 1992). Traditionally, deep lignite coal mining has been the motor of economic growth in the Ruhr district. In 1988 the total area covered by Ruhr mining was 3044 km², 64% of which was mined out. The overall volume of coal extracted from 1800 to 1990 is estimated to be 9.54 billion tonnes, i.e. about 5% of the world's production (Meyer, 1993). In 1990, 100 000 miners extracted 54.6 million tonnes of coal from seams of 0.6-4.5 m thickness at an average depth of 920 m. The reserves of first grade coal are estimated to be 20 billion tonnes (Fig. 1) in seams thicker than 0.6 m, 40% of which are minable with today's technology (Jacobi *et al.*, 1992).

The extraction of coal so far has led to considerable subsidence. The environmental consequences are immense. Today we start thinking about the implications and introduce remediation measures, the benefits of which future generations will appreciate.

HISTORY OF SUBSIDENCE

In the Ruhr, subsidence resulting from mining has been a matter of concern since the middle of the century. Since mining took place at increasing depths mainly in the form of longwall mining, the cause of damage at the surface was no longer restricted to the mined out working. In order to be able to assess the justification to arising claims for damage, altimetry was increasingly conducted from about 1860 on, and measuring lines were laid out over the panels. In particular, these measurements were on behalf of railway companies and home and property owners. At the end of last century subsidence

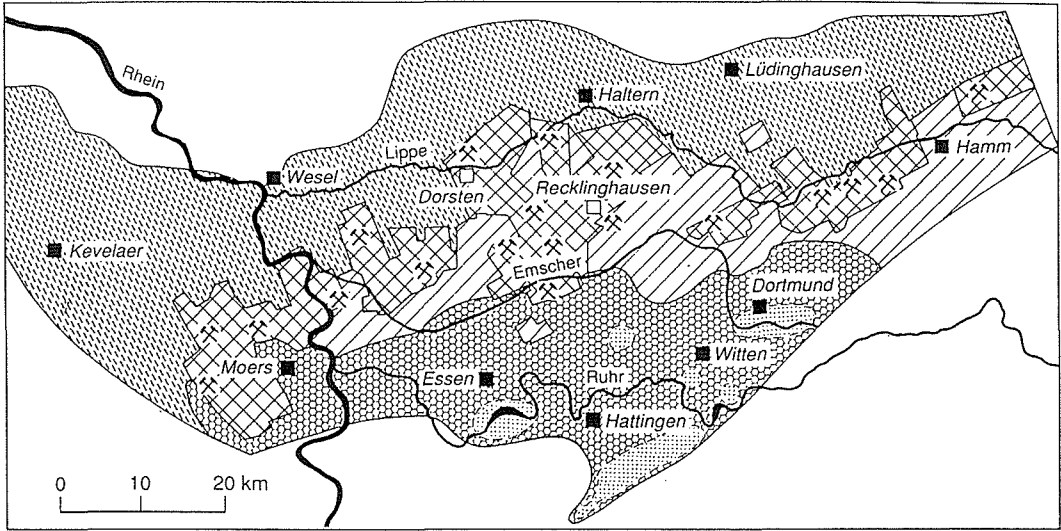


Fig. 1 Coal mining in the Ruhr district. Dotted = medieval mining, honeycombs = mining at the end of the 10th century, solid hatching = today's mines, crossed hatching = active mining, dashed hatching = reserves (Jacobi *et al.*, 1992).

has caused the reversal of natural drainage in extensive areas. This gave rise to severe sanitary problems and eventually triggered an epidemic increase of typhus and cholera cases. To restore public health the authorities were urged to take action. In 1904 the Emschergenossenschaft (Emscher Cooperative Society) was founded. Their initial task was the design and construction of systems to control and treat the increasing amount of sewage and to rearrange the existing but distorted drainage pattern. The assessment of surface observation lines enabled the Emschergenossenschaft to make predictions on future subsiding at the surface. Thus conducting and evaluation of altimetry formed the actual basis for later surface damage research. In the course of time, experience and theoretical findings on subsidence provided the basis for developing the science of surface damage (Niemczyk, 1949; Kratzsch, 1974), which has been a subject at German mining schools since 1931. Not only is the science of surface damage concerned with land movement and strata structure analyses, it also includes mining laws, land laws and also mining technology and engineering. Also covered are aspects of hydrology and hydraulics, agricultural-, town- and traffic-planning.

The extent to which subsidence becomes apparent and possibly leads to damage depends primarily on natural conditions such as the number, thickness and inclination of the mined seams, the tectonics and petrographic state of the hanging wall. Furthermore, the course of mining and stowing are of decisive significance. However, it must be pointed out that even the optimum stowing will not prevent subsidence and consequent damage.

AMOUNT OF SUBSIDENCE

The total amount of coal mined allows a back calculation of the voids created (Meyer, 1993). The 9.54 billion tonnes of coal extracted are equivalent to 7 km^3 . Adding 2.5 km^3

of refuse gives a total of up to 9 km^3 of extraction mainly from longwall mining. Since stowing is applied only in special cases the overall subsidence ranges from 80 to 90% of the seam thickness, thus resulting in an overall subsidence volume of some 8 km^3 .

The maximum subsidence observed so far is 24 m. Compression and extension at the subsidence troughs may reach up to 10 mm m^{-1} . The inclination of surface structures may be as high as 30 mm m^{-1} (Szelag & Weber, 1993).

EFFECTS OF MINE SUBSIDENCE

The extent of damage resulting from mining-related earth movements is strongly dependent upon the way the site is used. For buildings and structures, for instance, damage will result foremost due to subsidence sloping, flexing and displacement at the site. In the case of traffic and supply facilities, it is particularly elevation changes and pressure or tension which are noticed. On the other hand, in the case of agricultural areas only the relative rise of the groundwater table as a consequence of subsidence will lead to damage.

The migration of mining in the Ruhr district which follows the deposits is a foreseeable development which has been taking place for over a century. It is a consequence of the geological situation where the seams of the (hard) coal deposits are exposed in the southern Ruhr area and which are covered northwards by strata of growing thickness. The gradual northward migration of mining has led to many southern areas now being free of mining activities. Subsidence that has strongly affected regions of the lower Emscher plain has now ceased. In this area, drainage conditions had already been extremely unfavourable and strained even before the development of mining activities. Floods often occur when there is a long period of continual rainfall. Additional subsidence has led to a situation where the predominant part of the Emscher regions are "Polderland". To protect these areas from flooding and swamping, they have to be drained with a large number of pumping stations.

Meanwhile similar conditions prevail in the eastern lowlands of the Lippe River so that a belt of subsidence areas stretches from the Rhine trend along the northern Ruhr area to Hamm. Surface subsidence has not ceased in this region but continues to occur or is even increasing.

According to the "Arbeitsgemeinschaft Rahmenkonzept Gewässersystem Emscher" (1990) in 1953 some 147 km^2 of the drainage area of the Emscher River were already poldered. In 1989 the Polderland comprised already 340 km^2 . Together with the drainage area of the Lippe River where 243 km^2 are poldered this adds up to about 600 km^2 (Meyer, 1993). For every tonne of coal mined today in the Ruhr district 1.6 m^3 of water have to be pumped. Figure 2 gives a comparison of the extraction of groundwater in the Ruhr district and the observed precipitation.

FORMATION OF SECONDARY BIOTOPES

Should a large area fall below the groundwater level due to mine subsidence, and should this be compatible with the objectives of regional and environmental planning, on the long term, a terrain will be formed which can be led back to human activity. However,

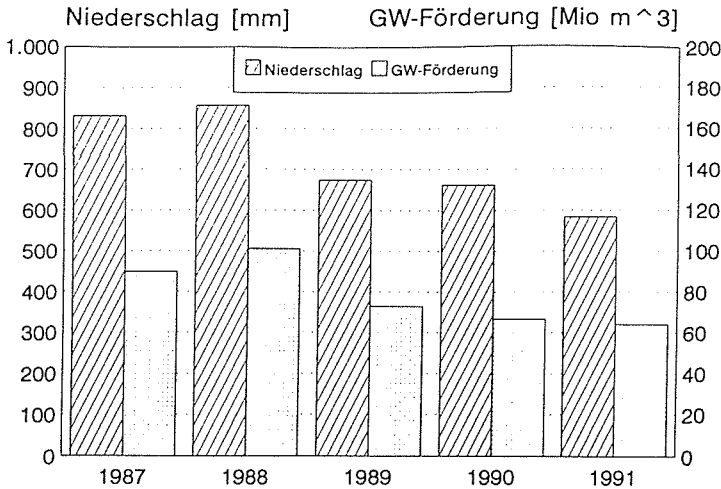


Fig. 2 Precipitation (Niederschlag) and extracted groundwater (GW-Förderung) in the Ruhr district from 1987 until 1991 (after Rathke, 1993).

the further development of vegetation and fauna will take a course which is predominantly free of human intervention, at least with the exception of eutrophic influences. Only few waters resulting from mine subsidence are situated in an open area, most are embedded in wooded areas. Water originates primarily from precipitation and flowing groundwater. Only very few lakes and ponds receive water from streams flowing into them.

Particularly in a densely populated region such as the Ruhr area, the number of natural unimpaired waters is extremely low. Thus the bodies of water formed due to mining activities could be of great importance for flora and fauna of the area. In the Ruhr area, a large share of the natural preserves and wildlife areas formed by water are so-called secondary biotopes that can be traced back to former mine subsidence.

Since the retreat of coal and steel industry in the 1970s and 1980s the demand of society for a more natural environment increased. Environmental awareness became a key issue and the Ruhr district was considered to be an ideal one-to-one scale laboratory to experiment with. The formation of secondary biotopes fits perfectly in this main stream of ideas.

THREE EXAMPLES

Lake Lanstrop in Dortmund-Lanstrop

The surface changes resulting from the former mining activities of the Gneisenau colliery in the area of Dortmund-Grevel and Dortmund-Lanstrop are referred to as an example. Here the coal seam is beneath a covering strata that is almost 300 m thick. This strata is composed of marl and chalk layers. Coal was first able to be mined in this area only after steam engines had solved the groundwater problems. In the area of severe mine subsidence, Dortmund-Lanstrop, where mining has largely come to an end, five coal seams at depths between 300 m and 500 m were mined in the past years. Impressive

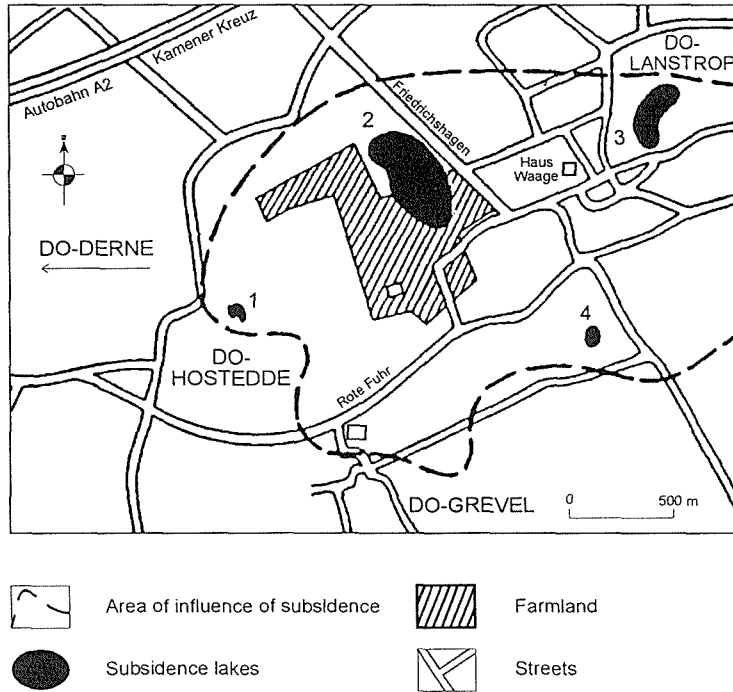


Fig. 3 Subsidence to the northeast of Dortmund.

evidence of this are several lakes and ponds formed only some years ago (Fig. 3).

A few were pumped off or filled up (as for No. 3 and 4 in Fig. 3). The largest of these lakes formed by subsidence, the so-called "Lake Lanstrop" (No. 2 in Fig. 3), with a width of 200 m and a length of 450 m, came into being between 1963 and 1967. The coal mining particularly concentrated at this site led to subsidence to the extent of about 9 m. Owing to this extreme subsidence, the ground level fell below the groundwater level thus forming the lake (Fig. 4).

Mine subsidence in the area investigated virtually involves all elements of land use: The formation of "Lake Lanstrop" led to sinking of the old Friedrichshagener Straße (road) and this had to be rerouted around the lake. Haus Wenge – an old moated castle situated directly adjacent to the lake – threatened to collapse and, as cultural-historical monument, had to be preserved at great expense. Some of the population of Lanstrop were also affected directly when sewerage from their homes was no longer able to flow off. Furthermore agricultural operations were strongly affected by the relative groundwater rise.

Besides the impairment to agriculture and structures mine subsidence has had also positive effects: The rapid formation of Lake Lanstrop was certainly of great interest to biologists since the settlement of plants and animals was able to be followed closely as if in a laboratory. After all, this lake represents an enrichment of the landscape and has already become a fishing centre which has been designated a conservation area by the authorities.

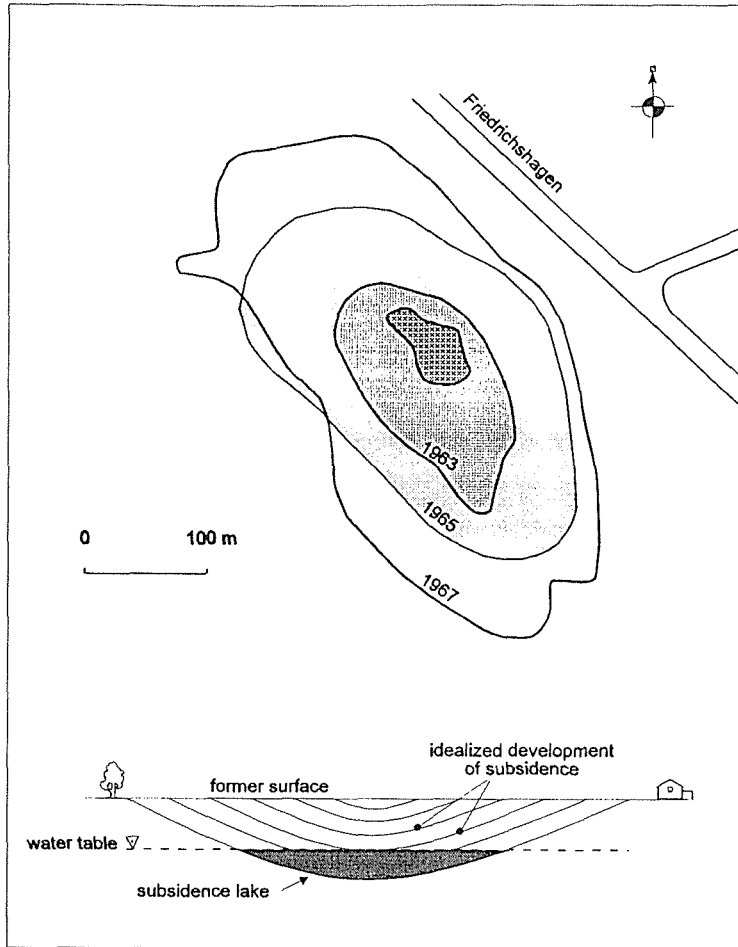


Fig. 4 Development of a subsidence lake (part of the drawing according to R. Kischkel, 1968).

Lake Hallerey in Dortmund-Dorstfeld

Marks (1993) reports on the formation of a subsidence lake in Dortmund-Dorstfeld. The formation of wetland was first observed around 1900 as a consequence of ongoing longwall mining. In 1920 the lake covered an area similar to that today, but the lake was drained, later used as a landfill site and finally as a flotation basin for coal refuse. Today, Lake Hallerey has the shape depicted in Fig. 5.

Highways and rail roads that were built over the years lead to a complete isolation of the site. This isolation caused a drastic decrease of fauna. From 1965 to 1991 some species were reduced to 10% of their original population, in some dramatic cases only 1% survived. Hallerey Lake became one of the most intensely studied nature reservation in Germany.

It became clear that a stable ecological balance is not easy to achieve in an area as populated as the Ruhr district. In this particular case a central problem is to harmonize

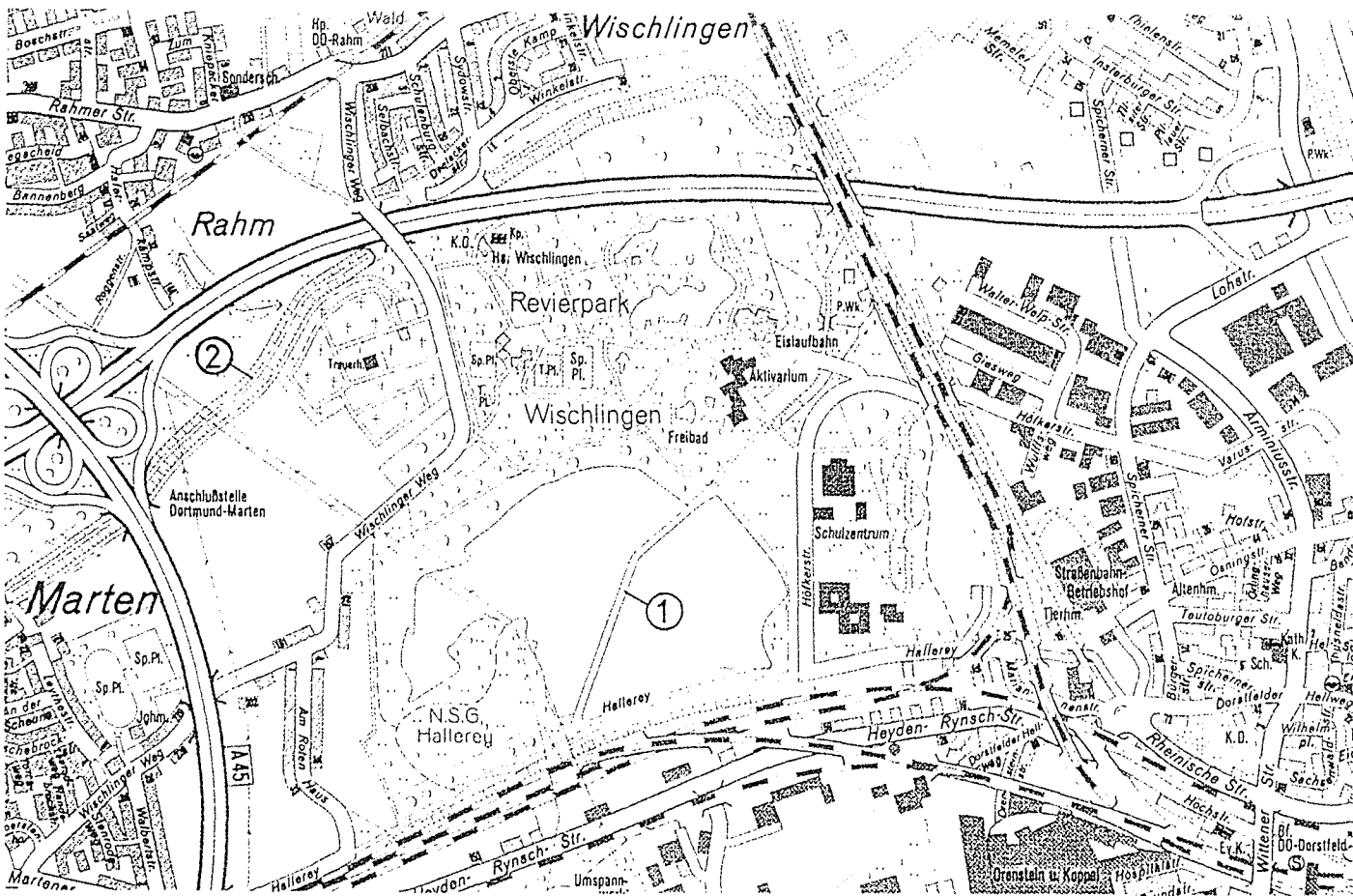


Fig. 5 Lake Hallerey, Dortmund-Dorstfeld (from Marks, 1993).

the introduction of shallow water zones to stimulate the development of fauna with the need of a large and deep fresh water body to allow dispersion and biological reduction of the abundant contamination. The research to achieve this goal is still going on. Migrating birds, however, have already accepted this secondary biotope: Hallerey lake has become one of their favourite resting places in northwest Germany.

Renaturation of the Dellwig creek, Dortmund-Lütgendortmund

An example typical for most creeks and rivers of the Ruhr district affected by subsidence is the Dellwig creek in Dortmund-Lütgendortmund (Grote, 1993). As mentioned above subsidence disturbed and reversed the flow direction of rivers, thus causing severe flooding and sanitary problems. Consequently, rivers had to be aligned and channelled, a fate Dellwig creek shared with a large number of Ruhr, Emscher, and Lippe tributaries. Around 1930 an artificial streambed for Dellwig creek was constructed, large enough to hold also the sewage of the surrounding communities.

In 1977 the area was declared a development zone for recreation, an attempt of the City of Dortmund to increase the quality of life in this area. Shortly after this decision the renaturation of Dellwig creek became an ecological pilot project of the State of North Rhine-Westfalia. The renaturation work started in 1982 (Fig. 6), spearheaded by

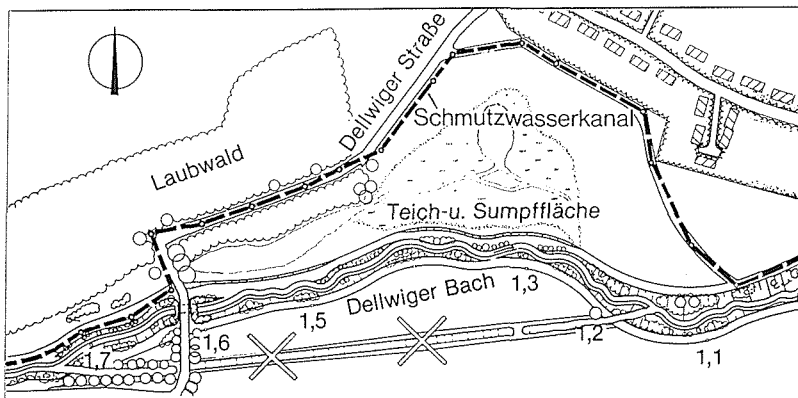


Fig. 6 Renaturation of Dellwig creek (from Grote, 1993 and unpublished documentation of Emschergenossenschaft).

the Emschergenossenschaft that 50 years ago aligned the river and turned it into a sewage canal. The variety of aspects to be considered in this renaturation project made it a complex and challenging task for the interdisciplinary team in charge of the project. The environmental consequence of the removal of the concrete lining of the canal had to be predicted, the hydrogeological effect on the groundwater table had to be discussed, the appropriate flora had to be prepared, all tasks where only little experience had been gained so far. The effort was not in vain: in 1986, after an investment of 5 million Ecu, the area became an officially protected state park.

CONCLUSIONS

The commitment to environmental issues as already formulated in the "Allgemeine Berggesetz für die preußischen Staaten" in 1865 has been finally taken up again. 120 years after the "Allgemeine Berggesetz" the European Community implemented the legal framework to carry out environmental impact studies for every major project connected with mining activities. In the Ruhr district international environmental programmes are utilized such as the European Fund for Regional Development (EFRE) that not only aids the remediation of abandoned industrial sites (Genske & Noll, 1995), but also supported the restoration of natural environments. With the instigation of additional projects such as the "Internationale Bauausstellung IBA Emscherpark" (the International Emscher Building Fair), the "Bundesgartenschau" (the National Garden Fair) the financial resources are now available to turn the Ruhr district into the "Greenest Industry Belt of the World" as postulated by the Government of North Rhine-Westfalia at the beginning of this decade. Already 207 national parks, i.e. 132 km² of recreation areas (Duckwitz, 1993) have been established.

REFERENCES

- Arbeitsgemeinschaft Rahmenkonzept Gewässersystem Emscher (1990) *Umgestaltung der Wasserläufe im Emschergebiet. Kurzgutachten und Berwertung*. Emscherpark Planungsgrundlagen, vol. 2/1. Selbstverlag Emscher genossenschaft, Essen.
- Duckwitz, G. (1993) Naturschutz im Ruhrgebiet – ein Widerspruch? In: *Vorort im Ruhrgebiet*, Geografisches Institut der Ruhr-Universität Bochum (ed.), 36-37. Verlag Peter Pomp, Essen.
- Genske, D. D. & Noll, P. (eds) (1995) *Brachflächen und Flächenrecycling*. Verlag Ernst & Sohn, Berlin.
- Grote, W. (1993) Renaturierung – Das Pilotprojekt Dellwiger Bach in Dortmund – Lütgendortmund. In: *Vorort im Ruhrgebiet*, Geographisches Institut der Ruhr – Universität Bochum (ed.), 54-57. Verlag Peter Pomp, Essen.
- Jacobi, H. E. & Hofmann, G. W. (1992) Aufgaben des Umweltmanagements im Steinkohlenbergbau. *Glückauf* 128(4), 249-258. Essen.
- Kratzsch, H. (1974) *Bergschadenkunde*. Berlin.
- Marks, R. (1993) Biotopmanagement – Das Beispiel Hallerey in Dortmund-Dorstfeld. In: *Vorort im Ruhrgebiet*, Geografisches Institut der Ruhr-Universität Bochum (ed.), 38-41. Verlag Peter Pomp, Essen.
- Meyer, D. (1993) Flächeninanspruchnahme und Massenverlagerung. In: *Steinkohlenbergbau* (ed. by Wiggering), 116-121. Ernst & Sohn, Berlin.
- Niemczyk, O. (1949) *Bergschadenkunde*. Essen.
- Rathke, K. (1993) Hydrologisch-hydrogeologische Beeinträchtigung. In: *Steinkohlenbergbau* (ed. by Wiggering), 137-148. Ernst & Sohn, Berlin.
- Szelag, S. & Weber, U. (1993) Bergsenkungen. In: *Steinkohlenbergbau* (ed. by Wiggering), 121-136. Ernst & Sohn, Berlin.

Land subsidence on Magnesian Limestone terrain in County Durham, England

M. R. GREEN

Soil Mechanics Ltd, Glossop House, Hogwood Lane, Finchampstead, Berkshire, UK

R. A. FORTH

Department of Civil Engineering, University of Newcastle upon Tyne, Newcastle upon Tyne NE1 7RU, UK

D. BEAUMONT

Durham County Council, UK

Abstract The east of County Durham, England, is underlain by a complex group of Permian age Magnesian Limestones. Under certain circumstances these limestones may be prone to dissolution by a range of processes; the result often being subsidence and collapse of roadways and other engineered structures. It has become important at the site investigation stage to reveal the presence of solution voids and conduits so as to avoid the possibility of subsidence or collapse occurring during construction or the economic life of the structure. A review of the controls on the processes of solution has been carried out and the findings are summarized. A study of investigation and exploration techniques is presented, along with a review of current construction practice and methods applicable to solution feature remediation. Associated case histories from County Durham are given. A weighted factor hazard map, showing the risk of encountering solution features, has been produced for the benefit of engineers and planners dealing with projects lying in limestone areas, and its main features are summarized.

INTRODUCTION

County Durham is situated in the northeast of England and much of the east of the county is underlain by a complex group of Permian age Magnesian Limestones. These limestones can be prone to dissolution by a range of processes. The result of which can often be the subsidence and, in extreme cases, the collapse of roadways and other engineered structures.

Remedial measures to rectify the effects of subsidence or collapse can be extremely costly and it is, therefore, desirable at the site investigation stage of a project to quantify the ground conditions on a site with as high a degree of confidence as possible, so that any likely problems can be taken into account and if necessary acted upon to minimize the possibility of subsidence or collapse occurring during the construction or economic life of the structure.

CONTROLS ON THE SOLUTION OF LIMESTONE

There are many different factors that affect the solution of limestone. The particular physical and chemical characteristics of a rock will affect the degree of weathering and erosional processes. These processes are many and varied but the most important factor that controls their effectiveness is the amount of surface area that exists in the rock which is penetrable by water. Thus the frequency and degree of jointing and bedding within a rock are very important in determining the amount of water that may enter the system facilitating dissolution and hydration. Discontinuities provide the major pathways for solutional and erosive waters, but deposition of metals and minerals often occurs in joints and fissures and this can effectively seal them, thereby reducing the overall permeability of the rock. The weatherability of a rock is increased with larger pore spaces within the fabric of the rock and thus the size of grains, their degree of interlocking and cementation between grains will all influence the weatherability.

The rate of dissolution depends on the total amount of calcium carbonate held in solution by water passing through the limestone. This in turn is dependent on the temperature and partial pressure of CO_2 with a low temperature and high pressure favourable for increased activity (Dickson, 1993).

In northern England limestone is dissolved chiefly by the direct act of acid rainwater and snow and by the action of CO_2 and humic acids in association with a cover of soil and vegetation (Sweeting, 1966). The Magnesian Limestones of County Durham are on the whole a dolomite rich limestone. Dolomite rocks tend to be more porous than calcitic rocks as a 12% reduction in molecular volume is effected when calcite is replaced by dolomite. However the solubility of a rock may not be a major factor in its erodibility as its petrological properties may be more important.

Other factors also affect the weatherability of the rocks. The age of a rock plays an important role as young unlithified rocks will erode differently due to shelly constituents with differing solubilities being present.

Environmental controls such as the availability of CO_2 and contact time between solvent and solid are also very important. These factors are controlled by the type and depth of soil cover, slope angles, temperature and rainfall regimes. Figure 1 shows the key variables in the control of limestone solution processes (Trudgill, 1985). A factor that may be particularly important in areas prone to snowfall, such as Durham, is the CO_2 content of snow which is very high and therefore may increase the solution potential of limestone. Dissolution rates can be controlled by either the rates of transport of ions or by the rate of the surface reactions. The dissolution rate is accelerated by the flushing of the solution products as a drop in the concentration of dissolved solute is achieved.

Other factors affect the solution processes to a lesser degree. Dissolution potential is increased when water leaches out acids from organic material such as leaf litter in woods. Solution erosion processes are more likely to operate at the top of slopes than at the foot of them due to mechanical slope processes producing alkaline lower slopes and acidic upper slopes. Altitude and aspect can affect biological processes. For example, soil CO_2 productivity is lower on north facing slopes and at higher altitudes.

It can be seen that the prediction of degrees of limestone solution in an area is difficult as the situation is multivariate. Dissolution potential in combination with water flow rate and volume provide the chief control on the solution of limestone. High

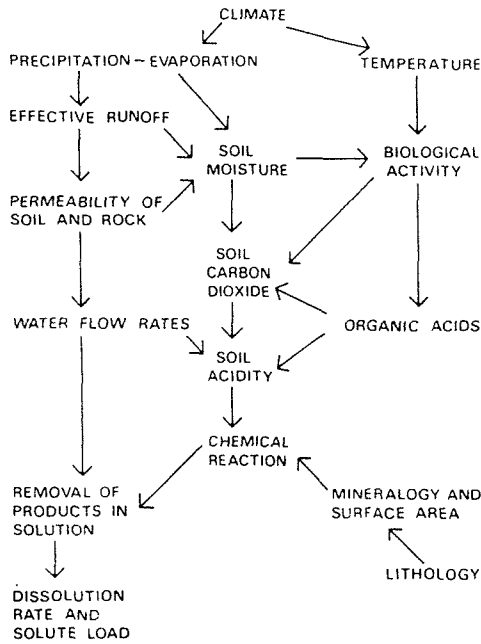


Fig. 1 Key variables in the control of limestone solution processes.

volumes of runoff increase limestone dissolution rates as does high soil acidity and high CO₂ productivity in permeable soils. The balance between dissolution potential and waterflow controls the overall rate of erosion of the limestone.

INVESTIGATION/EXPLORATION OF LIMESTONE SITES

The most important step before undertaking investigations is to define the scope and nature of the proposed development. Limestone terrain is prone to solution features such as sinkholes and dolines and as such the investigation should aim to locate these features and define their profile and stability.

The first stage in any investigation should be a review of all geological information, aerial photographs and historical information. At this stage a reconnaissance walk over survey of the area should also be carried out (Fischer *et al.*, 1987).

At Stage 2 of an investigation consideration of the planning alternatives that are available based on the information gained from Stage 1 should be addressed. Possible or probable development problems can be identified and the next stage of the investigation can be tailored to prove or disprove these.

Stage 3 should employ both direct and indirect methods of exploration. Stage 4 is further detailed to increase the confidence of any previous findings and also to obtain any planning or design parameters. At all times during the investigation it is critical that the programme is flexible to take account of unforeseen ground conditions.

The following parameters may need to be determined in an investigation:

- (a) depth, thickness and engineering properties of the soils and rock stratum;
- (b) groundwater levels, any fluctuation and direction of movement;

- (c) rock joint distribution;
- (d) nature and extent of defects.

The initial site investigation should aim to delineate groundwater regimes and forecast any changes in these regimes that are likely to occur due to any construction works. All site investigation work should be followed up with laboratory testing to give an indication of the susceptibility of a formation to dissolution. Investigation techniques can be divided into direct (boring/penetration tests, etc.), indirect (remote sensing/geophysics) and statistical methods.

In terms of cost per km² coverage, indirect and statistical methods are more effective than direct methods. Table 1 shows some of the many methods available for cavity detection.

Table 1 Methods available for cavity detection.

Direct methods	Indirect methods
Percussion drilling	Aerial photographs
Diamond drilling	Thermal imagery
Pumping tests	Satellite imagery
Trial pits	Multispectral scanning
Percussion probe	Microgravity
CPT	Radar
	Electrical resistivity
	Electromagnetic
	Seismic reflection
	Spontaneous potential

CONSTRUCTION AND REMEDIATION PRACTICE

When building on ground that is prone to solutional features, several different approaches can be taken to minimize the effect of these features:

- (a) optimization of site location,
- (b) correction or mitigation of any defects that are present,
- (c) use of modified shallow foundations allowing for defects,
- (d) use of deep foundations to overcome defects,
- (e) minimization of future activation of defects.

Often a degree of uncertainty exists as to the exact location of solution features so it is not uncommon to find more than one of the above design approaches being adopted to take account of any uncertainty that does exist. The approach or approaches that are taken should correct or mitigate the existing solution features and minimize the activation of old features whilst halting the development of new features.

There are numerous methods that are applied to either correct or treat ground that contains solution features, including correcting the hazards by filling or collapsing them, bridging over small hazards, reinforcing the rock, bypassing shallow hazards with deeper foundations and minimizing activation of the processes that form the hazards (Savers, 1984).

Any found improvement measures that are adopted need to take into account three major factors:

- the aerial extent of the surface depression,
- depth of bedrock,
- the size of the cavity in the bedrock (Parate, 1984).

There are several methods that can be used to remediate solution features, including grouting, dental filling, high volume grouting, compaction grouting, dynamic compaction, vibrocompaction and vibroreplacement. Structures can be strengthened so they do not deflect if nearby cavities fail and existing cavities may be cleaned out and a series of engineered filters and fills used to stabilize them. Foundations may be engineered to bridge any cavities with beams, geogrids, reinforced earth or rock. When relocation of a construction is not feasible and shallow foundations are not suitable, deep piled foundations are often used to overcome the real surface defects in the underlying limestone. Future defect development can be minimized by preventing access of water by using cutoffs or diverting flows. Water can also be chemically altered to stop it being corrosive, although this is usually prohibitively expensive.

County Durham is currently undergoing a large programme of redevelopment and this involves the construction of several new link roads to existing main routes. The nature of the Magnesian Limestone in certain areas may lead to instability of batter slopes and a loss of integrity in the carriageway (Buist & Ineson, 1992). In County Durham the Magnesian Limestone possesses a well developed system of vertical or near vertical joints with a regional trend. Where the limestone is underlain by coal workings the joints may develop into open fissures as a result of subsidence and chemical weathering (Shadbolt & Mabe, in Buist & Ineson, 1992).

Reactivation of Pleistocene fractures can be caused by the mining subsidence and this is likely to have occurred in the East Durham area. Where fracturing occurs in the limestones the following recommendations for cuttings have been made by Buist & Ineson (1992):

- for areas of little fracturing a near vertical slope may be cut into the limestone;
- for moderately fractured rock a 60° slope is considered to be safe;
- for highly fractured rock a 45° slope is considered safe;
- where gulls or fissures are present all slopes should be cut to less than 45°.

Embankment stability can be affected by flooding within sinkholes and solution features which saturate the embankment toe. Collapse features often occur along the edge of highways if unpaired ditches are employed as the method of drainage and they approach the soil rock interface.

A contributory factor to all the above is that highway development often causes an increase in the drainage volumes (Moore, 1984).

Where void development is a possibility, tensile reinforcement is often used to support earth structures to resist complete collapse into the void and secondly to limit deformations so that serviceability of structure is maintained.

CASE HISTORIES FROM COUNTY DURHAM

Fox Cover, Dawdon Redevelopment

The Fox Cover site in the east of the county has been chosen for the development of an industrial estate. A link road is planned to connect the development to existing major

routes. The planned route of the roads has been found to lie very close to solution features mapped during a reconnaissance survey by Dickson (1993) and a further investigation by Green (1994) (Fig. 2).

It is noted that in the south west of the area a fault is believed to exist and trends NNW-SSE, and the depressed ground areas appear to run on the inferred position of the fault. From preliminary borings limestone appears to be close to the surface in this area and solutional features and ground movements correlate closely with areas where limestone is close to the surface. A sewerage interceptor tunnel is being bored in the immediate vicinity and the local water company has been pumping considerable volumes of water to assist in this boring. It is believed that the pumping of water from within the limestone is leading to solution as limes are washed out. This may be a contributory factor of the solution features, particularly where faults/joints and fissures extend to the surface.

Previous experience in the East Durham area has shown that problems with dissolution of the limestone occur when construction has led to exposure of the Magnesian Limestone resulting in rainfall causing rapid erosion of the weaker material along joints and fissures. For this reason it is important that the limestone is not exposed for long periods during construction work.

The probable cessation of pumping in the area following the closure of the last coal pits will lead to groundwater rebound which in turn may increase the rate of dissolution of the limestone, especially along joints and faults. Current dissolution rates are in the order of $0.05 \text{ mm year}^{-1}$.

The tunnelling contractor for the water company described the limestone they were encountering as soft yellow dolomite that was able to be mined out with picks. Hard bands were also encountered but soft rock was dominant.

A report by local consulting engineers notes that rainfall is low in the area and significant solution of the limestone is taking place at the present time and most of the solution features observed developed during periods of heavier rainfall in the Quaternary. Small areas of collapse are unlikely to be caused by mining subsidence as the limestone covering the coal deposits is greater than 100 m thick.

As a precaution, the following recommendations have been made for the Dawdon redevelopment scheme.

- (a) All buildings should be built on reinforced raft foundations.
- (b) All new drainage should be a closed system with flexible jointing or contain impervious linings to prevent infiltration of water into the underlying limestone.
- (c) No surface water drainage should be taken into soakaways.
- (d) During construction all foundations should be kept dry and protected from inflows of surface or groundwater at all times. This can be achieved by the use of a concrete binding layer.
- (e) Development should avoid linear problem areas.
- (f) Reducing ground levels where Magnesian Limestone is at or near surface should be avoided, if possible.
- (g) Any sand layers with flowing water encountered at foundation depth should be replaced with concrete.
- (h) Any loose completely weathered powdery limestone encountered should be removed and replaced with suitably compacted granular fill material.
- (i) Slopes with completely weathered limestone should be protected by a clay capping.

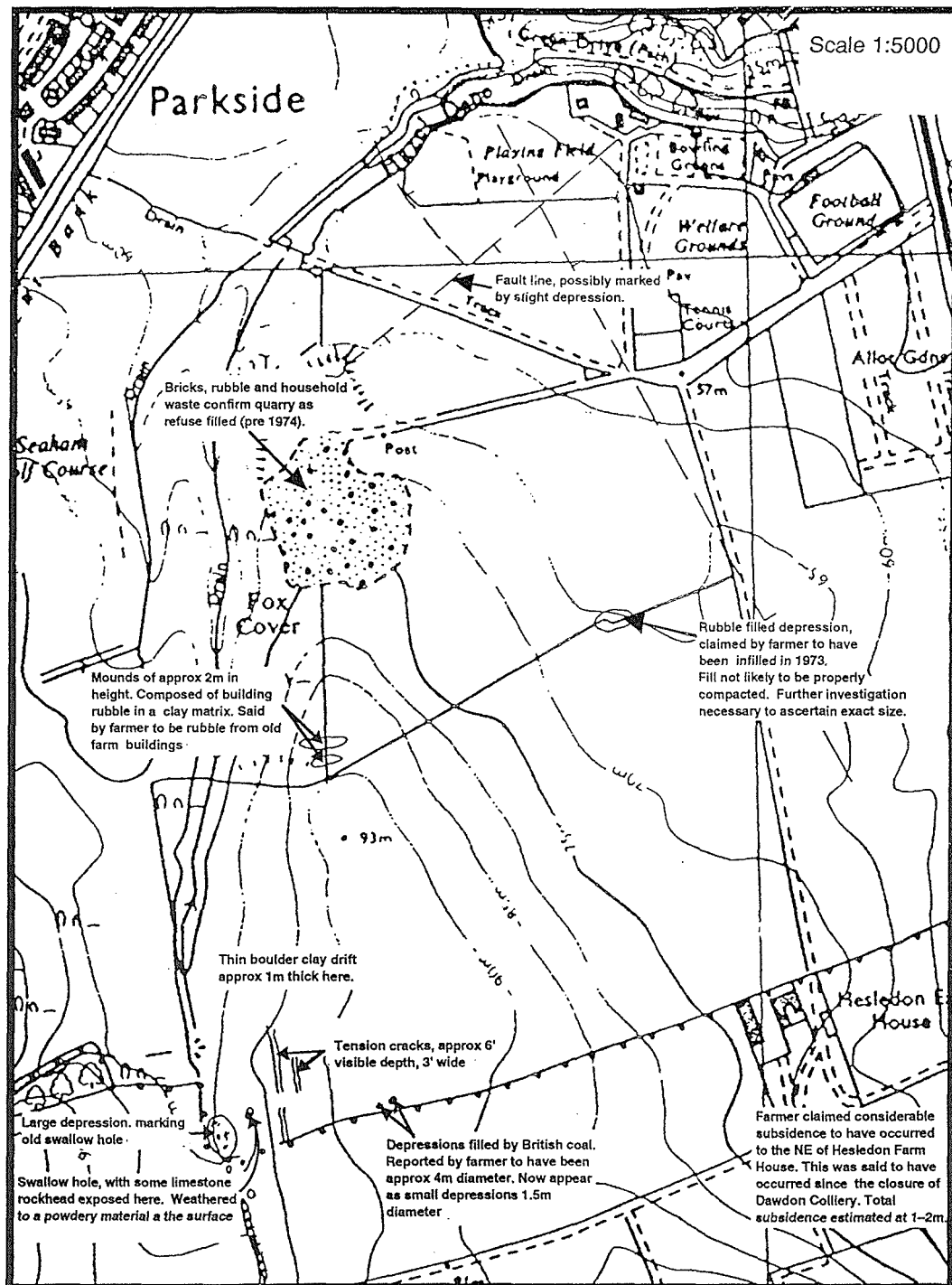


Fig. 2 Detailed plan of features observed at Fox Cover.

Wheatley Hill Bypass Scheme (A181)

This road scheme passes through several cuttings and in these Type 1 subbase (local Dolomite Limestone) has been laid directly upon the dolomitic country rock. This country rock appears to be well fissured and jointed and there is also some evidence of karstic activity.

The site investigation for the road revealed that the limestone is bedded and close to the surface (0.4 to 4.0 m below ground). Water seepage was detected in silt layers in the area. During construction of the carriageway for the bypass the subbase material settled within fissures in the Magnesian Limestone and was subsequently washed out leaving voids which could promote subsidence of the flexible pavement material above. Voids formed, the largest being some 2 m ϕ . As a remedial measure, the fissures were grouted with concrete or filled with granular material. It was deemed necessary for a survey to be carried out along the road to identify any further open fissures or voids that existed beneath the pavement which might lead to failure in the flexible pavement. The method of investigation chosen was non-destructive indirect impulse radio echo sounding.

The transducers used in the survey were selected for their penetration range and resolution which would allow the detection of the construction materials, any voiding of the subbase/rockhead boundary and any deeper features within the bedrock.

The results of the survey indicate that there are areas of homogeneous rock but the majority of the limestone appears to contain discontinuities, with the high amplitude responses obtained being consistent with a well jointed fractured rock into which the overburden has penetrated. These areas highlighted by the survey showed larger features which appear to plot transversely to the pavement and are possibly a result of karstic solution. There is evidence of vertical formations and also orientations in the bedding planes indicating that regional folding may also be important. All the possible solution features were located where the road has been laid directly on the bedrock.

Large features that are associated with high amplitude signals that are consistent with the presence of voids or fissures were found and these features may warrant further investigation and probable remedial action.

Remedial measures have been adopted as a result of this survey and take the form of:

- (a) grouting the fissures by drilling through the road surface;
- (b) excavating to formation level and then grouting;
- (c) excavating to roadbase level and laying a continuously reinforced concrete slab overlain by a macadam basecourse. This option is very expensive but any voids would be spanned, maintaining serviceability of the road.

No further action was taken as deflectograph testing showed the road to be well supported.

HAZARD MAP

Whatever the methodology used for the estimation of hazard, a useful hazard map should be:

- (a) *Applicable* – dynamics of the sinkhole must be clear so that adequate assumptions

about the type and magnitude of the sinkholes can be used to predict distribution of events.

- (b) *Reliable* – database should accurately reflect the past distribution of sinkholes.
- (c) *Flexible* – parameters should be easily changed when new data becomes available to provide new information.
- (d) *Rapid* – hazard maps should be produced in a short enough time to be effective and usable.

The area of County Durham included in the study was some 600 km². Due to the large area and time constraints, the method of weighted factors was chosen. In this method a whole series of factors that may be contributing to sinkhole/solution feature development are assessed and mapped onto individual maps. A database was set up on a grid square basis, every square being 1 km² in this study.

Each factor that affects, or is believed to affect, sinkhole development is scored or weighted according to its degree of importance. The degree of importance is decided upon by a combination of visual examination, professional experience and literature studies. If a factor occurs in a square a value is attributed to that square. This is done for all factors on all squares. A totals of risk values is obtained and a contour plot can then be produced. A plan using risk, based on a 1 km² area, was produced for the benefit of engineers and planners.

With this method, choice of weighting factors was subjective and the method would have benefited from a probability analysis of the factors causing dissolution. The method would have been better suited to a site specific investigation where all factors could be subjected to a rigorous statistical analysis.

Time dependency is not important in this application as it is the location of sinkholes that is important for planners. The hazard maps produced give the user an indication of the likelihood of encountering a solution feature that already exists. It does not indicate when new sinkholes will develop or the likely severity of the problem if a sinkhole is encountered.

REFERENCES

- Buist, D. S. & Ineson, P. R. (1992) Problems in highway construction in Magnesian Limestone – a case history from Pleasley, Derbyshire. *Highways and Transportation*, April 1992, 23-26.
- Dickson, R. (1993) East Durham Regeneration Scheme site investigation. MSc Dissertation, University of Newcastle upon Tyne (unpublished).
- Fischer, J. A., Greene, R. W., Ottoson, R. S. & Graham, T. C. (1987) Planning and design considerations in karst terrain. *Proc. of the Second Multidisciplinary Conf. on Sinkholes and the Environmental Impacts of Karst* (Orlando, Florida, 9-11 February). A. A. Balkema, Rotterdam.
- Moore, H. L. (1984) Geotechnical considerations in the location, design and construction of highways in karst terrain – the Pellissippi Parkway extension, Knox Blount Counties, Tennessee. *Proc. of the First Multidisciplinary Conf. on Sinkholes* (Orlando, Florida, 15-17 October). A. A. Balkema, Rotterdam.
- Parate, N. S. (1984) Sinkhole subsidence damage and protective measures. *Proc. of the First Multidisciplinary Conf. on Sinkholes* (Orlando, Florida, 15-17 October). A. A. Balkema, Rotterdam.
- Sweeting, M. M. (1966) The weathering of limestones. In: *Essays in Geomorphology* (ed. by G. H. Dury). Heinemann, London.
- Trudgill, S. T. (1985) *Limestone Geomorphology*. Longman, London.

The large scale development of land subsidence in northwest Jakarta and north Tangerang, Indonesia

RIK HOOGEVEEN

Witteveen + Bos Consulting Engineers, PO Box 2719, Jakarta Pusat, Indonesia

BERNARD VAN LEEUWEN

Witteveen + Bos Consulting Engineers, PO Box 233, 7400 AE Deventer, The Netherlands

Abstract A large area of approximately 10 000 ha is being developed along the northwest shore of Jakarta (Indonesia). Approximately 50% of the area is located onshore and 50% offshore. The future number of inhabitants amounts to approximately 500 000 to 600 000. The upper soil layer onshore and under the seabed consists, in large parts of the area, of soft marine sediments, overlaying medium stiff to stiff clay and silts. During recent years (1974/1978 until 1989/1990), along the entire northern coast of Jakarta, subsidence due to groundwater mining has been monitored, and found to range between 0.2 and 0.7 m. The present development plan needs to take account of this land subsidence. Because the area will be developed as a polder, the sea defence is of major importance. Also the drainage requirements of the upstream area are under pressure.

SITUATION

General description

Along the northwest coast of the Indonesian capital Jakarta and the westerly, neighbouring city of Tangerang, large-scale land reclamation is planned (Fig. 1). The area is partly located onshore and partly offshore (Fig. 2). The onshore area consists of typical coastal wetlands, at present mainly in use as fish pond areas. The offshore area stretches to the 5 m depth contour (i.e. LLWS - 5 m). The area comprises approximately 10 000 ha and runs approximately 29 km along the coast with a width ranging between 2 and 6 km.

The tidal levels range between MSL - 0.5 m (LLWS) and MSL + 0.5 m (HHWS). Storm surges, with an occurrence frequency of 10^{-4} per year, can add up to 1.2 m, depending on the wind direction. The future sea level rise over a period of 50 years is assessed at 0.3 m.

The future land levels range between MSL - 5.5 m and MSL + 3 m. The main onshore area lies at approximately MSL + 0.5 m.

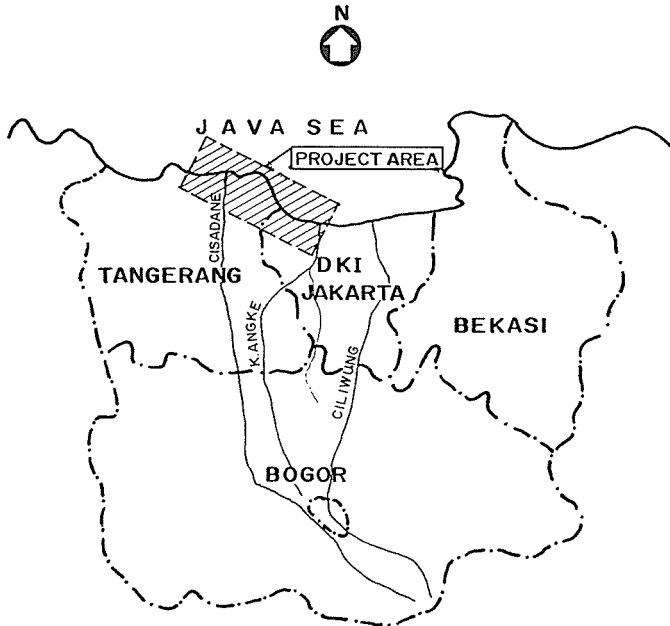


Fig. 1 Location of the project area, along the north coast of the cities Jakarta and Tangerang, on the island Java, Indonesia.

REGIONAL SUBSIDENCE

Soil

From available soil data it is concluded that the coastal zone is composed of a basin fill of predominantly clay and clayey sediments with a thickness of several hundred metres. The depth of the upper marine sediment layer is about 10 m, on some places overlain by coastal swamp deposits and humic flood plain clays. It covers a late Pleistocene layer of volcanic origin with a thickness of more than 35 m.

Below this layer a distinction in soil profile has to be made between the area east and west of the Cisadane River, more or less following a deeper fault. At the eastern side of the Cisadane River a thick complex of Pleistocene deltaic, coastal and alluvial clays and silts are present up to 200 m below ground level. Only minor beds of intercalated sands are present. Below the Pleistocene basin fill impermeable Tertiary rock formations are found. At the western side of the Cisadane, west of the Cisadane fault, where the Pleistocene basin fill is missing, permeable Tertiary rock is present. Below the permeable Tertiary rock impermeable Tertiary rock formations are found, belonging to the same geological formation. The upper silty clayey marine soils are very soft and compressible.

Geohydrology

The stratigraphy cannot easily be characterized by clearly distinguishable high permeable layers (aquifers) and low permeable layers (aquitards). Groundwater mining

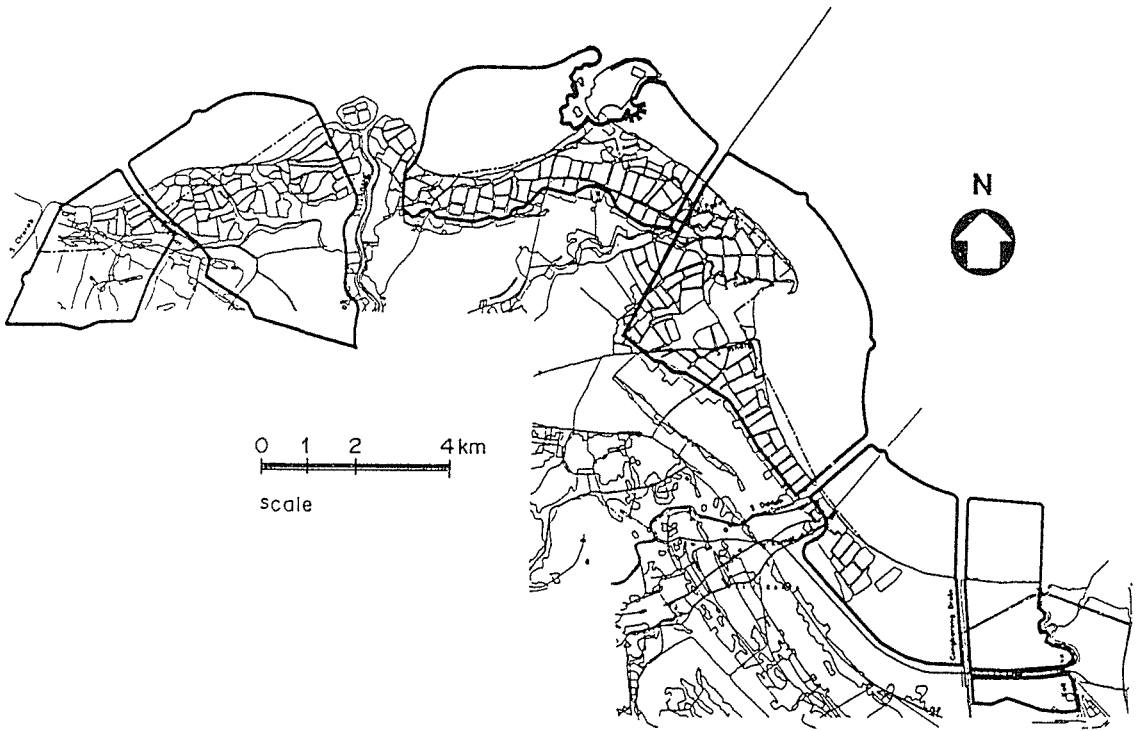


Fig. 2 Lay-out of the planned land development project.

in the upper layers, mainly for domestic use, takes place over large areas of Jakarta by means of shallow wells, causing a decline of the groundwater head. Deep wells (up to more than 100 m below land level) are mainly used for industrial purposes. The hydraulic head declined more than 30 m in a period of 75 years.

Subsidence

Studies indicate that the coastal zone suffers from subsidence due to the extraction of groundwater from a depth between 40 and 120 m. The results of these studies have been converted to the offshore and nearshore reclamation areas. In future about 0.2-0.3 m of subsidence might be expected from the influence of urbanization.

POLDERS

Conceptual design

The land development design foresees the division of the area in six separate polders. A polder is a reclamation area, surrounded by a closed loop of flood protection elements (sea defences, dikes, water management system) to separate the water regime inside the polder areas from the water regime outside and to control the water table inside the area.

A partial landfill is applied to improve the accessibility in the polder area.

The concept of a polder comprises the following elements:

- A macro drainage system that consists of canals and outlets to intercept the runoff from the adjacent areas and the discharge of the rivers, and to divert this runoff towards the rivers and macro drainage outlets between the polders.
- Flood protection measures to retain the high water levels outside the polder and to protect the coastline against erosion. The flood protection measures comprise the dikes facing the sea, the dikes along the rivers, a landward dike bordering the interception drain and a separation dike between the shallow polders on the existing land and the deeper polders in the present offshore area (Fig. 3).
- A water management system to control the water table inside the polder. It comprises collector drains, retention basins, pumping stations and subsurface drainage to control the open water and the groundwater table.

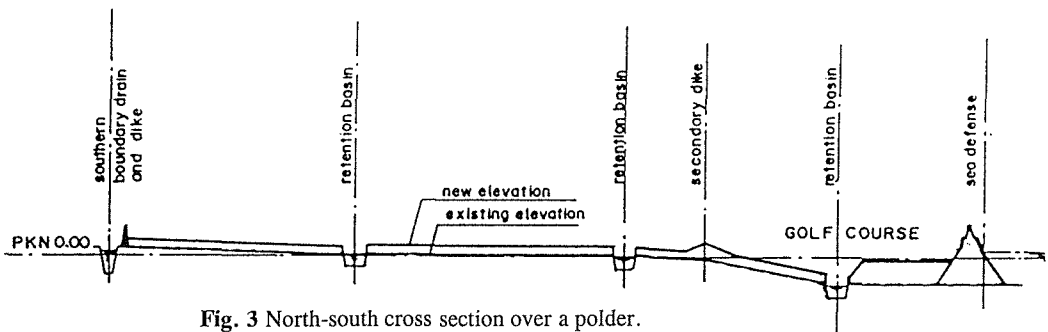


Fig. 3 North-south cross section over a polder.

Flood protection

The polders are surrounded by one of the following types of dike:

- Sea defence dikes along the new shoreline, that is the present 5-m depth contour. These dikes are subject to tidal water level fluctuations, and attack and run-up of waves from the Java Sea.
- River dikes along the seaward part of the drains, intersecting the subsequent polders, between the present shoreline and the sea defences. These dikes are protecting the lower part of a polder. The river dikes are under the influence of fluctuations of the water level due to tides and due to the backwater effects of river and drain discharges, but wave attack is only minor. The dikes will therefore differ in type of outer slope protection and in crest level.
- River dikes along the landward part of the intersecting drains. These dikes are also under attack from both tides and backwater effects, but the dikes protect the upper part of a polder.
- Dikes along the boundary drains. These dikes are along the southern project boundary of the polders.
- Separation dike. This is a dike along the present coastline that protects the lower section against flooding from the upper reclamation section.

The dike structures are subject to consolidation settlement of the order of 1.5-2.5 m due to compression of the marine topsoil. Dike construction along the 5-m depth contour

will be phased to allow a substantial part of the settlements to occur before finalizing the crest structure of the sea defence dike. Still, between 0.5 and 1 m of residual settlement has to be considered. In the settlement predictions a semi-probabilistic approach has been chosen, taking into account the variation coefficient of the consolidation parameters.

Earthworks inside the polder areas

The local topsoils at the future reclamation area mainly consist of soft silty clay, plant remains and debris. Beyond the present shoreline the topsoils mainly consist of very soft organic silty clay with shells. These topsoils are not very desirable for a future housing/commercial area and have poor drainage properties. Therefore the sector will be filled by a sand layer approximately 1.5 m thick. This sand layer serves as a foundation for roads and the housing/commercial area, and also as a drainage layer. Due to the low permeability of the local soils, the settlement process may take several months.

For the onshore area, settlement analysis was carried out assuming no groundwater lowering. The present groundwater table ranges from 0.5 to 1.5 m below ground level. After filling and the construction of settlements the groundwater table will lie between 1.5 and 3.0 m below the future ground level. The mean characteristic values with a probability of exceedance of 5% have been used for the settlement analysis to avoid underestimating the future ground level.

The retention basin plays an important role in the drying of the reclamation area. Until 1 m above the sea bed the water can be easily pumped out, but below this level the retention basin has to be used as the main drainage provision.

First, the retention basin will be excavated by grab dredgers. The slopes that will form under water are about 1:4. Along the future basin embankment at the north side a sand fill will be placed under water over a width of about 20 m. The excavated material from the retention basin will be deposited between the sand fill and the landward slope of the sea defence on top of a 1-m-thick sand fill. The lowest part of the future reclamation area, at the landward foot of the sea defence, is thus effectively reduced. After the reclamation area has been pumped dry, the retention basin can be further deepened and the embankment slopes protected against erosion.

Settlement of grab dredged soil from the retention basin

The *in situ* properties of the material from the retention basin will change due to the excavation by a grab dredger. The material is loosened by the dredging process and will absorb additional water. The excavated material will reduce in volume due to the drying process after filling. It is estimated that the disposed local soil will reduce 60% in volume.

The analysis reported here has been based on soil borings spaced about 1000 m apart. Additional borings will be made to upgrade the soil data. In 1995 the conceptual designs will be worked out. A more detailed construction schedule will be prepared. It is envisaged to build a test section of the sea defence structure to confirm the estimates and to optimize the design.

Land subsidence and other environmental impacts due to groundwater extraction from fractured hard rocks in Sri Lanka

U. de S. JAYAWARDENA

University of Peradeniya, Civil Engineering Department, Peradeniya, Sri Lanka

M. J. SARATHCHANDRA

National Water Supply and Drainage Board, Kandy, Sri Lanka

Abstract Groundwater extraction and distribution for the general public from two borehole wells which have been drilled through metamorphic rocks at Ampitiya, Kandy, was started in 1991. After two years the paddy fields and dug wells began to dry up and land subsidence was observed in the surrounding. In addition, the formation of cracks in the was seen in some houses in the neighbourhood. People in the area explained the other possible environmental effects. Land subsidence was greater close to the production wells. The dewatering cone extending along a linear rock fracture is related to the drying out of surface water resources. This situation indicates the extraction of groundwater from metamorphic hard rocky terrains also creates environmental problems for the people who utilize this groundwater for domestic purposes. To avoid this situation the average annual groundwater withdrawal should be kept constant, below the estimated recharge volume.

INTRODUCTION

General

Land subsidence is not a common geo-related hazard in Sri Lanka. It sometimes occurs in gem mining areas where horizontal tunnels or adits are made to remove gem bearing gravels. The first event on the Island of land subsidence due to groundwater extraction has been recorded from the Ampitiya production intake in Kandy. It was a very rare event because most of the boreholes have been drilled in metamorphic rocky terrains where the overburden thicknesses are comparatively low. Since there was an absence of environmental impacts, groundwater is being extracted from deep fractured rocks continuously without considering its effects on the overburden. After many complaints from the people living within the affected area, even though these same people benefit from the groundwater supply, a survey was carried out to assess the damage and other environmental impacts which are seriously affecting them. This paper shows the land subsidence and other environmental impacts due to groundwater extraction from hard rocky areas. The survey was carried out in 1993.

The project

After introducing the deep well concept to Sri Lanka in 1978, a number of foreign organizations have started to tap the deep groundwater resources in the crystalline hard rocks. Under this programme, hydrogeological investigations were carried out by "Kandy District Water Supply and Sanitation Project (KDWSSP)" for locating groundwater resources and for the determination of their properties for the realization of water supply in the area.

After feasibility investigations, deep boreholes were drilled at selected suitable locations. Groundwater from higher yielding wells was supplied for distribution through delivery pipes. Ampitiya scheme is one of the major groundwater supply schemes under KDWSSP.

Ampitiya is located southeast of Kandy city (Fig. 1). The area is a small, broad valley surrounded by gentle sloping hills. The elevation of the valley bottom is around 500 m above mean sea level. The wells have been drilled in the paddy fields. A narrow stream is flowing nearby. The mean annual precipitation at the closest station is 1959 mm. The population density of the area is 966 persons per km² (Plancenter Limited, Finland, 1981).

HYDROGEOLOGICAL SETTING

Geology

Geologically the intake is situated in the eastern limb of the Uduwela anticline, within a lineament along the northeast direction and also in a band of crystalline limestone (marble). The major rock types in the area are crystalline limestone, quartzite, quartz-feldspathic gneiss and interbanded charnockitic gneiss. The rocks dip towards the northeast.

Groundwater system

The lithological data of two boreholes indicate that the maximum thickness of soil overburden is 8 m. Highly fractured rocks have been noted between 20 and 25 m below the surface level. One interesting feature is the variable penetration rates of drilling through this marble. Penetration rates of highly weathered overburdens are about 20 minutes per metre. Slower rates are usually encountered when drilling through unfractured crystalline rocks. At some depths the penetration rates during the drilling of the boreholes was about 3 minutes per metre. This faster penetration rate, together with the samples collected, indicated the occurrence of highly fractured rocks in the marble. As faster penetration rates are found through fractured rocks than through the overburden, this points to the occurrence of narrow sinkholes within the marble. And also there were no samples at some depths. Lithological data indicate that this is an unconfined aquifer system and the principal aquifers in fractured rocks vary from 25 m to 40 m in thickness down to 60 m depth from the surface. Recharge to the principal aquifers is primarily from the hilly areas. Water may enter from all directions to this unconfined aquifer system.

LEGEND

-  Flow lines
-  Water level contours above "S.L.
-  Boundary for classify the effected areas
-  Location of borehole with elevation

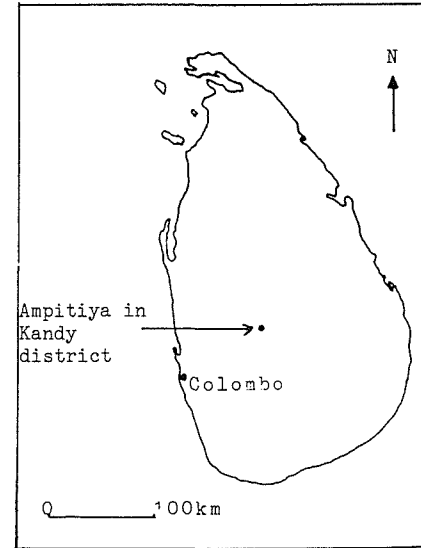
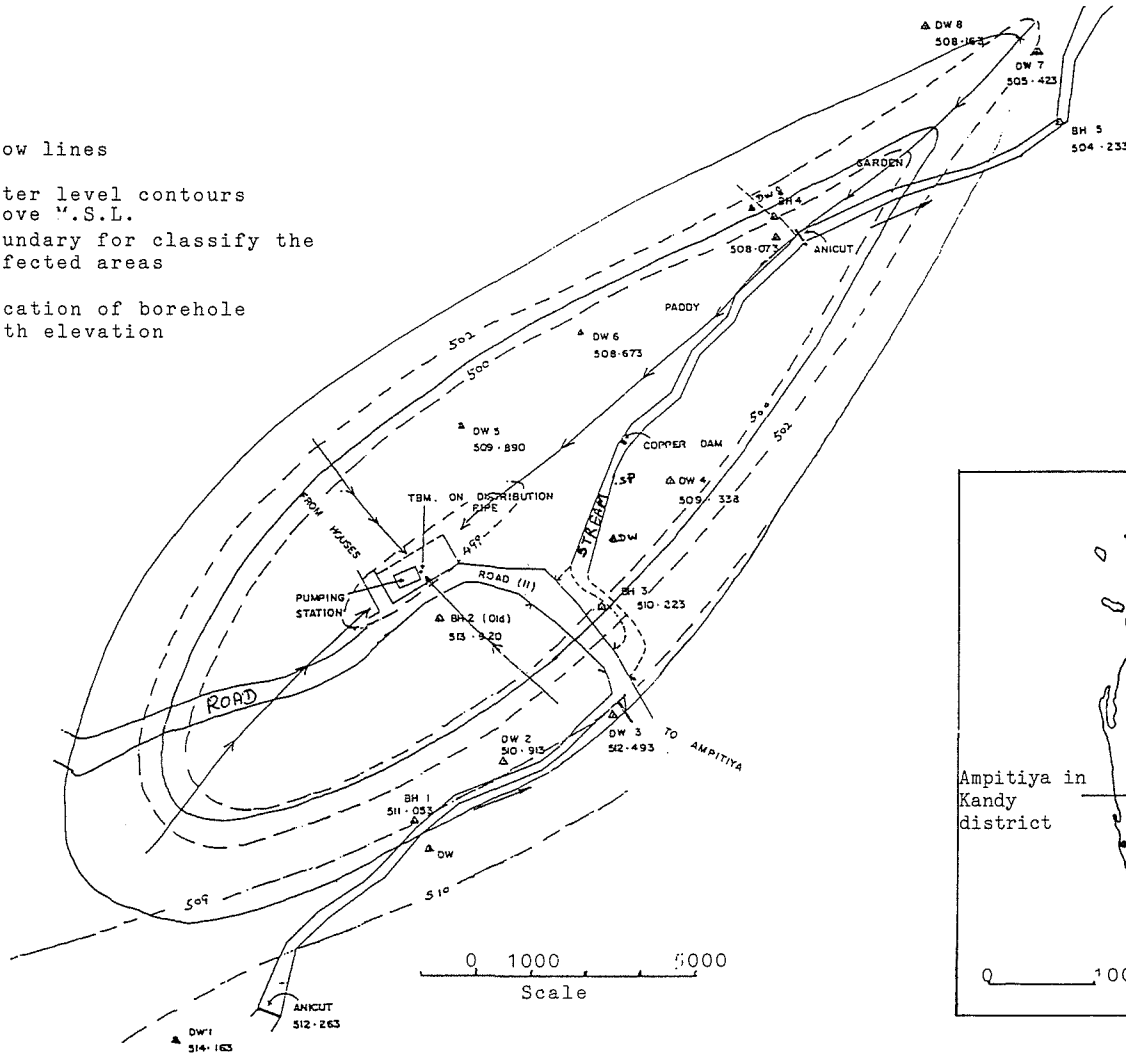


Fig. 1 The location of the project area, water level contours and flow lines around the intake and the boundaries of effected and non-effected areas due to groundwater withdrawal.

Groundwater pumping

Borehole drilling was completed in June 1990. In April 1991 the distribution of water for the public commenced. The collected data indicated that the average pumping rate in 1991 was $75.1 \text{ m}^3 \text{ h}^{-1}$ for a 17 h daily pumping period. In 1992, the groundwater withdrawal rate was $85.2 \text{ m}^3 \text{ h}^{-1}$ for 17 hours daily. This shows an increase of annual withdrawal in the second year. But the actual recharge amount per year has not been calculated. Therefore the higher extraction in the second year was purely in response to an increase in water demand.

Water level declines

Monitoring of dug wells and observation boreholes were carried out in 1993. Based on a study of water levels during this short period, water level contours were drawn for the peak drought at the beginning of April 1993. The level of water in boreholes have declined as much as 5 m in the first year and it has further declined by about another 5 m within the second year after pumping began. This is due to the higher withdrawal from the aquifer.

Dynamic water level contours and flow lines around the intake are shown in Fig. 1. It also indicates the situation of water levels along the lineament during pumping. The cone of depression is elongating and extending along the lineament which lies along the northeast direction. The dewatering cone along the lineament was related to the drying out of surface water sources. The difference between dynamic water level and static water level is about 19 m. The cone of depression extends along the lineament and covers an area of approximately $20\,000 \text{ m}^2$ (Fig. 1).

ENVIRONMENTAL IMPACTS

Subsidence

As mentioned earlier, groundwater level monitoring was not undertaken in the areas due to the lack of experience of similar events in Sri Lanka. While the test pumping programme was going on before distribution started, about 100 m^2 of the land surface around the borehole suddenly collapsed and the surface level dropped by about 1 m. This was the first subsidence event recorded in this well field. After the commencement of continuous pumping changes of ground surface spread further away from the borehole. Some cracks and holes were seen on the public road which crosses the area. About one year later some cracks on the walls and foundations of nearby buildings and gardens were noticed. Many complaints were forwarded after the appearance of these cracks. A detailed survey of the environmentally affected areas due to pumping of groundwater was undertaken for the benefit of the people living there. Figure 2 indicates the adversely affected areas where the buildings and gardens have been damaged due to groundwater withdrawal. These areas lie along the lineament and cone of depression. In general, about 1.5 m of land has subsided close to the pumping well and no subsidence was noticed in non-affected areas. But changes of the surface levels were not

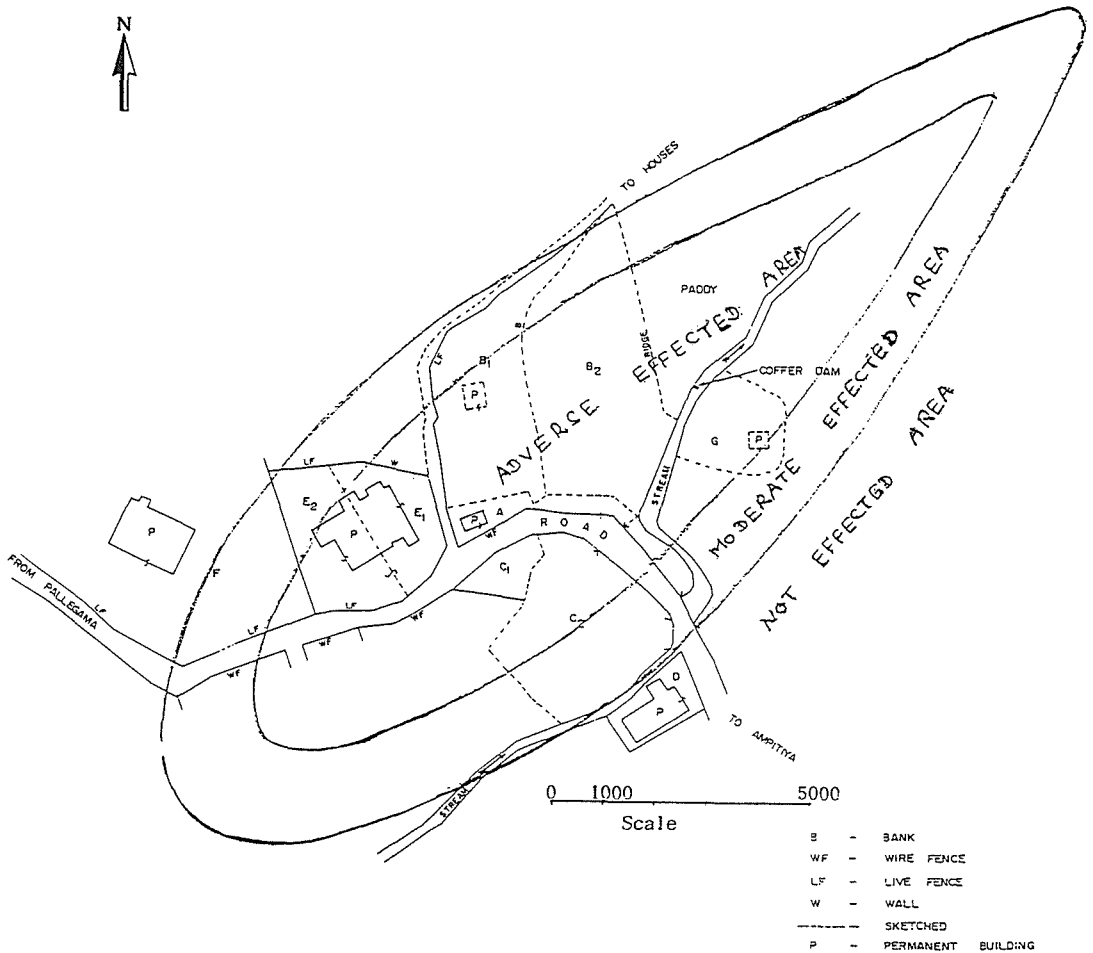


Fig. 2 The boundaries of the effected areas due to groundwater withdrawal.

monitored and therefore the actual amount of subsidence is not known. The badly affected areas were subsequently filled by compacted layers of soils. The project is still in operation. Structural damage related to land subsidence has been a common occurrence since this project was started.

Other impacts

The other major environmental impacts in the area were drying out of paddy fields and dug wells and lower crop yields from homestead plots. The local people reported their experiences of the situation in the paddy fields before and after groundwater extraction from the boreholes. The normally wet muddy paddy fields have dried up completely and it is difficult to work on the hard dry surfaces. Most of the dug wells have completely dried up. The crop yields in the homestead cultivation plots have decreased and they are comparatively very low after the commissioning of production pumping.

CONCLUSION

Land subsidence and the other environmental effects of the Ampitiya area in Kandy district, Sri Lanka, are directly related to the groundwater withdrawal from the deep boreholes. This groundwater mainly occurs in the fractured hard rocks and possible sinkholes in crystalline limestone. This is an unconfined aquifer system. To minimize the environmental damage and the future effects, the average annual groundwater withdrawal must be kept constant and should be less than the estimated average annual recharge. Still there is no system to find the changes of land surface. Therefore a proper technical management system to maintain the scheme is needed. This situation should be considered for the future projects to minimize the environmental hazards.

Acknowledgement The authors thank the management of Kandy District Water Supply and Sanitation Project for providing the permission and facilities and data to carry out this investigation. Thanks are extended to Mr U. Wickramasinghe for reading and correcting the manuscript.

REFERENCE

Plancenter Limited, Finland (1981) Interim Report of Kandy District Water Resources Potential Study, Kandy, Sri Lanka.

Legal aspects of catastrophic subsidence

PHILIP E. LaMOREAUX

P. E. LaMoreaux & Associates, Inc., PO Box 2310, Tuscaloosa, Alabama 35403, USA

Abstract Phosphate mining in Florida requires large quantities of water for processing. Beneath the Central Florida Phosphate district the Floridan Aquifer is capable of producing millions of litres per day from individual wells in limestone. The present combined use of groundwater by the phosphate industry exceeds 1134 million litres per day. The production of this water, plus that used for industrial, agricultural, and municipal uses has resulted in large overlapping cones of depression in the Floridan Aquifer. In addition to problems of water rights, there are associated environmental problems such as subsidence, diversion of streams, pollution, property damage, and litigation. In the United States, federal legislation may require companion legislation and rules in each state.

INTRODUCTION

Two striking examples illustrate the legal aspects of water supply development and catastrophic subsidence in karst terrains. The first in central Florida is related to the very large development of groundwater for municipal, agricultural, industrial, and mining purposes that has resulted in the development of protective legislation requiring very detailed and extensive hydrogeological studies. The second is related to dewatering for the quarrying of limestone in Alabama. Rights to water, groundwater depletion and catastrophic subsidence are related to dewatering practices. These examples illustrate the sensitivity of a limestone or karst area and the need for adequate environmental geoscience knowledge to deal with these problems.

PHOSPHATE MINING IN FLORIDA

Phosphate mining in Florida requires large quantities of water for processing. Beneath the Central Florida Phosphate District the Floridan Aquifer is capable of producing millions of litres of water per day from wells. The production of this water, plus that used for industrial, agricultural, and municipal uses has resulted in large overlapping cones of depression in the Floridan Aquifer, an area referred to by the press as the "big red hole."

A Consumptive Use Permit (CUP), the result of legislative action, was developed for a large farmer-owned cooperative that supplies fertilizer and other agriculturally-oriented products to its members over the United States. The project illustrates the kind of information required in Hardee County, Florida (Fig. 1).

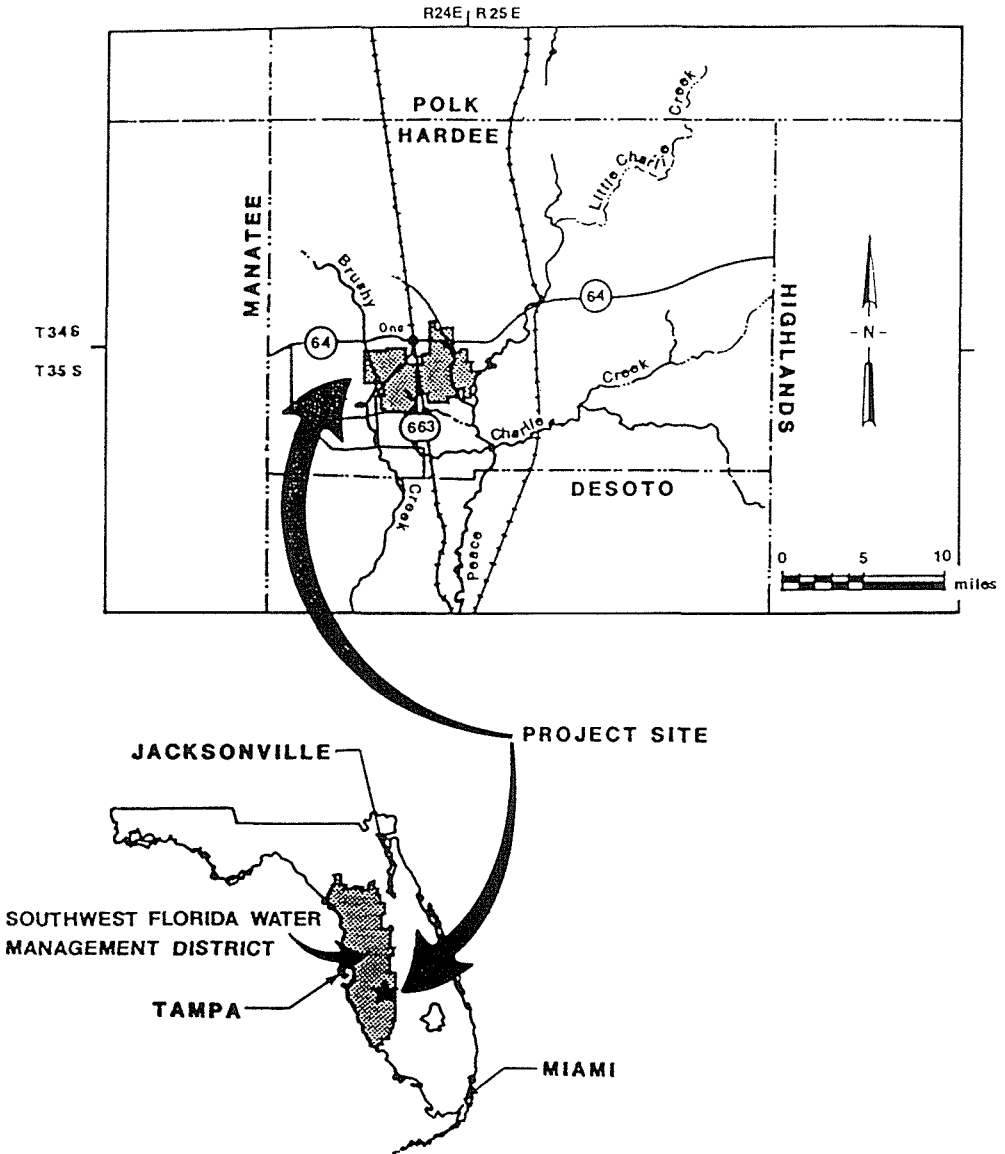


Fig. 1 Location of farm cooperative – Hardee County, Florida.

Florida groundwater law

The State of Florida passed legislation and has developed regulations to be applied to the development of groundwater. These regulations require strict adherence to defining the impact on the surface water, the shallow Surficial Aquifer, and the deeper Intermediate and Floridan Aquifers. Regulations require the Development of a Regional Impact Statement (DRI). Extensive pumping tests, surface water and groundwater studies, monitoring for discharge, water levels, and quality of water are required to identify

these impacts. This article describes the results of a study required to obtain a Consumptive Use Permit (CUP) for the Cooperative Fertilizer Facility in the Southwest Florida Water Management District (SWFWMD), the regional regulatory district of the Florida Department of Environmental Regulations (DER).

The SWFWMD in its Code Section 16, C3-0.15 (5)(A) provides that, "The water crop, in the absence of data to the contrary, is 1000 gallons per day per acre" (*9360 litres per day per hectare*). The cooperative's project tract is 3160 hectares and the water crop established legally for the acreage involved is more than needed for the proposed projected mining operations. However, "the 5-3-1 Criteria" which also applies requires that a determination be made to show that there will not be more than a 1.5-m average decline in water level in the Floridan Aquifer at the boundary of the property, not more than 0.3-m decline in the Surficial Aquifer at the boundary, and no more than a 1-m decline in the nearest water body (pond, lake, etc.). In addition, surface water flow in streams of the area must not be decreased more than 5% unless a variance to the rule is obtained.

Surface water flow is effected by differences in soils, geology, vegetation cover, altitude, elevation, and precipitation intensities for the various surface water basins within the tract. Each year, within the project area, streams recede to low flows, from April to June. Therefore, a seasonal distribution of average monthly flow must be determined. The annual minimum instantaneous or daily flow is subject to alterations by transient, natural, or manmade causes and therefore the lowest 7-day average flow each year, is used as a reference period for low flows. The yearly minimum 7-day low flows are determined from data collected by the US Geological Survey at gauging stations strategically located over the state. One or more of these long-term gauging station records provide the 7-day minimum flows. Regression models are used to obtain a site-specific extension of the annual flows to an equivalent 40-year period.

Description of project area

The cooperative's tract of land is east of the town of Ona. It is a 3155-ha tract that is intersected by S.R. 663 and the Peace River on the east. State Road S.R. 64 crosses the northern portion of the area. Surface water drainage of the area is by three small tributaries (which flow in a south/south-east direction) and discharge to the Peace River. The present land is used for range land, pasture, and citrus groves. An environmental concern is that part of the project area adjoining Troublesome Creek and the Peace River, known as the Oak Creek Islands, is a unique wetland that drains to Oak Creek.

The project duration will be 20 years and the mine will require that approximately 101 ha be mined each year. Of the 3155 ha, 2133 ha will be mined and 1022 ha will be left undisturbed. The Oak Creek Islands and the flood plain forest of Troublesome Creek and Peace River will not be disturbed.

CATASTROPHIC SUBSIDENCE FROM DEWATERING A QUARRY IN ALABAMA

Induced sinkholes (catastrophic subsidence) are those caused, or accelerated, by human activities. These sinkholes commonly result from a water level decline due to pumpage.

Construction activities in a cone of depression greatly increases the likelihood of sinkhole occurrence. Almost all occur where cavities develop in unconsolidated deposits overlying solution openings in carbonate rocks. Triggering mechanisms resulting from water level declines are (1) loss of buoyant support of the water, (2) increased gradient and water velocity, (3) water-level fluctuations, and (4) induced recharge. Construction activities triggering sinkhole development include ditching, removing overburden, drilling, movement of heavy equipment, blasting, and the diversion and impoundment of drainage. Triggering mechanisms include piping, saturation, and loading.

Induced sinkholes resulting from human water development/management activities are most predictable in a youthful karst area impacted by groundwater withdrawals. Shape, depth, and timing of catastrophic subsidence can be predicted in general terms.

Remote sensing techniques can be used in prediction of locations of catastrophic subsidence. This provides a basis for design and relocation of structures such as a gas pipeline, dam, or building. Utilization of techniques and a case history of the relocation of a pipeline are described.

Shelby County-triggering subsidence

In this hydrogeologic setting the following processes or activities are generally recognized as causing or accelerating subsidence following a decline of the water table.

- (a) The loss of buoyant support exerted by groundwater to unconsolidated materials overlying bedrock. Based on comparative specific gravities, for instance, this support to an unsaturated clay overlying a bedrock opening would amount to about 40% of its weight.
- (b) An increase in the velocity of groundwater movement resulting from an increased hydraulic gradient toward a discharge point. This water velocity results in the flushing of sediments filling openings in the cavity system. This, in turn, results in the downward movement of overburden into bedrock openings that forms a sinkhole.
- (c) The weakening of unconsolidated bridging materials and downward erosion of these materials caused by alternate repeated addition and subtraction of buoyant support and alternate wetting, drying, and lubrication brought about by water level fluctuations.
- (d) Induced recharge to previously water-filled bedrock cavities by infiltrating surface water passing through and eroding overlying unconsolidated material downward. This process, most active during periods of heavy or prolonged rainfall, is the same process described by many authors as "piping" or "subsurface mechanical erosion."
- (e) Grading, ditching, or other human-related disturbances that result in thinning of overburden or concentrations of drainage at the surface or in the subsurface. These activities induce more water to move more rapidly along preferential flow patterns through soils or overburden and into bedrock. Triggering mechanisms are piping, saturation, and loading. Other examples include leaking pools, pipes, gutters, irrigation, and broken lined canals or ditches. Collapses resulting from leakage from underground pipes are well documented in the literature. Such a collapse in a gold mining district in South Africa resulted in the loss of a three-story building and the lives of 29 men.

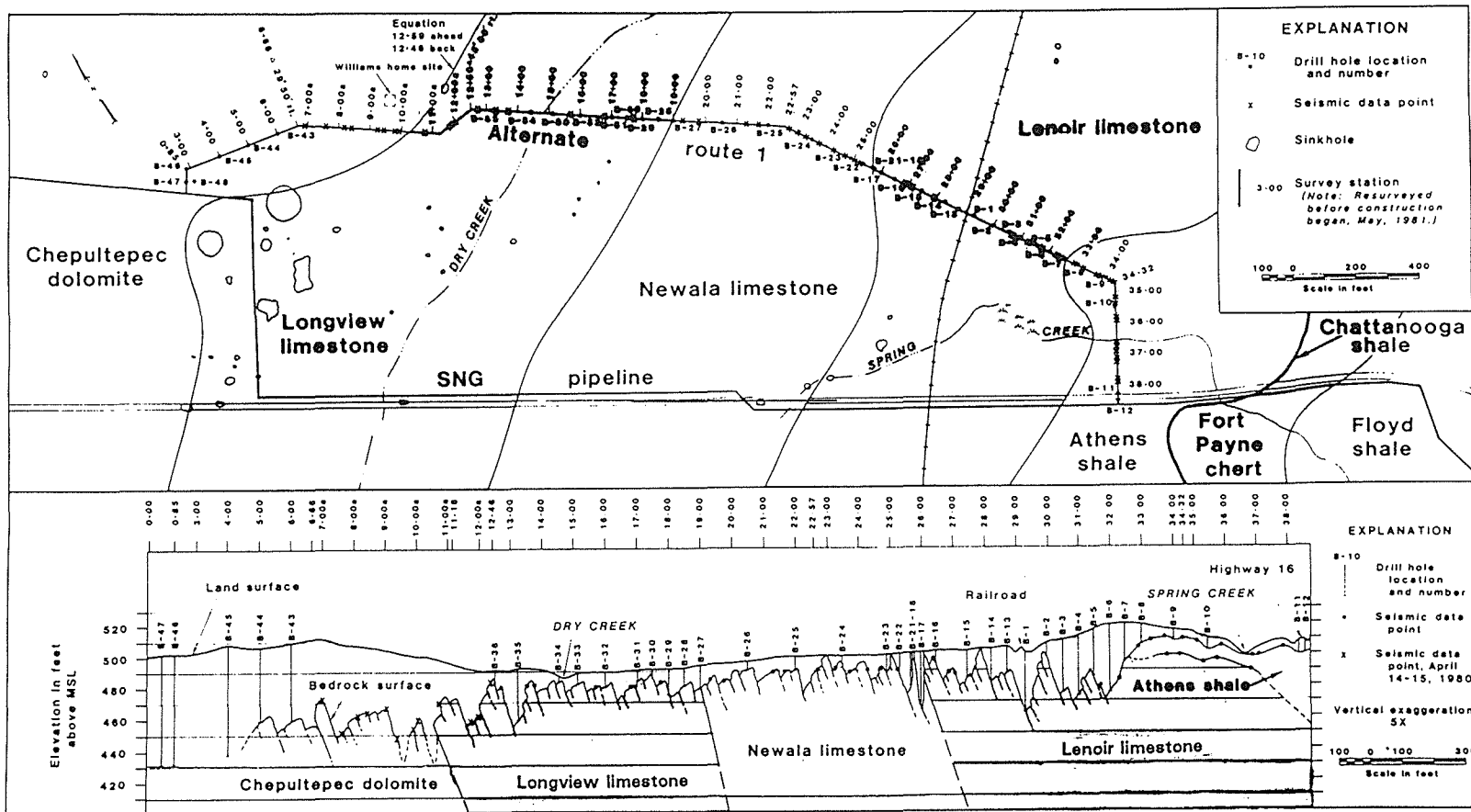


Fig. 2 Geological map and cross section, Shelby County, Highway 16.

- (f) Heavy construction, traffic, or explosives that disturb the soil or overburden and trigger its downward movement into solution openings in bedrock.
- (g) Removal of vegetation or the planting of large deep-rooted trees that increases recharge by creating avenues for more rapid movement of water from the land surface through soils and overburden to bedrock.
- (h) Drilling, auguring, or coring where surface water gains access to uncashed or unsealed holes. These activities cause erosion of overburden into underlying openings in bedrock. This occurrence has resulted in collapses at and near drill rigs or the holes created.
- (i) Impounding of water results in saturation of overburden and loss of cohesiveness of unconsolidated deposits overlying bedrock openings. This, accompanied by loading caused by the weight of impounded water, results in the collapse of unconsolidated

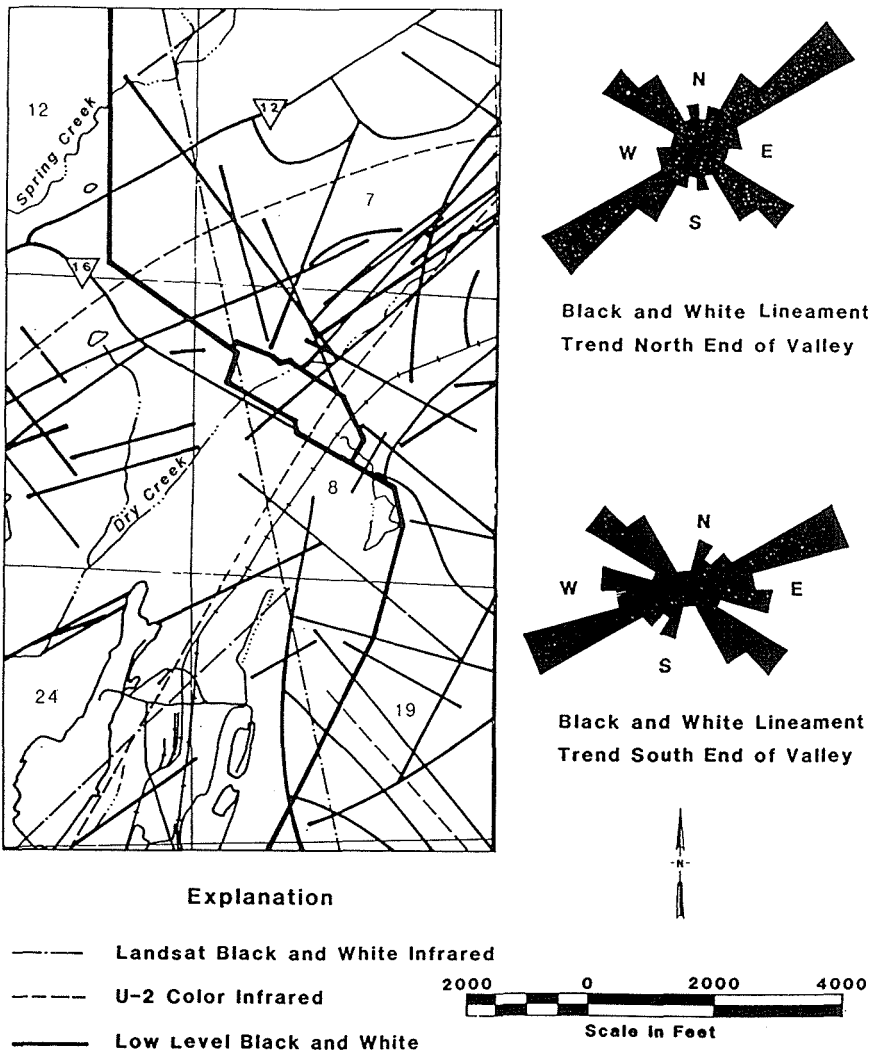


Fig. 3 Lineaments interpreted from aerial photographs.

material into a bedrock opening. Similar collapses beneath impoundments are also caused by piping. This occurs where the water table has declined below the top of bedrock and where openings at the surface are interconnected with those in bedrock. Collapses resulting from saturation and loading have been described by Aley *et al.* (1972) and those resulting from saturation and piping have been described by Warren (1974). Collapses resulting in draining of impoundments in cones of depression are not uncommon.

LEGAL ASPECTS OF SUBSIDENCE

In Shelby County, Alabama, USA, no local, state, or federal law specifically addressed catastrophic subsidence. Therefore, the determination of occurrence, risk, and damages had to be determined by the companies and landowners to reach a mutual settlement or by the courts.

Determining the geographic distribution, frequency, and probability of catastrophic sinkhole occurrence was accomplished by the following work:

- (a) Preparation of a detailed map of the geology and structure along the pipeline in the critical areas of subsidence (Fig. 2).
- (b) Mapping of exposures of bedrock limestone in quarries, road cuts, and sinkholes to determine dip and strike of bedding and joint and fault trends to relate to preferential solution zones and groundwater flow patterns.
- (c) Acquisition and analysis of satellite imagery and high- and low-altitude aerial photography (black and white, black and white infrared, colour infrared, colour). Resulting regional and local geological structural trends, lineaments, and sinkhole and drainage alignments were studied to project preferential groundwater flow patterns and solution zones in bedrock limestone (Fig. 3).
- (d) Use of seismic geophysical studies and test drilling to define the top of bedrock and overburden thickness along the alternate pipeline route (Fig. 2).
- (e) Determination of geology along the new pipeline route before construction, which was verified during its construction to ensure that the pipeline was securely connected to bedrock.
- (f) Monitoring of sinkhole-subsidence occurrence on a monthly basis over a period of 38 months. Each month, photography from an overflight was analysed and subsidence features located were checked in the field and documented.

REFERENCES

- Aley, T. J., Williams, J. H. & Masselo, J. W. (1972) Groundwater contamination and sinkhole collapse induced by leaky impoundments in soluble rock terrace. *Missouri Geological Survey, and Water Resources Engineering Geology Series no. 5, Rolla, Missouri, USA.*
- Warren, W. M. (1974) Retention basin failures in carbonate terrains. *Wat. Resour. Bull.* 10(1), 22-31.

The effect of land subsidence on the embankment of the new second freeway in Taiwan

LIN PING-SIEN

National Chung-Hsing University, Department of Civil Engineering, Taiwan, R.O.C.

CHAO CHI-SHENG, CHEN FU-SHENG & HO TAI-YUAN

China Engineering Consultants, Inc., Department of Geotechnical Engineering, R.O.C.

Abstract Economical development in Taiwan has rapidly grown in recent years, and this has greatly increased the demand for groundwater for the fish ponds, located mainly around the mid-southern coastline of Taiwan. The great demand for groundwater has led to extensive pumping which has brought about substantial surface subsidence around the area of Nanjou, Linbian, Jiadoan and Fungliao in Pingtung County, as well as Yulin and the outlet of Beigang Creek in Jiai County. This paper: (a) looks at the literature related to ground subsidence; (b) predicts the rate of subsidence and ground surface settlement; (c) evaluates the effect of ground surface settlement on the construction of the second freeway from Nanjou to Linbian; (d) presents measures to prevent or lessen the influence of subsidence on the second freeway. It also attempts to present design criteria for the new second freeway.

INTRODUCTION

Due to the safe yield of groundwater not being thoroughly understood and lack of proper management on its general use in Taiwan, many serious problems have resulted, including the excessive withdrawal of groundwater, a reduction of the effectiveness of flood control measures, decreased safety of embankments, sea-water intrusion, difficult drainage of downtown sewage, settlement of buildings, lower efficiency of irrigation system, destruction of tap water and wells, etc. For these reasons a high social cost must be paid by the local population. Thus, the purpose of this study is to find out the influence of land subsidence, resulting from the excessive withdrawal of groundwater, on the construction of the freeway passing through the Pingtung region. This paper aims to:

- (a) Look at literature related to ground subsidence in the region.
- (b) Perform a site investigation, selecting boreholes and taking undisturbed samples of soil for laboratory experiments or conducting *in situ* tests, to understand soil characteristics and strata in the region.
- (c) Use boreholes to install monitoring instruments such as observation wells, piezometers and settlement gauges to undertake a long-term observation programme.
- (d) Analyse the land subsidence by the three-dimensional finite-difference computer

programs MODFLOW and INTERBED based on the soil stratum and its characteristics, in order to predicting the ground surface settlement, the rate of subsidence, and the ranges affected according to the profile and the changes of groundwater table.

- (e) Evaluate the influence of land subsidence on the construction of the freeway based on the literature and numerical analysis.
- (f) Consult successful cases inside or outside Taiwan and draw up available precautions against land subsidence.

LITERATURE REVIEW

The geographic environment of the research area

The research area is located mainly around the southwest coastline in Pingtung County including Linbian, Linyuan, Nanjou, and Cinbe. Owing to the rapid development of pisciculture, serious land subsidence from the excessive withdrawal of groundwater has resulted. According to the results measured by the Taiwan Conservancy Bureau (Taiwan Conservancy Bureau, 1976), the strata in the region started to subside in 1961. The problem of settlement has become more serious since January 1979, and the rate of settlement was very rapid in the drought period in the first half of 1980, reaching an average rate of about 5 cm per month. The greatest settlement accumulated up till April 1992 was 2.35 m on the right outlet of the Linbian River in Linbian village. Moreover, it spread all around. After land subsidence, the low-lying areas in the region tend to suffer backward flow of seawater.

Distribution of soil and stratum

Most of the research area is covered by old underconsolidated alluvial deposits which have not undergone diagenesis and so have poor cementation and high permeability. In the primary region of aquifers the soil is composed of sand which is interbedded with thick silt or clay. The underground stratum is mainly composed of silty sand (SM), sandy silt (SP-SM), silty clay (MC), and clay (CL). The grain sizes of the soil are mostly from 0.3 to 0.01 mm, which are between fine sand and silt; the content of clay is not high. Therefore, silt is the primary soil for land subsidence in the region and most of them are on the condition of normal consolidation. Due to the large voids and compressibility, settlement will result from pumping or surcharge.

ANALYTICAL RESULTS AND PREDICTION OF LAND SETTLEMENT

Consolidation theory

In 1925, Terzaghi proposed a one-dimensional consolidation theory (Terzaghi, 1943). He used Darcy's law to describe the state that water drained from soil pores and assumed the drainage passage and the compression of soil were one-dimensional. Afterwards, this theory has been used widely for calculating the consolidated settlement

of soil. However, some hypotheses based on this theory often caused the restriction of its applicability. After Terzaghi, many scholars corrected and elaborated the one-dimensional hypothesis theory. Among them, the more consummate ones are the diffusion equation, as well as three-dimensional consolidation theory announced by Biot (1941). They provide more consummate analytic basis for analysing land subsidence. However, both Biot's three-dimensional consolidation theory and the diffusion equation are quite complicated. Thus, the US Geological Survey initiated numerical models to simulate land subsidence. It can solve the various properties of the region by means of finite-difference method and simulate different boundary conditions. This research adopted the MODFLOW program compiled by McDonald & Harbaugh (1988). The program primarily uses a three-dimensional finite-difference method to analyse the pattern of underground flow. In addition, it matches with the INTERBED storage package compiled by Leake & Prudic (1988) to calculate stratum settlement of clay in an aquifer caused by the consolidation resulting from the change in water head.

The analytic method of land subsidence

The prediction of land subsidence caused by excessive withdrawal of groundwater Two programs – MODFLOW and INTERBED – were used; the former simulates the rising and falling heads of groundwater and the latter simulates land subsidence caused by the falling groundwater head. Simplified stratum and relative soil parameters are developed based on the boring data, laboratory testing results, geological

depth (m)		soil classification	conductivity coeff. K (m/day)	transmissivity coeff. T (m ² /day)	specific storage coeff. S	elastic modulus E (t/m ²)
0m	G.L					
G.W.L 2m		SM	20			0.21
5m	confined aquifer					
24m	silt or clay(19m thick)	ML	0.0001			0.49
38m	confined aquifer	SM	20	130	0.001	
42m	silt or clay(4m thick)	ML	0.0001			0.42
59m	confined aquifer	SM	20	700	0.001	
77m	silt or clay(18m thick)	ML	0.0001	420	0.001	
87m	confined aquifer	SM	20			
98m	silt or clay(11m thick)	ML	0.0001	380	0.001	
116m	confined aquifer	SM	20			
136m	silt or clay(20m thick)	ML	0.0001	260	0.001	
149m	confined aquifer	SM	20			

Fig. 1 Simplified soil profile and parameters.

condition and related studies. The hydrologic data are not available easily and land settlement is closely related to pumping and dry climate. According to the survey by Taiwan Conservancy Bureau, it is pointed out that the drought cycle in Taiwan is twelve years. The annual pumping quantity from May 1979 to June 1991 was back-calculated by comparing the settlement from the *in situ* benchmark with the change in groundwater table. The five aquifers are in proportion of 2.5:10:40:40:7.5 measured by extensimeters and piezometers. Supposing that the quantity of yearly overextraction is 100% and the recharge is 80%, the land subsidence can then be predicted from the pumping simulation data at an increasing rate of 2.5% every cycle.

- (a) *The soil profile*: On the basis of stratum acquired by *in situ* boring, the simplified soil profile and parameters are shown in Fig. 1.
- (b) *Finite-difference mesh*: Considering the planned route of the new second freeway land subsidence contours, the research area is divided into 20×12 cells, each cell having an area of 200 m x 200 m. The cells are classified as having constant head or variable head based on the records of subsidence or non-subsidence (Lin et al., 1992).
- (c) *Change of groundwater head*: According to the report on groundwater level by Lin et al. (1992), the pumping ratio of the five aquifers is 2.5:10:40:40:7.5. Since May is the month with the lowest water level, for simulation purposes it is used as the point at which a year is divided into two periods. The period after May is considered the recharge period. Assuming that the yearly overextraction is 100%, the recharge would be 80% with one cycle of twelve years, it will increase 2.5% per cycle. From these assumptions, the variation in groundwater head is simulated.

Estimation of settlement caused by embankment surcharge After constructing the embankment for the new freeway, the surface will be paved. The problem of land subsidence caused by the construction of the embankment must be taken into consideration. The settlement can be calculated for different heights of fill ($H = 4, 6, 8$ m) based on:

- (a) Calculating consolidation settlement of silt from Terzaghi's consolidation theory.
- (b) Calculating the immediate settlement of each soil layer. By assuming that the settlement corresponds with one-dimensional elastic strain conditions, based on the E value suggested by Lin et al. (1992), the immediate settlement can be estimated.
- (c) Estimating the consolidation time of a silt or clay layer based on Terzaghi's 1-D consolidation theory.
- (d) Estimating secondary compression: Due to the discovery that $C\alpha/Cc$ has a certain ratio and adopting the silt characteristics suggested by Mesri & Godlewski (1977): $C\alpha/Cc = 0.03 \sim 0.06$, which is 0.045 in this study. Therefore, the secondary compression index $C\alpha$ is equal to 0.09. Besides, secondary compression settlement can be calculated from Mesri & Godlewski's formula. In this study, the secondary compression 50 years later is estimated.
- (e) Estimating the settlement of the ground surface: The total settlement of the stratum can be determined from $S_t = S_i + S_c + S_s$.

Results using the MODFLOW-INTERBED programs

Comparing the simulation results using MODFLOW-INTERBED in cells No. 19 and 11 with the measured values, for the period from 1979 to 1992 the error is about 6%. The settlement is estimated to be about 1.52 m after 55 years based on the pumping quantities from 1979 to 1991, which is about $227 \times 10^{12} \text{ m}^3 \text{ km}^{-2}$. The water head is decreasing about 23 m every layer. In recent years, the problem tend to alleviate gradually. If analysing the subsidence due to pumping during the period from 1987 to 1991 with the annual increment rate of 2.5%, overextraction of 100%, and recharge of 80%, the settlement after 50 years is estimated to be about 0.45 m, which is less serious than expected.

The settlement due to the construction of the embankment

The consolidation settlements due to the construction of the embankment are shown in Table 1. The time for 98% consolidation is calculated, except for the depth of 116 ~ 136 m, the consolidation is only 88% within the design period (50 years). The secondary compression for a 8 m high embankment and the immediate settlement due to embankment surcharge are also computed.

The land subsidence from pumping and embankment surcharge

Supposing that the construction of the embankment will be finished in May 1996, the greatest settlement of the ground surface will be 2.14 m, 2.43 m and 2.59 m after 50 years for embankment heights of 4, 6 and 8 m, respectively. Table 2 and Fig. 2 are the results for an embankment of height 8 m.

Considering that before the completion of constructing the embankment (before May 1996), the immediate settlement and most of the primary consolidation settlement will

Table 1 The consolidation settlement caused by embankment surcharge.

Depth (m)	$H = 6 \text{ m}$						$H = 8 \text{ m}$					
	Settlement (cm):						Settlement (cm):					
	1	2	3	4	5	6	1	2	3	4	5	6
5-24	3.0	9.3	29.4	57.2	68.1	64.9	3.6	10.7	33.3	67.0	83.2	81.7
38-42	1.3	2.0	2.9	3.7	4.2	4.0	1.6	2.5	3.6	4.7	5.4	5.3
59-77	5.6	7.0	8.3	9.4	9.9	9.7	7.1	8.9	10.7	12.2	13.0	12.9
87-98	1.9	2.1	2.4	2.5	2.6	2.6	2.4	2.8	3.1	3.4	3.5	3.5
116-136	2.4	2.6	2.7	2.9	2.9	2.9	3.1	3.4	3.6	3.8	1.5	3.9
Ground surface settlement	14.1	23	45.7	75.8	87.8	84.2	17.8	28.3	54.4	91.1	108.9	107.2

Table 2 The results of land subsidence by numerical simulation ($H = 8$ m).

Duration (year)	Consolidation settlement caused by embankment (cm)	Immediate settlement (embankment) (cm)	Secondary compression (embankment) (cm)	Total settlement caused by embankment (cm)	Land subsidence due to pumping (cm)	Estimated total settlement (cm)	Land subsidence after embankment construction (cm)
5	95.78	16.8	1.9	114.48	23.57	138.05	35.47
10	105.04	16.8	18.3	140.14	30.8	170.94	50.1
15	105.47	16.8	37.6	159.87	38.6	197.47	76.62
20	105.82	16.8	46.3	168.92	41.62	210.54	88.27
30	106.29	16.8	56.7	179.79	50.34	230.13	107.51
40	106.36	16.8	63.1	186.26	58.61	244.87	121.78
50	106.48	16.8	67.9	191.18	81.34	259.08	149.36

have taken place, the stratum settlement would include the subsidence caused only by pumping, secondary compression and the remaining consolidation settlement after completing the embankment. Therefore, the greatest stratum settlement will be about 1.49 m after 50 years for the heights of 6 and 8 m, as shown in the last column of Table 2.

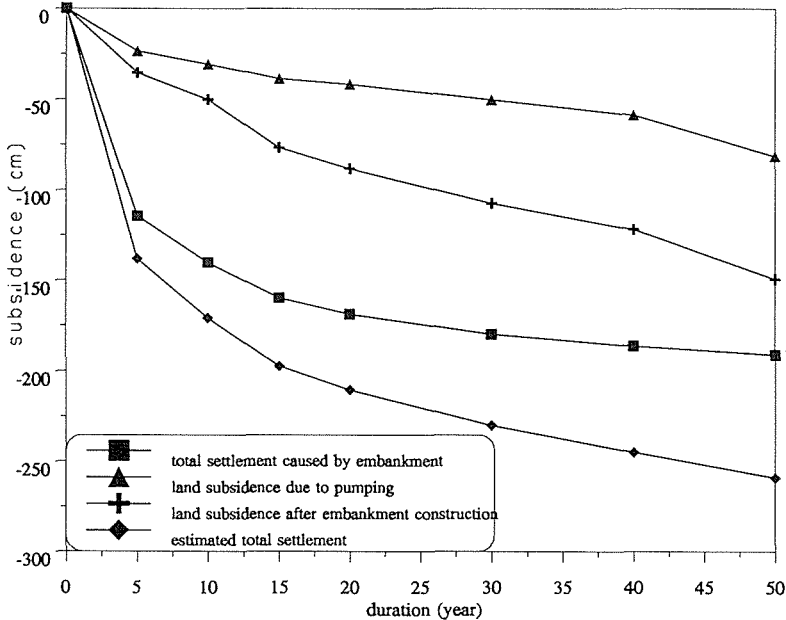


Fig. 2 The results of land subsidence by numerical simulation.

PREVENTIVE MEASURES AGAINST THE FREEWAY BEING AFFECTED BY SUBSIDENCE

The embankment settlements are caused by the embankment surcharge and the excessive withdrawal of groundwater. The former will cause a stability problem in the soft strata, which could be solved by filling soil at a slow rate, ensuring sufficient construction time of the embankment and using specific handling methods. The latter is the focus of this study.

The treatment of extensive stratum subsidence

Stratum subsidence due to excessive withdrawal of groundwater is a kind of "extensive stratum subsidence". According to experiences in Japan, it is very difficult to control subsidence within the permissive range even though they adopted the methods of vertical drainage or ground improvement via sand drains, wick drains, etc. It will be uneconomical and time-consuming if the land subsidence is controlled within the permissive extent by ground improvement methods.

As to the subsidence treatment methods from the above experience, if the embankment stability is ensured, easy-maintenance structures or non-worn-susceptible structure patterns due to subsidence, as shown in Table 3, are recommended instead of ground improvement methods. However, if the allowable settlement of underlain pipeline is not satisfactory or the maintenance is difficult, suitable treatment methods are still needed after considering the economy and effectiveness of construction.

Table 3 The treatment methods of freeway construction extensive land subsidence.

Type of subsidence treatment methods	Case 1: deep layer only	Case 2: deep and shallow layers
Increased embankment height	○	△
Low fill	×	△
Increased culvert clear height	○	○
Temporary pavement	○	○
Approach slab	△	○
Patching	△	○
Overlay	○	○
Ground modification methods for	×	△

○ necessary; × unnecessary; △ conditional.

Consideration on pile foundation

If the thickness of the alluvium is greater than 15 m and the rate of land subsidence is larger than 2 cm year⁻¹, the negative skin friction should be considered when pile foundations are adopted. In the region the land subsidence rate is greater than 2 cm year⁻¹, and the use of deep pile foundations should be avoided. However, the pile foundations are still needed, so the negative skin friction should be considered carefully in the design procedure. At shallow layers, because of the water supply from the surface, the general groundwater pressure presents a static state, and the overextraction of groundwater has little impact. The adoption of "friction piles" when ensuring the shallow layer in the research area has no problem of extensive land subsidence.

The treatment of differential settlement

The embankment settlement is uniform if the extensive land subsidence is at the deep layer. However, differential settlement will occur when the extensive land subsidence is at the shallow layer. This differential settlement will affect the smoothness of the paved surface of the freeway. The treatment methods for differential settlement can be divided into two categories, basic and auxiliary, as shown in Table 4.

Table 4 The treatment methods for the smoothness of freeway.

Treatment methods		General embankment	Culvert pipeline	Abutment
Basic treatment methods	accelerated consolidation	○	○	○
	surcharge	○	○	○
	sand compaction			○
	preload		○	○
	long time placement	○	○	
	temporary pavement, overlay, patching,	○	○	○
Auxiliary treatment methods	increased embankment height	○	○	
	increased clear height cross section		○	
	drainage	○		
	voids treatment			○
	approach slab			○
	negative skin friction treatment			○

○ applicable.

The influence of extensive land subsidence on the local hydrologic environment

- (a) Coastal stratum subsidence will cause sea water to flow backwards. The embankment could be submerged or eroded by sea-water encroachment. Therefore, liplap or buttresses at the base of the embankment must be installed as protection measures.
- (b) If there are no extensive drainage measures within the area of extensive land subsidence, the water level will rise because the rivers cannot easily flow into the sea, and the speed of the current will decrease. In order to solve the problem caused by rising water levels and decreasing current velocity, the cross section of the drainage culvert must be increased accordingly in the freeway design.
- (c) When the cross section of drainage culverts is increased due to the rising water level, the design height of the embankment must be increased if necessary to ensure the proper overburden depth of the box culvert.
- (d) Since the planned route of the second freeway runs roughly parallel to the Linbian River and is perpendicular to the coastline, it will not be an obstruction when flooding due to heavy rainfall or seawater occurs. Therefore, constructing the freeway will not negatively affect the hydrologic environment of the extensive region.

CONCLUSIONS AND SUGGESTIONS

- (a) According to the above discussion, in Nanjou and Linbian, land subsidence due to overpumping of groundwater only occurs in the deep layer (below 60 m below ground level). Therefore, the subsidence at shallow layers due to the construction of the embankment surcharge and the deeper subsidence due to overpumping of groundwater can be considered separately. Their summation is the total settlement.
- (b) Because the extensive land subsidence in Nanjou and Linbian is at a deep level, specific ground modification methods (e.g. soil improvement) are not recommended when constructing the freeway. However, in the study region, if the shallow layer is soft soil, the general considerations of embankment design criteria in the soft compressible stratum should be examined to check that the consolidation settlement is within the permissible range.
- (c) Because the extensive land subsidence at a deep level is uniform, it will not influence the smoothness of the road surface. Therefore, when considering the effect of subsidence on constructing the freeway, treatment measures as suggested in Tables 3 and 4 can be adopted. Temporary pavements and overlays should be used if possible. In this region there are many drainage culverts and bridges (passing bridges and drainage bridges at eight places). Based on the estimated settlement, the bottom of drainage culverts should be lifted or their heights should be increased in order to increase their drainage capacity.
- (d) If bridge abutments are supported by pile foundations the effect of negative friction must be considered. However, if the friction pile and its frontage does not penetrate the extensive land subsidence at a deep level, the consideration of negative friction can be omitted (a pile length within 30 m is recommended). At the junction of embankment and bridge abutment, differential subsidence may occur, which can be treated by patching, overlays and approach slabs.

- (e) Propose that the government make and enforce restrictions on pumping groundwater. As far as the basic solution is concerned, we should make more efforts to survey and collect basic data, including setting up a groundwater data centre in Taiwan, making a survey of wells, setting up a monitoring system of groundwater levels, quality and land subsidence. With regard to groundwater withdrawals, we should open up new substitutes for water resources, plan restricted areas, disperse wells, execute present regulations and laws, promote groundwater conservation, and distribute groundwater reasonably.

REFERENCES

- Biot, M. A. (1941) General theory of three-dimensional consolidation. *J. Appl. Phys.* **12**(2), 155-164.
- Leake, S. A. & Prudic, D. E. (1988) Documentation of a computer program to simulate aquifer-system compaction using the modular finite-difference ground-water flow model. *US Geol. Survey Report no. 88-482, Tucson, Arizona.*
- Lin, Ming-Huang et al. (1992) *An Investigation on the Land Subsidence in Hukuao area of Yunlin Hsian and Linbian Area of Pingdong Hsian*, 108-151. Industrial Technology Research Institute.
- McDonald, M. G. & Harbaugh, A. W. (1988) A modular three-dimensional finite-difference ground-water flow model. *US Geol. Survey Report no. 83-875.*
- Mesri G. & Godlewski, P. M. (1977) Time- and stress-compressibility interrelationship. *J. Geotech. Engng Div. ASCE* **103**(GT5), 417-430.
- Taiwan Conservancy Bureau (1976) *An investigation on the subsidence of land in Pinyngtung County 11 (Linbian, Chiatung, Fangliao), Taiwan.*
- Terzaghi, K. (1943) *Theoretical Soil Mechanics*. John Wiley & Sons, Inc., New York.

Problems of subsidence and their mitigation in Saga Plain, Japan

NORHIKO MIURA, SHIGENORI HAYASHI

Saga University, Department of Civil Engineering, 1 Honjo, Saga 840, Japan

MADHIRA R. MADHAV

Indian Institute of Technology, Department of Civil Engineering, Kanpur 208016, India

YOICHIRO HACHIYA

Saga Prefectural Office, Saga 840, Japan

Abstract Saga Plain is a lowland affected by 6 m tides of the Ariake Sea. The plain is underlain by 15-40 m of soft, compressible and highly sensitive marine (Ariake) clay below which aquifers of water bearing strata exist. Land subsidence started about 35 years ago due to groundwater withdrawal. Subsidence of the order of 80 cm to 1 m has been observed. The rate of subsidence accelerated to 16 cm year⁻¹ due to an extremely hot summer and great demand for water in 1994. Medium and heavy structures built on piles bearing on dense gravel layers lead to large differential settlements between pile supported structure and the surrounding ground due to land subsidence. This paper summarizes the geotechnical characteristics of Saga Plain, and the variety of ground improvement techniques adapted to mitigate problems arising from subsidence.

INTRODUCTION

The Ariake Sea is located near the centre of Kyushu, the southern most main island of Japan. It is a large bay (Fig. 1) covering an area approximately 1700 km², with a central axis of length of about 98 km, of an average width of 18 km and a depth of 20 m. The characteristic feature of the Ariake Sea is the vast tidelands exposed at low tide. The Saga-Shiroishi Plain of today is formed either by natural action of alluvial rivers and tidal currents or by reclamation of land from the sea. The original coastline is believed to be approximately 20 km inland from the present one. Reclamation work in this area dates from 1185 AD (Watanabe, 1988). The different stages of reclamation are depicted in Fig. 1. Typhoons that strike the area during the post monsoon period (July-September) each year, have posed a serious threat to the dikes. Consequently, the design and construction of these dikes are modified from the conventional vertical wall type to a gently sloping embankment that can soften the impact of oncoming waves.

GEOLOGY

The Saga Plain is surrounded (Oshima, 1988) in the north by Mesozoic granites and a small amount of metamorphic rocks, in the east by Sangun metamorphic rocks, in the

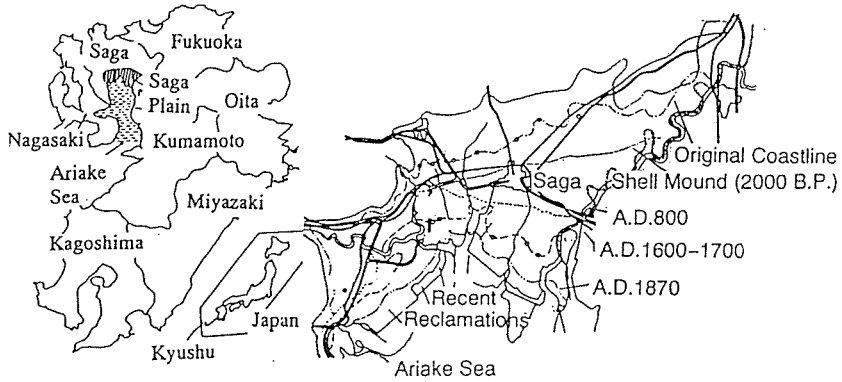


Fig. 1 Ariake Sea and reclamation in Saga Plain.

the west by Palaeogenic sediments, diluvial volcanic rocks, diluvial terraces and alluvial fan, and in the east by the small hills of Kishimayama. The alluvial delta less than 4 m in altitude, is underlain by unconsolidated sediments.

The Saga lowland consists of an alluvial delta, with the limit of the tidal river stretching as far out as the root of the delta region. The south of Saga lowland is reclaimed land making the best use of top set of the delta in the tidal flat, by drainage. The succession of unconsolidated sediments are divided into A, B, C, D, E and F formations (Fig. 2). Formation A is Ariake clay deposited in alluvial transgression and regression and it consists mainly of soft silt and clay occasionally accompanied by sand. Formation B is a diluvial marine deposit, mainly composed of sand. C formation is a pumice-bearing volcanic ash formation formed about 33 000 years ago, from the pyroclastic flows from Mt Aso. Marine sands and silts constitute formations D, E and F (undivided diluvial beds). Formation F has compact silts and fossils of wood. All the formations are inclined from the land to the sea with inclination increasing downward, indicating compression of the basin in the early stages of deposition of the thick unconsolidated deposits.

GEOTECHNICAL PROPERTIES

The Ariake clay deposits vary in thickness from 15 to 42 m. Based on the fossil assemblages investigated, it is surmised that the clay layers in the top 10-11 m were deposited under marine environment while the lower layers were formed under brackish conditions (Ohtsubo *et al.*, 1988). Smectite is the predominant mineral which exists along with vermiculite, illite and kaolinite, in the clays. The geotechnical and chemical properties from a typical site in Saga Plain is shown in Fig. 3. The liquid limit and the plasticity index vary in the ranges 60-125 and 25-80 respectively. The natural water content ranging between 80-140 is higher than the liquid limit. Liquidity index value could be high as 2.5. The sensitivity of the soil is less than 100 in the top 10 m but could be as high as 500 or more at depths below 10 m. Thus, the clays can be classified as quick or extra quick according to Rosenquist's (1953) classification and salt leaching is identified as the primary cause for the sensitivity of the clays (Fig. 4). The salt concentration in the pore water ranges between 0.05-1.08 g l⁻¹ for extra quick

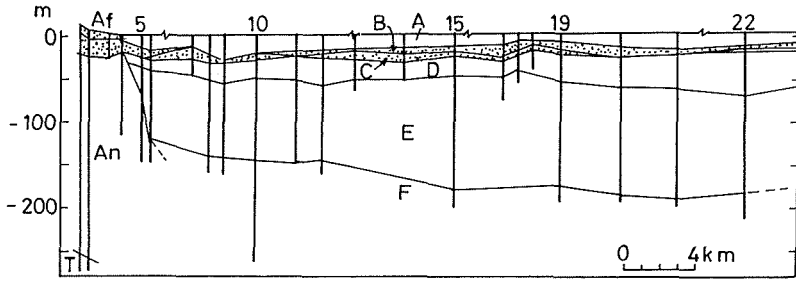


Fig. 2 Geologic profile of Saga Plain (after Oshima, 1988).

clays and $1.02-10.4 \text{ g l}^{-1}$ for quick clays. The undrained strength of the clays could be as low as 5 kPa near the ground surface and increases with depth to a value of about 25 kPa at 15 m.

The compression index, C_c , of Ariake clay ranges between 0.5 and 2.5, and the coefficient of consolidation from $3.5 \cdot 10$ to $1.5 \cdot 10^2 \text{ cm}^2 \text{ day}^{-1}$ (Sanaka, 1990). The values of S_u , the undrained strength, q_c , the cone penetration resistance, $S_{uf(v)}$, the field vane and q_u , the unconfined compression strengths together with σ_y' , the preconsolidation stress from standard oedometer test are presented in Fig. 5 from Hanzawa *et al.* (1990). The undrained strength of upper clay increases linearly with depth while that of lower clay increases more rapidly with depth. The preconsolidation stress, σ_y' , agrees closely with the effective overburden stress, σ_{vo}' , particularly for the upper clay indicating that it is in normally consolidated state. σ_y' values for the lower clay layer are somewhat greater than σ_{vo}' at its lower end. The variation of S_u with depth is consistent with that of σ_y' with depth.

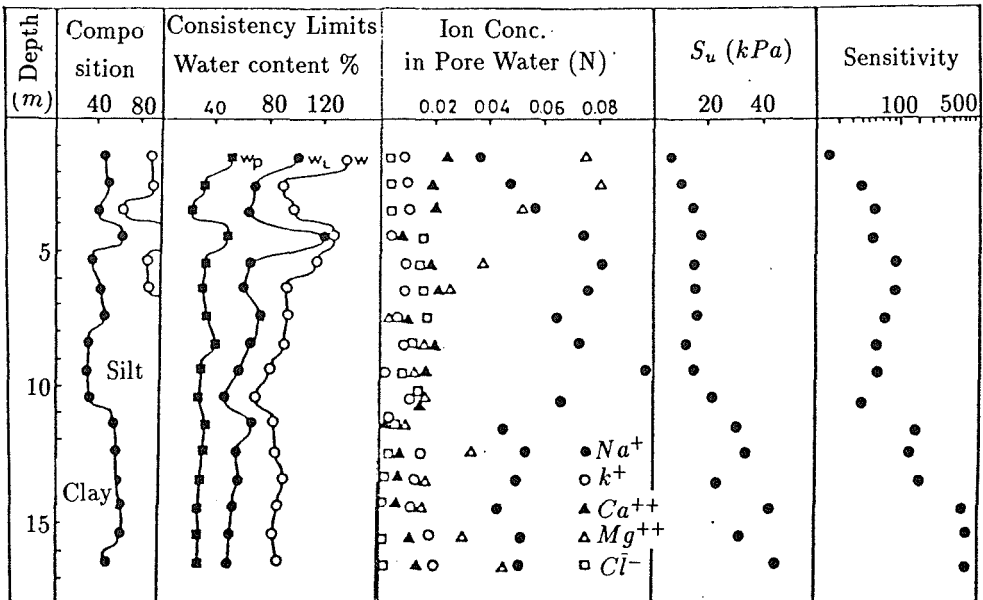


Fig. 3 Typical geotechnical and chemical properties of Ariake clay (after Ohtsubo *et al.*, 1988).

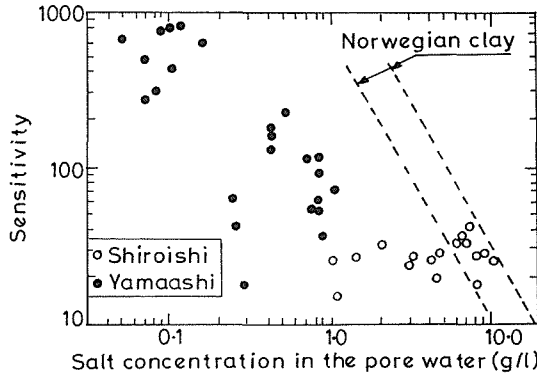


Fig. 4 Salt content versus sensitivity (after Ohtsubo et al., 1988).

SUBSIDENCE

When groundwater had been pumped out from the sand layer, the first aquifer, the sea water had intruded into it increasing the Cl ion content to a value above the permissible one. Subsequently, groundwater from the second and third diluvial layers is being utilized for domestic, agricultural and industrial purposes. The quality of groundwater from the third aquifer in Shiroishi area appears to be affected.

As a consequence of groundwater pumping, Saga Plain is subjected to subsidence due to induced consolidation of soft normally consolidated Ariake clay (Miura et al., 1988). Even though subsidence initiated from 1950s, precisely monitored values from the year 1971 for Saga and Shiroishi districts are shown in Fig. 6. The settlements

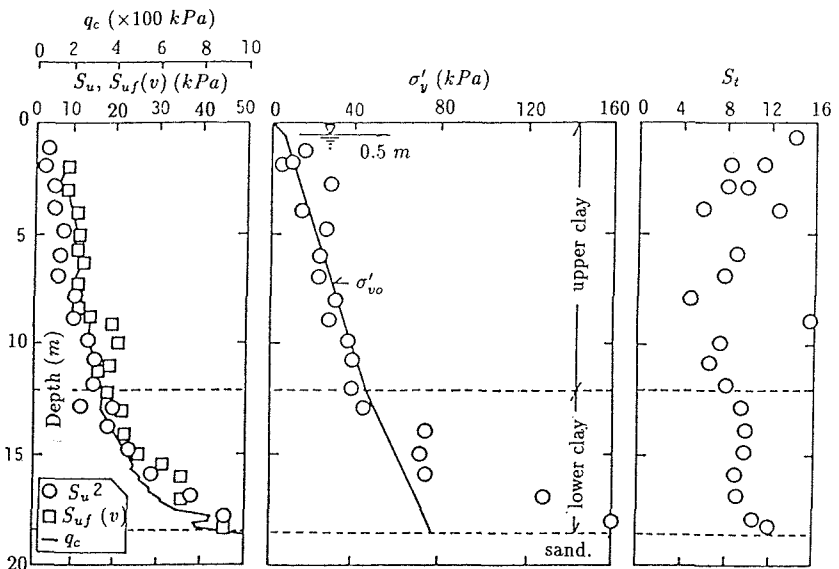


Fig. 5 Undrained strength (S_u), yield stress (σ'_v) and sensitivity (S_t) from unconfined, field vane, oedometer and cone penetration tests (after Hanzawa et al., 1990).

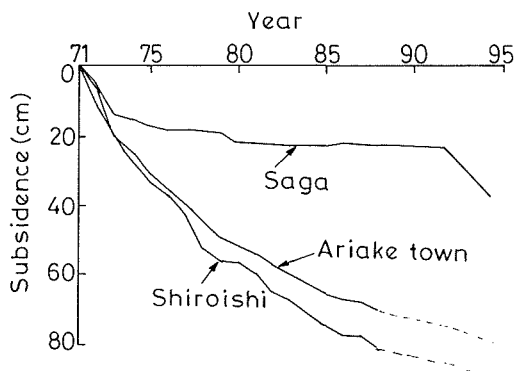


Fig. 6 Subsidence in Saga Plain.

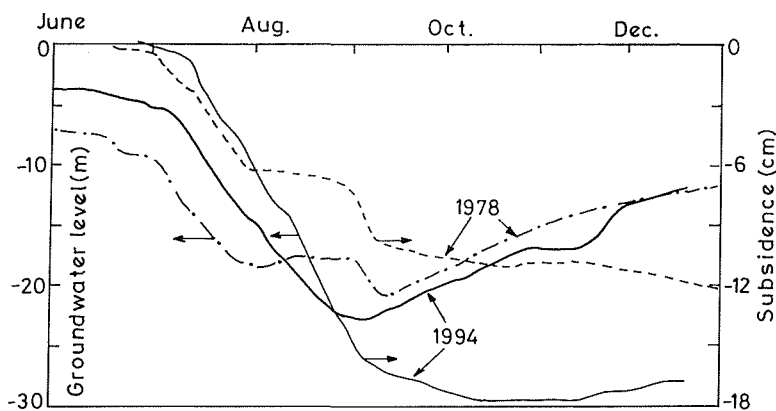


Fig. 7 Groundwater level and subsidence in the years 1978 and 1994.

observed from 1971 to 1988, are of the order of 30 cm in Saga and 80 cm in Shiroishi. The movement of the ground level corresponds to that of the groundwater level with a small time lag, the rates being more during the summer months because of increased pumping rates. In periods of small rainfall, the subsidence rate per year has been as high as 10 cm in Saga and 13 cm in Shiroishi. Saga Plain has experienced in 1994 the severest summer for the last 50 years with the maximum temperature reaching a record level of 40.6°C. The movement of groundwater and ground levels from June to December 1994 are depicted in Fig. 7 and compared with those for the year 1978 which was the next most severe summer. In Shiroishi area, while the groundwater level fell by about 20 m, the subsidence has been nearly 18 cm in four months.

DAMAGE DUE TO SUBSIDENCE

Most of the structures in Saga Plain have been built on piles that are made to rest on the dense sand/gravel layers below the soft clay. However, because of subsidence,

serious differential settlement appears between the pile supported structures and the surrounding ground. A typical example is a box culvert and the approach roads on both sides of the culvert, the different settlements in this case reached 80 cm because of an overlay of asphalt concrete which was added occasionally to reduce the differential settlement. The piles are also subjected to down drag.

FLEXIBLE AND COMPATIBLE FOUNDATIONS

The basic principle of the flexible foundation system is that the structure deforms in conformity with the differential settlement of the ground, which is reinforced by floating foundations (Miura & Madhav, 1993). Two foundation types, viz. timber pile-grid system (Type A) and improved soil column-grid system (Type B), are adopted. Type A foundation system (Fig. 8) uses timber piles as skin resistance piles with a geogrid reinforced granular pad on top to serve as a pile cap and to restrain lateral displacements. Camber provided minimizes excess differential settlements.

In Type B foundation system, improved soil-lime columns of 1 m diameter are made by the Dry Jet Mixing (DJM) method (Fig. 9), a mechanical method of mixing quicklime with clay *in situ*. The area of the soil-lime columns is 30% of the total area of the ground. A reinforced granular base course with a single layer of polymer grid and with camber is provided as in the Type A system.

To make the structure (sluice way in this case) flexible, its body is separated into several blocks which are connected by flexible/multilayer rubber joints. Figure 10

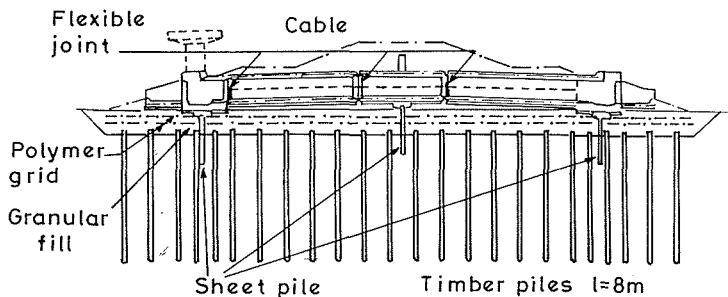


Fig. 8 Floating timber pile-reinforced granular fill system.

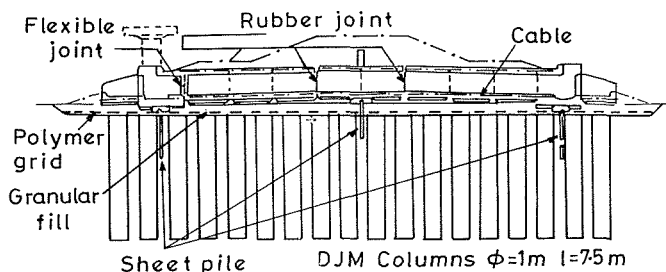


Fig. 9 DJM column-reinforced granular fill system.

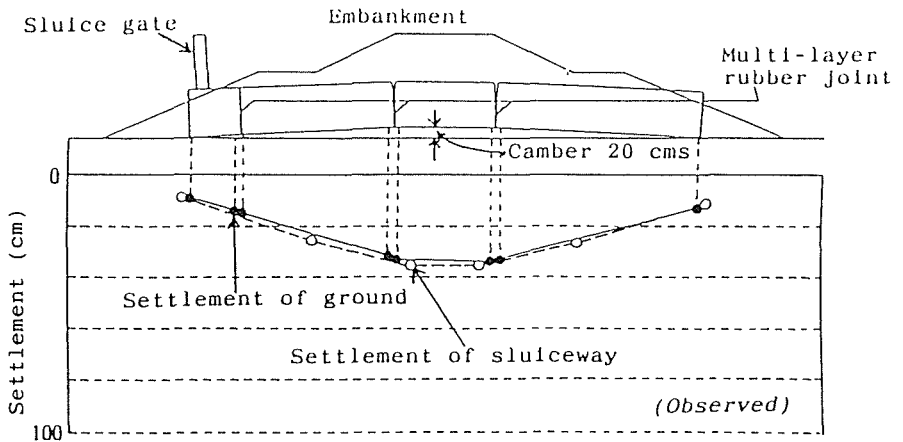


Fig. 10 Compatible deformation of structure and soil.

confirms that the settlements of the structure and the ground are compatible and consistent.

CONCLUSIONS

The lowlands reclaimed from the tidal range of Ariake Sea, Japan, are subjected to subsidence due to groundwater withdrawal. The Ariake clay whose thickness varies from 15 to 40 m is very soft, highly compressible and extremely sensitive due to leaching of salts from the pore water. Subsidence of the order of 80-100 cm causes large differential settlements especially adjacent to structures built on end bearing piles. A new flexible and compatible foundation system consisting of timber piles or DJM columns and polymer grid reinforced granular fill, are shown to function extremely well.

REFERENCES

- Hanzawa, H., Fukaya, T. & Suzuki, K. (1990) Evaluation of engineering properties for an Ariake clay. *Soils and Foundations* 80, 11-21.
- Miura, N. & Madhav, M. R. (1993) Performance of a new system of flexible sluiceway with floating foundation in highly compressible ground. In: *Proc. Int. Symp. on Prediction versus Performance in Geotechnical Engineering* (Bangkok), 15-28.
- Miura, N., Taesri, Y., Sakai, A. & Tanaka, M. (1988) Land subsidence and its influence to geotechnical aspects in Saga plain. In: *Proc. Int. Symp. on Shallow Sea and Low Land* (Saga), 151-158.
- Oshima, T. (1988) Geological structure of Saga Plain. In: *Proc. Int. Symp. on Shallow Sea and Low Land* (Saga), 139-144.
- Ohtsubo, M., Takayama, M. & Egashira, K. (1988) Mineralogy, chemistry and geotechnical properties of Ariake marine clays. In: *Proc. Int. Symp. on Shallow Sea and Low Land* (Saga), 145-150.
- Rosenquist, I. Th. (1953) Considerations on the sensitivity of Norwegian quick clays. *Geotechnique* 3, 195-200.
- Sanaka, N. (1990) Saga Airport Project on reclaimed lowland in Ariake clay. In: *Proc. Int. Seminar on Geotechnical and Water Problems in Lowland* (Saga), 97-108.
- Watanabe, K. (1988) Overview of the Ariake Sea and its surrounding areas. In: *Proc. of the Int. Symp. on Shallow Sea and Low Land* (Saga), 1-7.

Recent countermeasures for land subsidence and groundwater resources in Japan

KUNIAKI SATO & NGUYEN VAN HOANG

Saitama University, Hydrosience and Geotechnology Laboratory, Faculty of Engineering, 255 Shimo-Okubo, Urawa, Saitama 338, Japan

Abstract The history of land subsidence in Japan can be traced back to the late 1930s. During the past century the suppression of the land subsidence has been a constant challenge in groundwater resources management. This paper deals with the latest measures for land subsidence. The current approach is rooted in optimizing the groundwater pumpage without land subsidence. Today, an adjusted approach is required for more groundwater to meet water shortages in the summer season.

INTRODUCTION

A history of land subsidence due to groundwater pumping in Japan can be traced back to the late 1930s. During World War II no land subsidence was observed because there was no increase in groundwater use and industry was suspended. Levelling results of land in several places in Osaka and Tokyo showed the response of land subsidence to the industrial and economical growth after the end of World War II. The demand for groundwater by industry since 1950 has increased tremendously and has brought serious land subsidence to several industrial areas. The use of water in 1993 in Japan is given in Table 1.

The lowland below sea level was a problem because of sea-water flooding caused by tidal storms and big typhoons. This became a serious social problem. The state and local governments started to request counter measure for land subsidence. The state law on industrial water has been enacted to control groundwater pumping in parts of some land subsidence areas since 1956. There have been no signs of a reduction in land subsidence, irrespective of whether the state law and regulation by local governments were enacted. Thus, the state law on industrial water has been revised to strengthen the control of groundwater withdrawals, and also the state government issued a law on groundwater pumping for building's cooling water, which was in force in 1962 (Environment Agency of Japan, 1990). Figure 1 shows the history of land subsidence and groundwater use.

Countermeasures for land subsidence were improved by the development of new water resources in place of groundwater resources as well as industrial water supply projects. Land subsidence has expanded to industrialized and newly-developed cities. The pollution of groundwater with salt-water intrusion in coastal aquifers increased because of so much groundwater extraction. After the 1970s a numerical groundwater simulation technique was used to predict and to plan countermeasures for land subsidence. It was the time when computers started to become popular. In those days, studies of the prediction of land subsidence and allowable pumping volume by means of

Table 1 Water resources and water use in 1993 in Japan (after Environment Agency of Japan, 1994).

Kind of use	Total volume:		Surface water and others:		Groundwater:	
	(10 ⁹ m ³ year ⁻¹)	(%)	(10 ⁹ m ³ year ⁻¹)	(%)	(10 ⁹ m ³ year ⁻¹)	(%)
Industrial	10.70	12.3	7.65	10.1	3.05	26.3
Service water	16.74	19.2	13.10	17.4	3.64	31.4
Agricultural	58.60	67.3	54.72	72.5	3.88	32.5
Others	1.02	1.2	0.00	0.0	1.02	8.8

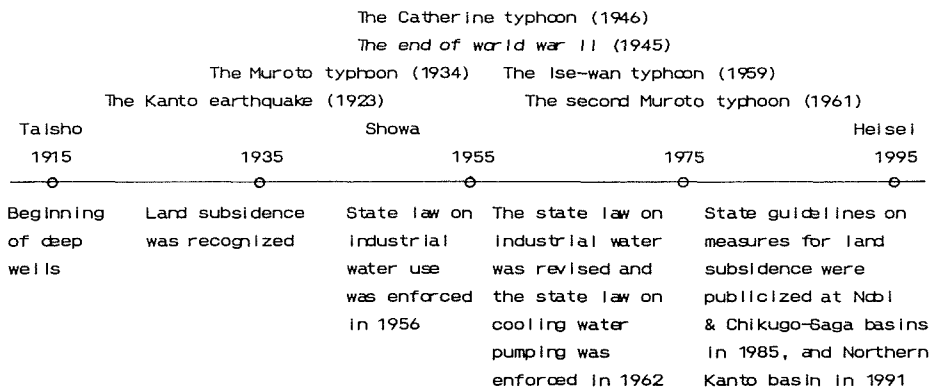
numerical groundwater simulation were reported from the cities of Tokyo and Osaka. In addition, the installation of new observation wells for measuring groundwater heads and land subsidence was required as groundwater simulation techniques became more advanced. Many of observation wells have been at depths of 100~300 m excepting those for deep geological boring wells.

The concept on optimal groundwater utilization and pumping for promoting the conservation of the groundwater as well as a countermeasure for land subsidence was investigated at the end of the 1980s. The state government tried to make a law on the conservation of groundwater, but it failed to pass the draft law because the common interests were not amended. A cabinet ministers' meeting on countermeasures for land subsidence (nine ministers were present at the meeting) was held in November 1981. The meeting confirmed the guidelines for countermeasures for land subsidence at three basins: Nobi and Chikugo-Saga (1985) and Northern Kanto (1991). The effectiveness of the measures can be illustrated by the changes of land subsidence in space and time presented in Fig. 2.

The priority policy in Northern Kanto basin is to develop new water resources in place of excessive groundwater use under optimal groundwater pumping. The rules for groundwater pumping are based upon:

- optimization of the allocation and distribution of regional pumping volume,
- optimization of well locations and depths,
- optimal operation of pumping wells.

In planning the optimization policy, numerical simulation coupled with linear programming theory has been applied (National Land Agency of Japan, 1993).

**Fig. 1** A short history of land subsidence and groundwater use.

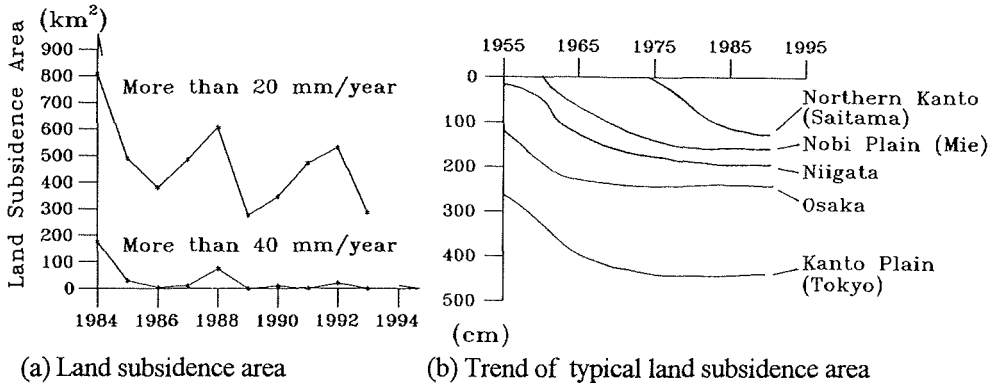


Fig. 2 Change of land subsidence in Japan: (a) land subsidence areas, (b) trends of a typical land subsidence area (after Environment Agency of Japan, 1994).

In the last decade Japan has experienced serious water shortages every three or four years. How to use groundwater resources in the drought season is one of the important considerations.

COUNTERMEASURES FOR LAND SUBSIDENCE IN NORTHERN KANTO BASIN

Hydrogeology and background of land subsidence

The location of the Northern Kanto basin is shown in Fig. 3(a). The basin covers five prefectures (Saitama, Gunma, Ibaraki, Tochigi and Chiba), and the population in it is about ten millions. Three big rivers (Tone-gawa, Ara-kawa and Edo-gawa) flow through the basin. The average rainfall is 1284 mm year⁻¹ (Kumagaya, Saitama), and the annual temperature is 13.9°C.

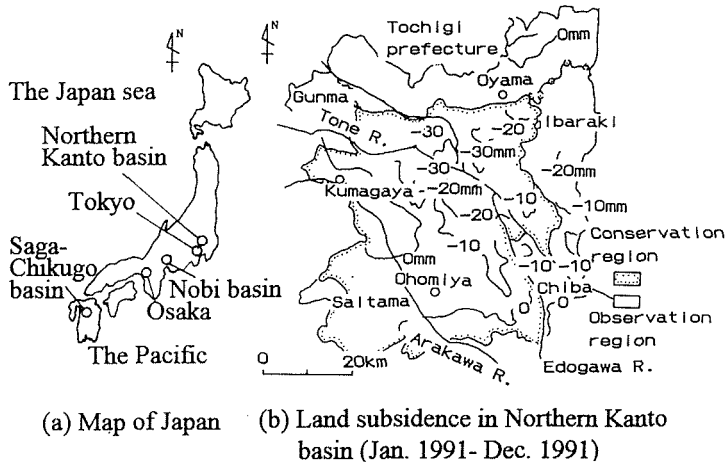


Fig. 3 Location of Northern Kanto basin and its land subsidence.

The basin consists of several terraces and hills, and an alluvial plain 30~60 m a.m.s.l. The geology of the basin is classified into alluvial and diluvial deposits, Tertiary deposits and a bottom set bed of the Miocene. The depth of the hydrogeological base may be in the range of 1500~2000 m below m.s.l. The basin is located at the centre of the Kanto basin. The alluvial deposits are mainly composed of soft clay and sand. The land subsidence caused by the groundwater withdrawal is mainly due to soft clay. The diluvial deposits consist of sand, gravel and consolidated clay. The strata of the basin are complex. Groundwater is extracted mainly from depths between 100 and 300 m. The largest land subsidence has occurred since 1980. The total pumping discharge of groundwater was 660 million m³ year⁻¹ in 1986. Figure 3(b) shows the Northern Kanto basin and land subsidence in 1991. The largest land subsidence contour is -40 mm in the northwest part of Saitama prefecture. The National Land Agency of Japan has determined a pumping goal of 480 million m³ year⁻¹ using the following process.

Determination of the goal for pumping discharge

One of the most important tasks for the state guidelines for the basin is to determine a goal for pumping discharge without the occurrence of land subsidence (Sato *et al.*, 1986; Specialist Committee on Preventive Measures for Land Subsidence, 1990). Two methods were adopted:

- empirical method based on relationship between land subsidence and pumping discharge;
- coupling numerical simulation with linear programming.

Empirical method based on relationship between land subsidence and pumping volume A pumping volume goal in a hydrogeological basin is defined as the sum of maximum (or allowable and optimal) pumping volumes without the occurrence of land subsidence in all sub-basins. The pumping volume goal must be less than the total recharge by precipitation.

The pumping volume can be determined from a set of relationships between land subsidence and pumping volume as follows. The average land subsidence s_i in sub-basin i ($i = 1, 2, 3, \dots, N$) from a total pumping volume per year q_i (Fig. 4) is calculated as:

$$\bar{s}_i = \frac{i}{M} \sum_{j=1}^M s_j^i \dots \quad (1)$$

in which j is the number of benchmarks for land levels ($j = 1, 2, 3, \dots, M$) at the i th sub-basin.

The total pumping discharge q_i from the i th sub-basin and the total pumping discharge Q from the basin are determined as follows:

$$q_i = \sum_{k=1}^L q_k \dots \quad (2)$$

$$q = \sum_{i=1}^N q_i \dots \quad (3)$$

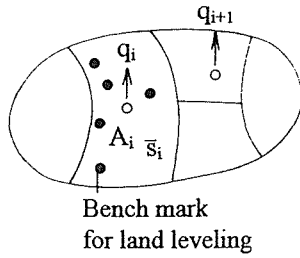


Fig. 4 Pumping discharge q_i and land subsidence \bar{s}_i in sub-basins.

where L is the number of pumping wells in the i th sub-basin and N is the number of sub-basins.

In practice the total pumping discharge per unit area ($\text{m}^3 \text{ year}^{-1} \text{ km}^{-2}$) is sometimes used. Based on several existing relationships between the total pumping discharge per unit area q_i and averaged land subsidence s_i in the i th sub-basin, a critical total pumping discharge q_{ci} corresponding to $s_i = 0$ will be found practical as shown in Fig. 5. The goal for pumping discharge Q_0 in the whole basin will be estimated by:

$$Q_0 = \sum_{i=1}^N A_i \bar{q}_{ci} \dots \tag{4}$$

in which A_i is the area of the i th sub-basin.

This method is applicable for estimating the maximum pumping discharge in a hydrological basin equipped with many benchmarks for land levels over a decade or more.

Method based on numerical simulation coupled with linear programming Let us consider an optimizing problem of groundwater pumping discharge in a hydrological basin. The basin consists of N sub-basins which usually are administrative districts as cities, towns or villages as shown in Fig. 6. The critical head at some sub-basins is specified and it is required to maximize the total sum of pumping discharges from the whole basin:

$$Q_0 = \sum_{i=1}^N q_{oi} \rightarrow \max \dots \tag{5}$$

$$h_i \geq h_{ci} \dots \tag{6}$$

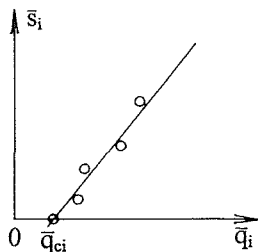


Fig. 5 Relationship between \bar{q}_i and \bar{s}_i .

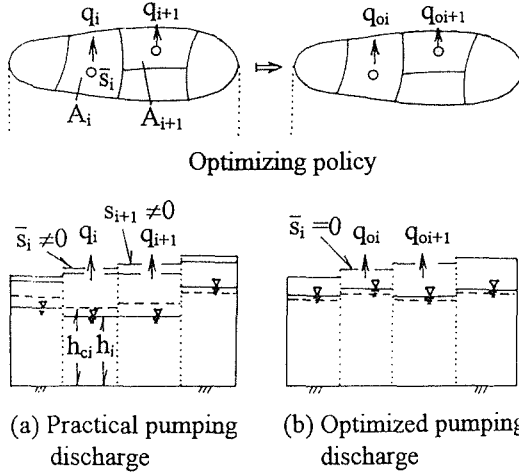


Fig. 6 Optimization of pumping discharge and its realization policy.

where q_{oi} is positive.

$$\frac{\partial}{\partial x} (T_k \frac{\partial h_k}{\partial x}) + \frac{\partial}{\partial y} (T_k \frac{\partial h_k}{\partial y}) + \frac{K_k}{b_k} (H - h_k) + \frac{K_{k+1}}{b_{k+1}} (h_{k+1} - h_k) + R - \sum_{k \in N_q} q_k \delta(x_k, y_k) = S_k \frac{\partial h_k}{\partial t} \dots \quad (7)$$

The basic equation of groundwater flow is where x, y are horizontal coordinates, T is transmissivity, h is groundwater head, K is permeability of the confining layer, b is thickness of the confining layer, H is groundwater head in unconfined aquifer, R is natural recharge rate, q is pumping discharge rate, N_q is number of pumping wells, d is Dirac delta, S is storativity, t is time and k is the number of the aquifer.

Applying FEM to equation (7) at the steady state results in a set of linear simultaneous equations expressing the relation between head h and pumping discharge q . Linear programming will give the optimal pumping discharge q_{oi} at each sub-basin i and the total pumping discharge goal Q_0 . The most important aspect in this method is the determination of the critical head h_{ci} because it often involves some legal and administrative matters as well as scientific reality. A typical application of this method is shown in Fig. 6. The overall methodology of the computation of the optimal pumping discharge and its distribution in terms of required groundwater use plan under restricted conditions is shown in Fig. 7.

OBSERVATION SYSTEMS OF GROUNDWATER AND LAND SUBSIDENCE

There are many groundwater observation wells all over Japan. They can be classified into three kinds: shallow wells for measuring shallow groundwater, deep wells which consist of double pipes and single pipe wells, which have been adopted from abandoned pumping wells. Usually, observation wells are less than 700 m deep, except those for seismic measurements, and most deep wells are 100 ~ 300 m. Geological, mechanical and hydraulic surveys are carried out by boring. Several wells with different depths are bored in the same place; the groundwater heads of different aquifers can then be

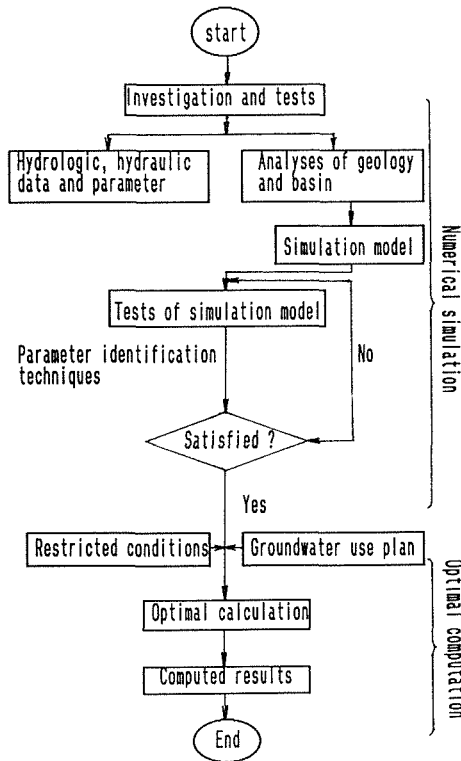


Fig. 7 Numerical computation procedure for groundwater use plans.

measured, as well as the land subsidence at each depth. There is also a number of shallow observation wells used to measure shallow groundwater behaviour up to depths of several tens of metres. The data give us precise information to estimate the natural recharge and infiltration by precipitation. Figure 8 shows a typical observation well and

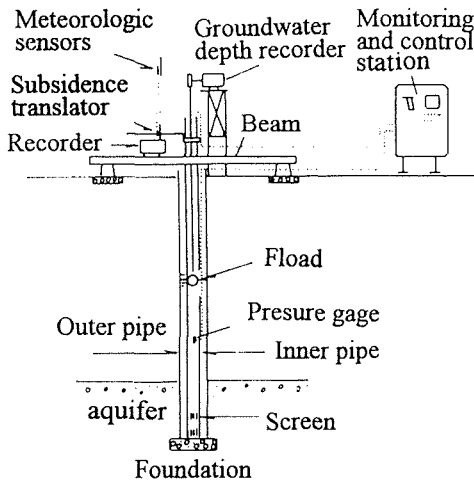


Fig. 8 A typical observation well and its recording devices.

its recording equipment. Monitoring and maintenance of wells are performed by several state ministries and agencies, and by many prefectural governments (Sato, 1988).

Recently, as the number of observation wells has increased in large basins and modern technology has advanced, automated observation systems are being introduced. Several new types of data processing equipment have been developed along a conceptual process (Fig. 9).

Real-time data collection and processing are useful for the achievement of safe groundwater utilization, preventing land subsidence.

Highly accurate level measurements are carried out in many basins once a year (in winter, when the land subsidence abates) to measure land subsidence. The results of these measurements are shown as contour lines on topographical maps. In addition, pumping volume and atmospheric data are collected in every city and basin. The simultaneous measurement of groundwater heads at a number of pumping wells can be performed whenever the occasion demands.

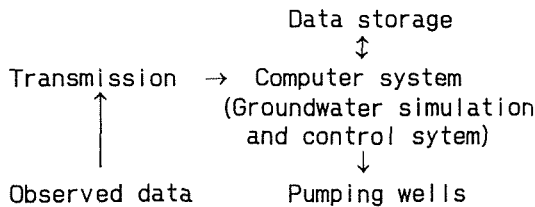


Fig. 9 Data processing concept.

CONCLUSION

In Japan there has been a long tradition of countermeasures for land subsidence for at least half a century. The history and current state are summarized as follows:

- The historical stages with respect to countermeasures for land subsidence were; a significant increase of land subsidence in big cities during about 10 years after World War II; regulation of industrial groundwater use by state and local government laws since 1956; and a localizing and land subsidence extending to local cities in the vicinity of big cities in later years.
- The state government (National Land Agency) issued guidelines in three different areas (Saga-Chikugo plain in Kyushu, Nobi plain and Northern Kanto plain on the main land) to arrest serious land subsidence.
- Most countermeasures for land subsidence have been planned through computers using numerical simulation techniques coupled with optimization theories. The use of computers been popular since the mid 1970s.
- The current concept of countermeasure for land subsidence is concentrated on optimal groundwater pumpage in the following ways: (i) optimization of local allocations or distribution in groundwater pumping volume, (ii) optimization of pumping wells in depth and location, and (iii) optimal operation of pumping wells in avoiding a rapid groundwater drop.

Finally, two future problems are foreseen. Most data collecting systems in Japan use traditional charts at observation sites. There is a need for a more systematic observation

of groundwater and land subsidence measurements. Another is land subsidence resulting from abnormal groundwater withdrawal in drought seasons. Some serious droughts have been experienced every three or four years in summer. The occurrence of abnormal land subsidence has been a matter of concern.

REFERENCES

- Environment Agency of Japan, Study Society on Preventive Measure for Land Subsidence (1990) *Land Subsidence and Its Preventive Measure* (in Japanese). Hakuha Book Comp.
- Environment Agency of Japan (1994) *An Outlook of Land Subsidence in Japan* (in Japanese). Environment Agency of Japan, December 1994.
- National Land Agency of Japan (1993) *Water Resources in Japan* (in Japanese). National Land Agency of Japan, August 1993.
- Sato, K. (1988) *Groundwater Resources and Characteristics of Groundwater Basins*, 45-52. Water Resources Development, vol. 4, Butterworths.
- Sato, K. *et al.* (1986) Investigation on optimal groundwater pumping in Saitama basin (in Japanese). *J. Soils and Foundations, Japan. Soc. Soil Mechan. & Foundation Engng (JSSMFE)* **1641**, November, 25-31.
- Specialists Committee on Preventive Measure for Land Subsidence, Saitama (1990) *On an Optimal Groundwater Pumping Volume Based on State Guideline of Preventive Measures for Land Subsidence in Northern Kanto Basin* (in Japanese). Report for Saitama Prefectural Government.

Groundwater rise and hydrocollapse: technical and political implications of "Special Geologic Report Zones" in Riverside County, California, USA

ROY J. SHLEMON

*Roy J. Shlemon & Associates Inc., Geological and Environmental Consultants,
PO Box 3066, Newport Beach, California 92659-0620, USA*

Abstract Rapid urbanization in the semi-arid southwestern part of Riverside County, California is made possible only by the large-scale importation of water for domestic use. The resulting irrigation run-off and infiltration has caused groundwater levels to rise over 20 m within the past few years, particularly in former, alluvium-filled channels. Soil hydrocollapse, differential settlement and ground fissures are now occurring, causing extensive damage to houses, schools and related infrastructure. Alleged property damages exceed 50 million (US) dollars, and litigation has ensued. For public safety, the County of Riverside established two Special Geologic Report Zones, each about 500 ha, deemed "California Oaks" and "Silverhawk," respectively. In retrospect: the formation of the zones has proven to be administratively time-consuming and expensive; the litigation between home-owners, builders, geotechnical firms and reviewing agencies is divisive; home values, even for undamaged structures, have been reduced owing to "disclosure" laws; and the geotechnical community now recognizes, from sad experience, that rapid urbanization and related water level rise accelerates the potential for soil hydrocollapse and extensive property damage.

INTRODUCTION

In 1989, land subsidence and ground fissures were first observed in a new residential area in southwestern Riverside County, about 125 km southeast of Los Angeles in southern California (Fig. 1). Urbanization, particularly centred around the towns of Murrieta and Temecula, has been very rapid, and the population has increased from a few thousand in 1980 to over 100 000 in 1990. This portion of Riverside County has a Mediterranean, semiarid climate, with rainfall generally less than about 400 mm year⁻¹. The potential for groundwater withdrawal is thus inherently limited. Indeed, where such withdrawal occurred nearby, faults were seismically rejuvenated, causing surface fissures and significant damage to residential and commercial structures (Shlemon & Davis, 1992). Rapid urban growth is therefore only possible by large-scale importation of water for residential and recreational use. However, it was soon determined that urban water run-off, particularly from landscaping and golf course maintenance, eventually saturated 35-m thick, previously "unwetted" alluvium that remained in deeply incised late-Pleistocene-age channels. Soil hydrocollapse thus ensued, causing local land subsidence and ground fissures, damage to over 50 homes and scores of unbuilt lots,

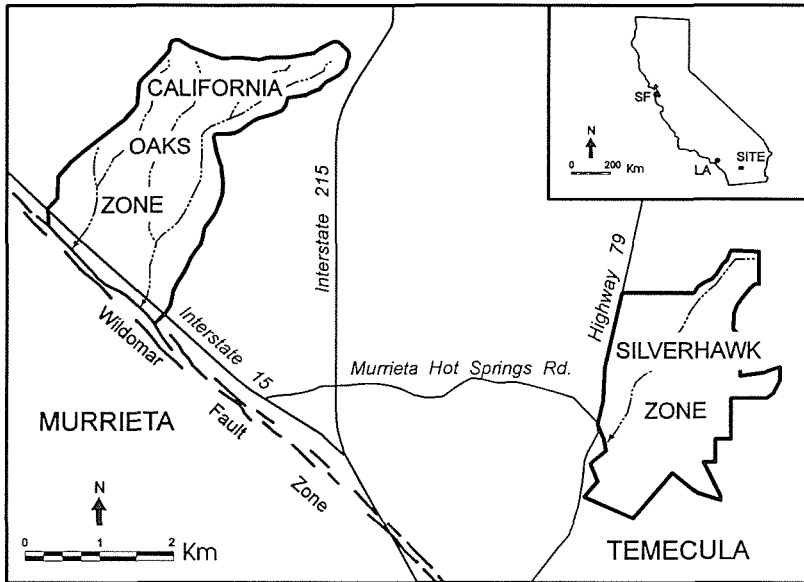


Fig. 1 Location of the California Oaks and Silverhawk Special Geologic Report Zones at Murrieta and Temecula in southwestern Riverside County, California. Major alluvium-filled channels within the zones shown by dashed lines. SF = San Francisco; LA = Los Angeles.

abandonment of a public school, and local disruption of sewage and water systems. Property damage, allegedly exceeding \$50 million (US) dollars, has now led to extensive litigation between water providers, property developers, home builders, home-owners, government agencies and geotechnical firms. The County of Riverside has now established two Special Geologic Report Zones informally deemed "California Oaks" and "Silverhawk," respectively (County of Riverside, 1991, 1994; Fig. 1).

SUBSIDENCE AND FISSURES: THE INFLUENCE OF SOIL HYDROCOLLAPSE

The California Oaks and Silverhawk Special Geologic Report Zones encompass over 1000 ha of slightly undulating terrain mostly underlain by granitic rocks, by the Plio-Pleistocene Pauba formation, and by alluvium-filled channels that trend westward across the active Wildomar fault zone (Fig. 1; Shlemon & Hakakian, 1992). Litigation-driven investigations (Pacific Soils Engineering, 1992) show that the principal cause of subsidence and fissures is hydrocollapse of previously unsaturated alluvium. Four principal factors, when occurring together, give rise to hydrocollapse-caused subsidence and fissures in this part of Riverside County:

- the presence of relatively thick, partially saturated alluvium;
- the occurrence of a relatively steep (usually more than about 2:1), alluvial-bedrock frontal slope, typically the outside of an ancient meander loop within the channel;
- the placement of an overlying load, usually compacted fill, across the bedrock-alluvial transition;
- the rapid rise of regional and perched groundwater levels (Fig. 2).

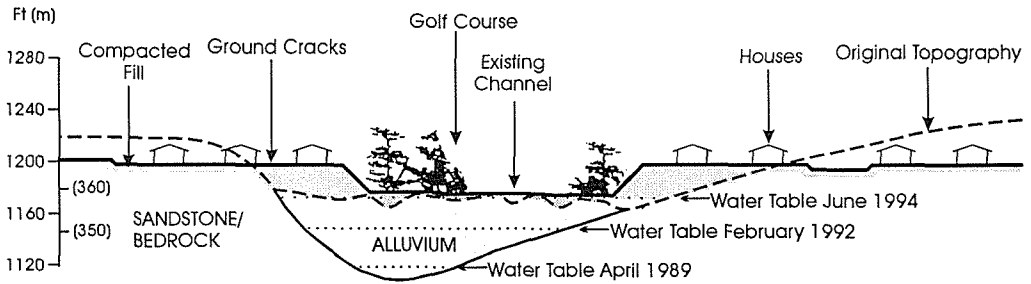


Fig. 2 Generalized section across a former alluvium-filled channel in the California Oaks Special Geologic Report Zone showing the 20-m, urban-induced rise in water levels, the location of hydro-collapsible alluvium, and the site of damaged houses and infrastructure.

The California Oaks Zone

The first of the two Special Geologic Report Zones, the California Oaks Zone, was established in 1991 and now is within the administrative jurisdiction of the City of Murrieta (Fig. 1). Well log data show that groundwater levels rose about 20 m in the two-year period between 1989 and 1992, a time of regional drought (Fig. 2). The ensuing hydrocollapse resulted in widespread differential settlement and ground fissures that particularly impacted "view" homes built on alluvial-bedrock transition zones and on bluffs overlooking golf courses constructed in the old Pleistocene channels (Fig. 3). Additionally, several roads failed, the infrastructure was impaired, a public school was severely damaged and ultimately torn down and, in one area, an entire street tilted resulting in either abandonment or non-sale of many new homes (Fig. 4).

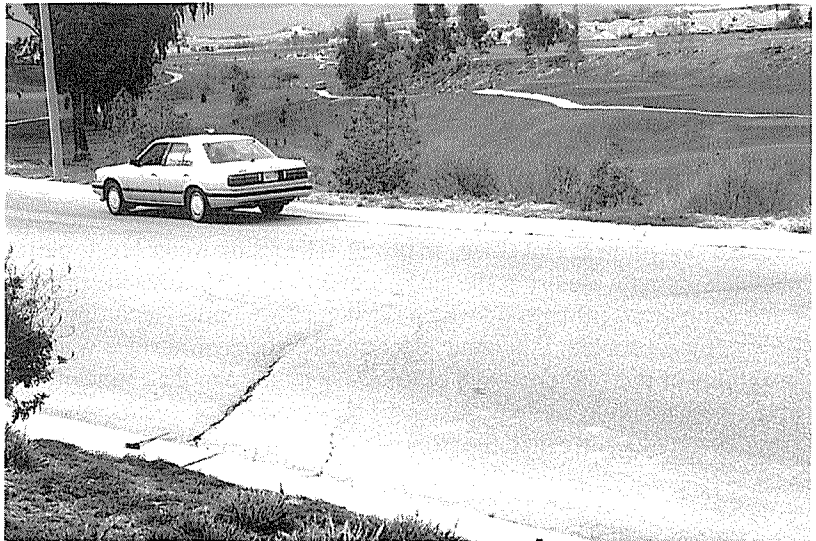


Fig. 3 Typical ground fissures disrupting roads, sewage and potable water lines in the California Oaks Zone. The fissures coincide with the subsurface alluvial-bedrock contact that define the margins of former alluvium-filled channels now encroached upon by housing tracts (background) and golf courses (middle-ground).



Fig. 4 Unsold or abandoned "new homes" distressed by ground fissures and differential settlement. Disruption of street paving (foreground) is caused by subsurface soil hydrocollapse resulting in street tilting and 10 cm of surface compression. The concrete curbing, acting as a temporary rigid beam, is now cracked.

Geotechnical mitigation for yet unbuilt lots has been mainly entailed the complete removal of all underlying alluvium and the rebuilding of slopes with up to 30 m of compacted fill, a very expensive undertaking. Elsewhere, where houses are tilted but are still structurally sound (generally those built with post-tensioned foundations), homeowners were paid a "fee" to be temporarily relocated. The structures were then relevelled using mud-jacking methods, the alluvium was stabilized by injection of grout, and an additional property warranty was provided to the owner. Such mitigation is similarly very expensive, often ranging from about one-third to one-half the original cost of the property.

The onset of "100-year" rainfall in January 1993 accelerated groundwater rise within the old alluvium-filled channels. This "natural" water was superimposed on anthropic (urban run-off) groundwater levels thereby contributing to hydrocollapse-induced damage (Shlemon & Hakakian, in press). The rising water level, particularly in the old channels, is now almost at the surface and, locally, has reached the typically 3 to 5 m thick compacted fill-caps on which the homes are built. Accordingly, another potential geotechnical problem is at hand. Specifically, the near-surface water levels, the nearby proximity of the Wildomar and other active faults, and the abundance of fine sand in the underlying alluvium has now increased the potential for seismically induced liquefaction from essentially nil, when the Zone was first investigated, to "very high."

The Silverhawk Zone

The Silverhawk Special Geologic Zone was more recently established by the County of Riverside (1994) following a technical-report "disclosure" of potential hydrocollapse

(Fig. 1). Here, however, neither differential subsidence nor ground fissures have yet been unequivocally attributed to rising water levels. Nevertheless, based on proximity to the California Oaks Zone where damages are extensive, and on the similar geologic setting, the County of Riverside – again in the interest of public safety and welfare – now requires the land developer, the home builder and the home owner, alike, to conduct additional geotechnical investigations to evaluate the potential for subsidence, ground fissures and ultimately for damage to habitable structures. The establishment of the Silverhawk Zone allegedly resulted in loss of sales and possible diminution of land values. Litigation has thus ensued. As in California Oaks, certain Silverhawk Zone builders and developers have brought suit against the County, against each other, and will soon likely seek financial redress from their respective geotechnical firms.

CONCLUSIONS

Lessons to be learned from establishment of subsidence and fissure-related Special Geologic Report Zones in Riverside County are many:

- Administratively, it is time consuming and expensive, although, in the interest of public safety and welfare, the County of Riverside was obliged to establish the California Oaks and the Silverhawk zones and thereby require land developers and home builders to conduct adequate geotechnical investigations for mitigation of potential differential settlement and ground fissures.
- Legally, the spate of litigation produces much ill will and seemingly provides few benefits other than to the legal profession (Corwin *et al.*, 1991).
- Financially, the home builders pay for the additional government-mandated investigations and reviews; and the home owner, according to California law, must disclose to any future buyer that his house is in a "Special Geologic Report Zone," thus potentially lowering the value of the property.
- Technically, from a professional "standard of care" viewpoint, the geological and engineering community now recognizes that the hydrocollapse potential is much more widespread than previously thought, particularly where rapid urbanization and related water importation and run-off may cause accelerated rise in regional groundwater levels. In retrospect, the establishment of Special Geologic Report Zones has proven to be socially "traumatic." However, the Riverside County experience shows that money spent for land subsidence and ground fissure investigations *prior* to urban development usually negates the need for such zones. The cost of such early investigations pale in comparison with those for damage repair, for seemingly endless litigation, and for loss of good will.

Acknowledgements I thank Consultant M. Hakakian and the Riverside County Geologist S. Kupferman for sharing their insights about extent and causation of subsidence and fissures in the zones. I likewise thank J. Hanson (Pacific Soils Engineering, Inc.) for providing unpublished water level data.

REFERENCES

- County of Riverside (1991) *Special geologic report zone, Resolution 91-125*. Department of Building and Safety (Riverside, California).
- County of Riverside (1994) *Special Geologic report zone, Resolution 94-125*. Department of Building and Safety (Riverside, California).
- Corwin, E., Alhadeff, S., Oggle, S. & Shlemon, R. (1991) Earth fissures, urbanization and litigation: a case study from the Temecula area, southwestern Riverside County, California. In: *Land Subsidence* (ed. by A. I. Johnson) (Proc. Fourth Int. Symp. on Land Subsidence, Houston, May 1991), 291-299. IAHS Publ. no. 200.
- Pacific Soils Engineering, Inc. (1992) Murrieta Special Geologic Report Zone – report, Murrieta, California. *Consultants' Technical Report 23* (for Builders' Cooperative Association, Murrieta, California).
- Shlemon, R. J. & Davis, P. (1992) Ground fissures in the Temecula area, southwestern Riverside County, California. In: *Engineering Geology Practice in Southern California* (ed. by B. W. Pipkin & R. J. Proctor), 275-288. Assoc. Engineering Geologists, Southern California Section Special Publ. no. 4, Star Publ. Co., Belmont, California.
- Shlemon, R. J. & Hakakian, M. (1992) Fissures produced both by groundwater rise and by groundwater fall: a geological paradox in the Temecula-Murrieta area, southwestern Riverside County. In: *Proc., Assoc. Engineering Geologists, 35th Ann. Meeting* (Long Beach, California) (ed. by M. L. Stout), 165-169.
- Shlemon, R. J. & Hakakian, M. (in press), Impact of the 1992-1993 winter storms on ground fissures and differential settlement, Murrieta area, southwestern Riverside County, California. In: *Impact of the 1992-1993 Winter Storms in Southern California* (ed. by R. Larson & J. Slosson). Geol. Soc. America Reviews in Engin. Geology.

Recent trend of land subsidence in Japan

SOKI YAMAMOTO

Tokyo Seitoku College, 1-7-13 Jujodai, Kitaku, Tokyo 114, Japan

Abstract Many areas of Japan are still affected by land subsidence. The author reviews and summarizes the history of land subsidence in Japan. Most areas of land subsidence are located on alluvial plains and hit the headlines as a result of natural disasters such as earthquakes, typhoons and droughts. Recently, new incidents of subsidence have occurred in areas where groundwater is used to melt thick snow on roads. An intergovernmental committee has been asked to propose solutions to this problem area by area.

INTRODUCTION

There are many land subsidence areas in Japan. According to the Environmental Protection Agency of Japan (1995), principal subsiding areas are distributed in 37 prefectures with 62 regions. The 11 areas where subsidence exceeds 20 mm year^{-1} amount to 276 km^2 . Although in general subsidence is slowly decreasing, some remarkable new incidents of subsidence have occurred in some areas. Last year (1994) Japan was suffered a severe drought and most of the reservoirs dried up. The shortfall in water resources for drinking and irrigation was supplied by groundwater, and this accelerated some remarkable incidents of land subsidence.

It noteworthy that recently Japan introduced the centimetre (cm) as a unit of subsidence amount instead of the millimetre (mm).

HISTORICAL REVIEW OF LAND SUBSIDENCE IN JAPAN

Deep well drilling started at the beginning of 1900. The drilling company "Nissaku" which adopted the western type drilling method was established in 1913. Taking advantage of the economic boom during the World War I, deep well drilling became popular in Japan.

The great Kanto earthquake which hit Tokyo in 1923 drew attention to land subsidence in Tokyo. Then attention was drawn to the subsidence at Osaka around 1928. Hirono & Wadachi (1989) pointed out that land subsidence was caused by the withdrawal of groundwater. Generally speaking, land subsidence in Japan is brought to our notice through natural disasters such as typhoons, earthquakes, heavy rainfalls and droughts.

Comparing the distribution of the areas of land subsidence in 1965 and 1994, no change is found, but differences can be seen in the size and amount of maximum subsidence (Fig. 1). The historical changes of subsidence are shown in Fig. 2. This

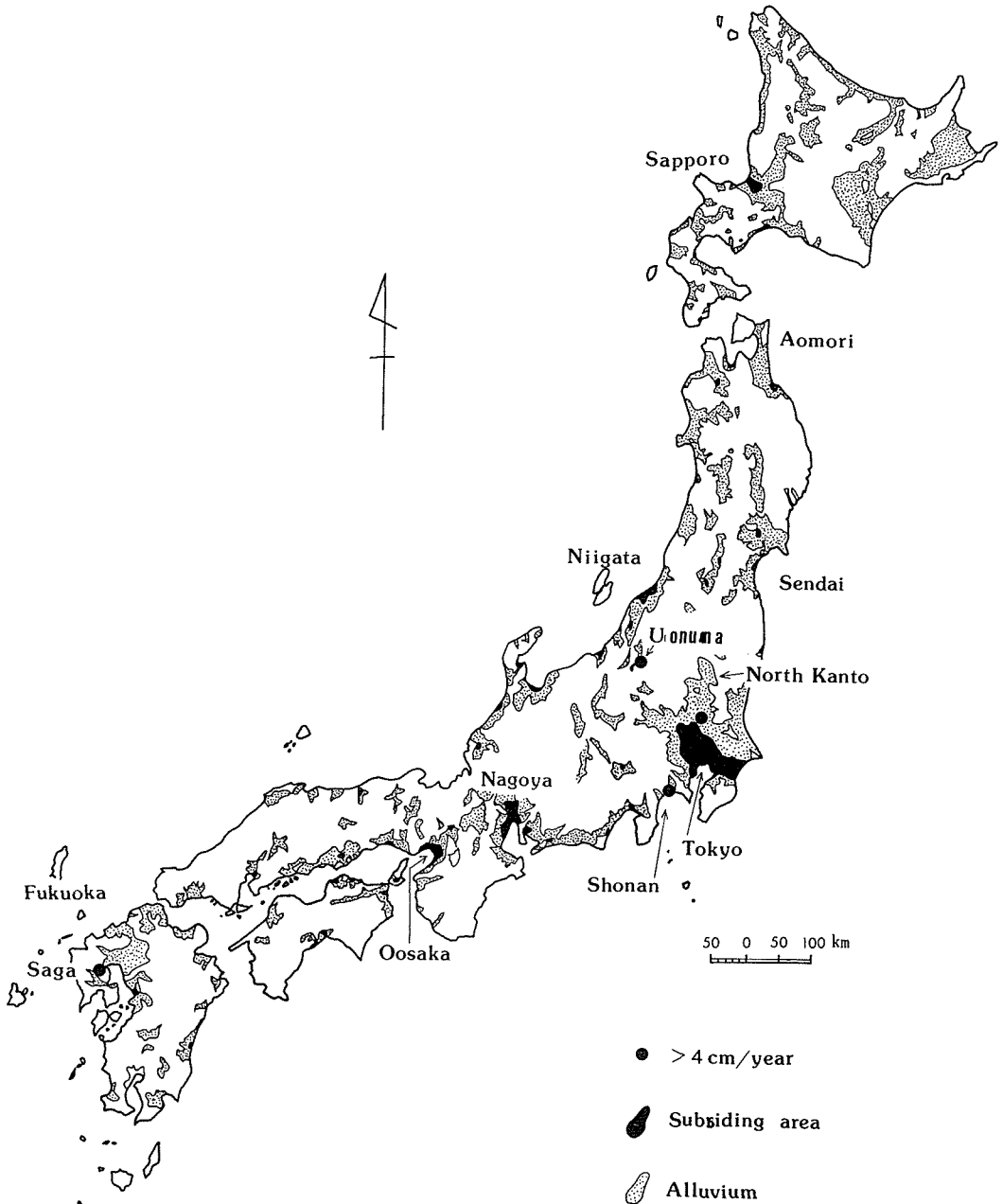


Fig. 1 The distribution of land subsidence areas and alluvial plains in Japan.

figure shows there are three types of change: slow, rapid and slowing-down components of sinking. The decline in water level is parallel to this sinking curve with the exception of two rises, one at the end of World War II and the other at the invocation of the subsidence regulation law. In response to these two rises, an interruption or slowing-down of subsidence can be seen.

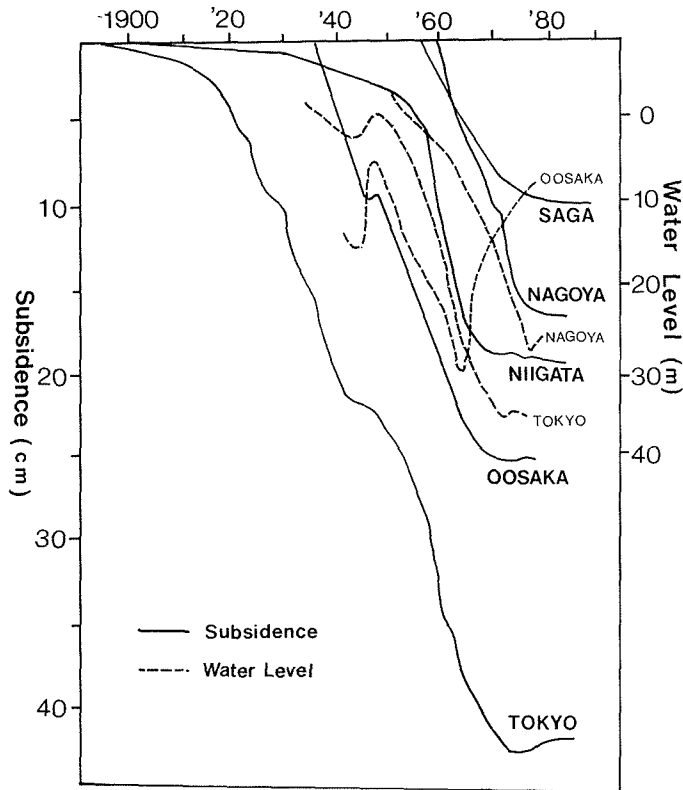


Fig. 2 Subsidence and change in piezometric head in selected areas.

There have been many discussions concerning the cause of land subsidence. The denial that the principal cause of subsidence in Niigata was due to gas water withdrawal was a famous one. But the gas water discharge in Kujukuri was approved with its iodine product in the sparsely populated region and recharge work of separated water. Later in the Niigata region, gas extraction was permitted on the condition that separated water was recharged into the aquifer when gas was extracted from the deep Tertiary formation.

Industrial Water Law (1956) and Building Water Law (1962) prevented land subsidence, and the establishment of the Japanese Environmental Protection Agency also contributed to stopping land subsidence in Japan. Present disastrous subsidence is occurring on agricultural land and regions of drinking water shortage because of an increase in groundwater withdrawals.

NEW ASPECTS OF LAND SUBSIDENCE

Recently the practice of using groundwater for melting snow is increasingly being used in Japan. Along the Japan Sea coast a thick snow-covered zone exists. Snow covers as deep as 7.3 m are recorded in the eastern part of Nagano. In winter time in this region, first-floor windows are used as doorways! It is very important to remove snow on the roads.

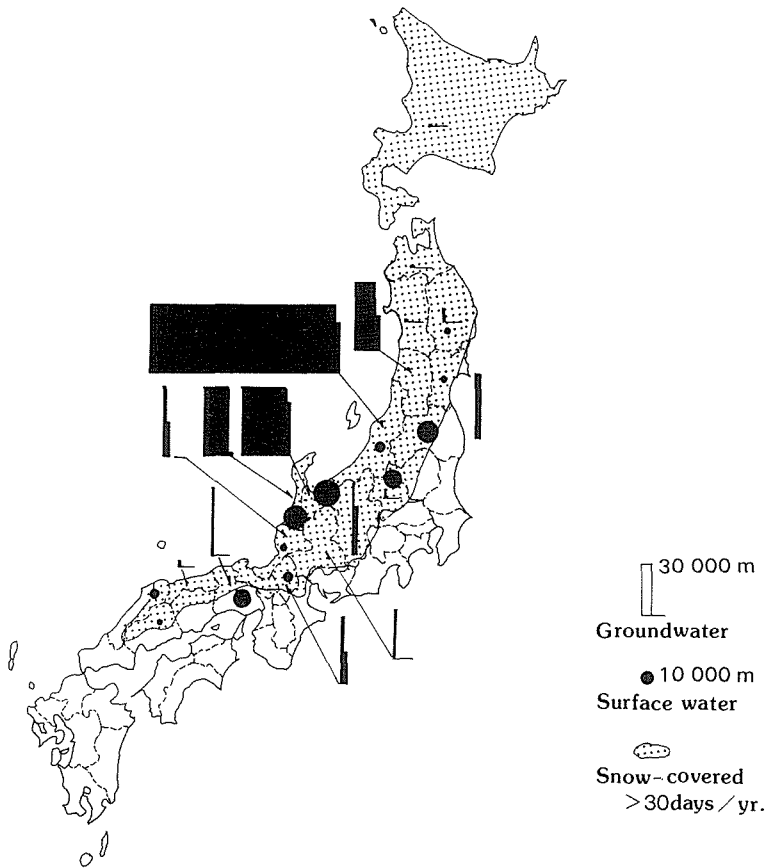


Fig. 3 Length of snowmelting pipes in Japan.

As a snow removal method, snowmelting pipes are installed under roads. Through nozzles located 10 cm apart in the pipes, water is sprinkled to remove the snow. The distribution of the snow removal pipeline is shown in Fig. 3. The length is considerable along the Japan Sea coast. Groundwater is more suitable than surface water for this purpose and groundwater is pumped intensively for four months in winter for this purpose.

Recently remarkable subsidence due to groundwater withdrawal has been observed at Muikamachi in the southern part of Niigata Prefecture. The maximum subsidence amounts to 73 mm year⁻¹ and area affected is estimated to be as much as 50-60 km². This is one of the worst incidents recently recorded in Japan. As Muikamachi is a thick snow-covered area, a tremendous amount of groundwater is used for melting snow. The total discharge of groundwater in this town is $126 \times 10^3 \text{ m}^3 \text{ day}^{-1}$ during winter time. The drawdown of water level at Bunkakaikan's well was 13.0 m and shrinkage of the clay layer amounted to 57 mm in 1993. The total amount of subsidence over 17 years reached 450 mm.

Muikamachi town is located on the alluvial valley of a tectonic origin. The maximum depth of the alluvial deposits, consisting of sand and gravel layers with two clay

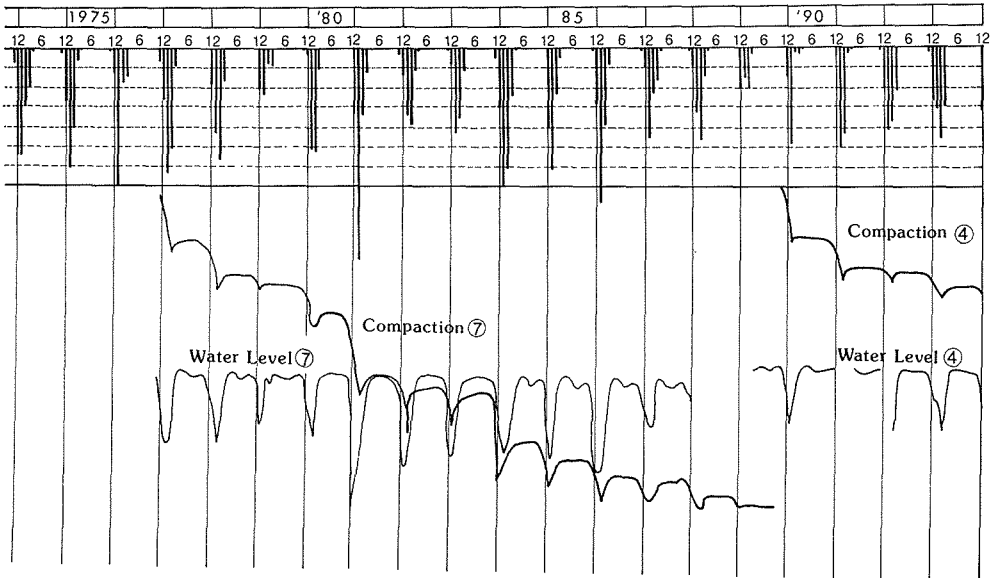


Fig. 4 Subsidence and water level changes at Minami-Uonuma.

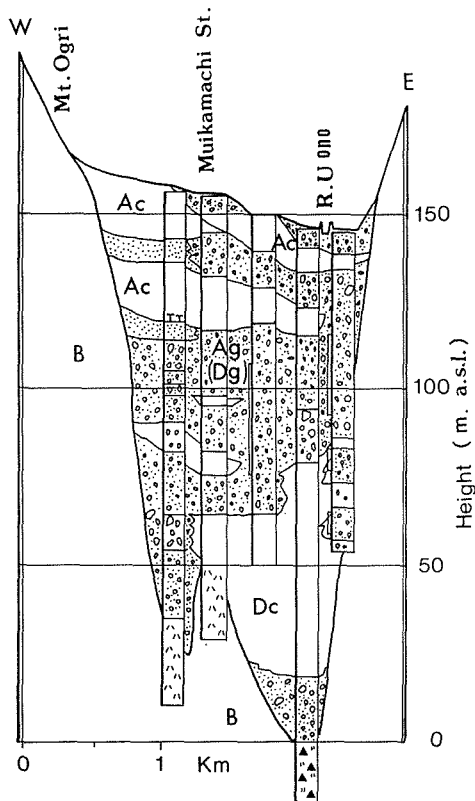


Fig. 5 Geological cross section at Minami-Uonuma.

layers, is about 150 m. The upper clay layer is situated at a shallow depth of 40 m and the other one of 50 m thickness is deeper than 80 m and underlain by sands and gravels (Fig. 4). The popular depth of wells ranges from 40 to 80 m, and most wells tap the upper confined aquifer of 40-80 m depth. The compaction of the upper clay layer is occurring.

Land subsidence of Muikamachi town is produced by the heavy pumping of groundwater for a limited period in winter time. It is noticed that the groundwater level recovers quickly after pumping has stopped, but that while subsidence continues to accelerate with no recovery. The town authorities are now considering the introduction of legal regulations to remedy this situation (Fig. 5).

RECENT NEW POLICY TO COPE WITH LAND SUBSIDENCE

Japan has two laws which regulate groundwater utilization for building and industrial use but none for drinking and irrigation use. Most local governments have municipal ordinance for groundwater. Recently our government organized an "Intergovernmental Committee for Land Subsidence". The Committee was composed of nine Ministers as members and nominated three specific regions – Nobi Plain (Nagoya), Chikushi Plain (Saga) and North Kanto (northeastern part of Tokyo) – where disastrous subsidence was still happening over large areas.

Several specialists were appointed as regional committee members. Discussions are underway to determine the tolerable cutback for each region and from computer analyses to decide the techniques of optimal pumping operation with regard to safety and permissive groundwater head. In addition to this effort, the author would like to see artificial groundwater recharge introduced in Japan.

REFERENCES

- Environmental Protection Agency (1995) *Brief Summary of Land Subsidence in Japan*.
Hirono, T. & Wadachi, K. (1989) *Land Subsidence in Western Osaka*, 1. Report of the Disaster Prevention Research Institute.